

Volume II Findings

Effects of Dredge Deposits on Seagrasses: An Integrative Model for Laguna Madre

Concluding Report



**INTERAGENCY COORDINATION TEAM
U.S. ARMY CORPS OF ENGINEERS, GALVESTON DISTRICT**

**The University of Texas Marine Science Institute
Texas A&M University Department of Oceanography
Texas Parks and Wildlife Department**

March 2003

FINAL

**EFFECTS OF DREDGE DEPOSITS ON SEAGRASSES:
AN INTEGRATIVE MODEL FOR LAGUNA MADRE**

Concluding Report

VOLUME II

Findings

March 2003

CITATION

Dunton, K.H., A. Burd, L. Cifuentes, P.M. Eldridge, and J.W. Morse. 2003. Concluding Report Effects of dredge deposits on seagrasses: an integrative model for Laguna Madre. Volume II: Findings. U.S. Army Corps of Engineers, Galveston District, Galveston, Texas.

Abstract

This report presents the results of an interdisciplinary collaborative effort to develop an integrative model for seagrass productivity in Laguna Madre. One of the major components of this integrative model is the Laguna Madre Seagrass Model (LMSM) which was designed to interface with other component models described in this report, including carbon and nitrogen allocation, sediment diagenesis, and spectral irradiance and radiative transfer. Linkage with hydrodynamic and sediment transport models provided a potentially valuable management tool to assess the effects of maintenance dredging and resuspension of dredged material deposits on seagrasses of Laguna Madre.

The development of the models described in this report required a substantial input of data for model calibration and when possible, verification. For the seagrass models, much of this data were available from previously published studies (*e.g.*, *Halodule wrightii*), but intensive field work, from April 1996 to December 1997, provided the additional data needed to develop the models presented in this report. We present the results of these field investigations, which were conducted at 24 transect-survey sites (12 stations paired by seagrasses and bare bottom) and six permanent stations to fill gaps in our knowledge of seagrass biology, variations in water column and sediment geochemistry, underwater irradiance, and the inherent optical properties of Laguna waters.

Studies on seagrass biology included delineation of the photosynthesis vs. irradiance (P vs. I) relationships for *Syringodium filiforme*, which were used in developing the LMSM for this species (P vs. I relationships have been previously published for *Halodule wrightii* and *Thalassia testudinum*). In addition, density and above- and below- ground biomass of the three grass species were collected over variable temporal and spatial scales at 12 transect sites and three permanent stations in Laguna Madre. Continuous measurements of photosynthetically active radiation (PAR) were also collected at the permanent sampling stations. Indices of carbon and nitrogen content were measured in leaves and below-ground tissues to provide data for the LMSM and allocation models for *Thalassia*.

Thousands of samples were analyzed in our efforts to better understand the complex geochemical relationships occurring within Laguna seagrass beds. We collected samples at 24 transect sites; in addition, sediment chemistry was examined in detail from vertical profiles conducted at four additional stations. Results demonstrated that most sediments in Laguna Madre are sandy with a relatively narrow range in their physical and geochemical characteristics and that the diagenetic activity takes place in the upper few centimeters of sediment (in contrast to most estuarine siliciclastic muds). This work also demonstrated that the flux of

ammonium from resuspended sediments (as occurs during dredging) can be substantial, thereby providing a large pulse of inorganic nitrogen that can fuel phytoplankton blooms. This finding is important, since measurements of water inorganic nitrogen levels are generally low ($<3 \mu\text{M}$) throughout the Laguna. Such low concentrations probably play an important role in regulating phytoplankton production, as reflected in water column chlorophyll levels that are $<10 \mu\text{g L}^{-1}$ in the Lower Laguna.

Knowledge of the inherent optical properties (IOPs) of Laguna Madre waters is critical in developing a radiative transfer model to link with the LMSM. Strong relationships were observed between IOPs and total suspended solids (TSS). TSS is likely to contribute most to water column light attenuation during dredging events, which can result in significant reductions in both light quality and quantity. Declines in light-driven photosynthetic oxygen evolution can have serious effects on seagrass health. Sediment geochemical model simulations suggested that root zone fluxes of O_2 (produced during photosynthesis) were essential to maintaining non-toxic levels of sulfide. In addition, model results indicate that seagrass beds overlain with even modest (cm) amounts of dredged material can experience rapid increases in sulfide concentrations that can be sustained at toxic concentrations for several months.

The LMSM was developed for *Halodule*, *Syringodium*, and *Thalassia*. Of the three models, the LMSM was able to reproduce many features of a continuous nine-year data set for *Halodule*, mainly because the *Halodule* set contained a prolonged period of light stress (brown tide event) interspersed between two periods of favorable light climates. Simulations using worst-case light attenuation profiles show that the seagrasses are able to withstand short periods (one to two weeks) of very high water column light attenuation. However, under prolonged periods of low PAR (ca. 100 days or more) of even moderate levels of water column attenuation, model predictions indicate potentially dangerous decreases in plant biomass.

Our efforts have produced an integrative and quantitative model that predicts the response of seagrasses to changes in their environment, particularly with respect to changes in light availability, based on extensive interdisciplinary field observations and experimental studies conducted over the past two years. Model simulations and *in situ* measurements of an actual dredging event strongly suggest that dredging operations are very likely to have a measurable negative impact on the health when (1) dredging activities occur over extended periods (weeks) when the plants are metabolically most active (spring through autumn), and (2) the dredging activity and/or disposal of materials occurs within 1 km of the grass bed.

The results of the LMSM depend, as does any model, upon a variety of inputs (in particular TSS) and assumptions that are used in the interpretation of simulation results. For example, the seagrass model was run at sites that were not immediately adjacent to disposal areas. This was done to simulate the impact of disposal on the Laguna as a whole. The Seagrass Model addresses a representative area and can be applied at any location along the length of the Laguna. Similarly, the hydrodynamic and sediment transport models cover the whole length of Upper and Lower Laguna Madre. Given such a wide spatial coverage in all three models, there will always be regions where differences occur between model output and observed data. The power of these models lies in providing information on long-term trends and large-scale spatial patterns. Consequently, when one evaluates the output from these models, consideration does need to be given to anecdotal observations that disagree with the model results. However, it is very difficult to gauge the importance of such observations without hard numerical data.

We stress that the output from our models needs to be interpreted in the context of long-term trends and large-scale spatial patterns. We are confident that the LMSM performs well in this respect. In addition, our conclusions on dredging impacts to seagrasses include results of additional model simulations based on data collected during actual dredging events (*e.g.*, model verification study at PA 235) and *in situ* observations of seagrass response to chronic reductions in underwater light regimes. We recognize that environmental, political, and economical factors are likely to play key roles in the management decisions regarding seagrass resources in Laguna Madre. Therefore, we recommend efforts be undertaken, however modest, to collect accurate measurements of environmental variables (*e.g.*, TSS, light attenuation) to directly verify model predictions at test sites where dredge activities and seagrass response can be directly measured and observed.

Contributors

PRINCIPAL INVESTIGATORS

Kenneth H. Dunton, Ph.D.
Marine Science Institute
The University of Texas at Austin
750 Channel View Drive
Port Aransas, Texas 78373

Adrian Burd, Ph.D.
Department of Marine Science
University of Georgia
Athens, Georgia 30602-3636

Luis Cifuentes, Ph.D.
Department of Oceanography
Texas A&M University
3146 TAMU
College Station, Texas 77843

Peter Eldridge, Ph.D.
US EPA-Western Ecology Division
Coastal Ecology Branch
2111 SE Marine Science Center Dr.
Newport, Oregon 97365

John Morse, Ph.D.
Department of Oceanography
Texas A&M University
3146 TAMU
College Station, Texas 77843

CO-AUTHORS

James E. Kaldy, Ph.D.
US EPA-Western Ecology Division
Coastal Ecology Branch
2111 SE Marine Science Center Dr.
Newport, Oregon 97365

Kun-Seop Lee, Ph.D.
Department of Biology
Pusan National University
Pusan 609-735, Korea

Robert A. Maffione, Ph.D.
Hydro-Optics, Biology and Instrumentation Labs
P.O. Box 859
Moss Landing, California 95039

Kelly Major, Ph.D.
Biological Sciences - LSCB #51
University of South Alabama
Mobile, Alabama 36688-0002

Jeff Morin
Department of Oceanography
Texas A&M University
3146 TAMU
College Station, Texas 77843

**EDITOR
&
PROJECT DIRECTOR
Kenneth H. Dunton**

Acknowledgments

The Principal Investigators would like to recognize the following individuals for their contribution to the Laguna Madre Seagrass Program:

To the co-authors of several chapters in this report, for their dedication and persistence over a period of several years in support of their colleagues, both in the field and in data synthesis: *Dr. James Kaldy, Dr. Kun-seop Lee, Dr. Robert Maffione, Dr. Kelly Major and Mr. Jeff Morin.*

To the numerous students and staff of Texas A&M University and The University of Texas Marine Science Institute for assistance in the field and in the processing of huge volumes of samples: *Kim Jackson, Joe Kowalski, Sharon Herzka, and Susan V. Schonberg.*

To *George Jackson* at Texas A&M University, for his critical support and constructive criticism in all aspects of this project.

To the U.S. Army Corps of Engineers staff, for their support, encouragement, patience, and objectivity under often difficult and awkward circumstances: *Dr. Terry Roberts, Carolyn Murphy, Martin Arhelger, Joseph Hrametz, and Robert Hauch.*

To the silent editor that made the completion of this extensive report possible: *Susan V. Schonberg.*

This work was funded under cooperative agreement 96-PL-03 between Texas A&M University and the U.S. Army Corps of Engineers (Galveston District).

Contents

Page

PART I: RESULTS

- R-1—R-55 **Final Model Results and Extended Model Simulations**
Adrian Burd

PART II: THE MODELS

- I-1—I-61 **The Seagrass Models**
Adrian Burd
- II-1 —II-26 **Carbon and Nitrogen Allocation Model for the Seagrass *Thalassia testudinum* in Lower Laguna Madre**
Peter M. Eldridge and James. E. Kaldy
- III-1—III-32 **Sediment Geochemical Model**
Peter M. Eldridge, James E. Kaldy, and Robert A. Maffione
- IV-1—IV-54 **Water Column Data and Spectral Irradiance Model**
Luis Cifuentes, Peter M. Eldridge, James E. Kaldy, and Robert Maffione
- V-1—V24 **Model Verification**
Adrian Burd and Peter Eldridge

PART III: BIOLOGICAL AND CHEMICAL MEASUREMENTS

- VI-1—VI-35 **Characterization of Seagrasses Responses, Light, and Water Column Parameters**
Kenneth H. Dunton
- VII-1—VII-51 **Sediment Geochemistry**
John W. Morse
- VIII-1—VIII-33 **Nutrient Release from Resuspended Sediments**
Jeff Morin and John W. Morse
- IX-1—IX-26 **Response of *Thalassia testudinum* to a Dredging Event**
Kun-Seop Lee and Kenneth H. Dunton
- X-1—X-28 **Photosynthesis in the Manatee Grass, *Syringodium filiforme***
Kelly Major and Kenneth H. Dunton

Preface

The Laguna Madre of Texas is only one of three hypersaline lagoons in the world. Seagrasses inhabit huge areas of the Laguna and provide a winter food resource for more than 75% of the world's population of redhead ducks. Because of the fundamental role that seagrasses play in the ecology of coastal ecosystems, activities that potentially threaten the productivity of the system have long been a cause for concern.

The Gulf Intracoastal Waterway (GIWW) is a 117-mile long, 12-foot deep by 125-foot wide navigation channel that bisects the entire length of the Laguna. The GIWW is maintained by the U.S. Army Corps of Engineers (USACE) by dredging activities based on an environmental impact statement (EIS) that was completed in October 1975. During the 1980s, the adequacy of the EIS was questioned by several State and Federal resource agencies and in 1993, the U.S. Army Corps of Engineers undertook the task of completing a series of Section 216 studies to address the problems and concerns along the GIWW. The National Audubon Society and others filed a lawsuit in 1994 to halt unconfined, open-bay disposal of dredged material in Laguna Madre before the 216 studies were completed. As a result of the suit, the Corps agreed to develop a long-term dredged material management plan (DMMP) for this section of the GIWW and to prepare a supplemental environmental impact statement (SEIS).

An Interagency Coordination Team (ICT) composed of the Corps, the National Marine Fisheries Service, U.S. Fish and Wildlife Service, U.S. Environmental Protection Agency, Texas Parks and Wildlife Department, Texas General Land Office, Texas Water Development Board, Texas Department of Transportation, and the Texas Natural Resource Conservation Commission (now the Texas Commission on Environmental Quality) was formed in February 1995 to help the USACE to develop the DMMP and SEIS. The U.S. Coast Guard, Padre Island National Seashore, and Coastal Bend Bays and Estuaries Program were invited to send members during subsequent meetings to provide information and advice to the ICT.

This report reflects the completion of one of about 35 studies that have been sponsored by the ICT and funded by the USACE to provide the latest scientific information on the impacts and benefits of the GIWW. In 1996, the USACE provided Texas A&M University, the University of Texas Marine Science Institute, and Texas Parks and Wildlife Department funds to conduct a study with the following objectives:

- 1) To collect additional field measurements to fill gaps in our knowledge related to the biology of seagrasses and their geochemical and physical environment, and
- 2) To develop an integrative model for seagrass productivity in Laguna Madre that could be used as a management tool to assess the effects of maintenance dredging.

In addition to this report, a number of peer-reviewed publications have resulted from this research (see below) and are available to the public.

PUBLICATIONS RESULTING FROM RESEARCH SUPPORTED UNDER THIS USACE SPONSORED PROGRAM

- Burd, A.B. and K.H. Dunton. 2000. Field verification of a light-driven model of biomass changes in the seagrass *Halodule wrightii*. *Marine Ecology Progress Series* 209:85-98.
- Eldridge, P.M. and J.W. Morse. 2000. A diagenetic model for sediment-seagrass interactions. *Marine Chemistry* 70:89-103.
- Lee, K-S. and K.H. Dunton. 1999a. Inorganic nitrogen acquisition in the seagrass *Thalassia testudinum*: development of a whole-plant nitrogen budget. *Limnology and Oceanography* 44(5):1204-1215.
- Lee, K-S. and K.H. Dunton. 1999b. Influence of sediment nitrogen availability on carbon and nitrogen dynamics in the seagrass *Thalassia testudinum*. *Marine Biology* 134:217-226.
- Lee, K-S. and K.H. Dunton. 2000a. Diurnal changes in pore water sulfide concentrations in the seagrass *Thalassia testudinum* beds: the effects of seagrasses on sulfide dynamics. *Journal of Experimental Marine Biology and Ecology* 255:201-214.
- Lee, K-S. and K.H. Dunton. 2000b. Effects of nitrogen enrichment on biomass allocation, growth, and leaf morphology of the seagrass *Thalassia testudinum*. *Marine Ecology Progress Series* 196:39-48.
- Major, K.M. and K.H. Dunton. 2000. Photosynthetic performance in *Syringodium filiforme*: seasonal variation in light-harvesting characteristics. *Aquatic Botany* 68:249-264.
- Major, K.M. and K.H. Dunton. 2002. Variations in light-harvesting characteristics of the seagrass, *Thalassia testudinum*: evidence for photoacclimation. *Journal of Experimental Marine Biology and Ecology* 275:173-189.
- Morin, J. and J.W. Morse. 1998. Ammonium release from resuspended sediments in the Laguna Madre estuary. *Marine Chemistry* 65:97-110.

Part I: Results

FINAL MODEL RESULTS

Contents

Abstract	4
Introduction	6
The Model	7
The Light Attenuation Model	10
Model Results Summary	12
Model Result Details	13
<i>Halodule</i> Sites	13
Site ULM-2 (node 2236)	13
Site 17 (node 4746)	15
Site 19 (node 3708)	17
Site 23 (node 1498)	19
Site WES-3 (node 17232)	21
<i>Thalassia</i> Sites	21
Site LLM-2 (node 16580)	23
Site 1 (node 16768)	25
Site 3 (node 17543)	27
Site 5 (node 15541)	29
Site 7 (node 16684)	31
Site PA-235a (node 176780)	33
Site PA-235b (node(17676)	37
Site PA-235c (node 17679)	39
Site PA-235d (node 17677)	39
Site JEK (node 16394)	39
Site WES-4 (node 16496)	41

Site WES-5 (node 16306)	43
Discussion	44
Conclusions	46
References	47

Tables

Table 1	Table of placement area locations	6
Table 2	Table of site locations and types	8
Table 3	Summary of Model Results	14

Figures

Figure 1	Map of site locations.	9
Figure 2	$K_d(\text{PAR})$ as a function of TSS.	12
Figure 3	Modeled TSS concentrations for Site ULM-2.	15
Figure 4	Model results for Site ULM-2.	16
Figure 5	Modeled TSS concentrations for Site 17.	17
Figure 6	Model results for Site 17.	18
Figure 7	Modeled TSS concentrations for Site 19.	19
Figure 8	Model results for Site 19.	20
Figure 9	Modeled TSS concentrations for Site 23.	21
Figure 10	Model results for Site 23.	22
Figure 11	Modeled TSS concentrations for Site WES-3.	23
Figure 12	Model results for Site WES-3.	24
Figure 13	Modeled TSS concentrations for Site LLM-2.	25
Figure 14	Model results for Site LLM-2.	26
Figure 15	Modeled TSS concentrations for Site 1.	27
Figure 16	Model results for Site 1.	28
Figure 17	Modeled TSS concentrations for Site 3.	29

Figure 18	Model results for Site 3.	30
Figure 19	Modeled TSS concentrations for Site 5.	31
Figure 20	Model results for Site 5.	32
Figure 21	Modeled TSS concentrations for Site 7.	33
Figure 22	Model results for Site 7.	34
Figure 23	Modeled TSS concentrations for Site PA-235a.	35
Figure 24	Model results for Site PA-235a.	36
Figure 25	Modeled TSS concentrations for Site PA-235b.	37
Figure 26	Model results for Site PA-235b.	38
Figure 27	Modeled TSS concentrations for Site JEK.	39
Figure 28	Model results for Site JEK.	40
Figure 29	Modeled TSS concentrations for Site WES-4.	41
Figure 30	Model results for Site WES-4.	42
Figure 31	Modeled TSS concentrations for Site WES-5.	43
Figure 32	Model results for Site WES-5.	44

Abstract

We present results from the production runs of the Laguna Madre Seagrass Model. These results combine output from the W.E.S. Hydrodynamic and Sediment Transport models in order to provide suitable forcing conditions for the Seagrass Biomass and Diagenesis Model. Using the results of the W.E.S. models, the Seagrass model predicts that, at the sites modeled, the seagrasses survive the impacts of disposal of dredge material. The results also indicate that seagrass beds closer to actual disposal sites will be impacted to a greater extent than those further away (as was seen in the results of the Verification Phase of this project).

Concentrations of TSS tend to be elevated during the spring and the fall, with lower values during the summer growth period. There is very little difference in TSS concentrations between the dredging and non-dredging scenarios. The time series of underwater irradiance reflects the changes in the TSS concentration; low light levels occur during the spring and fall months and increase during the summer.

Biomass at the *Halodule wrightii* stations tends to increase and values at the end of the simulation are higher than those observed in the Laguna Madre. The model predicts above-ground biomass values for *Thalassia testudinum* that generally lie between 100 and 150 gdw m⁻³; these fall within the range of measured biomass in the Laguna Madre.

Root-zone HS⁻ concentrations are low except at a few sites in the Upper Laguna Madre. Typical values predicted by the model are between 5 and 10 μM, though in the Upper Laguna, concentrations can reach as high as 400 μM. The model predicts root-zone concentrations that lie between 100 and 350 μM which are within the range of measured values. Both the HS⁻ and NH₄⁺ concentrations predicted by the model are not sufficient to significantly affect the growth and production of the plants. Thus, available irradiance is the dominant factor affecting seagrass growth and production.

The model assumes that the only factors contributing to attenuation of light in the water column are the water itself and TSS. The effects of other factors such as algal mats and phytoplankton blooms are not accounted for. The model also does not account for the burial of seagrasses by sediment.

The results of the model, and the caveats underpinning it, strongly suggest that long term

monitoring of light levels and water quality in the Laguna Madre is advisable. The results of such a program, together with the results from this study, would provide an invaluable guide to managers in deciding when to schedule dredging activities. In addition, the presence of a buffer zone between the placement area and nearest seagrass bed should be considered.

Introduction

The aim of the Laguna Madre Seagrass Model is to investigate the effects of dredging on seagrasses in the Laguna Madre. In order for realistic predictions to be made using the model, time series of irradiance at canopy level and deposition of sediment on the benthos are required. Irradiance at canopy level requires knowledge of the attenuation of light as it propagates through the water column from the surface. One important component contributing to this attenuation is the concentration of Total Suspended Solids (TSS) in the water column. Modeled time series of TSS and bed elevation were provided by the combined Hydrodynamic and Sediment Transport models developed at WES.

Two runs of the Hydrodynamic and Sediment Transport Model were made (Allen Teeter, personal communication); one with no disposal of dredge material and the other with disposal at six sites, PA's 187, 197, 202, 211, 221, and 233 (Table 1. The quantities of material deposited at each site were 88, 655, 512, 680, 844, and 380 keyds respectively. In the model simulations, 70% of the disposed material was placed on the bed and remaining 30% was placed in suspension immediately above the disposal site. This suspended fraction was finer than the material placed on the bed (Allen Teeter, personal communication).

Table 1: Table of placement area locations. The latitude and longitude values in the table refer to the centers of the disposal areas (Allen Teeter, pers. comm.).

PA	Latitude	Longitude
187	27°27'00"	97°20'06"
197	27°17'30"	97°24'18"
202	27°10'12"	97°25'54"
211	26°47'06"	97°27'54"
221	26°29'42"	97°23'24"
233	26°11'06"	97°15'54"

The Seagrass model was run at sites containing *Thalassia testudinum* or *Halodule wrightii* (Table 2 and Figure 1). The model was not run for sites having bare areas or for sites with *Syringodium*

filiforme (see Chapter I).

The model was run for a period of three years; during the disposal runs, disposal occurred at the start of the first year followed by two years using forcings identical to those used in the first year but without disposal.

The Model

The Laguna Madre Seagrass Model actually consists of several different models that either work together or supply information to one another. These models are:

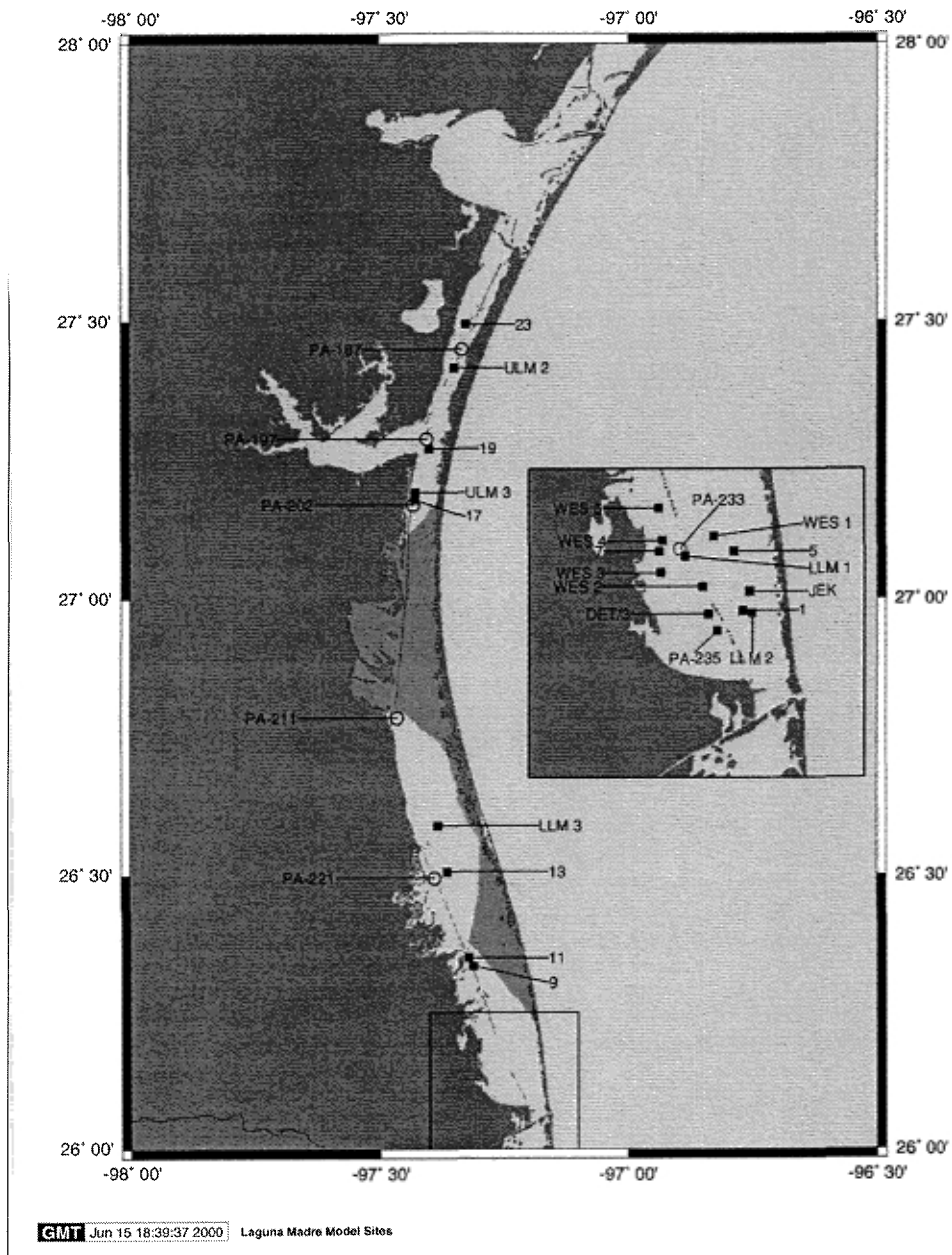
- **Hydrodynamic Model:** calculates current flows and water depths within the Laguna Madre. It was developed and operated by the U.S. Army Corps of Engineers at W.E.S.
- **Sediment Transport Model:** relies on information from the hydrodynamic model and predicts the movement and deposition of sediment within the Laguna Madre. This model was also developed and run by the U.S. Army Corps of Engineers at W.E.S. by Allen Teeter.
- **Light Attenuation Model:** predicts the irradiance at the depth of the seagrass canopy within the water column. The model was developed by Adrian Burd and relies on information from the hydrodynamic model (water depth), the sediment transport model (water column total suspended solids) and the model of light absorption developed by Robert Maffione (Chapter IV of this report). This model is described below.
- **Biomass and Diagenesis Model:** predicts the production and biomass of seagrasses and changes in sediment chemistry. This model was developed by Adrian Burd and Peter Eldridge and is described in Chapters I and III of this report.

TSS concentrations and water depth for 26 sites were extracted from two different simulations of the Hydrodynamic and Sediment Transport models. The two simulations represented a) a one year period during which there was not disposal of dredging material and b) a one year simulations identical to a) except that disposal of dredging material occurred on the first day of the simulation. These data were used to drive the Light Attenuation Model and the Biomass and Diagenesis Model.

Table 2: Table of site location and types.

Node	Station	Latitude	Longitude	Mean Depth (m)	Type
2236	ULM-2	27°25'00" W	97°21'00" N	1.0	<i>Halodule</i>
4798	ULM-3	27°11'33" W	97°25'42" N	1.0	Bare
16845	LLM-1	26°10'45" W	97°15'36" N	1.15	Bare
16580	LLM-2	26°08'00" W	97°12'00" N	1.3	<i>Thalassia</i>
7511	LLM-3	26°35'25" W	97°22'57" N	1.27	<i>Syringodium</i>
16768	1	26°08'06" W	97°12'31" N	1.2	<i>Thalassia</i>
17543	DET/3	26°07'57" W	97°14'21" N	1.65	<i>Thalassia</i>
15541	5	26°11'00" W	97°13'00" N	1.3	<i>Thalassia</i>
16684	7	26°11'00" W	97°17'00" N	1.15	<i>Thalassia</i>
13072	9	26°20'05" W	97°18'45" N	0.9	<i>Syringodium</i>
13928	11	26°21'00" W	97°19'20" N	0.7	<i>Syringodium</i>
10037	13	26°30'23" W	97°21'53" N	0.8	<i>Syringodium</i>
6725	15	24°40'00" W	97°24'00" N	0.8	<i>Syringodium</i>
4746	17	27°10'47" W	97°25'45" N	1.1	<i>Halodule</i>
3708	19	27°16'20" W	97°24'00" N	1.1	<i>Halodule</i>
1498	23	27°29'42" W	97°19'42" N	1.2	<i>Halodule</i>
17680	PA235a	26°07'05" W	97°13'50" N	1.3	<i>Thalassia</i>
17676	PA235b	26°07'23" W	97°13'44" N	1.3	<i>Thalassia</i>
17679	PA235c	26°07'13" W	97°13'40" N	1.3	<i>Thalassia</i>
17677	PA235d	26°07'21" W	97°13'48" N	1.3	<i>Thalassia</i>
16394	JEK	26°09'03" W	97°12'09" N	1.2	<i>Thalassia</i>
15556	WES-1	26°11'43" W	97°14'03" N	1.5	Bare
17393	WES-2	26°09'16" W	97°14'40" N	1.65	Bare
17232	WES-3	26°09'56" W	97°16'55" N	1.5	<i>Halodule</i>
16496	WES-4	26°11'30" W	97°16'48" N	1.2	<i>Thalassia</i>
16306	WES-5	26°13'05" W	97°17'01" N	0.9	<i>Thalassia</i>

Figure 1: Locations of the sites used in the model production runs. The squares indicate the sites at which the Seagrass Model was run; open circles represent the disposal sites used in the model. The shaded area represents the land cut.



The coupled biomass–diagenesis model was written in FORTRAN-77. The Light Attenuation Model and all post-processing and graphics for the Light Attenuation and Biomass and Diagenesis Models were programmed using Matlab™.

The Light Attenuation Model

The Light Attenuation Model was developed to predict the irradiance at the depth of the seagrass canopy given the concentration of TSS in the water column. Irradiance at canopy level will depend upon the light at the air-water interface, the depth of the water, the concentration of total suspended solids (TSS) in the water. The absorption characteristics of TSS are wavelength dependent so a spectral irradiance model was required to accurately predict light levels in the water column.

Irradiance at the air-water interface was calculated using a model of spectral solar irradiances for cloudless maritime atmospheres (Gregg and Carder, 1990). The model used a standard model of the solar spectrum and takes into account absorption by ozone, oxygen, water vapor and Rayleigh scattering. Aerosol scattering and absorption were accounted for using a modified version of the U.S. Navy marine aerosol model. Surface reflectance from a flat air-water interface was included in the model, the effects of surface waves being small for zenith angles less than about 60°(Kirk, 1994).

The effects of cloud cover on surface irradiance are not included in the model of Gregg and Carder (1990). Empirically generated corrections for cloud cover can be made (*e.g.*, Iqbal, 1983) if measurements of cloud cover are available. However, there are severe problems in applying this approach to the Seagrass Model. Firstly, the seagrass model requires hourly light data and no comprehensive data set of hourly cloud coverage for the region was found. Secondly, estimates of cloud cover do not give information as to which parts of the sky are covered. Thirdly, reflection of solar radiation from the edges and sides of clouds can increase surface irradiance to values greater than the extra-terrestrial radiation.

For these reasons, a simpler approach was taken. Average surface irradiance values had been obtained in the Laguna Madre and are presented in Figure 2 of Chapter I of this report. A correction factor was derived by taking the ratio of the maximum observed surface PAR and the maximum calculated surface PAR; the value of this ratio was 0.6. This factor was then applied uniformly to

the model results.

Irradiance within the water column is affected by water depth, absorption by the water and absorption and scattering by TSS. Hourly water depth was taken from results of the hydrodynamic model provided by Allen Teeter (W.E.S.). The effects of water and TSS were calculated using the following model developed by Robert Maffione (Chapter IV of this report)

$$K_d(\lambda) = \frac{a_w(\lambda)}{\cos(\theta)} + (0.0255 + 0.537 \exp(-0.00441 \lambda)) \text{ TSS} \quad (1)$$

In this equation, λ (nm) is the wavelength of the light, $K_d(\lambda)$ is the wavelength dependent attenuation coefficient (in units of m^{-1}), $a_w(\lambda)$ is the spectral absorption coefficient of water (Smith and Baker, 1981), θ is the zenith angle (degrees) and TSS the concentration of total suspended solids (mg l^{-1}).

The spectral irradiance at the canopy level was calculated using

$$I_\lambda(z) = I_\lambda(0) \exp(-K_d(\lambda)z) \quad (2)$$

where z is the depth of the seagrass canopy, $I_\lambda(z)$ is the spectral irradiance at depth z and $I_\lambda(0)$ is the spectral irradiance at the air-water interface.

The spectral irradiance at the depth of the canopy was integrated over the wavelength range 400-700 nm to obtain the photosynthetically active radiation (PAR)

$$I_{\text{PAR}}(z) = \int_{400}^{700} I_\lambda(z) d\lambda \quad (3)$$

and this was used as a forcing function for the seagrass production model.

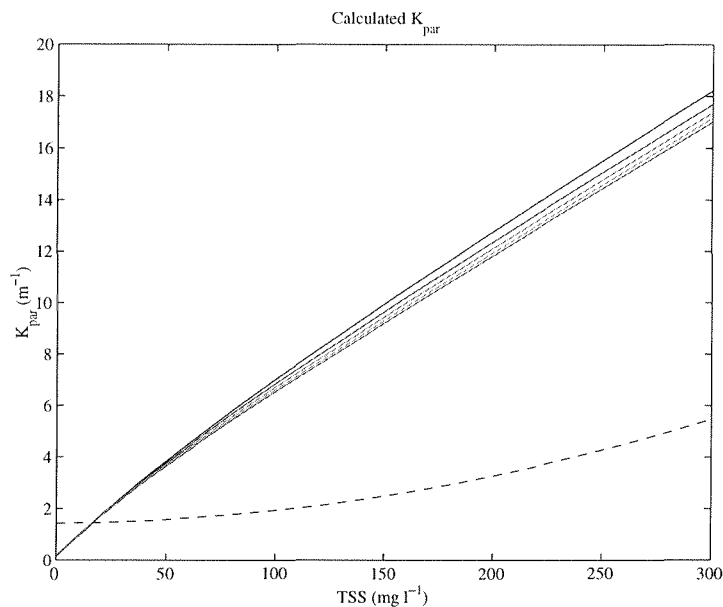
An estimate of the diffuse attenuation coefficient over the PAR wavelength range was made using

$$K_d(\text{PAR}) = -\frac{1}{z} \ln \left(\frac{I_{\text{PAR}}(z)}{I_{\text{PAR}}(0)} \right) \quad (4)$$

where $I_{\text{PAR}}(0)$ was calculated using Equation 3 with $z = 0$. A plot $K_d(\text{PAR})$ as a function of TSS concentration is shown in Figure 2 for various values of z .

To put this curve in context, the minimum light requirements for seagrasses are often quoted in terms of percent surface irradiance (%SI). For example, for *H. wrightii*, a minimum light requirement of 18% SI was determined by Dunton (1994). For a water depth of 1m, this implies a diffuse attenuation coefficient of $K_d(\text{PAR}) = 1.7$ which is attained for a TSS concentration of

Figure 2: The relationship between $K_d(\text{PAR})$ and TSS (solid curves) for depths 1, 1.5, 2 and 2.5m, with the top-most curve representing the case for 1m, the next curve 1.5m etc. The dashed curve represents the $K_d(\text{PAR})$ –TSS relationship obtained by Brown and Kraus (1997).



approximately 25 mg l^{-1} . These light levels are **average** light levels required during the growing season of the plant. Daily, or instantaneous irradiances can be far greater, so long as the average over the spring and summer months satisfies the above limits.

Model Results Summary

The seagrass model was run at 17 sites using TSS concentrations supplied by Allen Teeter from the sediment transport model. These sites were those containing *Thalassia* and *Halodule* listed in Table 2. As discussed in Chapter I of this report, no model was available for *Syringodium*. There were a total of 12 sites at which the *Thalassia* model was run, and 5 sites at which the *Halodule* model was run.

There is little difference in the modeled TSS concentrations between the dredging and non-dredging scenarios. This can be seen by examining the figures in Section or from Table 3. The table shows the fraction of a single year during which the TSS concentration was $< 50 \text{ mg l}^{-1}$, between 50 and 150 mg l^{-1} and $> 150 \text{ mg l}^{-1}$; these boundaries were chosen arbitrarily based on

visual examination of the curves shown in Section ; the top row of each entry corresponds to the single year with dredging and the bottom row to the single year without dredging. Only sites in Upper Laguna Madre show TSS concentrations greater than 150 mg l^{-1} and only one of these sites shows an appreciable difference between dredging and non-dredging scenarios.

Previous experience with the Biomass and Diagenesis model indicated that if there was an impact on seagrasses in one year, the effects of impact would disappear by the second or third year. This, together with the small differences in TSS concentrations between the dredging and non-dredging cases suggested that the Biomass and Diagenesis model should be run for three years. During the first year, the TSS concentrations corresponding to the dredging scenario were used; for the second and third years, the TSS concentrations appropriate for a non-dredging year were used.

Seasonal changes in the TSS led to seasonal patterns in the underwater irradiance. Elevated TSS concentrations tended to appear in the spring and the fall, reducing the canopy level irradiance during these times. Summer irradiances were high, allowing the seagrasses to grow.

At those sites for which the model was run, the seagrass survived the increased TSS resulting from the dredging. The biomass of *Halodule* tended to increase over the three-year simulation; the biomass of *Thalassia* tended to stabilize such that the above-ground biomass was between 100 and 150 gdw m^{-3} . Sulfide levels remained low in all the simulations. Site 17 showed the highest values and this is also the site that showed the greatest difference in TSS concentrations between dredging and non-dredging scenarios.

Model Result Details

Halodule Sites

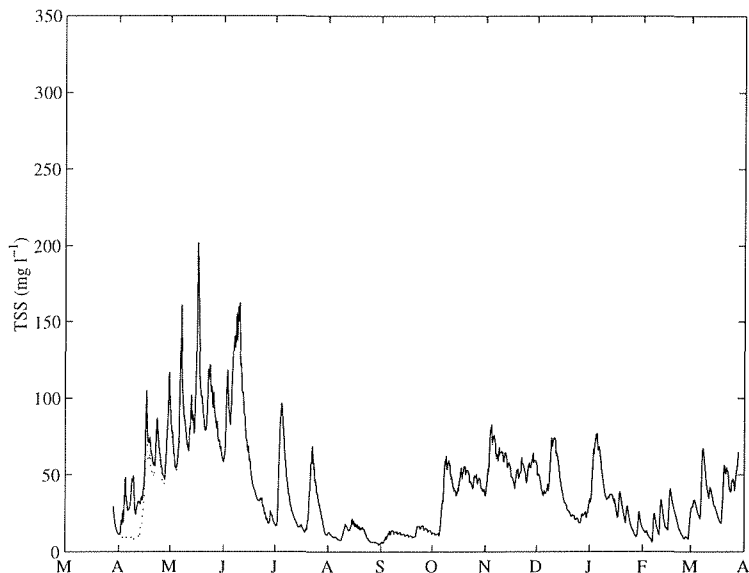
Site ULM-2 (node 2236)

There is very little difference in TSS concentrations between dredging and non-dredging scenarios (Figure 3). Concentrations of TSS reach as high as 200 mg l^{-1} during May and then fall to remain below 100 mg l^{-1} from July through to the following spring.

Table 3: Summary of model results. The sites for each species are listed from northernmost to southernmost. The distance column lists the distance (in statute miles) from the model site to the closest disposal area (see Figure 1); the three TSS columns give the fraction of one year within the specified range - top row dredged scenario, bottom row non-dredged; F_{HS} is the fraction of the three year simulation for which HS^- concentrations exceed the minimum inhibition threshold.

	Site	Distance (miles)	TSS ($mg\ l^{-1}$)			F_{HS}
			< 50	50 – 150	> 150	
<i>Halodule</i>	23	3.1	0.76	0.24	0	0.04
			0.76	0.24	0	
	ULM-2	2.5	0.67	0.32	0.01	0.04
			0.68	0.31	0.01	
	19	0.8	0.42	0.46	0.12	0.01
			0.47	0.43	0.1	
	17	1.2	0.29	0.58	0.13	0.2
			0.48	0.47	0.05	
	WES-3	2.3	0.57	0.43	0.0	0.0
			0.62	0.38	0.0	
<i>Thalassia</i>	WES-5	3.2	0.64	0.36	0.0	0.0
			0.66	0.34	0.0	
	WES-4	1.90	0.55	0.45	0.0	0.0
			0.6	0.4	0.0	
	5	2.1	0.51	0.49	0.0	0.0
			0.52	0.48	0.0	
	7	2.1	0.61	0.39	0.0	0.0
			0.66	0.34	0.0	
	JEK	3.7	1.0	0.0	0.0	0.0
			1.0	0.0	0.0	
	1	4.2	1.0	0.0	0.0	0.0
			1.0	0.0	0.0	
	LLM-2	4.6	1.0	0.0	0.0	0.0
			1.0	0.0	0.0	
	3	3.6	0.46	0.54	0.0	0.0
			0.48	0.52	0.0	
	PA-235b	4.4	0.79	0.21	0.0	0.0
			0.80	0.2	0.0	
	PA-235d	4.4	0.69	0.31	0.0	0.0
			0.90	0.3	0.0	
PA-235c	4.6	0.80	0.20	0.0	0.0	
		0.81	0.19	0.0		
PA-235a	4.7	0.72	0.28	0.0	0.0	
		0.73	0.27	0.0		

Figure 3: Modeled TSS concentrations (mg l^{-1}) for site ULM-2 (node 2236 - *Halodule*). The solid line shows the results of the simulation with dredging and the dotted line shows the results of the simulation without dredging (model data courtesy of Allen Teeter).



The underwater irradiance ranged from 1 to $50 \mu\text{mol m}^{-2} \text{s}^{-1}$ (Figure 4a). High light levels were seen between July and October of each year, reflecting the low values of TSS during those times. Both above and below-ground biomass increased to very high values (Figure 4b) because of the optimum light levels available. Because of the high, increasing biomass, both the root-zone HS^- and NH_4^+ increased. Although the root-zone HS^- and NH_4^+ values were high, they were not sufficiently high to cause the feedbacks to have adverse affects on the plant growth.

Site 17 (node 4746)

The modeled concentration of TSS at this site is generally greater than that at site ULM-2 (Figure 5). This is because one of the placement areas was in the vicinity. There was also a pronounced difference between the dredged and non-dredged scenarios. TSS concentrations reached values greater than 350 mg l^{-1} at the start of the dredged scenario in April. TSS concentrations decreased between July and October.

Underwater irradiance reaches very low levels during the late spring and early summer months

Figure 4: Model results for site ULM-2 (node 2236 - *Halodule*): a) canopy level irradiance ($\text{mol m}^{-2} \text{d}^{-1}$); b) biomass (gdw m^{-2}) - solid line for above-ground and dashed line for below-ground; root-zone HS concentration (μM); d) root-zone NH_4^+ concentration (μM).

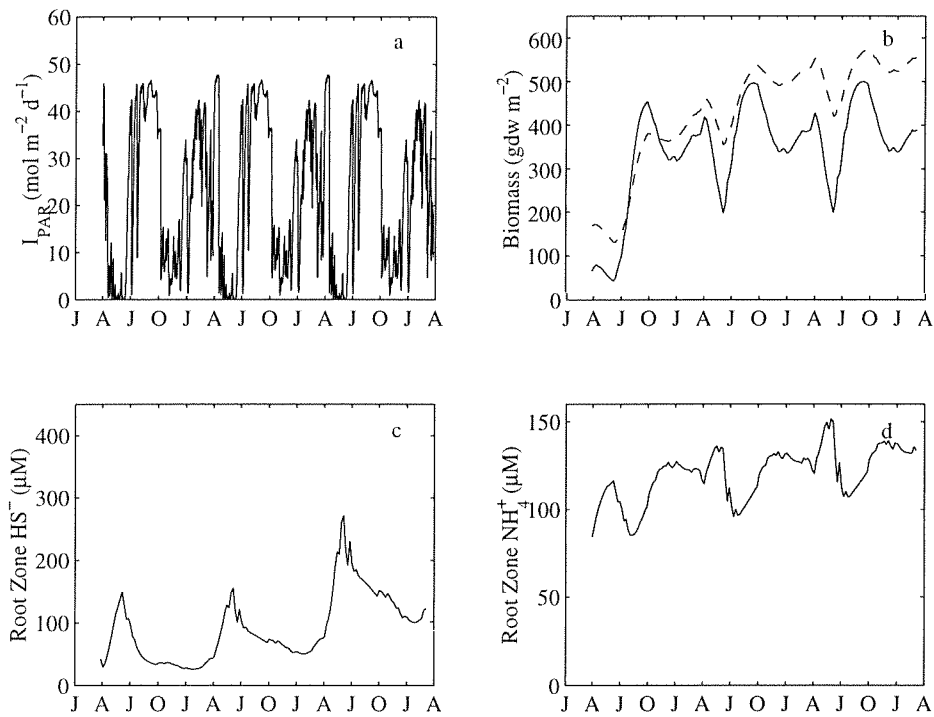
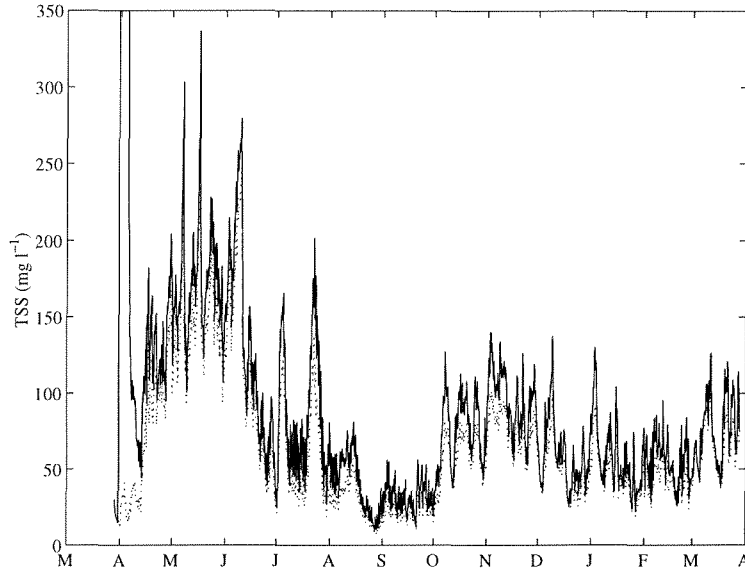


Figure 5: Modeled TSS concentrations (mg l^{-1}) for site 17 (node 4746 - *Halodule*). The solid line shows the results of the simulation with dredging and the dotted line shows the results of the simulation without dredging (model data courtesy of Allen Teeter).



(Figure 6a) when the TSS concentrations are high. Between July and and October when the TSS values are generally low, the underwater irradiance is high allowing the plants to grow. Above and below-ground biomass remains high throughout the year (Figure 6b) and root-zone HS^- (Figure 6c) and NH_4^+ (Figure 6d) values are also high, though follow a seasonal cycle.

Site 19 (node 3708)

Modeled TSS concentrations at site 19 (Figure 7) show a similar pattern to those at site 17 and are generally a little lower; peak TSS concentrations are about 300 mg l^{-1} . Differences between the dredging and the non-dredging scenarios are smaller at this site than at site 17.

Underwater irradiance (Figure 8a) show the familiar pattern of high values during the late spring and into the summer with low values between April and July when the TSS concentrations are highest. Biomass (Figure 8b) increases showing a regular seasonal growing cycle with biomass values that are high. Root zone sulfide (Figure 8c) and ammonia (Figure 8d) concentrations remain below levels at which any significant feedback would affect plant growth.

Figure 6: Model results for site 17 (node 4746 - *Halodule*): a) canopy level irradiance ($\text{mol m}^{-2} \text{d}^{-1}$); b) biomass (gdw m^{-2}) - solid line for above-ground and dashed line for below-ground; root-zone HS concentration (μM); d) root-zone NH_4^+ concentration (μM).

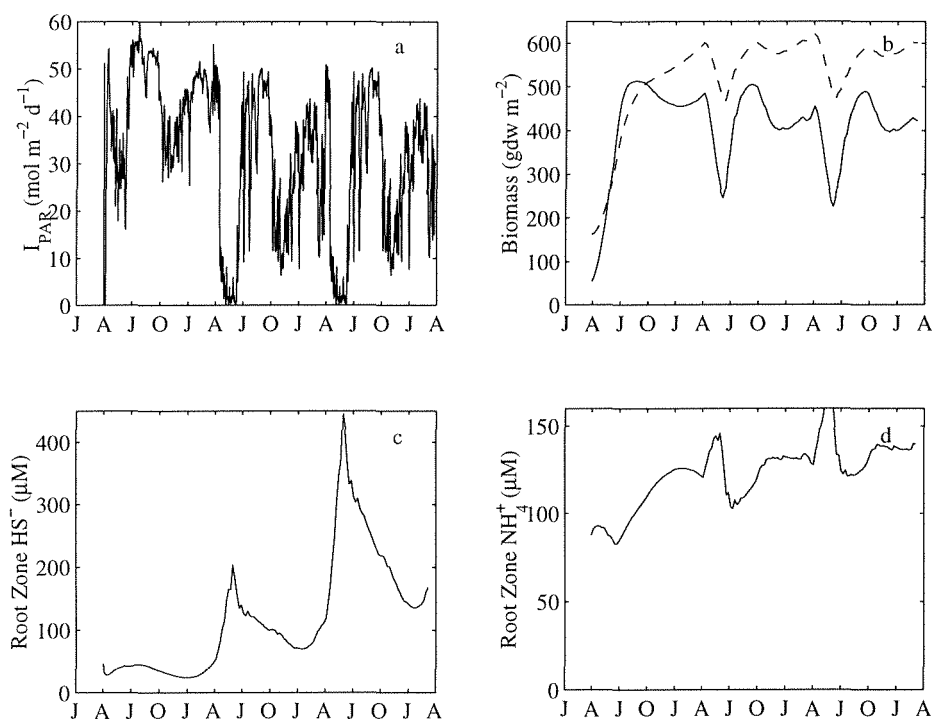
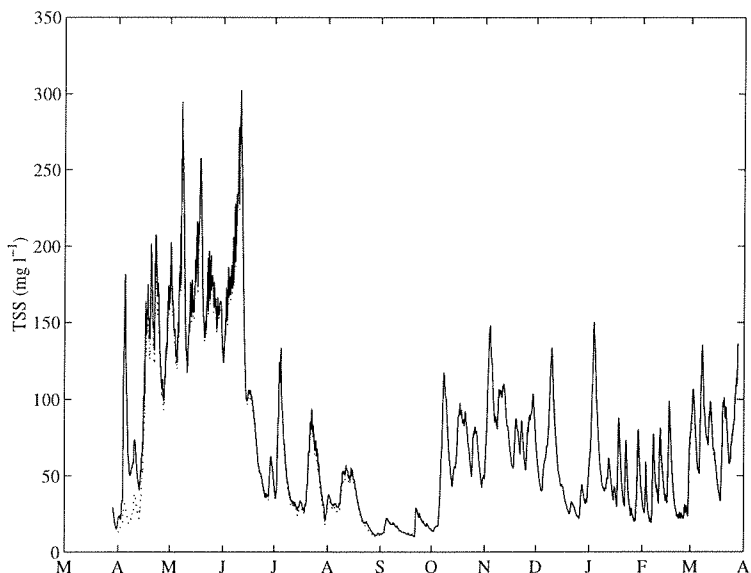


Figure 7: Modeled TSS concentrations (mg l^{-1}) for site 19 (node 3708 - *Halodule*). The solid line shows the results of the simulation with dredging and the dotted line shows the results of the simulation without dredging (model data courtesy of Allen Teeter).



Site 23 (node 1498)

Site 23 is the northernmost site at which seagrasses were modeled. The modeled TSS concentrations (Figure 9) are generally lower than at sites ULM-2, 19, and 17 with maximum concentrations of 150 mg l^{-1} occurring between April and June; concentrations during the summer and winter are typically below 50 mg l^{-1} .

The underwater irradiance (Figure 10a) shows the normal pattern with high values (approaching $45 \mu\text{mol m}^{-2} \text{ s}^{-1}$) corresponding to the times of low TSS concentrations (July to October and January to April). The above and below-ground biomass has seasonal cycle superimposed on a pattern of continuous growth (Figure 10b). Modeled biomass values are higher than observed *Halodule* biomass in the Laguna (*c.f.*, values in Figure 13, Chapter V). The high biomass also leads to high concentrations of root-zone HS^- (Figure 10c) and NH_4^+ (Figure 10d) but these values are not sufficient to lead to significant inhibitions on the seagrass growth.

Figure 8: Model results for site 19 (node 3708 - *Halodule*): a) canopy level irradiance ($\text{mol m}^{-2} \text{d}^{-1}$); b) biomass (gdw m^{-2}) - solid line for above-ground and dashed line for below-ground; root-zone HS concentration (μM); d) root-zone NH_4^+ concentration (μM).

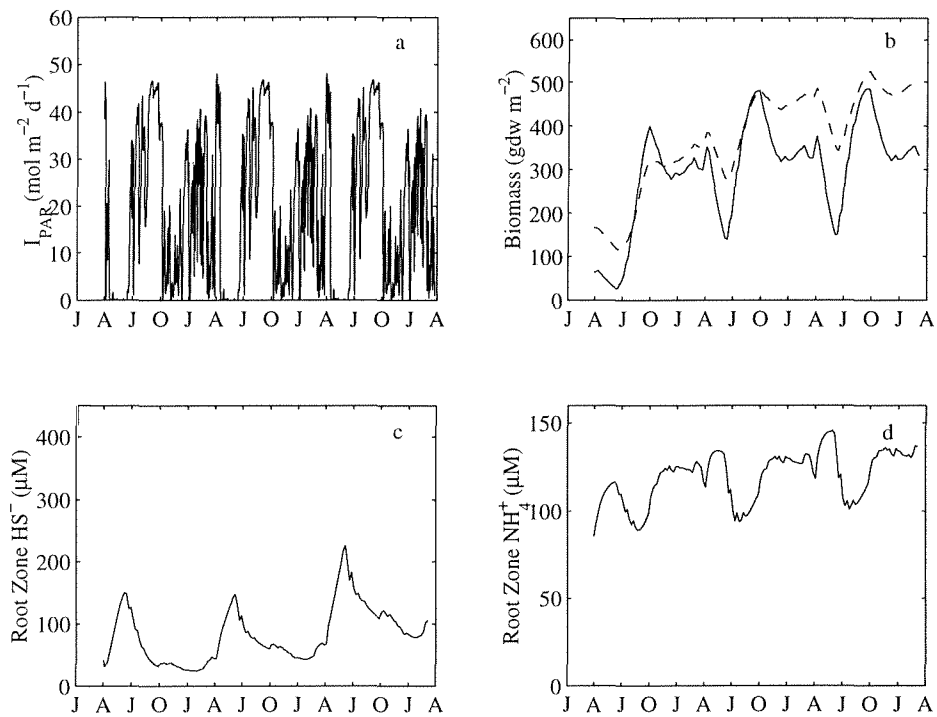
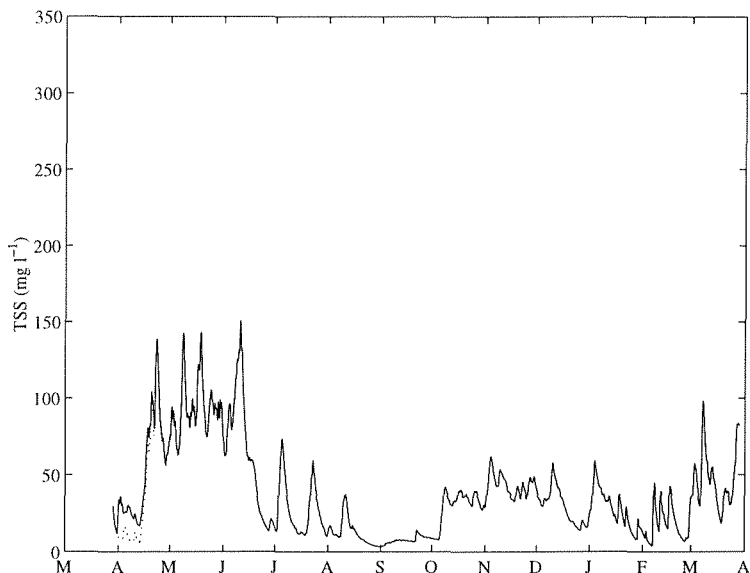


Figure 9: Modeled TSS concentrations (mg l^{-1}) for site 23 (node 1498 - *Halodule*). The solid line shows the results of the simulation with dredging and the dotted line shows the results of the simulation without dredging (model data courtesy of Allen Teeter).



Site WES-3 (node 17232)

This is the only *Halodule* site in the Lower Laguna Madre that was modeled. Maximum modeled TSS concentrations (Figure 11) were low compared with the other *Halodule* sites; spring-time concentrations reached approximately 100 mg l^{-1} . The lower concentrations of TSS occurring through the summer and winter were comparable with the *Halodule* sites in Upper Laguna Madre.

Levels of underwater irradiance were generally high ($40 - 50 \mu\text{mol m}^{-2} \text{s}^{-1}$) throughout the year, with low values occurring only during the time of TSS between April and July (Figure 12a). Biomass steadily increased over the three years, but did not attain the values seen in the model results for sites in the Upper Laguna Madre (Figure 12b). The root-zone HS^- (Figure 12c) and NH_4^+ (Figure 12d) concentrations were not sufficient to impact the growth of the plants.

Thalassia Sites

All the nodes at which *Thalassia* was modeled were in the Lower Laguna Madre.

Figure 10: Model results for site 23 (node 1498 - *Halodule*): a) canopy level irradiance ($\text{mol m}^{-2} \text{d}^{-1}$); b) biomass (gdw m^{-2}) - solid line for above-ground and dashed line for below-ground; root-zone HS concentration (μM); d) root-zone NH_4^+ concentration (μM).

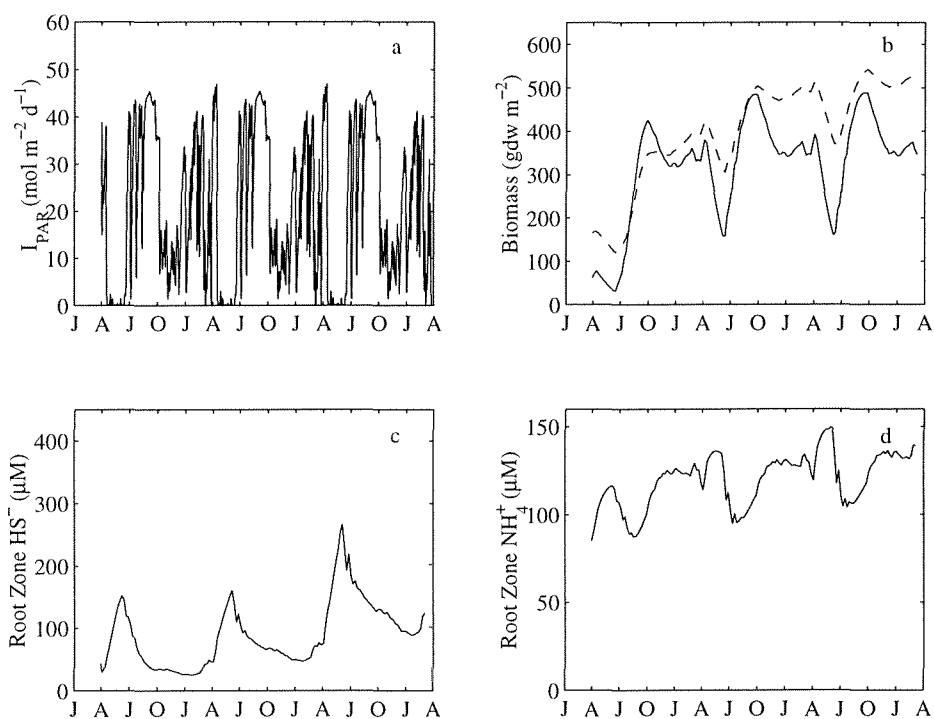
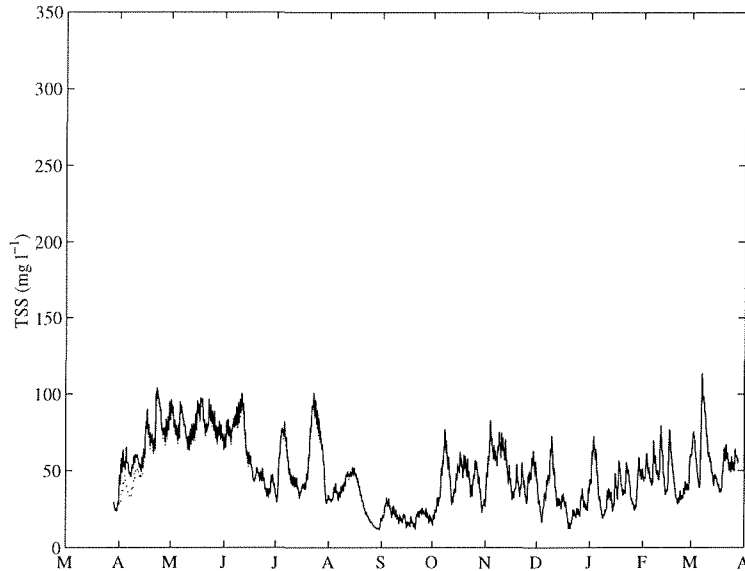


Figure 11: Modeled TSS concentrations (mg l^{-1}) for site WES-3 (node 17232 - *Halodule*). The solid line shows the results of the simulation with dredging and the dotted line shows the results of the simulation without dredging (model data courtesy of Allen Teeter).



Site LLM-2 (node 16580)

Concentrations of TSS at LLM-2 were very low compared with sites in Upper Laguna Madre (Figure 13). TSS values were rarely greater than 50 mg l^{-1} and typically were between 10 and 20 mg l^{-1} . The high values of TSS between April and May that were characteristic of the Upper Laguna Madre are absent, though there are elevated TSS concentrations between October and January. There is no discernible difference between the dredging and the non-dredging scenarios.

The underwater irradiance (Figure 14a) reflects the changes in the TSS concentrations. Maximum irradiances are approximately $50 \mu\text{mol m}^{-2} \text{ s}^{-1}$. The irradiance is lowest between October and January, the period of elevated TSS concentrations, reaching values lower than $10 \mu\text{mol m}^{-2} \text{ s}^{-1}$. The above-ground biomass shows seasonal fluctuations about a value of approximately 140 gdw m^{-3} (Figure 14b); this value is within the range of measured values in the Laguna Madre, especially when one takes into account that most of the plant's biomass is in the below-ground tissue.

Root-zone HS^- values (Figure 14c) are much lower than those at the modeled *Halodule* sites.

Figure 12: Model results for site WES-3 (node 17232 - *Halodule*): a) canopy level irradiance ($\text{mol m}^{-2} \text{d}^{-1}$); b) biomass (gdw m^{-2}) - solid line for above-ground and dashed line for below-ground; root-zone HS concentration (μM); d) root-zone NH_4^+ concentration (μM).

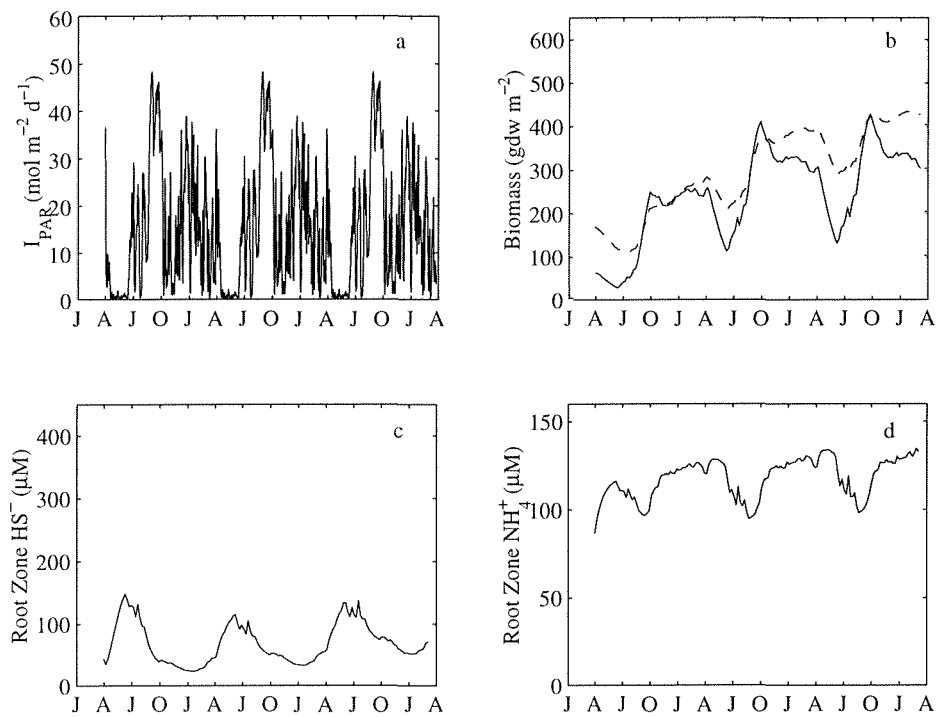
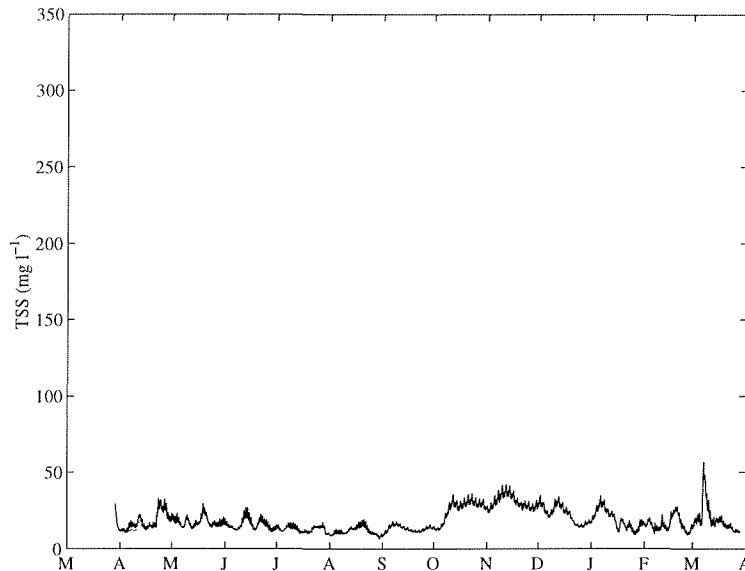


Figure 13: Modeled TSS concentrations (mg l^{-1}) for site LLM-2 (node 16580 - *Thalassia*). The solid line shows the results of the simulation with dredging and the dotted line shows the results of the simulation without dredging (model data courtesy of Allen Teeter).



Values at LLM-2 are between 5 and 10 μM and are well below the levels required for any toxic effects on the plant. Ammonia (Figure 14d) levels are higher, varying between 350 and 450 μM . At the higher concentrations, a small inhibition effect is possible.

Site 1 (node 16768)

The model results for this site are very similar to those for site LLM-2 because both sites are located very close to each other. The concentrations of TSS are very low (Figure 15), rarely rising above 50 mg l^{-1} and most typically remaining near approximately 10 mg l^{-1} . Elevated concentrations of TSS occur between October and January and there is a spike in March. There is no discernible difference between the modeled TSS concentrations for the dredging and the non-dredging scenarios.

Since the TSS concentrations at Site 1 are so similar to those at Site LLM-2, the underwater irradiance and resulting plant biomass and sediment chemistry are also very similar (Figure 16).

Figure 14: Model results for site LLM-2 (node 16580 - *Thalassia*): a) canopy level irradiance ($\text{mol m}^{-2} \text{d}^{-1}$); b) above-ground biomass (gdw m^{-2}); root-zone HS concentration (μM); d) root-zone NH_4^+ concentration (μM).

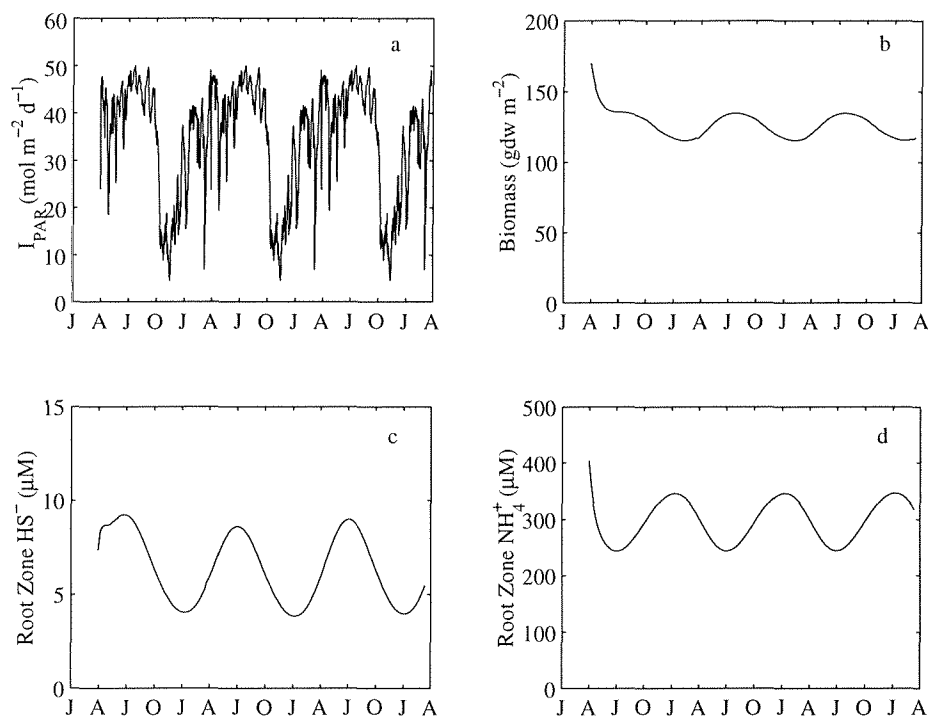
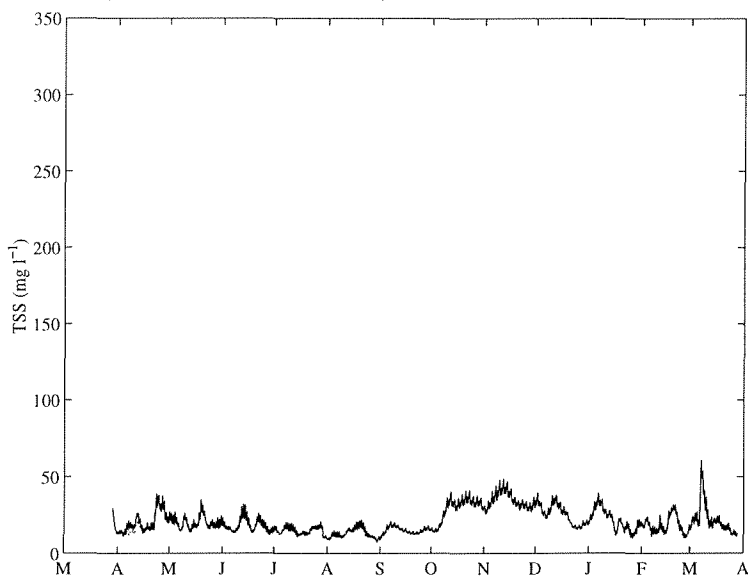


Figure 15: Modeled TSS concentrations (mg l^{-1}) for site 1 (node 16768 - *Thalassia*). The solid line shows the results of the simulation with dredging and the dotted line shows the results of the simulation without dredging (model data courtesy of Allen Teeter).



Site 3 (node 17543)

Modeled concentrations of TSS at this site were generally higher than those at LLM-2 and Site 1 (Figure 17). Maximum concentrations were greater than 100 mg l^{-1} and values were generally elevated between April and August and between October and January. The variation in TSS concentrations was also greater than at the previous two sites with rapid changes of TSS in a few days (*e.g.*, the drop in TSS from 100 mg l^{-1} to less than 25 mg l^{-1} at the end of July).

The underwater irradiance at this site shows pronounced lows of less than $10 \mu\text{mol m}^{-2} \text{ s}^{-1}$ during two parts of the year: April through July and October through January (Figure 18a). Between July and October, the modeled irradiance at canopy level reaches $45 \mu\text{mol m}^{-2} \text{ s}^{-1}$ and between January and April it gets as high as $30 \mu\text{mol m}^{-2} \text{ s}^{-1}$; these levels are generally lower than the underwater irradiances at site 1 (Figure 16a). The above-ground biomass at site 3 (Figure 18b) is also lower than that at site 1 because of the lower light levels. The biomass is greatest in October and reaches its lowest values in late spring; both correspond to fluctuations in the TSS concentrations.

Figure 16: Model results for site 1 (node 16768 - *Thalassia*): a) canopy level irradiance ($\text{mol m}^{-2} \text{d}^{-1}$); b) above-ground biomass (gdw m^{-2}); c) root-zone HS concentration (μM); d) root-zone NH_4^+ concentration (μM).

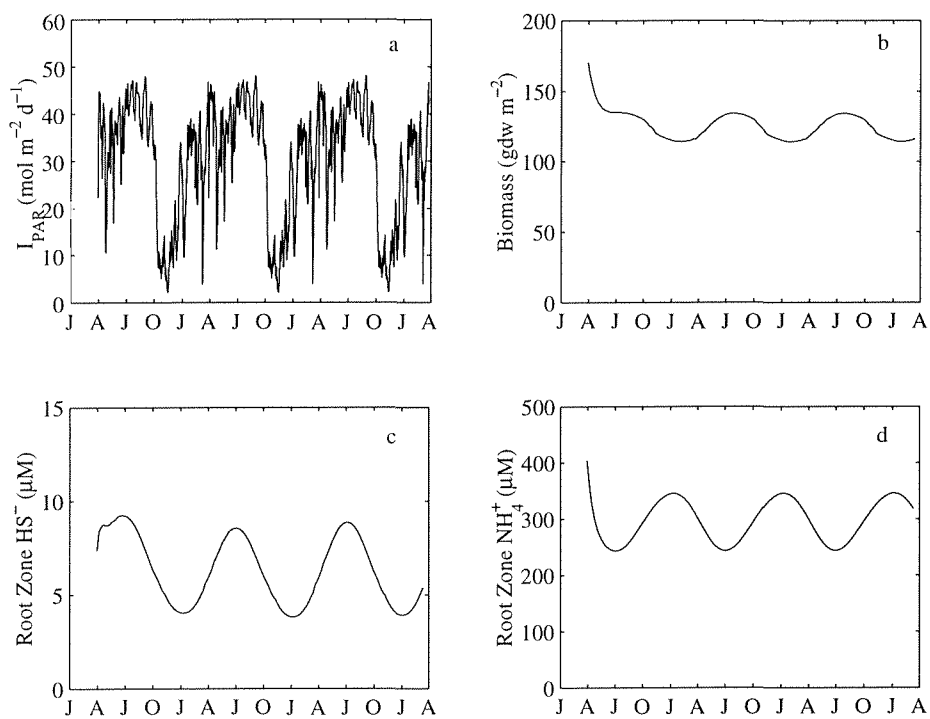
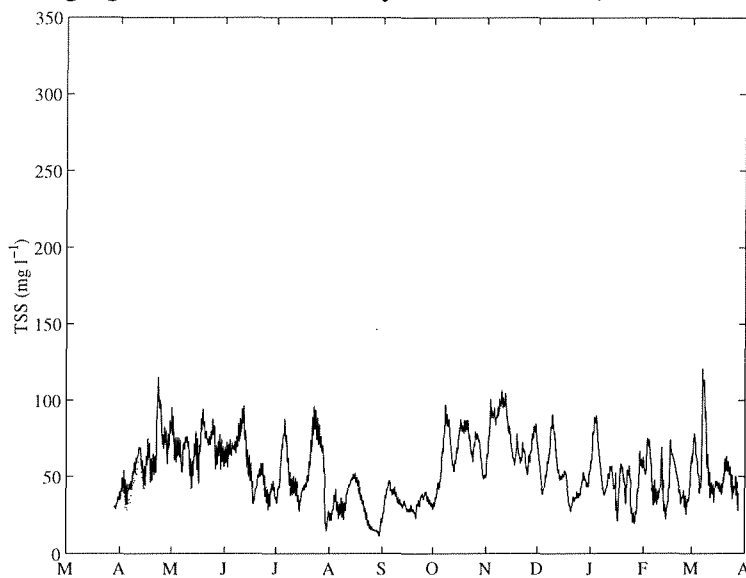


Figure 17: Modeled TSS concentrations (mg l^{-1}) for site 3 (node 17543 - *Thalassia*). The solid line shows the results of the simulation with dredging and the dotted line shows the results of the simulation without dredging (model data courtesy of Allen Teeter).



The root-zone HS^- levels are low (Figure 18c), varying between 5 and 10 μM with the peaks occurring in late spring (April–May). The root-zone NH_4^+ concentrations (Figure 18d) are similar to those seen at other sites and are sufficiently low as to not lead to significant inhibitions to plant growth.

Site 5 (node 15541)

Modeled concentrations of TSS vary between approximately 20 and 120 mg l^{-1} (Figure 19). There is appreciable difference between the dredging and the non-dredging scenarios. Maximum TSS concentrations occur in late April and early March, with lower values between August and September.

Modeled underwater irradiance (Figure 20a) reflects the changes in the TSS concentration. High irradiances (approximately 45 $\mu\text{mol m}^{-2} \text{s}^{-1}$) occur between July and October. The minimum irradiances ($< 10 \mu\text{mol m}^{-2} \text{s}^{-1}$) occur during two periods of the year; between October and September and between April and July. Modeled above-ground biomass values (Figure 20b)

Figure 18: Model results for site 3 (node 17543 - *Thalassia*): a) canopy level irradiance ($\text{mol m}^{-2} \text{d}^{-1}$); b) above-ground biomass (gdw m^{-2}); root-zone HS concentration (μM); d) root-zone NH_4^+ concentration (μM).

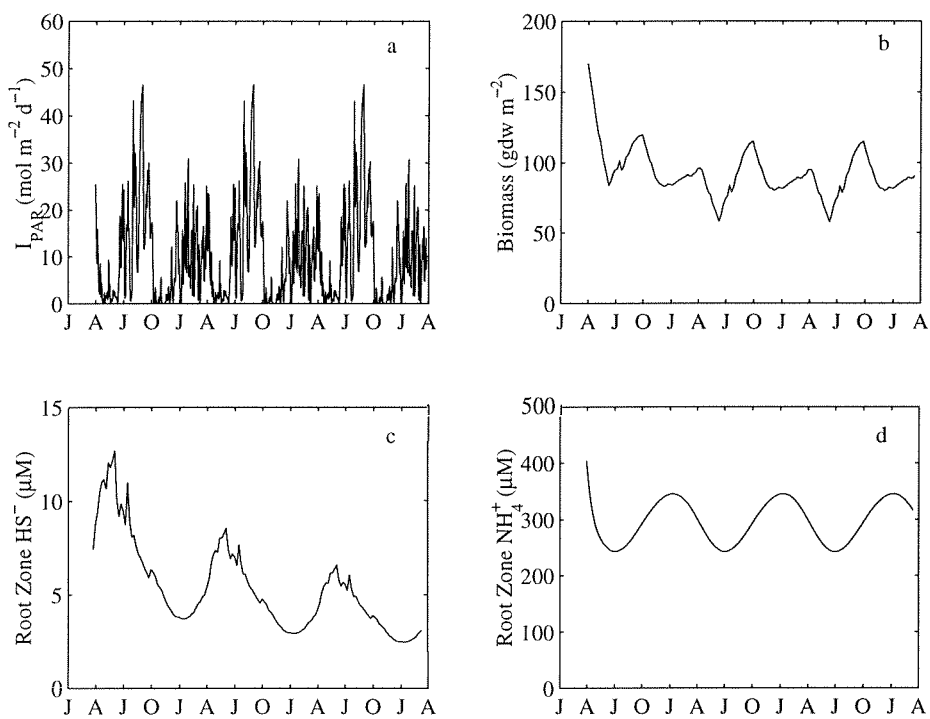
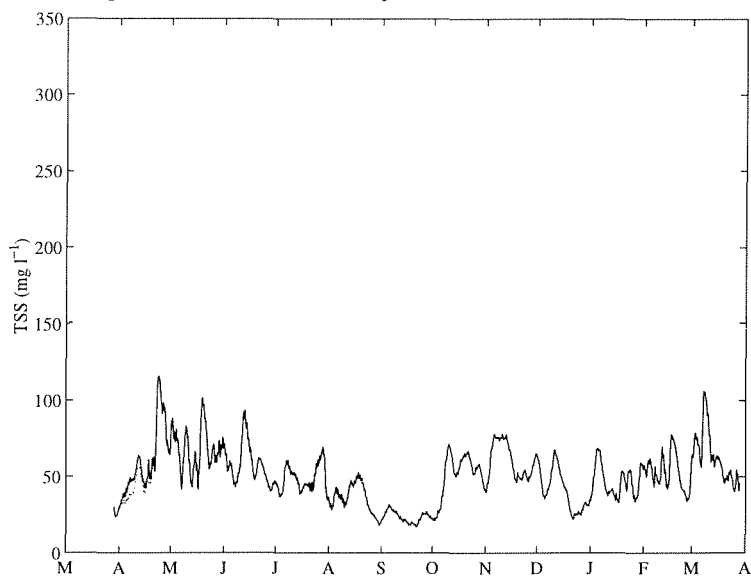


Figure 19: Modeled TSS concentrations (mg l^{-1}) for site 5 (node 15541 - *Thalassia*). The solid line shows the results of the simulation with dredging and the dotted line shows the results of the simulation without dredging (model data courtesy of Allen Teeter).



show small peaks between July and October (when the irradiance is greatest) and has a minimum value between April and July when the irradiance is also a minimum. The above ground biomass varies between about 75 and 125 gdw m^{-3} .

Root zone HS^- (Figure 20c) and NH_4^+ (Figure 20d) concentrations are similar to those at site 3. Sulfide concentrations vary between about 5 and 10 μM with peaks in the spring when the biomass is lowest. Ammonia levels vary between approximately 250 and 350 μM and are below the level which would result in an inhibition to growth.

Site 7 (node 16684)

Site 7 has modeled TSS concentrations that peak at about 100 mg l^{-1} (Figure 21). These concentrations are elevated during the spring (April to July). The minimum TSS concentrations occur between September and October. Apart from the first half of April, there is negligible difference between the TSS concentrations in the dredging and the non-dredging scenarios.

The underwater irradiance (Figure 22a) follows the patterns in the TSS concentrations. The

Figure 20: Model results for site 5 (node 15541 - *Thalassia*): a) canopy level irradiance ($\text{mol m}^{-2} \text{d}^{-1}$); b) above-ground biomass (gdw m^{-2}); root-zone HS concentration (μM); d) root-zone NH_4^+ concentration (μM).

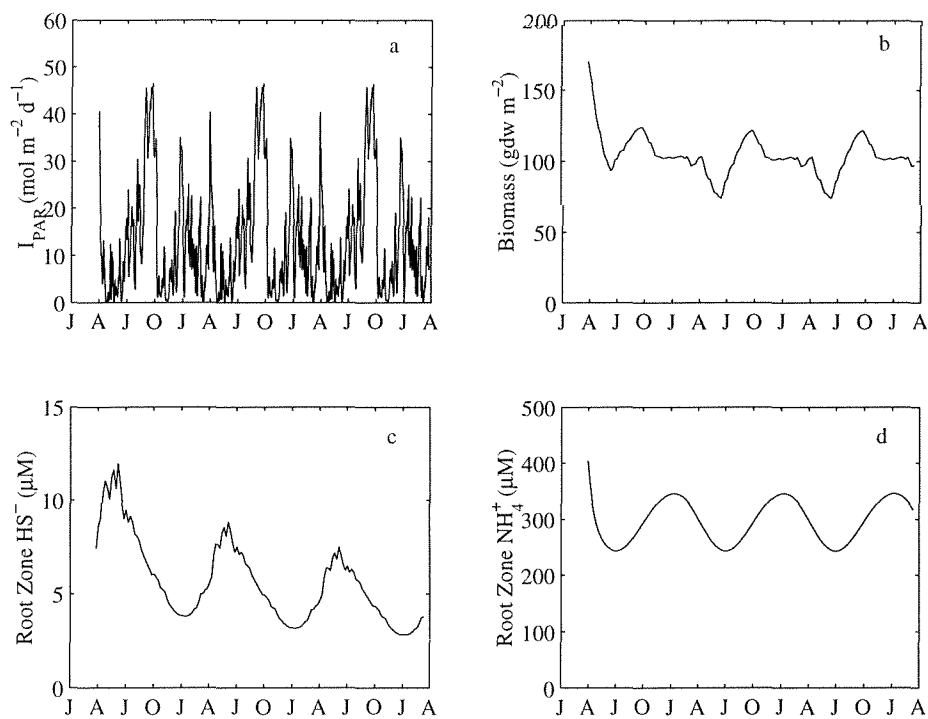
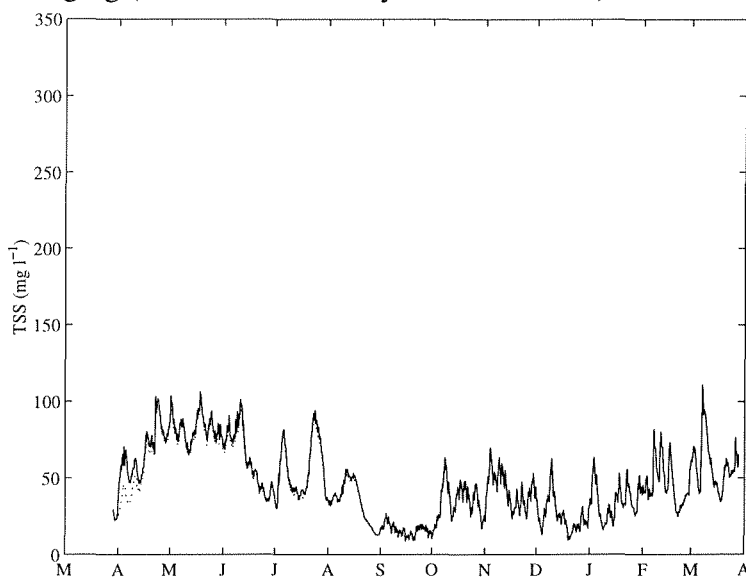


Figure 21: Modeled TSS concentrations (mg l^{-1}) for site 7 (node 16684 - *Thalassia*). The solid line shows the results of the simulation with dredging and the dotted line shows the results of the simulation without dredging (model data courtesy of Allen Teeter).



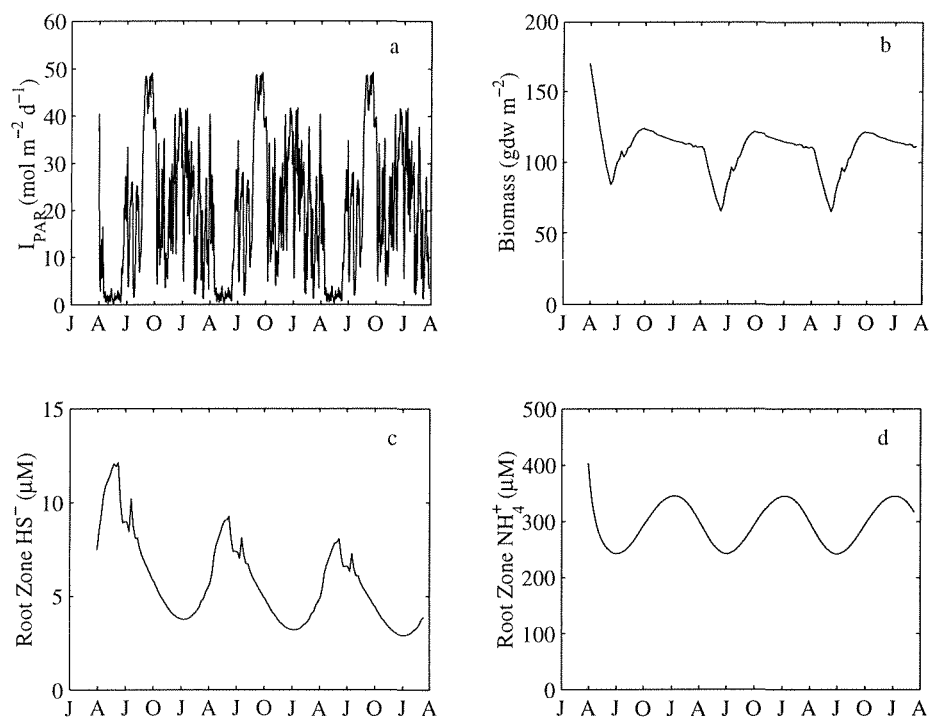
maximum irradiance ($\sim 50 \mu\text{mol m}^{-2} \text{s}^{-1}$) occurs during September when the TSS concentration is lowest, and the minimum irradiance is between April and July during the period of elevated TSS concentrations. The above-ground biomass shows a peak in October and has a minimum in the late spring (Figure 22b). Typical above-ground biomass is 100gdw m^{-3} with a minimum value of approximately 75gdw m^{-3} and a maximum of approximately 120gdw m^{-3} .

The model shows root-zone HS^- levels with a peak in the spring and minimum in the fall (Figure 22c). There is also a generally decreasing trend in HS^- concentrations over the three years. Root-zone NH_4^+ concentrations (Figure 22d) are very similar to those seen at site 5; peaks in the winter and minima in the summer and maximum concentrations insufficient to initiate inhibition of plant growth.

Site PA-235a (node 176780)

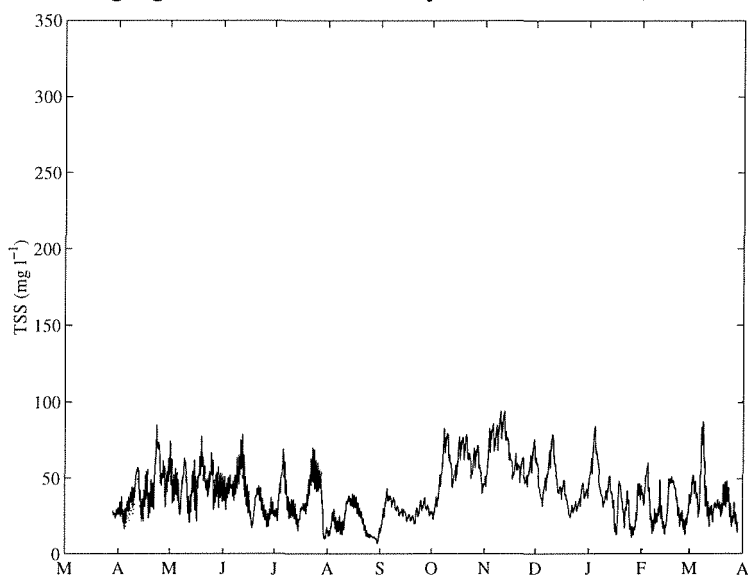
Modeled TSS concentrations (Figure 23) for site PA-235a are below 100mg l^{-1} for the whole year. Elevated TSS values occur between October and January and minimum concentrations occur

Figure 22: Model results for site 7 (node 16684 - *Thalassia*): a) canopy level irradiance ($\text{mol m}^{-2} \text{d}^{-1}$); b) above-ground biomass (gdw m^{-2}); c) root-zone HS concentration (μM); d) root-zone NH_4^+ concentration (μM).



between August and October. There is very little difference between the TSS concentrations in the dredging and the non-dredging scenarios.

Figure 23: Modeled TSS concentrations (mg l^{-1}) for site PA-235a (node 17680 - *Thalassia*). The solid line shows the results of the simulation with dredging and the dotted line shows the results of the simulation without dredging (model data courtesy of Allen Teeter).

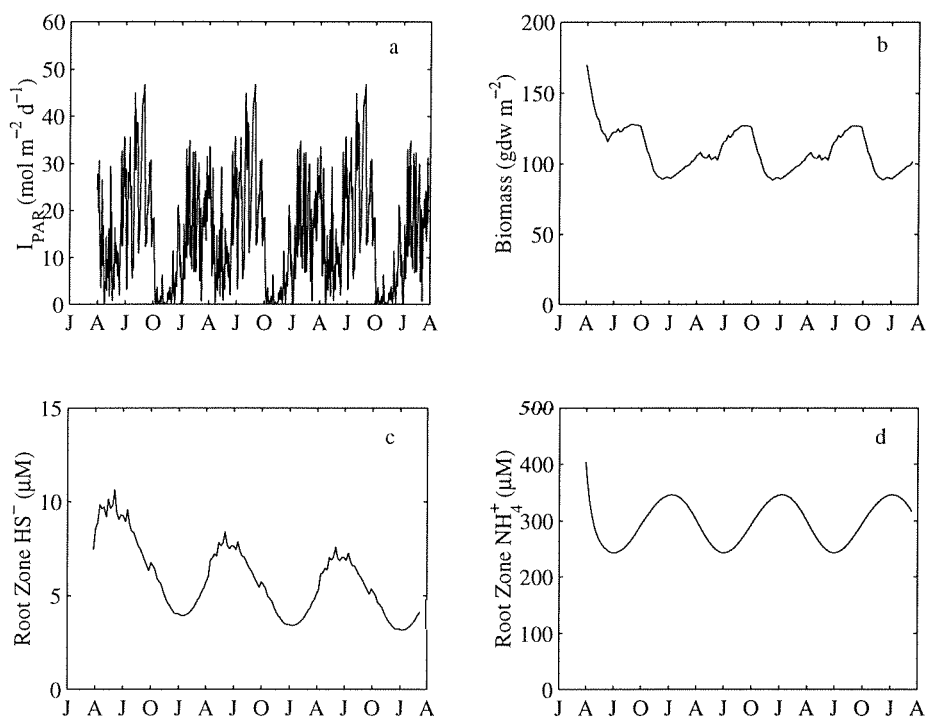


The modeled underwater irradiance (Figure 24a) is dictated by the TSS concentration. The minimum underwater irradiance ($< 5 \mu\text{mol m}^{-2} \text{s}^{-1}$) occurs between October and January (the period of elevated TSS concentrations at this site). The peak irradiances ($\sim 45 \mu\text{mol m}^{-2} \text{s}^{-1}$) occur between July and October (the period of minimum TSS concentrations).

The modeled above-ground biomass varies between approximately 90 and 120 gdw m^{-3} (Figure 24b). The peak biomass is at the end of the summer (September–October) and the minimum biomass is in the winter. The sudden decrease in biomass in October is a consequence of the irradiance resulting from the increased TSS concentrations at that time.

Root-zone HS^- concentrations (Figure 24c) remain low, varying between about 4 and 10 μM with a gradual decreasing trend over the three years of the simulation. The modeled root-zone NH_4^+ concentrations (Figure 24d) oscillate about 300 μM with peaks in the winter and maxima during the summer months.

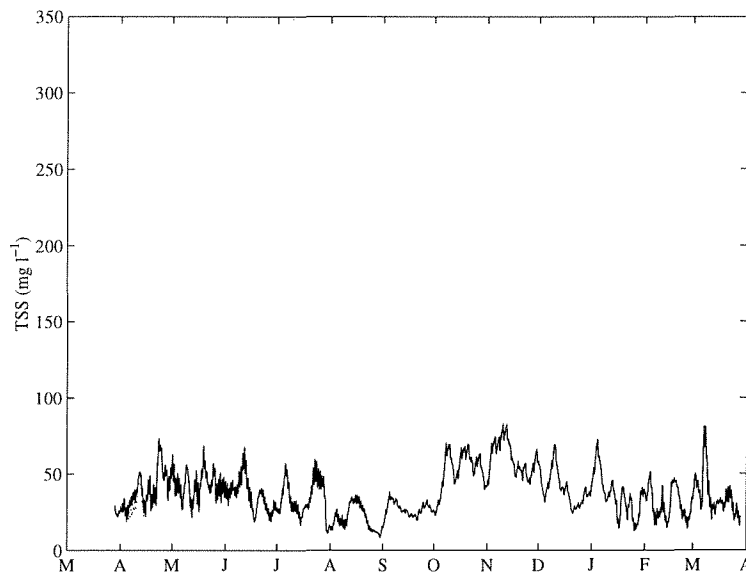
Figure 24: Model results for site PA-235a (node 17680 - *Thalassia*): a) canopy level irradiance ($\text{mol m}^{-2} \text{d}^{-1}$); b) above-ground biomass (gdw m^{-2}); root-zone HS concentration (μM); d) root-zone NH_4^+ concentration (μM).



Site PA-235b (node(17676))

Modeled TSS concentrations are below 100 mg l^{-1} (Figure 25). As with site PA-235a, elevated TSS concentrations occur between October and January preceded by a period between August and September of minimum values. There is little discernible difference between TSS concentrations in the dredging and the non-dredging scenarios.

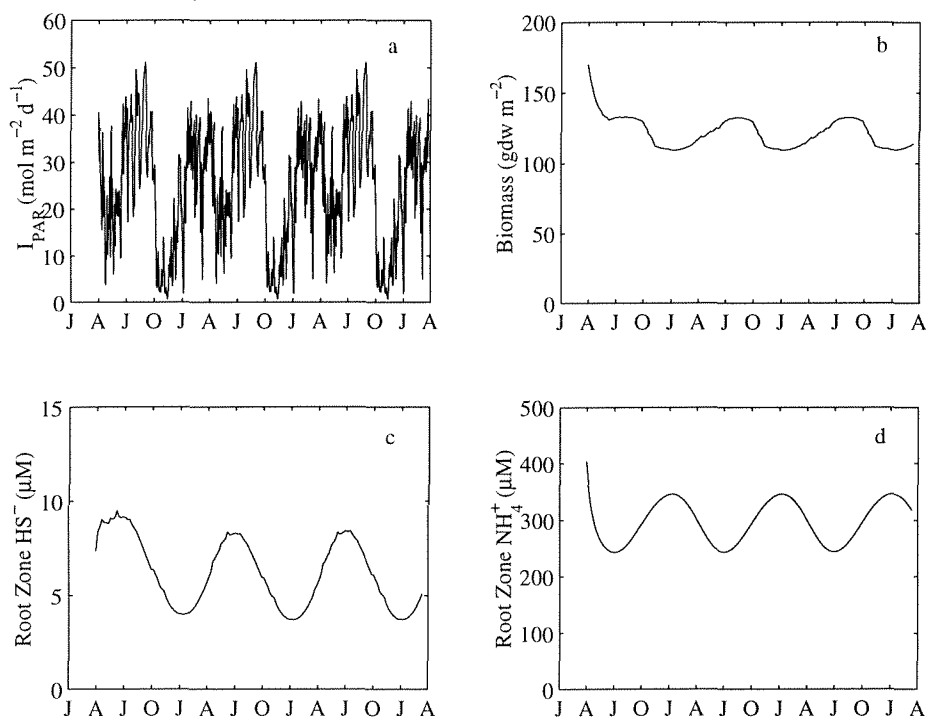
Figure 25: Modeled TSS concentrations (mg l^{-1}) for site PA-235b (node 17676 - *Thalassia*). The solid line shows the results of the simulation with dredging and the dotted line shows the results of the simulation without dredging (model data courtesy of Allen Teeter).



Maximum underwater irradiance occurs between July and October (Figure 26a) with values reaching $50 \text{ mol m}^{-2} \text{ d}^{-1}$. The underwater irradiance sharply drops to values below $15 \text{ mol m}^{-2} \text{ d}^{-1}$ in October. This drop corresponds to the increase in TSS at the same time. Irradiance values increase again during the winter.

The modeled root-zone HS^- and NH_4^+ are little different from those at previous sites. The HS^- varies between about 5 and $10 \text{ } \mu\text{M}$ (Figure 26c) while the NH_4^+ oscillates about $300 \text{ } \mu\text{M}$ (Figure 26d).

Figure 26: Model results for site PA-235b (node 17676 - *Thalassia*): a) canopy level irradiance ($\text{mol m}^{-2} \text{d}^{-1}$); b) above-ground biomass (gdw m^{-2}); root-zone HS concentration (μM); d) root-zone NH_4^+ concentration (μM).



Site PA-235c (node 17679)

The model results (TSS concentration, biomass, HS^- and NH_4^+) for site PA-235c are all almost identical to those of PA-235b.

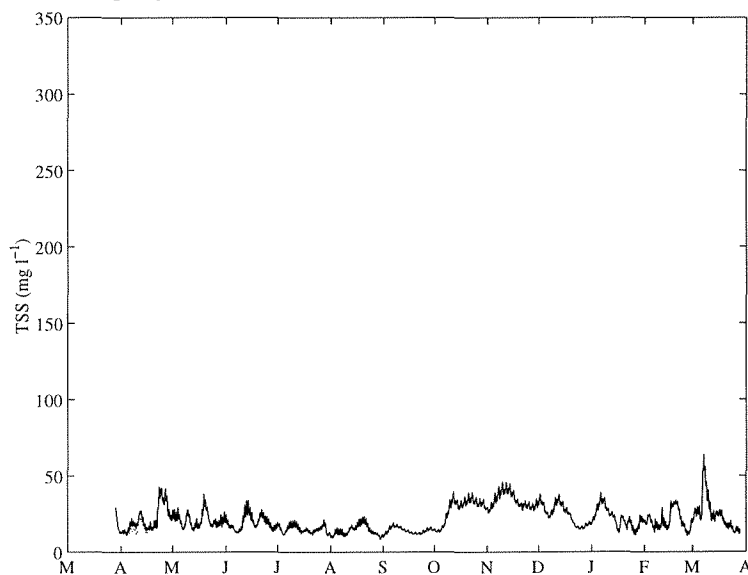
Site PA-235d (node 17677)

The model results (TSS concentration, biomass, HS^- and NH_4^+) for site PA-235d are all almost identical to those of PA-235b.

Site JEK (node 16394)

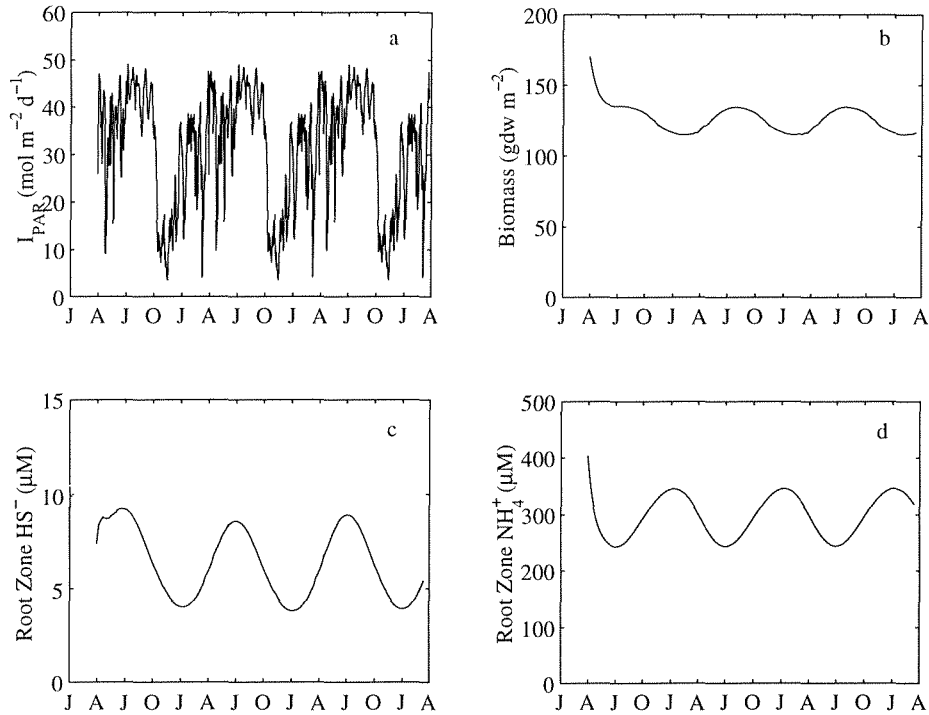
Modeled TSS concentrations remain below 50 mg l^{-1} except during March (Figure 27) when concentrations can get slightly greater than 50 mg l^{-1} . Generally elevated TSS concentrations occur between October and January. There is little discernible difference in TSS concentrations between the dredging and the non-dredging scenarios.

Figure 27: Modeled TSS concentrations (mg l^{-1}) for site JEK (node 16394 - *Thalassia*). The solid line shows the results of the simulation with dredging and the dotted line shows the results of the simulation without dredging (model data courtesy of Allen Teeter).



Modeled underwater irradiance reaches maximum values ($\sim 50 \mu\text{mol m}^{-2} \text{s}^{-1}$) between July and October each year (Figure 28a). Irradiance falls to about $10 \mu\text{mol m}^{-2} \text{s}^{-1}$ in October and the steadily rises throughout the rest of the year.

Figure 28: Model results for site JEK (node 16394 - *Thalassia*): a) canopy level irradiance ($\text{mol m}^{-2} \text{d}^{-1}$); b) above-ground biomass (gdw m^{-2}); root-zone HS concentration (μM); d) root-zone NH_4^+ concentration (μM).



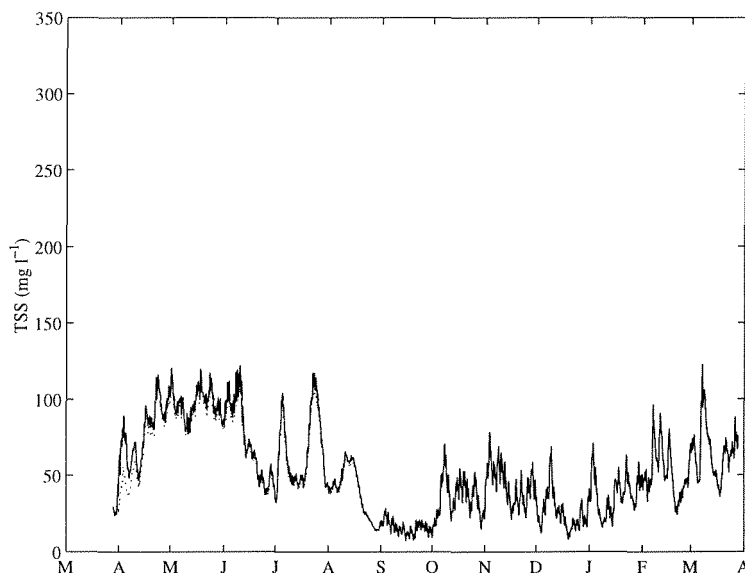
Modeled above-ground biomass (Figure 28b) is reasonably constant, varying between approximately 115 and 140 gdw m^{-3} . Peak biomass occurs during July with minimum values during January.

Root-zone HS^- and NH_4^+ show regular oscillations. The HS^- concentration varies between approximately 4 and 9 μM with peaks during the summer and minimum values during the winter (Figure 28c). Ammonia concentrations show the opposite behavior, with peaks during the winter and minimum values during the summer (Figure 28d). Both HS^- and NH_4^+ concentrations are insufficient to result in growth-inhibition of the plant.

Site WES-4 (node 16496)

Modeled TSS concentrations at WES-4 (Figure 29) are similar, but slightly higher than those at WES-3 (Figure 11). Elevated TSS concentrations occur between April and July, with values reaching 100 mg l^{-1} . Concentrations reach minimum values between September and October and then rise again in the winter with the maximum TSS occurring as a peak in March. There is no discernible difference in TSS concentrations between the dredging and the non-dredging scenarios, except for slightly lower concentrations during April in the non-dredging case.

Figure 29: Modeled TSS concentrations (mg l^{-1}) for site WES-4 (node 16496 - *Thalassia*). The solid line shows the results of the simulation with dredging and the dotted line shows the results of the simulation without dredging (model data courtesy of Allen Teeter).

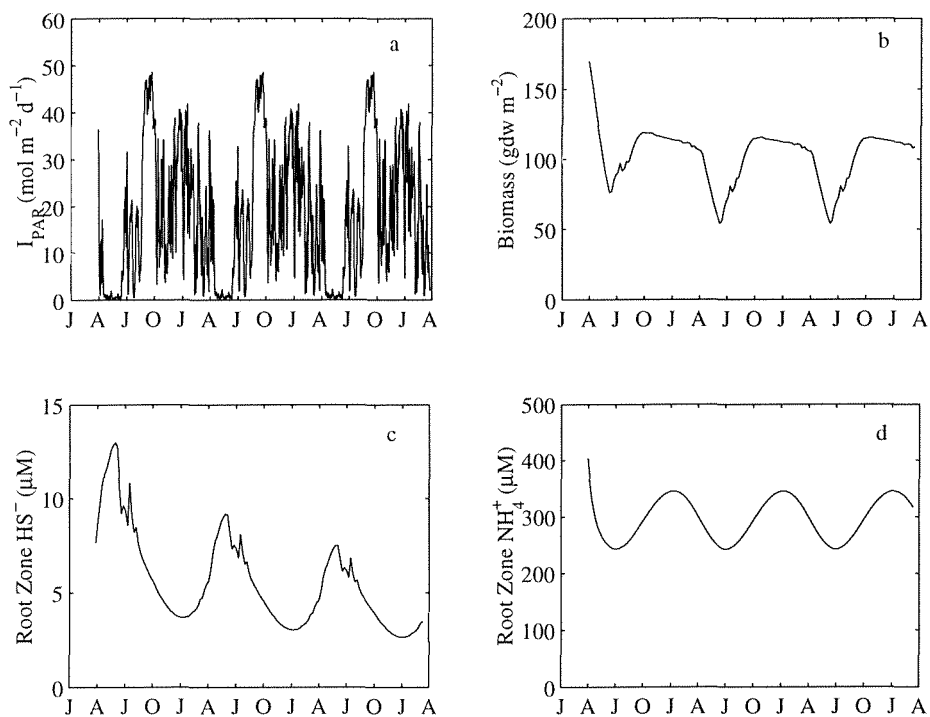


Modeled underwater irradiance reflects the changes in the TSS concentrations with maximum values ($\sim 50 \mu\text{mol m}^{-2} \text{ s}^{-1}$) in September and October and minimum values ($< 5 \mu\text{mol m}^{-2} \text{ s}^{-1}$) between April and July (Figure 30a).

Above-ground biomass varies between approximately 50 and 120 gdw m^{-3} throughout the year (Figure 30b) with maximum values in the summer and minimum values in the late spring.

The root-zone HS^- varies between about 10 and $4 \mu\text{M}$ with maximum values between April and July and minimum values in January (Figure 30c). These low HS^- values are not sufficient to

Figure 30: Model results for site WES-4 (node 16496 - *Thalassia*): a) canopy level irradiance ($\text{mol m}^{-2} \text{d}^{-1}$); b) above-ground biomass (gdw m^{-2}); c) root-zone HS concentration (μM); d) root-zone NH_4^+ concentration (μM).



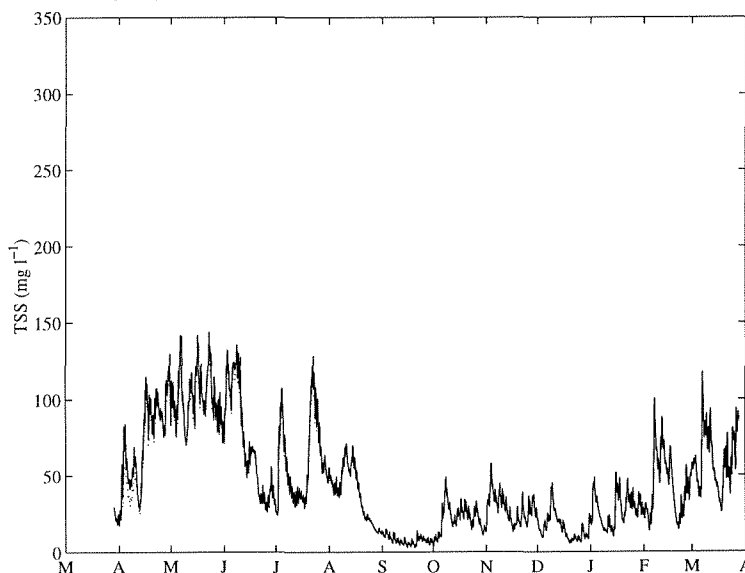
result in any toxic effects on the plant.

The root-zone NH_4^+ varies between approximate 250 and 350 μM with maximum values in the winter and minimum values in the summer (Figure 30d). These values are also too small to be toxic to the plant.

Site WES-5 (node 16306)

The modeled TSS concentrations at this site reach almost 150 mg l^{-1} during the spring (Figure 31). Elevated concentrations of TSS occur during between April and July, followed by minimum values in September and October. TSS concentrations remain below about 50 mg l^{-1} between October and February, then gradually increase again. The non-dredging scenario produces TSS concentrations that are slightly lower those in the dredging scenario during certain parts of the year.

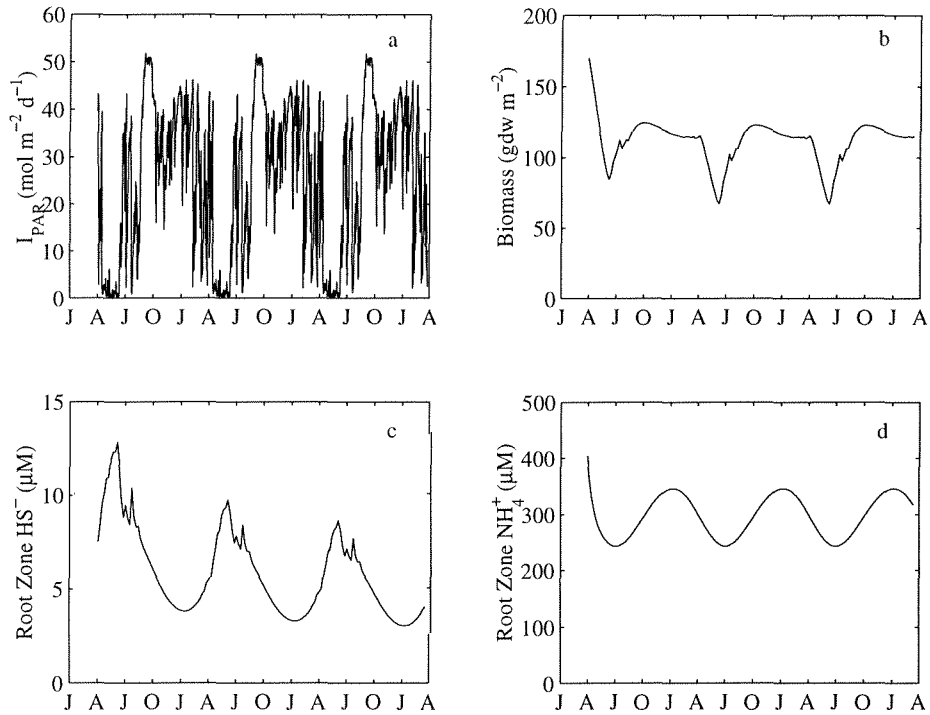
Figure 31: Modeled TSS concentrations (mg l^{-1}) for site WES-5 (node 16306 - *Thalassia*). The solid line shows the results of the simulation with dredging and the dotted line shows the results of the simulation without dredging (model data courtesy of Allen Teeter).



The modeled underwater irradiance (Figure 32a) reflects the changes in the TSS concentrations with maximum values ($> 50 \mu\text{mol m}^{-2} \text{s}^{-1}$) in September and October during the period of low TSS, and low irradiances ($< 5 \mu\text{mol m}^{-2} \text{s}^{-1}$) between April and July during the period of elevated TSS.

TSS.

Figure 32: Model results for site WES-5 (node 16306 - *Thalassia*): a) canopy level irradiance ($\text{mol m}^{-2} \text{d}^{-1}$); b) above-ground biomass (gdw m^{-2}); c) root-zone HS concentration (μM); d) root-zone NH_4^+ concentration (μM).



Above-ground biomass varies between approximately 60 and 120 gdw m^{-3} (Figure 32b) with maximum values in the summer and minimum values in the late spring. Root-zone HS^- shows slightly higher values during the dredging year, but values are still low varying between 4 and 12 μM . Root-zone NH_4^+ concentrations vary between 250 and 350 μM .

Discussion

For the forcing conditions used in these simulations, seagrasses at all the modeled sites survived. At all the sites in both Upper and Lower Laguna Madre, the seagrasses were exposed to irradiance levels greater than or equal to the saturation irradiance for almost the whole simulation.

The model predicts root-zone HS^- concentrations for the *Thalassia* sites that are generally lower than those observed in field (Tables 2 and 6, Chapter VI). This may be due to the lack of

a detailed below-ground biomass compartment in the model for this species. Root-zone NH_4^+ concentrations are within the range of those measured in the field for both *Halodule* and *Thalassia* sites, but tend to lie on the high end of this range. The model predicts NH_4^+ concentrations that lie between 100 and 350 μM . Observed root-zone NH_4^+ concentrations tend to be less than 100 μM , but some sites show concentrations greater than 1000 μM .

The maximum underwater irradiances predicted by the model fall within the range 40 – 60 $\mu\text{mol m}^{-2} \text{s}^{-1}$. These values are consistent with those observed in Lower Laguna Madre (Figure 11, Chapter I; Figures 10-12, Chapter V) but are higher than those seen in Upper Laguna Madre (Figure 8, Chapter I; Figures 7-9, Chapter V). One reason for this is that modeled attenuation of light in the water column comes only from the water and TSS. Other causes of light attenuation (*e.g.*, phytoplankton bloom, algal mats) are not accounted for in the model.

The *Halodule* biomass predicted by the model is higher than that observed, often by a factor of 2. The model was developed from data taken in Upper Laguna Madre (Chapter I). The data showed the effects of reduced light levels resulting from a persistent brown tide. This affected the calibration of the model such that the model recovered from reduced light levels more rapidly than was actually seen in the data (Figure 14, Chapter I). This tendency of the model to predict higher plant growth and productivity during periods of high irradiance may explain the high biomasses produced in these simulations.

The model only predicts above-ground *Thalassia* biomass. For the simulations presented here, the predicted above-ground biomass lies between approximately 100 and 150 gdw m^{-3} . The measured ratio of above to below-ground biomass (the root-shoot ratio) for *Thalassia* lies between approximately 3 and 6 (Figure 13, Chapter V). So, total biomass from the model therefore lies in the range 500 to 1000 gdw m^{-3} . This compares very favorably with *Thalassia* biomass measured in the Laguna Madre (Figure 13, Chapter V).

Two different results were seen in the verification experiment (Chapter V). At sites PA-235a and PA-235b the seagrasses were buried by material and subsequently died. Seagrasses at the nearby sites PA-235c and PA-235d, although affected by the decreased light, recovered at the end of the year. These observations do not contradict the results of the simulations in this chapter. The reason being that the verification sites were close (within a few hundred meters) to the disposal site, whereas most of the sites used in the model were greater than 1 mile from disposal areas;

the site closest to a disposal area was Site 19 which was 0.8 miles from PA-197 (Table 3 and Figure 1). This supports the idea of having a “buffer zone” between the placement area and the nearest seagrass bed. The extent of such a zone is hard to determine from the available information.

Conclusions

The model results presented here indicate that under the conditions used to force the model (*i.e.*, TSS concentrations, irradiances etc.) the seagrasses survive at the sites where the model was run. Several caveats need to be placed on this conclusion:

- Only light attenuation by TSS and water were accounted for in the model. The presence of other factors contributing to light attenuation (*e.g.*, phytoplankton blooms and algal mats) would decrease the light available to the seagrasses and compound any stresses affecting the seagrasses as a result of dredging activities.
- Burial of seagrasses by dredge material is not accounted for in the model. The Verification study of this project demonstrated that burial of seagrasses will kill the plants within a short period of time. The model results presented here need to be interpreted in the context of prolonged, chronic effects of dredging.
- Only certain sites were modeled. These sites are varying distances from the disposal sites and the results from the sites in Upper Laguna Madre strongly suggest that seagrasses in the immediate vicinity of a disposal site maybe impacted more than those further away.
- In the case of *Halodule* the model appears to over-estimate the plants recovery from adverse conditions. This implies that over successive periods of adverse and good conditions, the model will produce an optimistic estimate of plant biomass. However, these estimates are within a reasonable range of realistic values.

The model predicts the survival of the seagrasses mainly because, although TSS concentrations can be high, these high values are not prolonged. The model results indicate that during the summer growth period, the TSS concentrations are very low, hence the irradiance at canopy level can

be high allowing the plants to prosper. Prolonged exposure to high TSS concentrations would adversely affect the plants.

References

- Brown, C.A. and N. C. Kraus (1997) *Environmental Monitoring of Dredging and Processes in Lower Laguna Madre, Texas: Final Report, Year 1*. Technical Report TAMU-CC-CBI-96-01 (Texas A&M University-Corpus Christi).
- Dunton, K.H. (1994) Seasonal growth and biomass of the subtropical seagrass *Halodule wrightii* in relation to continuous measurements of underwater irradiance. *Marine Biology* **120**:479-489.
- Gregg, W.W. and K.L. Carder (1990) A simple spectral solar irradiance model for cloudless maritime atmospheres. *Limnol. Oceanogr* **35**, 1657-1675.
- Iqbal, M (1983) *An Introduction to Solar Radiation* (Academic Press, San Diego).
- Kirk, J.T.O. (1994) *Light and Photosynthesis in Aquatic Ecosystems* 2nd Edition (Cambridge University Press, Cambridge).
- Mobley, C.D. (1994) *Light and Water: Radiative Transfer in Natural Waters* (Academic Press, San Diego, US).
- Smith, R.C. and K. Baker (1981) Optical properties of the clearest natural waters. *Applied Optics* **20**, 247.

Extended Model Simulations

Addendum: Extended Simulations

Two series of additional simulations were performed using field data collected during the Verification Experiment from site PA-235. Both series of simulations were run for three years. The first had simulated a dredging event in the first and the third years while the second simulated a dredging event in the first year only. Both series of simulations were run with a variety of root-zone depths, root-zone widths, and percentages of reactive and refractory carbon (see Table 1).

Table 1. Table of model sediment and root-zone parameters used in both extended simulations. Root zone depth and width distributions are similar to those shown in Lee and Dunton (2000). The proportions of reactive and refractory carbon sum to that measured during the Verification Experiment in Lower Laguna Madre.

Line type	Root zone depth (cm)	Root zone width (cm)	Reactive carbon (%)	Refractory carbon (%)
Red solid line	5	3	0.35	0.735
Green solid line	7	3	0.37	0.715
Blue solid line	9	3	0.40	0.685
Red dashed	5	4	0.35	0.735
Green dashed	7	4	0.37	0.715
Blue dashed	9	4	0.40	0.685
Red dotted	5	5	0.35	0.735
Green dotted	7	5	0.37	0.715
Blue dotted	9	5	0.40	0.685

Time series of underwater irradiance were synthesized using field observations collected during the Verification Experiment (see Chapter V). Underwater irradiance for a year with a simulated dredging event was taken to be that collected at sites PA-235c and PA-235d (see Chapter V). For years with no dredging, underwater light profiles collected at the same time but at station FIX-2

were used (see Chapter V). This was done because the underwater irradiance at FIX-2 indicates that it was apparently unaffected by dredging activities during the field observations.

The model used in these simulations was that described in Chapter V. The disposal of dredged material was simulated by adding 7.0 cm of dredged material to the surface layer in the simulation. Different percentages of reactive and refractory carbon were used in describing the dredged material (Table 1), but in all cases, the total organic carbon equaled that measured during the Verification Experiment. Root zone depths and widths for *Thalassia* were taken from Lee and Dunton (2000).

The aims of these simulations were:

1. To examine the seagrass model (independently of the hydrodynamic and sediment transport models) to see if its long-term behavior matched that observed at site PA-235. This site was chosen for its proximity to a dredged material disposal area (see Chapter V) and for the availability of data at the site.
2. To compare the modeled effect of a single dredge event against alternating years of dredging and non-dredging.
3. To estimate the time that *Thalassia testudinum* requires to recover between dredging events.

Results

Dredging in the first year only

If dredging occurs in the first year only, the plants have two years to recover. The simulation shows that at the end of the third year, the above-ground plant biomass is recovering (Figure 1). The above-ground biomass at the end of the simulation is approximately 50% of the initial above-ground biomass and has an increasing trend indicating continued growth. In the second year of the simulation, the above-ground biomass drops to almost zero as a result of both low irradiance and high root-zone sulfide concentrations. The maximum root-zone sulfide concentrations are approximately 2 mM and maximum ammonium concentrations are approximately 750 μM . Concentrations of root-zone sulfide and ammonium decline throughout the second and third years allowing the *Thalassia* biomass to recover. It is also apparent from the

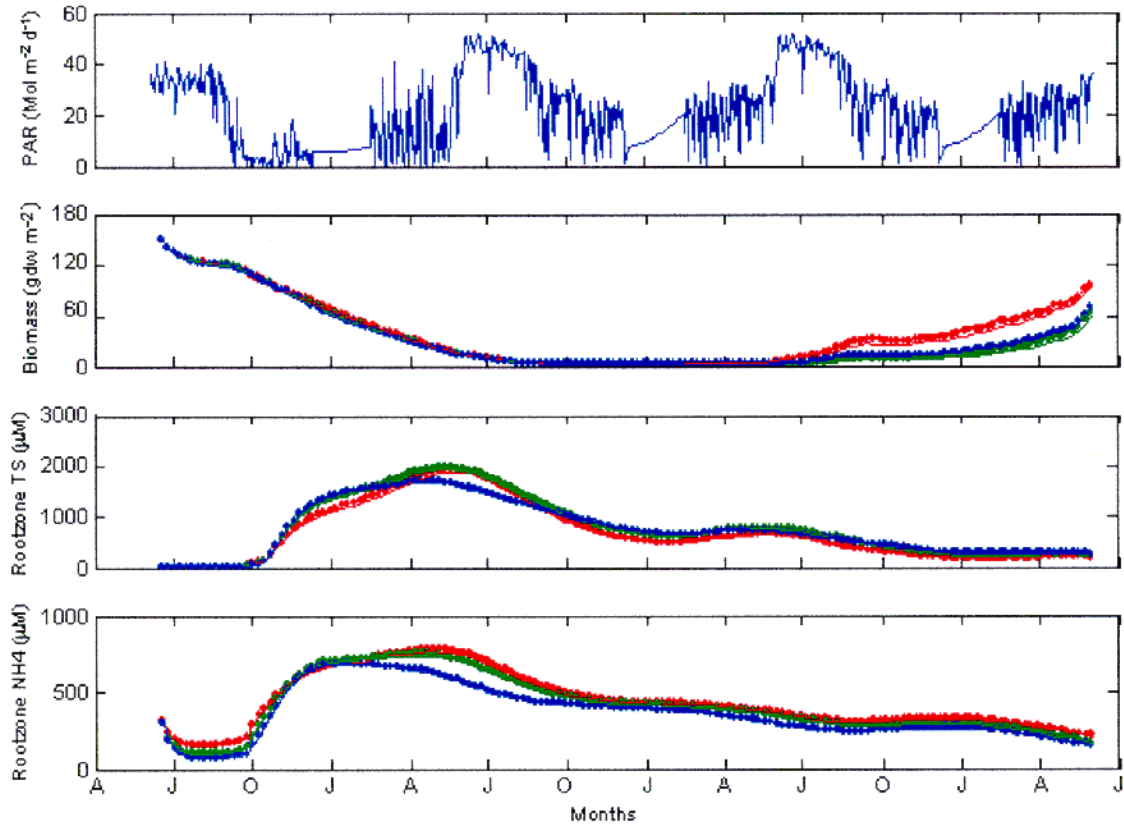


Figure 1. Underwater irradiance, above ground biomass, root-zone total sulfides and ammonia for a three year simulation with dredging occurring only in the first year. See Table 1 for the key between the different curves.

curves in Figure 1 that the model has greatest sensitivity to the root-zone depth (the red, green and blue curves).

Dredging in alternate years

If dredged material disposal occurs in the same site on alternate years, then *Thalassia* has a harder job surviving and will most likely die-off in that area (Figure 2).

The above-ground seagrass biomass starts to decline from the time of the initial dredging event and at the same time, the root-zone sulfide and ammonium concentrations increase. As with the first simulation, these concentrations decline during the second year, but unlike the previous simulation, they increase dramatically in the third year at the onset of the second dredge event. Although the above-ground biomass appears to be increasing, the decrease in underwater

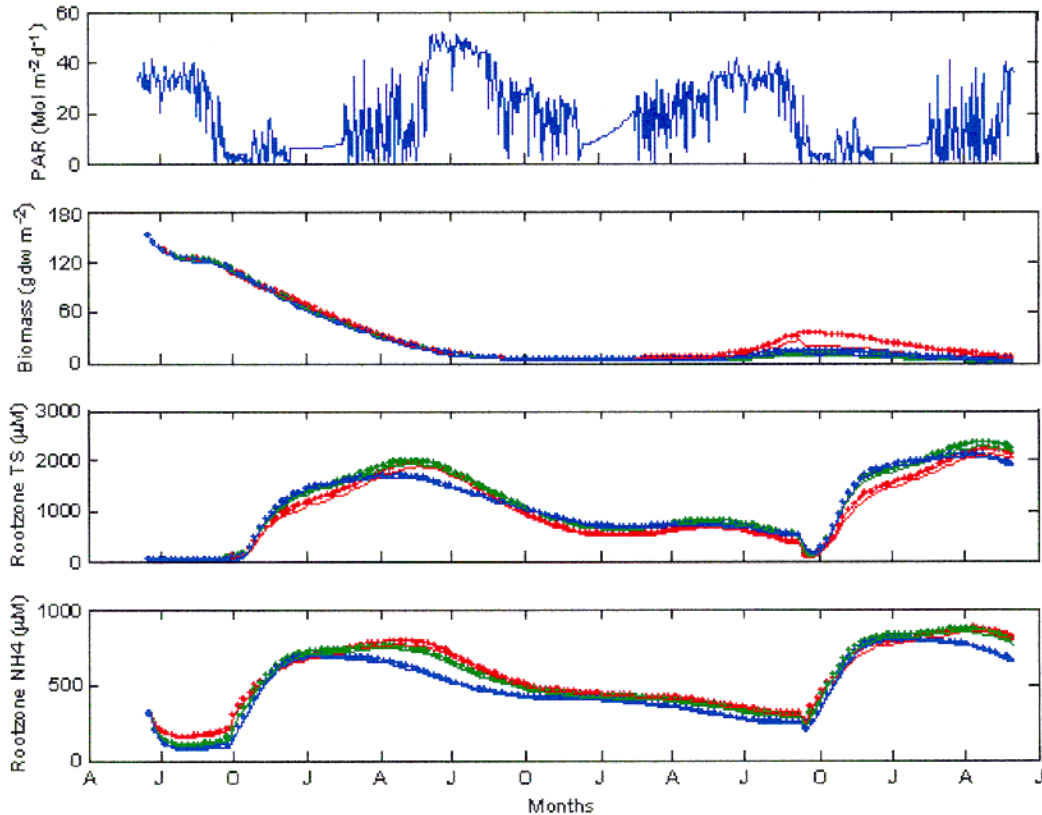


Figure 2. Underwater irradiance, above-ground biomass, root-zone sulfide and ammonium concentrations for a three year simulation with dredging occurring in the first and third years. See Table 1 for a description of the line types.

irradiance combined with the increase in sediment sulfide and ammonium reverse the recovery of the plants. After the second dredging event, the maximum sulfide and ammonium concentrations reached in the root-zone appear to be slightly larger than those following the first dredging event. This is because the root-zone has insufficient time to reduce these concentrations to their pre-dredging levels. Additional dredged material deposited on top of the sediments therefore compounds the existing concentrations.

Discussion

Seagrasses are complex organisms and their response to a nearby dredging event is not simple. The plants respond to a combination of both irradiance (which drives plant photosynthesis and growth) as well as sediment sulfide and ammonium concentrations (high values of which are toxic to the plant). Unfortunately, these two factors are not independent of each other. This is

clearly seen in the first year in both simulations where the increase in sulfide and ammonium concentrations occurs in conjunction with the decrease in underwater irradiance. The reason for this is that the plants use some of the oxygen from photosynthesis to convert the sediment sulfides into sulfates, which the plant can tolerate more easily. As the underwater irradiance levels decline, the level of photosynthesis declines and the amount of oxygen generated is insufficient to keep the sediment sulfide concentrations low. So, not only does the plant suffer from lower levels of photosynthesis (and hence is unable to grow or even metabolically support its existing tissues), but it also suffers from increased sediment toxicity. The combination of these two effects results in seagrass die-off unless the plants can resume their previous levels of photosynthetic activity.

The reverse of the above scenario allows the plants to recover in the single-dredge scenario (Figure 1). Normal levels of irradiance in the second and third years lead to increased photosynthetic activity and declining sediment sulfide and ammonium concentrations. If a second dredging event occurs before the plants have had time to sufficiently recover, then they will decline further (Figure 2). It would appear from the simulations that this period is longer than one year since alternating years of dredging and non-dredging do not appear to allow the plants sufficient time to recover. Even after two years (Figure 1) the biomass has not returned to its pre-dredging level and the sediment total sulfide (TS) concentration remains high. Determining the exact length of time required for the seagrasses to recover is difficult, especially since the simulation results become less meaningful the longer the period of time being simulated.

The model results appear to be relatively insensitive to the width of the *Thalassia* root-zone as well as to the percentages of reactive and refractory carbon in the dredge material. The model is sensitive to the depth of the root-zone.

Caveats

Great care has to be taken over the interpretation and use of these model results. There are several crucial assumptions that have been used in this modeling effort, and each assumption affects the conclusions in different ways.

Hydrodynamics and sediment transport

This model was run *without* input from any hydrodynamic or sediment transport model. This means that erosion, re-suspension and deposition of dredged material were not realistically incorporated into the model. This has several important consequences:

1. The 7 cm layer of dredge material used in this model is incorporated into the sediments. In reality, some of this material will be re-suspended and deposited elsewhere in the system thereby reducing the input of new material into the sediment. However, in being re-suspended, some of this material will contribute to a reduction in the underwater irradiance thereby reducing the photosynthetic activity of the plant and hence its ability to pump oxygen into the sediments. This lack of information concerning re-suspension is overcome to some degree by using the underwater irradiance measured at site PA-235 during a dredging event. The time series contains within it the effects of suspended material in the water column. However, this does not provide any extra information about the time evolution of the depth of the dredge material layer.
2. The lack of information about sediment re-suspension becomes more acute as the length of the simulation increases. For a one year simulation (as presented in Chapter V) the availability of detailed irradiance information may in part make up for the lack of sediment transport data. However, over a period of three years (the length of the simulations presented here) significant sediment erosion and deposition can take place, which will not be reflected in the irradiance time series used nor in inputs to the sediments.
3. The model as it stands is site specific. At a different location, different currents will produce differing amounts of sediment re-suspension. The time series of underwater irradiance will therefore be different from that used in this model.

Results from the hydrodynamic and sediment transport models show that there is little difference in the underwater irradiance between dredging and non-dredging scenarios. If this is the case, then greater confidence can be placed in the results of the simulations presented here. However, the site, PA-235, used in these simulations was close to a dredged material disposal area (see

Chapter V). The underwater irradiance data used here are most likely inappropriate for other sites in the Laguna Madre.

Underwater irradiance

The time series of underwater irradiances used in these simulations consists of two parts. For the years when dredging occurs, the time series developed in Chapter V for site PA-235 was used. This time series in itself was constructed from time series collected at two sets of stations during non-overlapping periods of time (see Chapter V for details). For the years when dredging did not occur, the time series of underwater irradiance collected at station FIX-2 was used. This has the following implications:

1. The final months of the time series at PA-235 are qualitatively and quantitatively different from the start of the time series at FIX-2. Underwater irradiance at PA-235 shows a lower mean value and greater oscillations about that mean than does FIX-2 (c.f. the irradiance between January and April with that between July and October of the first year in Figure 1). This may be a result of the effects of dredging, or it may simply be a consequence of yearly differences in the winds. Either way, there is an appreciable change in mean light levels between the two cases.
2. As with the lack of hydrodynamic and sediment transport information, the use of these irradiance time series make implications from these model results site specific.
3. The disposal of dredged material occurs at the same time (September) each year in the simulations. If disposal were to occur at any other time, the time series of underwater irradiance would be different.

Conclusions

Any conclusions from these models *must* be taken with the above caveats firmly in mind. In particular, it must be remembered that the site, PA-235, chosen for the validation and hence for these simulations, was very close to a dredged material disposal area. Consequently, one cannot draw generic conclusions about the fate of seagrass beds throughout the Laguna Madre based solely on the results of the two simulations presented in Figures 1 and 2.

1. The model results appear to agree with long-term field observations at site PA-235. Three years after the dredge event, seagrass biomass is recovering, with *Thalassia* above-ground biomass approximately 50% of the value prior to the dredge event (Figure 1).

2. Root-zone sulfide and ammonium concentrations reach maximum, toxic, levels within a few months of the dredge event after which they steadily decline (Figure 1).
3. The model demonstrates that seagrasses close to a dredged material disposal area would die-off if dredging occurred every other year (Figure 2).
4. A single year between dredge events appears to be insufficient time to allow the sediments to return to their prior state. What is more, the effects of dredging in alternate years is additive, so that maximum concentrations of sulfides and ammonium in the sediment are greater in after the second dredging event (Figure 2).
5. The results of these simulations indicate that a period of significantly greater than two years is required for a *Thalassia* seagrass bed to recover from a dredging event close by. Exactly how long this period needs to be is hard to determine using the current model.
6. Seagrasses having deeper root-zones do not recover as readily as those with shallower root-zones.

Part II: The Models

CHAPTER I: THE SEAGRASS MODELS

Contents

Introduction	4
The Laguna Madre Seagrass Models in General	7
The Light Field and Self Shading.....	10
Temperature Effects.....	21
Model Equations	22
Data Requirements and Availability.....	23
Biomass and Irradiance	23
Physiological Parameters.....	33
The Halodule Model.....	35
The Thalassia Model	37
The Syringodium Model.....	39
The Production Model.....	42
Results	43
Conclusions	57
References	58

Tables

Table 1. Photosynthetic, respiratory and mortality rates used in the seagrass models.	34
Table 2. Model parameter values obtained in the calibration of the model with data for each of the species.....	41

Figures

Figure 1. General structure of the Laguna Madre Seagrass Model.	9
Figure 2. A comparison of daily surface irradiance	14
Figure 3. An area randomly seeded with plants	16
Figure 4. The calculation of the shadow.	17

Figure 5. A comparison between hourly *Halodule* production rates with and without self-shading 18

Figure 6. A comparison of hourly production rates for a *Halodule* seagrass bed..... 19

Figure 7. A comparison between hourly production rates in a *Halodule* seagrass bed. 20

Figure 8. Underwater irradiance at the level of the seagrass canopy for site LM-151 25

Figure 9. Observations of above and below ground biomass for *Halodule wrightii* 26

Figure 10. Above and below ground biomass for *Thalassia testudinum* 27

Figure 11. Underwater irradiance at the canopy level in a *Thalassia testudinum* bed 28

Figure 12. Above and below ground biomass for *Syringodium filiforme* 29

Figure 13. Biomass calculated from a sequence of 10 cores taken at the same site of a *Thalassia* bed. 32

Figure 14. Comparison of 8 years of the *Halodule wrightii* data set with the model. 36

Figure 15. Parameterization of the *Thalassia* model against the 1995 data set. 38

Figure 16. Verification of *Thalassia* model 39

Figure 17. Calibration of the *Syringodium filiforme* model. 40

Figure 18. The baseline *Halodule wrightii* production model. 43

Figure 19. Production model run for *Halodule wrightii* with one week of enhanced water column attenuation 44

Figure 20. Production model run for *Halodule* with two weeks of enhanced water column attenuation 45

Figure 21. Production model run for *Halodule wrightii* with 50 days of enhanced water column attenuation 46

Figure 22. Production model run for *Halodule wrightii* with 100 days of enhanced water column attenuation. 47

Figure 23. The baseline *Thalassia testudinum* production model. 49

Figure 24. Production model run for *Thalassia* with one week of enhanced water column attenuation 50

Figure 25. Production model run for *Thalassia* with 50 days of enhanced water column attenuation 51

Figure 26. Production model run for *Thalassia* with 100 days of enhanced water column
attenuation 52

Abstract

The Laguna Madre Seagrass Model (LMSM) is a single component of a suite of models developed to assist in management decisions concerning maintenance dredging in the Laguna Madre. The objective of the seagrass component was to be able to predict trends in seagrass biomass and productivity resulting from changing environmental conditions. In particular, the model predicts how the plants respond to changes in irradiance that might arise from increases in suspended material in the water column.

The model was developed for three seagrass species, *Thalassia testudinum*, *Halodule wrightii* and *Syringodium filiforme* that are found in the Laguna Madre. The model was developed and calibrated using extensive data sets for the three species. In particular, a 9 year data set of biomass and hourly light data was used for the *Halodule* model with smaller data sets being used for *Thalassia* and *Syringodium* (approximately two years for each). The *Halodule* data set fortuitously contained a prolonged period during which a brown tide affected the area thus stressing the plants.

The LMSM is able to reproduce many features of the *Halodule* data set, including the effect of light stress on the below ground biomass and the rapid recovery of root and rhizome tissue after the brown tide disappeared. The *Thalassia* model reproduces the observed seasonal cycle of the plants which, unfortunately, the *Syringodium* model was not able to do.

Simulations using worst-case light attenuation profiles show that the seagrasses are able to withstand short periods (one to two weeks) of very high water column attenuation. Prolonged periods of approximately 100 days result in a dangerous decrease in plant biomass at moderate levels of water column attenuation.

Introduction

The Laguna Madre Seagrass Model has been developed as part of an interdisciplinary project to examine the effects of maintenance dredging on the health of seagrass beds. The model described here is one part of a suite of models developed for the Laguna Madre that include a hydrodynamics model, a sediment transport model, a water-column light model and a sediment diagenesis model (Eldridge, Chapter III of this report).

The objective of the modeling effort was to determine the effects of a variety of dredging scenarios upon the health of seagrass beds. The model will be used as a management tool to assist in decisions concerning the timing of maintenance dredging and the placement of dredged material. The separate modules of the modeling effort (the hydrodynamic, sediment transport, water column light, sediment diagenesis and seagrass models) share information. For example, the seagrass model described here requires information from the water column light model, which in turn depends upon input from the sediment transport model.

For the seagrass model, the objective was to provide a model of above and below ground biomass that would be able to successfully predict trends in seagrass biomass and productivity in response to external conditions. In particular, dredging activities may affect a seagrass bed in several ways. The most direct impact of dredging is the placement of dredged material on top of seagrass beds. In this case, unless this material is removed, the plants will die. A more subtle effect is the reduction in available light arising from an increase in suspended material. In this case the effect on the seagrasses will depend upon the severity and duration of the reduction in light levels.

Any model relies on field data for its formulation, calibration and verification. In the case of physical models, such as the hydrodynamic model, the basic theory underpinning the model is known and mathematical formulations (e.g., the Navier Stokes Equations) of the theory are well established. For biological models this is not necessarily the case and one has to resort to parameterizing processes using field data. For plant models, some parameterizations are well established (e.g., those used to represent production as a function of irradiance); others are not on

such firm ground. Any model which attempts to represent these processes can only be as accurate as the data used to set up the model.

Existing seagrass models (e.g., Dennison and Alberte, 1985; Kuhn, 1992; Short, 1980; Verhagen and Nienhuis, 1983) are semi-empirical, being based upon regression analysis of observations local to the site of interest. Such models work well within the constraints of the data used to form the model, but may give results with increasing uncertainty for predictions outside of that range. The model most relevant for our purposes is the Chesapeake Bay model (Kuhn, 1992) which includes interactions between the plants and the sediments. The Chesapeake Bay Seagrass model deals with *Zostera marina* (a species not found in the Laguna Madre) and has interactions between the plant and water-column as well as the plant and the sediment. Many of these interactions are parameterized from data collected both *in situ* in the Chesapeake as well as in the laboratory. A detailed examination of the model formulations revealed that some of these parameterizations were not applicable to seagrasses in the Laguna Madre. As a result it was decided to develop a new model, based on the Chesapeake model, for the three species *Thalassia testudinum*, *Halodule wrightii* and *Syringodium filiforme* found in the Laguna Madre.

Research on seagrasses is in its infancy compared to that of terrestrial plants. Terrestrial grassland models (e.g., Hurley Grassland Model (Thornley and Cannell, 1997)) require over one hundred parameters to be determined before the model can be run. Even then, the model output often differs from observations by a factor of two or three. Such a detailed model is impossible for seagrasses given the current state of knowledge about the plants.

Even within the field of seagrass research, not all species have been studied uniformly. Seagrasses are found throughout the world, and the most studied and modeled species is *Zostera marina*, a temperate species. Within this project, we are concerned with the sub-tropical species *Thalassia testudinum*, *Halodule wrightii* and *Syringodium filiforme*. Of these, the most is known about *Thalassia* and *Halodule*.

The major influences on seagrass growth are however known. The most important of these is light (Wetzel and Penhale, 1983; Dennison and Alberte, 1985). The surface light field is attenuated as it passes through the water column; water molecules, algae and suspended solids

contribute to this attenuation. The plant canopy itself also modifies the light being received by an individual leaf through shading of one leaf by another (Ross, 1981; Myneni *et al.*, 1989); this self-shading depends on the canopy architecture as well as the leaf density. A knowledge of the light field at the depth of the plant canopy provides sufficient information to predict the gross production of the plant. In order to determine the biomass resulting from such production, one needs to know how the plant allocates its various resources under differing conditions. The mechanisms controlling this allocation are generally unknown though some hypotheses and simple models have been proposed (Wilson, 1988; Thornley and Johnson, 1990; Thornley, 1995).

This chapter describes the Laguna Madre Seagrass Model (LMSM) which consists of the plant biomass and productivity modules of the modeling effort. The model contains parts that are common to the three seagrass species being examined, and these are discussed in the next section. After that, the data needs for the model are discussed. Differences, and their rationales, in the model for individual species are discussed. Although full model production runs cannot be made at present, some initial test runs are presented which give a good indication of the range of behaviors expected. Finally, the model and its predictions are discussed.

The Laguna Madre Seagrass Models in General

The Laguna Madre Seagrass Model has been constructed to allow its application to the three main seagrass species found in the region (*Thalassia testudinum*, *Halodule wrightii* and *Syringodium filiforme*). Models for each of the species examined in this project followed the same general structure (Figure 1) though there are differences between species, especially for *Thalassia*. The model computes changes in above and below ground biomass resulting from changes in the production of the plant; changes in plant production can arise from temperature effects as well as changes in the light environment.

Plant models generally use either carbon or nitrogen as their currency. The LMSM makes use of carbon, with required nitrogen concentrations and demands being obtained from measured C:N ratios of the plant material. Many plant models preferentially follow nitrogen (e.g., Sheehy *et al.*, 1996) since nitrogen limitation is a crucial aspect for plants. Carbon was followed in this model

since much of the required information for a nitrogen based model was unavailable. For example, seagrasses obtain most (if not all) of their nitrogen from the sediments (e.g., Zimmerman *et al.*, 1987) through the roots. In order to follow nitrogen uptake by the plant one needs to know the root biomass of the plant as well as how the specific uptake rate changes with nitrogen concentration. For both *Halodule* and *Syringodium* the plant architecture makes measurement of the root biomass an almost impossible task.

The inputs to the model consist of initial above and below ground biomass and the irradiance at the canopy level of the plants. The irradiance used is the photosynthetically active radiation (PAR) that is incident at the top of the plant canopy. Once this has been determined, the amount of carbon produced by the plant can be calculated if the photosynthetic response of the plant is known. Photosynthetic parameters for all three species of seagrass were obtained either through experiments conducted as a part of this project, e.g., for *Syringodium* (Major, 1998) or from published values for *Halodule* (Dunton and Tomasko, 1994) and *Thalassia* (Herzka and Dunton, 1997).

Both above and below ground biomasses experience losses through respiration and mortality. Respiration values for both above and below ground tissue were obtained from literature values for *Halodule* (Dunton and Tomasko, 1994) and *Thalassia* (Herzka and Dunton, 1997). *Syringodium* values were obtained from experiments conducted as part of this project (Major, 1998). In the model (Figure 1), the term mortality refers to any mechanism that will lead to a loss of structural material from the plant. Examples include leaf-blade loss through blades dying as well as through wave action. Values for the mortality rate were not available, but estimates were used based on field observations.

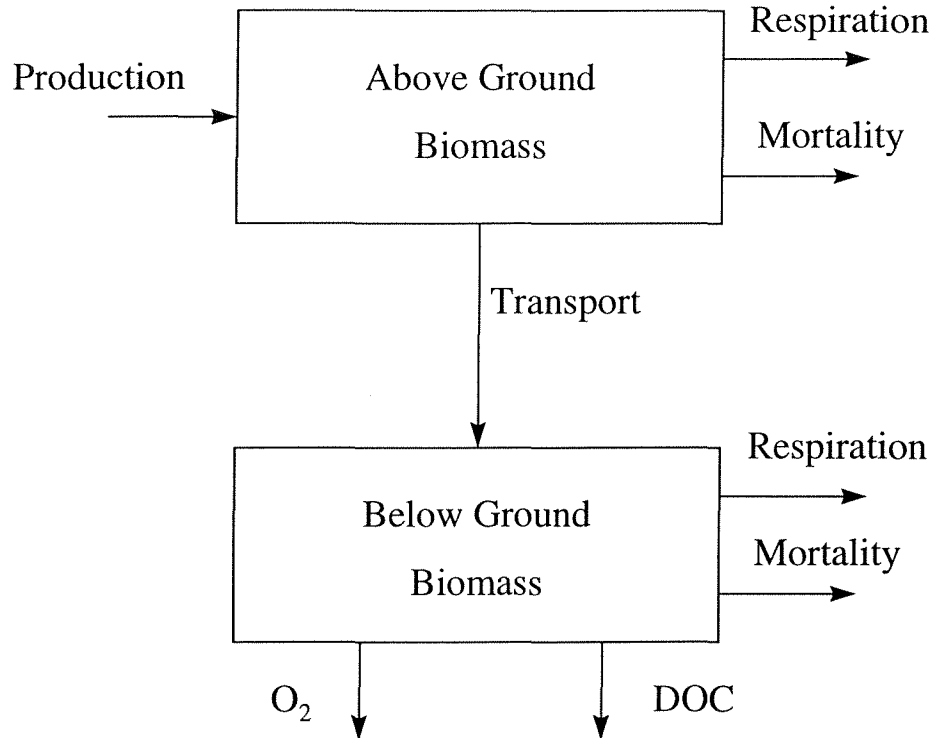


Figure 1. General structure of the Laguna Madre Seagrass Model. The model tracks both above and below ground biomass with transport of material from the above ground to the below ground compartments. Losses from the system include respiration, mortality and exudation of DOC into the sediments. The major input to the model is the underwater irradiance from which gross primary production is calculated.

Carbon used to generate below ground biomass is obtained through translocation from the above ground photosynthetic tissue. How the plant determines the allocation of this carbon is as yet only vaguely known, so a detailed model is not possible without an extensive laboratory program. Measurements that have been made and are available in the literature show a wide range of transport rates under varying conditions. Wetzel and Penhale (1979) measure less than 1% of the carbon fixed by *Thalassia* leaves being transported to the roots and rhizomes after 8 hours of incubation under conditions of saturated oxygen, high light and high temperatures. Moriarty *et al.* (1986) measured carbon allocation for *Halodule* under light saturating conditions. They found that after 3 hours, between 6% and 26% of the fixed carbon had been translocated to the roots and rhizomes; after 4 hours, 7% had been translocated and after 6 hours, 28% had been transported. The lack of available data for transport under various environmental conditions meant that we had to estimate the translocation rate, the procedure for doing this is given below.

The root zone exudes both dissolved organic carbon (DOC) and oxygen. Again, insufficient measurements are available to formulate a detailed model. Brylinsky (1977) measured DOC release from the whole *Thalassia* plant under both high light as well as dark conditions. Under high irradiances, *Thalassia* exuded approximately 1% of the fixed carbon as DOC; under dark conditions, approximately 7% of the fixed carbon was released. Moriarty *et al.* (1986) measured DOC release amounting to 0.5% of the fixed carbon for *Halodule*, though as much as 17% of the fixed carbon found its way into the sediments in one form or another.

Except for *Thalassia* both above and below ground biomass was modeled; and even in the case of *Thalassia* below ground growth was modeled indirectly. Certain parameters required for the models were obtained from the literature and from work done in association with this project. Certain parameters however could not be obtained, and these were determined by optimizing the model against available data sets. This was done by varying the unknown parameters in the models to obtain the best agreement between the model biomass predictions and the observed biomass.

The Light Field and Self Shading

Light is the primary input for the plants, determining the rate of carbon production. As light passes through the water column it is attenuated via absorption and scattering by water molecules and material (e.g., inorganic solids and phytoplankton) suspended in the water column. Dredging can affect the light attenuation by increasing the amount of suspended material in the water column, thereby increasing the attenuation coefficient and hence the light reaching the plant canopy.

There are several ways to calculate the irradiance received by the plants. For model calibrations and testing, the measured irradiance at the top of the plant canopy was used. For production runs of the model either an idealized irradiance or a typical irradiance calculated from surface observations was used, with details given below.

For the initial production runs of the model, the surface irradiance has to be determined and then the propagation of the light through the water column can be calculated once a light attenuation is given. Two separate surface irradiances were used. The first is a synthetic irradiance determined from equations governing the amount of light received at a given latitude for both a clear sky and an overcast sky.

This synthetic light field was produced using simple, standard equations for a clear sky (Kirk, 1994). The solar declination (in degrees) is determined by the empirical equation

$$\delta = 0.39637 - 22.9133 \cos(\eta) + 4.02543 \sin(\eta) - 0.3872 \cos(2\eta) + 0.052 \sin(2\eta)$$

where η is the Julian Day Number calculated as an angle in degrees, $\eta = 360(\text{Day}/365)$. The angular distance of the sun above the horizon (the solar elevation, β) at a latitude l and for a time, t (in hours) is given by

$$\sin(\beta) = \sin(l) \sin(\delta) - \cos(l) \cos(\delta) \cos(\tau) \quad (1)$$

where $\tau = t(360/24)$. The solar azimuthal angle, φ , is given by

$$\cos(\varphi) = \frac{\sin(\beta) \sin(l) - \sin(\delta)}{\cos(\beta) \cos(l)} \quad (2)$$

The time of sunrise is calculated using (Kirk, 1994)

$$t_{\text{sunrise}} = \arccos(\tan(l) \tan(\delta))$$

with the day length (in hours) given by

$$N = 0.133 \arccos(-\tan(l) \tan(\delta))$$

The irradiance on a horizontal surface by direct sunlight is then

$$I_0 = (S / 2f) \cos(\pi / 2 - \beta)$$

where $S = 1373 \text{ W m}^{-2}$ is the Solar Constant and $(\pi/2 - \beta)$ is the solar zenith angle. The factor of 1/2 arises from the fact that we are interested in PAR which accounts for about half the solar output and the factor f (approximately 2, (Kirk, 1994)) from atmospheric attenuation.

The diffuse component of the surface irradiance is harder to model since it is dependent on meteorological conditions at the site. An approximate, angular dependence for the diffuse component can be obtained from the *Standard Overcast Sky* (Monteith and Unsworth, 1990)

$$I_d(\sigma) = I_d(0) \frac{1 + B \cos(\sigma)}{1 + B}$$

where $I_d(0)$ is the fraction of the clear sky irradiance measured directly overhead, σ is the solar zenith angle and B is in the range 1.1 to 1.4 .

The surface of the water is assumed to be flat (i.e., no surface waves) so that the transmission of the light through the air-water interface is determined by Snell's Law and Fresnel's Equations. To a first level of approximation, waves and white caps have a small impact on light levels (including their effects leads to about a 10% change, (Kirk, 1994)). Snell's Law predicts the change in direction of a beam of light as it passes through an air water interface,

$$\frac{\sin(\theta_a)}{\sin(\theta_w)} = \frac{n_w}{n_a}$$

where θ_a, θ_w are the angles of the light ray from the vertical in air and water respectively and n_a, n_w are the refractive indices of air and water. For seawater, the refractive index is 1.33 and for air it is 1 (Kirk, 1994). Fresnel's Equations determine the proportions of light reflected and transmitted at the air-sea interface. The reflectance, r , of unpolarized light is

$$r = 0.5 \frac{\sin^2(\theta_a - \theta_w)}{\sin^2(\theta_a + \theta_w)} + 0.5 \frac{\tan^2(\theta_a - \theta_w)}{\tan^2(\theta_a + \theta_w)}$$

The reflectance is low for small θ_a , increasingly slowly up to about 50° , above which it increases rapidly.

Attenuation within the water column is modeled using Beer's Law

$$I(z) = I(0)\exp(-kz)$$

where z is the depth below the surface of the water. The attenuation coefficient, k , is initially taken to be constant, though in the later models this will be determined from the sediment transport model and the water column properties.

A second light field was calculated from observed surface irradiance at site LLM-2 over a period of about 3 years. Hourly irradiances for a year were calculated by taking the same hour in each year of the data record and averaging over those values. This results in a year long representative surface irradiance that includes typical cloud cover, fronts etc. This averaged light record was used in the production runs of the model presented later in this chapter. A comparison of the different irradiances used is given in Figure 2.

Given the irradiance at the plant canopy, the gross production of the plant can be calculated. Production of carbon in plants varies according to the amount of irradiance the plants receive and several possible parameterizations are available. Two relations between gross production and irradiance were used:

$$P = P_{\max} \tanh\left(\frac{I}{I_k}\right) \quad (3)$$

$$P = P_{\max} \left(\frac{\alpha I}{\sqrt{P_{\max}^2 + (\alpha I)^2}} \right) \quad (4)$$

where P_{\max} is the maximum gross production of the plant, I_k is the saturation irradiance of the

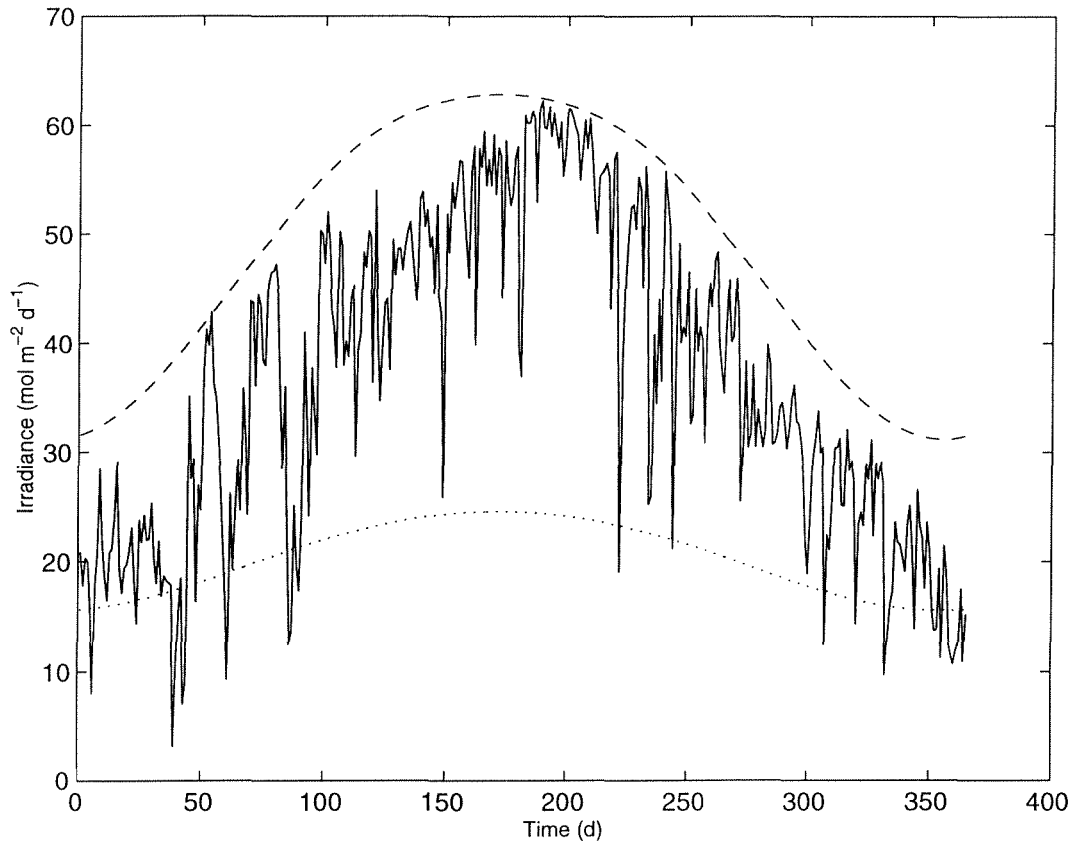


Figure 2. A comparison of daily surface irradiance calculated using a clear sky model (dashed line), a standard overcast sky (dotted line) and an average of surface observations (solid line). The clear sky model provides an upper envelope for the surface irradiance but often overestimates irradiance since local conditions (e.g., cloud cover, marine aerosol concentrations etc) are not taken into account. The standard overcast sky (dotted line) provides a reasonable estimate for the lower limit to surface irradiance.

plant and $\alpha = P_{\max} / I_k$. These three parameters were determined experimentally for each plant species and their values are listed in Table 1. Equation (3) was used for *Halodule* and Equation (4) for *Thalassia* and *Syringodium* since these were the forms used in the determination of the parameters (Herzka and Dunton, 1997; Dunton and Tomasko, 1990; Major 1998). The actual forms for the P vs. I curve for *Thalassia* used by Herzka and Dunton (1997) were somewhat more general but measurements of *in situ* observations were made at only two times of the year.

As a result, photosynthetic parameters measured for late summer were used in this study with the simpler form for the P vs. I curve.

So far the architecture of the seagrass canopy has not been taken into account. Leaves can shade each other, so that an individual leaf will not perceive the full irradiance at that depth in the water column. In addition, leaves can scatter and reflect radiation, making radiative transfer within the canopy extremely complicated. Various approximations to full radiative transfer can be made, depending on the quantities one wishes to calculate. To estimate photosynthesis, the leaves may be considered *black*; i.e., they absorb all radiation falling on them without scattering or reflection (Norman, 1980; Shultis and Myneni, 1988).

To simulate a seagrass bed, a rectangular region was “seeded” with shoots whose positions were selected randomly (Figure 3). The leaves can be inclined at any angle to the horizontal, but for the purposes of the simulations presented here, the leaves were assumed to be vertical. For this simulation, each shoot had only one leaf. Periodic boundary conditions were used to simplify the problem, making the effective size of the simulated seagrass bed infinite. Average, species-specific values for the length and width of each leaf blade were used.

The irradiance at the top of the canopy was calculated using Beer’s Law and the direction of the direct beam light was given by the beam azimuth and zenith angle, calculated from Equations (1) and (2). To calculate the effects of an individual shadow on the surrounding leaves, a chaining mesh is formed together with a linked list (Hockney and Eastwood, 1988). This allows the model to keep track of individual leaves and their neighbors. For a given beam direction, the shadow cast by a leaf was calculated (Monteith and Unsworth, 1990) (Figure 4).

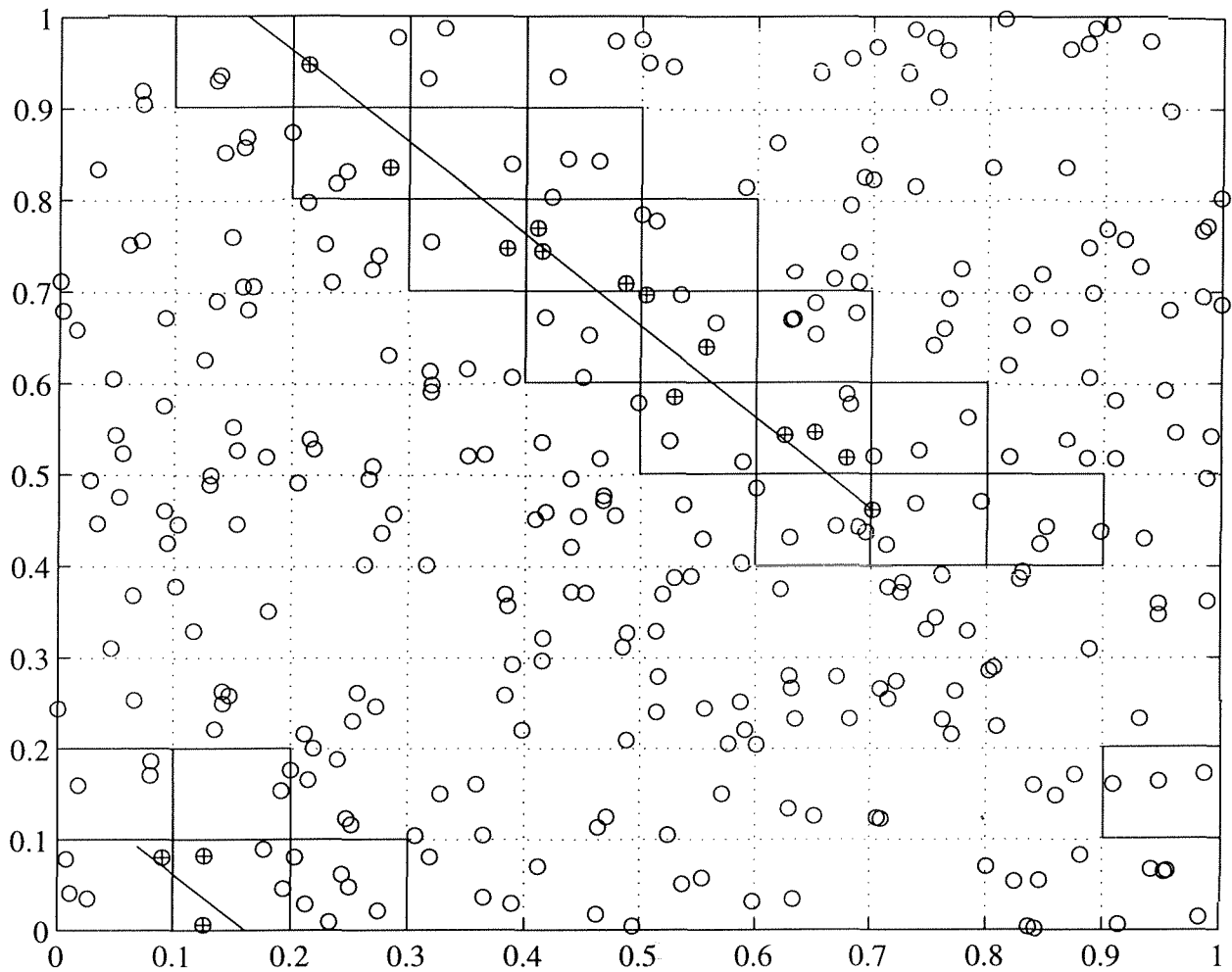


Figure 3. An area randomly seeded with plants (open circles). The area is divided into smaller rectangles (cells – solid rectangles in the figure) and the plants within each of these cells are kept track of using a linked list. The center line of the shadow of an individual leaf is shown. Once the shadow has been determined, a pattern of cells is established and these are searched for those plants that are affected by the shadow in question.

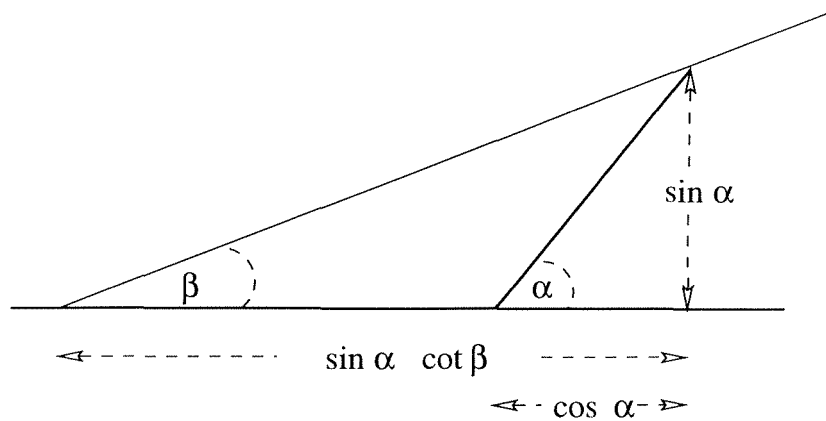


Figure 4. The calculation of the shadow. The seagrass blade is inclined at an angle α to the horizontal and the light is striking the blade at an angle β to the horizontal.

Each leaf, though, will reduce the size of the shadow until either the shadow reaches its proper length, or the shadow has been used up. The shadow cast by the leaf will impinge upon other leaves. Using the linked lists, those leaves that are affected by each shadow were found (Figure 3). The area of each leaf that is shaded by this shadow was calculated and stored. This procedure is repeated for each plant in the randomly seeded area. At the end of this procedure, the area of each leaf covered by shadow (taking into account that shadows can overlap) was calculated and stored. This information was then used to calculate the gross production and the effects of self shading.

Self-shading within the seagrass canopy reduces the light received by the plants and hence the daily production. The effects of self-shading within the canopy are most noticeable during mid-morning (about 9 a.m.) and mid-afternoon (about 4 p.m.) with reductions of about a factor of 1.5 in the productivity (Figure 5 and Figure 6). The extent of the self shading increases with shoot density. For the simulations shown here (using a canopy geometry similar to *Halodule*) self shading becomes negligible for shoot densities below about $1,000 \text{ m}^{-2}$ (Figure 7).

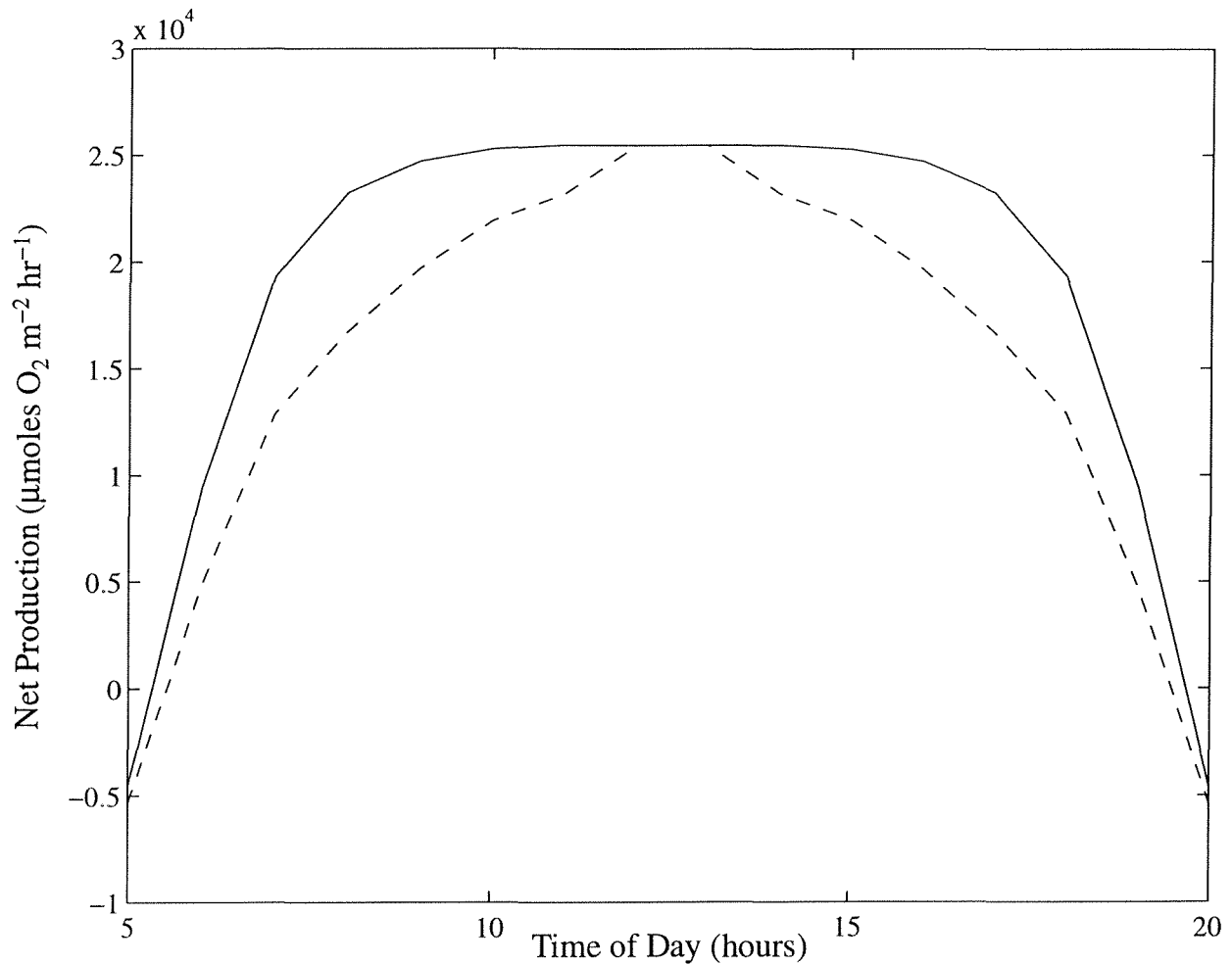


Figure 5. A comparison between hourly *Halodule* production rates without self-shading (solid line) and with self-shading (dashed line). The simulation was run for June 21st with a water column attenuation coefficient of $k = 0.5 \text{ m}^{-1}$ and the top of the seagrass canopy at a depth of 1.8 m. The shoot density was $10,000 \text{ m}^{-2}$. The total daily production without self-shading was $0.3 \text{ mol C m}^{-2} \text{ d}^{-1}$ and with self-shading was $0.23 \text{ mol C m}^{-2} \text{ d}^{-1}$.

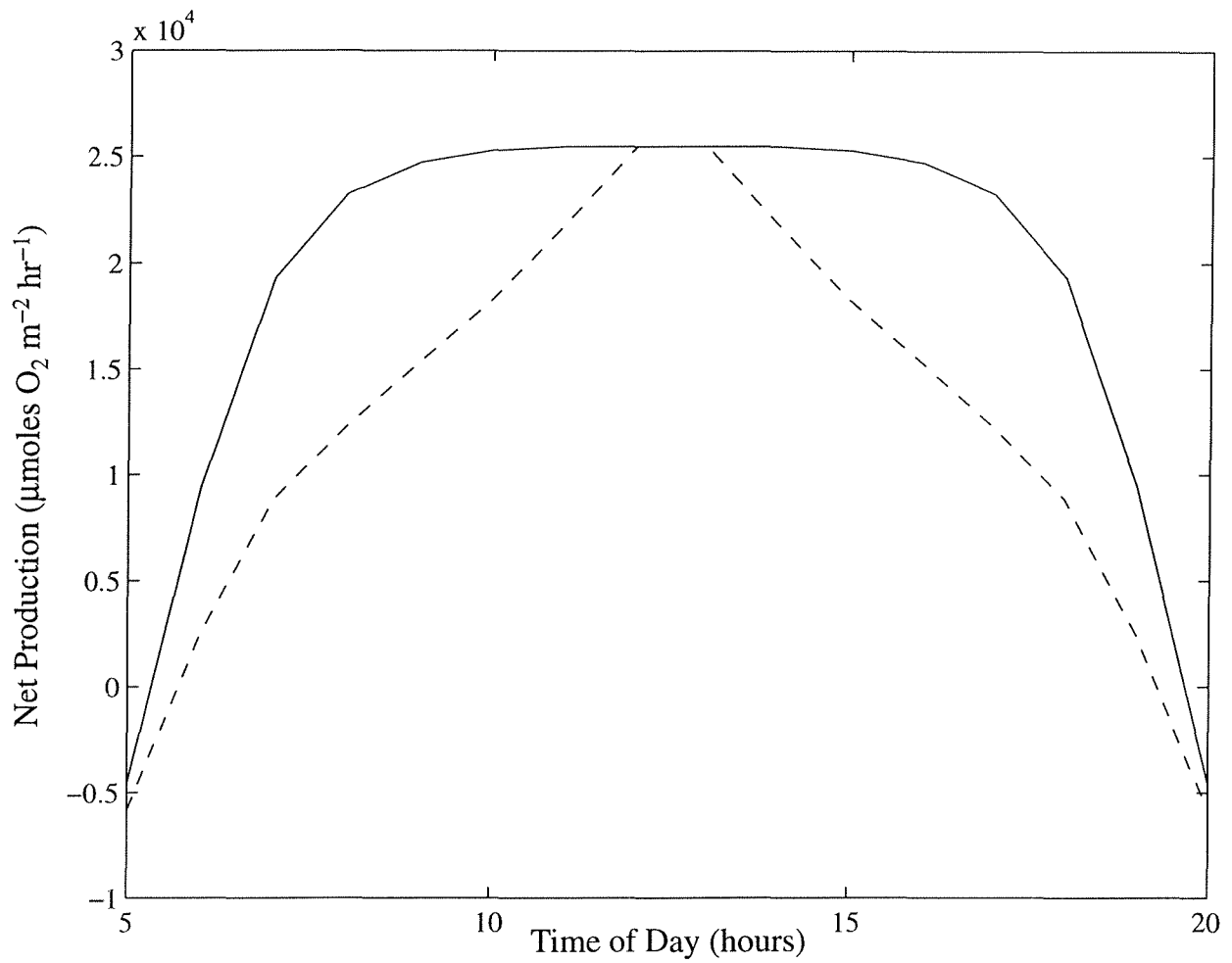


Figure 6. A comparison of hourly production rates for a *Halodule* seagrass bed with a shoot density of 20,000 m⁻². All other parameters have the same values as in Figure 5.

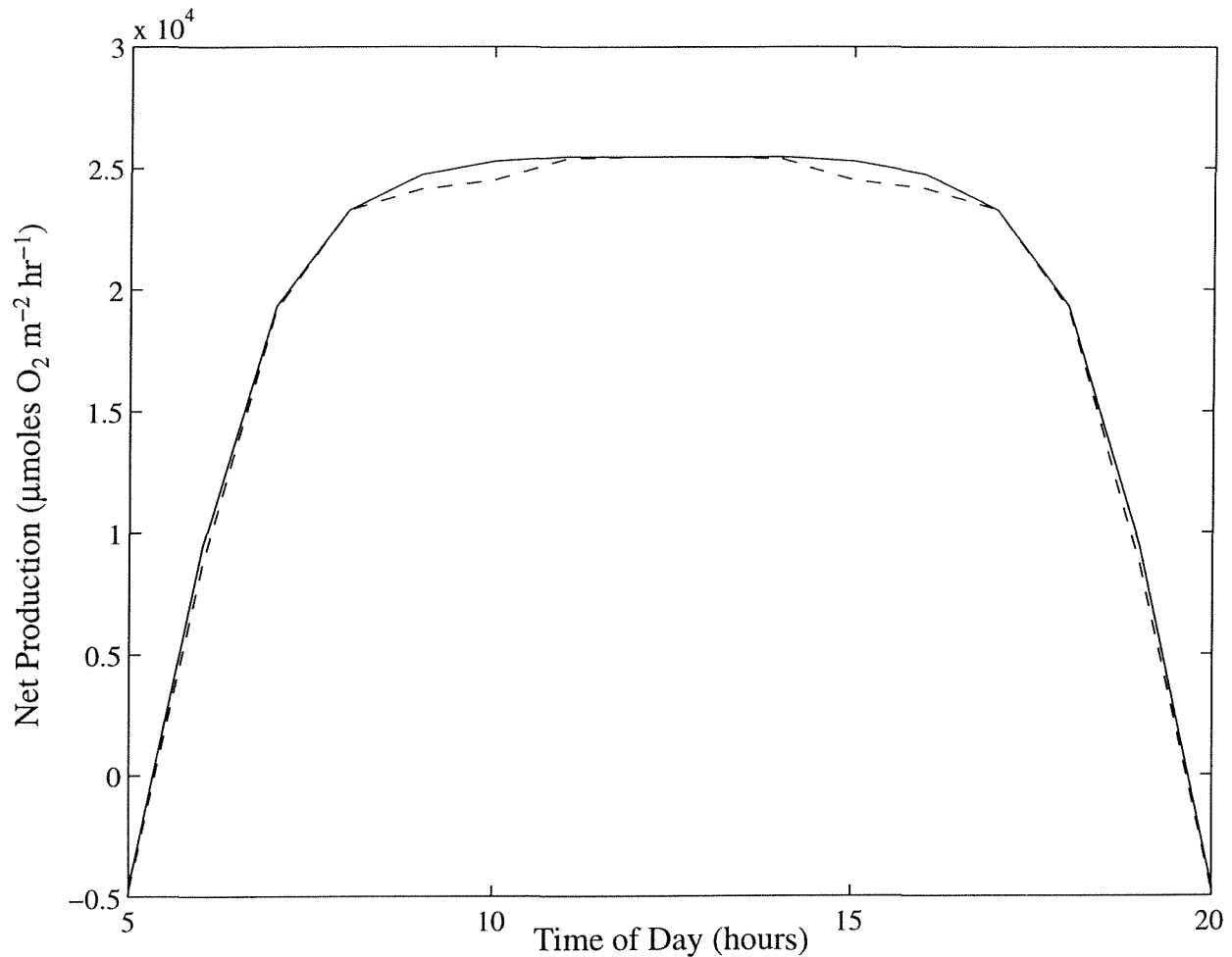


Figure 7. A comparison between hourly production rates in a *Halodule* seagrass bed with and without self-shading. All parameters are the same as in Figures 5 and 6 except that here the seagrass shoot density is only $1,000 \text{ m}^{-2}$.

Self shading is important for determining the plant biomass, especially at high shoot densities. Without taking it into account, the seagrasses can potentially increase their biomass to unrealistically large values. Detailed measurements of the attenuation of light as it propagates through a seagrass canopy have never been made. This makes the construction of a detailed canopy light model largely speculation. However, as the above simulations show, self-shading must be taken into account. So, in order to model the upper biomass limit imposed by the density of the canopy, we used a logistic term for the productivity

$$P = P_{\max} \tanh\left(\frac{I}{I_k}\right) \left(1 - \frac{C_a}{\kappa}\right) \quad (5)$$

where C_a is the above ground biomass and κ is the carrying capacity of the system (i.e., the maximum above ground biomass that the system can support). The logistic term provides a feedback between the canopy biomass (C_a) (and hence the shoot density) and the production of the plant.

Temperature Effects

It is well known that rates of physiological processes depend on ambient temperature. For example, one expects respiration rates to increase with temperature. Often the parameters describing these processes also depend upon other factors, and isolating the influence of temperature alone from the available data is difficult. Both *in situ* and laboratory measurements have been made of the temperature dependence of gross production and respiration for *Thalassia testudinum* (Herzka and Dunton, 1997), *Halodule wrightii* (Dunton and Tomasko, 1994; Dunton, 1996) and *Syringodium filiforme* (Major, 1998). Comparison between laboratory and *in situ* measurements for *Thalassia* showed that *in situ* measurements and whole-plant production measurements were more realistic than laboratory measurements (Herzka and Dunton, 1997). Unfortunately, *in situ* production measurements display the greatest intrinsic variability making the isolation of any temperature effect extremely problematic. For example, production vs. irradiance measurements for *Halodule* in Upper Laguna Madre show the production in January 1990 (at 20 °C) to be more than twice that measured during July 1989 or July 1990 (at 30 °C). One's expectation would be for the January measurements to be lower than the July ones.

Temperature effects on physiological processes such as respiration are traditionally modeled using an Arrhenius type formulation (e.g., Thornley and Johnson, 1990). Here the effect of temperature is modeled using an exponential function, $R = R_0 e^{k(T-T_0)}$ where R is the physiological parameter of concern, T_0 is the temperature, R_0 is the value of the parameter at the temperature T_0 and k is a parameter. The value of k chosen in this study is that which corresponds to a Q_{10}

value of 2 (where Q_{10} is an indication of the dependence of the rate in question on temperature and can be interpreted as the increase in the rate for a 10° change in temperature).

Model Equations

The equations determining the evolution of the above ground (C_a) and below ground (C_b) biomass are:

$$\frac{dC_a}{dt} = (1 - \tau) P(I) \exp(k_0 \Delta T) C_a \left(1 - \frac{C_a}{\kappa}\right) - R_a \exp(k_0 \Delta T) C_a - M_a C_a$$

$$\frac{dC_b}{dt} = (\tau - \delta) P(I) \exp(k_0 \Delta T) C_a \left(1 - \frac{C_a}{\kappa}\right) - R_b \exp(k_0 \Delta T) C_b - M_b C_b$$

where $\Delta T = T(t) - 31$ is the temperature difference between the current temperature in the simulation ($T(t)$) and a reference temperature at which the photosynthetic and respiratory parameters were measured (in this case 31°C). The current temperature is given by

$$T(t) = 21 + 9.0 \left(\sin \left(\frac{2\pi t}{365} - \frac{\pi}{2} \right) \right)$$

and was determined by a fit to observed water temperatures in the Laguna Madre (Brown and Kraus, 1997), with t being the day number. The parameter $k_0 = 0.07$ and was chosen to represent a value of $Q_{10} = 2$. The function $P(I)$ is given by either Equation 3 or Equation 4 depending on the species in question. The parameters $R_{a,b}$ and $M_{a,b}$ represent above and below ground plant respiration and mortality respectively. Parameters τ , δ and κ are determined in the model calibration and represent respectively the rate of material transport from above to below ground tissue, the rate of DOC release into the sediments and the carrying capacity.

The *Thalassia* model contained the below ground component only implicitly. For *Thalassia* no below ground equation was used, so that the only parameters that had to be estimated were τ and

κ. The estimates one obtains for τ can be expected to be approximate in this case since below ground processes such as exudation of DOC are not accounted for.

Data Requirements and Availability

A model of any natural phenomenon, be it seagrass growth or water currents in a bay, depends heavily on data. Data are required for the formulation of the model since one needs to know what it is that has to be explained. For many models, mathematical expressions of the mechanisms underlying the processes being modeled are unknown. In these cases, data are required for the parameterization of these processes. Lastly, data are required in order to test the model against reality. The degree to which the model represents reality therefore depends upon the accuracy of the data used to formulate and validate the model. If the data used are an accurate representation of reality, then comparisons between data and model results can be made with some confidence. If accurate data are not available, then identifying those areas in the model which need to be improved becomes harder.

Many processes contribute to the production of seagrass biomass. Mechanisms and models for most of these are as yet undetermined. Therefore, only those processes that have the largest effect on the seagrasses can be taken into account. To set up the model and parameterize it, data on the above and below ground biomass of the plant are required as well as the canopy level light field measured at the same place and over the same period. Once the models have been developed, only initial above and below ground biomasses are required along with time series of irradiance at the surface of the water and attenuation of light in the water column.

Biomass and Irradiance

The longest relevant data set available to us was for *Halodule wrightii*. These data were collected at the site LM151. This was a nine year data set, during which the plants were heavily affected by a brown tide (*aurcoubra lagunensis* (DeYoe *et al.*, 1997)) which was found in the Laguna Madre between 1989 and 1997. Light levels showed a dramatic decrease between 1989 and

1995; peak underwater irradiance reached almost $40 \text{ mols m}^{-2} \text{ d}^{-1}$ during 1989 and about $15 \text{ mols m}^{-2} \text{ d}^{-1}$ during 1995. Underwater light levels increased rapidly in 1996 and 1997 giving peak values of approximately $34 \text{ mols m}^{-2} \text{ d}^{-1}$ in 1997 (Figure 8). Both above and below ground biomass showed a response to these changing light levels, with the more dramatic response being a decrease in the below ground biomass. Possible explanations for this decrease in below ground biomass include: a decrease in transport of carbon from above to below ground such that dying below ground tissue was not replaced sufficiently fast to maintain the below ground biomass; the plant made use of material stored in the rhizome to supplement its carbon production under conditions low light. For *Thalassia* (Lee and Dunton, 1996), the amount of stored soluble carbohydrate available for use by the plant amounts to only about 10% of the rhizome biomass. If this result also applies to *Halodule*, then there would appear to be too little storage material to account for the large changes in below ground biomass. Between 1989 and 1992, biomass samples were taken approximately every two months. After 1992, the sampling rate dropped to four (or less) samplings in a year. (Figure 9)

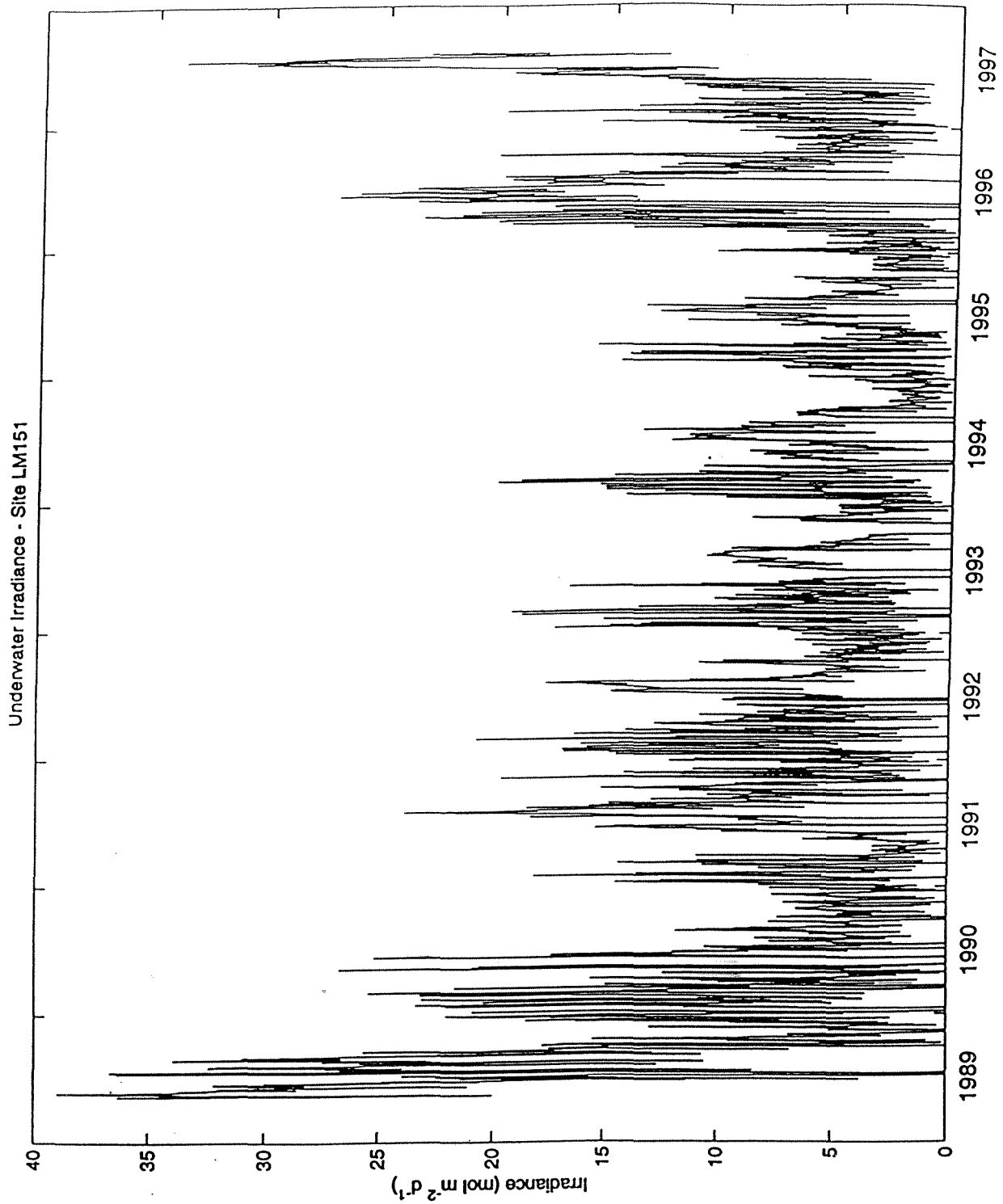


Figure 8. Underwater irradiance at the level of the seagrass canopy for site LM-151 (*Halodule wrightii*). The light levels show the effect of the brown tide that affected Upper Laguna Madre between 1989 and 1997; light levels begin to return to normal in 1996 with a continuing recovery to almost pre-brown tide levels in early 1997.

brown tide. Unlike the *Halodule* data set, the *Thalassia* data set contained no information on the behavior of the plants during periods of light limitation.

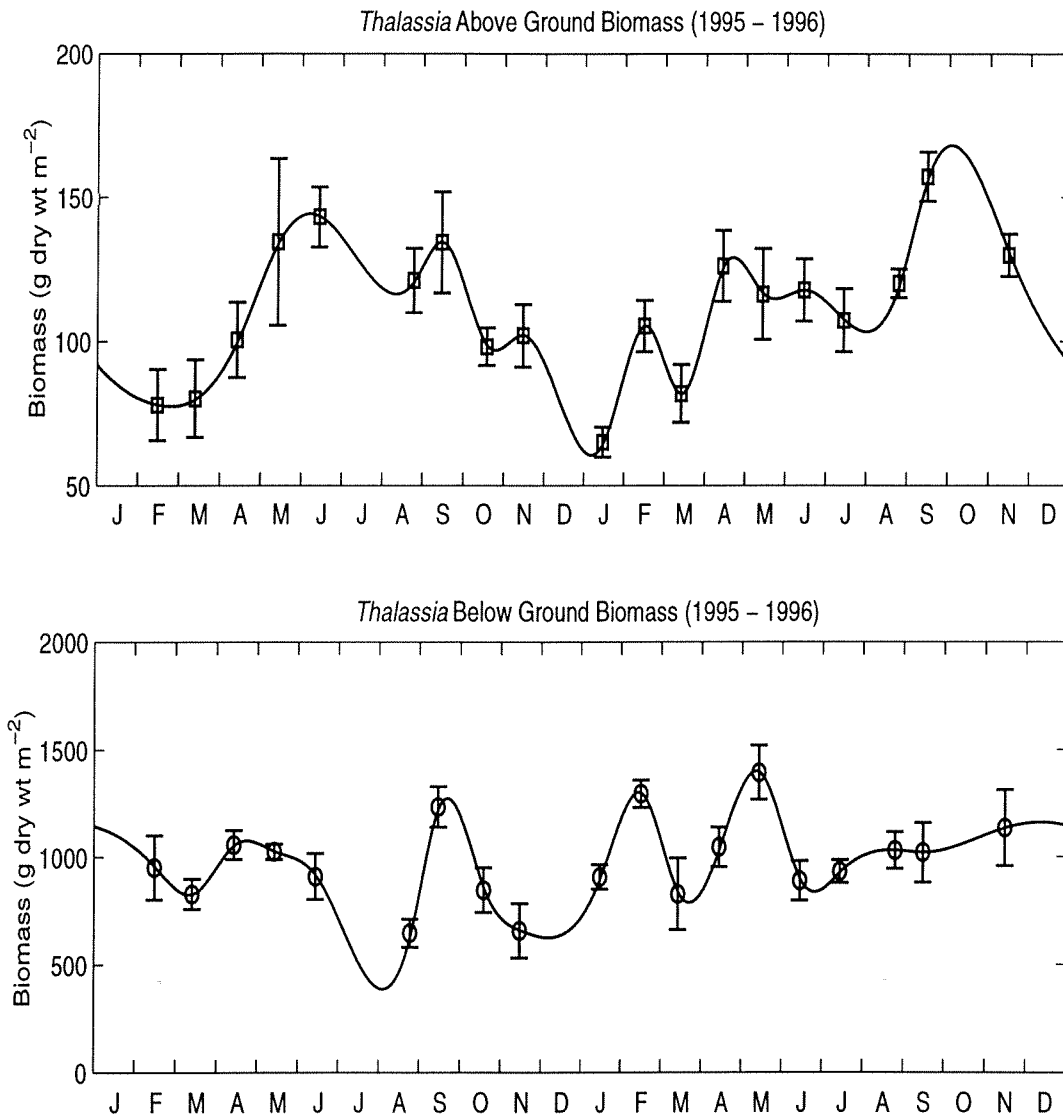


Figure 10. Above and below ground biomass for *Thalassia testudinum* collected over a two year period (1995-1996) in Lower Laguna Madre (Kaldy, 1997). The continuous curve is a spline curve fitted to the data as a visualization aid. Both above and below ground biomass compartments show non-seasonal fluctuations, with the magnitude of changes in the below ground compartment at times being more than 500 gdw m⁻² over a month (i.e., the below ground biomass almost doubling in 30 days – e.g. August and September 1995).

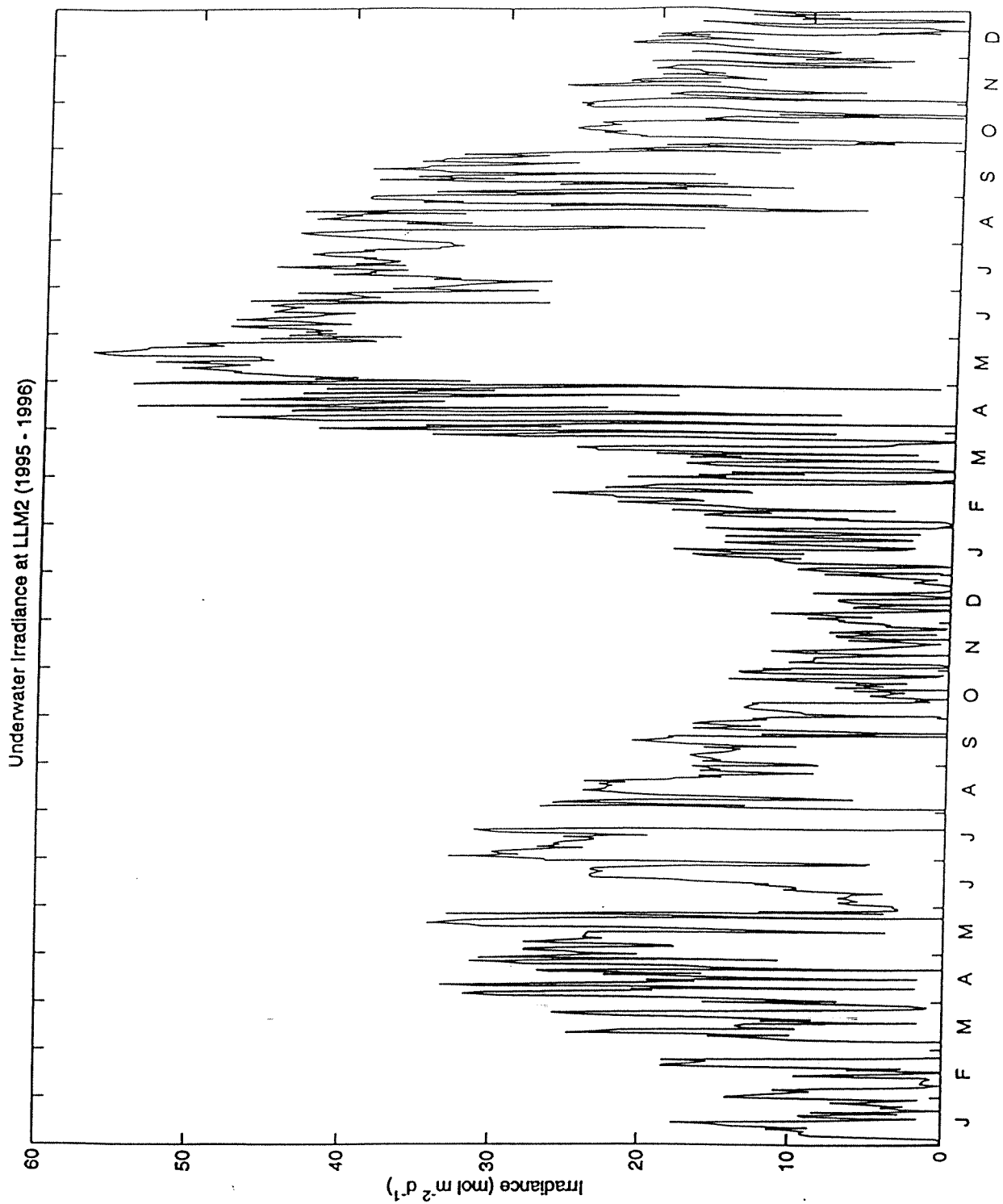


Figure 11. Underwater irradiance at the canopy level in a *Thalassia testudinum* seagrass bed in Lower Laguna Madre collected during 1995-1996 (Kaldy, 1997). Not only is the seasonal signal in the irradiance apparent, but also the difference between the two years is striking. In comparison with the light levels recorded at the *Halodule* site, there was no brown tide affecting the area.

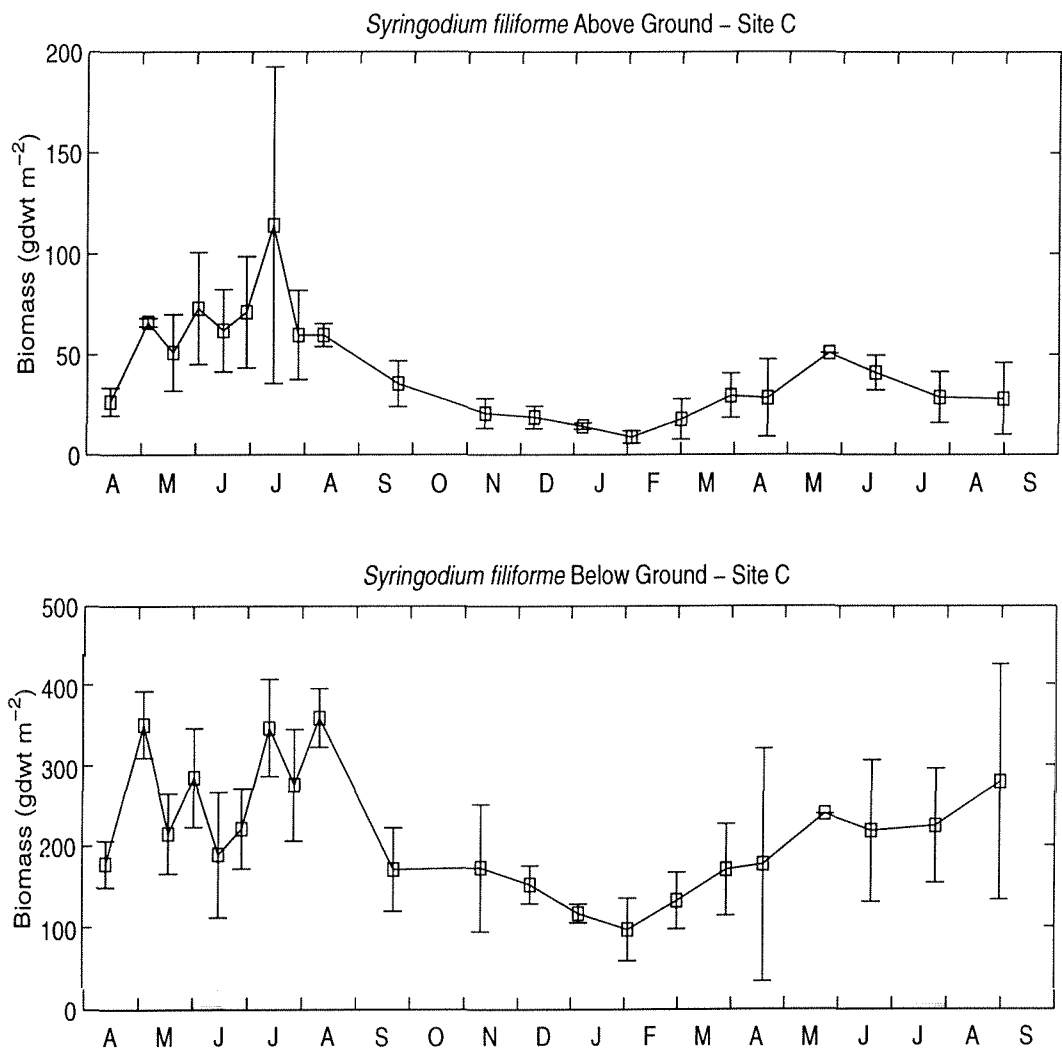


Figure 12. Above and below ground biomass for *Syringodium filiforme* collected in Lower Laguna Madre from April 1996 through August 1997 (Krull, 1998). The curve fitted to the data is a simple spline to assist in visualization. The below ground biomass exhibits strong fluctuations during the period April to August 1996 (c.f. measurements of *Thalassia* below ground biomass), after which both the above and below ground biomass change smoothly. The fluctuations in the below ground measurements are not repeated during the same period in 1997.

The *Syringodium* model was developed using data obtained by C. Krull (University of Texas, Pan American) from site C in Lower Laguna Madre (Krull, personal communication, unpublished data). This consists of a 16 month time series of above and below ground biomass - the below ground biomass was not divided into root and rhizome tissue. The light data were the same as for *Thalassia*.

All three biomass data sets exhibit fluctuations. For the above ground *Halodule* biomass these are primarily seasonal fluctuations; fluctuations in the above ground biomass follow fluctuations in the light field. For example, during the summer of 1991, the underwater irradiance drops from about 15 to below 5 $\text{mols m}^{-2} \text{d}^{-1}$ and the results of this can be seen in both the above and below ground biomass records. A similar correspondance can be seen in the *Thalassia* data, though the larger irradiances recorded in 1996 do not appear in the biomass records. This is probably due to the fact that at these light levels the plants are healthy and light saturated (implying that an increase in light level does not translate to an increase in production and hence biomass). This indicates that light is the controlling factor in determining seagrass production and hence biomass. This agrees with the conclusions of other researchers (e.g., Dennison and Alberte, 1985).

The *Syringodium* biomass data also exhibited large fluctuations, but only in the first half of the time series. As in the case of *Thalassia* the changes in biomass associated with some of these fluctuations were greater than the gross production of the plant. Curiously, the fluctuations in above and below ground *Syringodium* biomass occur only between April and August of 1996. After that, the biomass follows a smooth curve, even during the same period in the following year.

The hourly light data did not form a complete record, but contained gaps – mostly of an hour or two, but occasionally lasting for more than a day. These gaps were filled using irradiance measurements taken from the record directly preceding the gap.

The high sampling frequency of the *Thalassia* biomass reveals strong fluctuations particularly in the below ground component. The below ground biomass can fluctuate by as much as 40% within a month (c.f. the period between January and May 1996); in fact, these below ground

fluctuations are greater than can be supported by the gross primary production of the plant. Various attempts were made to smooth the data using a variety of numerical filters, but none produced results that could be successfully modeled. These rapid biomass fluctuations do not appear to be reflected in the availability of light but rather arise from the inherent inhomogeneity of the biomass distribution. This inherent heterogeneity prevents modeling the *Thalassia* below ground biomass.

The standard method employed, by all seagrass researchers, to determine plant biomass is to take a number of cores from a region and measure above and below ground biomass in all the cores. This strategy rests on the hope that the number and size of cores being taken leads to a representative estimate of plant biomass in the seagrass bed. Each seagrass bed exhibits some degree of natural heterogeneity which can lead to sampling problems. Heterogeneity in the below ground architecture of *Thalassia* results from the presence of large rhizomes with a smaller root system. The below ground biomass of these plants is dominated by the rhizome (Lee and Dunton, 1996; Kaldy, 1997) and yet this tissue is not uniformly distributed horizontally throughout the sediments.

The inherent heterogeneity of a seagrass bed also hinders the accurate measurement of biomass. Most of the biomass data used in developing the Laguna Madre Seagrass Model were collected using between two and four cores for each measurement. A series of 10 cores collected at the same *Thalassia* site reveals the problem of heterogeneity (Kaldy and Burd, 1998). Figure 13 shows the cumulative average total plant biomass for the sequence of 10 cores. As the number of cores contributing to the calculated average biomass in the seagrass bed increases, the plant biomass asymptotes to a constant value. This would indicate that at least 10 cores are required to accurately determine the average biomass within a *Thalassia* bed. The standard deviations of the average measured values increase rapidly from 1 to 4 cores, and remains constant between 5 to 10 cores. This indicates that there is some inherent heterogeneity in the seagrass bed, though after 5 cores, the individual cores can be regarded as being statistically independent. The range of the standard deviations however covers a two-fold range. These large standard deviations imply that any measurement of *Thalassia* biomass is only accurate to plus or minus 50%. For example, a *Thalassia* biomass measurement of 800 gdw m⁻² may correspond to a biomass lying between

approximately 550 and 1050 gdw m^{-2} . Both the plant heterogeneity and sampling inadequacies are also manifested in the shoot density fluctuations.

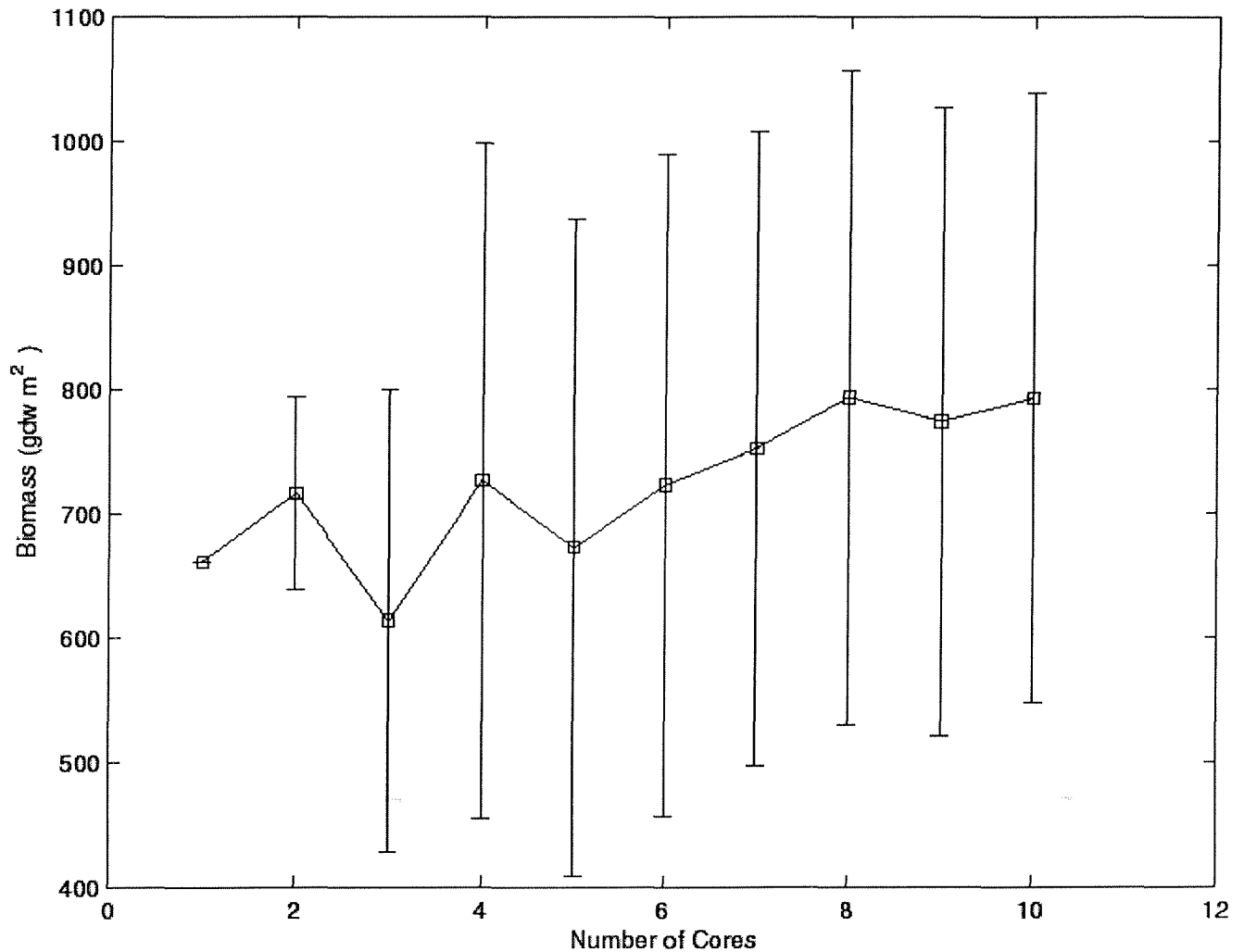


Figure 13. Biomass calculated from a sequence of 10 cores taken at the same site of a *Thalassia* bed. The estimate of biomass for each core number is calculated as the accumulative average of all preceding cores including that one. The average values (indicated by squares) appear to asymptote to a value of approximately 800 gdw m^{-2} . However, the standard deviations of the accumulated sum do not decrease as the number of cores increases. This indicates the presence of an inherent inhomogeneity in the seagrass bed which the coring device is too small to average over (Kaldy and Burd, 1998).

Figure 13 shows that to accurately sample the seagrass biomass requires at least 10 cores for each measurement. Sampling of this magnitude would probably severely impact (perhaps even destroy) the seagrass bed being studied.

Physiological Parameters

Plant production of carbon depends on the irradiance at the depth of the plant canopy and on the response of the plant to the irradiance. The latter is determined experimentally by producing a relationship between gross production (P) and irradiance (I). This is done by fitting the data to an appropriate functional form to determine the maximum production (P_{\max}) and the saturation irradiance (I_k). These parameters were determined for each species and their values are given in Table 1.

Plant respiration rates are required if net production is to be calculated. Respiration rates for *Thalassia*, *Halodule* and *Syringodium* for both above and below ground material are also given in Table 1.

The model determines the change in biomass by calculating the residual between carbon production from photosynthesis and a variety of loss mechanisms. These losses include respiration, mortality, and exudation of DOC into the sediments by below ground tissues. Values for the specific respiration of the plants were obtained from the literature and from experiments performed as part of this project. Mortality rates represented a loss of carbon to the seagrasses through, for example, loss of leaves and death of root/rhizome tissue. This has never been measured though some estimates can be made from field observations. Estimations of above and below ground mortality are given in Table 1.

	<i>Halodule</i>	<i>Thalassia</i>	<i>Syringodium</i>
P_{\max} ($\mu\text{mol O}_2 \text{gdw}^{-1} \text{h}^{-1}$)	422	195	308
I_k ($\mu\text{mol m}^{-2} \text{s}^{-1}$)	319	281	149
R_a ($\mu\text{mol O}_2 \text{gdw}^{-1} \text{h}^{-1}$)	41.5	35	33
R_b ($\mu\text{mol O}_2 \text{gdw}^{-1} \text{h}^{-1}$)	16.1	NA	9
M_a (d^{-1})	0.004	0.0052	0.004
M_b (d^{-1})	0.0004	NA	0.0004

Table 1. Photosynthetic, respiratory and mortality rates used in the seagrass models. Photosynthetic and respiratory parameter values for *Halodule* were taken from Dunton and Tomasko (1994) and Dunton (1996), *Thalassia* values from Herzka and Dunton (1997) and *Syringodium* values from Major (1998). In all cases mortality values were estimates (Dunton, private communication; Kaldy private communication). R_{ab} and R_{be} are the above and below ground respiratory rates, M_{ab} and M_{be} the above and below ground mortality rates.

Seagrasses absorb nutrients primarily through their root system (e.g., Zimmerman *et al.*, 1987). Seagrass nutrient uptake depends on several factors including the root biomass, the substrate nutrient concentration, the nutrient requirements of the plant and the kinetics of the uptake process; the latter is required to calculate the rate at which the plant takes nutrients from the sediments. Only minimal information concerning the nutrient uptake rates of the seagrasses being studied was available. In addition, the lack of information about root biomass for *Halodule* and *Syringodium* meant that no nutrient uptake component could be incorporated into the model.

The below ground biomass of seagrasses consists of root material and rhizome material. The rhizome material is used chiefly for storage and anchoring the plant; the root material, and in

particular the root hairs, are primarily associated with nutrient uptake (Barnabas and Arnott, 1987; Roberts, 1993).

In order to parameterize the model, a constrained optimization routine was used to perform a least squares minimization between the data and the results from the model. This procedure was carried out using Matlab™ and the Mathworks Optimization Toolbox. Different tolerances and optimization parameters were used in multiple trials in order to obtain the best agreement between data and model results.

The Halodule Model

The *Halodule* model was based upon a 9 year time series (Dunton 1996; Dunton unpublished data) of above and below ground biomass collected at site LM151 (Figure 9). The time series extended from 1989 through mid 1997 during which time the effects of a brown tide are evident. Light data were also collected at the site over the same period of time (Figure 8). The brown tide affects the light and biomass data from 1990/1991 up until early 1997; this has both advantages and disadvantages. The advantages are that there exists a data set of biomass (both above and below ground) and irradiance collected during a protracted period of light stress. The disadvantages are that only one year or so of data were collected under normal conditions, and there are no data on the change in physiological parameters associated with the light stress.

The *Halodule* model was parameterized in the manner described above with the 1989/1990 part of the data set. These data were relatively unaffected by the brown tide and can be assumed to represent the plant under normal conditions. After model parameters were determined, the model was run in a predictive mode using the first biomass measurements as initial conditions and being forced with the 9 year light time series. The output from this model was then compared with the above and below ground biomass that was measured. The results of this experiment are shown in Figure 14.

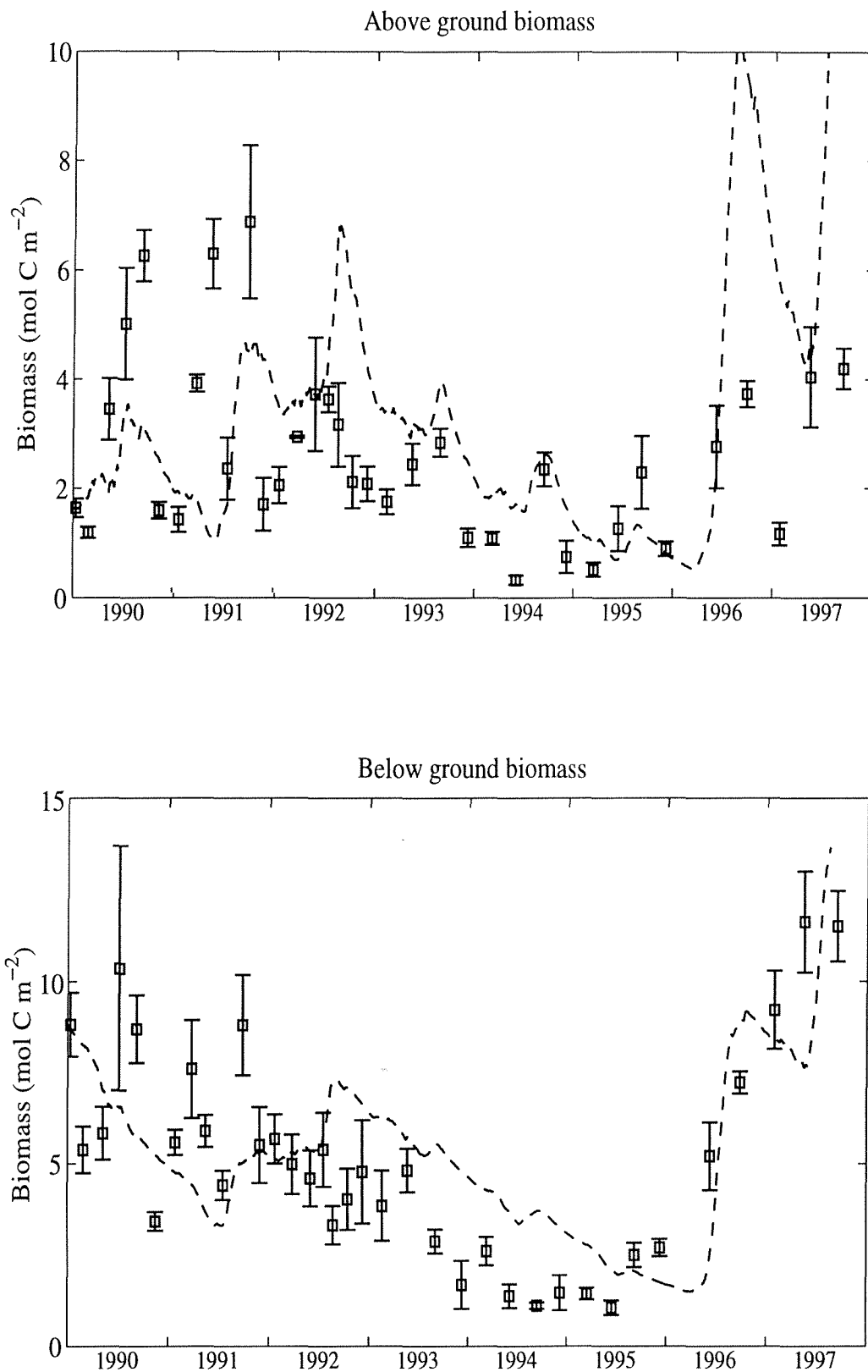


Figure 14. Comparison of 8 years of the *Halodule wrightii* data set with the model. The model was calibrated using data from 1989 and was then forced with the irradiance data for 1990-1997. The model captures the decline in biomass resulting from the brown tide. The model also reproduces the recovery of the below ground biomass at the end of the brown tide between 1996 and 1997. The symbols correspond to data points and the dashed line to the model results.

The model tracks trends in the observed data quite well. In particular, the effects of the brown tide are apparent in both above and below ground biomass numbers produced by the model. What is more encouraging is that the model also tracks the rapid recovery of both the above and below ground biomass at the end of the brown tide in 1996/1997. The seasonal signal in above ground biomass is present, and its effects can be seen in the below ground biomass as well. Whilst the model tracks the below ground biomass reasonably faithfully, the model under-predicts the above ground biomass during 1990/1991 and over-predicts the above ground biomass in 1997.

The *Thalassia* Model

The *Thalassia* model was parameterized using a two year data set collected by J. Kaldy (Kaldy, 1997) during 1995-1996. This data set was collected at the LLM2 site and was unaffected by light limitation. In fact, the plants were light saturated for the two year period. This is good news for parameterization purposes but does not provide a good validation of the model. The model was parameterized using the first year of the data (Figure 15) and then validated against the second year of the data (Figure 16). The *Thalassia* model only considers the above ground biomass explicitly for the reasons given above, otherwise the model is similar to the *Halodule* model. The model agrees well with 1996 data, showing the approximate doubling in above ground biomass between January and February (Figure 16).

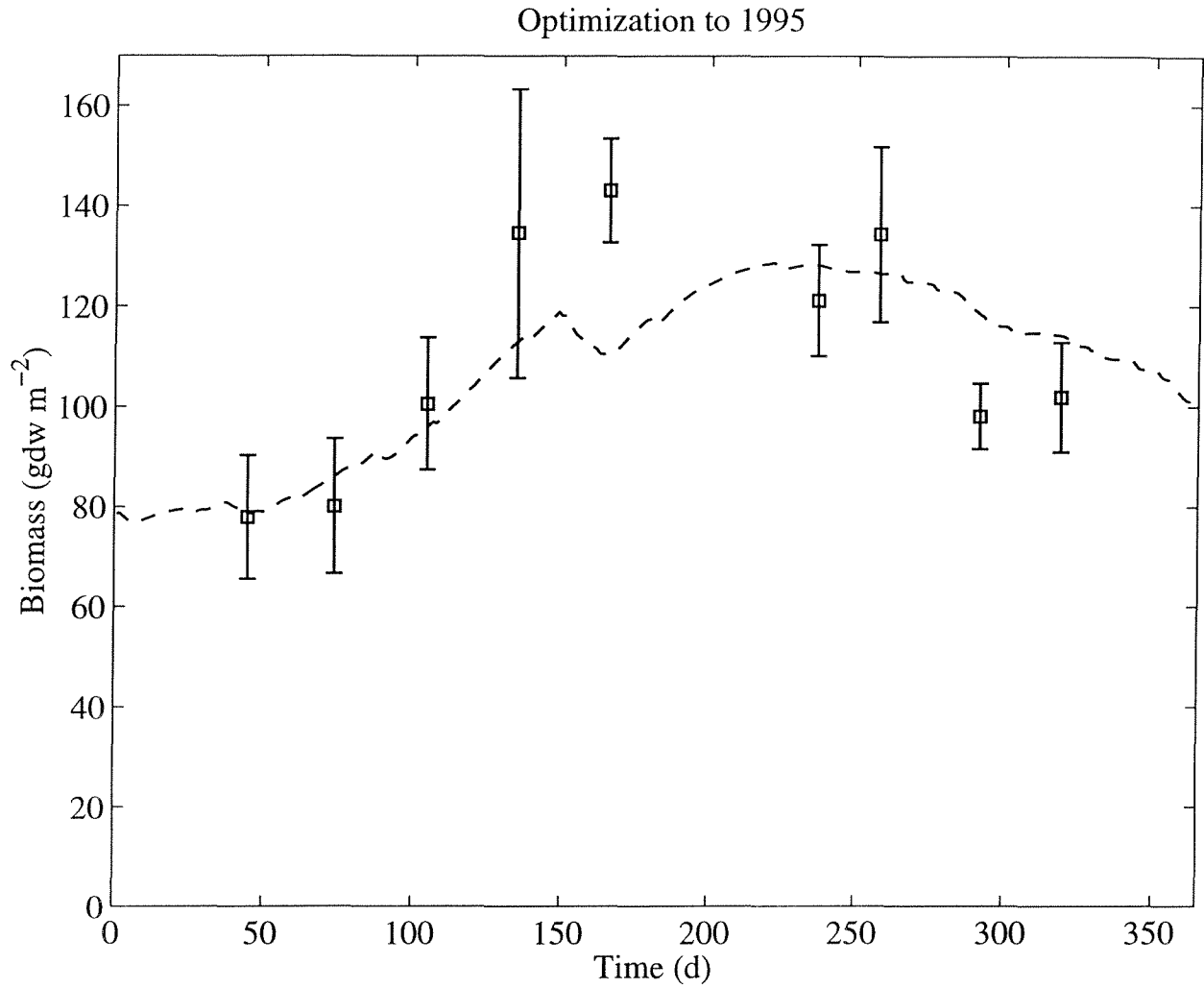


Figure 15. Parameterization of the *Thalassia* model against the 1995 data set. Only the above ground biomass is used in the *Thalassia* model. The model shows a clear seasonal signal. Symbols represent observations and the dashed line the model results.

Model Comparison for 1996

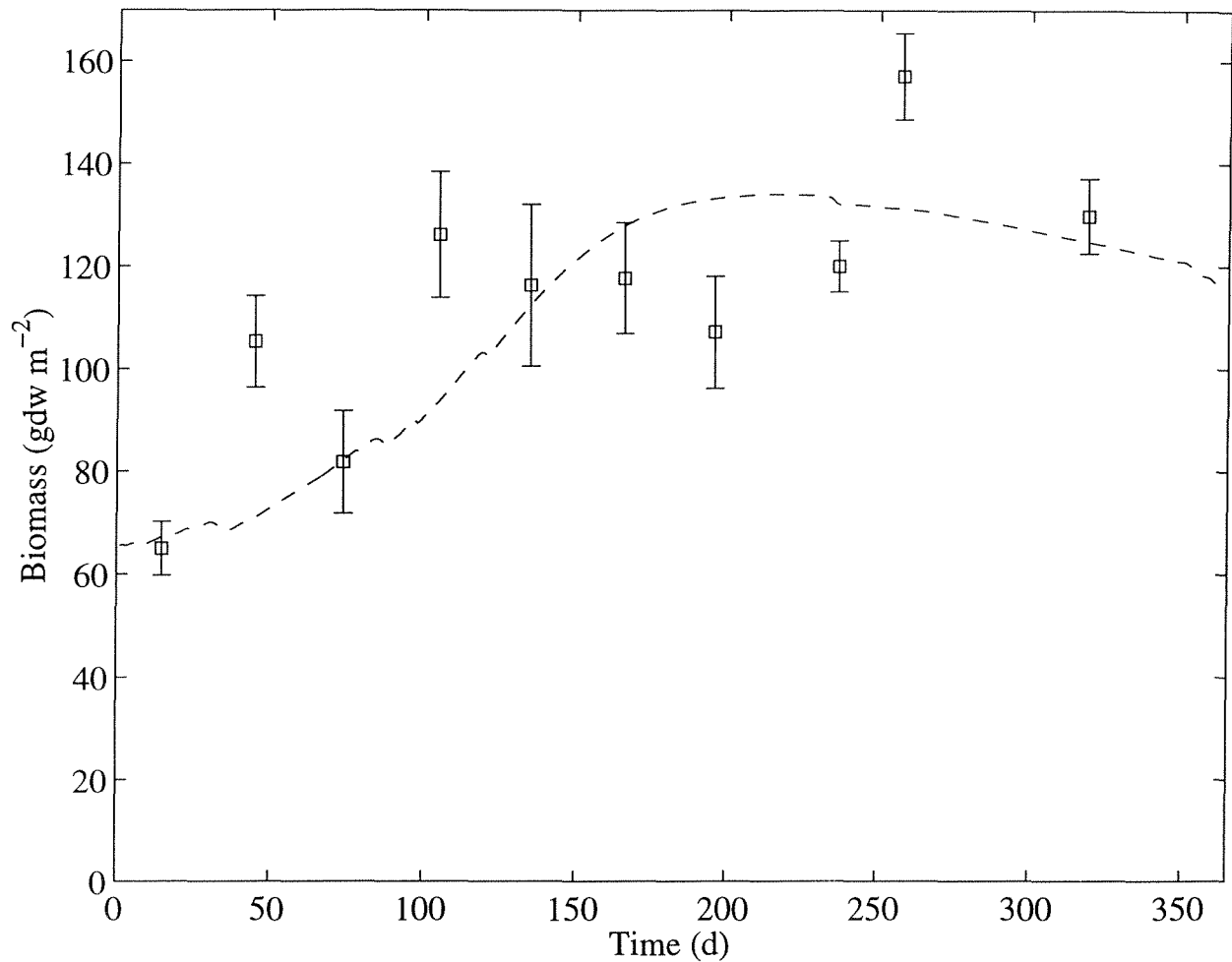


Figure 16. Verification of *Thalassia* model against the 1996 data set using the calibration showed in Figure 11. Symbols represent the observed biomass and the dashed line the model results.

The Syringodium Model

The *Syringodium* model was identical in structure to that used for *Halodule*. Unfortunately, less than 18 months worth of data were available. For this model, parameterizations attempted without smoothing the data led to failure of the optimization procedure. In order to successfully parameterize the model, the biomass data were smoothed using a 3 point convolution. The best fit to the observations is shown in Figure 17.

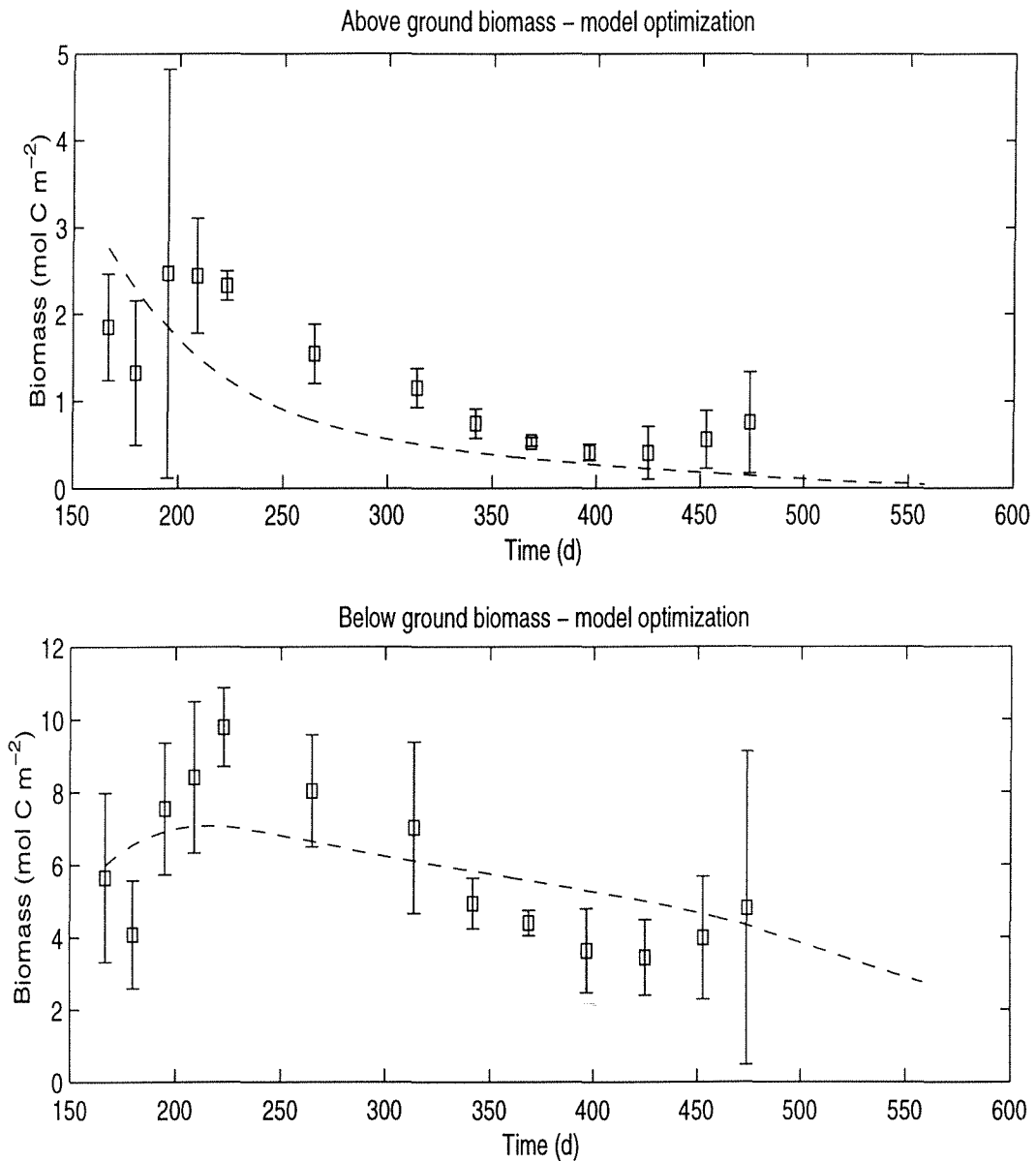


Figure 17. Calibration of the *Syringodium filiforme* model using part of the *Syringodium* data set. The model does not capture the seasonal cycle in the data and has the above ground biomass asymptoting to zero. The model for the below ground biomass shows a steady decline after a maximum in summer of the first year. Symbols represent the observations and the dashed line the model results.

The resulting parameterized model does not perform well in following the observed biomasses. The seasonal signal in both the above and below ground biomasses is absent, and the model shows the above ground biomass asymptoting to zero, whereas the observations show above and below ground biomass increasing in the first part of the second year. The below ground biomass observations show a clear seasonal signal, with high biomass in the summer and lower biomass in the winter. This is only hinted at the in the model results.

A summary of the parameter values found for the calibration of each species is given in Table 2.

	<i>Halodule</i>	<i>Thalassia</i>	<i>Syringodium</i>
κ	20.0	5.49	27.76
τ	0.34	0.125	0.89
δ	0.001	NA	0.11

Table 2. Model parameter values obtained in the calibration of the model with data for each of the species. The units of τ and δ are d^{-1} and the units for κ are $mol\ C\ m^{-2}$.

The *Halodule* model produced a minute small amount of DOC exudation which must be compared with the relatively large (~10% of gross primary production) that the *Syringodium* model produced. The carrying capacities of both *Halodule* and *Syringodium* were significantly larger than that for *Thalassia*. The above ground biomass of *Halodule* and *Thalassia* are similar, yet *Thalassia* has to support a larger below ground biomass and this may account for the smaller carrying capacity. The transport coefficients for *Halodule* and *Thalassia* are both reasonable (c.f. Wetzel and Penhale, 1979; Moriarty *et al.*, 1986), but that for *Syringodium* appears to be unrealistically large.

The Production Model

Without detailed sediment transport and aquatic radiative transport models, the effects of dredging upon the irradiance experienced by the plants is hard to determine. In order to examine the effects of dredging on the health of seagrass beds, the models derived above for the three seagrass species were run with varying values and duration of the attenuation coefficient.

The observed attenuation coefficient (k) in the Laguna Madre varies seasonally and geographically. In Upper Laguna Madre (site LM-151) over a period from 1989 to 1993, an average value of $k \sim 1 \text{ m}^{-1}$ was measured with values occasionally getting as high as 2 m^{-1} for short periods of time (Dunton, 1994). In Lower Laguna Madre (site LLM-1) between April 1996 and February 1997 the attenuation coefficient was highly variable on a daily basis. Values between June and November 1996 averaged about 2 m^{-1} with daily excursions as high as 4 and 5 m^{-1} (Dunton, 1997). Elsewhere in Lower Laguna Madre (LLM-2), the attenuation coefficient was almost constant at an average value of approximately 0.5 m^{-1} , with rare daily excursions to values as high as 5 m^{-1} (Dunton, 1997). During 1994/1995, attenuation coefficients during dredging activities fluctuated between $k=2 \text{ m}^{-1}$ and 7 m^{-1} with the higher values continuing through the summer (Brown and Kraus, 1997).

For the simulations shown here a representative baseline attenuation coefficient of $k = 1 \text{ m}^{-1}$ was chosen; attenuation coefficients of 2, 4, 7 and 9 m^{-1} were superimposed on this. These values were taken as covering a representative range determined from Dunton (1994, 1997) and Brown and Kraus (1997). These larger attenuation coefficients were imposed for times of 7, 14, 28 and 100 days. The increased attenuation coefficients started in late spring on day 150.

For each of these conditions, the model was run for a period of a year and the biomass distribution determined. The health of the seagrass bed was determined qualitatively by observing whether the seagrass biomass at the end of the year was greater, the same as, or less than the biomass at the beginning of the year. These exploratory production runs were made only for *Thalassia* and *Halodule* since the model parameterization for *Syringodium* was not to the same standard. *Syringodium* is similar to *Halodule* in many respects and so one might expect behavior similar to that obtained from the *Halodule* model (Dunton, personal communication).

Results

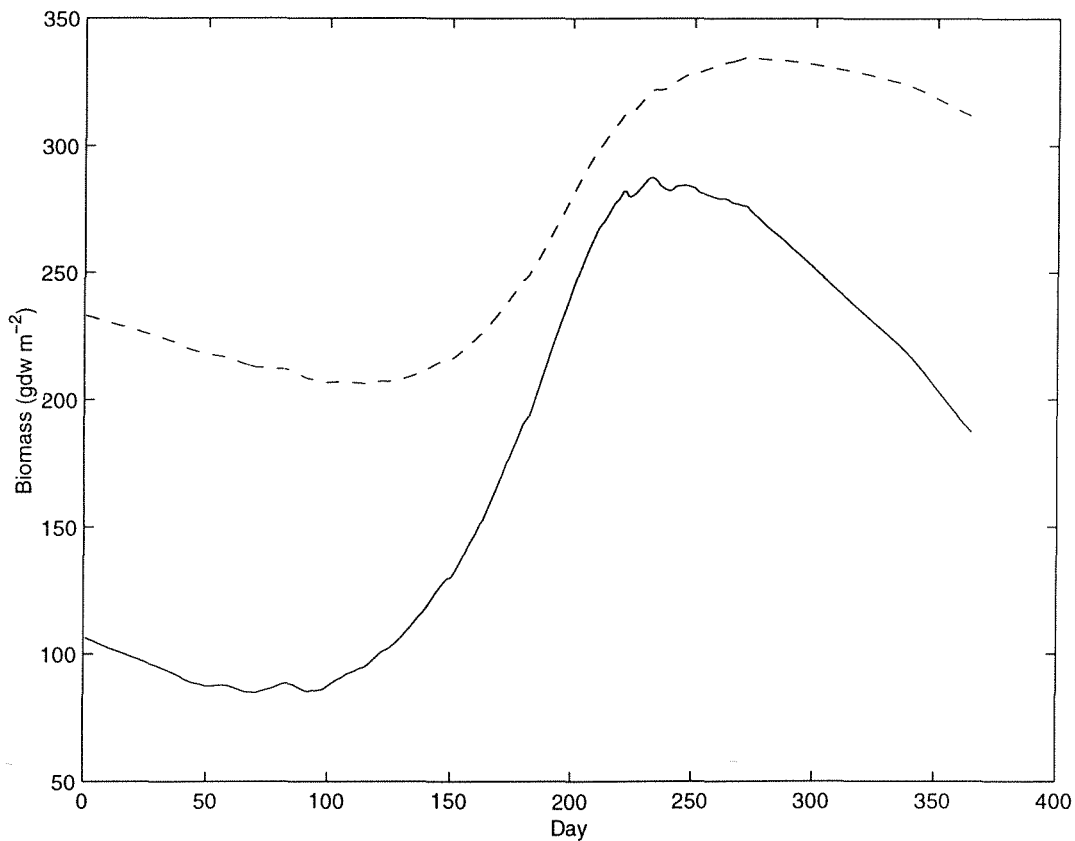


Figure 18. The baseline *Halodule wrightii* production model. This model uses the calibrations determined in the previous section and is forced with the surface irradiance assembled from surface observations and shown in Figure 2. In this, and the subsequent four sets of graphs, the dashed line represents the below ground biomass component and the solid line the above ground biomass. The water column attenuation in this baseline run is set to $k = 1 \text{ m}^{-1}$ throughout the whole simulation; i.e., there is no increase in water column attenuation due to dredging activities.

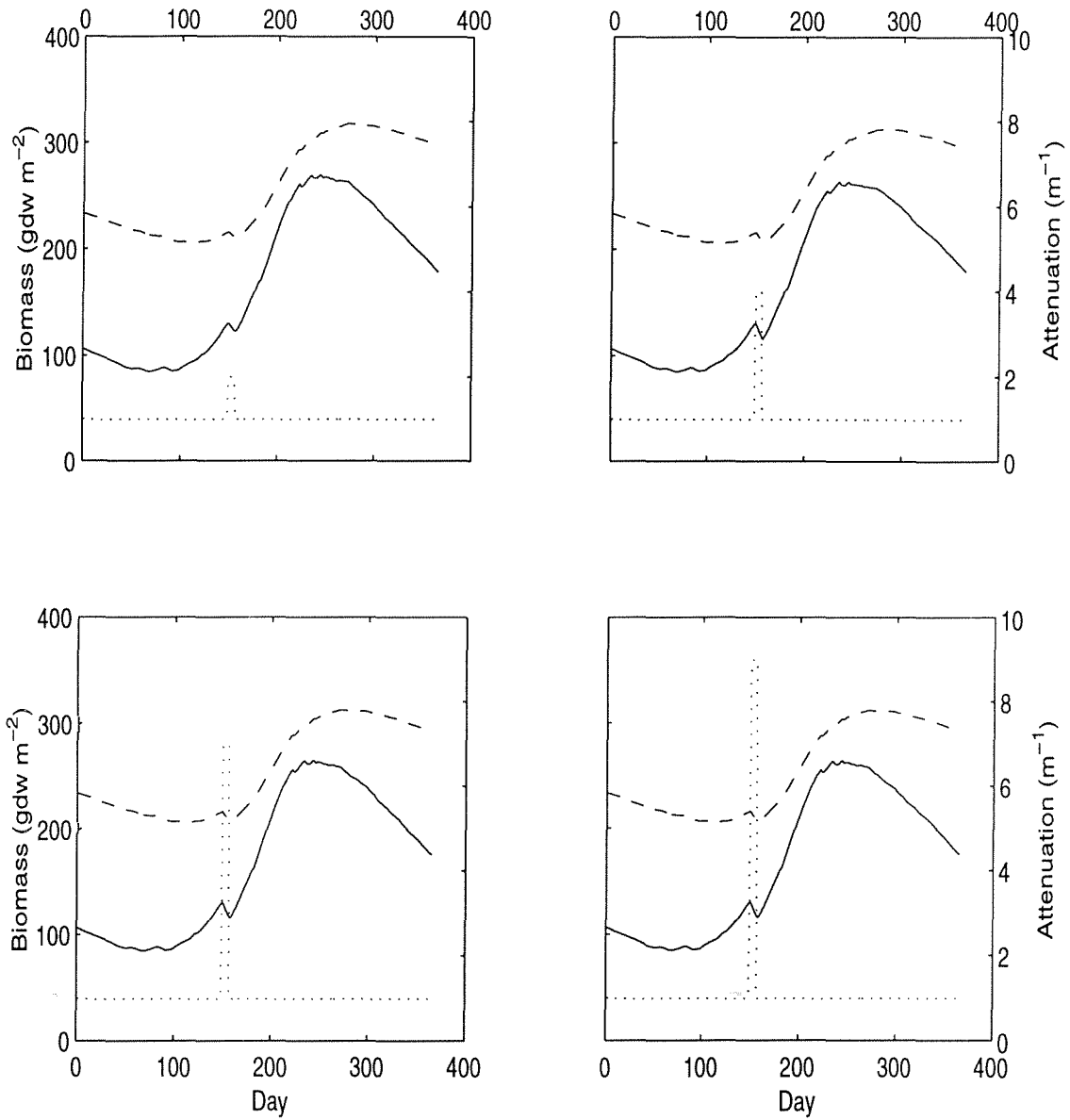


Figure 19. Production model run for *Halodule wrightii* with one week of enhanced water column attenuation of various levels. In each panel the dashed line represents below ground biomass, the solid line above ground biomass and the dotted line the attenuation coefficient.

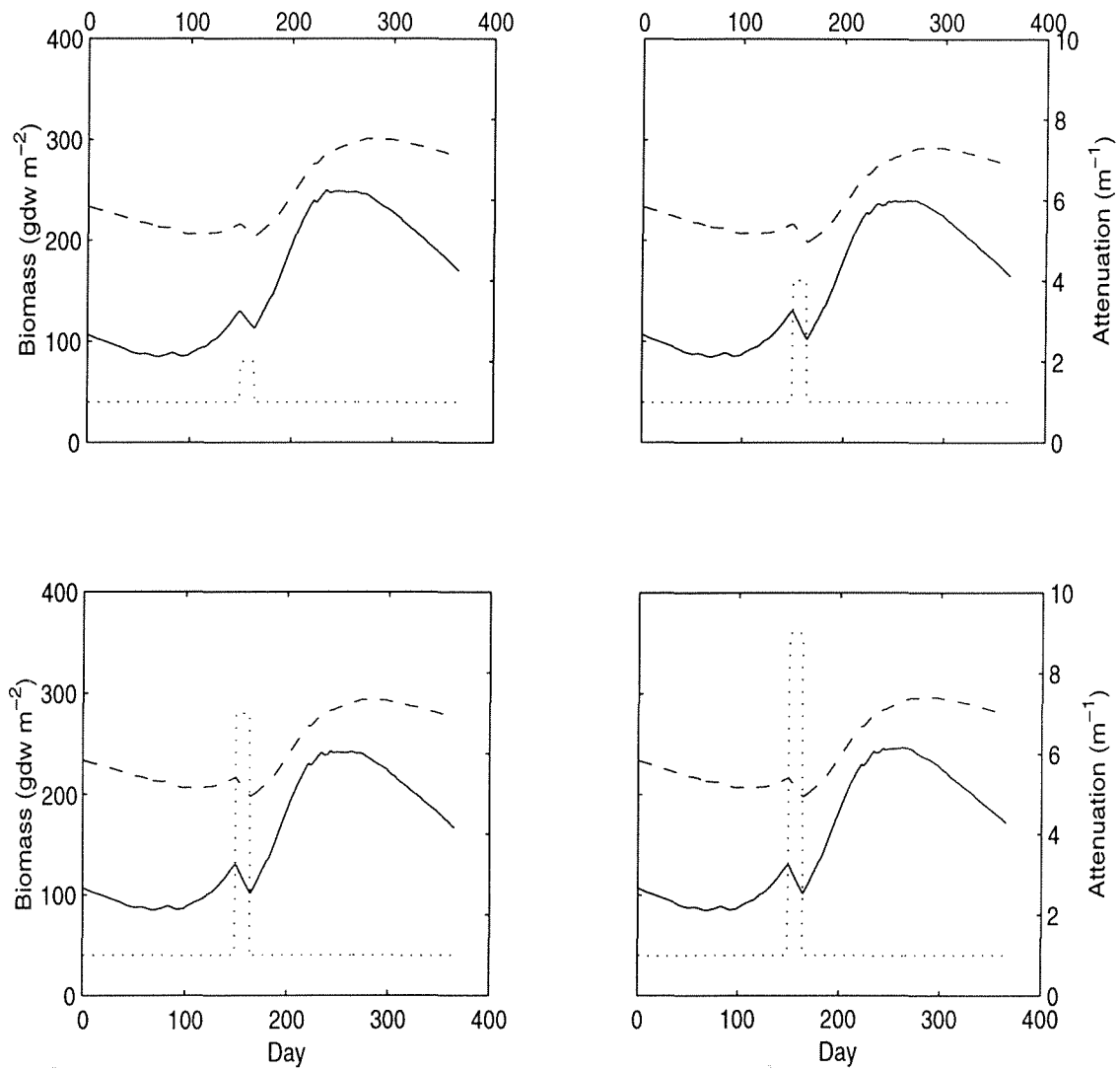


Figure 20. Production model run for *Halodule* with two weeks of enhanced water column attenuation of various levels. In each panel the dashed line represents the below ground biomass, the solid line the above ground biomass and the dotted line the water column attenuation coefficient.

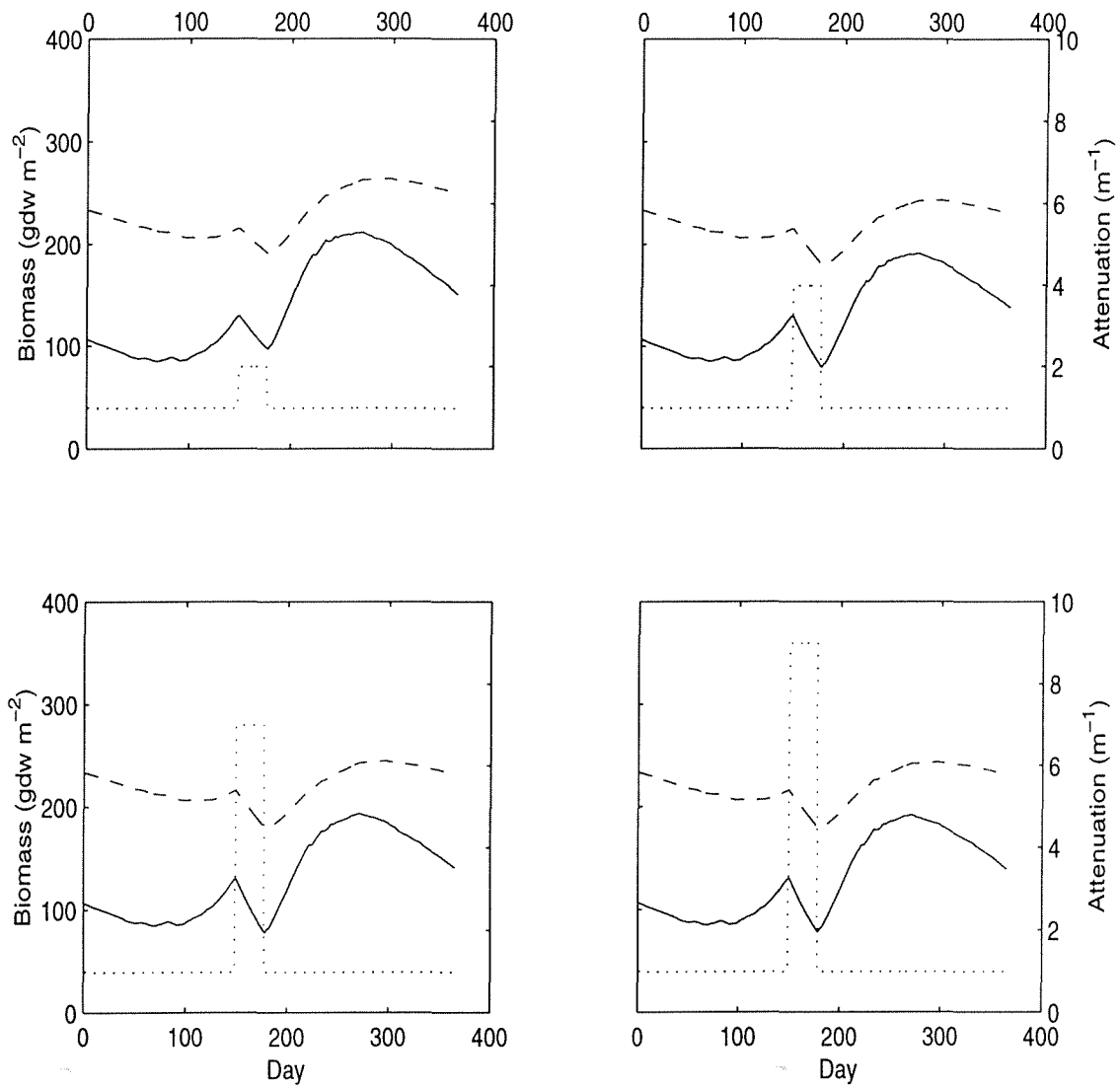


Figure 21. Production model run for *Halodule wrightii* with 50 days of enhanced water column attenuation of various levels. In each panel the dashed line represents the below ground biomass, the solid line the above ground biomass and the dotted line the water column attenuation coefficient.

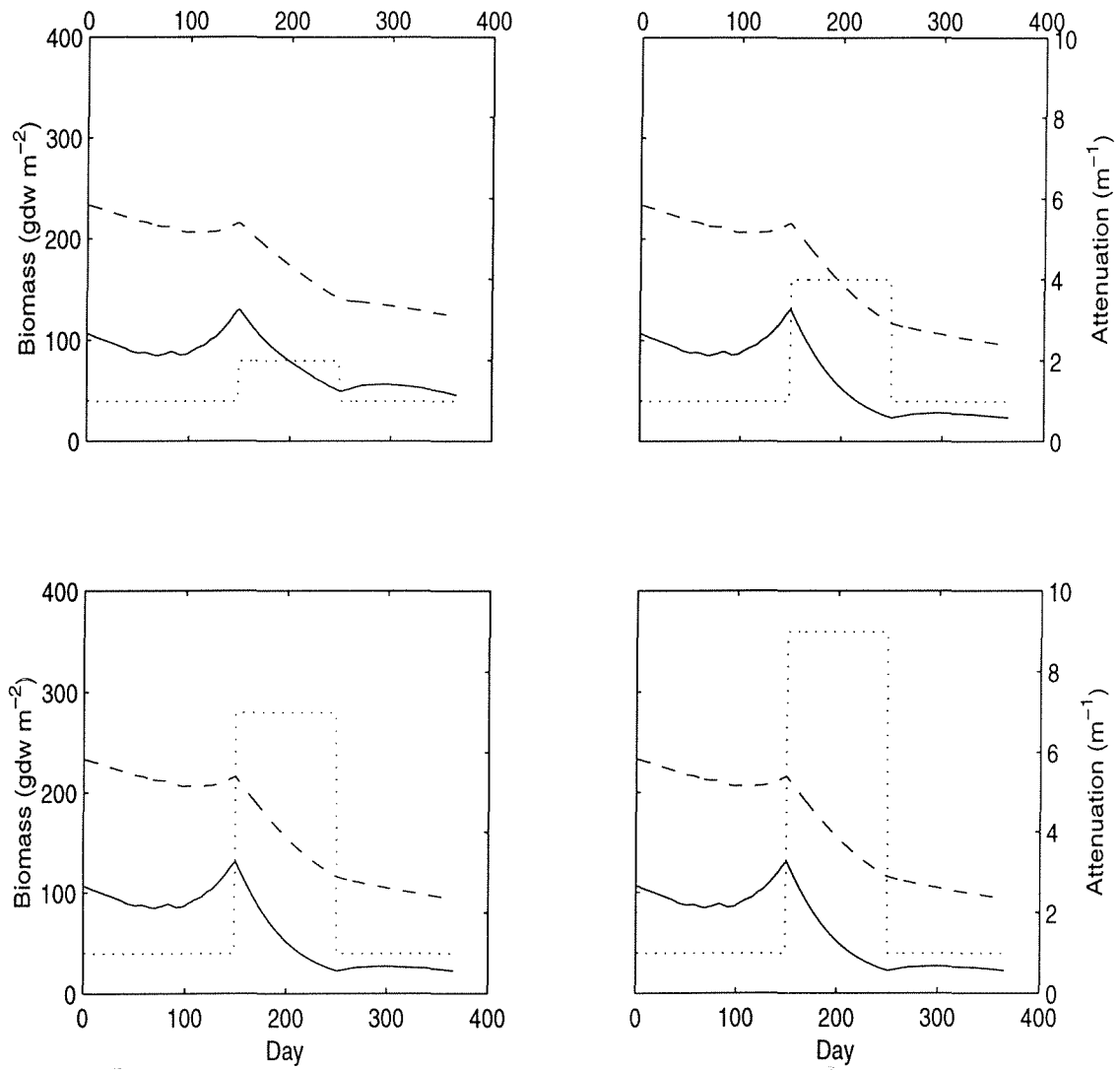


Figure 22. Production model run for *Halodule wrightii* with 100 days of enhanced water column attenuation. In each panel the dashed line represents below ground biomass, the solid line above ground biomass and the dotted line water column attenuation coefficient.

The model indicates that *Halodule wrightii* can successfully withstand short period (one to two weeks) of quite high water column attenuation (i.e., conditions of low light) without significant change in biomass. The initial above and below ground biomasses for the *Halodule* model were 106 and 233 gdw m⁻² respectively; the final biomasses in the *Halodule* baseline model run (Figure 18) were 187 and 311 gdw m⁻² respectively. The final below ground biomasses for one and two weeks of enhanced attenuation varied between 274 and 296 gdw m⁻², and the above ground biomasses between 164 and 179 gdw m⁻². Whilst lower increases in biomass are seen with the increased attenuation, the decrease does not threaten the survival of the plant.

The situation for *Halodule* is not so clear with 50 days of increased attenuation (Figure 21). The final below ground biomasses vary between 228 and 249 gdw m⁻², in the same range as the initial above below values. The above ground biomass appears to fare better, with year-end values between 138 and 150 gdw m⁻². For this duration of enhanced attenuation, the model predicts that the overall plant biomass remains approximately constant between the beginning and the end of the year. Presumably the plants will recover easily.

Increased attenuation coefficients for a period of 100 days have a dramatic effect on *Halodule* (Figure 22). Above ground biomasses at the end of the year range from 22 to 45 gdw m⁻², a decrease of up to 80%. The below ground biomass does not suffer so much, with year-end biomasses ranging between approximately one third and one half of the initial value.

Similar results hold for *Thalassia testudinum*. Short periods of one to two weeks of increased water column attenuation do not irreparably harm the plants (e.g. Figures 19 and 20). Decreased light at the plant canopy lasting approximately 100 days or more does have a significant impact on the biomass, with final above ground biomasses being approximately the same as those at the start of the simulation (Figure 26).

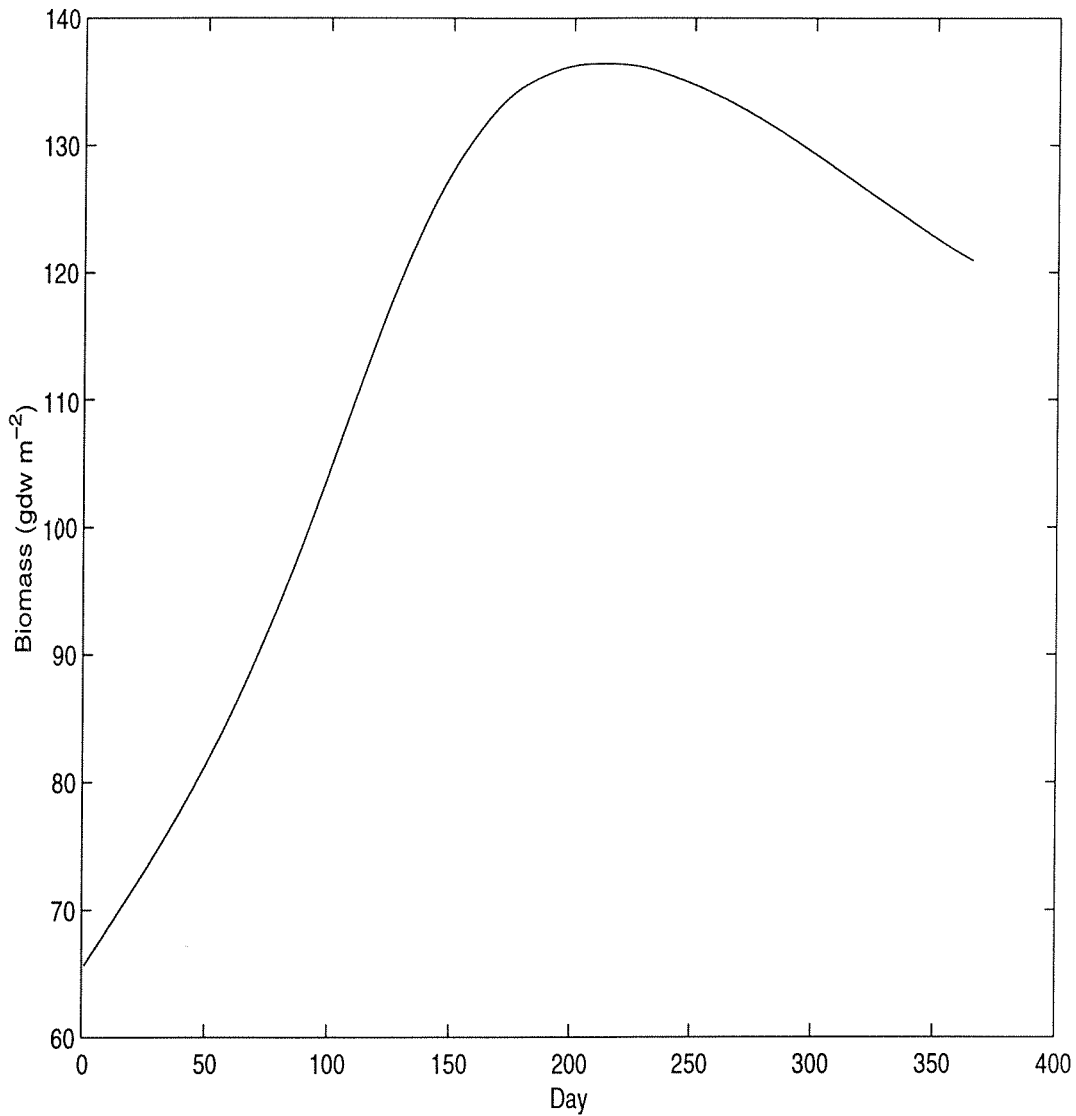


Figure 23. The baseline *Thalassia testudinum* production model. This model uses the calibration determined in the previous section and is forced with the surface irradiance assembled from surface observations (shown in Figure 2). Like the *Halodule wrightii* baseline model, the water column attenuation is set to $k = 1 \text{ m}^{-1}$ throughout the baseline simulation.

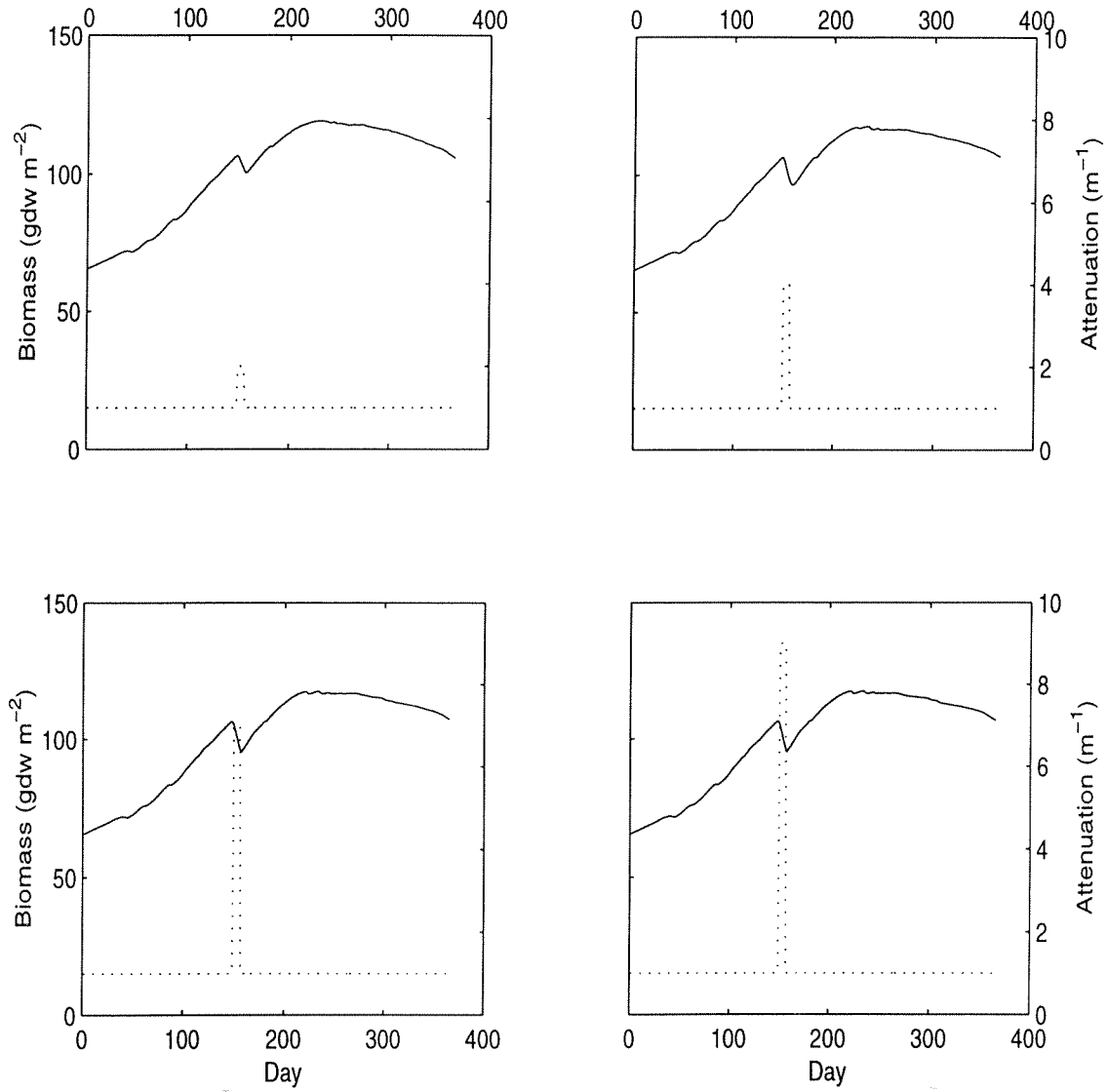


Figure 24. Production model run for *Thalassia testudinum* with one week of enhanced water column attenuation at various levels. In each panel the solid line represents the above ground biomass and the dotted line the water column attenuation coefficient.

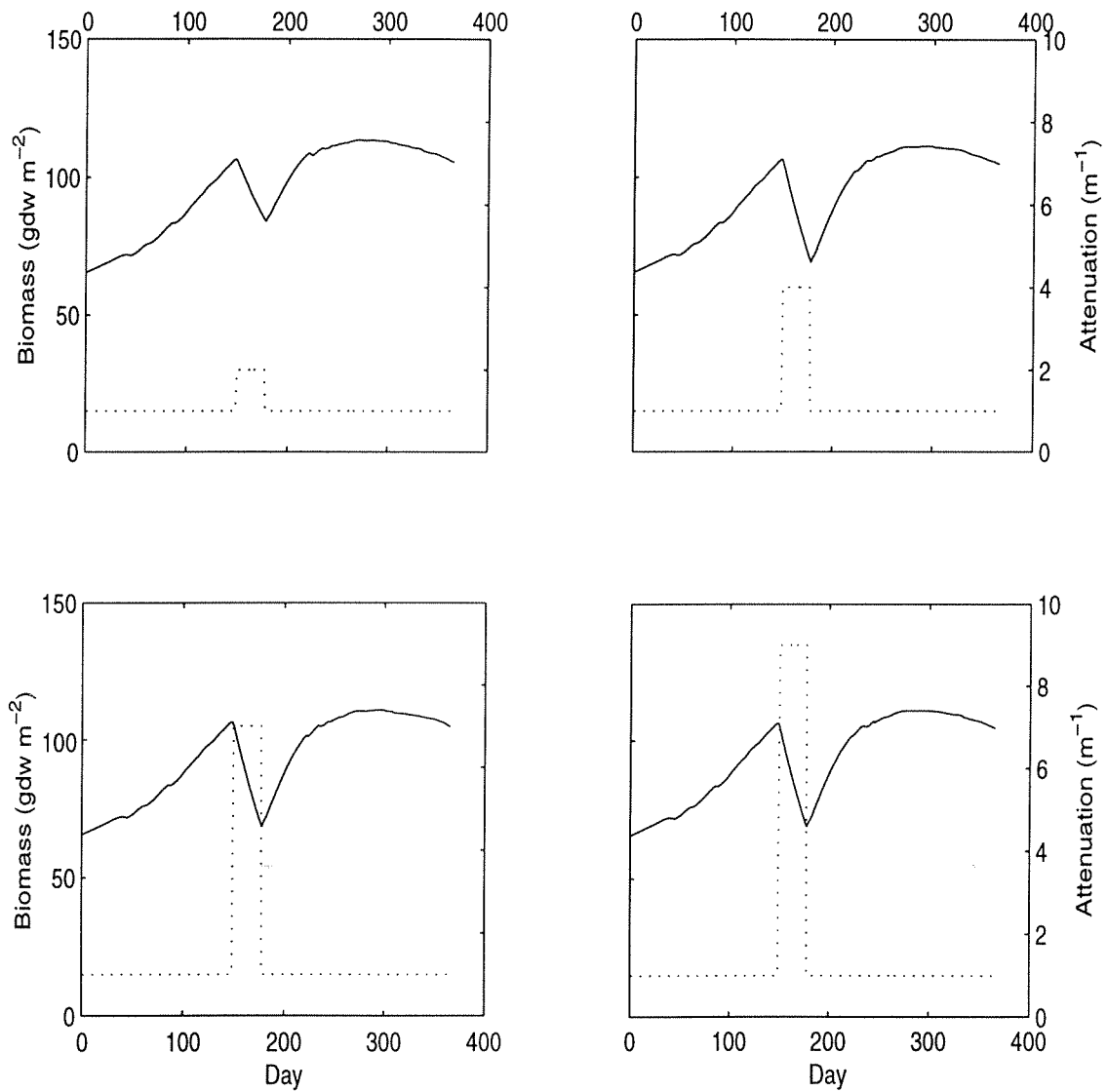


Figure 25. Production model run for *Thalassia testudinum* with 50 days of enhanced water column attenuation coefficient. In each panel, the solid line represents the above ground biomass and the dotted line the water column attenuation coefficient.

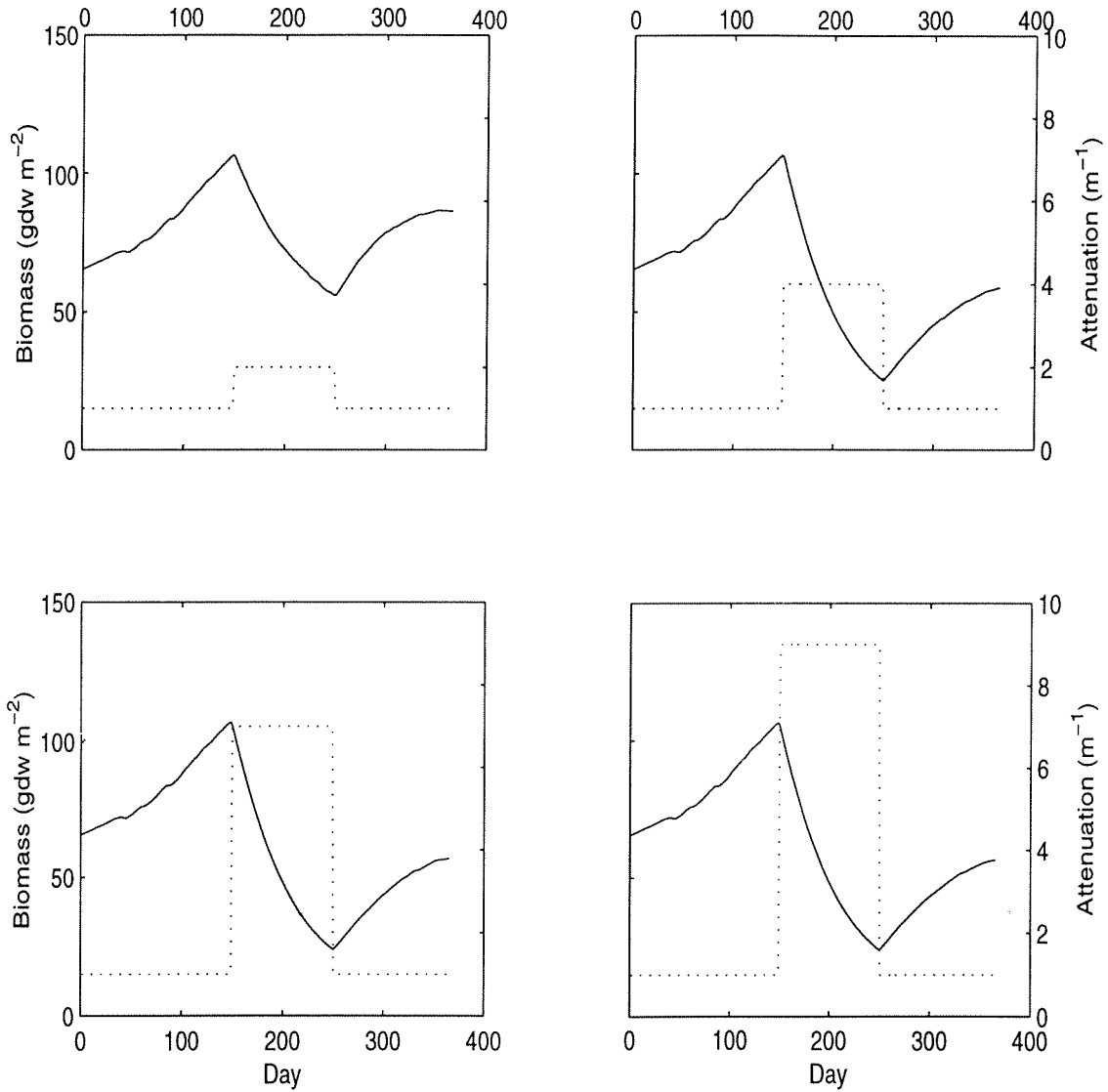


Figure 26. Production model run for *Thalassia testudinum* with 100 days of enhanced water column attenuation coefficient. In each panel, the solid line represents the above ground biomass and the dotted line the water column attenuation coefficient.

Discussion

The objective of the seagrass modeling effort was to provide a computer model that would indicate the effects of various dredging scenarios on the long term health of the seagrass beds in Laguna Madre. Light is the primary factor in determining the productivity and health of the seagrass beds and dredging activities can affect the light attenuation in the water column, thus affecting the seagrasses. Although the model presented here demonstrates that over the course of a year seagrass beds can withstand short periods of very high attenuation, these results should be interpreted with some degree of caution.

The development of a quantitative model requires a mathematical description of the processes being modeled. The mathematical representation of fluid flow (the Navier Stokes equations) is well known and its predictions compared with observation over many decades. There are few, if any, similar mathematical formulations for the processes involved in plant growth. Plant productivity as a function of incident irradiance can be represented using one of a number of standard semi-empirical curves (e.g., Thornley and Johnson 1990). Similarly, the temperature dependence of most metabolic processes is modeled using a Boltzmann exponential function. Beyond this, there are few firm models.

The construction of these mathematical formulations requires the analysis of data sets. Broad principles, such as the conservation of mass and the law of mass action, help in developing these formulations. Unfortunately, for seagrasses there is a lack of detailed data covering a wide range of environmental conditions. Mathematical models describing various processes can be formulated, but without the data to support them they must remain hypotheses.

The architecture of the plants hinders making accurate measurements using current sampling strategies. *Thalassia testudinum* has thick rhizomes which can strongly bias any determination of below ground biomass using coring methods. This bias is probably responsible for the strong fluctuations seen in the measured below ground biomass. *Halodule wrightii* and *Syringodium filiforme* suffer from a different problem; the root tissue consists of fine hairs and it is practically impossible to separate out root biomass from rhizome material. For all three species examined,

the plant architecture makes accurate determination of the components in the below ground biomass very hard.

Once a model has been formulated it needs to be calibrated against an existing data set. In this case, for each species the model was calibrated using a biomass data set. If this biomass represents the real seagrass biomass to within a factor of two or three, then additional uncertainty is introduced into the model.

What confidence can we have in the results from the seagrass model as it stands? This is a difficult question to answer quantitatively, partly for the reasons given above. The most extensive tests were made with the *Halodule* version of the model. The biggest feature in this data set is the decline in both above and below ground *Halodule* biomass as a result of the brown tide. A similar effect is seen in both the above and below ground biomass predicted from the model (Figure 14). The model successfully tracks changes in biomass resulting from long term decreases in the availability of light. Before the onset of the brown tide, the model is generally under predicting both above and below ground biomass by a factor of 2 or 3. The model accurately reproduces the recovery of the below ground biomass after the end of the brown tide, but over-predicts the above ground biomass again by about a factor of 3.

So far we are unable to explain the asymmetry between pre and post brown tides for the above ground biomass. One possibility is that the plants' physiological parameters (such as specific respiration, transport etc.) might change when they experience dramatic changes in ambient conditions. If this is the case, then one might hope that if continuing observations were available, the model and observations would converge again.

Alternatively, some of the parameters that are taken as being constant in the model may actually change with external or internal factors. For example, the rate of release of dissolved organic carbon into the sediments is taken as being a constant proportion of gross primary production. This may not be so, and the plant may exude varying proportions of DOC into the sediments according to external environmental conditions or the health of the plant. Without knowing more about how the plants respond to environmental stresses we cannot say for certain which hypothesis (if either) is true.

The *Thalassia* model is based on data taken during a time when the plants were not suffering any stresses. Therefore, the biomass measurements display a response to only the seasonal changes in the irradiance. The model does likewise. This is in many ways unsatisfactory since the aim of the model is to examine and predict the response of the plants under stressed conditions arising from maintenance dredging. Any changes in physiological parameters arising from external stresses are not included in the model since the model was calibrated under ideal, as opposed to stressed conditions.

The model for *Syringodium filiforme* is disappointing. The best model calibration does not reproduce the observed biomass, but instead gives an almost exponentially decreasing biomass. The large value of the transport coefficient ($\tau = 0.89$) indicates that the optimization model wants to place most of the carbon produced by the plant into the below ground tissue. This is not surprising once it is acknowledged that the fluctuations in the plants' below ground biomass control the calibration procedure.

The water column light model used in the model to date uses only photosynthetically active radiation (PAR). Zimmerman and Mobley (1997) have convincingly shown that PAR models over-estimate the plant production and that spectral models should be used. The information being collected in the project addendum (Cifuentes *et al.*, 1997) should help in addressing this problem for the Laguna Madre Seagrass Model.

The *Halodule* and *Thalassia* models were verified using the same data sets that were used to calibrate the models. In each case, separate parts of the data sets were used for the calibration and verification. This situation is not satisfactory since the model has not been tested against intra-site variations. One would hope that these would not affect the long term responses of seagrasses to stresses resulting from dredging activity.

The biggest unknown factor in the models is the allocation of material within the plant. The carbon produced by photosynthesis occurring in the above ground compartment finds itself in both above and below ground biomass. There is very little information about the mechanism that plants use to allocate their resources. This is true even for terrestrial plants. Some tentative models have been proposed (see Wilson, 1988) and these have been incorporated into larger

grassland models. The allocation models themselves however have not been rigorously tested against observations. In addition, physiological adaptations (e.g. the presence of lacunae) by seagrasses to the marine environment may make these models inapplicable.

Without self-shading, the net daily production for *Halodule* varies between about 43 and 26 mg C (gdwt leaf)⁻¹ d⁻¹. Above ground biomass densities for *Halodule* vary between 40 and 115 gdwt m⁻² (Tomasko and Dunton, 1995). If these densities correspond approximately to the maximum and minimum production rates, then the simulation gives net daily production rates between 0.38 and 0.08 mol C m⁻² d⁻¹. Observed values in the Laguna Madre lie between 0.44 and 0.04 mol C m⁻² d⁻¹ (Tomasko and Dunton, 1995). The model is predicting values which are close to those observed. However, the growth module of the model has yet to be implemented, nor was the canopy architecture taken into account in this version of the model.

The light received by the photosynthetic parts of the leaves depends on the light propagating through the water column as well as the structure of the plant canopy (Ross, 1981; Myneni *et al.*, 1989). The self-shading contribution to the light attenuation will depend on the number density of leaves as well as on their shape and size. For *Halodule wrightii*, shoot densities can get as high as 10,000 m⁻² (Dunton, 1996). For such densities, the plants self shade each other for most of the day; only around solar-noon is the self-shading negligible (Figure 8). For plant densities of 1,000 m⁻² the separation between individual plants is sufficient to make self shading negligible (Figure 9). Shoot densities of 20,000 m⁻², self shading reduces the daily production by one third (from 0.3 to 0.2 mole C m⁻² d⁻¹ (Figure 9). For shoot densities as low as 1,000 m⁻², the effects of self-shading on hourly production are negligible (Figure 10). Shoot densities measured over a six year period (1989 to 1994) show shoot densities averaging approximately 6,000 m⁻² only dropping as low as 2,000 m⁻² in 1994. This indicates that for *Halodule wrightii* self-shading is a dominant factor in determining the upper shoot density of the plants. An important adaptation of seagrass beds to increased water column attenuation would be to decrease plant areal coverage.

Conclusions

A model for the production and biomass of seagrasses in the Laguna Madre has been constructed. The model works well for *Halodule wrightii*, showing the decline in above and below ground biomass during the brown tide and the recovery of the plants biomass after the brown tide had disappeared. The model for *Thalassia testudinum* is less complete in that a meaningful model incorporating below ground biomass was not found. The model for *Syringodium filiforme* performs the worst of the three models. The *Halodule* and *Thalassia* models are able to successfully predict seasonal cycles in the plant biomass and trends in the biomass distribution resulting from changes in the light environment.

The formulation, development and parameterization of these models relied heavily upon data and to a large extent the quality and quantity of this data determines the accuracy of the models. The best data set, in terms of duration and data quality, is that used for the *Halodule* model and it is therefore no real surprise that this model performs better.

The data set of *Thalassia* biomass suffers from significant fluctuations over short periods of time. Fluctuations in the below ground component are due in part to the inhomogeneity of the below ground architecture. Fluctuations in the above ground component appear to arise from inhomogeneities in the above ground biomass on scales larger than the coring device. A more extensive verification of the models should be performed so that their accuracy can be assessed and limitations in the models identified.

References

- Barnabas, A. D. And H. J. Arnott (1987) *Zostera capensis* Setchell: root structure in relation to function. *Aquatic Botany* **27**, 309-322
- Brown, C. A. and N. C. Kraus (1997) *Environmental Monitoring of Dredging and Processes in Lower Laguna Madre, Texas*
- Brylinsky, M (1977) Release of dissolved organic matter by some marine macrophytes. *Marine Biology*, **39**, 213-220
- Cifuentes, L., K. Dunton, P. Eldridge and J. Morse (1997) *A Radiative Transfer Model for Light in the Laguna Madre: Proposal Addendum.*
- Dennison, W.C. and R.S. Alberte (1985) Role of daily light period in the depth distribution of *Zostera marina* (eelgrass). *Marine Ecology Progress Series*, **25**, 51-61.
- DeYoe, H. R. and C. A. Suttle (1994) The inability of the Texas brown tide algae to use nitrate and the role of nitrogen in the initiation of a persistent bloom of this organism. *J. Phycol.*, **30**, 800-806.
- Dunton, K.H. (1994) Seasonal growth and biomass of the subtropical seagrass *Halodule wrightii* in relation to continuous measurements of underwater irradiance. *Marine Biology*, **120**, 479-489.
- Dunton, K.H. (1996) Photosynthetic production and biomass of the subtropical seagrass *Halodule wrightii* along an estuarine gradient. *Estuaries*, **19**, 436-447.
- Dunton, K. H. (1997) Seagrass, light and chlorophyll, Ch. 1 in *The effect of dredge deposits on the distribution and productivity of seagrasses: an integrative model for Laguna Madre (Interim Report).*

- Dunton, K.H., and D. A. Tomasko (1994) *In situ* photosynthesis in the seagrass *Halodule wrightii* in a hypersaline subtropical lagoon. *Marine Ecology Progress Series*, **107**, 281-293.
- Herzka, S. Z., and K. H. Dunton (1997) Seasonal photosynthetic patterns of the seagrass *Thalassia testudinum* in the western Gulf of Mexico. *Marine Ecology Progress Series*, **152**, 103-117.
- Hockney, R.W. and J.W. Eastwood (1988) *Computer Simulation Using Particles*. Institute of Physics Publishing, Bristol, UK.
- Kaldy, J. E. (1997) *Production Dynamics, Reproductive Ecology and Demography of Thalassia testudinum (Turtle Grass) from the Lower Laguna Madre, Texas*, Ph.D. thesis, University of Texas.
- Kaldy, J. E. and A. Burd (1998) The consequences of heterogeneity in a seagrass bed for the development of seagrass models. (*in preparation*)
- Krull, C (1998) Unpublished data.
- Kirk, J.T.O. (1994) *Light and Photosynthesis in Aquatic Systems*. Cambridge University Press, second edition.
- Kuhn, W.A. (1992) Interacting effects of light and sediment sulfide on Eelgrass (*Zostera marina* L.) growth. Master's thesis, University of Maryland.
- Lee, K. -S., and K. H. Dunton (1996) Production and carbon reserve dynamics of the seagrass *Thalassia testudinum* in Corpus Christi Bay, Texas, USA. *Marine ecology Progress Series*, **143**, 201-210.
- Major, K. (1998) personal communication.
- Monteith, J.L. and M.H. Unsworth (1990) *Principles of Environmental Physics*. Edward Arnold.

- Moriarty, D. J. W., R. L. Iverson and P. C. Pollard (1986) Exudation of organic carbon by the seagrass *Halodule wrightii* Aschers. and its effect on bacterial growth in the sediment. *Journal of Experimental Marine Biology and Ecology*, **96**, 115-126.
- Myneni, R.B., J. Ross, and G. Asrar (1989) A review of the theory of photon transport in leaf canopies. *Agricultural and Forest Meteorology*, **45**, 1-153.
- Norman, J.M. (1980) Interfacing leaf and canopy light interception models. In J. D. Hesketh and J. W. Jones, editors, *Predicting Photosynthesis for Ecosystem Models*, volume 2, chapter 3, pages 49-67. CRC Press, Boca Raton, FL.
- Roberts, D. G. (1993) Root-hair structure and development in the seagrass *Halophila ovalis* (R. Br.) Hook. f. *Australian Journal of Marine and Freshwater Research* **44**, 85-100.
- Ross, J. (1981) *The Radiation Regime and Architecture of Plant Stands*. Dr. W. Junk Publishers, The Hague, The Netherlands.
- Sheehy, J. E., F. Gastal, P. L. Mitchell, J. -L. Durand, G. Lemaire and F. I. Woodward (1996) A nitrogen-led model of grass growth. *Annals of Botany* **77**, 165-177.
- Short, F.T. (1980) A simulation model of the seagrass production system. In R. C. Phillips and C. P. McRoy, editors, *Handbook of Seagrass Biology: An Ecosystem Perspective*, chapter 15, pages 277-295. Garland STPM Press, New York.
- Shultis, J.K. and R. B. Myneni (1988) Radiative transfer in vegetation canopies with anisotropic scattering. *Journal of Quantum Spectroscopy and Radiative Transfer*, **39**, 115-129.
- Thornley, J.H.M. (1995) Shoot:root allocation with respect to C, N, and P: an investigation and comparison of resistance and teleonomic models. *Annals of Botany*, **75**, 391-405.
- Thornley, J.H.M. and I. Johnson (1990) *Plant and Crop Modelling: A mathematical approach to plant and crop physiology*. Oxford University Press.

- Thornley, J. H. M. and M. G. R. Cannell (1997) Temperate grassland responses to climate change: and analysis using the Hurley Pasture Model. *Annals of Botany*, **80**, 205-221
- Tomasko, D.A. and K.H. Dunton (1995) Primary productivity in *Halodule wrightii*: A comparison of techniques based on daily carbon budgets. *Estuaries*, **18**, 271-278.
- Verhagen, J.H.G. and P.H. Nienhuis (1983) A Simulation Model of Production, Seasonal Changes in Biomass and Distribution of Eelgrass (*Zostera marina*) in Lake Grevelingen. *Marine Ecology Progress Series*, **10**, 187-195.
- Wetzel, R. L. and P. A. Penhale (1979). Transport of carbon and excretion of dissolved organic carbon by leaves and roots/rhizomes in seagrasses and their epiphytes. *Aquatic Botany*, **6**, 149-158.
- Wetzel, R.L. and P.A. Penhale (1983) Production ecology of seagrass communities in the lower Chesapeake bay. *Marine Tech. Soc. J.*, **17**, 22-31.
- Wilson, J.B. (1988) A review of evidence on the control of shoot:root ratio, in relation to models. *Annals of Botany*, **61**, 433-449.
- Zimmerman, R. C., R. D. Smith and R. S. Alberte (1987) Is growth of eelgrass nitrogen limited? A numerical simulation of the effects of light and nitrogen on the growth dynamics of *Zostera marina*. *Marine Ecology Progress Series*, **41**, 167-176.
- Zimmerman, R. C. And C. D. Mobley (1997) Radiative transfer within seagrass canopies: impact on carbon budgets and light requirements. *Ocean Optics XIII*, 331-336.

CHAPTER II: CARBON AND NITROGEN ALLOCATION MODEL FOR THE SEAGRASS *THALASSIA TESTUDINUM* IN LOWER LAGUNA MADRE

Contents

Abstract.....	4
Introduction.....	5
Methods.....	6
Inverse Model Methods	6
Solving the Inverse Problem.....	7
Model Structure	7
Assumptions of the Model	8
Optimization Model	8
Data input and sources.....	9
Model Formulation	9
Inverse analysis for <i>Thalassia</i>	14
Tracer Analysis	14
Results and Discussion	15
Carbon allocation	15
Nitrogen allocation.....	18
Carbon-nitrogen relationships.....	18
Tracer Analysis	22
References Cited.....	23

Tables

- Table 1. Data used to model *Thalassia testudinum* during the summer (May through September) in Lower Laguna Madre. Data includes either mean \pm SE or range of data. Number of replicates (n) for each measurement and the source are also reported. We converted SE to SD to develop the constraint relationships (Table 4). Reference numbers are (1) Herzka & Dunton, 1997; (2) Chapter 6 this report; (3) Lee & Dunton, 1999; (4) Kaldy, 1997; (5) Vermaat et al., 1995; (6) Opsahl and Benner 1993.....10
- Table 2. Data ranges converted to model units ($\text{mmol-C m}^{-2} \text{d}^{-1}$), that were used to develop the model constraints system. Production gains represent the movement of carbon from one biological pool into another. Respiration losses represent loss of carbon as a result of detrital sloughing or respiratory processes.11
- Table 3. Equations of mass balance for the different model compartments. Carbon and nitrogen flow are designated with C and N followed by a descriptor of the source and sink. Example — $C_{gp,lf}$ is primary production allocated to leaf materials. Subscripts are as follows: lf = leaf, ss = short shoot, rr = root/rhizome, gp = gross production, co = respiration, de = detritus, gr = growth, do = dissolved organic carbon.12
- Table 4. Description of the constraint system used for the model of carbon and nitrogen allocation in *Thalassia testudinum*. Nomenclature is as described in Table 3. Note that because there was essentially no variation in the measured C:N ratio of young leaf material we used an equation (Table 3) to mandate this C:N relationship instead of using a set of constraints13
- Table 5. Results of the nitrogen and carbon ($\text{mmol m}^{-2} \text{d}^{-1}$) allocation model. Showing the percent of gross primary production allocated to each seagrass component, and the C:N of each flow within the seagrass plant.....16
- Table 6. Carbon consumption and release by seagrass as total plant and by leaf and non-photosynthetic tissue. Flows are in $\text{mmol-C m}^{-2} \text{d}^{-1}$. Production, respiration, and organic loss efficiencies are calculated for each seagrass tissue type and for the seagrass as a whole.....16

Figures

- Figure 1. *Thalassia* carbon flow diagram. Arrows indicate direction and numbers (in bold) show the amount of the flow ($\text{mmol-C m}^{-2} \text{d}^{-1}$) to other seagrass component, to losses (i.e., respiration, excretion, etc.) or to growth18
- Figure 2. *Thalassia* flow diagram as in Figure 1, with transport expressed as percent of material entering each seagrass component— leaf, short shoot, and root/rhizome .19
- Figure 3. *Thalassia* nitrogen flow diagram. Same as Figure 1, except for nitrogen20
- Figure 4. Distribution of carbon tracer in the seagrass. One percent of the DIC pool is added as ^{13}C tracer. The model shows how a tracer would move through a seagrass plant. To fit the Wetzel and Penhale (1979) tracer results for *Thalassia* , we set the exchangeable pool to 5% of the total pools of leaf, short shoot, and root/rhizome. This assumes that seagrass like other grass species is composed of structural, storage, and soluble pools that exchange at different rates (Sheehy et al., 1996).22

Abstract

Much of our understanding of seagrass physiology is based on crude estimates of production and biomass. To better understand the complex physiological relationships between the plants and the environment we developed a model of carbon and nitrogen allocation in *Thalassia testudinum* plants from Lower Laguna Madre, Texas. This optimization model is composed of linear equations and inequality constraints which describe material flows between the seagrass tissues (e.g., leaf, short shoot, and roots/rhizomes) and the environment (e.g., water column and sediments). Model results showed that carbon fixed in the leaves (i.e., primary production) was partitioned equally between growth of leaf and non-photosynthetic tissues, with the greatest proportion of non-photosynthetic material going to the root and rhizome tissue. The below-ground growth/storage rate was about 30% lower than above ground growth even though there was 5 times more below-ground tissue than leaf tissue. Losses from the leaf compartment were primarily a result of old leaf material sloughing off to form detritus. Continued loss of leaf detritus in the autumn and winter, when gross primary production is low would account for the yearly cycles in leaf biomass. Losses as a percent of carbon allocated to below-ground tissues were equivalent to those in the leaves but were predominately in the form of dissolved organic material (DOM). The relatively constant year round biomass of below-ground seagrass tissue would suggest that the DOM loss rate must be directly tied to seagrass primary production.

Nitrogen was preferentially allocated to leaf growth, consequently, below-ground tissues had high C:N ratios. The model predicted high C:N ratios for leaf detritus which was confirmed with preliminary quantitative analyses. Furthermore, the model predicts that DOM released below-ground will be nearly depleted of nitrogen. We suggest that *Thalassia testudinum* conserves nitrogen resources through translocation from old leaf tissue (i.e., internal recycling) and preferential release of nitrogen depleted DOM from below-ground tissue.

Introduction

The development of energy balance models (Short, 1980; Wetzel and Neckles, 1986; Dennison and Alberte, 1986; Zimmerman et al. 1994; Herzka and Dunton 1997) have helped to establish relationships between seagrass distribution and light availability by estimating relative rates of productivity and respiration (Denison and Alberte 1985, Denison 1986, Fourqurean and Zieman 1991, Kenworthy and Fonseca 1996, Lee and Dunton 1996, 1997, Herzka and Dunton 1998, Kaldy & Dunton *in press*). Other models have been developed to assess how carbon concentration changes in response to variations in the light environment (Zimmerman et al., 1995; Chapter I). Those modeling strategies examine temporal scales over which light attenuation due to dredging, natural sediment transport process, and phytoplankton may affect seagrass. However, none of these analyses provide information about how seagrasses interact with other (non-light) components of their physical and chemical environment.

Although light is probably the major factor affecting seagrass distribution (Onuf, 1996) in Laguna Madre, other secondary factors including nutrient limitation and sulfide toxicity may effect overall seagrass "health". In some areas of Lower Laguna Madre, seagrass growth may be limited by sediment porewater NH_4^+ concentration (Lee and Dunton, 1999). Even though sulfides rarely reach toxic concentrations in Laguna Madre seagrass beds, this phenomenon has been observed in Florida Bay *T. testudinum* populations (Carlson et al, 1992). Kuhn (1992) developed empirical relationships among seagrass growth, NH_4^+ uptake, and sulfide toxicity in the sediments and used them to estimate the response of the seagrass to changing environmental conditions. The accuracy of this approach, however, is hampered by the large natural variation found in estuarine seagrass and sediment geochemical parameters (see Chapters I, VI, and VII). Modelling seagrass physiology therefore requires better descriptions of both the plants' biology and the biogeochemical environment.

The goal of this analysis was to bridge the gap between the biomass model developed for Chapter I and the sediment geochemistry model described in Chapter III. For this purpose, the model provides a description of carbon and nitrogen allocation within the seagrass and details their interaction with the water-column and sediment environment. Our specific objectives were to

develop an inverse model of carbon and nitrogen flow through the seagrass *Thalassia testudinum* and to provide a data set for the parameterization of the production models.

Methods

The analysis is comprised of an inverse (optimization) model that describes carbon (C) and nitrogen (N) flows within the seagrass (e.g., leaf, short-shoot, and root-rhizome) and between the seagrass and its environment (e.g., production, excretion, and detritus). Tracer analysis was conducted using the carbon flow network from the inverse model and Wetzel and Penhale's (1979) *Thalassia* tracer data to estimate the size of exchangeable C pools in the seagrass leaf, short-shoot and root/rhizomes. This analysis calculates the accumulation rates of the tracer in various sediment geochemical pools.

Inverse Modeling Method

The power of an inverse analysis is its ability to include constraints when describing a biological system. Combining a set of linear equations describing pathways within the seagrass plant system, inequalities containing physiological information and data, and an objective function that can be minimized (i.e., a norm), produces a solution that reasonably defines the energy and nutrient relationships in the plant. As in any linear system, all mass flows must sum to zero (i.e., the system must balance mass). In the model, the requirement that flows entering and leaving a seagrass compartment balance was expressed as a linear equation involving the relevant flows while the requirement that all compartments balance was expressed as a system of linear equations. Measured fluxes were expressed using equations in which the relevant fluxes equal the measured values. All of these equality relationships were combined into a matrix equation of the form

$$Ax = b \quad (1)$$

where x was the vector of all the flows, b was the vector of all the constants, usually data values, and A was a matrix of coefficients describing the equations.

Historical information about respiration, growth efficiency, and C/N ratios were expressed as a combination of fluxes occurring over a range of values. The system of such inequality relationships can then be expressed in matrix form as

$$Gx \geq h \quad (2)$$

where h was the vector of all constants and G was a matrix of coefficients describing the inequalities.

Solving the inverse-problem

When there are n components of x and A has rank $k < n$, the inverse technique was used to solve for the minimum Euclidean length of flow vector x that satisfies Eq. 1 subject to Eq.2. The problem was solved in stages. First the model uses a singular value decomposition (SVD) routine to solve for the minimum length vector x_0 consistent with Eq. 1. This result was expressed in terms of a set of k basis vectors, y_0 , which span the subspace for which $A y_0 \neq 0$. The SVD decomposition also returns the basis vectors for the null space, the space consisting of all vectors for which $A y = 0$. Because of this property, they can be added to x_0 to form a new x which was no longer the minimum length but which still satisfied Eq. 1. The two sets of vectors completely described any x . The null space basis vectors, suitably transformed, were used to find the smallest additional length which yielded a solution that satisfied Eq. 2. When combined with x_0 , they form the shortest vector which satisfied Eqs. 1 and 2. Vezina and Platt (1988) provide a more complete description of these calculations.

Model structure

Primary production (photosynthetic carbon fixation) provided all the energy resources for the seagrass which were then partitioned in the analysis to leaf, short shoot, and root/rhizome material. Short shoot refers to the vertical rhizome (stem) connecting the leaves with the roots and horizontal rhizome. For convenience and because of the relative paucity of data, roots and rhizomes were combined into a single root/rhizome compartment for this analysis. The result was a description of seagrass physiology, specifically carbon and nitrogen resource partitioning, sorted by important above- and below-ground structures. Interactions between seagrass compartments were described by the rates of material flows between them and by the nitrogen and carbon relationships implicit

in these flows. Carbon flows can be thought of as surrogates for energy flows: organic nitrogen flows can be considered surrogates for the nutritional aspects of seagrass material (sensu Eldridge and Jackson, 1993). The set of all flows is a vector which was solved using the inverse technique (see above). Biomass and scalar flows used as the model inputs were provided by direct measurements and from the literature.

Assumptions of the Model

We made several simplifying assumptions for this analysis. Ammonium (NH_4^+) is the only form of dissolved inorganic nitrogen (DIN) assimilated and this occurs exclusively through the root/rhizome compartment. Extensive research has shown that seagrasses preferentially assimilate ammonium over other nitrogenous compounds (Short 1980, Lee and Dunton 1999). We assumed that short shoot tissue was non-photosynthetic. Further, no respiration or excretion occurred through the short shoot compartment but was instead incorporated into the results for the root/rhizome compartment. Available data were generally partitioned between photosynthetic and non-photosynthetic tissue making the partitioning of respiration and excretion somewhat arbitrary. Allometric constraints based on the relative size of the short shoot and root/rhizome compartments and temperature (Vezina and Platt, 1988) could have been used to partition these flows but the authors felt uncomfortable with this approach because of the high concentration of storage tissue in these structures.

Optimization Model

The analysis shown here describes *Thalassia testudinum* only during the summer months (May-Sept.). The optimization analysis provides a snap-shot of material flows within a seagrass plant, which can be used to help parameterize the production models. Since temperature and light have a strong effect on both the physiology of the seagrass and diagenetic processes in sediments, we had to select a time of year for the analysis during which the seagrass physiology would remain reasonably constant and during which sediment diagenetic processes would be most active. Diagenesis refers to changes in the chemical composition of sediments after deposition (sensu Schlesinger 1991).

Data inputs and sources

The natural variation in seagrass biomass measurements and flux rates is large even in comparison to other marine biological systems e.g., benthic and pelagic food webs (Jackson and Eldridge, 1992; Eldridge and Jackson, 1993). Because it is a constrained optimization, the inverse analysis is uniquely able to incorporate data ranges. The data consisted of biomass measurements, O₂ evolution rates, respiration rates, and various tissue growth and turnover rates collected in Lower Laguna Madre (Table 1). All data was converted to consistent units (mmol-C or -N m⁻² d⁻¹) using simple arithmetic relationships between biomass and specific rates and turnover times (Table 2). Quantitative measures of tissue C:N ratios were used in the conversions (Chapter VI), where appropriate. We assume a 1 to 1 stoichiometry for O₂ to C conversion. Bounded ranges of data used in the model were either the actual range of data or the means ± standard deviation (SD) as defined in Table 1. We used the mean value for the C:N ratio of young leaf biomass (Table 5, Chapter VI) and; the excreted DOM from leaf and root/rhizome. There was no variation in the C:N ratio for young leaves (Chapter VI) and the variation in DOM excretion was not reported (Wetzel and Penhale, 1979).

Model Formulation

As discussed above, at steady state, the sum of all flows into a compartment equals the sum of the flow out of that compartment. When growth or death is included in the model, actual growth or death rate of each seagrass compartment must be added to the appropriate equations. In this way the analysis is translated into a growth model while still meeting the assumptions of the steady state system. Furthermore, since the plant assimilates carbon and nitrogen at a known ratio, fixed C:N ratios for flows can then be expressed using linear equations.

Model flows were related to each other and to biomass through physiological relationships based on data from this project and from the literature. These relationships exist as bounded ranges and were expressed using inequality relationships (Tables 3 & 4).

Table 1. Data used to model *Thalassia testudinum* during the summer (May through September) in Lower Laguna Madre. Data includes either mean \pm SE or range of data. Number of replicates (n) for each measurement and the source are also reported. We converted SE to SD to develop the constraint relationships (Table 4). Reference numbers are (1) Herzka & Dunton, 1997; (2) Chapter 6 this report; (3) Lee & Dunton, 1999; (4) Kaldy, 1997; (5) Vermaat et al., 1995; (6) Opsahl and Benner 1993.

Parameter	Values	n	Reference
primary production ($\mu\text{mol O}_2 \text{gdw}^{-1} \text{hr}^{-1}$)	208 to 270	4-5	1
range of above ground biomass (g m^{-2})	129 \pm 13.7	5	2
range of below-ground biomass (g m^{-2})	581 \pm 122	5	2
range of root biomass (g m^{-2})	79.98 \pm 9.83	5	2
wt % carbon in above ground biomass	36.2 \pm 3.4	12	2
wt % nitrogen in above ground biomass	1.78 \pm 0.34	12	2
wt % carbon in below-ground biomass	35.9 \pm 0.66	12	2
wt % nitrogen in below-ground biomass	0.77 \pm 0.13	12	2
wt % carbon in young leaf biomass	37.83 \pm 2.09	3	3
wt % nitrogen in young leaf biomass	2.16 \pm 0.11	3	3
wt % carbon in mature leaf biomass	37.81 \pm 2.16	3	3
wt % nitrogen in mature leaf biomass	2.10 \pm 0.08	3	3
wt % carbon in old leaf biomass	33.76 \pm 2.49	3	3
wt % nitrogen in old leaf biomass	1.12 \pm 0.13	3	3
NH ₄ ⁺ uptake in leaf material $\mu \text{mol gdw}^{-1} \text{hr}^{-1}$	2.5*	1	3
NO ₃ ⁻ uptake in leaf material $\mu \text{mol gdw}^{-1} \text{hr}^{-1}$	1.0*	1	3
NH ₄ ⁺ uptake in below-ground material $\mu \text{mol gdw}^{-1} \text{hr}^{-1}$	5.0*	1	3
leaf turn-over time (d^{-1})	0.015 to 0.025	10	4
short shoot turn-over time (yr)	2-3		4
short shoot growth (nodes yr^{-1})	10 to 16		4
biomass per short shoot node (mg dry wt node ⁻¹)	3.2		4 & 5
above ground net production $\text{gC m}^{-2} \text{mo}^{-1}$	23.0 \pm 5.3	5	4
below-ground net production $\text{gC m}^{-2} \text{mo}^{-1}$	14.2 \pm 1.7	5	4
range of respiration for leaf material ($\text{gdw}^{-1} \text{hr}^{-1}$)	26.0 to 34.7	4-5	1
range of respiration for root/rhizome material ($\text{gdw}^{-1} \text{hr}^{-1}$)	3.7 to 4.7	4-5	1
dissolved organic carbon (DOC) released as a percent of gross primary production to leaf	1	2-8	6
DOC released as a percent of gross primary production to root/rhizome	8	2-8	6

* N uptake rates were conducted in September 1997. Ambient concentrations in the water column were 1.5 $\mu\text{M-NH}_4^+$ and 1.0 $\mu\text{M-NO}_3^-$. Sediment porewater concentration was 35 $\mu\text{M-NH}_4^+$.

Table 2. Data ranges converted to model units ($\text{mmol-C m}^{-2} \text{d}^{-1}$), that were used to develop the model constraints system. Production gains represent the movement of carbon from one biological pool into another. Respiration losses represent loss of carbon as a result of detrital sloughing or respiratory processes.

Production gains	value	Respiration losses	value
Gross production, min	$C_{gp_{lo}}=288.1$	Leaf loss to detritus, min	$Clf_{lo}=48.1$
Gross production, max	$C_{gp_{hi}}=462.8$	Leaf loss to detritus, max	$Clf_{hi}=77.5$
Leaf production, min	$Clf_{p_{lo}}=49.1$	Leaf loss to resp., min	$Clf_{r_{lo}}=65.1$
Leaf production, max	$Clf_{p_{hi}}=78.6$	Leaf loss to resp., max	$Clf_{r_{hi}}=119.6$
Short shoot prod, min	$C_{ssp_{lo}}=0.2$	Root/rhiz to detritus, min	$Crr_{lo}=12.3$
Short shoot prod, max	$C_{ssp_{hi}}=0.36$	Root/rhiz to detritus, max	$Crr_{hi}=29.4$
Root/rhiz prod, min	$Crr_{p_{lo}}=34.0$	Root/rhiz resp., min	$Crr_{r_{lo}}=40.82$
Root/rhiz prod, max	$Crr_{p_{hi}}=44.9$	Root/rhiz resp., max	$Crr_{r_{hi}}=79.41$

Table 3. Equations of mass balance for the different model compartments. Carbon and nitrogen flow are designated with C and N followed by a descriptor of the source and sink. Example — C_{gp,lf} is primary production allocated to leaf materials. Subscripts are as follows: lf = leaf, ss = short shoot, rr = root/rhizome, gp = gross production, co = respiration, de = detritus, gr = growth, do = dissolved organic carbon.

Model structure		
Leaf (lf)	$C_{gp,lf} - C_{lf,ss} - C_{lf,co} - C_{lf,de} - C_{lf,gr} - C_{lf,do} + C_{ss,lf}$	=0
Short shoot (ss)	$C_{lf,ss} + C_{rr,ss} - C_{ss,rr} - C_{ss,lf} - C_{ss,de} - C_{ss,gr}$	=0
Root/rhizome (rr)	$C_{ss,rr} - C_{rr,ss} - C_{rr,co} - C_{rr,do} - C_{rr,lf} - C_{rr,de} - C_{rr,gr}$	=0
Leaf (lf)	$N_{ss,lf} - N_{lf,ss} - N_{lf,do} - N_{lf,de} - N_{lf,gr}$	=0
Short shoot (ss)	$N_{lf,ss} + N_{rr,ss} - N_{ss,lf} - N_{ss,rr} - N_{ss,de} - N_{ss,gr}$	=0
Root/rhizome (rr)	$N_{nh,rr} + N_{ss,rr} - N_{rr,ss} - N_{rr,do} - N_{rr,de} - N_{rr,gr}$	=0
 Data equations		
Leaf DOM release	$0.01C_{gp} - C_{lf,do}$	=0
Root/rhizome DOM release	$0.08C_{gp} - C_{rr,do}$	=0
C:N leaf growth	$C_{lf,gr} - R_{loy} N_{lf,gr}$	=0

Table 4. Description of the constraint system used for the model of carbon and nitrogen allocation in *Thalassia testudinum*. Nomenclature is as described in Table 3. Note that because there was essentially no variation in the measured C:N ratio of young leaf material we used an equation (Table 3) to mandate this C:N relationship instead of using a set of constraints.

1.	gross Prod., min	$C_{gp,lf} - C_{gp,lo}$	≥ 0
2.	gross Prod., max	$-C_{gp,lf} + C_{gp,hi}$	≥ 0
3.	leaf growth, min	$Clf,gr - Clf,de - Clf,lo$	≥ 0
4.	leaf growth, max	$-Clf,gr + Clf,de + Clf,hi$	≥ 0
5.	short shoot growth, min	$C_{ss,gr} - C_{rr,de} - C_{ssp,lo}$	≥ 0
6.	short shoot growth, max	$-C_{ss,gr} + C_{rr,de} + C_{ssp,hi}$	≥ 0
7.	root/rhizome growth, min	$C_{rr,gr} - C_{rr,lo}$	≥ 0
8.	root/rhizome growth, max	$-C_{rr,gr} + C_{rr,hi}$	≥ 0
9.	leaf detritus, min	$Clf,de - Clf,lo$	≥ 0
10.	leaf detritus, max	$-Clf,de + Clf,hi$	≥ 0
11.	root/rhizome detritus, min	$C_{rr,de} - C_{rr,lo}$	≥ 0
12.	root/rhizome detritus, max	$-C_{rr,gr} + C_{rr,hi}$	≥ 0
13.	leaf respiration, min	$Clf,co - Clf,lo$	≥ 0
14.	leaf respiration, max	$-Clf,co + Clf,hi$	≥ 0
15.	root/rhiz respiration, min	$Clf,co - C_{rr,lo}$	≥ 0
16.	root/rhiz respiration, max	$-C_{rr,co} + C_{rr,hi}$	≥ 0
17.	C:N root/rhiz growth, min	$C_{rr,gr} - R_{lob} N_{rr,gr}$	≥ 0
18.	C:N root/rhiz growth, max	$-C_{rr,gr} + R_{hib} N_{rr,gr}$	≥ 0
19.	C:N transfer, min	$Clf,rr - R_{lob} N_{lf,rr}$	≥ 0
20.	C:N transfer, max	$-Clf,rr + R_{hib} N_{lf,rr}$	≥ 0
21.	C:N leaf excret, min	$Clf,do - R_{loa} N_{lf,do}$	≥ 0
22.	C:N leaf excret, max	$-Clf,do + R_{hia} N_{lf,do}$	≥ 0
23.	C:N root/rhiz excret, min	$C_{rr,do} - R_{lob} N_{rr,do}$	≥ 0
24.	C:N root/rhiz excret, max	$-C_{rr,do} + R_{hib} N_{rr,do}$	≥ 0
25.	C:N leaf detritus, min	$Clf,de - R_{lod} N_{lf,de}$	≥ 0
26.	C:N leaf detritus, max	$-Clf,de + R_{hid} N_{lf,de}$	≥ 0
27.	C:N root/rhiz detritus, min	$C_{rr,de} - R_{lob} N_{rr,de}$	≥ 0
28.	C:N root/rhiz detritus, max	$-C_{rr,de} + R_{hib} N_{rr,de}$	≥ 0

Inverse Analysis for *Thalassia*

We solved the inverse problem with a procedure that minimizes the sum of the squares of the results vector (norm-2) in a way that is consistent with our set of equations and constraint relationships (Haskell and Hanson, 1981). As nitrogen flows are smaller than those of carbon, the technique preferentially decreased carbon flows while it increases those of nitrogen even though each is in the same units (Eldridge and Jackson, 1993). Therefore the nitrogen flows were normalized to C-equivalents using a multiplication factor of 12. Earlier pelagic and benthic food web analyses used the Molar Redfield ratio (6.6) (Jackson and Eldridge, 1992; Eldridge and Jackson, 1993), but the higher average C:N of seagrass (Table 1) material requires a larger factor. The result of the procedure is a flow vector with the minimum Euclidean length that satisfies the equations (Table 3) subject to the constraints specified by the inequalities (Table 4). We used Matlab from Mathworks to solve the analysis.

Simulated tracer analysis

The flows out of a compartment can be expressed as the compartment biomass times a kinetic rate constant. This constant can be used to calculate the rate at which a simulated tracer moves through the various seagrass structures (e.g., leaf, shoot, root/rhizome). We calculated kinetic rate constants for those compartments where biomass values existed using flows derived from the inverse model and biomass measurements from Chapter VI and Kaldy (1997). Morse (Chapter VII) provides sediment geochemical measurements for this analysis. Because all these measurements were taken from the same site (LLM-2) during one study, we have a consistent set of data for this analysis. Wetzel and Penhale (1979) provide ^{14}C tracer accumulation data for *Thalassia*. This information is very useful for the determination of exchangeable pool size within each seagrass structure. Seagrass structures are composed of tissue specialized for transport, structure, and storage. Each of these tissues exchange C with other tissues at different rates and the total rate of exchange may be determined predominately by a few tissue types (e.g., a transport tissue). Thus, the exchange rate becomes a function of specific tissue biomass and not the total biomass of a compartment. Given the accumulation rates of a few compartments

(Wetzel and Penhale, 1979) and the inverse analysis, we can estimate both the size of the exchangeable pools in each tissue and tracer accumulation rates in other pools.

The tracer model was conducted to simulate the movement of a ^{13}C tracer added to an incubation chamber of the type typically used to measure *in situ* photosynthesis (Dunton and Tomasko, 1994). The chamber is clear acrylic, has a volume of 5 l and covers 113 cm^2 (12 cm diameter) of a *Thalassia* bed. The dissolved inorganic carbon concentration ([DIC]) was 2.3 mM and we assumed that all DIC uptake was by *Thalassia*. This assumption is reasonable because the water column is net heterotrophic (Ziegler and Benner 1999) and epiphyte biomass is typically $<5\text{ mg epiphytes sht}^{-1}$ (Kowalski unpub. data). The biomass in each compartment was incrementally reduced by an integer factor until 7% and 2% of the tracer resides in the leaf and root/rhizomes respectively (6.9 and 1.7 % respectively in Wetzel and Penhale, 1979) after 8 hrs. This provided the model calibration to known data and provided estimates of the "exchangeable pool" size. The model was then run for 20 days.

Results and Discussion

An aspect of seagrass ecology that is often neglected in seagrass models is the community response to changes in seagrass production. The seagrass community may extend beyond the confines of the seagrass bed itself. Benthic infauna and epi-fauna in and adjacent to seagrass depend on seagrass litter and particulate detritus for food (Thayer et al., 1984; Zieman and Zieman, 1989; Phillips, 1984) while red drum fisheries expropriate these organism for their needs (Rooker et al 1997). Although the direct contribution of seagrass detritus to secondary production (directly or indirectly) has not been quantified (Wetzel 1977), it is certain that much of the fisheries in Laguna Madre is dependent in part on seagrass production (Hoss and Thayer, 1993).

Carbon allocation

The inverse optimization technique provided a set of flows that was consistent with the lowest allowable primary productivity i.e., $G_{pgi_0} = 288.16$ (Table 5). The relatively few feasible

solutions we found indicates that the actual solution space for the analysis is small, even though, individual parameters often had a broad set of values between their upper and lower bounds.

Carbon assimilated by the leaves was partitioned approximately equally between growth of leaves and below-ground tissues (Fig. 1). During this time period C flow was unidirectional, from the leaves to the below-ground storage organs (i.e. roots and rhizome). Losses to excretion and respiration were relatively small. However, when detrital leaf losses were included, about 25% of the primary production was lost (Table 6). Short shoots functioned as a conduit for carbon and nitrogen exchange between leaves and the roots and rhizomes with minimal losses to detritus. Growth and detrital loss of short shoot tissue was less than that found in other tissues (Fig. 1). This is consistent with the role of short shoots as perennial structures for leaf growth. The short shoot apical meristem initiates leaf growth, while an intercalary meristem causes leaf elongation. In the root/rhizome tissue more organic carbon was lost to DOC than to detritus (Fig. 2). This may contribute to the high DOC concentrations found in the seagrass sediments (Morse, see Chapter VI).

During summer the net flow of carbon was from the leaf to the below-ground tissue as a result of a positive energy balance in the seagrass at that time. The production efficiency which is a measure of the magnitude of the energy balance can be estimated from the inverse analysis flow network. For the whole seagrass plant the production efficiency was 50% with a lesser value in the non-photosynthetic tissue and a greater value for the leaf tissue (Table 6). During this time of year seagrass growth was at its annual maximum (Chapter I). To estimate the range of *Thalassia* production efficiencies that is still consistent with our data set (Table 1), we imposed the upper bound for gross primary production ($C_{g_{ph}}=462.85$) on the analysis. This produced a production efficiency of 31%. Thus, this sensitivity test suggests that the production efficiency lies between 31-50%.

Table 5. Results of the nitrogen and carbon ($\text{mmol m}^{-2} \text{d}^{-1}$) allocation model. Showing the percent of gross primary production allocated to each seagrass component, and the C:N of each flow within the seagrass plant.

Flow	C	N	% of Primar Productivity.	C/N
Primary production to leaf	288.16	7.93		36.33
Leaf to CO_2	16.59	-	5.8	-
Root/rhizome to CO_2	40.82	-	14.2	-
Leaf to short shoot	123.31	1.84	42.8	66.84
Short shoot to root/rhizome	110.47	1.65	38.3	67.09
Root/rhizome to short shoot	0.00	8.13	0.0	-
Leaf to DOM	2.88	0.09	1.0	32.04
Root/rhizome to DOM	23.05	0.34	8.0	66.96
Leaf to detritus	48.14	1.23	16.7	39.12
Short shoot to detritus	0.27	0.00	0.1	66.96
Root/rhizome to detritus	12.35	0.18	4.3	66.96
Leaf to growth	97.24	4.77	33.7	20.40
Short shoot to growth	12.57	0.39	4.4	32.04
Root/rhizome to growth	34.25	1.07	11.9	32.04

Table 6. Carbon consumption and release by seagrass as total plant and by leaf and non-photosynthetic tissue. Flows are in $\text{mmol-C m}^{-2} \text{d}^{-1}$. Production, respiration, and organic loss efficiencies are calculated for each seagrass tissue type and for the seagrass as a whole.

	Whole seagrass	Leaf	Non- photo
Flows			
inputs (C)	288.2	288.2	123.3
respiration (R)	57.4	16.6	40.8
detritus (F)	60.8	48.1	12.6
DOC (U)	25.9	2.9	23.1
P=C-R-F-U	144.1	220.5	46.8
Efficiencies (%)			
P/S inputs x 100	50	77	38
S R/S inputs x 100	20	6	33
(F+U)/S inputs x 100	30	18	29

The leaf and non-photosynthetic tissue partitioned C losses quite differently. Organic carbon losses were much greater in the leaf tissues (mostly as detritus), while the below-ground tissue seem to split C losses about equally between organic and inorganic C.

Nitrogen allocation

Allocation of nitrogen flows generally paralleled carbon flows (Fig. 3). While carbon enters the seagrass through the leaves, most nitrogen enters through the root system. We calculated the relative contribution of leaf and root zone N-uptake using NH_4^+ and NO_3^- uptake data (Lee and Dunton, 1999) scaled to our biomass data. About 85% of the dissolve inorganic nitrogen (DIN) entered through the root system providing justification for a model structure with DIN uptake occurring only through the root system.

The transport of DIN through the below-ground tissue and presumably returned back to the non-photosynthetic tissues as organic nitrogen, suggests that internal recycling is an important adaptation to nutrient limitation (Fig. 1 & 3). About 25% of the nitrogen in the leaves was returned below-ground, most of which was allocated to the root/rhizome tissue. Substantially more N went to new growth than to losses (i.e., detritus or DON leakage), which indicates that the plants are very efficient at using nitrogen. Non-photosynthetic N flows were small (excluding uptake) with most of the nitrogen being allocated to growth. Detrital and DON losses of non-photosynthetic nitrogen were minimal, which may account for the high C:N ratio of DOM found in seagrass bed sediments (Chapter VII),

Carbon-nitrogen relationships

The C:N in seagrass is substantially greater than found in plants of the pelagic zone. Above ground biomass had an average C:N by atoms of 25 while below-ground tissue had an average of 60 (Chapter VI). This compares with a Redfield ratio of 6.6 typical of phytoplankton in estuarine and oceanic systems (Redfield, 1958). Most of the C:N material flows in this analysis were even higher than the average seagrass biomass, the leaf tissue had a C:N of 36, while detritus and DOM had a C:N ratio of 32 and 39 respectively. Material shunted below-ground had a C:N ratio of 67.

Figure 1. *Thalassia* carbon flow diagram. Arrows indicate direction and numbers (in bold) show the amount of the flow ($\text{mmol-C m}^{-2} \text{d}^{-1}$) to other seagrass component, to losses (i.e., respiration, excretion, etc.) or to growth.

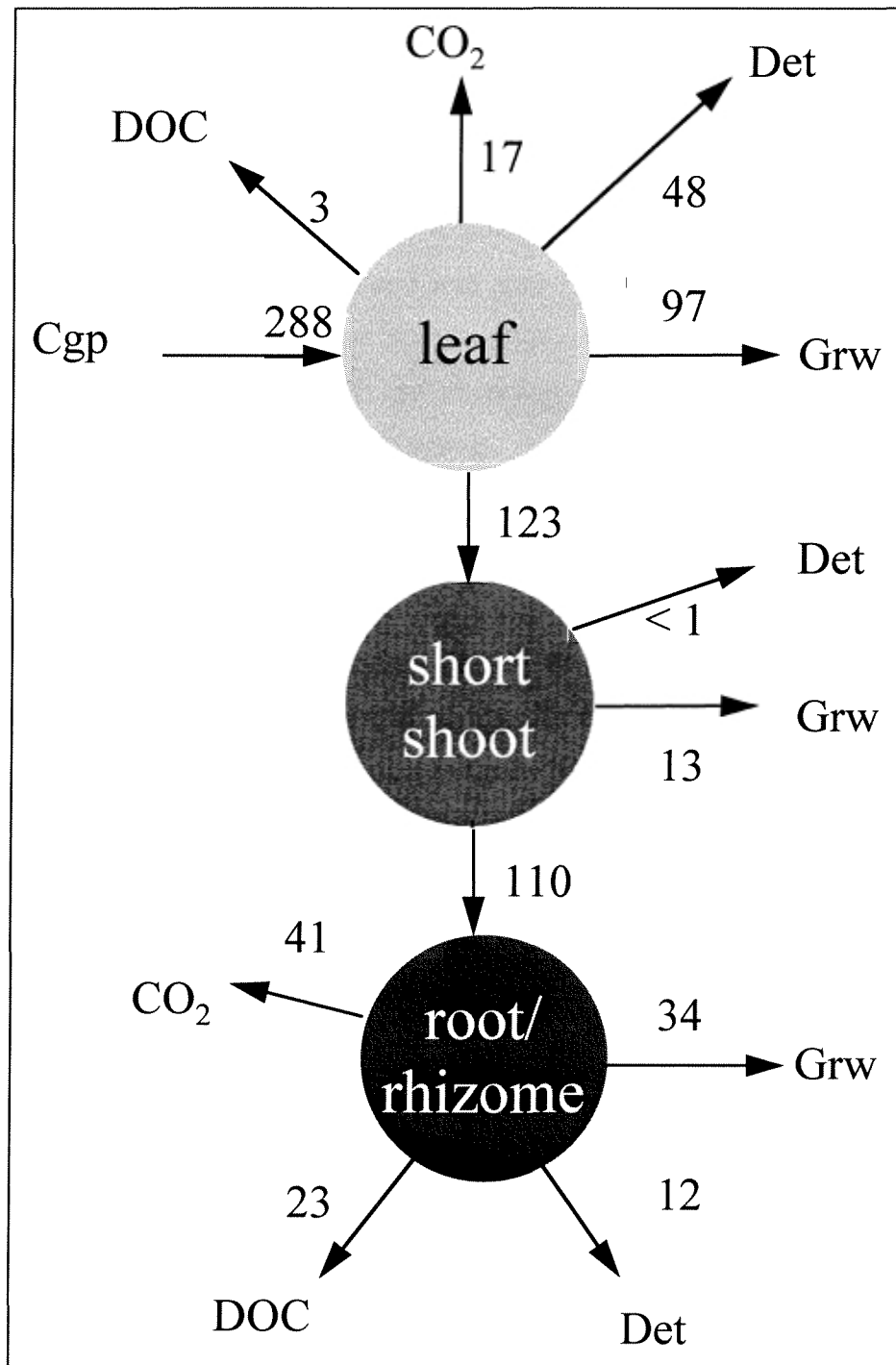


Figure 2. *Thalassia* flow diagram as in Figure 1, with transport expressed as percent of material entering each seagrass component— leaf, short shoot, and root/rhizome.

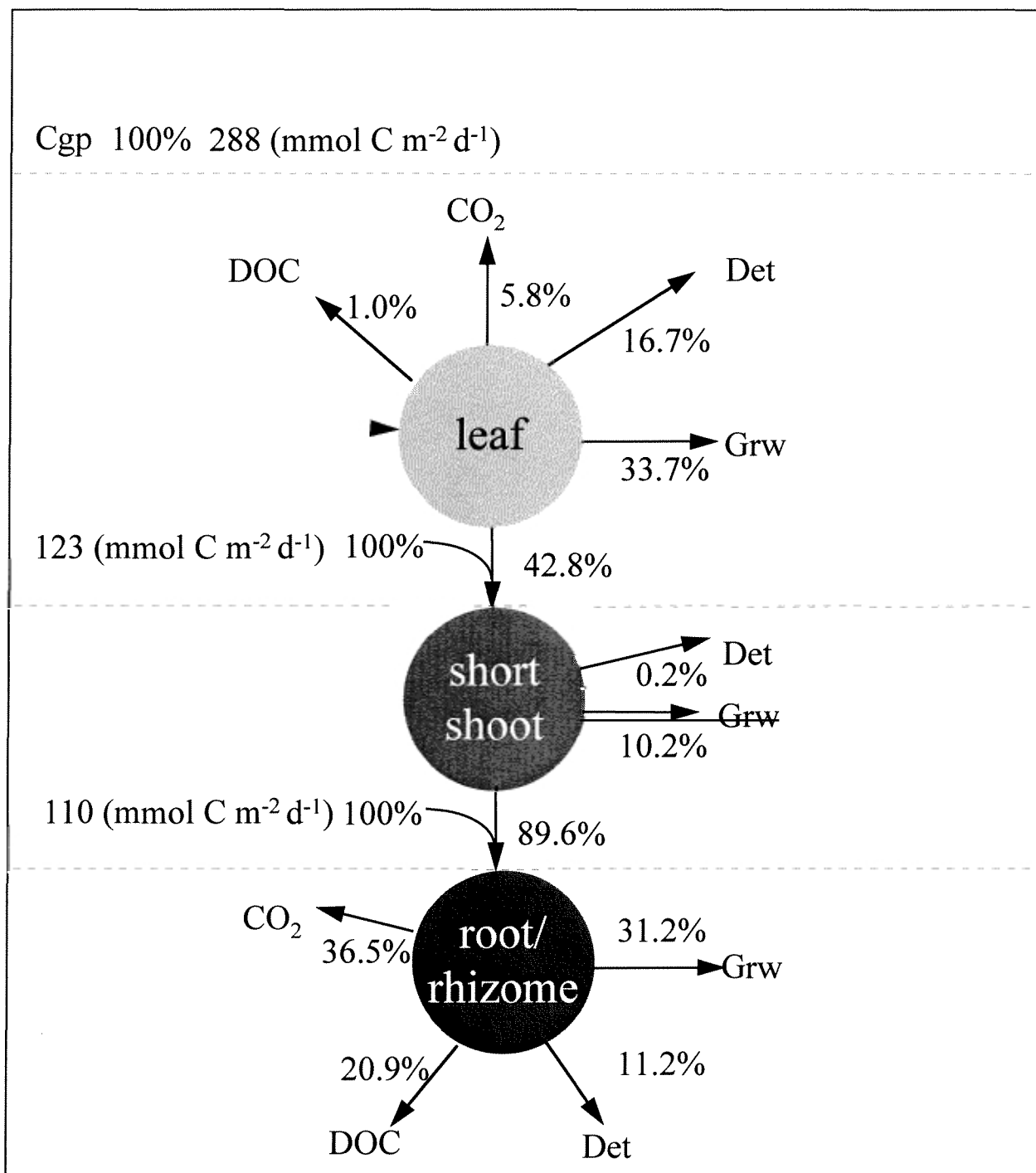
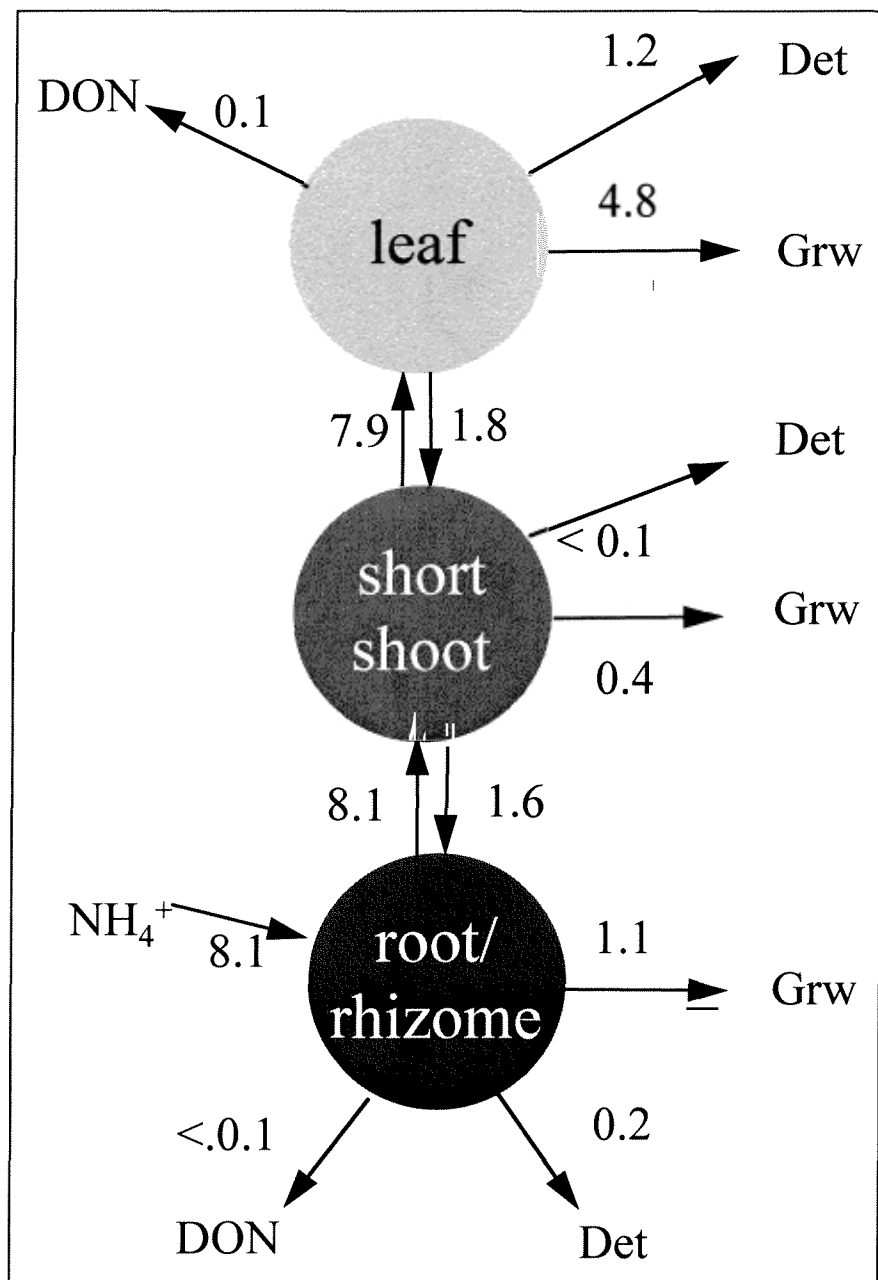


Figure 3. *Thalassia* nitrogen flow diagram. Same as Figure 1, except for nitrogen.



Only new leaf growth had a relatively low C:N ratio of 20 (Lee and Dunton 1999; Chapter VI). The high nitrogen content of new leaf material and limited role of dissolution during the aging of leaf material suggests that substantial amounts of nitrogen are re-allocated from old leaf material back to the plant.

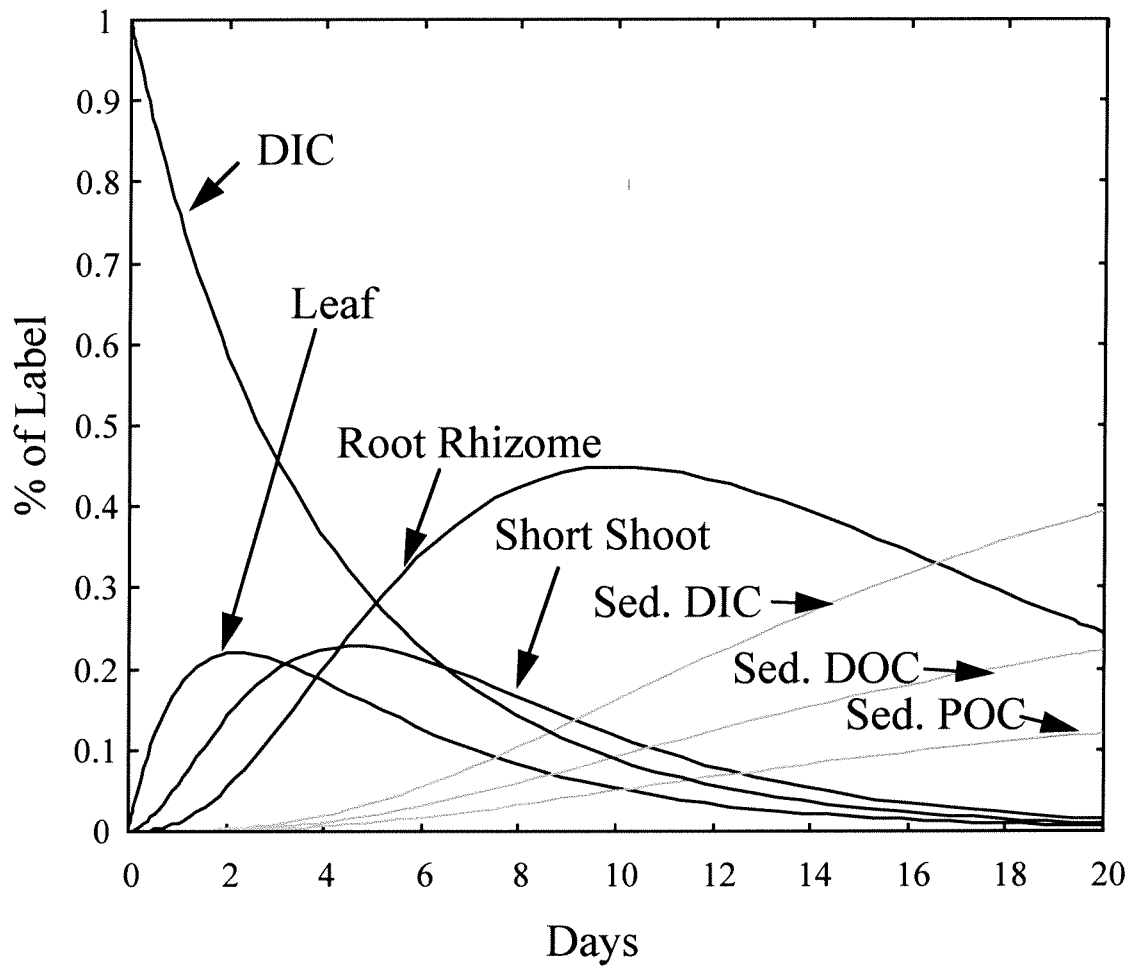
Tracer analysis.

Carbon tracer initially placed in the DIC pool within the incubation chamber moved rapidly into the seagrass leaf compartment reaching a maximum concentration in about 2 days (Fig. 4). Carbon flows from leaf to short shoot and then to short shoot and root/rhizome redistributed the C tracer so that maximum accumulations occurred in the short shoots in 4 days and in the root/rhizomes in about 10 days. The maximum concentration of tracer was greatest in the root/rhizome compartments because of its large size relative to other compartments.

Tracer accumulation in sediment DIC, DOC, and POC were not significant until day 5, low rates of detrital loss from the roots/rhizomes produced little tracer accumulation in the sediment POC pool. However substantial tracer was allocated to the sediment DIC and DOC pools. Since the model does not include microbial assimilation of the tracer, actual sediment POC accumulations would probably be larger than that predicted by the model.

The sum of all the tracers in the pools at the end of 20 days is about 80% (Fig 4). Losses of tracer occurred through leaf detritus for which we had no biomass measurements and hence could not include in the analysis.

Figure 4. Distribution of carbon tracer in the seagrass. One percent of the DIC pool is added as ^{13}C tracer. The model shows how a tracer would move through a seagrass plant. To fit the Wetzel and Penhale (1979) tracer results for *Thalassia*, we set the exchangeable pool to 5% of the total pools of leaf, short shoot, and root/rhizome. This assumes that seagrass like other grass species is composed of structural, storage, and soluble pools that exchange at different rates (Sheehy et al., 1996).



References Cited

- Carlson, P. R. Jr, L. A., Yarbrow, and T. R. Barber. 1992. Relationship of sediment sulfide to mortality of *Thalassia testudinum* in Florida Bay. SYMPOSIUM ON FLORIDA KEYS REGIONAL ECOSYSTEM. Bull. Mar. Sci. 54: 733-746,
- Dennison, W. C. 1987. Effects of light on seagrass photosynthesis, growth and depth distribution. Aquatic Botany 27: 15-26.
- Dennison, W. C. and R.S. Alberte. 1985. Role of daily light period in the depth distribution of *Zostera marina* (eelgrass). Marine Ecology Progress Series 25: 51-61.
- Dennison, W.C. and R.S. Alberte. 1986. Photoadaptation and growth of *Zostera marina* L. (eelgrass) transplants along a depth gradient. Journal Experimental Marine Biology Ecology 98: 265-282.
- Dunton, K. H. and D. A. Tomasko. 1994. *In situ* photosynthetic performance in the seagrass *Halodule wrightii* in a hypersaline subtropical lagoon. Mar. Ecol. Prog. Ser. 107: 281-293.
- Eldridge, P. M., and J. A. Jackson. 1993. Benthic trophic dynamics in California coastal basin and continental communities inferred using inverse analysis. Mar. Ecol. Prog. Ser. 99: 115-135.
- Fourqurean, J.W. and J.C. Zieman. 1991. Photosynthesis, respiration and whole plant carbon budget of the seagrass *Thalassia testudinum*. Marine Ecology Progress Series 69: 161-170.
- Haskell, K. H., Hanson, R. J. 1981. An algorithm for linear constrained least squares problems with equalities and nonnegativity constraints. Math. Program. 21: 98-118.
- Herzka, S.Z. and K.H. Dunton. 1997. Seasonal photosynthetic patterns of the seagrass *Thalassia testudinum* in the western Gulf of Mexico. Marine Ecology Progress Series 152: 103-117
- Herzka, S.Z. and K.H. Dunton. 1998. Light and carbon balance in the seagrass *Thalassia testudinum*: evaluation of current production models. Marine Biology. In press.
- Hoss, D.E. and G. W. Thayer. 1993. The importance of habitat to the early life history of estuarine dependent fishes. Am. Fish Soc. 14: 147-158.
- Jackson, J. A. and P. M. Eldridge. 1992. Foodweb analysis of a planktonic system off southern California. Prog. Oceanogr. 30: 223-251.
- Kaldy, J. 1997. Production dynamics, reproductive ecology and demography of *Thalassia testudinum* (Turtle Grass) from the Lower Laguna Madre, Texas. Dissertation. Submitted to the Faculty of the Graduate School of the University of Texas at Austin.
- Kaldy, J.E. and K.H. Dunton. *In press*. Above- and below-ground production, biomass and reproductive ecology of *Thalassia testudinum* (Turtle grass) in a subtropical coastal lagoon. Marine Ecology Progress Series.
- Kenworthy, W.J. and M.S. Fonseca. 1996. Light requirements of seagrasses *Halodule wrightii* and *Syringodium filiforme* derived from the relationship between diffuse light attenuation and maximum depth distribution. Estuaries 19: 740-750.
- Kuhn, W. A. 1992. Interacting effects of light and sediment sulfide on Eelgrass (*Zostera marina* L. : Growth. Thesis. Submitted to the Faculty of the Graduate School of the University of Maryland.
- Lee, K.S. and K.H. Dunton. 1996. Production and carbon reserve dynamics of the seagrass *Thalassia testudinum* in Corpus Christi Bay, Texas, USA. Marine Ecology Progress Series 143: 201-210.

- Lee, K.S. and K.H. Dunton. 1997. Effects of *in situ* light reduction on the maintenance, growth and partitioning of carbon resources in *Thalassia testudinum* Banks ex König. *Journal Experimental Marine Biology Ecology* 210: 53-73.
- Lee, K.S. and K.H. Dunton. 1999. Influence of sediment nitrogen-availability on carbon and nitrogen dynamics in the seagrass *Thalassia testudinum*. *Marine Biology* 134: 217-226.
- Onuf, C.P. 1996. Seagrass responses to long-term light reduction by brown tide in Upper Laguna Madre, Texas: distribution and biomass patterns. *Marine Ecology Progress Series* 138: 219-231.
- Opsahl, S. and R. Benner. 1993. Decomposition of senescent blades of the seagrass *Halodule wrightii* in a subtropical lagoon. *Marine Ecology Progress Series* 94: 191-205.
- Phillips, R.C. 1984. The ecology of eelgrass meadows in the Pacific Northwest: a community profile. US Fish Wildlife Service. FWS/OBS-84/24.
- Redfield, R.C. 1958. The biological control of chemical factors on the environment. *Am. Sci.* 46: 205-221.
- Rooker, J. R., G. J. Holt, and S. A. Holt. 1997. Condition of larval and juvenile Red Drum (*Sciaenops ocellatus*) from estuarine nursery Habitat. *Marine Biology*. 127 :387-394.
- Schlesinger, W.H. 1991. Biogeochemistry: an analysis of global change. Academic Press, San Diego.
- Sheehy, J.E., F. Gastal, T.L. Mitchell, J.L. Duran, G. Lemaire, F.I. Woodward. 1996. A nitrogen led model of grass growth. *Annals of Botany* 77: 165-177.
- Short, F.T. 1980. A simulation model of the seagrass production system. Pp. 277-295. *In*: R.C. Phillips and C.P. McRoy (eds.). Handbook of seagrass biology: an ecosystem perspective. Garland STPM Press, New York.
- Thayer, G.W., W.J. Kenworthy and M.S. Fonseca. 1984. The ecology of eelgrass meadows of the atlantic coast: a community profile. US Fish and Wildl. Serv. FWS/OBS-84/02.
- Wetzel, R. L. 1977. Carbon resources of a benthic salt marsh invertebrate *Nassarius obsoletus* (Mollusca: Nassariidae) *In*: Wiley. M (ed) *Estuarine processes*, Vol. 2. Academic press, New York, p. 293-308.
- Wetzel, R.L. and H.A. Neckles. 1986. A model of *Zostera marina* L. photosynthesis and growth: simulated effects of selected physical-chemical variables and biological interactions. *Aquatic Botany* 26: 307-323.
- Wetzel, R.L. and P. A. Penhale. 1979. Transport of carbon and excretion of dissolved organic carbon by leaves and roots/rhizomes in seagrasses and their epiphytes. *Aquatic Botany*. 6: 149-158.
- Vermaat. J. E., N. S. R. Agawin, C. M. Duarte, M. D. Fortes, N. Marba, J. S. Uri. 1995. Meadow maintenance, growth and production of a mixed Phillipine seagrass bed. *Mar. Ecol. Prog. Ser.* 124: 215-225.
- Vezina, A. F., Platt, T. 1988. Food web dynamics in the ocean. I. Best-estimates of flow networks using inverse methods. *Mar. Ecol. Prog. Ser.* 42: 269-287.
- Ziegler, S. and R. Benner. 1999. Dissolved organic carbon cycling in a subtropical seagrass-dominated lagoon. *Marine Ecology Progress Series* 180: 146-160.
- Zieman, J.C. 1982. The ecology of the seagrasses of South Florida: a community profile. U.S. Fish and Wildl. Serv., Office of Biol. Serv., Washington D.C. FWS/OBS-82/25. 158 pp.
- Zieman, J.C. and R.T. Zieman. 1989. The ecology of the seagrass meadows of the West coast of Florida: a community profile. U.S. Fish and Wildl. Serv. Biol. Rep. 85(7.25). 155 pp.

- Zimmerman, R.C., A. Cabello-Pasini, R.S. Alberte. 1994. Modelling daily production of aquatic macrophytes from irradiance measurements: a comparative analysis. *Marine Ecology Progress Series* 114: 185-196.
- Zimmerman, R.C., D.G. Kohrs, D.L. Stellar and R.S. Alberte. 1995. Carbon partitioning in eelgrass. *Plant physiology* 108: 1665-1671.

CHAPTER III: SEDIMENT GEOCHEMICAL MODEL

Contents

Abstract	3
Introduction	4
Methods	5
Reactions	5
Transport processes	9
Boundary conditions	15
Rootzone fluxes	15
Results and Discussion	16
Model simulations	20
Differences in seagrass sediment chemistry	23
Conclusions	25
References	30

Tables

Table 1. Solid and dissolved species	6
Table 2. Diagenetic reactions	7
Table 3. Rate equations used in the reaction scheme	9
Table 4. Reactions involving each model constituent	10
Table 5. Units for model parameters	12
Table 6. Root zone fluxes	17
Table 7. Conditions for sensitivity test	18
Table 8. Root mean square difference test of model accuracy	22

Figures

Figure 1. Sensitivity of model to changes in bioturbation and burial rate.....	21
Figure 2. <i>Syringodium filiformi</i> . site sediment geochemistry	26
Figure 3. <i>Thalassia testudium</i> . site sediment geochemistry.	27
Figure 4. <i>Halodule wrightii</i> site sediment geochemistry	28
Figure 5. Bare area sediment geochemistry	29

Abstract

The objective of this modeling effort was to better understand the dynamic relationship between seagrass beds and their sedimentary environment using a diagenetic model. The model was developed and optimized for sediments in the Laguna Madre, TX, which is one of the world's largest (~140 km long) negative estuaries with close to 85% of the basin floor covered with seagrass beds. Although high levels of organic matter decomposition occur in the near-surface sediments, the model was unable to produce enough metabolism to satisfy dissolved inorganic carbon (DIC) profiles from organic matter oxidation alone, suggesting the presence of an additional DIC source. Carbon isotope analyses of DIC verified that carbonate mineral dissolution contributes more than 50% of DIC added to porewaters during early diagenesis and is especially important below ~5 cm.

In comparison to unvegetated areas, a common characteristic of seagrass bed sediments was their low sulfide concentrations in the seagrass rootzone. Model simulations indicate that rootzone fluxes of O_2 are essential to maintaining non-toxic levels of sulfide and consequently promote healthy conditions for seagrass growth. Further, the model simulations suggest that the position of maximum organic matter metabolism relative to the position of the seagrass rootzone can be used to predict several properties of seagrass sediment geochemistry. These predictions include the comparative role of anaerobic and aerobic metabolism, the sulfide to ammonium ratio, and the presence or absences of sulfides in the rootzone.

In summary, the results of this model clearly demonstrate a dynamic interaction between seagrasses and diagenetic processes in the underlying sediments. The primary impact of these interactions is to lower sedimentary sulfide concentrations below toxic levels for seagrasses. Such interactions not only modify the sedimentary record but also play an important role influencing the health and productivity of seagrasses.

Introduction

Laguna Madre is one of the world's largest negative estuaries stretching close to 140 km from south of Corpus Christi, Texas, to near the U.S.-Mexican border. It is generally quite shallow (~1 m) with much (~85%) of the bottom covered with a variety of seagrass species growing on poorly sorted sandy sediments. The climate is subtropical with water temperatures commonly ranging from 10°C in the winter to over 30°C in the summer. Because seagrass beds are so plentiful, there is considerable potential for them to influence sediment geochemistry. The seagrass roots and rhizomes, provide nitrogen, phosphorus and other nutrients to the photosynthetic part of the plant while energy-rich organic material is returned below ground to sustain growth and metabolism.

Sediments can limit growth or inhibit seagrass colonization when they are depauperate in growth limiting nutrients, contain toxic materials, or have some physical property that slows growth. (Zimmerman *et al.*, 1987; Pulich, 1989). Both physical properties, such as consolidation and grain size, and chemical characteristics, including high concentrations of sulfides, ethanol, and metals, may lead to the degradation or stunted growth of seagrass beds (Carlson *et al.*, 1994; Pulich, 1989). In the Laguna Madre low porewater ammonium may also contribute to reduced production while in other areas of Laguna Madre ammonium may actually be high enough to reach toxic levels (Morse *et al.*, in prep.).

Conversely, seagrass have the potential to alter their sedimentary environment. For example, seagrass leaf detritus can enhance both the percent concentration and quality of organic matter in the sediments. The nitrogen content and increased lability of seagrass leaf detritus may stimulate ammonium production through metabolism of the organic matter. Some of this recycled ammonium then becomes available for seagrass growth (Zimmerman *et al.*, 1987). The seagrass can also pump photosynthetically produced O₂ through a transport structure (lacunae) that leads through the root system and into the sediments. This O₂ loading has the potential to re-oxidize sulfides and other porewater and solid constituents in the rootzone.

The goal of our geochemical modeling was to produce a quantitative description of the interactions between seagrasses and sediment geochemistry. This allows us to predict changes in sediment

chemical properties due to seagrass production and colonization, and the possible toxic effects of sediment sulfide and ammonia on the seagrass plants.

Methods

General

Data and observations of general geochemical relationships for sediments in Laguna Madre given in Morse *et al.* (Chapter VII) are used to parameterize our diagenetic model. The model uses a numerical simulation for vertical transport that borrows heavily from Boudreau's (1996) general diagenetic model, while the reactions involving particulate organic matter (POM) mineralization and generation are derived mostly from the Van Cappellen and Wang (1996) model. Our diagenetic model departs from these earlier models, which were primarily designed to address sedimentary processes in oceans, in its treatment of sediment interactions with a biotic component—the seagrass. This requires the linking of the Laguna Madre sedimentary environment to seagrass nutrient uptake, dissolved organic matter (DOM) release, and O₂ transport from the roots to the sediments. The model represents oxidation of POM and DOM as coupled reactions in successively deeper sedimentary layers to reduction by oxygen, nitrate, iron, and sulfate. Manganese was found in very low concentrations in Laguna Madre and therefore was not included in this analysis. The use of each oxidant within the model is predicated on the Gibb's free energy (ΔG) released by the organic matter (OM)-oxidant reaction. We are able to maintain these energy relationships by assuming that within each layer of the sediment, populations of bacteria will specialize in using specific oxidants while becoming inhibited by more energetic oxidants (Boudreau, 1996). These energy relationships and the specificity of bacteria make it possible to formulate a generalized and consistent set of equations, for each oxidant, that is valid for all sediment strata (Rabouille and Gaillard 1991; Dhakar and Burdige, 1996; Soetaert *et al.*, 1996; and Boudreau, 1997).

Reactions

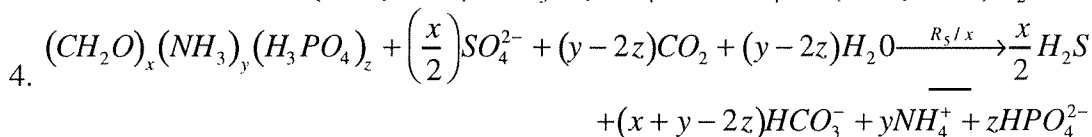
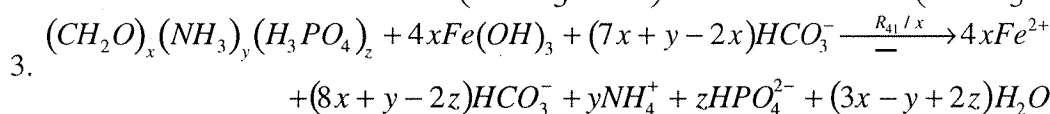
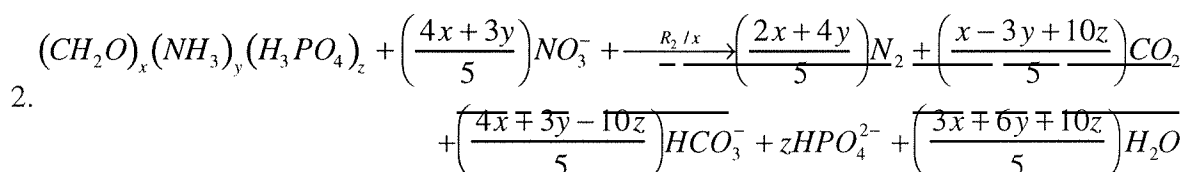
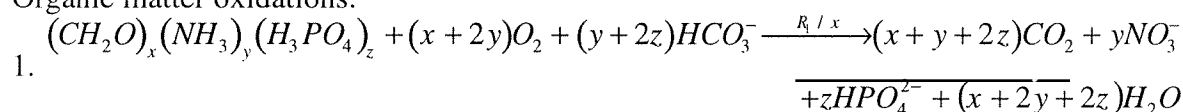
There are many pathways by which organic matter may be oxidized and the oxidation may form various organic intermediates (Lovley and Phillips, 1989; Kristensen and Blackburn, 1987; Postma and Jakobsen, 1996). To keep the analysis manageable, only one generalized biogenic reaction for

Table 1. Solid and dissolved species found in the sediment diagenesis model. The model assumes an oxidation state of zero for organic material. C:N:P of surface flux is that of seagrass above ground biomass. Rootzone flux C:N:P is that of the below ground biomass.

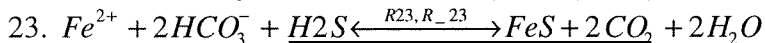
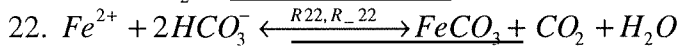
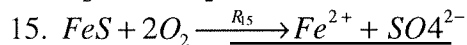
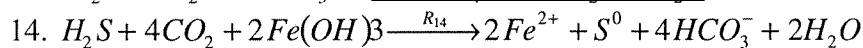
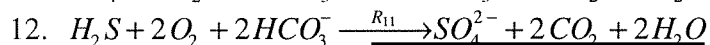
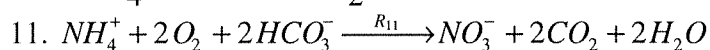
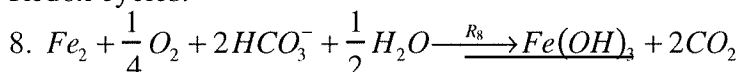
<u>Explicit species</u>		
OM1	labile organic matter	Solid
OM2	refractory organic matter	Solid
DOM	dissolved organic matter	Porewater
O ₂	oxygen	Porewater
NO ₃ ¹⁻	nitrate	Porewater
NH ₃	ammonia	Porewater
SO ₄ ²⁻	sulfate	Porewater
TS	total sulfides	Porewater
Fe(OH) ₃	amorphous	Solid
Fe ²⁺	ferrous	Porewater
FeS ₂	pyrite	Solid
DIC	dissolved inorganic carbon	Porewater
ALK	total alkalinity (treated as species)	Porewater
<u>Implicate (calculated) species</u>		
HS ⁻	sulfide species	Porewater
H ₂ S	sulfide species	Porewater
CO ₂ *	sum of hydrated and unhydrated carbonic acid	Porewater
HCO ₃ ⁻	bicarbonate	Porewater
CO ₃ ²⁻	carbonate	Porewater
ALK _c	carbonate alkalinity	Porewater
pH	—	Porewater

Table 2. Shows the diagenetic reactions simulated in the model. Equations 1 through 4 are replicated for refractory and labile organic matter. x, y, z are the component of oxidation contributed by CH₂O, NH₃, and H₃PO₄ respectively. Because we did not include all but reactions from Van Cappellen and Wang (1996) the numbers in table to are not sequential, but refer to the numbering scheme used by these authors).

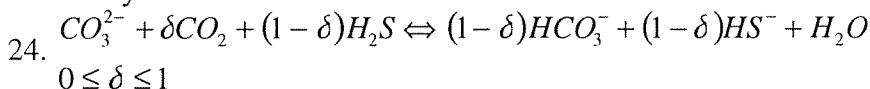
Organic matter oxidations:



Redox cycles:



Alkalinity:



each oxidant is included and we assume the reaction goes to completion (CO_2 and water). The relationships between growth and substrate concentration are implemented in this model using hyperbolic Monod relationships, while inhibition is modeled with a hyperbolic feedback (see equations 58 through 62 in Boudreau, 1996).

The sediment diagenetic model has 13 geochemical compartments covering solid and porewater organic and inorganic species that are important in the diagenesis of Laguna Madre sediments (Table 1). We also calculate the equilibrium distributions of solutes in aquatic carbonate solution and the equilibrium system for porewater sulfides. A simplified stoichiometry for the oxidation of OM is provided to reduce the number of species modeled, and the number of equations in the model (Table 2; EQ. 1-4). We also assume the organic matter species oxidation reactions are biologically mediated.

Once the reduced products are formed, they can become titrated through reactions with other constituents or transported by diffusion and bioturbation back into upper strata of the sediments to be used in a series of redox reactions (Table 2; EQ 8-15). We included most of the coupled redox reactions considered in other recent diagenetic models (Boudreau, 1996; Van Cappellen and Wang, 1996), but with a slightly different feedback for FeS production and loss (Table 3).

Among the numerous constituents modeled, H_2S and DIC are the most important because sulfide can be toxic to seagrass and DIC is an indicator of total carbon metabolism in sediments. DIC concentration is the consequence of equilibrium reactions (Table 4) and provides a “whole system” estimate of the model accuracy when results are compared to measurements. When DIC or alkalinity is not known, pH is also required for Table 2, EQ 1 to 4 (Morse and Mackenzie, 1990). The model uses the Whitfield and Turner (1986) relationship for salinity and temperature dependence of equilibrium constants and the Stumm and Morgan (1981) closed system ionization fractions to predict the distribution of solutes in aqueous carbonate solution. Data in this study (Chapter VII) included vertical profiles of pH, however, the model also has the capacity to model pH using formulations from Van Cappellen and Wang (1996).

Table 3. Rate equations used in the reaction scheme (Revised from Van Cappellen and Wang, 1996). TS= [H₂S] + [HS⁻]. Indexes on equation are the same as used by Van Cappellen and Wang 1996. N.A. indicates that the reaction referenced with the corresponding index in Van Cappellen and Wang 1996 was not used.

$R_1 = k_g rO_2$	$R_{10} = \text{N.A.}$	$R_{21} = \text{N.A.}$
$R_2 = k_g rNO_3$	$R_{11} = k_{11} [NH_4^+] [O_2]$	$R_{21} = \text{N.A.}$
$R_3 = \text{N.A.}$	$R_{12} = k_{12} \text{TS} [O_2]$	$R_{21} = \text{N.A.}$
$R_4 = k_g rFe$	$R_{13} = \text{N.A.}$	$R_{22} = \text{N.A.}$
$R_5 = k_g rSO_4$	$R_{14} = k_{14} \text{TS} [Fe(OH)_3]$	$R_{22} = \text{N.A.}$
$R_6 = \text{N.A.}$	$R_{15} = k_{15} [FeS] [O_2]$	$R_{23} = K_{23} \sigma_{23} (\Omega[FeS]-1)$
$R_7 = \text{N.A.}$	$R_{16} = \text{N.A.}$	$R_{23} = K_{23} \sigma_{23} [FeS] (1-\Omega_{FeS})$
$R_8 = k_8 [Fe^{2+}] [O_2]$	$R_{17} = \text{N.A.}$	
$R_9 = \text{N.A.}$	$R_{21} = \text{N.A.}$	

where:

$$\Omega_{FeS} = \frac{[Fe^{2+}][HS^-]}{[H^+] + K_{H^+}} K'_{FeS}$$

$$\Omega_{FeS} > 1: \delta_{23} = 1, \delta_{-23} = 0$$

$$\Omega_{FeS} \leq 1: \delta_{23} = 0, \delta_{-23} = 1$$

Transport processes

Solids (C_s , $\mu\text{mol cm}^{-3}$) and porewater (C_w , $\mu\text{mol cm}^{-3}$) constituents are subject to advective and diffusive transport within the sediments and at the sediment/water interface. Because of the different affects compaction, molecular diffusion, bioturbation, and irrigation have on solids and porewater constituents, they are transported within the sediments at different rates. Bioturbation and burial (ω) are the processes that displace solids within the sediment column. While the effect of burial is obvious, the transport by bioturbation is less clear. In this model, we assume that the displacement or disturbance caused by a single infaunal deposit feeder is small relative to the total bioturbation within the sediment column. Given this assumption Boudreau (1997) used

Table 4. Reactions involving each model constituent $\sum R_{C_r}(x)$ (revised from Van Cappellan and Wang 1996).

$$R_{OM} = -(R_1 + R_2 + R_3 + R_4 + R_5)$$

$$R_{O_2} = \frac{1-\phi}{\phi} \left(\frac{-x+2y}{x} R_1 - \frac{R_7}{2} - 2R_{15} \right) - \left(\frac{R_8}{4} + 2R_{12} \right)$$

$$R_{NO_3^-} = \frac{1-\phi}{\phi} \left(\frac{y}{x} R_1 - \frac{4x+3y}{5x} R_2 \right) + R_{11}$$

$$R_{Fe^{2+}} = \frac{1-\phi}{\phi} (4R_4 - 2R_{10} + R_{15} - R_{23} + R_{-23}) - R_8$$

$$R_{SO_4^{2-}} = \frac{1-\phi}{\phi} \left(-\frac{R_5}{2} \right) + R_{12} - R_{17}$$

$$R_{NH_4^+} = \frac{1-\phi}{\phi} \frac{y}{x} (R_3 + R_4 + R_5) - R_{11}$$

$$R_{Fe(OH)_3} = -4R_4 + \left(\frac{\phi}{1-\phi} \right) R_8 + 2R_{10} - 2R_{14}$$

$$R_{FeS} = -R_{15} + R_{23} - R_{-23}$$

$$R_{TC} = \frac{1-\phi}{\phi} (R_1 + R_2 + R_3 + R_4 + R_5)$$

$$R_{TS} = \frac{1-\phi}{\phi} \left(\frac{R_5}{2} - R_{13} - R_{14} - R_{23} + R_{-23} \right) - R_{12}$$

$$R_{ALK} = \frac{1-\phi}{\phi} \left(\begin{array}{l} -\frac{y+2z}{x} R_1 + \frac{4x+3y-10z}{5x} R_2 + \frac{4x+y-2z}{x} R_3 + \frac{8x+y-2z}{x} R_4 \\ \frac{x+y-2z}{x} R_5 - 2R_{10} + 2R_{13} + 4R_{14} - R_{23} + R_{-23} \\ -2R_8 - 2R_{11} - 2R_{12} \end{array} \right)$$

a Reynolds decomposition and time-averaging scheme to show that bioturbation transport can be modeled as a diffusion process (biodiffusion, D_b) (EQ 25).

$$\frac{\partial [C_s]}{\partial t} = \frac{1}{\phi_s} \frac{\partial}{\partial x} \left[\phi_s D_b \frac{\partial [C_s]}{\partial x} - \phi_s \omega [C_s] \right] + \sum R_{C_s}(x) \quad \text{EQ 25}$$

Profiles of porosity (ϕ) are used in the diagenetic equation to determine the rate of solid compaction with depth. In this analysis, we assume steady state compaction (EQ 26) to simplify both the parameterization of ω and porewater velocity (v), and to reduce the number of derivatives that need to be calculated (Berner, 1980).

$$\frac{\partial((1-\phi_w)\omega)}{\partial x} = \frac{\partial(\phi_w v)}{\partial x} = 0 \quad \text{EQ 26}$$

Conversion of organic and inorganic solids occurs through the reactions ($\sum R_{C_s}(x)$) (Table 4). The equations in table 4 includes conversion between solids and porewater units where needed. Expansion and simplification based on steady-state compaction results in an equation that can be converted to a finite difference and solved numerically (EQ 27).

$$\frac{\partial [C_s]}{\partial t} = D_b \frac{\partial^2 [C_s]}{\partial x^2} + \frac{1}{\phi_s} \left[\left(\frac{\partial \phi_s}{\partial x} D_b + \phi_s \frac{\partial D_b}{\partial x} - \phi_s \omega \right) \frac{\partial [C_s]}{\partial x} \right] + \sum R_{C_s} \quad \text{EQ 27}$$

The porewater transport equation, although similar to that used for solids, has the added complexity of molecular diffusion (D_w), tortuosity (θ^2), and irrigation (α). Molecular diffusion is constant over depth and is calculated for all constituents, except DOM, using the subroutine DIFCOEF provided by Boudreau (1996). This subroutine uses the Stokes-Einstein relationship and other data (see Boudreau, 1996) to estimate “free-solution” molecular/ionic diffusion (D_w) from salinity, temperature and pressure. DOM has a spectrum of molecular weights which varies

Table 5. Model parameters.

Description	Symbol	Units
Biodiffusion or mixing coefficient	D_b	$\frac{cm^2}{y}$
Velocity of porewater burial	v	$\frac{cm}{y}$
Velocity of solid particle burial	ω	$\frac{cm}{y}$
Porosity	ϕ	$\frac{cm_w^3}{cm_b^3}$
Porewater irrigation constant (nonlocal)	$\alpha(x)$	y^{-1}
Tortuosity	θ	dimensionless
Density	ρ	$\frac{g}{cm_s^3}$
Generic solid concentration	C_s	$\frac{\mu mol}{cm_s^3}$
Generic porewater concentration	C_w	$\frac{\mu mol}{cm_w^3}$
Rate constant	k	y^{-1}

temporally and spatially within Laguna Madre (Opsahl and Benner, 1993). The DOM solution free diffusion coefficient can only be estimated from first principles when we know the size and shape of all the molecules that compose it (Berg, 1983). Given the heterogeneity of the DOM, a first principle estimate is not possible and an experimental estimate would not be meaningful on the scale of the Lagoon. The Einstein-Smoluchowski equation shows an inverse relationship between the free-solution diffusion rate and molecular weight. Because of the generally high molecular weight of DOM, we picked a low diffusion rate for DOM (1/2 that of sulfide) and ran simulations that encompassed 1 order of magnitude below this diffusion rate. The normalized root-mean square difference (i.e., S.D.(prediction – field data)/ mean(field data)) varied among

these test cases from 0.34 to 0.48 with virtually no change in the normalized root-mean square difference (NRMSD) in any of the other porewater or solid species. Further, simulations showed that the high porewater irrigation rates in Laguna Madre effected the DOM concentration profile more than diffusion, causing the model to be robust against changes in the DOM diffusion rate. We do not expect that diagenetic models will be robust against changes in DOM diffusion rate in other coastal ocean sites where irrigation or advection are not dominate transport processes.

We include both biodiffusion and molecular diffusion in the porewater diagenetic equation. This is not necessary in most coastal or ocean sediments where biodiffusion rates are low, however in estuaries biodiffusion coefficients can be similar in magnitude to molecular diffusion (Berner, 1980). Tortuosity, however, is only applied to the free-solution molecular diffusion coefficient since interface mixing through biodiffusion (Boudreau, 1997) does not increase the distance a molecule or ion must travel relative to the free-solution diffusion rate. Tortuosity is calculated using the modified Weissberg relationship $\theta^2 = 1 - b \ln(\phi)$. The molecular diffusion rates in the diagenetic equation are constant over depth, while the other parameters change with depth, requiring additional derivatives in the transport equation (EQ 28).

Irrigation in this analysis is assumed to occur through non-local exchange with the water-column or exchange with a benthic boundary layer composed of unconsolidated seagrass leaf litter. Irrigation is therefore a function of the difference between these concentrations and the actual concentration of each constituent in the sediment profile (Emerson et al, 1984; Boudreau, 1984; and Boudreau, 1997) (e.g. third term RHS, EQ 28). Again the reaction $\sum R_{C_w}$ unit conversions for solids and porewater constituents are shown in table 4. The positive sign on the reaction term signifies that the reactions proceed according to the equations in Table 4. The last term on the RHS of EQ 28 ($\sum RF_{C_w}$) are the fluxes of O_2 , DOM, NH_4^+ , and NO_3^- between sediment and the seagrass roots.

$$\frac{d[C_w]}{dt} = \frac{1}{\phi} \frac{\partial}{\partial x} \left[\phi \left(D_b + \frac{D_w}{\theta^2} \right) \frac{d[C_w]}{dx} - \phi v [C_w] \right] + \alpha(x) ([C_w]_0 - [C_w]_x) + \sum R_{C_w} + \sum RF_{C_w} \quad \text{EQ 28}$$

Once again expansion of the equation and simplification based on steady state compaction provides an equation that can be formulated into a finite difference scheme. This process reduces the total number of calculations in the model (EQ 29). Units of the parameters in EQ 25 through 29 are shown in Table 5.

$$\begin{aligned} \frac{d[C_w]}{dt} = & \left(D_b + \frac{D_w}{\theta^2} \right) \frac{\partial^2 [C_w]}{\partial x^2} \\ & + \frac{1}{\phi} \left[\frac{1}{(\theta^2)^2} \left(\theta^2 \frac{\partial \phi}{\partial x} - \phi \frac{\partial (\theta^2)}{\partial x} \right) + D_b \frac{\partial \phi}{\partial x} + \phi \frac{\partial D_b}{\partial x} - \phi v \right] \frac{d[C_w]}{dx} \quad \text{EQ 29} \\ & + \alpha(x) \left([C_w]_0 - [C_w]_x \right) + \sum R_{C_w} + \sum RF_{C_w} \end{aligned}$$

We used a simple linear relationship for $D_b(x)$ (EQ 30) and its derivative (EQ 31) (Boudreau, 1997),

$$\begin{aligned} x < x_1 & \quad D_b(x) = D_b(0), \\ x \geq x_1 \geq x_2 & \quad D_b(x) = D_b(0) \frac{(x_2 - x)}{(x_2 - x_1)}, \\ x > x_2 & \quad D_b(x) = 0. \end{aligned} \quad \text{EQ 30}$$

Here, we assume the derivative of bioturbation ($DD_b(x)$) is zero to depth x_1 and is constant to x_2 (see Boudreau, 1997)

$$\begin{aligned} x < x_1 & \quad DD_b(x) = 0., \\ x \geq x_1 \geq x_2 & \quad DD_b(x) = -\frac{D_b(0)}{(x_2 - x_1)}, \\ x > x_2 & \quad D_b(x) = 0. \end{aligned} \quad \text{EQ 31}$$

Boundary conditions

At the sediment-water interface, two types of boundary conditions are defined, a flux condition for OM and a concentration boundary for all other constituents. The model incorporates options for switching between concentration and flux boundaries depending on the data available. The flux boundary (FC_s) has the form (EQ 32):

$$-\varphi D_b(0) \frac{d[C_s]}{dx} + \varphi \alpha(0) [C_s] = FC_s \quad \text{EQ 32}$$

while the other constituents are set to a known interface (C_{io}) concentration (EQ 33)

$$C(0) = C_{io} \quad \text{EQ 33}$$

For all constituents the bottom boundary condition assumes that the diffusive flux has diminished to zero (no gradients) (EQ 34),

$$\frac{d[C_i]}{dx} = 0, \quad \text{EQ 34}$$

where i is a solid or pore-water constituent (Boudreau, 1996). An alternative option for this bottom condition is a concentration boundary similar to EQ 33 when there is sufficient data available.

Rootzone fluxes

Below ground seagrass release of O_2 , and dissolved organic material (DOM) are dispersed through molecular diffusion in the rootzone according to a Gaussian probability distribution (Berg, 1983) (EQ 35),

$$P(J, \mu, \sigma) = \frac{1}{2\pi\sigma^2} e^{-\frac{(j-\mu)^2}{2\sigma^2}}; (1 \geq x \geq np), \quad \text{EQ 35}$$

where j is the index for each gridpoint, np is the number of gridpoints, μ is the gridpoint in the center of the rootzone and 2σ dictates the number of gridpoints over which the flux occurs. In turn, the flux at each grid point is shown by EQ 36:

$$RF_{C_w}(x)_i = \frac{P(i, \mu, \sigma) F_T}{\Delta x}, \quad \text{EQ 36}$$

where F_T is the total flux, i are the constituents transported via the root system, and Δx is the length between each gridpoint. Berg (1983) has shown that the Gaussian distribution is the most accurate probability distribution for diffusion of large numbers of small molecules from a single source such as the rootzone of a seagrass plant. With this probability model the user can input any rootzone depth or width that is consistent with the total depth of the analysis.

Model Results and Discussion

Our goal is to determine how seagrass, through root-zone fluxes and leaf detrital formation, modify geochemical sediment profiles. As discussed in the methods, the model simulates exchange between the seagrass rootzone and sediments. Comparing the model results with the actual sediment chemical profiles provides an assessment of the seagrass interaction with sediment geochemistry. Removal of the seagrass model flux in some treatments of the model then provides a means to quantify how the seagrasses modify sediment chemistry.

Vertical sediment geochemical profiles were collected by Morse *et al.*, (Chapter VII.) in 2.0 cm increments in *Syringodium filiformi*, *Thalassia testudinum* and *Halodule wrightii* seagrass beds and in adjacent bare areas in Laguna Madre for comparison with the model results. Although, seagrass rootzone fluxes are estimated by adjusting these fluxes in model sensitivity tests, we still required an initial set of root-zone fluxes for each seagrass species. Demographic studies (Kaldy and Dunton, in press) and production studies (Herzka, and Dunton, 1997; Lee et al., 1997) were used in an optimization model (Chapter II) to estimate these fluxes for *Thalassia testudinum*. There are no similar demographic studies for *Halodule wrightii* or *Syringodium filiformi* in Laguna Madre,

Table 6. Rootzone fluxes ($\text{mmol m}^{-2} \text{d}^{-1}$) as estimated from the inverse analysis (Chapter 2). Case 2 and 3 scenarios provide 1/2 and the full rootzone fluxes estimates.

Species	O ₂	DOM	POC	DIC	NH ₄ ⁺
<i>Halodule</i>	288	35	48	41	8.0
<i>Thalassia</i>	288‡	35§	48§	41§	5.0†
<i>Syringodium</i>	260	35	48	41	12

† Rootzone uptake from Kuo Su Lee as $\mu\text{mol -N g}^{-1} \text{dry-wt}^{-1} \text{h}^{-1}$ (per comm, 1998)

‡ Summer *Thalassia* production predicted from inverse modelling (Chapter 2).

§ Predicted carbon allocation estimates of carbon release from inverse modeling (Eldridge and Kaldy, in prep.).

although photosynthetic, production, and respiration rates (Dunton and Tomasko, 1994; Tomasko and Dunton, 1995) are available. Summer *Halodule* photosynthesis was 100-400 $\text{mmol C m}^{-2} \text{d}^{-1}$ (Tomasko and Dunton, 1995) which is similar to the 288 $\text{mmol C m}^{-2} \text{d}^{-1}$ estimated by the optimization technique for summer *Thalassia* photosynthesis (sediment geochemistry sampling was in June). Similarly, *Halodule* respiration bracketed the *Thalassia* inverse model estimate of respiration (Dunton and Tomasko, 1994). *Syringodium* photosynthesis and respiration also appear to be similar (Nojima and Mukai, 1996). Thus, in our simulations we used the same root fluxes for *Halodule*, *Thalassia*, and *Syringodium* (Table 6), but varied O₂ flux to the rootzone as a percent of primary production (Fig. 2-4). The model was run to a steady state and the results were compared to the collected data.

A number of free parameters were then adjusted to match observed profiles for each seagrass species (Table 7). Two important parameters that were examined over a range of “reasonable” values for a coastal system were the sedimentation and bioturbation rates. These rates cannot be reasonably measured due to the dynamic conditions that prevail in shallow lagoons (e.g., storms and hurricanes) that result in movement and resuspension of sediments. Over 400 model runs were

Table 7. Conditions for sensitivity test. Three conditions are tested including no flux and 2 flux rates from the rootzone ($\text{mmol C m}^{-2} \text{d}^{-1}$). Parameters with the same value as in the column to the left are given an *.

Type	Parameter	<i>Halodule</i>	<i>Syringodium</i>	<i>Thalassia</i>	<i>Bare</i>	
Physical	Temperature	30.0	*	*	*	
	Pressure	35.0	*	*	*	
	Surface pH	7.9	*	*	*	
	Surface D_b ($\text{cm}^3 \text{yr}^{-1}$)	5.0	*	*	*	
	Depth D_b starts to decrease (cm)	5.0	*	*	*	
	Depth D_b goes to zero (cm)	9.0	*	*	*	
	sediment advection rate (cm yr^{-1})	0.20	*	*	*	
	Coef. of irrigation	85.0	200	*	*	
	Depth of irrigation	12.0	*	*	7	
	Porosity -surface	0.80	0.60*	0.80	.7	
	Porosity -asyptotic	0.50	*.53	0.50	*	
	Porosity exponential coef. (see text)	0.15	*	*	*	
	Max Depth of simulation (cm)	12.0	*	*	*	
	Mean depth of rootzone	4.0	3.5	*	-	
	Width of rootzone	2.5	3.5	*	-	
	boundary	Sediment Organic Flux - labile	18.6	8.8	8.2	1.4
	conditions	Sediment Organic Flux – refractory	6.8	8.9	24.7	22.6
DOM mM		20.0	38	36	6.0	

Table 7 continued

Type	Parameter	<i>Halodule</i>	<i>Syringodium</i>	<i>Thalassia</i>	<i>Bare</i>
	DOM advected by irrigators mM	5.0	65	50.0	2.0
	O ₂ μM	270.0	250	200	*
	NO ₃ ⁻ μM	4.0	*	*	*
	NH ₄ ⁺ μM	40.0	100	*	*
	SO ₄ ²⁻ mM	29.0	*	*	34.0
	H ₂ S μM	2.0	*	*	10.0
	Fe ³⁺ (Solid) mM kg ⁻¹	5.0	*	*	1.0
	Fe ²⁺ μM	1.0	*	*	*
	FeS (Solid) mM/kg	9.5		*	25.0
	DIC mM	2.8	2.6	3.6	2.0
Rate constants	Organic material-labile yr ⁻¹	15.5	8.5	6.5	6.5*
	Organic material-refractory yr ⁻¹	0.15	0.06	0.10	.30
	DOM yr ⁻¹	0.25	6.0	4.0	4.0
	Dissolution rate	0.15	*	*	*
	k ₈	8.0E6	*	*	*
	k ₁₁	3.0E3	*	*	*
	k ₁₂	2.6E8	*	*	*
	k ₁₄	8.0E3	*	*	*
	k ₁₅	3.0E3	*	*	*
	k ₂₃	2.0E3	*	*	*
	k ₋₂₃	1.0E-4	*	*	*

Table 7 continued

Type	Parameter	<i>Halodule</i>	<i>Syringodium</i>	<i>Thalassia</i>	<i>Bare</i>
Monod constants	KO ₂ μM	4.0	*	*	*
	KNO ₃ ⁻ μM	10.0	*	*	*
	KSO ₄ ⁻ μM	85.0	*	*	*
	KFe ³⁺ μM	100.0	*	*	*
Conditional Equation	FeS	6.3E3	*	*	*
C:N:P (atom)	Organic material-labile	105: 12: 0.2	105: 6: 0.2	105: 9 : 0.2	*
	Organic material-refractory	105: 4 : 0.1	105: 6 : 0.1	105 : 8 : 0.1	*
	DOM	105 : 3 : 0.1	105 : 3 : 0.1	105 : 3 : 0.1	*

made using a combination of sedimentation rates from 0.05 to 0.5 cm yr⁻¹ and bioturbation rates of 5 to 100 cm² yr⁻¹. Results indicated that model agreement with maximum DIC and H₂S concentrations was relatively insensitive to bioturbation rates and agreed best with intermediate values for sedimentation rates (Fig 1). Values of 0.2 cm yr⁻¹ and of 5 cm² yr⁻¹ were used respectively for sedimentation and bioturbation rates in subsequent model runs.

Model simulations

For each seagrass species we developed three simulations: 1) a simulation with no rootzone fluxes, 2) a simulation with one half the estimated rootzone flux, and 3) a simulation with the full rootzone flux. Results of the simulations when no root flux occurred (Fig. 2-4, case 1) were consistent with what one might expect in coastal sediments (see Berner, 1980). The modeled [O₂] did not penetrate more than a few millimeters beyond the sediment/water interface (unpublished microelectrode measurements, Joye per. comm.) and POM had a continuously decreasing trend (Fig. 2-4). [H₂S] increases sharply with depth (~4 cm) and was well in excess of all seagrass rootzone data while [DIC] was increasingly underestimated with depth by the model.

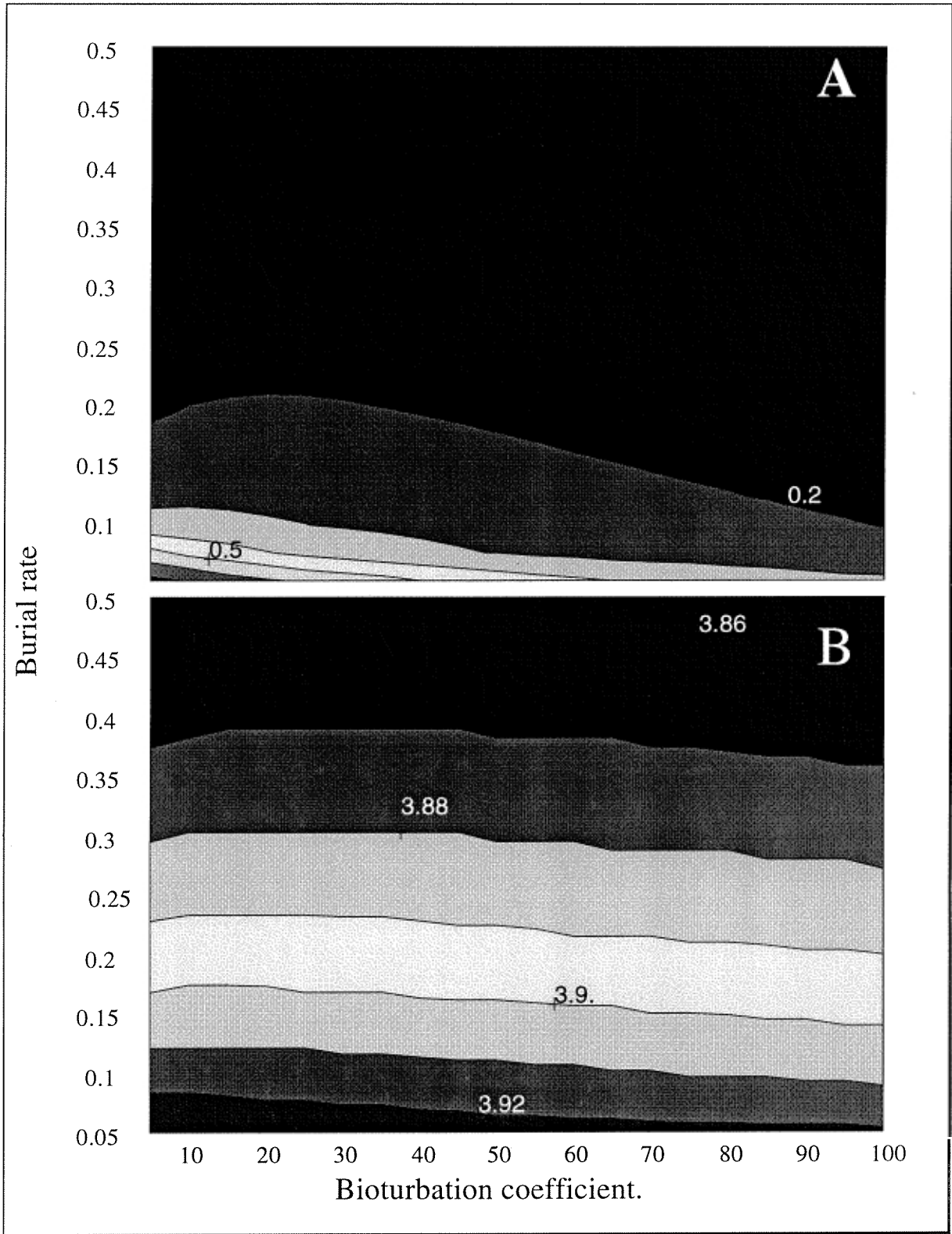


Figure 1. Sensitivity of model A) porewater sulfide concentration (μM), and B) DIC concentration (mM) to changes in bioturbation and burial rate (see table 5 for units).

Table 8. Normalized root mean squared differences between model predictions and field data.

Species	No rootzone flux		One-half estimated rootzone flux		Estimated rootzone flux	
	H ₂ S	DIC	H ₂ S	DIC	H ₂ S	DIC
<i>Halodule</i>	0.77	0.11	0.66	0.10	0.66	0.09
<i>Thalassia</i>	1.11	0.18	0.15	0.14	0.11	0.14
<i>Syringodium</i>	0.95	0.28	0.52	0.14	0.08	0.08

When the rootzone fluxes were applied (Fig. 2-4, case 2 and 3), the model was still unable to provide reaction rates sufficient to support the measured DIC concentration profile without producing unrealistically high H₂S concentrations. In order to overcome these difficulties, it was necessary to have both a means of oxidizing porewater H₂S and supplying DIC from a source other than organic matter oxidation. The second major source for DIC was demonstrated to be carbonate mineral dissolution, based on $\delta^{13}\text{C}$ values of porewater DIC (see Chapter VII, for discussion). Results indicate that well over half the DIC added to the porewaters is coming from carbonate mineral dissolution and that below about 6 cm depth close to all additional DIC comes from carbonate mineral dissolution. With the additional processes of carbonate mineral dissolution and rootzone flux, the model calculated maximal reaction rates in the top few centimeters of the *Thalassia* and *Halodule* analyses which resulted in dramatic changes in [DIC], [NH₄⁺], and [H₂S] in these simulations (Fig. 3-4). Surficial reaction rates (top 2 cm of sediment) were also high in the *Syringodium* simulation, although even higher reaction rates due to labile DOM in the rootzone complicated this analysis (Fig 2).

We used the root mean squared difference between the model results and a cubic spline interpolation of the field data to estimate the error in the simulation fit to the field data. This quantity was then normalized by the larger of the average value of the data or model predictions. This kept the normalized error from going to infinity when the field data or model results approached zero. The normalized root mean squared difference (NRMSD) of the *Thalassia* and

Syringodium model fit the measured H₂S and DIC data better when rootzone fluxes were applied (Table 8). Other than DIC, NH₄⁺ and H₂S, the model constituents were insensitive to rootzone fluxes (Fig 2-4) and generally fit the trends in observed data.

The NRMSD for the model validation runs (Chapter V) were actually better than that obtained during the analysis presented here. The validation model is a time dependent analysis for which the seagrass model (see Chapter I) is linked to the sediment diagenetic model (this Chapter). While the model parameters in our sensitivity test were adjusted to provide the best fit between the model and the data, the model validation required that the model parameters not be changed – only the initial conditions of the model could be changed to fit the dredge site conditions. Even though the validation model parameters were fixed, the NRMSD was between 10 to 30 percent more accurate than the steady state model presented in this chapter. The model presented here assumes that sediment processes are constant with time (i.e., steady state), while the linked model (see Chapter V) varies root zone input in response to seasonal changes in seagrass productivity. The comparison of NRMSD suggests that the coupling of the seagrass model to the sediment model significantly increases the accuracy of the sediment model.

Differences in seagrass sediment chemistry

The interaction between rootzone fluxes and [H₂S], and [DIC] profiles in all the seagrass species was sensitive to the relative position of rootzone and the depth of maximum metabolism in the sediments. In the *Syringodium* simulation the two zones coincided (Fig. 2). In this simulation, irrigation transported labile DOM from the benthic boundary layer directly into the rootzone, resulting in rootzone metabolic rates that exceeded the surficial metabolism by ~20%. Although there was no O₂ in the sediments below the first centimeter in any test cases (Fig. 2), simulations with rootzone O₂ fluxes (cases 2 and 3) had a larger percentage of the organic matter entering the aerobic metabolic pathways (47% for case 1, 62% for cases 2, and 91% for case 3). The result was a clear separation in [H₂S] and [DIC] sediment profiles for each rootzone flux case (Fig. 2) with up a 150 μM difference in [H₂S] between the simulation with and without seagrass root-zone fluxes.

In the *Thalassia* simulation, the surficial sediment metabolism exceeded the rootzone metabolism by 43% percent. Again the O₂ rootzone flux provided an oxidant for the more muted rootzone metabolism, thereby maintaining a low sulfide to NH₄⁺ ratio in test cases 2 and 3. However the difference in position of major sites of metabolism, the surficial sediments and the rootzone, reduced the impact of the rootzone fluxes on metabolism. Hence, the [DIC] concentration profiles were indistinguishable in all the *Thalassia* simulations (Fig. 3).

Finally, in the *Halodule* simulation nearly all (84 %) of the carbon metabolism occurred within the surficial sediments (0-2 cm). The separation between the depth zone where metabolism dominated and where the rootzone fluxes occurred was sufficient to uncouple sediment metabolism from rootzone dynamics (Fig. 3). The [DIC] or [H₂S] porewater profiles for all cases (with and without rootzone fluxes) were therefore the same. The high rates of surficial metabolism (more than twice that of *Syringodium* or *Thalassia*) resulted in very sharp gradients in [DIC] and [H₂S] and a clear separation in modeled [DIC] profiles with and without carbonate dissolution (Fig. 4).

The POC in the bare area simulation was less reactive than in the seagrass beds (Fig. 5). Our simulation for the bare area (Table 7) essentially used a single intermediately reactive POM component. This contrasts with the seagrass sediments where model results suggest that there was substantial input of labile POM (Table 7). The initial decomposition rates of seagrass is rapid (Opsahl and Benner, 1993) and export rates from seagrass beds are low (Stapel et al., 1996), suggesting that much of the litter production is used within the seagrass bed and not exported to adjacent bare areas. The lower reactivity of bare area POM is consistent with this description if only seagrasses are considered. However, the gross primary production (GPP) of benthic microalgae in bare areas is about one-half the seagrass production (Ziegler and Benner, 1999).

Microalgae biomass incorporated into the sediments might have provided a labile POM component that the model was unable to account for either due to the resolution of the model and data, or because benthic microalgae was consumed before diagenetic decomposition occurred. The model results suggest that there was a source of labile DOM in the sediments that might have its origin in

microalgae biomass, either through cell lysis or sloppy feeding by consumer organisms. Microalgae has less structural material than seagrass and DOM derived from microalgae is quite reactive (Aminot et al., 1990)

Conclusion

The model simulations indicate that rootzone fluxes of O₂ are essential to maintaining non-toxic levels of sulfide (<200 μM) in *Thalassia* and *Syringodium* seagrass beds in Laguna Madre. *Halodule* rootzone fluxes in these simulations were less effective in reducing sediment sulfide concentrations. Toxic concentrations of sulfide (Pulich, 1989) and ammonium are only likely to occur when O₂ transport to the rootzone is reduced by low rates of photosynthesis. Rootzone geochemical fluxes generally have little effect on sediment diagenesis other than to reduce the sulfide concentrations and alter DIC porewater profiles. Carbonate mineral dissolution is a major contributor to DIC in these sediments, and has generally not been considered in previous models for early diagenesis in siliciclastic sediments

Our model simulations suggest that knowledge of the depth and rate of maximum organic matter metabolism and the depth of the seagrass rootzone can be used to predict several features of seagrass habitat sediment geochemistry. These features include the relative role of anaerobic and aerobic metabolism, the sulfide to ammonium ratio and the presence or absence of sulfides in the rootzone.

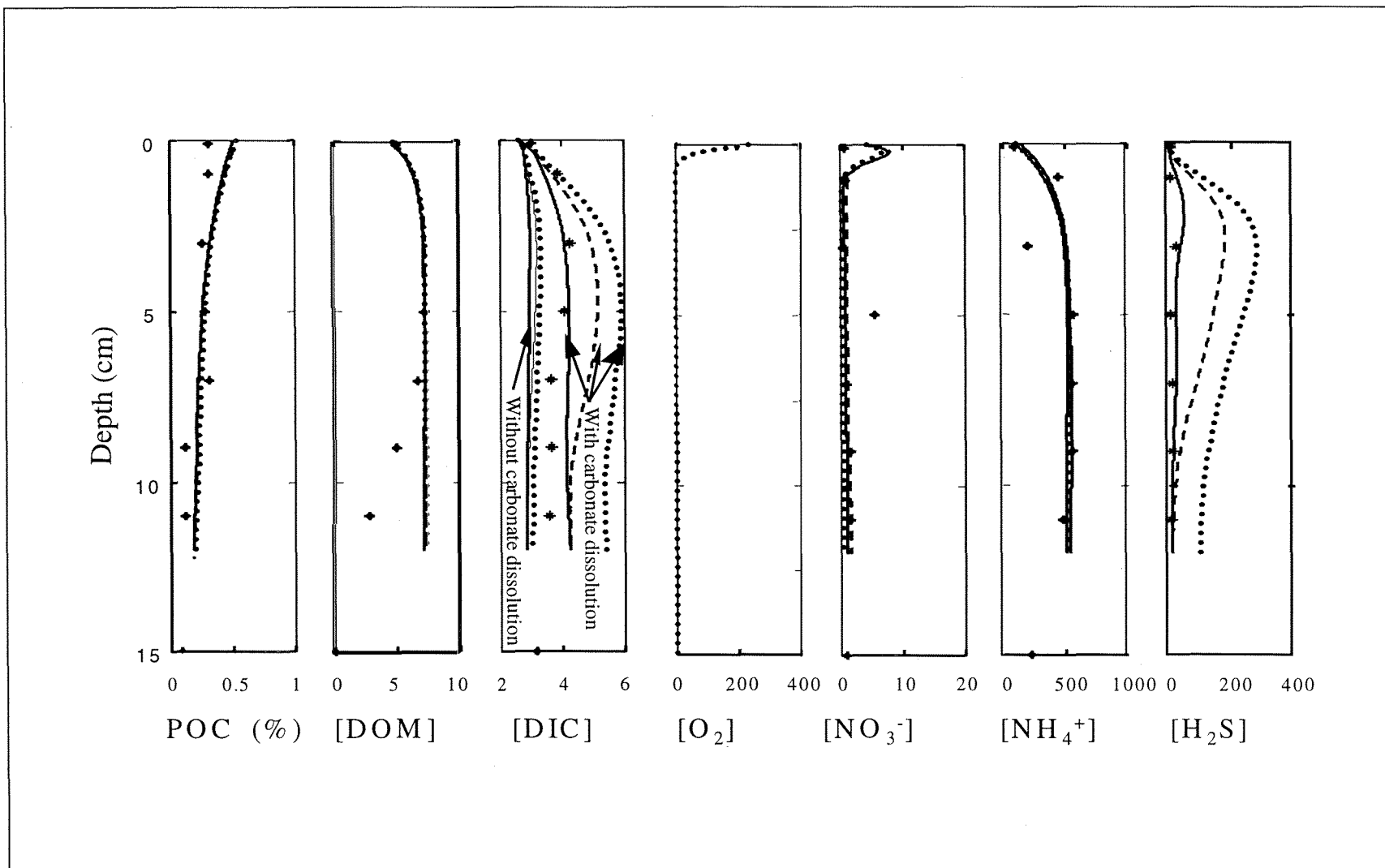


Figure 2. *Syringodium filiforme* site sediment geochemistry. Estimated flux of DOM, POC, and NH_4^+ , flux to the rootzone is estimated using fractions of primary production estimated in the *T. Testudium* optimization multiplied by the mean summer *S. filiforme* production. Dotted line simulation has no rootzone fluxes (case 1), dashed lines are one half the estimated rootzone flux (case 2), and the lines are model results with the estimated rootzone fluxes (case 3). Asterisks are data collected at LLM3 in September 1996. [DOC] and [DIC] as mM, POC in percent solid, [O₂], [NO₃⁻], [NH₄⁺], and [H₂S] μM.

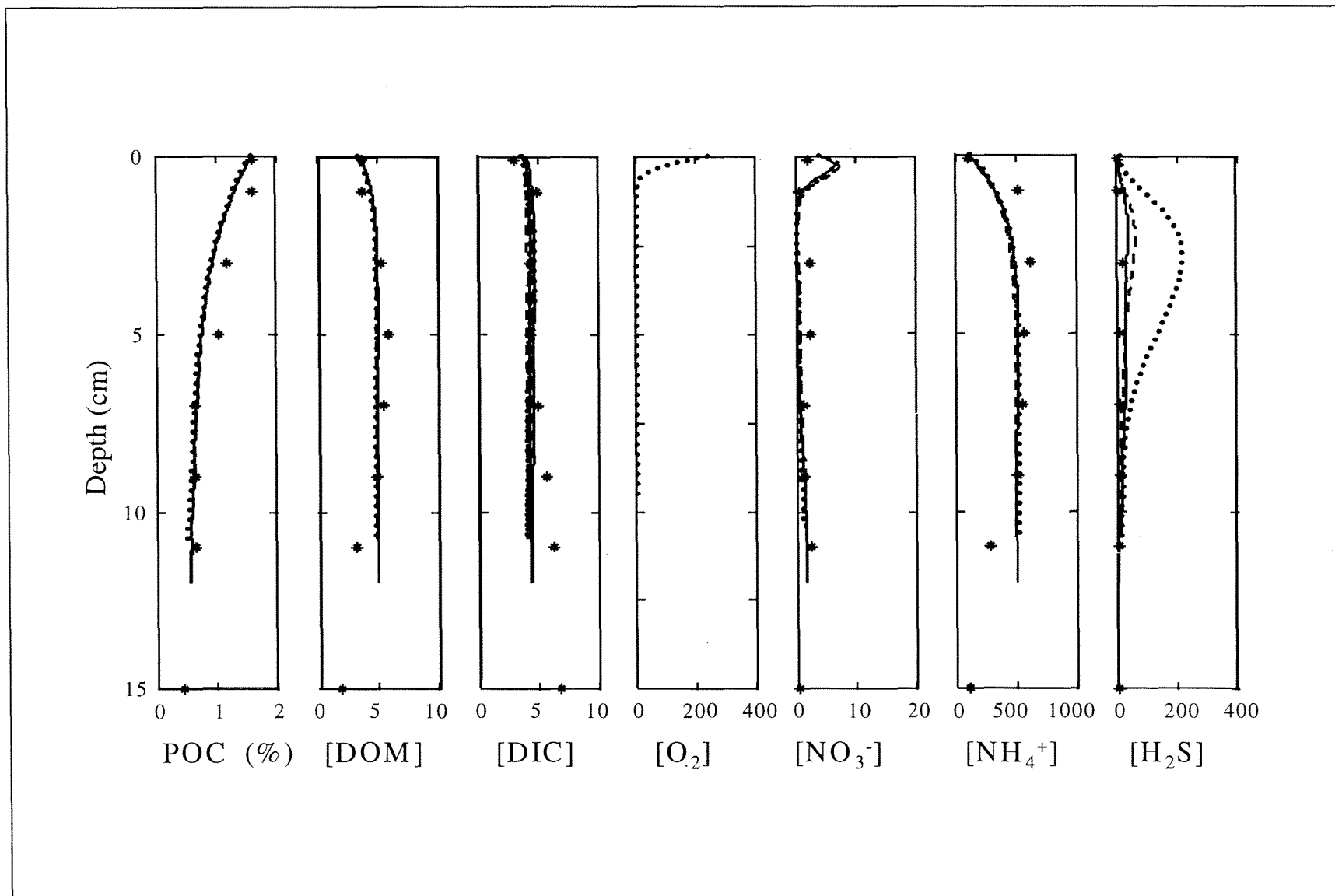


Figure 3. *Thalassia testudium*. site sediment geochemistry. Estimated fluxes and model simulations are as in Figure 1. Asterisks are data collected at LLM2 in September 1996.

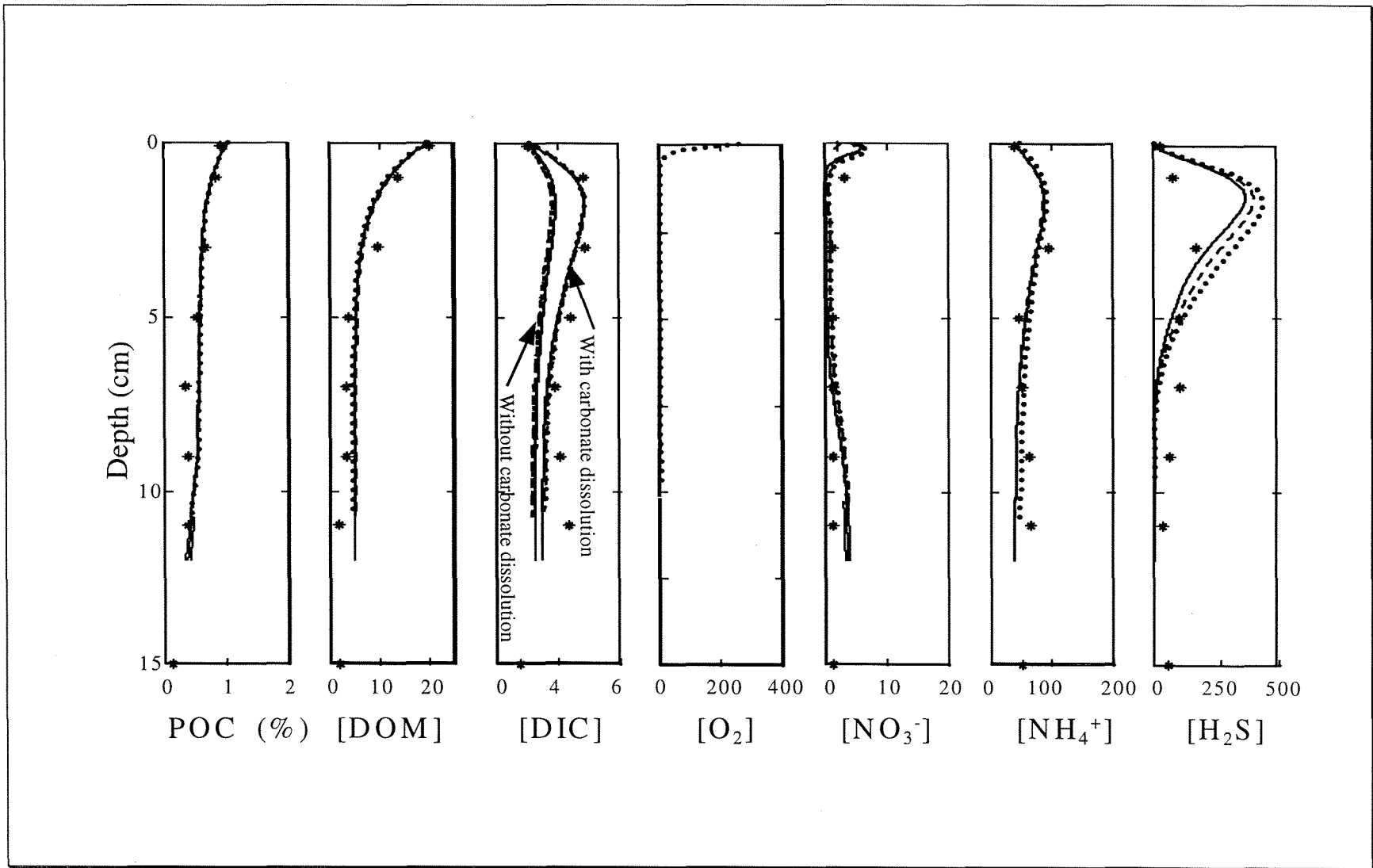


Figure 4. *Halodule wrightii* i. site sediment geochemistry. Estimated fluxes and model simulations are as in Figure 1. The asterisks are data collected at ULM2 during June 1996.

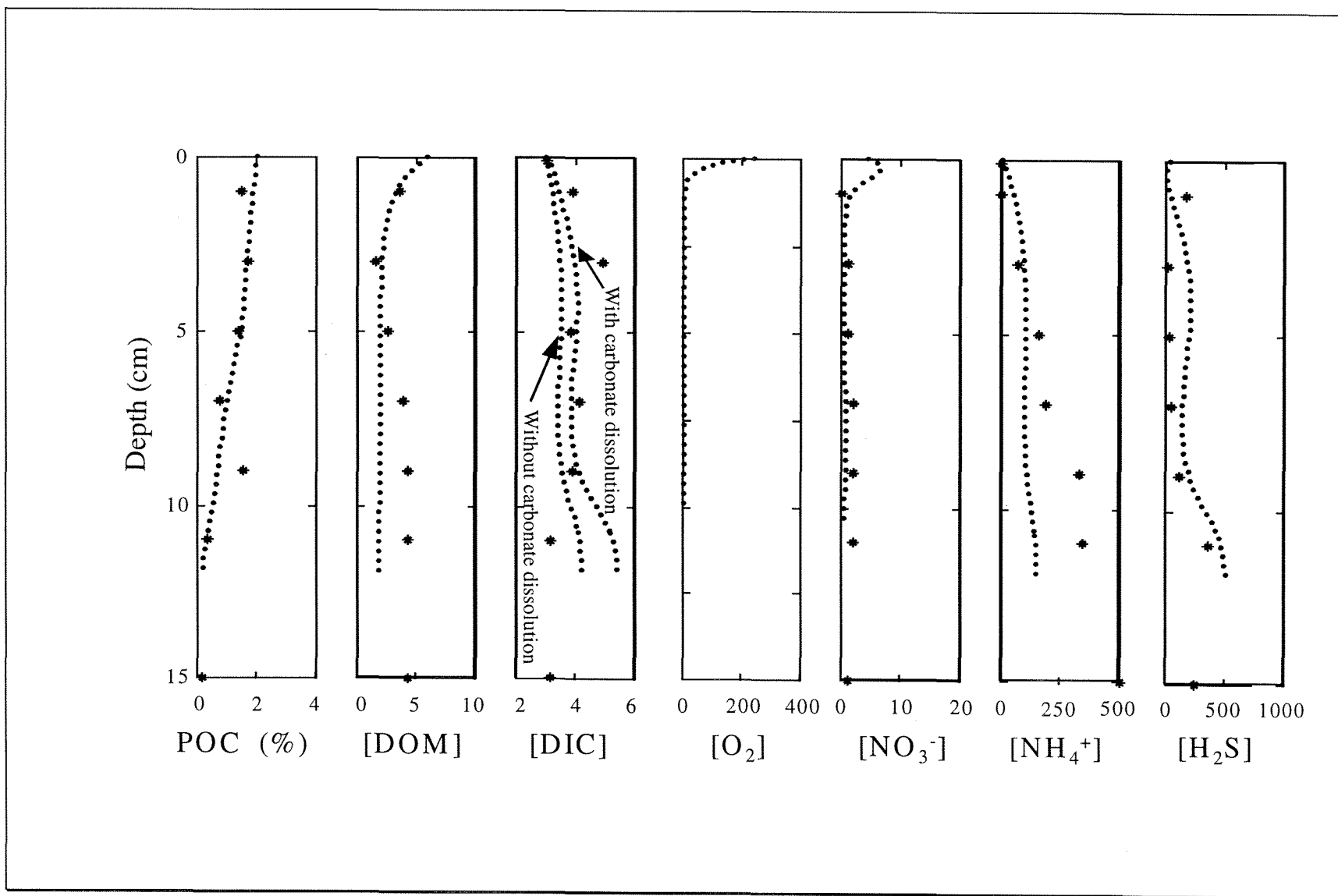


Figure 5. Bare area sediment geochemistry. Lines are model results and asterisks are data collected at LLM3 in September 1996.

References Cited

- Aminot, A., A. El-Sayed Monhamed, and R. Kerouel. (1990) Fate of natural and anthropogenic dissolved organic carbon in the macrotidal Elorn Estuary, France. *Mar. Chem.* 29: 255-275.
- Berg, H. C. 1983. *Random Walks in Biology*. Princeton University Press. Princeton, New Jersey, 142 p.
- Berner, R. A. (1980) *Early Diagenesis: a theoretical approach*. Princeton University Press. Princeton, New Jersey, 241 p.
- Boudreau, B. P. (1984) On the equivalence of nonlocal and radial-diffusion models for porewater irrigation models for porewater irrigation: *J. Mar. Res.* 42: 731-735.
- _____, __, _ (1996) A method-of-lines code for carbon and nutrient diagenesis in aquatic sediments. *Computers & Geosciences* 22: 479-496.
- _____, __, _ (1997) *Diagenetic models and their implementation: modelling transport and reactions in aquatic sediments*. Springer-Verlag, Berlin, Heidelberg, 414 p.
- Carlson, P. R., L. A. Tarbro and T. R. Barber. (1994) Relationship of sediment sulfide to mortality of *Thalassia testudinum* in Florida Bay. *Bulletin of Marine Science* 54: 733-746.
- Dhakar, S. P. and D. J. Burgide. (1996) A coupled, non-linear, steady state model for early diagenetic processes in pelagic sediments. *Amer. J. Science.* 296: 296-330.
- Dunton, K. H. and D. A. Tomasko. (1994) *In situ* photosynthesis in the seagrass *Halodule wrightii* in a hypersaline subtropical lagoon. *Mar. Ecol. Prog. Ser.* 107: 281-293.
- Emerson, S., R. Jahnke and D. Heggie. (1984) Sediment-water exchange in shallow water estuarine sediments. *J. Mar. Res.* 42: 709-730.
- Herzka, S. Z. and K. H. Dunton. (1997) Seasonal photosynthetic patterns of the seagrass *Thalassia testudinum* in the western Gulf of Mexico. *Mar. Ecol. Prog. Ser.* 152: 103-117.
- Koepfler, E. T., R. Benner, P. A. Montagna. (1993) Variability of dissolved organic carbon in sediments of a seagrass bed and an unvegetated area within and estuary in south Texas. *Estuaries.* 16: 391-404.
- Kristensen, E. and T. H. Blackburn, (1987) The fate of organic carbon and nitrogen in experimental marine sediments: influences of bioturbation and anoxia. *J. Mar. Res.* 45: 23-257.

- Lee, Kum-Seop, K. H. Dunton. (1997) Effects of *in situ* light reduction on the maintenance, growth and partitioning of carbon resources in *Thalassia testudinum*. Journal of Experimental Marine Biology and Ecology. 210: 53-73.
- Lovely, D.R., E.J.P. and E. J. P. Phillips (1989) Requirements for a microbial consortium to completely oxidize glucose in Re(III)-reducing sediments. Appl. Environ. Microbiol. 54: 3234-3236
- Morse, J. W and F. T. Mackenzie. (1990) Geochemistry of sediment carbonates. Amsterdam, Elsevier, 707 p.
- Nojima, S. and H. Mikai. (1996) The rate and fate of production of seagrass debris in cages over a *Syringodium isoetifolium* (Aschers.) Dandy Meadow, in Fiji. In: J. Kuo, R. C. Phillips., D. I. Walker and H. Kirkman. Seagrass biology: proceedings of an international workshop. Rottneest Island, W. Australia, 25-29 January. pp 149-154.
- Opsahl, S. and R. Benner. (1993) Decomposition of senescent blades of the seagrass *Halodule wrightii* in a subtropical lagoon. Mar. Ecol. Prog. Ser. 94: 191-205.
- Postma, D. and R. Jakobsen. (1996) Redox zonation: Equilibrium constraints on the Fe(III)/SO₄-reduction interface. Geochimica et Cosmochimica Acta. 60: 3169-3175.
- Pulich, W. M. (1989) Effects of rhizosphere macronutrients and sulfide levels on the growth physiology of *halodule wrightii* Aschers. and *Ruppia maritima* L. s.l. J. Exp. Mar. Biol. Ecol. 127: 69-80.
- Rabouille C. and J. Gaillard (1991) Towards the Edge: Early diagenetic explanation. A model depicting the early diagenesis of organic matter, O₂, NO₃, Mn, and PO₄. Geochimica et Cosmochimica. 55: 2511-2525
- Tomasko, D. A. and K. H. Dunton (1995) Primary productivity in *Halodule wrightii*: a comparison of techniques based on daily carbon budgets. Estuaries 18: 271-278.
- Soetaert, K., P. M. J. Herman, and J. J. Middelburg. (1997) A model of early diagenetic processes from the shelf to abyssal depths. Geochim. Cosmochim. Acta. 57: 1473-1488.
- Stapel, J., R Nijboer and B. Philipsen. (1996) Initial estimates of the export of leaf litter from a seagrass bed in the Spermonde Archipelago, South Sulawesi, Indonesia. In: J. Kuo, R. C. Phillips., D. I. Walker and H. Kirkman. Seagrass biology: proceedings of an international workshop. Rottneest Island, W. Australia, 25-29 January. pp 155-162..

- Stumm, W. and J. J. Morgan. (1981) Aquatic Chemistry. 2nd ED. Wiley-Interscience, 780 p.
- Van Cappellen. P., and Y. Wang. (1996) Cycling of iron and manganese in surface sediments: a general theory for the coupled transport and reaction of carbon , oxygen, nitrogen, sulfur, iron, and manganese. Amer. J. Science 296: 197-242.
- Whitfield, M. and D. R. Turner. (1986) The carbon dioxide system in estuaries— and inorganic prespective. The science of the Total Environment. 49: 235-255.
- Ziegler, S, and R. Benner. (1999) Dissolved organic carbon cycling in a subtropical seagrass-dominated lagoon. Mar. Ecol. Prog. Ser. 180:149-160.
- Zimmerman, R. C., R.D. Smith, R. S. Alberte. (1987) Is Growth of eelgrass nitrogen limited? A numerical simulation of the effects of light and nitrogen on the growth dynamics of *Zostera marina*. Mar. Ecol. Prog. Ser. 41: 167-176.

CHAPTER IV: WATER COLUMN DATA AND SPECTRAL IRRADIANCE MODEL

Contents

Abstract.....	7
Introduction.....	8
Laguna Madre Pigment and Nutrient Data.....	9
Sampling and Analyses.....	9
Nutrients.....	9
Water column pigments.....	9
Seagrass pigments.....	10
Laboratory pigment data.....	10
Results and Discussion.....	10
Nutrients.....	10
Water column pigments.....	12
Seagrass pigments.....	20
Laboratory pigment data.....	24
Laguna Madre Optical Properties.....	26
AC9 Measurements.....	27
PRR Measurements.....	29
TSS Measurements.....	30
AC9 versus TSS.....	30
Hydrolight Model.....	36
Preliminary Spectral Irradiance Model.....	44
Model Description.....	44
Influence of Light Quality on Production.....	45

References.....	49
Appendix.....	51

Tables

Table 1. Water column nutrient data for the summer 1996 cruise. Data are shown as mean concentration and standard deviation of quadruplicate samples taken at each station.....	11
Table 2. List of pigments observed in this study and their taxonomic-physiological significance (adapted from Bidigare 1989).....	14
Table 3. Water column HPLC pigment data for the summer 1996 cruise. Data are shown as mean concentration and standard deviation of quadruplicate samples taken at each station. The “brown tide” station was taken in upper Laguna Madre during a “brown tide” bloom. Abbreviations: B.D. = below detection; 19-But = 19-butanoyloxofucoxanthin.....	15
Table 4. Seagrass HPLC pigment data for the summer 1996 cruise. Data are shown as mean concentration and standard deviation of quadruplicate samples taken at each station. See text for description of dominant seagrasses at each site. Included are the ratios of chlorophyll b to chlorophyll <i>a</i> (Chl <i>b</i> /Chl <i>a</i>) and lutein to chlorophyll <i>a</i> (Lutein/Chl <i>a</i>). A potential outlier is shown in bold type.....	24
Table 5. HPLC pigment data for “brown tide” alga. Data for <i>Aureococcus anophagefferens</i> are from Bidigare (1989). Abbreviations: a=chlorophyll <i>a</i> ; c=chlorophyll <i>c</i> ₁ , <i>c</i> ₂ ; bf=19’-butanoyloxyofucoxanthin; f=fucoxanthin; dn=diadinoxanthin; z=zeaxanthin; B.D.=below detection.....	25
Table 6. Cases used in the comparison of the spectral irradiance model (P_{SPECTRAL}) with the standard PAR model (P_{PAR}). $P_{\text{SPECTRAL}}/P_{\text{PAR}}$ is the ratio of water column integrated production. Also, a_c and a_s are phytoplankton and sediment absorption coefficients, respectively.....	46

Figures

Figure 1. Ammonium (μM) and chlorophyll <i>a</i> ($\mu\text{g/L}$) concentrations along a transect through the Upper and Lower Laguna Madre during summer 1996.....	11
Figure 2. Phosphate (μM) and silicate (μM) concentrations along a transect through the Upper and Lower Laguna Madre during summer 1996.....	13
Figure 3. Dissolved inorganic nitrogen (DIN=nitrate+nitrite+ammonium; μM) versus phosphate (μM) concentrations in Upper and Lower Laguna Madre during summer 1996. Solid line represents the “Redfield Ratio”.....	13
Figure 4. Contour plot of chlorophyll <i>a</i> concentration at the fixed sampling stations in Laguna Madre from North (ULM1) to South (LLM2) during the period January to November 1997.....	17
Figure 5. Contour plot of fucoxanthin concentration at the fixed sampling stations in Laguna Madre (from North to South) during the period January to November 1997.....	17
Figure 6. Contour plot of chlorophylls <i>c</i> ₁ and <i>c</i> ₂ concentration at the fixed sampling stations in Laguna Madre (from North to South) during the period January to November 1997.....	18
Figure 7. Contour plot of diadinoxanthin concentration at the fixed sampling stations in Laguna Madre (from North to South) during the period January to November 1997.....	18
Figure 8. Contour plot of zeaxanthin concentration at the fixed sampling stations in Laguna Madre (from North to South) during the period January to November 1997.....	19
Figure 9. Contour plot of 19' butanoyloxyfucoxanthin concentration at the fixed sampling stations in Laguna Madre (from North to South) during the period January to November 1997.....	19
Figure 10. Pigment ratios for the most prevalent pigments relative to chl <i>a</i> at station ULM1 (Corpus Christi Bay) from June 1996 to November 1997. Missing data points are a result of pigment concentrations below the detection limit of HPLC.....	21

Figure 11. Pigment ratios for the most prevalent pigments relative to chl *a* at station ULM2 (South of Bird Island Basin) from June 1996 to November 1997. Missing data points are a result of pigment concentrations below the detection limit of HPLC.....21

Figure 12. Pigment ratios for the most prevalent pigments relative to chl *a* at station ULM3 (North of the Land Cut) from June 1996 to November 1997. Missing data points are a result of pigment concentrations below the detection limit of HPLC.....22

Figure 13. Pigment ratios for the most prevalent pigments relative to chl *a* at station LLM3(near Port Mansfield) from June 1996 to November 1997.....22

Figure 14. Pigment ratios for the most prevalent pigments relative to chl *a* at station LLM1(dredged material placement area 233) from June 1996 to November 1997. Missing data points are a result of pigment concentrations below the detection limit of HPLC.....23

Figure 15. Pigment ratios for the most prevalent pigments relative to chl *a* at station LLM2 (seagrass bed near South Padre Island Convention Center) from June 1996 to November 1997. Missing data points are a result of pigment concentrations below the detection limit of HPLC..... 23

Figure 16. Comparison of pigment ratios for *Aureoumbra lagunensis* from Upper Laguna Madre during a “brown tide” bloom and the isotype culture (TBA-2).....25

Figure 17. Absorption coefficient a (m^{-1}) versus wavelength (nm).....28

Figure 18. Beam attenuation coefficient c (m^{-1}) versus wavelength (nm).....28

Figure 19. Downwelling irradiance ($watts\ m^{-2}\ nm^{-1}$) versus wavelength (nm) for TSS = 4.54 mg/L at a depth of 0.77 m.....31

Figure 20. Downwelling irradiance ($watts\ m^{-2}\ nm^{-1}$) versus wavelength (nm) for TSS = 15.6 mg/L at a depth of 0.5 m.....31

Figure 21. Beam attenuation coefficient c (m^{-1}) versus TSS (mg/L) at a wavelength of 412 nm.....32

Figure 22. Beam attenuation coefficient c (m^{-1}) versus TSS (mg/L) at a wavelength of 440 nm.....32

Figure 23. Absorption coefficient a (m^{-1}) versus TSS (mg/L) at a wavelength of 412 nm.....	34
Figure 24. Absorption coefficient a (m^{-1}) versus TSS (mg/L) at a wavelength of 440 nm.....	34
Figure 25. Total scattering coefficient coefficient $b(m^{-1})$ versus TSS (mg/L) at a wavelength of 412 nm.....	35
Figure 26. Total scattering coefficient coefficient $b(m^{-1})$ versus TSS (mg/L) at a wavelength of 440 nm.....	35
Figure 27. Slope ($L\ mg^{-1}\ m^{-1}$) versus wavelength (nm) for the beam attenuation coefficient.....	37
Figure 28. Slope ($L\ mg^{-1}\ m^{-1}$) versus wavelength (nm) for absorption.....	37
Figure 29 Slope ($L\ mg^{-1}\ m^{-1}$) versus wavelength (nm) for the total scattering coefficient.....	38
Figure 30. Measurements of the total scattering coefficient $b(589\ nm)$ vs. concomitant measurements of TSS concentration at Laguna Madre.....	39
Figure 31. Specific scattering coefficient b^* as a function of wavelength derived from Laguna Madre measurements.....	39
Figure 32. Measurements of the absorption coefficient $a(589\ nm)$ vs. concomitant measurements of TSS concentration at Laguna Madre.....	41
Figure 33. Specific absorption coefficient a^* as a function of wavelength derived from Laguna Madre measurements	41
Figure 34. Downwelling attenuation coefficient $K_d(580\ nm)$ as a function of TSS derived from Eq. 4 using output from Hydrolight.....	43
Figure 35. Specific downwelling attenuation coefficient $\bar{K}_d^*(\lambda)$ as a function of wavelength derived from Hydrolight and Laguna Madre measurements	43

Figure 36. Our simplified radiance transfer model (downwelling light only) predicts spectral irradiance ($\mu\text{mols}/\text{m}^2/\text{d}/\text{nm}$) as a function of depth for (left to right) filtered Laguna Madre water, Laguna Madre water with added chrysophyte ($30 \mu\text{g chl a/L}$) and Laguna Madre water with added sediment (50 mg/L). The coefficients, a_w , a_d , a_c , a_s and a_t , are for water, DOM, phytoplankton, sediment and total absorption, respectively. In the latter two cases, a_t is equivalent, which means PAR is also equal at all depths. However, as is evident from the shapes of the curves, spectral quality is quite different, particularly at 650 to 700 nm.....47

Figure 37. Results of conceptual model showing the ratio of predictions by our spectral irradiance model to predictions by the PAR model (Jassby and Platt, 1976) ($P_{\text{SPECTRAL}}/P_{\text{PAR}}$) as a function of depth (m) for additions of phytoplankton (in $\mu\text{g chl a/L}$) and sediment (mg/L).....48

Abstract

Water samples collected monthly, for 18 months, from six sites in the Laguna Madre were analyzed to identify and quantify phytopigments using High Performance Liquid Chromatography (HPLC). In addition, water column pigment and nutrient data were acquired at 12 stations in Upper (ULM) and Lower Laguna Madre (LLM) during the summer 1996 cruise. The spatial and temporal scale of sampling provide a unique perspective on the dynamics of phytoplankton communities within the Laguna Madre. Phytopigment identification from field samples was consistent with the known pigment complex for *Aureoumbra lagunensis*, Texas brown tide. Pigment identification and pigment ratios indicate that the dominant phytoplankter at most sites was brown tide; however, other groups were also present. Extreme pigment ratios in Lower Laguna during September 1997 may be the result of a red tide bloom or a wind event suspending benthic diatoms. Additionally, this data set documents the decline of brown tide in the Upper Laguna. Nutrient data collected along a transect through the Laguna indicates that Baffin Bay and Arroyo Colorado may be sources of anthropogenic nutrients. Pigments were identified and quantified for the major seagrass species in Laguna Madre. Pigment ratios for the seagrasses were substantially higher than published values, because HPLC is more sensitive than traditional methods.

Inherent optical properties (IOPs) of Laguna Madre waters were studied in August 1997, and March and November 1998. Measurements of absorption and backscattering coefficients were performed along with analyses of total suspended solids (TSS) and pigment concentrations in both Upper and Lower Laguna Madre. Strong relationships were observed between IOPs and TSS, which were ultimately used to compute spectral irradiance in the water with the radiative transfer numerical model called Hydrolight. Finally, we describe a simple spectral irradiance productivity model that can use data provided by Hydrolight to estimate algal productivity in the water column. Comparisons with standard PAR models suggest light quality is important to understanding productivity in Laguna Madre waters.

Introduction

Light attenuation occurs as a result of scattering and absorbance by water as well as suspended and dissolved materials (Kirk, 1994). Suspended solids, including phytoplankton, are responsible for the majority of light attenuation (Voss 1992). In addition to attenuation, the presence of phytoplankton pigments and dissolved organic materials (e.g., humics) can cause dramatic spectral shifts (Smith and Baker 1978, Yentsch 1980, Pierce et al. 1986). Laguna Madre has been disrupted by an extensive bloom of *Aureoumbra lagunensis*, Texas “brown tide” (DeYoe et al. 1997), which caused a 50% reduction in underwater light levels in some portions of the Laguna (Dunton 1994). Shading from the brown tide has resulted in the loss of seagrass from deeper portions of the Upper Laguna Madre (Onuf 1996). Although, *A. lagunensis* has been the dominant phytoplankton in some regions, other phytoplankton is important in Laguna Madre.

Pigment composition is often used as a taxonomic indicator for plankton and algae. High Performance Liquid Chromatography (HPLC) can detect low concentrations of pigments and can be used to identify characteristic accessory pigments. The presence and abundance of particular accessory pigments can be used to identify major taxonomic groups contributing to water column primary productivity. Thus, HPLC analysis is a sensitive tool to identify the major phytoplankton groups responsible for light attenuation and to quantify the abundance of phytoplankton. Traditional spectrophotometric analysis is limited to quantifying the relative abundance of organisms containing chlorophyll *a*.

Photosynthesis, the energy gathering mechanism of seagrasses, is primarily dependent on the availability of radiant energy and nutrients. The fluxes of these rate-limiting factors are governed by optical properties of the water column, hydrodynamic and sediment transport, and biological processes (Bidigare et al. 1987). Because chlorophyll and other pigments absorb light quanta selectively from the light spectra, photosynthetic production will depend on the spectral quality of the light in the water and on the types of pigments found in the plants.

This chapter presents water column nutrient and pigment and seagrass pigment (obtained by HPLC) data collected in Upper and Lower Laguna Madre during summer 1996 cruise. Additionally, we present water column HPLC pigment data obtained at the permanent sampling stations (i.e., "Blucher platforms") from June 1996 through November 1997 and HPLC pigment data from the type culture (TBA-2) of *Aureoumbra lagunensis*. The long-term water column pigment data collected at the platforms presents a unique opportunity to examine the temporal and spatial dynamics of phytoplankton in the Laguna Madre. Also included is a report on inherent optical properties measured in Laguna Madre waters based on samplings that took place in August 1997 and March and November 1998. These data were used to describe the light field in the water column with a model called Hydrolight. Finally, initial testing of a spectral irradiance model is included, which may lead to better estimates of seagrass production.

Laguna Madre Pigment and Nutrient Data

Sampling and Analyses

Nutrients

Water column nutrient data were acquired at 12 stations in Upper (ULM) and Lower Laguna Madre (LLM) during the summer 1996 cruise. Samples were collected in quadruplicate in 1 L acid-washed Nalgene™ bottles. After rinsing, bottles were filled three-quarters full with surface water and frozen. In the laboratory, samples were thawed and filtered. Nutrient analyses on the filtrate were conducted according to Biggs et al. (1982).

Water column pigments

Surface waters were filtered through 47 mm GF/F filters and the volume recorded (about 100 to 1000 ml). At each site and date replicate ($n = 4$) samples were obtained, filtered and subsequently analyzed. Samples were filtered under low light conditions, filters were enclosed in aluminum foil and, when possible, frozen immediately in liquid nitrogen. Filter samples were kept frozen prior to analysis. Pigments were extracted in 100% acetone and measured by High Performance Liquid Chromatography using a modification of the Mantoura and Llewellyn (1983) method. A Shimadzu diode-array detector (model SPD-M10AV) was used to detect absorbance.

Absorbance peaks were then used to calculate pigment concentration ($\mu\text{g L}^{-1}$) based on extraction and sample volume. Canthaxanthin ($1 \mu\text{g ml}^{-1}$), a xanthophyll pigment not found in algae, was added to all samples and blanks as an internal standard.

Seagrass pigments

Seagrass samples, *Thalassia testudinum*, *Syringodium filiforme* and *Halodule wrightii*, were extracted in the laboratory of Dr. K. Dunton, UTMSI, and an aliquot of the extract was shipped to Texas A&M for analysis. Pigments were measured by High Performance Liquid Chromatography using a modification of the method of Mantoura and Llewellyn (1983).

Laboratory pigment data

Dr. R. Greene at Texas A&M University provided samples of the Texas "brown tide" organism (clone TBA-2) for pigment analysis. Cells were grown in batch culture in f/2 media at six phosphate and ammonium concentrations at 30°C and about $100 \mu\text{mol quanta/m}^2/\text{s}$. Pigments were extracted and measured as previously described.

Results and Discussion

Nutrients

During June 1996, nutrient concentrations were low compared to eutrophic estuaries; e.g., Chesapeake Bay (Table 1). Ammonium was the most abundant form of inorganic nitrogen and its concentration ranged from 0.52 to $4.42 \mu\text{M}$. Maxima were observed at Station 20 in the ULM and Station 25 in the LLM (Fig. 1). The former is in the vicinity of Baffin Bay, whereas the latter is in the vicinity of the Arroyo Colorado. Both of these areas are likely sources of nitrogen-rich waters, owing to anthropogenic nutrient inputs. Baffin Bay is bordered by agricultural lands treated with fertilizers and pesticides. Additionally, Baffin Bay receives several intermittent sources of freshwater, some of which are contaminated with treated wastewater. The Arroyo Colorado originates at the Harlingen wastewater treatment plant, receives effluent from shrimp farms and is the largest source of freshwater to Lower Laguna Madre. In contrast, oxidized forms of nitrogen, nitrate and nitrite, were below $0.3 \mu\text{M}$ throughout the region.

Table 1. Water column nutrient data for the summer 1996 cruise. Data are shown as mean concentration and standard deviation of quadruplicate samples taken at each station.

Station	Ammonium (μM)		Phosphate (μM)		Urea (μM)		Nitrate (μM)		Nitrite (μM)		Silicate (μM)	
	Conc.	Std.	Conc.	Std.	Conc.	Std.	Conc.	Std.	Conc.	Std.	Conc.	Std.
13	1.30	0.27	0.43	0.19	0.82	0.23	0.19	0.10	0.01	0.01	45.9	8.53
16	0.87	0.28	0.29	0.22	0.80	0.19	0.21	0.21	0.01	0.01	35.1	24.6
18	1.88	0.62	0.31	0.09	1.30	0.78	0.11	0.08	0.01	0.01	25.7	2.69
20	4.42	6.19	1.92	2.70	3.98	5.89	0.23	0.12	0.04	0.04	53.5	6.99
22	1.98	3.05	0.98	1.58	1.63	1.88	0.12	0.08	0.04	0.03	43.0	4.04
24	0.52	0.24	0.11	0.04	0.64	0.11	0.31	0.16	0.01	0.01	52.2	5.77
25	2.26	0.50	0.24	0.07	0.92	0.57	0.21	0.11	0.07	0.04	41.3	12.0
26	1.00	1.07	0.17	0.14	0.83	0.54	0.15	0.08	0.03	0.04	39.7	7.93
27	0.46	0.16	0.09	0.04	0.16	0.11	0.04	0.03	0.02	0.01	7.96	2.19
28	0.64	0.60	0.14	0.02	0.50	0.32	0.06	0.01	0.02	0.00	7.28	0.76
29	0.72	0.60	0.13	0.07	0.61	0.54	0.06	0.05	0.02	0.02	6.89	1.57
30	1.43	1.66	0.15	0.08	0.83	0.90	0.07	0.04	0.03	0.02	5.88	2.01

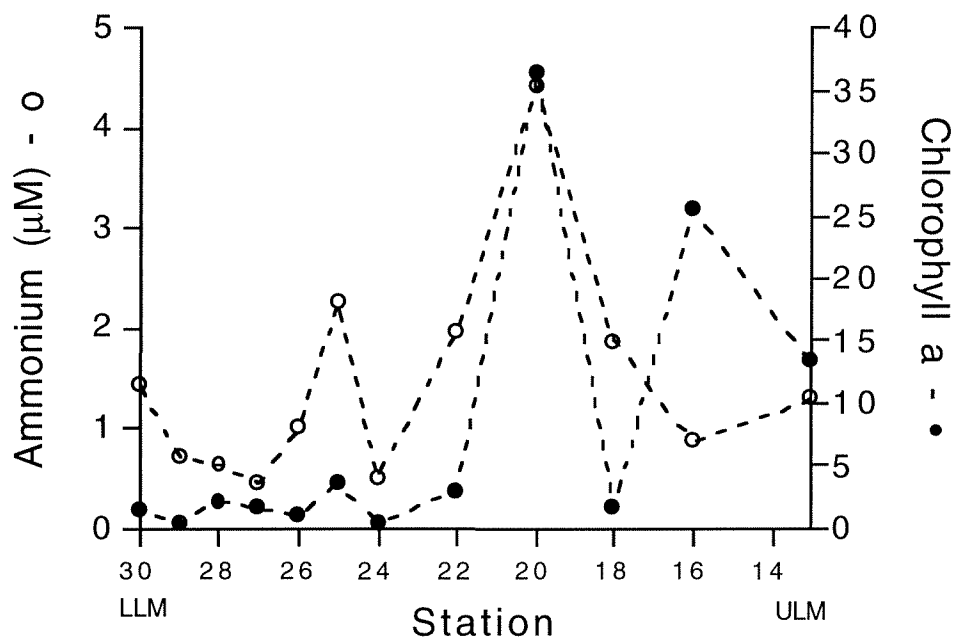


Figure 1. Ammonium (μM) and chlorophyll *a* ($\mu\text{g/L}$) concentrations along a transect through the Upper and Lower Laguna Madre during summer 1996.

Surprisingly, urea, an organic form of nitrogen, was found at high concentrations, varying from 0.2 to 3.98 μM . High abundance of urea was also documented in sediment porewater, which may have been the source for the overlying waters.

Phosphate concentrations ranged from 0.09 to 1.92 μM . Overall, the trend for phosphate appeared to be decreasing values from ULM to LLM (Fig. 2) with a significant maximum found at the same ULM region (near Baffin Bay) where the highest ammonium concentration was measured. At least during this period of the year, N:P were always lower than Redfield ratio (16:1) (Fig. 3). This suggests that additional nitrogen could lead to increases in algal abundance. Finally, silicate values were never low in either portion of the Laguna ($> 5 \mu\text{M}$ throughout), but decreased significantly to the west of Station 26 (Fig. 2).

Water column pigments

The HPLC analyzer was configured to detect chlorophylls *a*, *b*, *c*₁ and *c*₂ as well as 12 accessory pigments including fucoxanthin, 19' butanoyloxyfucoxanthin, diadinoxanthin, prasinoxanthin, lutein, zeaxanthin and Beta-carotene. The time series data set (Appendix 1) from the fixed stations (ULM 1-3 and LLM 1-3) represents 392 samples taken over an 18 month period. The five most prevalent pigments, besides chl *a*, were chl *c*₁*c*₂, fucoxanthin, 19' butanoyloxyfucoxanthin, diadinoxanthin and zeaxanthin. The taxonomic groups associated with the particular accessory pigments measured in the Laguna Madre are presented in Table 2. Comparisons between chlorophyll *a* measurements by HPLC and spectrophotometric methods were discussed in Chapter V.

During the summer 1996 cruise, chl *a* values ranged from 0.43 to 25.60 $\mu\text{g/L}$. Chlorophyll *a* values during the summer 1996 cruise were higher in the ULM compared with the LLM (Fig. 1, Table 3), and while there was no obvious correlation with nutrient abundance, concentrations of both were higher in the ULM (Figs. 2 & 3).

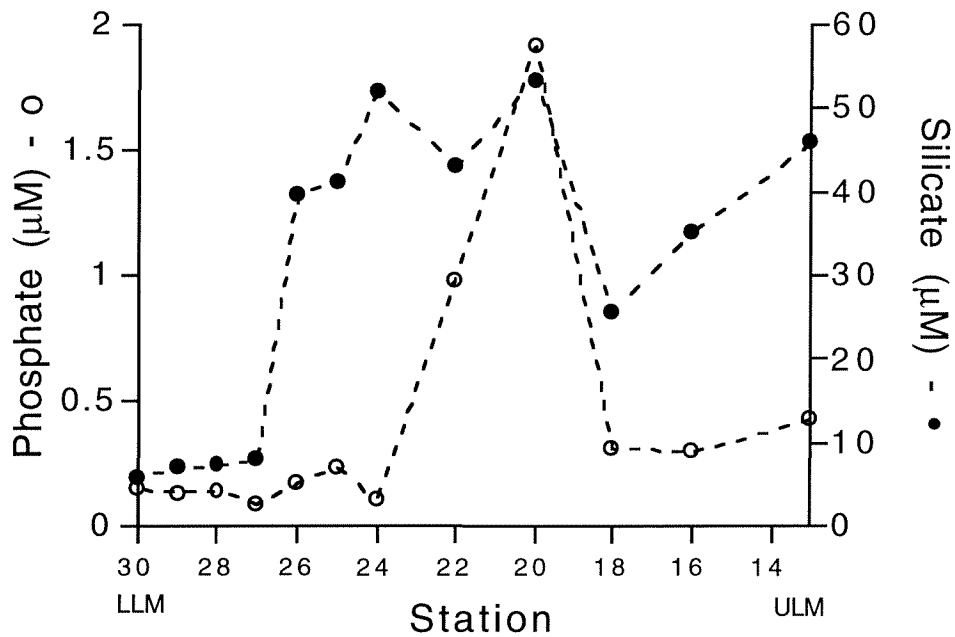


Figure 2. Phosphate (μM) and silicate (μM) concentrations along a transect through the Upper and Lower Laguna Madre during summer 1996.

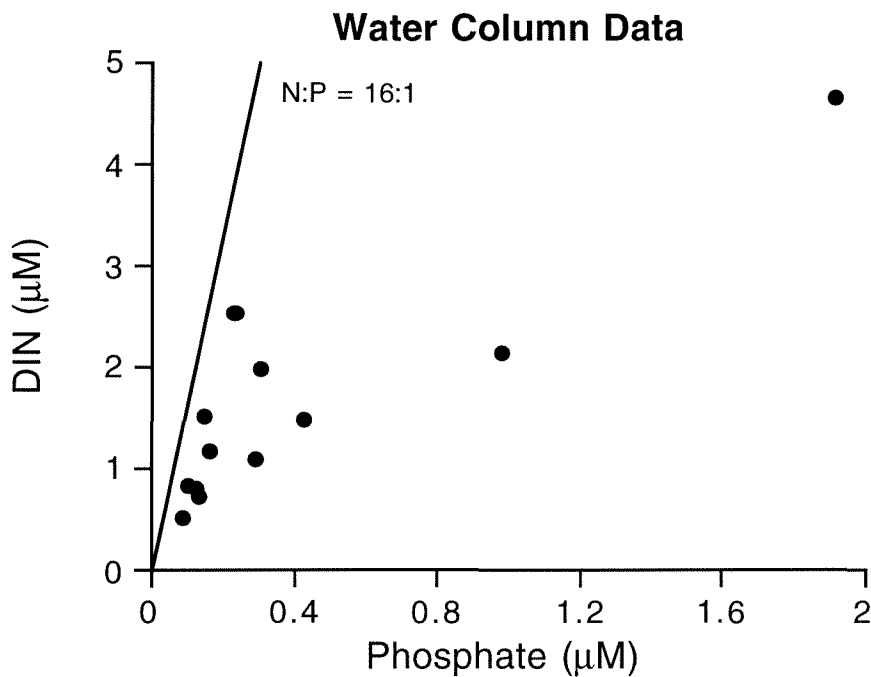


Figure 3. Dissolved inorganic nitrogen (DIN=nitrate+nitrite+ammonium; μM) versus phosphate (μM) concentrations in Upper and Lower Laguna Madre during summer 1996. Solid line represents the “Redfield Ratio”.

Table 2. List of pigments observed in this study and their taxonomic-physiological significance (adapted from Bidigare 1989).

Pigment	Significance
Physiological Markers	
Chlorophyll <i>a</i>	Algal biomass and photosynthetic potential
Diadinoxanthin Zeaxanthin	Photo-protectant
Golden-brown algae	
Fucoxanthin Chlorophyll <i>c</i> ₁ , <i>c</i> ₂	Diatoms (and some chrysophytes and prymnesiophytes)
19'-butanoyloxofucoxanthin Fucoxanthin	Chrysophytes
Chlorophyll b-containing algae	
Lutein	Chlorophytes ¹
Prasinoxanthin	Prasinophytes ¹
Zeaxanthin	Prochlorophytes ¹
Phycobilin-containing algae	
Zeaxanthin	Cocoid cyanobacteria

¹also contain small amounts of zeaxanthin

Table 3. Water column HPLC pigment data for the summer 1996 cruise. Data are shown as mean concentration and standard deviation of quadruplicate samples taken at each station. The “brown tide” station was taken in upper Laguna Madre during a “brown tide” bloom. Abbreviations: B.D. = below detection; 19-But = 19-butanoyloxafucoanthin.

Station	Date	Chlorophyll a ($\mu\text{g g}^{-1}$)		Chlorophyll c ($\mu\text{g g}^{-1}$)		Chlorophyll b ($\mu\text{g g}^{-1}$)		Lutein ($\mu\text{g g}^{-1}$)	
		Conc.	Std.	Conc.	Std.	Conc.	Std.	Conc.	Std.
13	6/1/96	13.41	1.36	2.00	0.03	B.D.	B.D.	0.43	0.12
16	6/1/96	25.60	1.77	1.99	0.17	1.85	0.20	B.D.	B.D.
18	6/1/96	1.65	0.04	B.D.	B.D.	B.D.	B.D.	B.D.	B.D.
20	6/1/96	36.35	2.44	2.06	0.44	B.D.	B.D.	B.D.	B.D.
22	6/1/96	3.08	0.25	B.D.	B.D.	B.D.	B.D.	B.D.	B.D.
24	6/1/96	0.43	0.11	B.D.	B.D.	B.D.	B.D.	0.17	0.01
25	6/1/96	3.68	0.53	B.D.	B.D.	B.D.	B.D.	B.D.	B.D.
26	6/1/96	1.06	0.10	B.D.	B.D.	B.D.	B.D.	0.11	0.02
27	6/1/96	1.66	0.06	B.D.	B.D.	B.D.	B.D.	B.D.	B.D.
28	6/1/96	2.23	0.05	B.D.	B.D.	B.D.	B.D.	B.D.	B.D.
29	6/1/96	0.46	0.04	B.D.	B.D.	B.D.	B.D.	B.D.	B.D.
30	6/1/96	1.60	0.07	B.D.	B.D.	B.D.	B.D.	B.D.	B.D.
“Brown Tide”	6/29/96	35.28	0.00	3.61	0.00	0.83	0.00	0.30	B.D.

Table 3. Continued.

Station	Date	Fucoxanthin ($\mu\text{g g}^{-1}$)		Zeaxanthin ($\mu\text{g g}^{-1}$)		Diadinoxanthin ($\mu\text{g g}^{-1}$)		19-But ($\mu\text{g g}^{-1}$)		Prasinoxanthin ($\mu\text{g g}^{-1}$)	
		Conc.	Std.	Conc.	Std.	Conc.	Std.	Conc.	Std.	Conc.	Std.
13	6/1/96	1.55	0.05	0.65	0.05	B.D.	B.D.	B.D.	B.D.	B.D.	B.D.
16	6/1/96	0.93	0.04	1.21	0.39	B.D.	B.D.	B.D.	B.D.	B.D.	B.D.
18	6/1/96	0.60	0.08	B.D.	B.D.	B.D.	B.D.	B.D.	B.D.	B.D.	B.D.
20	6/1/96	6.18	0.58	1.39	0.10	B.D.	B.D.	B.D.	B.D.	B.D.	B.D.
22	6/1/96	0.66	0.07	0.21	0.01	B.D.	B.D.	B.D.	B.D.	B.D.	B.D.
24	6/1/96	0.13	0.08	B.D.	B.D.	B.D.	B.D.	B.D.	B.D.	B.D.	B.D.
25	6/1/96	1.08	0.12	0.15	0.05	B.D.	B.D.	B.D.	B.D.	B.D.	B.D.
26	6/1/96	0.27	0.60	B.D.	0.00	B.D.	B.D.	B.D.	B.D.	B.D.	B.D.
27	6/1/96	0.30	0.04	0.10	0.00	B.D.	B.D.	B.D.	B.D.	B.D.	B.D.
28	6/1/96	0.85	0.04	0.28	0.01	B.D.	B.D.	B.D.	B.D.	B.D.	B.D.
29	6/1/96	B.D.	B.D.	B.D.	B.D.	B.D.	B.D.	B.D.	B.D.	B.D.	B.D.
30	6/1/96	0.06	0.02	B.D.	B.D.	B.D.	B.D.	B.D.	B.D.	B.D.	B.D.
Brown Tide	6/29/96	10.59	0.00	0.42	B.D.	2.41	B.D.	6.11	B.D.	0.17	B.D.

Contour plots provide a unique perspective on the spatial and temporal dynamics of pigment concentrations in Laguna Madre. As expected the pigment composition changed as a function of both location and time (Figs. 4 through 9). Chlorophyll *a* values were high at all sampling locations during winter and spring 1997 (Fig. 4). At LLM2, which typically has very low chlorophyll levels (e.g. $<3 \mu\text{g L}^{-1}$), chl *a* values were around $10 \mu\text{g L}^{-1}$ from April to June and elevated concentrations persisted until September 1997 (Fig. 4). Elevated levels ($> 2.5 \mu\text{g L}^{-1}$) of fucoxanthin occurred at most sites between February and May 1997. High fucoxanthin concentrations (i.e., $10 \mu\text{g L}^{-1}$) correspond with chlorophyll *a* values in excess of $30 \mu\text{g L}^{-1}$ (Figs. 4 and 5).

Elevated chl *c*₁*c*₂ concentrations also occurred at most sites between February and May and the highest concentrations ($0.5 \mu\text{g L}^{-1}$) coincide with chlorophyll *a* values in excess of $30 \mu\text{g L}^{-1}$ (Figs. 4 and 6). The pigments diadinoxanthin, zeaxanthin and 19' butanoyloxyfucoxanthin (Figs. 7, 8 and 9) also exhibited maxima that coincided with high chl *a* concentrations (Fig. 4). All of these accessory pigments are components of the light harvesting complex associated with the Texas "brown tide" *Aureoumbra lagunensis* (DeYoe et al. 1997). Bidigare (1989) reported that *Aureococcus anophagefferens*, New England "brown tide", had significant amounts of fucoxanthin, chlorophyll *c*, 19'-butoyloxyfucoxanthin, and a small quantity of diadinoxanthin.

Although *A. lagunensis* was the dominant phytoplankton during the spring, other phytoplankton were present and important contributors to primary production. The presence of diatoms is indicated by the combination of fucoxanthin and chlorophyll *c*₁*c*₂. Both of these pigments were observed in most samples, and the presence of diatoms would be consistent with the concentrations of silicate in these waters (Fig. 2). The other pigments, lutein, zeaxanthin and prasinoxanthin, suggest the presence of chlorophytes, prasinophytes and cyanobacteria, respectively (Table 2). It must be stated that this type of information can also be obtained, and with more detail, from microscopy counts. However, our main reason for measuring pigment composition was our interest in modeling radiative transfer of light in the Laguna water column.

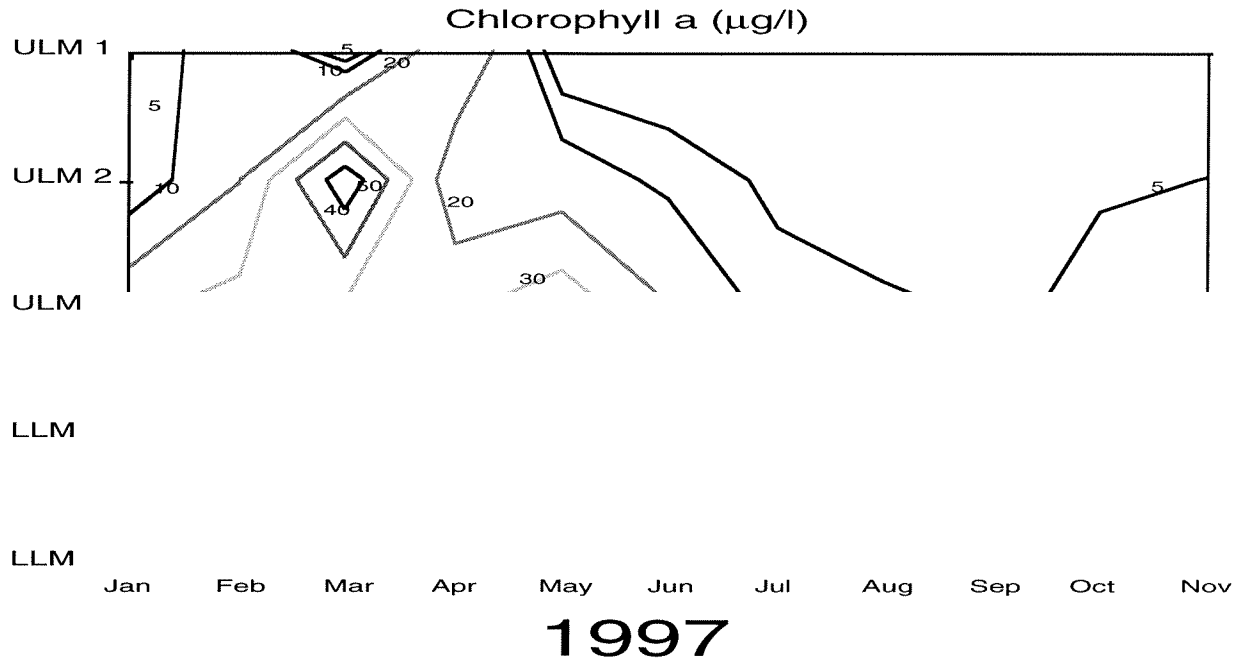


Figure 4. Contour plot of chlorophyll *a* concentration at the fixed sampling stations in Laguna Madre from North (ULM1) to South (LLM2) during the period January to November 1997.

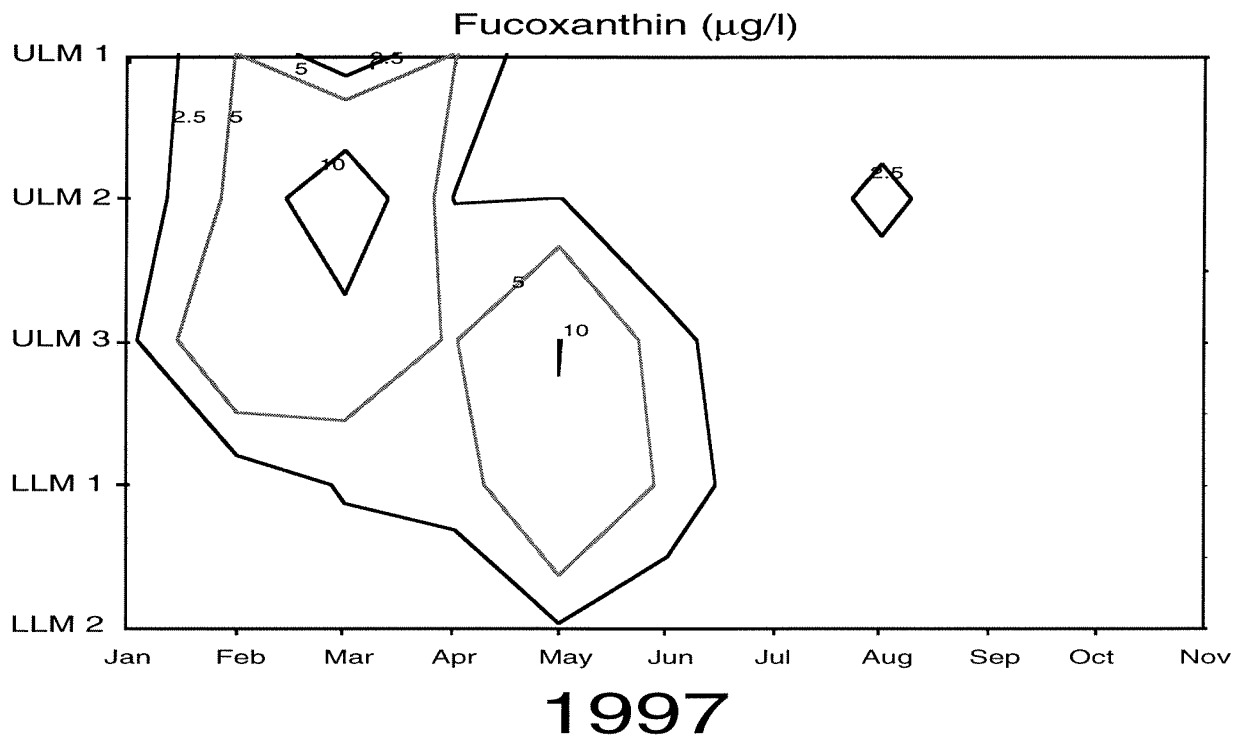


Figure 5. Contour plot of fucoxanthin concentration at the fixed sampling stations in Laguna Madre (from North to South) during the period January to November 1997.

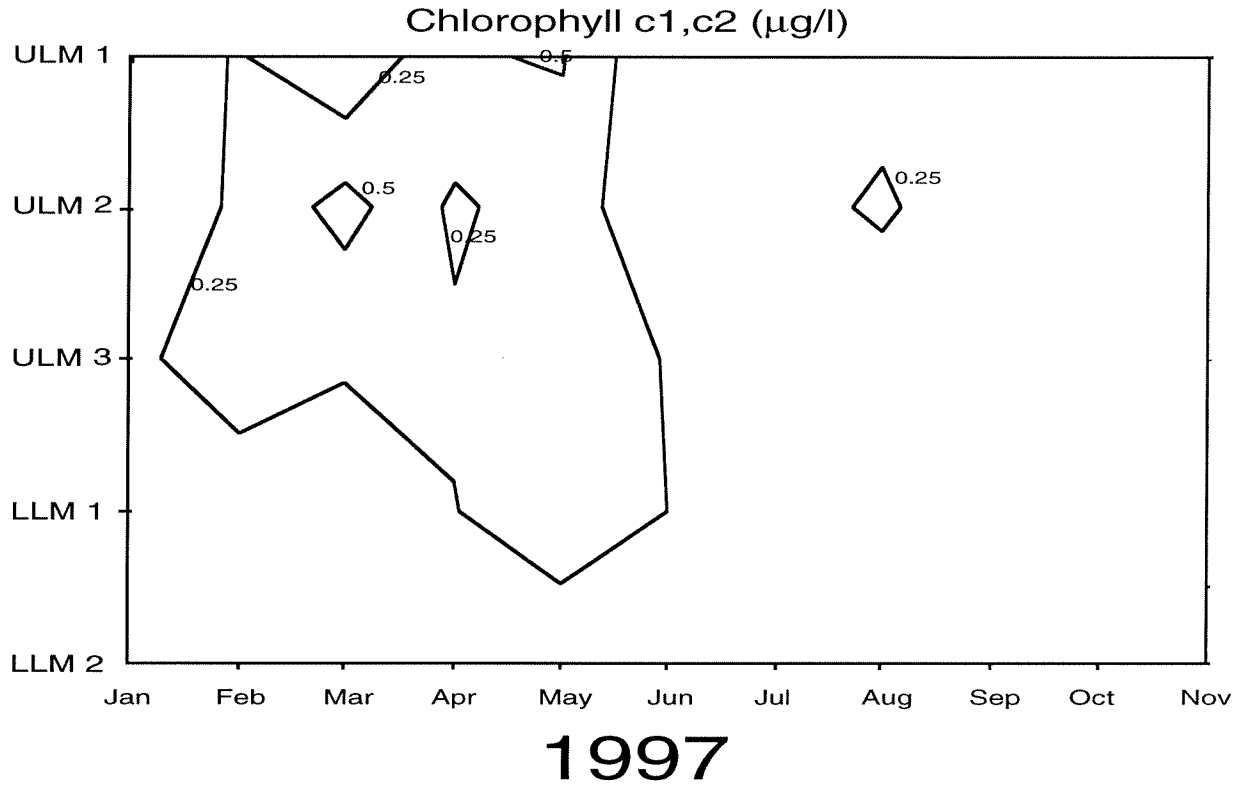


Figure 6. Contour plot of chlorophylls c_1 and c_2 concentration at the fixed sampling stations in Laguna Madre (from North to South) during the period January to November 1997.

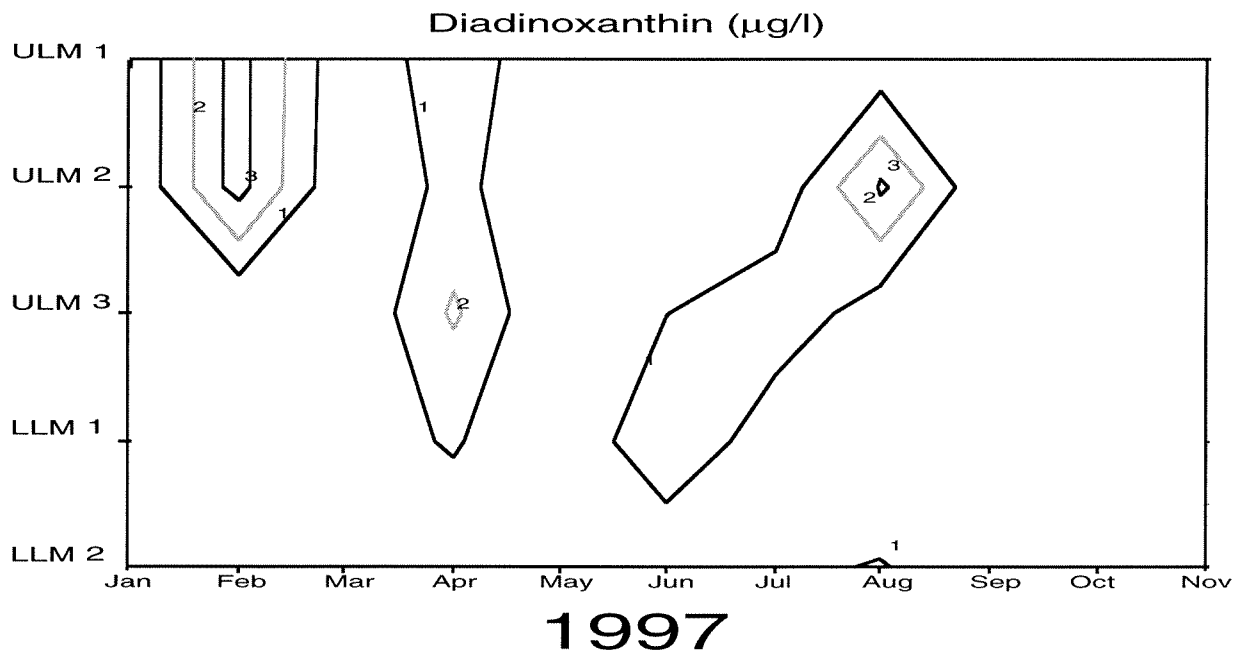


Figure 7. Contour plot of diadinoxanthin concentration at the fixed sampling stations in Laguna Madre (from North to South) during the period January to November 1997.

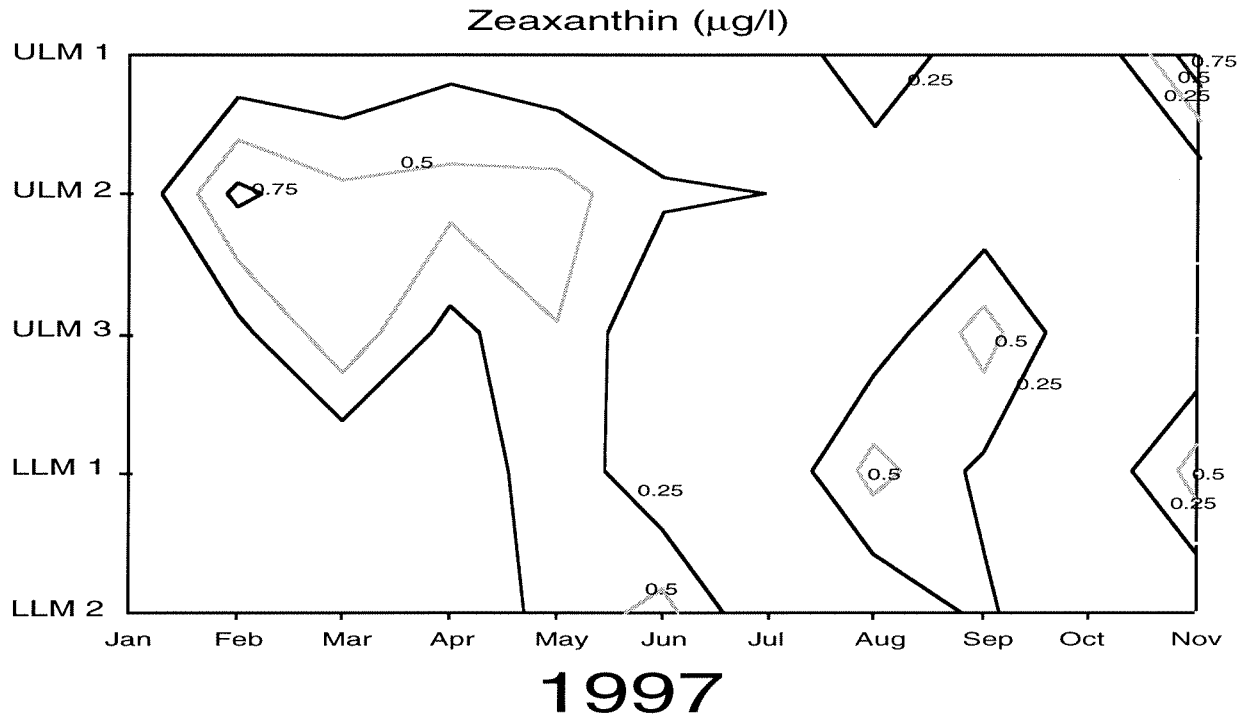


Figure 8. Contour plot of zeaxanthin concentration at the fixed sampling stations in Laguna Madre (from North to South) during the period January to November 1997.

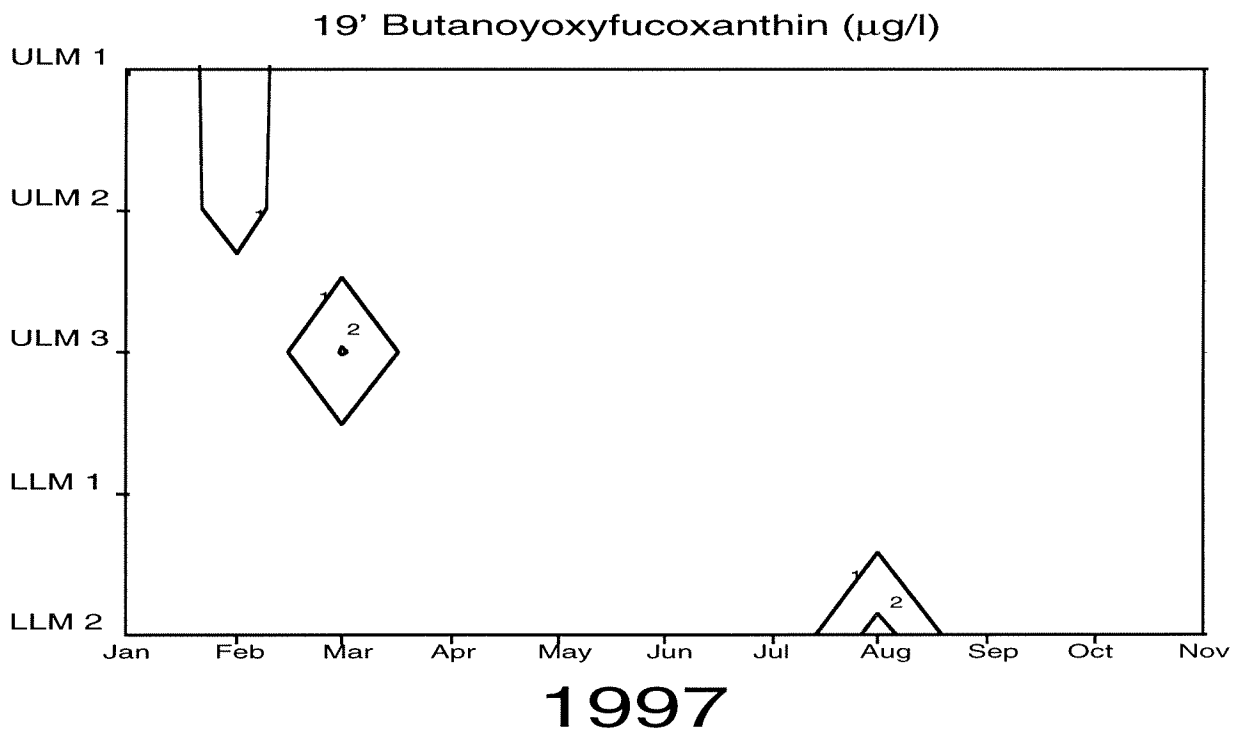


Figure 9. Contour plot of 19' butanoyloxyfucoxanthin concentration at the fixed sampling stations in Laguna Madre (from North to South) during the period January to November 1997.

The ratio of accessory pigments to chlorophyll *a* in a sample provides a technique to examine the relative contribution of various algal groups. Particular algal groups often have characteristic pigment ratios. For example, DeYoe et al. (1997) used pigment ratios, in part, to delineate between *A. anophagefferens*, *A. lagunensis* and *P. calceolata*, which are all members of the class Pelagophyceae. *A. lagunensis* characteristically has chl *c*:chl *a* ratio of 0.1, a fucoxanthin:chl *a* ratio of about 0.3 and a diadinoxanthin:chl *a* ratio around 0.1 (DeYoe et al. 1997). Using these values as a guideline, *A. lagunensis* appears to be the dominant phytoplankter at all of the sampling stations, with a few notable exceptions (Figs. 10 through 15). At LLM 1 during September 1997, the fucoxanthin:chl *a* and diadinoxanthin:chl *a* values were about 6.0, which are indicative of either diatoms or dinoflagellates. These extreme pigment ratios may have been related to the red tide bloom (*Gymnodinium breve*) that occurred at about the same time or to a wind event suspending benthic diatoms. The first winter fronts (i.e., wind events) generally occur during late September (Brown and Kraus 1997).

Seagrass pigments

Concentrations of chlorophyll *a*, chlorophyll *b* and lutein are shown for seagrasses in Table 4. Stations 13-20 were characterized by *Halodule wrightii*, stations 22-26 were dominated by *Syringodium filiforme* and stations 27-30 were dominated by *Thalassia testudinum*. Ratios of chlorophyll *b* to chlorophyll *a* varied from 0.51 to 0.80, but did not seem to vary with location in the Laguna. Although an order of magnitude smaller, .049 to .080, the range of values were similar for lutein to chlorophyll *a* ratios. Chlorophyll *b* to chlorophyll *a* ratios can be used as an indicator of light stress in seagrasses. High chl *b*:*a* ratios indicate that the plants have invested energy in an accessory pigment (i.e., chl *b*) in an attempt to maximize the light harvesting potential of the chloroplast. The chl *b*:*a* ratios calculated using spectrophotometric data, ranging between 0.3 and 0.5 (Czerny and Dunton 1995, Lee and Dunton 1996) were substantially lower than values calculated using HPLC methods (Table 4). This discrepancy is probably a result of the HPLC method's higher sensitivity and resolution.

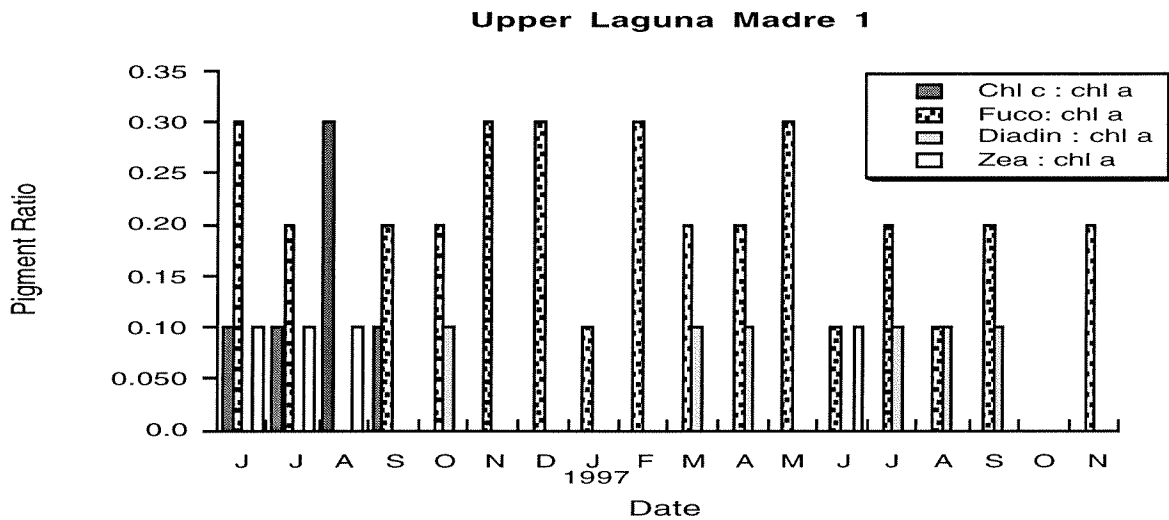


Figure 10. Pigment ratios for the most prevalent pigments relative to chl *a* at station ULM1 (Corpus Christi Bay) from June 1996 to November 1997. Missing data points are a result of pigment concentrations below the detection limit of HPLC.

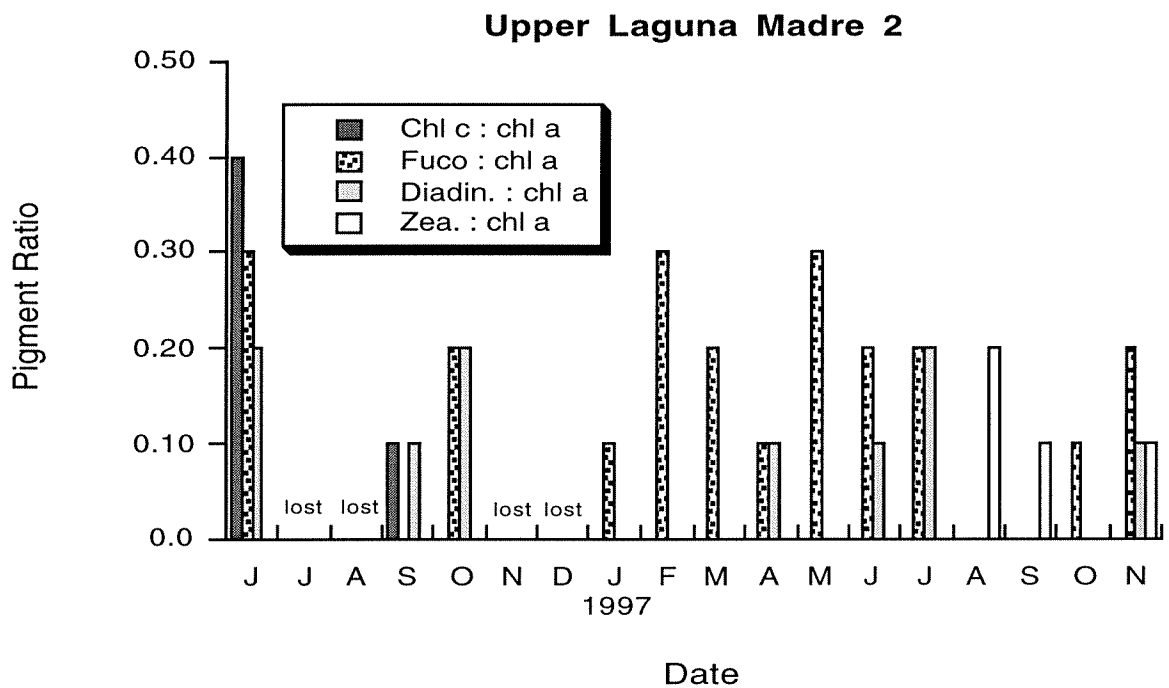


Figure 11. Pigment ratios for the most prevalent pigments relative to chl *a* at station ULM2 (South of Bird Island Basin) from June 1996 to November 1997. Missing data points are a result of pigment concentrations below the detection limit of HPLC.

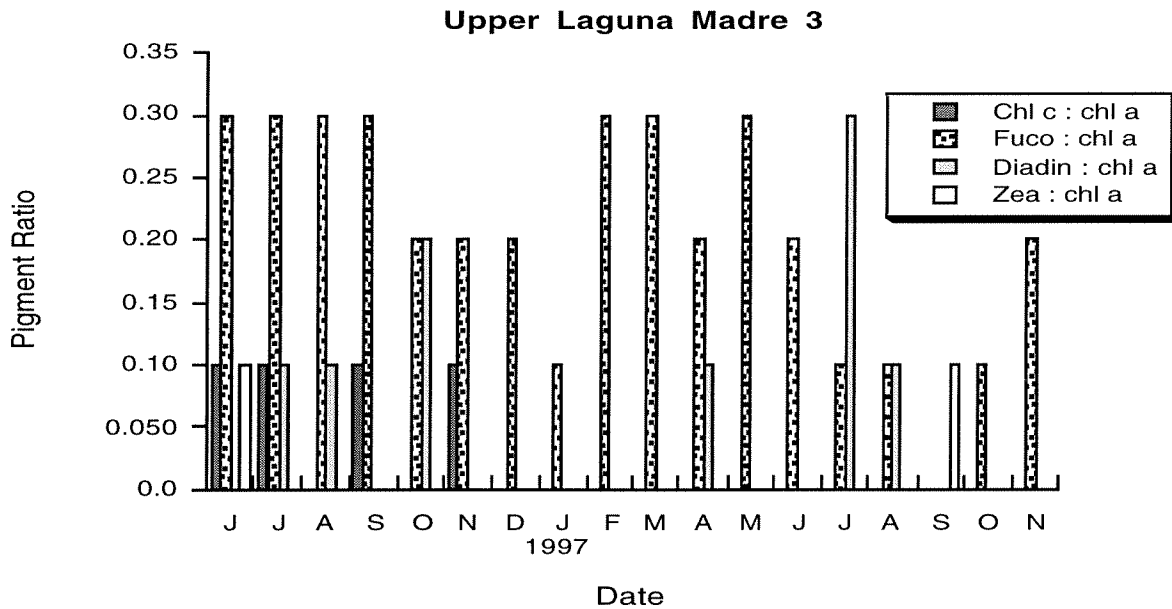


Figure 12. Pigment ratios for the most prevalent pigments relative to chl *a* at station ULM3 (North of the Land Cut) from June 1996 to November 1997. Missing data points are a result of pigment concentrations below the detection limit of HPLC.

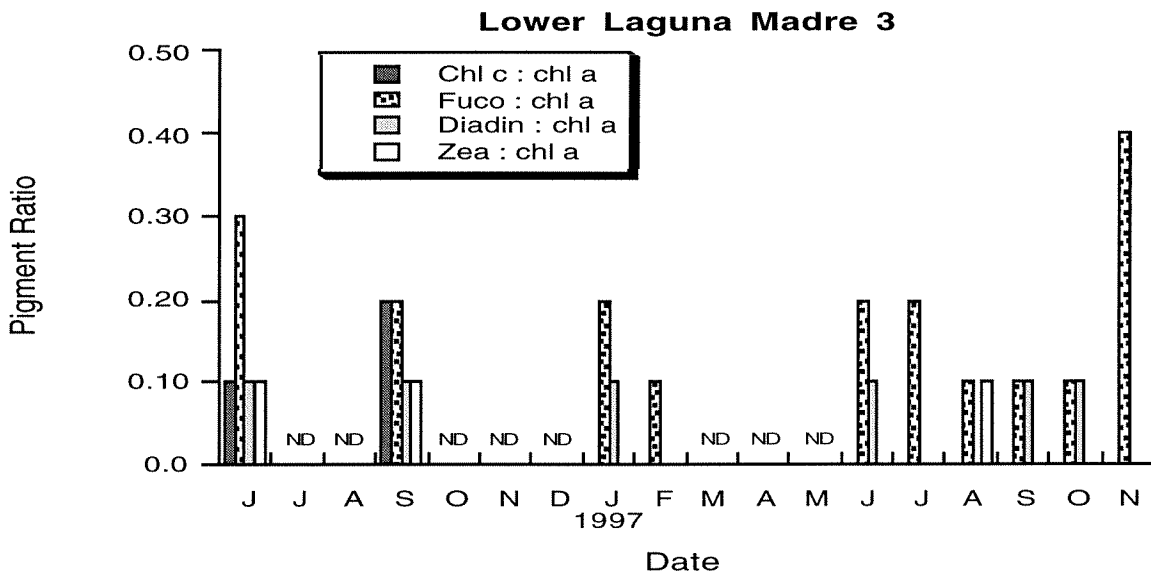


Figure 13. Pigment ratios for the most prevalent pigments relative to chl *a* at station LLM3(near Port Mansfield) from June 1996 to November 1997.

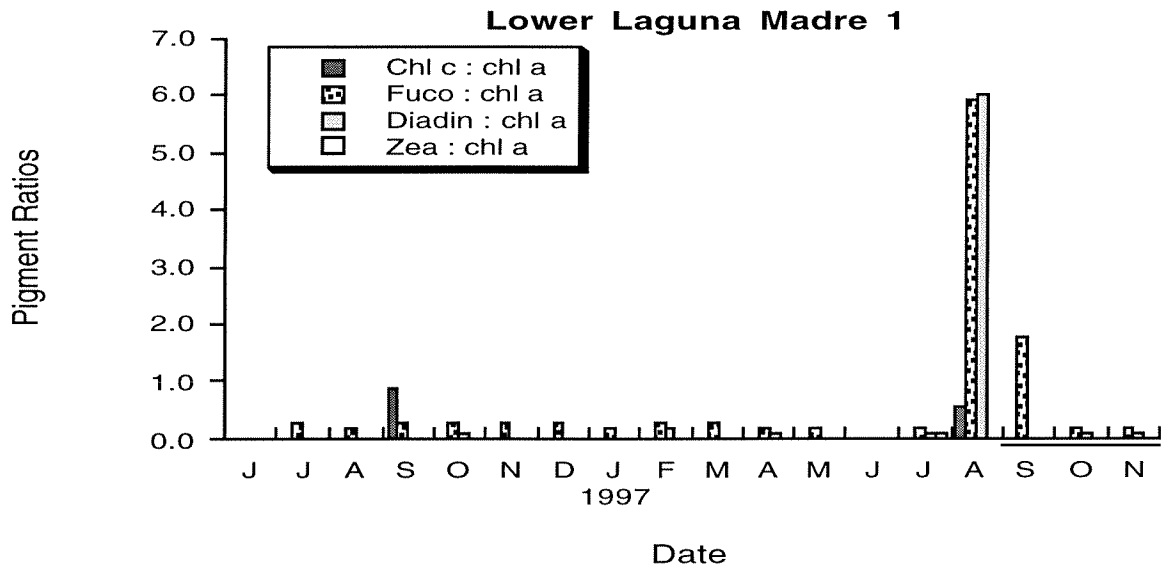


Figure 14. Pigment ratios for the most prevalent pigments relative to chl *a* at station LLM1 (dredged material placement area 233) from June 1996 to November 1997. Missing data points are a result of pigment concentrations below the detection limit of HPLC.

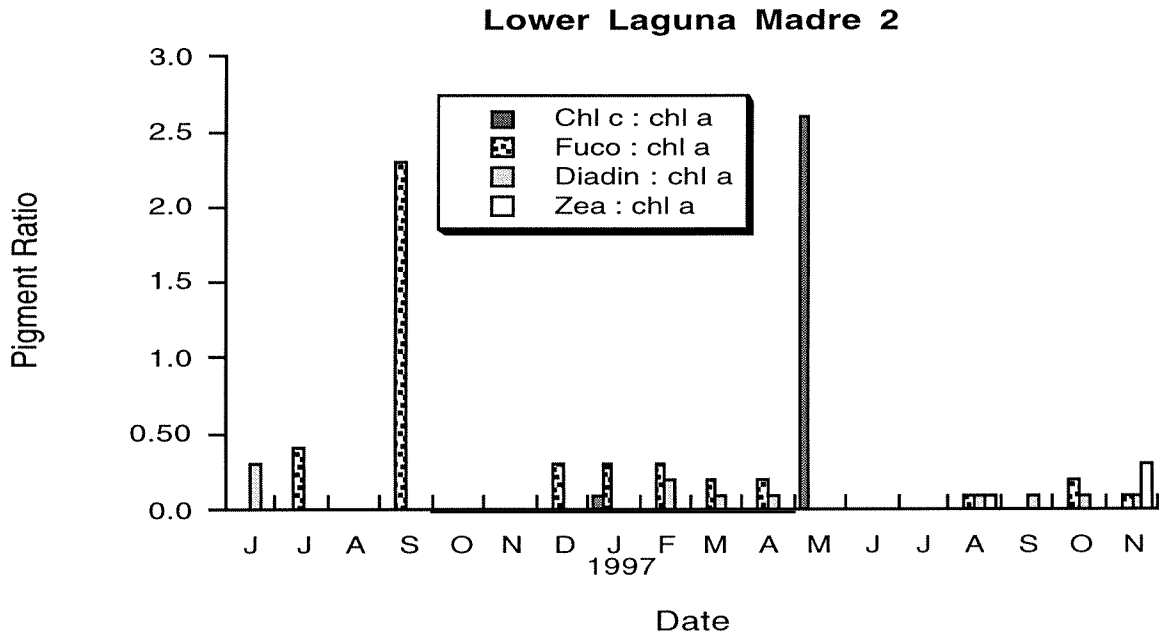


Figure 15. Pigment ratios for the most prevalent pigments relative to chl *a* at station LLM2 (seagrass bed near South Padre Island Convention Center) from June 1996 to November 1997. Missing data points are a result of pigment concentrations below the detection limit of HPLC.

Table 4. Seagrass HPLC pigment data for the summer 1996 cruise. Data are shown as mean concentration and standard deviation of quadruplicate samples taken at each station. See text for description of dominant seagrasses at each site. Included are the ratios of chlorophyll b to chlorophyll a (Chlb/Chla) and lutein to chlorophyll a (Lutein/Chla). A potential outlier is shown in bold type.

Station	Species	Chlorophyll a ($\mu\text{g g}^{-1}$)		Chlorophyll b ($\mu\text{g g}^{-1}$)		Lutein ($\mu\text{g g}^{-1}$)		Chlb/ Chla	Lutein/ Chla
		Conc.	Std.	Conc.	Std.	Conc.	Std.		
13	<i>Hw</i>	1804	140.1	915.6	53.38	95.30	25.22	0.51	0.053
16	<i>Hw</i>	1496	353.0	1107	748.7	92.96	23.82	0.74	0.062
18	<i>Hw</i>	1865	690.7	3009	3743	106.6	39.10	1.61	0.057
20	<i>Hw</i>	2126	439.4	1092	263.6	118.2	26.43	0.51	0.056
22	<i>Sf</i>	250.7	64.78	179.4	46.76	20.16	5.079	0.72	0.080
24	<i>Sf</i>	460.5	90.04	289.5	49.38	36.30	6.193	0.63	0.079
25	<i>Sf</i>	742.2	323.5	476.3	200.8	51.74	20.42	0.64	0.070
26	<i>Sf</i>	602.1	370.2	394.6	150.4	40.56	16.00	0.66	0.067
27	<i>Tt</i>	484.3	301.5	389.2	457.1	29.65	13.05	0.80	0.061
28	<i>Tt</i>	496.3	97.73	320.5	283.2	24.56	4.174	0.65	0.049
29	<i>Tt</i>	734.0	173.3	501.7	405.8	38.13	10.44	0.68	0.052
30	<i>Tt</i>	663.2	129.8	430.9	299.3	37.22	9.204	0.65	0.056

Laboratory pigment data

As mentioned earlier, Bidigare (1989) reported on the pigment composition of an *Aureococcus anophagefferens* culture (New England “brown tide”) obtained from E.M. Coper at SUNY, Stony Brook. We measured the pigment composition of a sample taken during a “brown tide” bloom in the ULM on 29 June 1996, and the type clone (TBA-2) of Texas “brown tide”. Samples of TBA-2 were obtained from Dr. Richard Greene at Texas A&M University. Comparisons of preliminary results are shown in Table 5 and Figure 16. These preliminary data indicate significant differences in pigment composition between field and laboratory samples of *A. lagunensis*. However, recent more thorough work, has shown a greater similarity in pigment ratios between cultured (TBA-2) and field samples of Texas “brown tide” (DeYoe et al. 1997). Furthermore, ribosomal RNA sequencing indicates that *A. anophagefferens* and *A. lagunensis* are distinct genera and species but both are distant relatives of *Pelagomonas calceolata* (DeYoe et al. 1995). The pigment composition of the Texas “brown tide” alga can be used in the spectral irradiance model to better describe light attenuation in the Laguna Madre.

Table 5. HPLC pigment data for “brown tide” alga. Data for *Aureococcus anophagefferens* are from Bidigare (1989). Abbreviations: a=chlorophyll *a*; c=chlorophyll *c*₁,*c*₂; bf=19'-butanoyloxyfucoxanthin; f=fucoxanthin; dn=diadinoxanthin; z=zeaxanthin; B.D.=below detection.

Sample	c:a	bf:a	f:a	dn:a	z:a
<i>Aureococcus anophagefferens</i> Bidigare (1989)	0.42	0.21	0.54	0.05	B.D.
Texas “brown tide” (clone TBA-2)	B.D.	B.D.	0.31	0.31	0.06
Sample from “brown tide” bloom	0.10	0.17	0.30	0.07	0.01

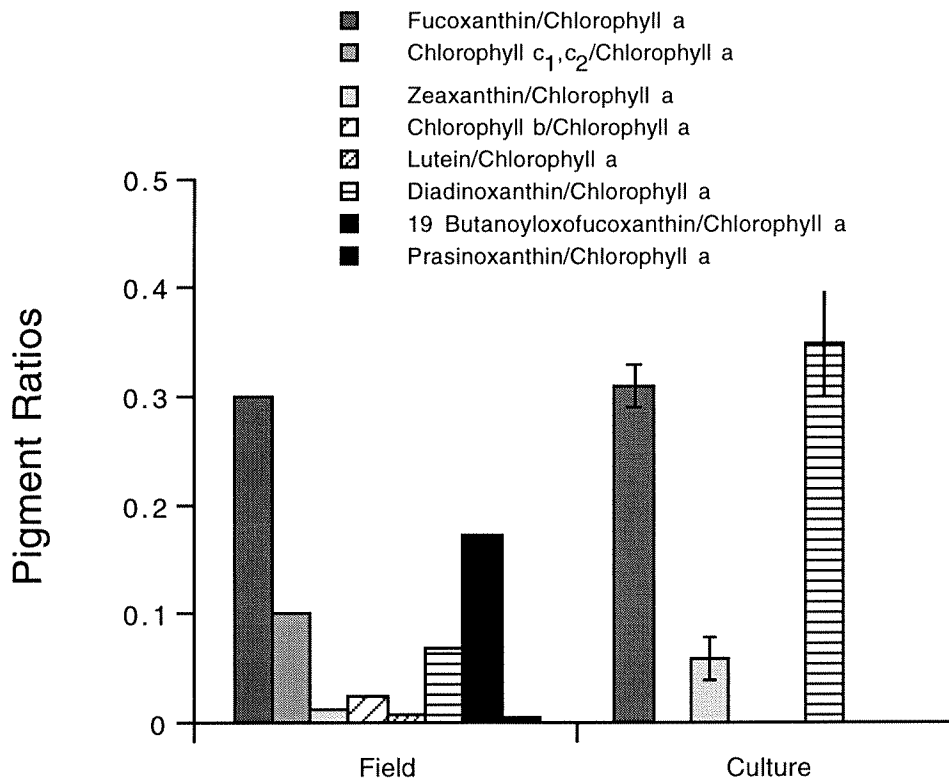


Fig. 16. Comparison of pigment ratios for *Aureoumbra lagunensis* from Upper Laguna Madre during a “brown tide” bloom and the isotype culture (TBA-2).

Laguna Madre Optical Properties

The overall goal of this effort was to develop accurate and efficient algorithms for computing the spectral downwelling irradiance incident on the bottom of Laguna Madre as a function of total suspended solids (TSS) concentration. Our approach was to first measure inherent optical properties (IOP's) along with TSS concentrations at a range of sites throughout Laguna Madre to obtain a functional database of IOP's versus TSS applicable to the region under study. From this database we were then able to derive a geo-optical model relating TSS to IOP's, or vice versa. Next, we computed the downwelling irradiance, $E_d(\lambda, z)$, at a bottom depth z for a range of TSS concentrations using the commercial software package Hydrolight, which numerically solves the radiative transfer equation. Our geo-optical model obtained from the Laguna Madre measurements allowed us to compute the IOP's, which serve as input parameters to Hydrolight, for the range of TSS concentrations that we used. Then, from E_d at the surface and bottom as computed by Hydrolight, we calculated the "bulk" downwelling, diffuse-attenuation coefficient, $\bar{K}_d(\lambda)$, over the photosynthetically active wavelength range, 400 – 700 nm. Finally, based on the computed database of $\bar{K}_d(\lambda)$ as a function of TSS, a direct relationship was derived between these two parameters.

Fundamentally, the logical flow of these relationships is $\text{TSS} \longrightarrow \text{IOP's} \longrightarrow E_d$. The first step, $\text{TSS} \longrightarrow \text{IOP's}$, is computed from the geo-optical model derived from the Laguna Madre measurements. The second step, $\text{IOP's} \longrightarrow E_d$, is computed with Hydrolight. It would be impractical, however, to incorporate Hydrolight directly into the L-M model because of the huge increase in computation time, complexity, and expense. Our approach was to use $E_d(\lambda)$ computed with Hydrolight to calculate a bulk $K_d(\lambda)$, denoted $\bar{K}_d(\lambda)$, which will be described below. Thus, using Hydrolight, we can take a third step, namely $E_d \longrightarrow \bar{K}_d$. Finally, we derived a direct relationship between $\bar{K}_d(\lambda)$ and TSS. Since the equation that relates E_d to $\bar{K}_d(\lambda)$

is easily inverted to obtain E_d from $\bar{K}_d(\lambda)$, we have, finally, the logical flow of our rapid model: $TSS \longrightarrow K_d \longrightarrow E_d$, with simple analytical equations represented by the connecting arrows.

AC9 Measurements

The AC9[®] measures the volume absorption and beam attenuation coefficients, denoted a and c , respectively, at nine wavelengths, where wavelength is denoted by λ . Absorption is measured by sending a known beam of light through a highly reflective sample cell to a detector. The light not reaching the detector is absorbed, because the high reflectivity permits measurement of scattered light. Backscattering is corrected using an empirical formula. Total attenuation (c) is measured by sending a known collimated light beam through an optically black sample cell to a detector. The attenuation is determined by the difference between the amount of light projected into the cell and the amount measured at the detector. The nine wavelengths are: 412, 440, 488, 510, 532, 589, 620, 676, 715 nm.

Because the AC9 is a flow-through, pumped system, a time series of a and c was measured at each station and the average values computed over a segment of each series. Examples of the spectra of a and c are shown in Figures 17 and 18. Note that both a and c yield exponential curves as a function of λ . This was consistent throughout all of the data sets and indicates that the dominant influence on the inherent optical properties (IOP's) is the total suspended solids (TSS), presumed to be primarily inorganic resuspended sediments.

For the purposes of modeling, we will parameterize the absorption coefficient $a(\lambda)$ and the total scattering coefficient $b(\lambda) = c(\lambda) - a(\lambda)$ with exponentials of the form:

$$a(\lambda) = a(\lambda_0) \exp[-\gamma_a(\lambda - \lambda_0)], \quad (\text{EQ 1})$$

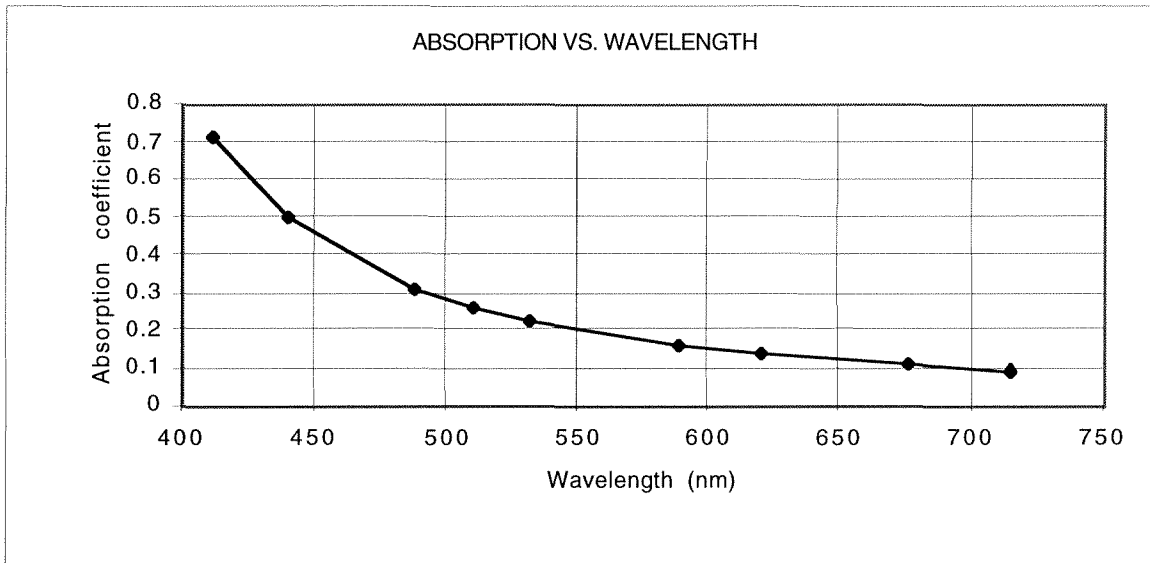


Fig 17. Absorption coefficient a (m^{-1}) versus wavelength (nm).

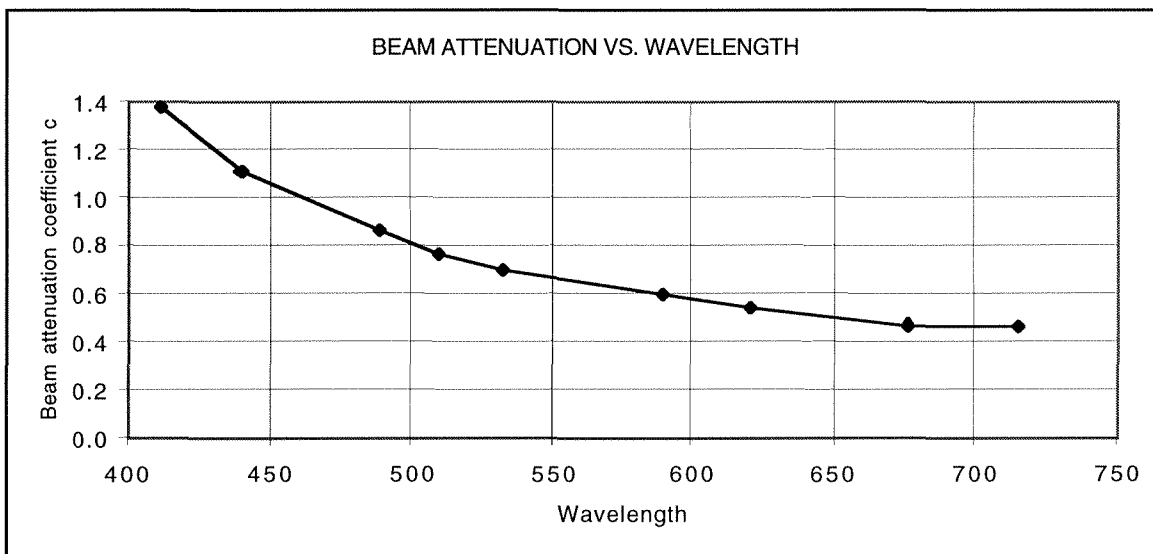


Fig 18. Beam attenuation coefficient c (m^{-1}) versus wavelength (nm).

$$b(\lambda) = b(\lambda_0) \exp[-\gamma_b(\lambda - \lambda_0)], \quad (\text{EQ 2})$$

where $\lambda_0 = 412$ nm is the reference wavelength and γ_a , γ_b are exponential coefficients for absorption and scattering. Note that, in general, γ_a , γ_b are functions of the type of sediment. For Laguna Madre, we assume that these coefficients are constant. Preliminary analysis of the data indicates that this is a good assumption.

The total scattering coefficient b is used instead of the beam attenuation coefficient c because b is a more fundamental optical property. Although c is measured directly with the AC9, it is a derivative optical quantity from a and b , namely $c = a + b$. It is the absorption and scattering properties of the suspended sediments, as characterized by a and b , that we wish to determine.

PRR Measurements

The PRR600 measures the spectral irradiance E_d at six wavelengths, plus PAR (photosynthetically available radiation), and the spectral radiance L_u at six wavelengths. The wavelengths are : 380, 412, 443, 490, 510, 555. In addition to the in-water radiometric measurements made with the PRR600, the downwelling spectral irradiance onto the surface of the water was measured with a surface radiometer. At most of the sites, these radiometric measurements were made at two depths. Measurements of E_d at two depths yield the downwelling diffuse attenuation coefficient, K_d . The relationship between $E_d(z)$, where z is the depth, and K_d is given by

$$E_d(z_2) = E_d(z_1) \exp[-K_d(z_2 - z_1)] \quad (\text{EQ 3})$$

assuming Beer's law. In this coordinate system, z is positive downward so the $z_2 > z_1$.

From these measurements and computations of K_d , which, it should be noted, is a function of λ , the solar irradiance incident on the bottom, or more importantly on a seagrass canopy, can be computed. One objective then is to relate $K_d(\lambda)$ to the TSS. Once K_d can be estimated or modeled for a given amount of resuspended sediments as quantified by TSS, the downwelling spectral irradiance incident on the bottom or a seagrass canopy can be computed.

Example spectra of $E_d(\lambda)$ measured at Laguna Madre with the PRR 600 are shown in Figures 19 and 20. Figure 19 shows the results of a relatively low concentration on TSS at a depth of 0.77 m and Figure 20 shows the results at a relatively high concentration at a slightly shallower depth of 0.5 m. Note not only the significantly lower values of E_d at the higher TSS concentrations, as expected, but also the change in the spectral curve in going from low to high concentrations of TSS. This effect is a result of exponential dependence of a , and especially b , on wavelength for inorganic resuspended sediments, as we found in Laguna Madre.

TSS Measurements

Total suspended solids were determined from bottle samples, which were taken directly from the water flowing through the AC9. The sample was filtered in duplicate. These averages were used in correlating TSS with a , b , and c .

AC9 versus TSS

To see how well the inherent optical properties (IOP's) correlated with TSS for the data collected at Laguna Madre, we plotted c , a , and $b = c - a$, versus TSS. Figures 21 and 22 show

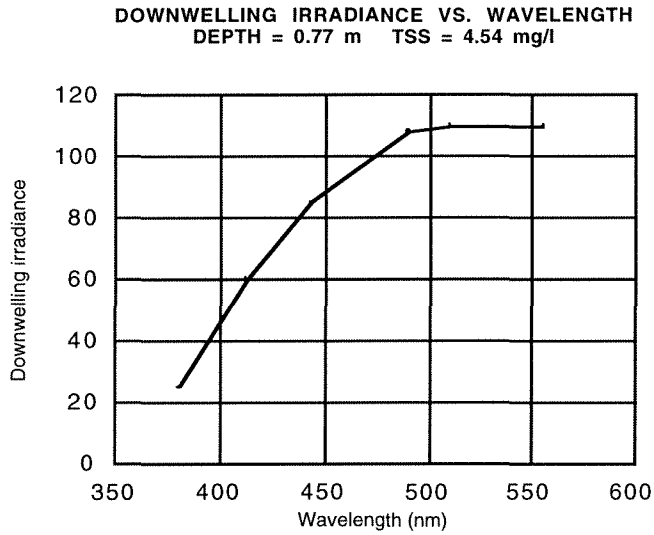


Fig 19. Downwelling irradiance ($\text{watts m}^{-2} \text{nm}^{-1}$) versus wavelength (nm) for TSS = 4.54 mg/L at a depth of 0.77 m

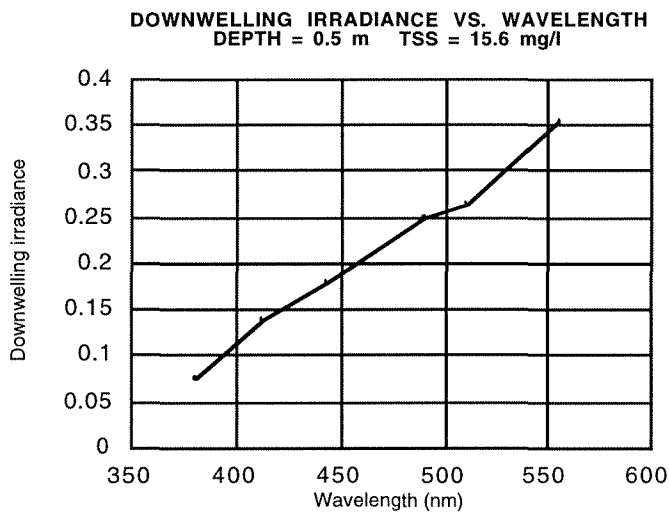


Fig 20. Downwelling irradiance ($\text{watts m}^{-2} \text{nm}^{-1}$) versus wavelength (nm) for TSS = 15.6 mg/L at a depth of 0.5 m

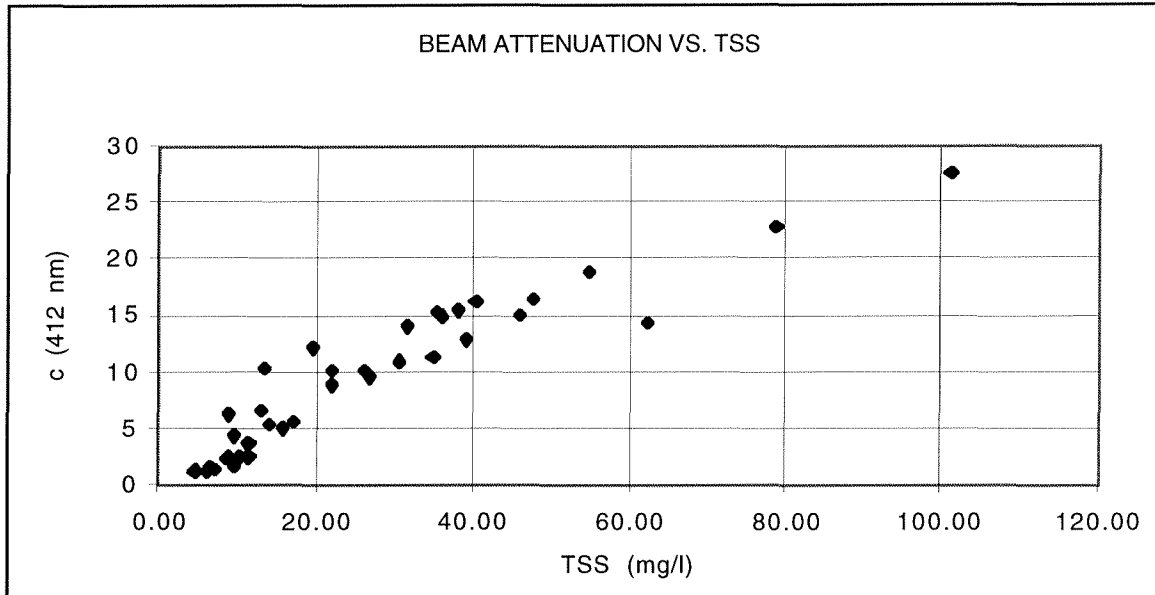


Fig 21. Beam attenuation coefficient c (m^{-1}) versus TSS (mg/L) at a wavelength of 412 nm.

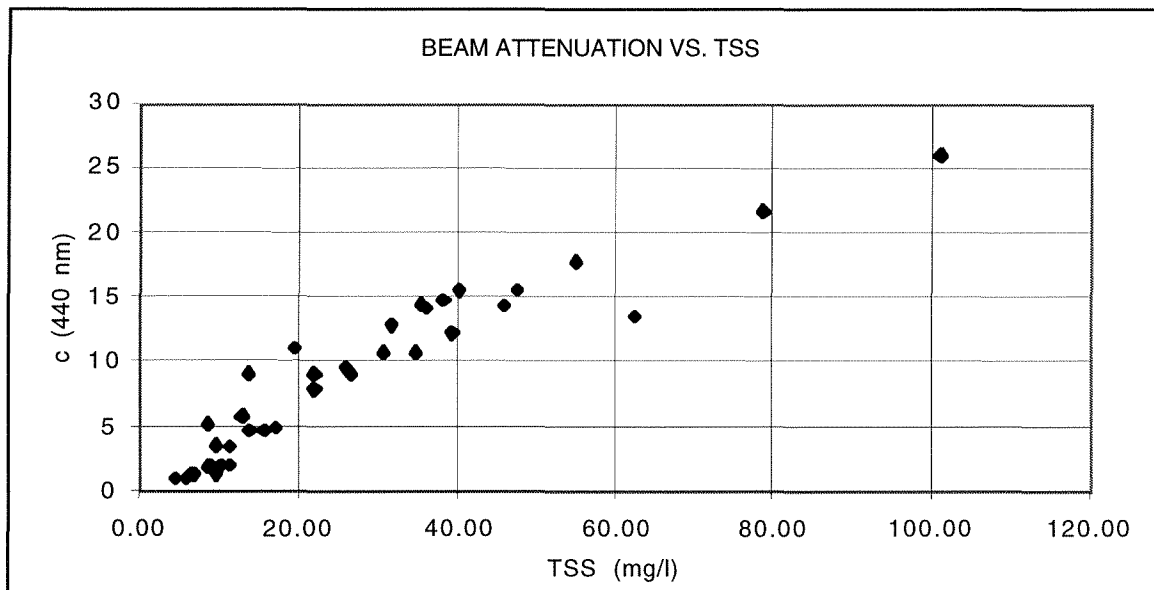


Fig 22. Beam attenuation coefficient c (m^{-1}) versus TSS (mg/L) at a wavelength of 440 nm.

beam attenuation at 412 and 440 nm, respectively, versus TSS. Note the surprisingly good correlation of c with TSS, including various locations and times at Laguna Madre. There are a few outliers, but if these outliers are considered to be accurate measurements, then perhaps they can be associated with anomalous field conditions.

Figures 23 and 24 show absorption at the same two wavelengths (412,440) versus TSS. Clearly the correlation is not nearly as good as with beam attenuation. It is possible that the scatter in the absorption versus TSS correlation is due to measurement errors in the absorption coefficient. The absorption measured by the AC9 is known to contain errors due to scattering. To some degree this error can be corrected, and was corrected in the data shown here. However, the scattering error cannot be removed completely. Nonetheless, due to the systematic nature of the scattering error, it is unlikely that most of the “scatter” in the plot of a versus TSS is due only, or even primarily, to the errors in the absorption measurement. There is a strong possibility that the absorption contained significant contributions from colored dissolved organic matter (CDOM) that was to some degree not correlated with the scattering caused by the suspended solids. Also, absorption by suspended sediments is not well known or characterized, and our results may simply reflect the natural variability in absorption by these inorganic particles, or a change of the fraction of organic versus inorganic solids that may have varied as a function of TSS concentration.

In Laguna Madre (excluding brown tide), it is clearly suspended solids, primarily inorganic, which have the largest effect on the water optical properties. These suspended sediment particles scatter much more light than they absorb (although the scattering does “enhance” the absorption via optical pathlength increase). It is to be expected that the magnitude of scattering increases in proportion to particle concentration. Thus, of the optical properties a , b , and c , we should expect b to yield the greatest correlation with TSS. Figures 25 and 26 show the total scattering coefficient b versus TSS. As with the beam attenuation coefficient c , the total scattering coefficient b shows a high correlation with TSS. This is to be expected since the largest

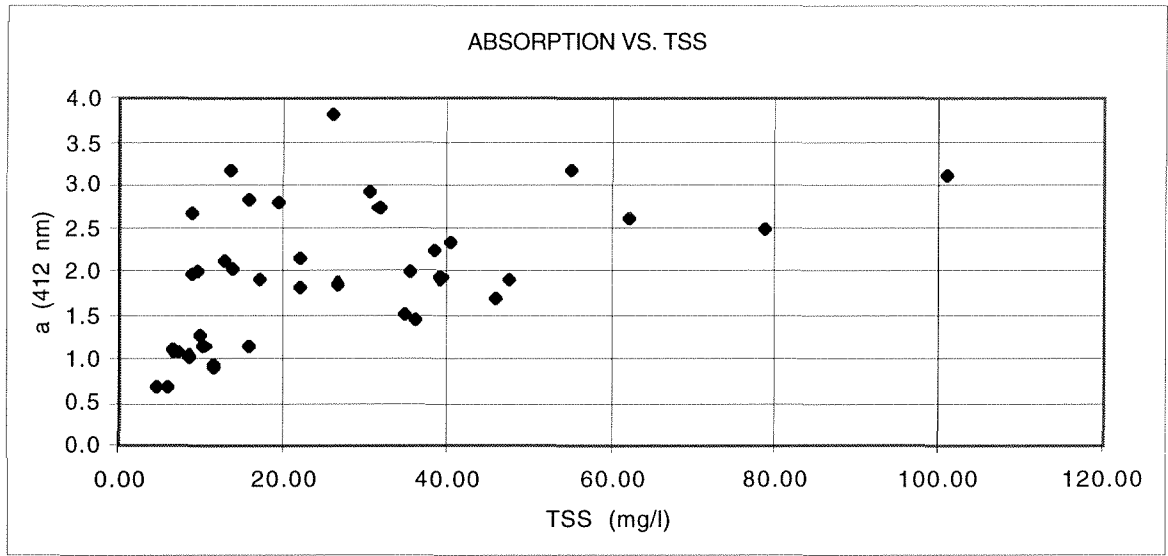


Fig 23. Absorption coefficient a (m^{-1}) versus TSS (mg/L) at a wavelength of 412 nm.

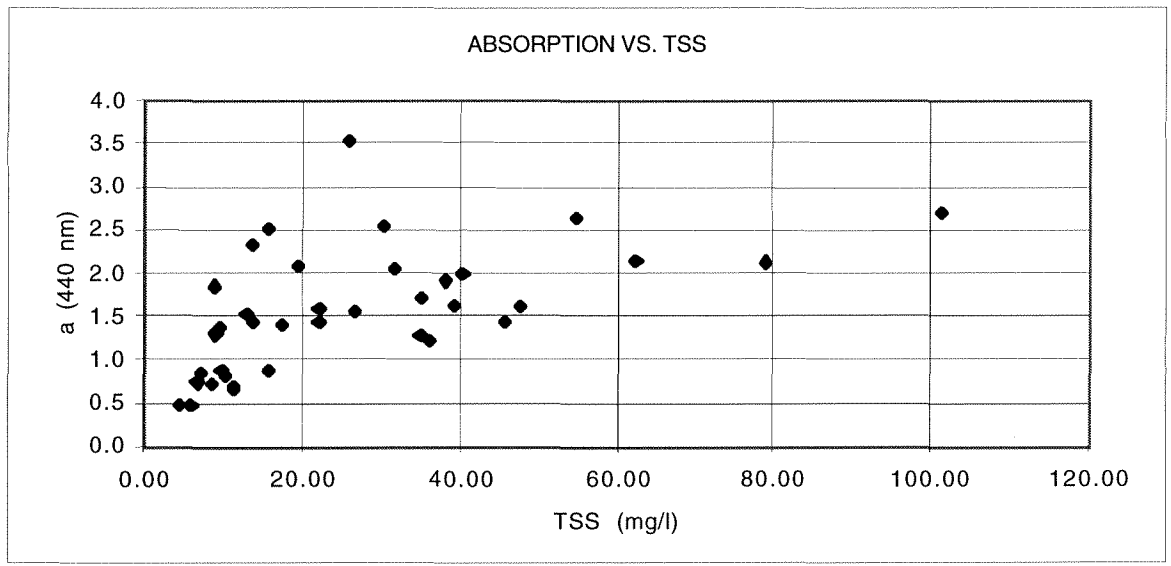


Fig 24. Absorption coefficient a (m^{-1}) versus TSS (mg/L) at a wavelength of 440 nm.

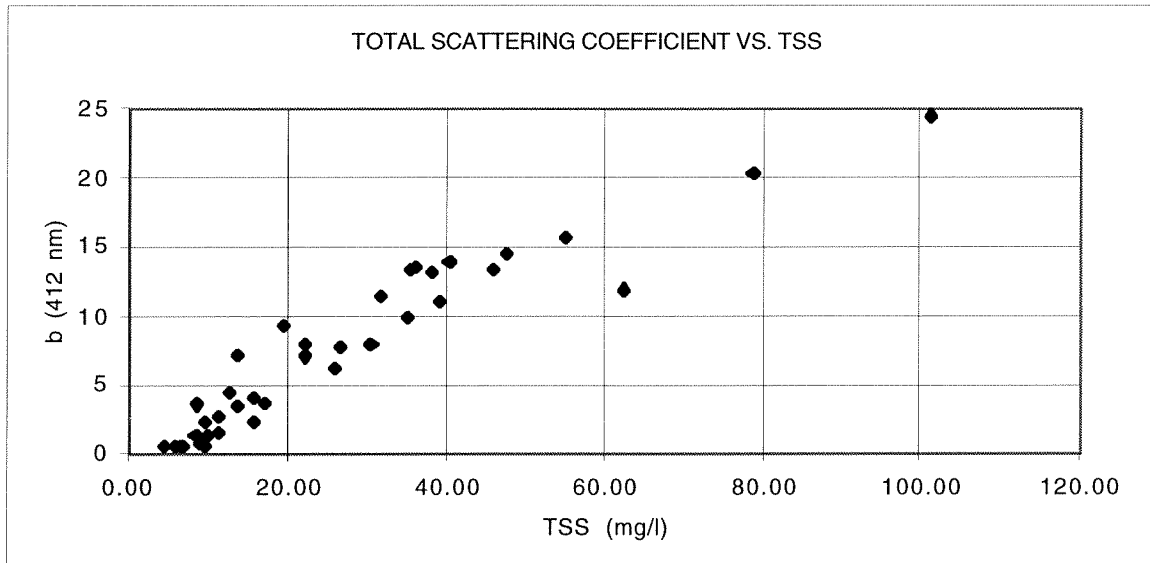


Fig 25. Total scattering coefficient coefficient $b(m^{-1})$ versus TSS (mg/L) at a wavelength of 412 nm.

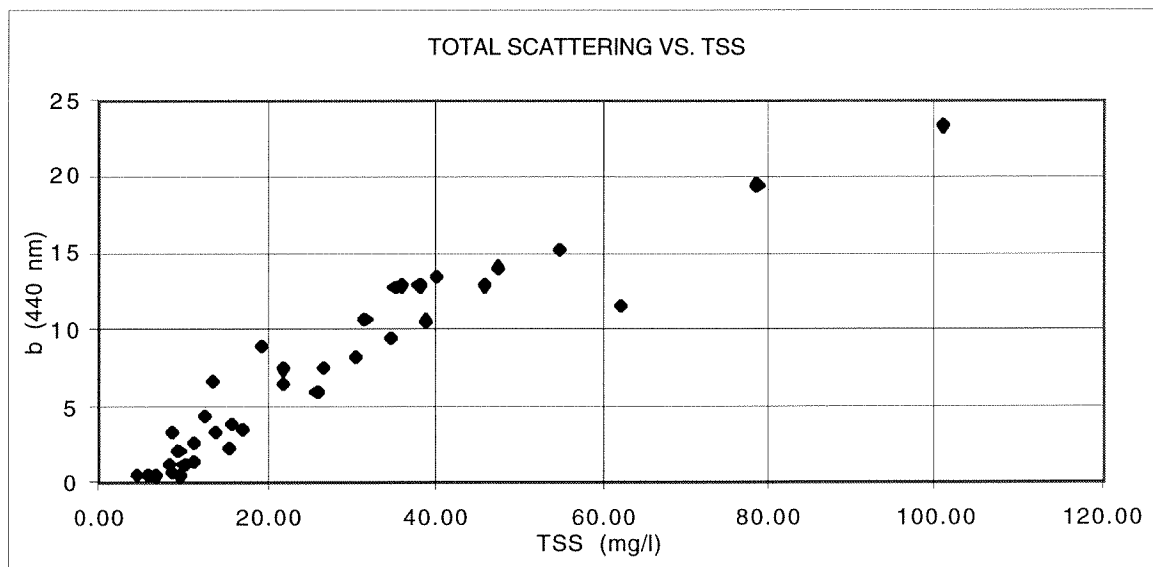


Fig 26. Total scattering coefficient coefficient $b(m^{-1})$ versus TSS (mg/L) at a wavelength of 440 nm.

contribution to c comes from b (recall that $c = a + b$). More importantly, b , unlike c , does not contain the effect of absorption, so the correlation of b with TSS is expected to be better than it is with c , which is indeed the case with our data set. Thus, except for probably a single outlier at about TSS = 61 mg/L, the Laguna Madre data set gives an excellent linear correlation of b with TSS. This result allows us to accurately model the effects of light attenuation due to scattering by suspended sediments in Laguna Madre.

It is of interest to calculate the slope of the IOP's versus TSS for various wavelengths, to investigate the wavelength dependence on the slopes. This is important for the overall modeling of PAR as a function of suspended sediment concentrations. Figures 27, 28, and 29 show these results for c , a , and $b = c - a$, respectively. Interestingly, the slope versus wavelength for c is nearly linear. For a , the slope dependence on wavelength is not as simple, but it is still surprisingly monotonic, although it should be remembered that the correlation of a with TSS was not very good. As should be expected, we obtain the "smoothest" relationship of slope versus wavelength for b .

Hydrolight Model

The first step was to develop the geo-optical model relating TSS to the IOP's, namely the spectral absorption and total scattering coefficients, $a(\lambda)$ and $b(\lambda)$, respectively. As stated earlier, in-situ measurements of a and b were performed at a range of sites in both the Lower and Upper Laguna. At all of these sites, bottle samples were taken and later analyzed for TSS concentration. Figure 30 shows an example of b versus TSS at 589 nm, which is one of the nine wavelengths (412, 442, 488, 510, 532, 589, 620, 676, 715) that the AC9 measures these coefficients. As expected, a simple linear regression best fit the data. The slope of this line is referred to as the specific scattering coefficient, b^* , and in this case has units of $L\ mg^{-1}\ m^{-1}$. The relationship between TSS and $b(\lambda)$ is then $b(\lambda) = b^*(\lambda)TSS$, where TSS is given in units of mg/L. Figure 31 shows the resulting graph of $b^*(\lambda)$ at all nine wavelengths. As can be seen in this figure, $b^*(\lambda)$ is accurately modeled by a linear function of wavelength. A linear regression yielded the result

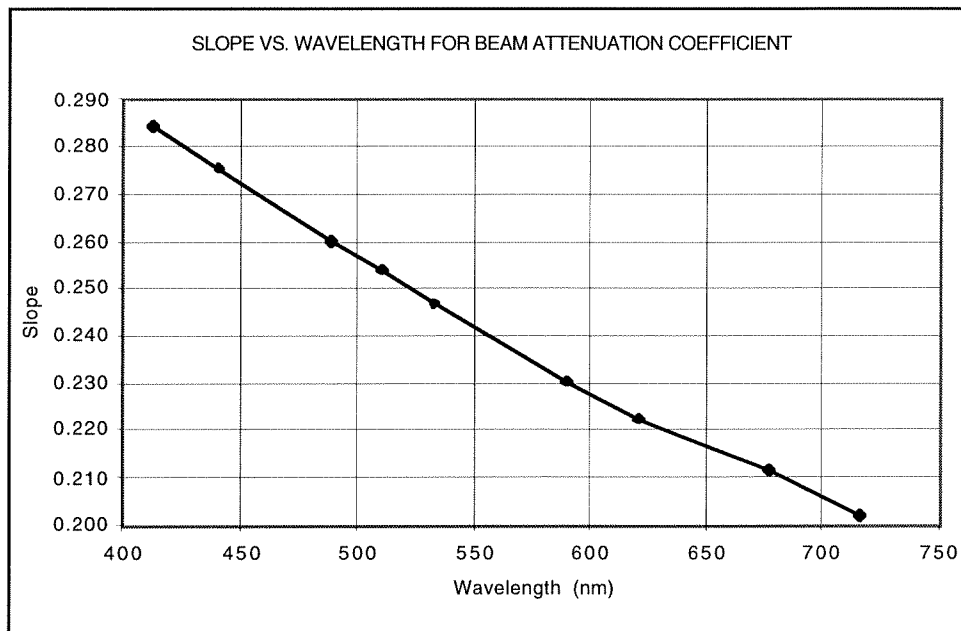


Fig 27. Slope ($L\ mg^{-1}\ m^{-1}$) versus wavelength (nm) for the beam attenuation coefficient.

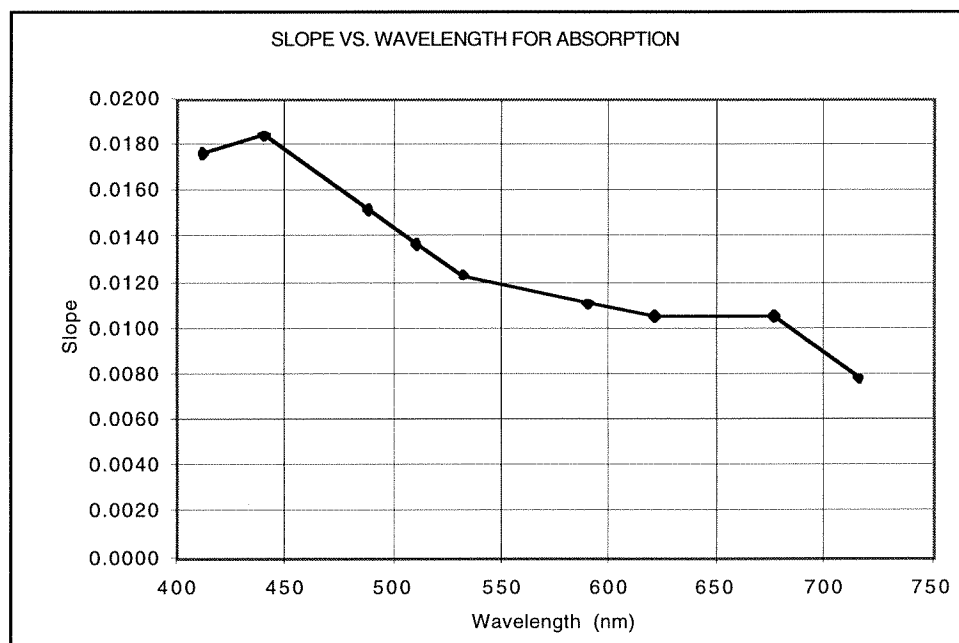


Fig 28. Slope ($L\ mg^{-1}\ m^{-1}$) versus wavelength (nm) for absorption.

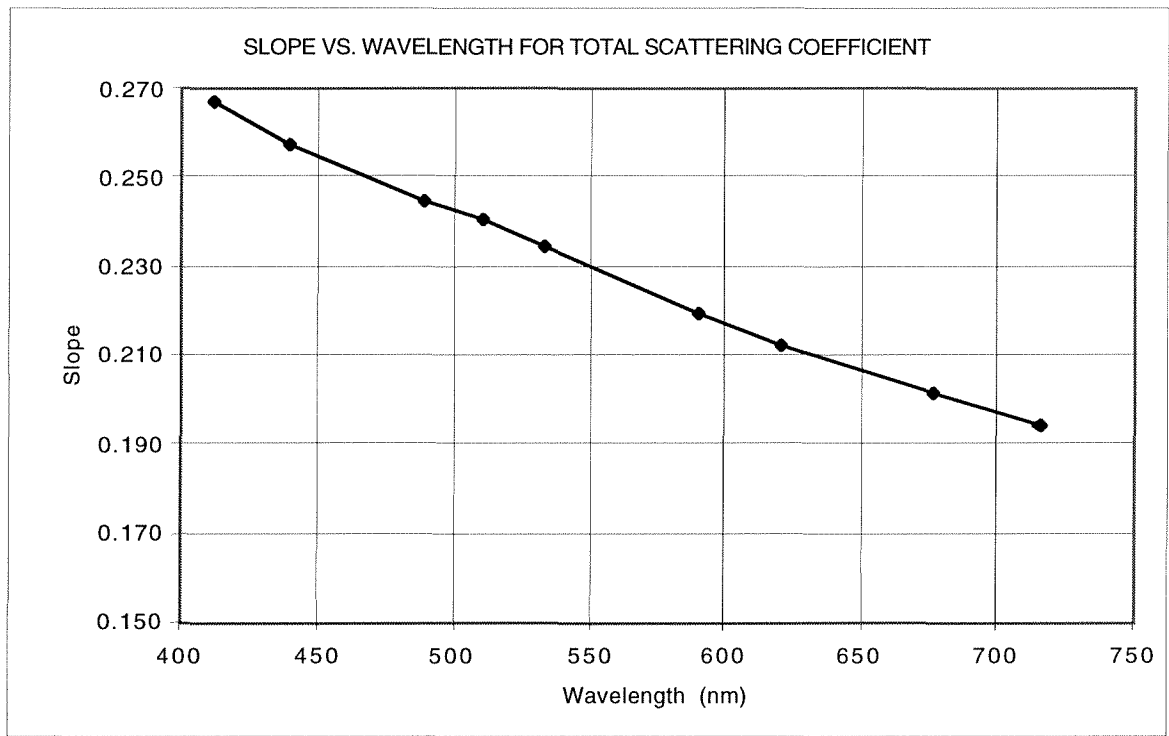


Fig 29. Slope ($L\ mg^{-1}\ m^{-1}$) versus wavelength (nm) for the total scattering coefficient.

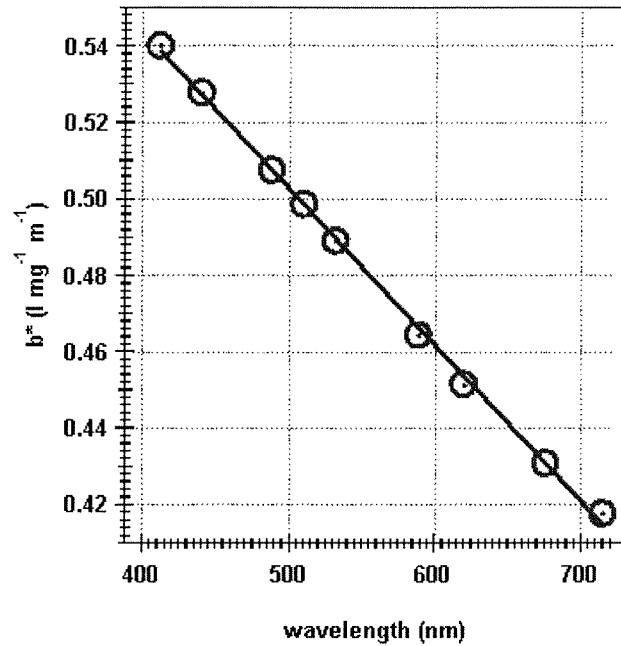


Fig 30. Measurements of the total scattering coefficient $b(589\text{ nm})$ vs. concomitant measurements of TSS concentration at Laguna Madre.

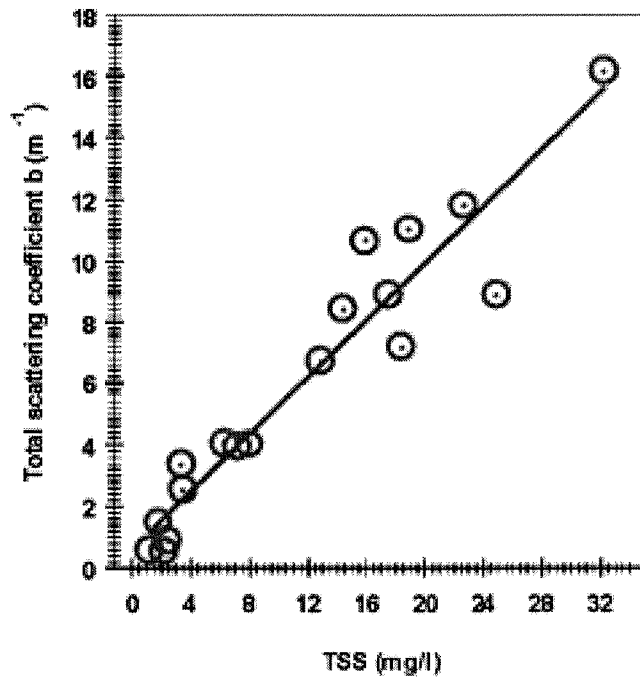


Fig 31. Specific scattering coefficient b^* as a function of wavelength derived from Laguna Madre measurements.

$$b^*(\lambda) = 0.707 - 0.000409\lambda \quad (\text{EQ 4})$$

where the wavelength λ is in units of nm.

The absorption coefficient was similarly modeled. Figure 32 shows an example of a versus TSS at 589 nm. The slope is the specific absorption coefficient a^* , which was computed at all nine wavelengths. Figure 33 shows the resulting graph of $a^*(\lambda)$. In this case we found that an exponential function best fit the data. An least-squares regression gave the result

$$a^*(\lambda) = 0.0191 + 2.69\exp(-0.0101\lambda). \quad (\text{EQ 5})$$

Equations 4 and 5 are the algorithms that allow one to compute the spectral total scattering and absorption coefficients for any given value of TSS concentration.

The next step was to compute the spectral total scattering and absorption coefficients for a range of TSS concentrations from 0 to 100 mg/L. Using this resulting database of $b(\lambda)$ and $a(\lambda)$ as input parameters to Hydrolight, we computed $E_d(\lambda, z)$ at a bottom depth $z = 2$ m. The spectral downwelling irradiance $E_d(\lambda, z)$ at depth z can be expressed by

$$E_d(\lambda, z) = E_d(\lambda, 0)\exp[-\bar{K}_d(\lambda)z] \quad (\text{EQ 6})$$

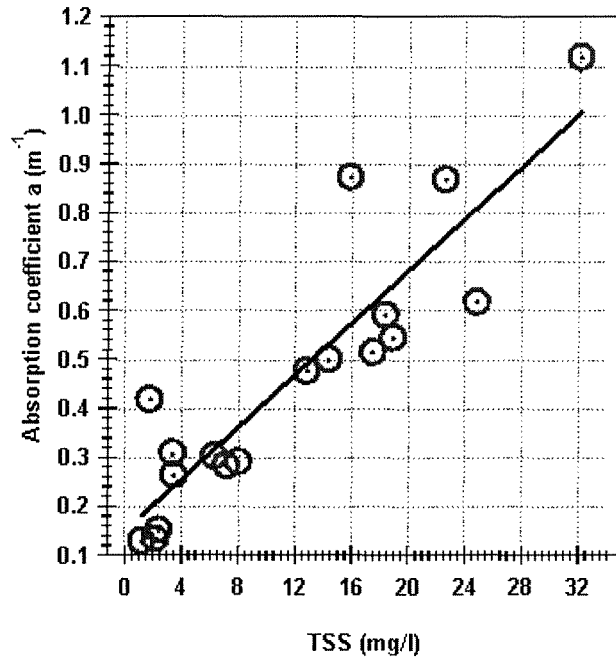


Fig 32. Measurements of the absorption coefficient $a(589 \text{ nm})$ vs. concomitant measurements of TSS concentration at Laguna Madre.

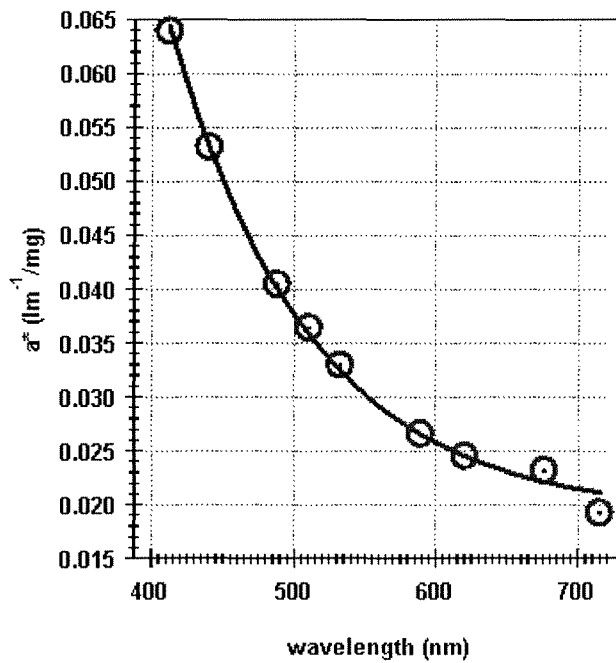


Fig 33. Specific absorption coefficient a^* as a function of wavelength derived from Laguna Madre measurements.

where $E_d(\lambda, 0)$ is the downwelling irradiance just below the surface and $\bar{K}_d(\lambda)$ is the “bulk” downwelling irradiance attenuation coefficient. Given values for the input parameters $b(\lambda)$ and $a(\lambda)$ and certain boundary conditions, Hydrolight provides as output $E_d(\lambda, 0)$ and $E_d(\lambda, z)$. From the Hydrolight output, $a(\lambda)$ can be computed by inverting EQ 6, namely,

$$\bar{K}_d = \frac{\ln[E_d(\lambda, 0) / E_d(\lambda, z)]}{z}. \quad (\text{EQ 7})$$

Since K_d results from a particular set of IOP's b and a , and b and a were derived from a particular TSS concentration, K_d can be directly related to TSS. An example for 580 nm is shown in Figure 34. Clearly, a linear relationship between K_d and TSS exists, and the slope is the specific downwelling attenuation coefficient, $\bar{K}_d^*(\lambda)$. Figure 35 shows the resulting graph of $\bar{K}_d^*(\lambda)$ as a function of wavelength for a particular set of boundary conditions. For all boundary conditions relevant to Laguna Madre, we found that an exponential function best fit the $\bar{K}_d^*(\lambda)$ versus TSS data. The most important boundary condition is the sun angle. After computing a multivariate database of $\bar{K}_d^*(\lambda)$ versus TSS for sun angles from 0 to 90 degrees, a least-squares regression gave the best fit equation,

$$\bar{K}_d(\lambda) = \frac{a_w(\lambda)}{\cos\theta_s} + [0.0255 + 0.537 \exp(-0.00441\lambda)]TSS \quad (\text{EQ 8})$$

where θ_s is the *refracted* sun angle and $a_w(\lambda)$ is the absorption coefficient of pure water (Pope and Fry, 1997). This model is valid from 400 to 700 nm and accurate for bottom depths in the range $0.5\text{m} \leq z \leq 4\text{m}$ and demonstrably valid in the TSS range $0 \leq \text{TSS} \leq 100\text{mg/L}$, although we are confident that the model is valid at TSS concentrations above 200 mg/L.

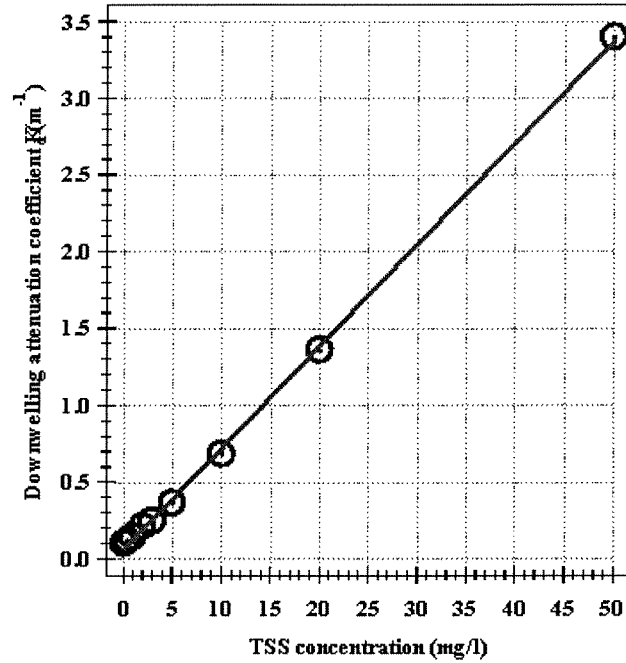


Fig 34. Downwelling attenuation coefficient $K_d(580 \text{ nm})$ as a function of TSS derived from Eq. 4 using output from Hydrolight.

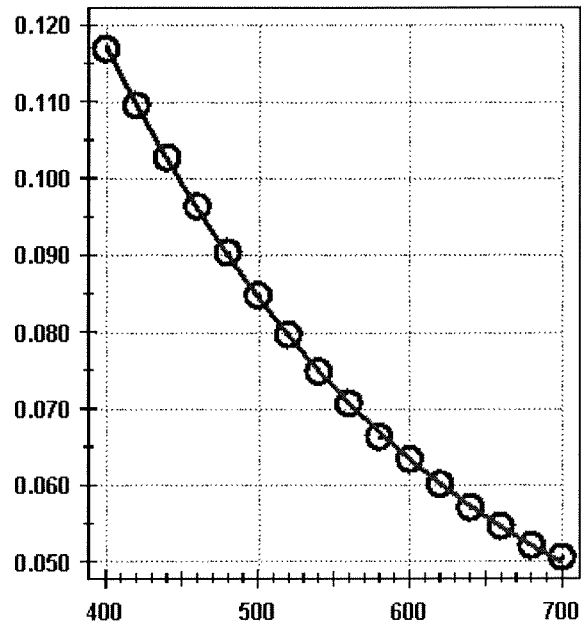


Figure 35. Specific downwelling attenuation coefficient $\bar{K}_d^*(\lambda)$ as a function of wavelength derived from Hydrolight and Laguna Madre measurements.

Preliminary Spectral Irradiance Model

Abundant seagrasses are a sign of healthy and productive coastal environments that support a biodiverse fauna. Unfortunately, seagrass densities have been declining in U.S. waters. Consequently, significant state and national resources are being devoted to the study and modeling of seagrasses. Our recent efforts strongly suggest that accepted modeling strategies are not appropriate for predicting the outcome of anthropogenic disturbances. Equivalent light absorption by either sediments or algae will affect seagrass growth differently because of their contrasting light absorbance properties. Although seagrasses have successfully evolved to take advantage of the light/nutrient environment found in Laguna Madre, man-made changes imposed by dredging, and the advent of algal blooms in the late 1980s have resulted in a significant alteration in the quantity and quality of light.

The seagrass modeling effort is only intended to determine the impacts due to changes in sediment concentration in the water column. Thus, it is important that the model discriminate between impacts due to increasing sediment concentration and those due to other factors (e.g., algal blooms). As shown in the preliminary modeling described below, models that account for the quality of light (spectral irradiance models), which is impacted differently by sediment and living material, will predict different growth rates compared to established PAR models. However, PAR models are extremely useful because they can employ the available data (PAR, attenuation coefficients, photosynthesis versus irradiance (P vs I) curves). A description of the PAR models used in the seagrass model under development can be found in Chapter I. We have initiated testing of a spectral irradiance model. This should allow us to make better predictions of the growth potential of seagrasses under predicted light fields and to assess the relative impact of sediment and living material on seagrass health.

Model Description

The seagrass model will ultimately have components for nutrient limitation and other sediment derived inhibition factors, but these matters will not be addressed in this chapter. Primary

production of phytoplankton, drift algae, and seagrass can be calculated from available irradiance, which is measured by the spectral radiometer:

$$P(z) = \phi(z) 12000 PHAR, \quad (\text{EQ 9})$$

where $P(z)$ is the daily production rate ($\text{mg-C m}^{-3} \text{ d}^{-1}$) at depth z , $PHAR$ is photosynthetically absorbed radiation ($\text{Einstein m}^{-3} \text{ d}^{-1}$), 12,000 is a conversion factor and $\phi(z)$ is the in situ quantum yield ($\text{Einstein mg Chla}^{-1} \text{ d}^{-1}$). $PHAR$ is calculated by quantifying photosynthetic absorption spectra of the plant based on the spectral quanta available:

$$PHAR = \int_{400}^{700} Q(z, \lambda) a(\lambda) Chla(z) d\lambda, \quad (\text{EQ 10})$$

where $Q(z, \lambda)$ is spectral quanta ($\text{Einstein s}^{-1} \text{ m}^{-2} \text{ nm}^{-1}$), $a(\lambda)$ are absorption coefficients (e.g. “brown tide”, seagrass, drift algae ($\text{m}^2 \text{ mg}^{-1}$)) and $Chla(z)$ (mg m^{-3}) is a proxy for biomass. In turn, $\phi(z)$ is a function of irradiance and cell physiology and can best be characterized by a variant of the Kiefer-Mitchell model (Bidigare et al. 1987). This formulation defines ϕ_m as the maximum quantum yield, and relates this quantity to $\phi(z)$ using a Monod-like negative feedback. For this purpose K_ϕ' is the P_m scaled by ϕ_m ($\text{Einstein mg chla}^{-1} \text{ d}^{-1}$):

$$\phi(z) = \phi_m \frac{(k'_\phi Chla(z))}{(k'_\phi Chla + PHAR(z))}. \quad (\text{EQ 11})$$

Influence of Light Quality on Production

To demonstrate the importance of light quality, we present a conceptual modeling exercise. Five concentrations of a chrysophyte (similar to Brown Tide alga) and of sediment were chosen, such that the resulting absorption coefficients, a_c and a_s , respectively, were similar (Table 6). The high concentrations of chl a and SPM represent extreme situations and are near the bounds of

what has been measured during extreme events in Laguna Madre. Absorption coefficients used in the model were taken from Roesler et al. (1989; opal glass method) and Mobley (1994). In turn, available light (PAR and spectral) was calculated as a function of depth (0 to 2 m) similar to those in the Laguna Madre. Although PAR versus depth was equivalent for each case (not shown), regardless of the source of turbidity, the quality of light differed (e.g., Fig. 36). Nutrients were assumed to be non-limiting. To simplify this example, we used the same spectral irradiance model for the chrysophyte and the seagrass (i.e., chlorophyll *a* was the most prevalent pigment in both).

The PAR-based productivity model (Jassby and Platt, 1976) predicted higher production compared to the spectral irradiance model, particularly at high concentrations of chrysophyte or sediment (Table 6). This difference was more evident at depths where seagrasses would grow (see Fig. 37). Also, the disparity between models was significantly greater when the chrysophyte was the source of turbidity because it absorbs light at wavelengths required by plants growing at depth. Finally, scattering was not considered, but this phenomenon should have accentuated this difference (G. Jackson. pers. comm.). Although simplistic, this modeling exercise demonstrates the potential importance of distinguishing the source of light absorption, particularly when comparing the impact of sediment resuspension to that of algal blooms or floating algal mats.

Table 6. Cases used in the comparison of the spectral irradiance model (P_{SPECTRAL}) with the standard PAR model (P_{PAR}). $P_{\text{SPECTRAL}}/P_{\text{PAR}}$ is the ratio of water column integrated production. Also, a_c and a_s are phytoplankton and sediment absorption coefficients, respectively.

Case	[Chl <i>a</i>] μg/L	[SPM] mg/L	a_c	a_s	Phytoplankton $P_{\text{SPECTRAL}}/P_{\text{PAR}}$	Sediment $P_{\text{SPECTRAL}}/P_{\text{PAR}}$
1	0	0	.00	.00	0.99	0.99
2	5	10	.10	.12	0.98	0.98
3	30	50	.61	.60	0.91	0.95
4	60	100	1.2	1.2	0.85	0.93
5	300	500	6.1	6.0	0.79	0.93

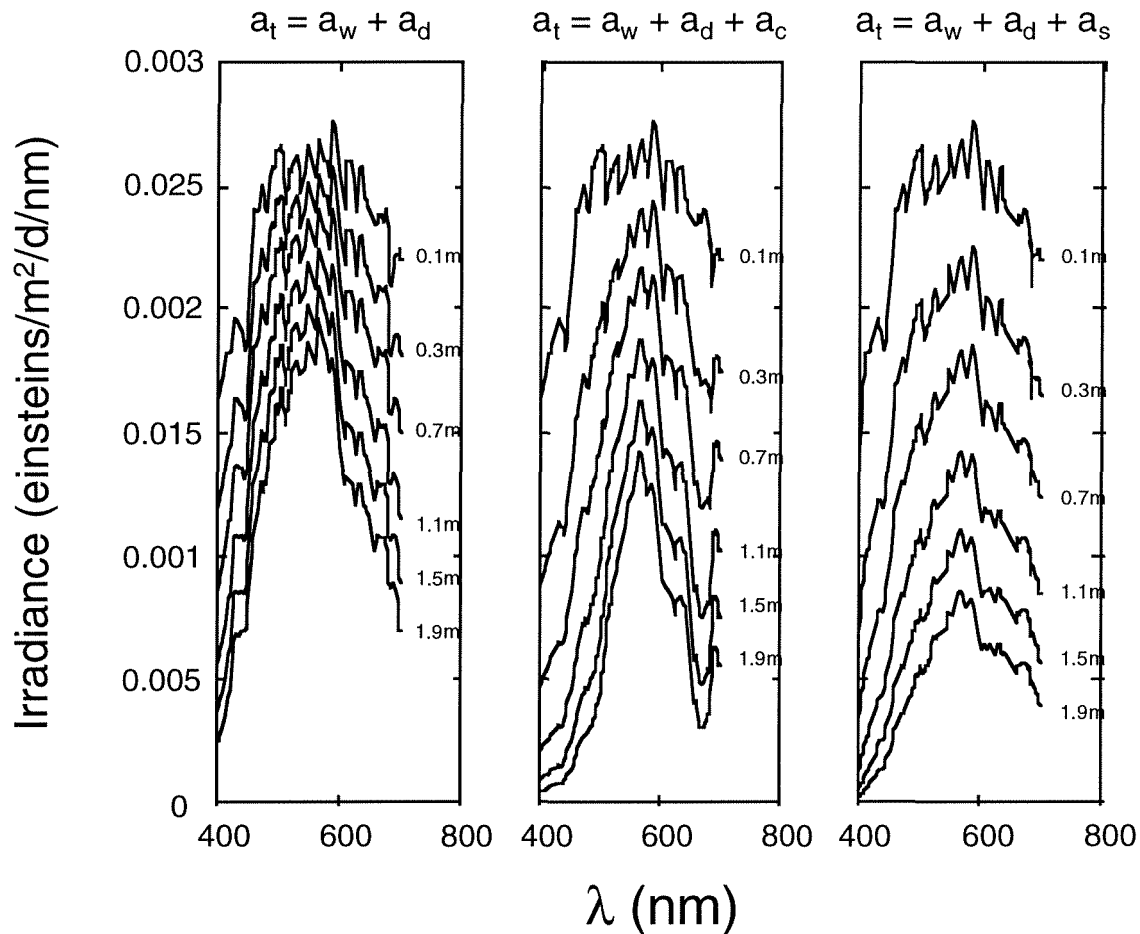


Figure 36. Our simplified radiance transfer model (downwelling light only) predicts spectral irradiance ($\mu\text{mols}/\text{m}^2/\text{d}/\text{nm}$) as a function of depth for (left to right) filtered Laguna Madre water, Laguna Madre water with added chrysophyte ($30 \mu\text{g chl a}/\text{L}$) and Laguna Madre water with added sediment ($50 \text{ mg}/\text{L}$). The coefficients, a_w , a_d , a_c , a_s and a_t , are for water, DOM, phytoplankton, sediment and total absorption, respectively. In the latter two cases, a_t is equivalent, which means PAR is also equal at all depths. However, as is evident from the shapes of the curves, spectral quality is quite different, particularly at 650 to 700 nm.

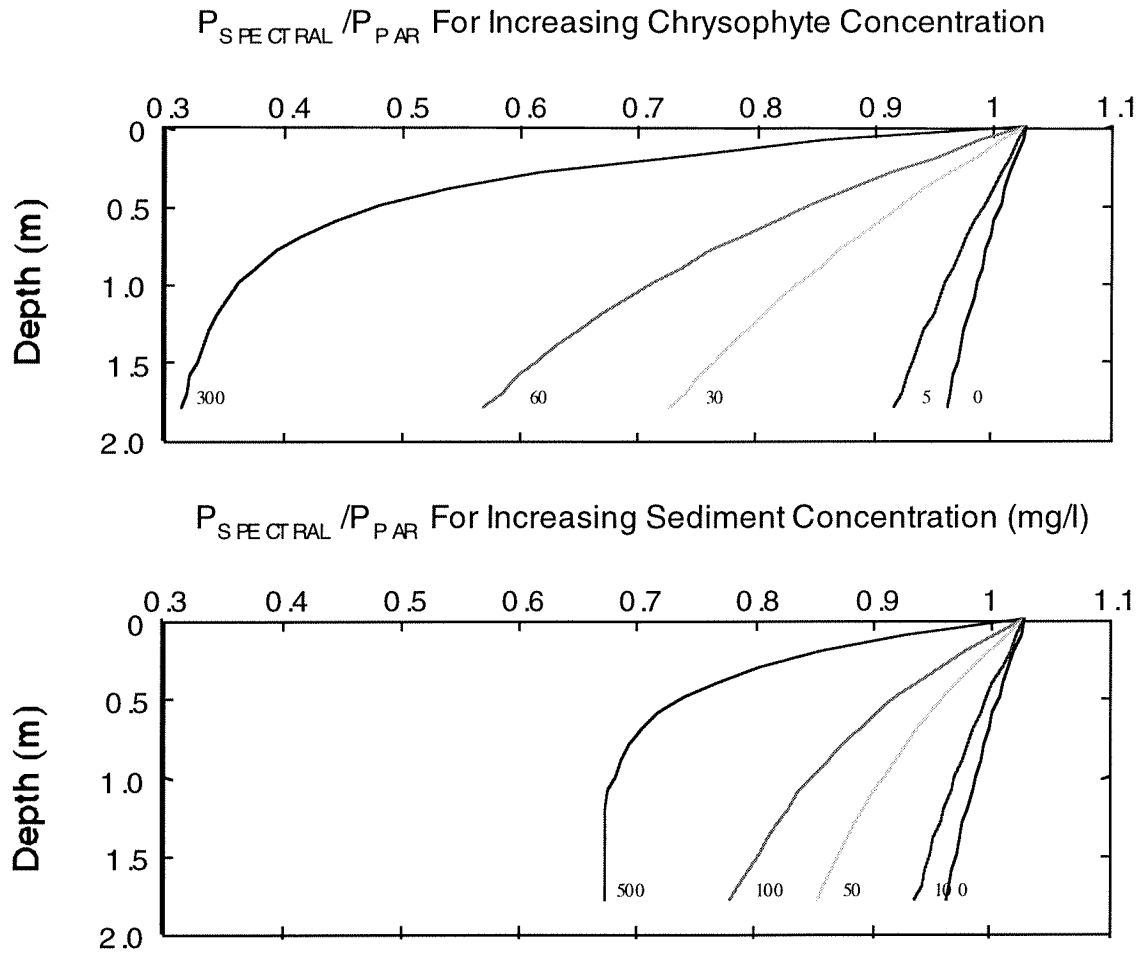


Figure 37. Results of conceptual model showing the ratio of predictions by our spectral irradiance model to predictions by the PAR model (Jassby and Platt, 1976) ($P_{\text{SPECTRAL}} / P_{\text{PAR}}$) as a function of depth (m) for additions of phytoplankton (in $\mu\text{g chla } a/L$) and sediment (mg/L).

References

- Biggs, D. C., Johnson, M. A., Bidigare, R. B., Guffy, J. D., Holm-Hansen, O. 1982. Shipboard autoanalyzer studies of nutrient chemistry. Tech. Rep. 82-11-T, Texas A&M Univ. Dept. Of Oceanogr., College Station, Texas.
- Bidigare, R.R. 1989. Photosynthetic pigment composition of the brown tide alga: Unique chlorophyll and carotenoid derivatives, pp. 57-85. In: Novel Phytoplankton Blooms (E.M. Cosper, V.M. Bicolj, E.J. Carpenter, Eds.). Elsevier.
- Bidigare, R. R., R. C. Smith, K. S. Baker, and J. Marra. 1987. Ocean primary production estimates from measurement of spectral irradiance and pigment concentrations. *Global Biogeochemical Cycles* 1: 171-186.
- Brown, C.A. and N.C. Kraus. 1997. Environmental monitoring of dredging and processes in Lower Laguna Madre, Texas. Final Report submitted to US Army Corps of Engineers, District Galveston, Galveston, TX. TAMU-CC-CBI-96-01.
- Czerny, A.B. and K.H. Dunton. 1995. The effects of in situ light reduction on the growth of two subtropical seagrasses, *Thalassia testudinum* and *Halodule wrightii*. *Estuaries* 18: 418-427.
- DeYoe, H. R., A.M. Chan and C.A. Suttle. 1995. Phylogeny of *Aureococcus anophagefferens* and a morphologically similar bloom-forming alga from Texas as determined by 18S ribosomal RNA sequence analysis. *J. Phycol.* 31: 413-418.
- DeYoe, H.R., D.A. Stockwell, R.R. Bidigare, M.Latasa, P.W. Johnson, P.E. Hargraves and C.A. Suttle. 1997. Description and characterization of the algal species *Aureoumbra lagunensis* gen. et sp. nov. and referral of *Aureoumbra* and *Aureococcus* to the Pelagophyceae. *J. Phycol.* 33: 1042-1048.
- Dunton, K.H. 1994. Seasonal growth and biomass of the subtropical seagrass *Halodule wrightii* in relation to continuous measurements of underwater irradiance. *Marine Biology* 120: 479-489.
- Jassby, A. D., and T. Platt. 1976. Mathematical formulation of the relationship between photosynthesis and light for phytoplankton. *Limn. Oceanogr.* 21: 540-547.
- Kirk, J.T.O. 1994. *Light and Photosynthesis in Aquatic Ecosystems*. Cambridge University Press.

- Lee, K.S. and K.H. Dunton. 1996. Production and carbon reserve dynamics of the seagrass *Thalassia testudinum* in Corpus Christi Bay, Texas, USA. Marine Ecology Progress Series 143: 201-210.
- Mantoura, R.F.C. and C. A. Llewellyn. 1983. The rapid determination of algal chlorophyll and carotenoid pigments and their breakdown products in natural waters by reversed-phase high-performance liquid chromatography. Anal. Chim. Acta 151: 297-314.
- Mobley, C. D. 1994. Light and water: Radiative transfer in natural waters. Academic Press. San Diego, CA. 592 pp.
- Onuf, C.P. 1996. Seagrass responses to long-term light reduction by brown tide in the Upper Laguna Madre, Texas: distribution and biomass patterns. Marine Ecology Progress Series 138: 219-231.
- Pierce, J.W., D.L. Correll, B. Goldberg, M.A. Faust and W.H. Klien. 1986. Response of underwater light transmittance in the Rhode River Estuary to changes in water-quality parameters. Estuaries 9: 169-178.
- Pope, R.M. and E.S. Fry. 1997. Absorption spectra (380-700 nm) of pure water: II. Integrating cavity measurements. Appl. Opt. 36: 8710-8723.
- Roesler, C. S., M. J. Perry, K. L. Carder. 1989. Modeling in situ phytoplankton absorption from total absorption spectra in productive inland marine waters. Limnology and Oceanography 34: 1510-1523.
- Smith, R.C. and K.S. Baker. 1978. Optical classification of natural waters. Limnology and Oceanography 23: 260-267.
- Voss, K.J. 1992. A spectral model of the beam attenuation coefficient in the ocean and coastal areas. Limnology and Oceanography 37: 501-509.
- Yentsch, C.S. 1980. Light attenuation and phytoplankton photosynthesis. Pp. 95-125. In: I. Morris (ed.). The physiological ecology of phytoplankton. University of California Press, Berkeley.

Appendix 1. Pigment data for the fixed sampling stations in Laguna Madre from June 1996 to November 1997. Values represent means and standard deviations. B.D. = below detection, NS = not sampled and several samples were lost as a result of analytical problems.

Site	date	Chl a	SD	Chl b	SD	Chl c1c2	SD	19 But.	SD	19 Hex	SD	Fuco	SD	Prasin	SD	Diadin	SD	Zea	SD
ULM 1	Jun. 96	21.0	1.0	3.1	0.2	1.8	0.3	3.9	0.1	B.D.	B.D.	5.7	0.3	B.D.	B.D.	B.D.	B.D.	1.4	0.5
ULM 2	Jun. 96	28.1	1.8	1.1	0.2	10.0	5.3	6.5	0.5	B.D.	B.D.	7.6	0.1	0.5	0.7	4.5	1.7	0.9	0.1
ULM 3	Jun. 96	43.7	2.2	5.3	0.4	4.0	0.2	8.0	0.3	B.D.	B.D.	12.7	0.7	B.D.	B.D.	B.D.	B.D.	2.3	0.2
LLM 1	Jun. 96	14.9	0.2	B.D.	B.D.	B.D.	B.D.	B.D.	B.D.	B.D.	B.D.	0.5	0.1	B.D.	B.D.	B.D.	B.D.	B.D.	B.D.
LLM 2	Jun. 96	4.5	0.5	B.D.	B.D.	B.D.	B.D.	B.D.	B.D.	B.D.	B.D.	B.D.	B.D.	B.D.	B.D.	1.5	0.4	B.D.	B.D.
LLM 3	Jun. 96	15.4	1.5	1.9	0.3	1.1	0.9	2.7	0.1	B.D.	B.D.	3.9	0.2	0.0	0.0	1.0	0.2	0.9	0.1
ULM 1	Jul. 96	7.8	0.8	B.D.	B.D.	0.8	0.1	0.8	0.1	B.D.	B.D.	1.2	0.2	0.1	0.1	B.D.	B.D.	0.7	0.1
ULM 2	Jul. 96	Lost	Lost	Lost	Lost	Lost	Lost	Lost	Lost	Lost	Lost	Lost	Lost	Lost	Lost	Lost	Lost	Lost	Lost
ULM 3	Jul. 96	45.7	1.5	B.D.	B.D.	4.7	0.2	4.9	0.2	B.D.	B.D.	12.9	0.6	1.1	0.2	2.6	0.1	1.1	0.0
LLM 1	Jul. 96	5.2	2.3	B.D.	B.D.	B.D.	B.D.	B.D.	B.D.	B.D.	B.D.	1.6	0.8	B.D.	B.D.	B.D.	B.D.	B.D.	B.D.
LLM 2	Jul. 96	0.6	0.2	B.D.	B.D.	B.D.	B.D.	B.D.	B.D.	B.D.	B.D.	0.3	0.1	B.D.	B.D.	B.D.	B.D.	0.0	B.D.
LLM 3	Jul. 96	NS	NS	NS	NS	NS	NS	NS	NS	NS	NS	NS	NS	NS	NS	NS	NS	NS	NS
ULM 1	Aug. 96	9.2	0.5	B.D.	B.D.	2.4	1.7	1.2	B.D.	B.D.	B.D.	B.D.	B.D.	B.D.	B.D.	B.D.	B.D.	0.6	0.1
ULM 2	Aug. 96	Lost	Lost	Lost	Lost	Lost	Lost	Lost	Lost	Lost	Lost	Lost	Lost	Lost	Lost	Lost	Lost	Lost	Lost
ULM 3	Aug. 96	61.6	7.0	B.D.	B.D.	0.6	0.1	B.D.	B.D.	3.6	0.4	18.6	2.5	2.3	0.2	7.2	1.1	B.D.	B.D.
LLM 1	Aug. 96	2.6	0.3	B.D.	B.D.	B.D.	B.D.	B.D.	B.D.	B.D.	B.D.	0.6	0.1	B.D.	B.D.	B.D.	B.D.	B.D.	B.D.
LLM 2	Aug. 96	0.8	0.2	B.D.	B.D.	B.D.	B.D.	B.D.	B.D.	B.D.	B.D.	B.D.	B.D.	B.D.	B.D.	B.D.	B.D.	B.D.	B.D.
LLM 3	Aug. 96	NS	NS	NS	NS	NS	NS	NS	NS	NS	NS	NS	NS	NS	NS	NS	NS	NS	NS
ULM 1	Sept. 96	43.3	6.3	B.D.	B.D.	2.5	0.2	5.2	1.8	B.D.	B.D.	9.4	3.7	0.5	0.8	1.7	B.D.	0.5	B.D.
ULM 2	Sept. 96	59.3	13.0	B.D.	B.D.	5.7	1.0	9.4	0.2	B.D.	B.D.	2.7	0.2	2.0	B.D.	5.8	1.3	0.4	0.1
ULM 3	Sept. 96	34.2	6.8	B.D.	B.D.	3.7	B.D.	5.5	B.D.	B.D.	B.D.	11.3	B.D.	2.3	B.D.	B.D.	B.D.	0.4	B.D.
LLM 1	Sept. 96	5.0	0.7	B.D.	B.D.	4.4	1.5	0.5	0.1	B.D.	B.D.	1.6	0.2	B.D.	B.D.	0.0	0.0	0.2	0.1
LLM 2	Sept. 96	0.6	0.2	B.D.	B.D.	B.D.	B.D.	B.D.	B.D.	B.D.	B.D.	1.4	1.6	B.D.	B.D.	B.D.	B.D.	B.D.	B.D.
LLM 3	Sept. 96	9.9	1.4	B.D.	B.D.	2.2	0.3	1.8	0.5	B.D.	B.D.	2.4	1.1	0.0	0.0	0.7	0.2	0.5	0.5
ULM 1	Oct. 96	5.5	0.3	B.D.	B.D.	0.2	0.0	B.D.	B.D.	B.D.	B.D.	1.2	0.0	B.D.	B.D.	0.4	0.0	B.D.	B.D.
ULM 2	Oct. 96	31.5	4.6	B.D.	B.D.	0.4	0.0	B.D.	B.D.	B.D.	B.D.	7.6	1.1	B.D.	B.D.	7.6	1.0	B.D.	B.D.
ULM 3	Oct. 96	34.1	4.0	B.D.	B.D.	0.4	0.0	B.D.	B.D.	B.D.	B.D.	8.3	1.2	B.D.	B.D.	7.5	0.9	B.D.	B.D.
LLM 1	Oct. 96	7.9	1.1	B.D.	B.D.	0.2	0.0	B.D.	B.D.	B.D.	B.D.	2.0	0.8	B.D.	B.D.	0.8	0.1	B.D.	B.D.
LLM 2	Oct. 96	0.9	0.1	B.D.	B.D.	B.D.	B.D.	B.D.	B.D.	B.D.	B.D.	B.D.	B.D.	B.D.	B.D.	B.D.	B.D.	B.D.	B.D.
LLM 3	Oct. 96	NS	NS	NS	NS	NS	NS	NS	NS	NS	NS	NS	NS	NS	NS	NS	NS	NS	NS
ULM 1	Nov. 96	4.8	0.9	B.D.	B.D.	B.D.	B.D.	B.D.	B.D.	B.D.	B.D.	1.4	0.3	B.D.	B.D.	B.D.	B.D.	B.D.	B.D.
ULM 2	Nov. 96	Lost	Lost	Lost	Lost	Lost	Lost	Lost	Lost	Lost	Lost	Lost	Lost	Lost	Lost	Lost	Lost	Lost	Lost

Site	date	Chl a	SD	Chl b	SD	Chl c1c2	SD	19 But.	SD	19 Hex	SD	Fuco	SD	Prasin	SD	Diadin	SD	Zea	SD
ULM 3	Nov. 96	38.1	2.1	B.D.	B.D.	3.3	0.4	B.D.	B.D.	B.D.	B.D.	9.1	1.7	B.D.	B.D.	B.D.	B.D.	Lost	Lost
LLM 1	Nov. 96	2.3	0.3	B.D.	B.D.	B.D.	B.D.	B.D.	B.D.	B.D.	B.D.	0.6	0.0	B.D.	B.D.	B.D.	B.D.	B.D.	B.D.
LLM 2	Nov. 96	0.7	0.3	B.D.	B.D.	B.D.	B.D.	B.D.	B.D.	B.D.	B.D.	B.D.	B.D.	B.D.	B.D.	B.D.	B.D.	B.D.	B.D.
LLM 3	Nov. 96	NS	NS	NS	NS	NS	NS	NS	NS	NS	NS	NS	NS	NS	NS	NS	NS	NS	NS
ULM 1	Dec. 96	7.4	0.4	B.D.	B.D.	0.2	0.0	0.2	B.D.	0.2	0.1	2.0	0.0	B.D.	B.D.	B.D.	B.D.	0.1	0.0
ULM 2	Dec. 96	Lost	Lost	Lost	Lost	Lost	Lost	Lost	Lost	Lost	Lost	Lost	Lost	Lost	Lost	Lost	Lost	Lost	Lost
ULM 3	Dec. 96	66.4	1.6	B.D.	B.D.	0.7	0.0	B.D.	B.D.	1.5	0.3	14.1	1.8	B.D.	B.D.	B.D.	B.D.	0.3	0.1
LLM 1	Dec. 96	4.3	1.5	B.D.	B.D.	B.D.	B.D.	B.D.	B.D.	B.D.	B.D.	1.3	0.5	B.D.	B.D.	B.D.	B.D.	0.1	0.0
LLM 2	Dec. 96	2.1	0.4	B.D.	B.D.	B.D.	B.D.	B.D.	B.D.	B.D.	B.D.	0.6	0.1	B.D.	B.D.	B.D.	B.D.	B.D.	B.D.
LLM 3	Dec. 96	NS	NS	NS	NS	NS	NS	NS	NS	NS	NS	NS	NS	NS	NS	NS	NS	NS	NS
ULM 1	Jan. 97	2.8	0.5	B.D.	B.D.	B.D.	B.D.	B.D.	B.D.	B.D.	B.D.	0.4	0.0	B.D.	B.D.	B.D.	B.D.	B.D.	B.D.
ULM 2	Jan. 97	13.1	2.2	B.D.	B.D.	B.D.	B.D.	B.D.	B.D.	B.D.	B.D.	0.9	0.2	B.D.	B.D.	0.5	0.1	B.D.	B.D.
ULM 3	Jan. 97	27.9	2.9	4.8	0.2	0.2	0.0	B.D.	B.D.	B.D.	B.D.	1.8	0.1	B.D.	B.D.	0.9	0.3	B.D.	B.D.
LLM 1	Jan. 97	3.2	1.0	B.D.	B.D.	B.D.	B.D.	B.D.	B.D.	B.D.	B.D.	0.7	0.3	B.D.	B.D.	B.D.	B.D.	B.D.	B.D.
LLM 2	Jan. 97	1.8	0.2	B.D.	B.D.	0.1	0.0	B.D.	B.D.	B.D.	B.D.	0.5	0.1	B.D.	B.D.	B.D.	B.D.	B.D.	B.D.
LLM 3	Jan. 97	40.5	2.2	5.8	0.4	0.5	0.0	B.D.	B.D.	1.1	0.1	7.9	0.7	B.D.	B.D.	2.7	0.5	B.D.	B.D.
ULM 1	Feb. 97	3.2	0.7	B.D.	B.D.	B.D.	B.D.	B.D.	B.D.	B.D.	B.D.	1.1	0.2	B.D.	B.D.	B.D.	B.D.	B.D.	B.D.
ULM 2	Feb. 97	3.1	0.3	B.D.	B.D.	B.D.	B.D.	B.D.	B.D.	B.D.	B.D.	0.8	0.1	B.D.	B.D.	B.D.	B.D.	B.D.	B.D.
ULM 3	Feb. 97	33.4	2.9	B.D.	B.D.	0.5	0.0	B.D.	B.D.	1.5	0.3	9.0	1.8	B.D.	B.D.	B.D.	B.D.	0.2	0.1
LLM 1	Feb. 97	19.8	1.8	B.D.	B.D.	0.3	0.0	1.4	0.2	B.D.	B.D.	5.8	1.1	B.D.	B.D.	3.4	0.5	0.8	0.2
LLM 2	Feb. 97	18.3	0.5	B.D.	B.D.	0.3	0.0	1.5	0.2	B.D.	B.D.	5.0	0.6	B.D.	B.D.	3.4	0.4	B.D.	B.D.
LLM 3	Feb. 97	21.3	0.9	1.5	0.2	0.2	0.0	B.D.	B.D.	B.D.	B.D.	2.6	0.2	B.D.	B.D.	B.D.	B.D.	B.D.	B.D.
ULM 1	Mar. 97	4.3	1.0	B.D.	B.D.	0.1	0.0	B.D.	B.D.	B.D.	B.D.	1.0	0.2	B.D.	B.D.	0.2	0.0	B.D.	B.D.
ULM 2	Mar. 97	14.2	1.0	2.8	0.3	0.2	0.1	B.D.	B.D.	0.4	0.1	2.7	0.3	B.D.	B.D.	0.6	0.0	B.D.	B.D.
ULM 3	Mar. 97	28.7	1.6	B.D.	B.D.	0.3	0.0	2.1	0.0	1.3	0.1	7.7	0.5	B.D.	B.D.	B.D.	B.D.	0.7	0.1
LLM 1	Mar. 97	56.5	0.5	B.D.	B.D.	0.6	0.1	B.D.	B.D.	1.2	0.1	14.9	0.2	B.D.	B.D.	B.D.	B.D.	0.6	0.0
LLM 2	Mar. 97	1.2	0.1	B.D.	B.D.	B.D.	B.D.	B.D.	B.D.	B.D.	B.D.	0.3	0.1	B.D.	B.D.	0.1	0.0	B.D.	B.D.
LLM 3	Mar. 97	NS	NS	NS	NS	NS	NS	NS	NS	NS	NS	NS	NS	NS	NS	NS	NS	NS	NS
ULM 1	Apr. 97	6.3	0.2	B.D.	B.D.	0.2	0.0	B.D.	B.D.	B.D.	B.D.	1.3	0.2	B.D.	B.D.	0.4	0.0	0.1	0.0
ULM 2	Apr. 97	21.7	3.2	2.2	0.3	0.2	0.0	B.D.	B.D.	B.D.	B.D.	3.0	0.9	1.5	0.3	1.1	0.2	B.D.	B.D.
ULM 3	Apr. 97	28.4	1.1	2.4	0.1	0.3	0.0	B.D.	B.D.	0.8	0.3	4.7	1.0	B.D.	B.D.	2.1	0.1	0.2	0.0
LLM 1	Apr. 97	12.0	1.3	1.1	0.1	0.2	0.0	0.9	0.1	B.D.	B.D.	2.4	0.2	B.D.	B.D.	1.3	0.3	0.6	0.1
LLM 2	Apr. 97	30.0	1.5	B.D.	B.D.	0.5	0.0	B.D.	B.D.	B.D.	B.D.	5.1	0.9	B.D.	B.D.	1.7	0.1	0.2	0.0
LLM 3	Apr. 97	NS	NS	NS	NS	NS	NS	NS	NS	NS	NS	NS	NS	NS	NS	NS	NS	NS	NS
ULM 1	May. 97	6.8	0.1	B.D.	B.D.	B.D.	B.D.	B.D.	B.D.	B.D.	B.D.	2.2	0.1	B.D.	B.D.	B.D.	B.D.	0.3	0.0
ULM 2	May. 97	33.6	0.8	B.D.	B.D.	0.5	0.0	B.D.	B.D.	1.4	0.1	9.8	0.3	B.D.	B.D.	B.D.	B.D.	0.5	0.0
ULM 3	May. 97	36.7	0.3	B.D.	B.D.	0.4	0.0	B.D.	B.D.	1.2	0.1	10.1	0.5	B.D.	B.D.	B.D.	B.D.	0.5	0.0

Site	date	Chl a	SD	Chl b	SD	Chl c1c2	SD	19 But.	SD	19 Hex	SD	Fuco	SD	Prasin	SD	Diadin	SD	Zea	SD
LLM 1	May. 97	14.9	0.8	B.D.	B.D.	0.4	0.0	B.D.	B.D.	B.D.	B.D.	2.5	0.4	0.7	0.1	B.D.	B.D.	0.6	0.0
LLM 2	May. 97	0.2	0.1	B.D.	B.D.	0.5	B.D.	B.D.	B.D.	B.D.	B.D.	B.D.	B.D.	B.D.	B.D.	B.D.	B.D.	B.D.	B.D.
LLM 3	May. 97	NS	NS	NS	NS	NS	NS	NS	NS	NS	NS	NS	NS	NS	NS	NS	NS	NS	NS
ULM 1	Jun. 97	7.9	0.3	1.3	0.1	B.D.	B.D.	B.D.	B.D.	B.D.	B.D.	0.7	0.2	B.D.	B.D.	B.D.	B.D.	0.6	0.0
ULM 2	Jun. 97	18.3	2.9	0.9	0.1	0.2	0.0	B.D.	B.D.	0.8	0.2	4.3	1.5	B.D.	B.D.	2.0	0.9	B.D.	B.D.
ULM 3	Jun. 97	20.8	0.7	1.7	0.1	0.2	0.0	B.D.	B.D.	0.4	0.1	3.2	1.1	B.D.	B.D.	1.0	0.1	B.D.	B.D.
LLM 1	Jun. 97	8.1	1.2	1.0	0.2	B.D.	B.D.	B.D.	B.D.	B.D.	B.D.	B.D.	B.D.	2.0	0.5	B.D.	B.D.	0.3	0.1
LLM 2	Jun. 97	0.4	0.2	B.D.	B.D.	B.D.	B.D.	B.D.	B.D.	B.D.	B.D.	B.D.	B.D.	B.D.	B.D.	B.D.	B.D.	B.D.	B.D.
LLM 3	Jun. 97	14.4	1.6	1.6	0.3	0.2	0.0	B.D.	B.D.	0.4	0.0	2.5	0.3	B.D.	B.D.	0.8	0.1	0.6	0.1
ULM 1	Jul. 97	5.6	0.4	B.D.	B.D.	B.D.	B.D.	B.D.	B.D.	B.D.	B.D.	1.1	0.1	B.D.	B.D.	0.8	0.1	B.D.	B.D.
ULM 2	Jul. 97	1.2	0.1	B.D.	B.D.	B.D.	B.D.	B.D.	B.D.	B.D.	B.D.	0.2	0.0	B.D.	B.D.	0.3	0.0	B.D.	B.D.
ULM 3	Jul. 97	6.8	0.2	B.D.	B.D.	0.1	0.0	B.D.	B.D.	B.D.	B.D.	0.6	0.1	B.D.	B.D.	1.7	0.1	B.D.	B.D.
LLM 1	Jul. 97	3.9	0.4	B.D.	B.D.	0.1	0.0	B.D.	B.D.	B.D.	B.D.	0.9	0.3	B.D.	B.D.	0.2	0.0	0.2	0.1
LLM 2	Jul. 97	0.1	0.2	B.D.	B.D.	B.D.	B.D.	B.D.	B.D.	B.D.	B.D.	B.D.	B.D.	B.D.	B.D.	B.D.	B.D.	B.D.	B.D.
LLM 3	Jul. 97	4.0	0.6	B.D.	B.D.	0.2	0.0	B.D.	B.D.	B.D.	B.D.	0.6	0.1	0.2	0.0	B.D.	B.D.	B.D.	B.D.
ULM 1	Aug. 97	10.2	0.2	B.D.	B.D.	0.2	0.0	2.4	0.6	0.4	0.1	0.5	0.1	B.D.	B.D.	1.1	0.0	B.D.	B.D.
ULM 2	Aug. 97	3.1	0.4	B.D.	B.D.	B.D.	B.D.	B.D.	B.D.	B.D.	B.D.	B.D.	B.D.	0.2	0.1	B.D.	B.D.	0.6	0.1
ULM 3	Aug. 97	6.2	0.8	1.0	0.1	B.D.	B.D.	B.D.	B.D.	B.D.	B.D.	0.9	0.0	0.2	0.1	0.5	0.1	0.1	0.0
LLM 1	Aug. 97	0.5	0.2	B.D.	B.D.	0.3	0.0	B.D.	B.D.	B.D.	B.D.	3.1	0.7	0.3	0.1	3.2	0.7	B.D.	B.D.
LLM 2	Aug. 97	4.8	0.2	B.D.	B.D.	0.1	0.0	B.D.	B.D.	B.D.	B.D.	0.5	0.0	B.D.	B.D.	0.2	0.0	0.5	0.0
LLM 3	Aug. 97	7.0	0.7	B.D.	B.D.	B.D.	B.D.	B.D.	B.D.	B.D.	B.D.	1.0	0.1	B.D.	B.D.	0.3	0.0	0.7	0.1
ULM 1	Sept. 97	6.5	0.5	B.D.	B.D.	B.D.	B.D.	B.D.	B.D.	B.D.	B.D.	1.0	0.2	B.D.	B.D.	0.3	0.0	0.3	0.0
ULM 2	Sept. 97	2.0	0.1	B.D.	B.D.	B.D.	B.D.	B.D.	B.D.	B.D.	B.D.	B.D.	B.D.	B.D.	B.D.	B.D.	B.D.	0.2	0.0
ULM 3	Sept. 97	4.1	0.1	B.D.	B.D.	B.D.	B.D.	B.D.	B.D.	B.D.	B.D.	B.D.	B.D.	B.D.	B.D.	B.D.	B.D.	0.6	0.0
LLM 1	Sept. 97	0.5	0.1	B.D.	B.D.	B.D.	B.D.	B.D.	B.D.	B.D.	B.D.	0.9	0.1	B.D.	B.D.	B.D.	B.D.	B.D.	B.D.
LLM 2	Sept. 97	3.0	0.3	B.D.	B.D.	B.D.	B.D.	B.D.	B.D.	B.D.	B.D.	B.D.	B.D.	B.D.	B.D.	0.2	0.0	B.D.	B.D.
LLM 3	Sept. 97	4.6	0.4	B.D.	B.D.	B.D.	B.D.	B.D.	B.D.	B.D.	B.D.	0.3	0.0	B.D.	B.D.	0.2	0.0	0.2	0.0
ULM 1	Oct. 97	1.9	0.3	B.D.	B.D.	B.D.	B.D.	0.5	0.1	B.D.	B.D.	B.D.	B.D.	B.D.	B.D.	B.D.	B.D.	B.D.	B.D.
ULM 2	Oct. 97	6.3	0.4	B.D.	B.D.	B.D.	B.D.	B.D.	B.D.	B.D.	B.D.	0.4	0.1	0.3	0.0	B.D.	B.D.	B.D.	B.D.
ULM 3	Oct. 97	6.0	0.9	B.D.	B.D.	B.D.	B.D.	B.D.	B.D.	B.D.	B.D.	0.5	0.1	B.D.	B.D.	0.3	0.1	B.D.	B.D.
LLM 1	Oct. 97	4.7	0.6	B.D.	B.D.	0.2	0.0	B.D.	B.D.	B.D.	B.D.	1.0	0.1	0.5	0.1	0.4	0.0	B.D.	B.D.
LLM 2	Oct. 97	2.0	0.1	B.D.	B.D.	B.D.	B.D.	B.D.	B.D.	B.D.	B.D.	0.5	0.0	B.D.	B.D.	0.3	0.0	B.D.	B.D.
LLM 3	Oct. 97	11.1	0.3	B.D.	B.D.	0.2	0.0	B.D.	B.D.	0.6	0.1	1.5	0.1	B.D.	B.D.	1.4	0.1	0.4	0.0
ULM 1	Nov. 97	3.7	0.1	B.D.	B.D.	B.D.	B.D.	B.D.	B.D.	B.D.	B.D.	0.6	0.0	B.D.	B.D.	B.D.	B.D.	B.D.	B.D.
ULM 2	Nov. 97	4.5	0.6	B.D.	B.D.	B.D.	B.D.	B.D.	B.D.	B.D.	B.D.	0.9	0.1	B.D.	B.D.	0.4	0.0	0.6	0.1
ULM 3	Nov. 97	7.0	0.5	B.D.	B.D.	B.D.	B.D.	B.D.	B.D.	B.D.	B.D.	1.4	0.1	B.D.	B.D.	B.D.	B.D.	B.D.	B.D.
LLM 1	Nov. 97	5.0	0.5	B.D.	B.D.	B.D.	B.D.	B.D.	B.D.	B.D.	B.D.	1.2	0.2	B.D.	B.D.	0.3	0.0	B.D.	B.D.

Site	date	Chl a	SD	Chl b	SD	Chl c1c2	SD	19 But.	SD	19 Hex	SD	Fuco	SD	Prasin	SD	Diadin	SD	Zea	SD
LLM 2	Nov. 97	3.8	0.3	B.D.	B.D.	B.D.	B.D.	B.D.	B.D.	B.D.	B.D.	0.4	0.0	B.D.	B.D.	0.3	0.0	1.0	0.1
LLM 3	Nov. 97	0.7	0.0	B.D.	B.D.	B.D.	B.D.	B.D.	B.D.	B.D.	B.D.	0.2	0.0	B.D.	B.D.	B.D.	B.D.	B.D.	B.D.

CHAPTER V: MODEL VERIFICATION

Contents

Abstract	3
Introduction	4
Verification Data	4
Model Verification	5
Verification for site FIX-2	5
Verification for the site PA-235a	16
Full model verification: comparison with site PA-235c	19
Conclusions	23

Tables

Table 1	Table of site locations	4
Table 2	Normalized root mean squared differences between the model and <i>Thalassia</i> field data after the dredge event.	23

Figures

Figure 1	Observed irradiances at all sites	6
Figure 2	Observed Biomass at PA-235a and PA-235b	7
Figure 3	Observed Biomass at PA-235c and PA-235d	8
Figure 4	Measured canopy irradiance at FIX-2	9
Figure 5	Measured above-ground biomass at FIX-2	10
Figure 6	Combined observed and modeled surface light	11
Figure 7	Estimated attenuation coefficient at FIX-2	12
Figure 8	Canopy level irradiance at FIX-2	13

Figure 9	Comparison between model and data at FIX-2	14
Figure 10	Observed biomass for FIX-2	15
Figure 11	Comparison of model with data at PA-235a	17
Figure 12	Comparison of model with data at PA-235a using new loss formulation	18
Figure 13	Compiled light profile used in verification at PA-235c	20
Figure 14	Comparison of predictions of above-ground biomass from the model with ob- servations at PA-235a	21
Figure 15	Model results of rootzone total sulfides and NH ₄ at site PA-235c.	22

Abstract

The scheduling of dredge operations in late 1988 provided an excellent opportunity to verify the model for *Thalassia testudinum*. Sampling of the sites, described in Chapter IX, was designed in association with the modelers so as to obtain the maximum amount of useful information possible. The model was run using measured light fields at the various sampling locations and the model results were compared with observed biomass at the same site.

Three verification runs were made. The first was with data collected at the control site (Fix-2) which did not show the effects of dredging. A second verification run was made for the sites PA-235ab where the seagrasses were buried and the model was altered to account for burial. In both of these cases only the seagrass biomass model was used. The full seagrass-sediment diagenesis model was verified using irradiance and sediment chemistry data collected at sites PA-235cd. The model shows good agreement with the available data.

Introduction

The Laguna Madre Seagrass Model described in Chapter I was formulated using a variety of available data sets: a 9 year time series of above and below-ground biomass and canopy level light for *Halodule wrightii*; a similar 2 year time series for *Thalassia testudinum*; and a 1 year data record for *Syringodium filiforme*. Of these, only the *Halodule wrightii* data set included the effects of light reduction, in this case from a persistent brown tide that affected Upper Laguna Madre. In this case, the model was able to reproduce the observed responses of the plant to the reduced light levels.

In order to provide further verification of the model, *Thalassia testudinum* sites (Table 1) were monitored during a dredging event in late 1998. A comparison between these data and results from the model is presented in this chapter.

Verification Data

Verification of the seagrass model was performed using data collected at 5 sites in the Laguna Madre between June 1998 and June 1999 (Table 1 and Figure 1 in Chapter IX).

Table 1: Table of site locations

Station Number	Latitude	Longitude	Seagrass
FIX-2	26° 10' 50.9" N	97° 15' 18.0" W	<i>Thalassia testudinum</i>
PA-235a	26° 07' 05" N	97° 13' 50" W	<i>Thalassia testudinum</i>
PA-235b	26° 07' 23" N	97° 13' 44" W	<i>Thalassia testudinum</i>
PA-235c	26° 07' 13" N	97° 13' 40" W	<i>Thalassia testudinum</i>
PA-235d	26° 07' 21" N	97° 13' 48" W	<i>Thalassia testudinum</i>

Above and below-ground biomass and canopy level irradiance were collected by Ken Dunton at all 5 sites and surface irradiance was collected at one site (FIX-2). Light data from the 5 sites are shown in Figure 1. A gap lasting approximately two months (from mid December 1988 through mid February 1999) exists in all the data records. The site FIX-2 was not impacted by dredging

and was used as a control site. Dredging activities occurred during September 9th and 10th 1998 (pers. comm., J. Kowalski).

Sites PA-235a and PA-235b are replicates of each other; similarly for sites PA-235c and PA-235d. Canopy level irradiance for sites PA-235a and PA-235b (Figure 1) reveal that the seagrasses were buried at this location by late October. Above and below-ground biomass was measured at sites PA-235a and PA-235b from the period June 1998 through June 1999 (Figure 2). After dredging occurred, the seagrasses at this site were buried (as can be seen from the light profiles in Figure 1). The above-ground biomass rapidly decreased to zero; the below-ground biomass decreased to almost zero but over a longer time (Figure 2). Biomass at sites PA-235c and PA-235d was measured only from November 1998 onwards. This site was established once it was realized that seagrasses at sites PA-235a and PA-235b were buried.

Dredging occurred between September 9th and September 10th 1998 (pers. comm. J. Kowalski). Seagrasses at site PA-235a were not buried by September 19th, but by September 26th a knee-deep colloidal layer was covering the sensor at this site (pers. comm. J. Kowalski).

Model Verification

Three different verifications were performed using the model and the available data. The first two verifications made use of the seagrass component of the model alone (as described in Chapter I). The third verification used the full seagrass-sediment diagenesis model:

1. Seagrass biomass model alone using data from FIX-2.
2. Seagrass biomass model alone using data from PA-235a
3. Combined seagrass-diagenesis model for site PA-235c.

Verification for site FIX-2

The data available from the FIX-2 site represented the most complete of the verification data sets. Unfortunately, it was also the control data set and so was not one of the disposal sites being monitored. It does however provide a good data set against which to test the *Thalassia* model.

Figure 1: Observed irradiances at the 5 verification sites for the period June 1998 to June 1999.

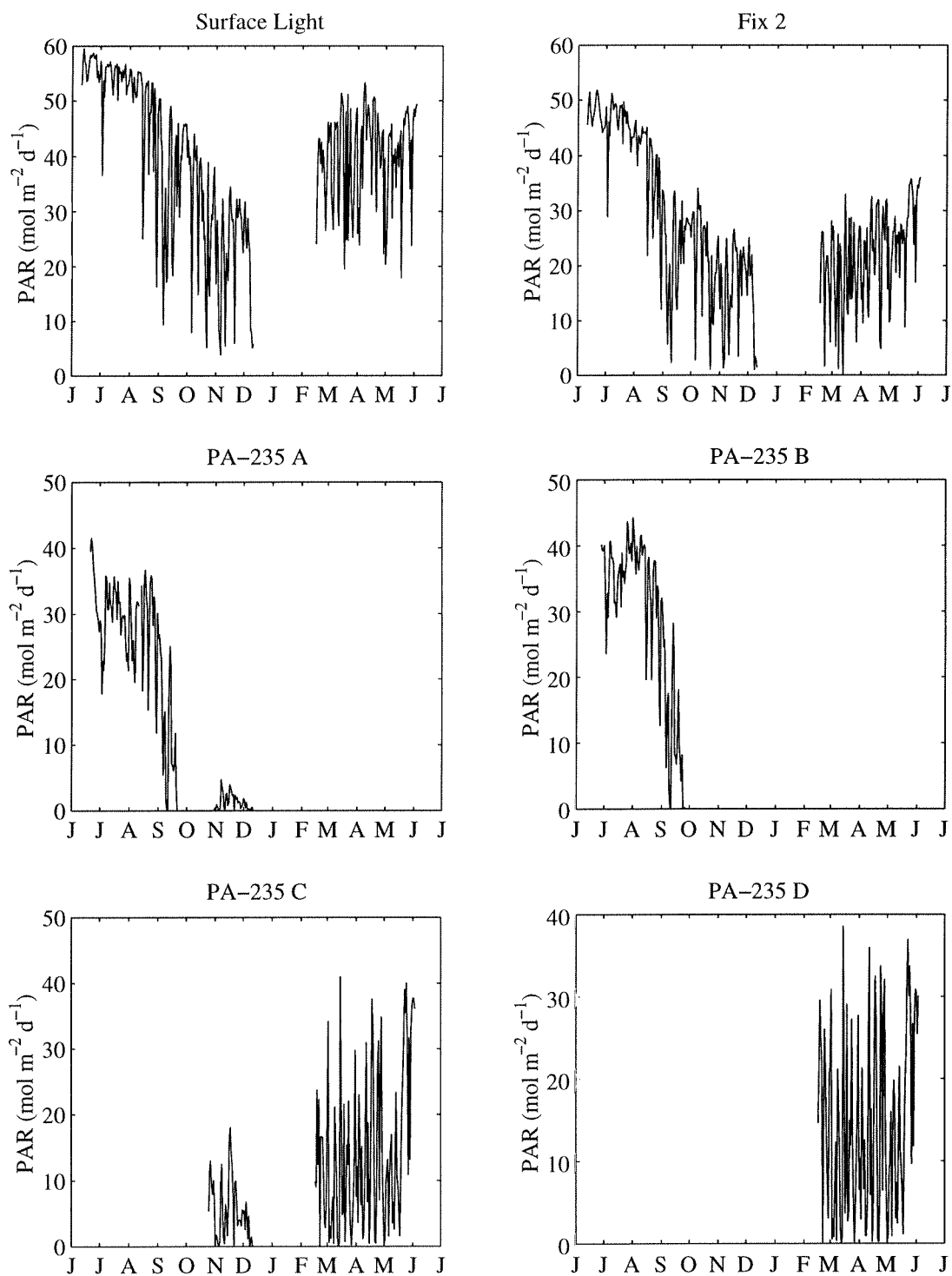


Figure 2: Measured shoot density (top row), above-ground biomass (middle row) and below-ground biomass (bottom row) at sites PA-235a (left hand column) and PA-235b (right hand column). Error bars represent standard deviations.

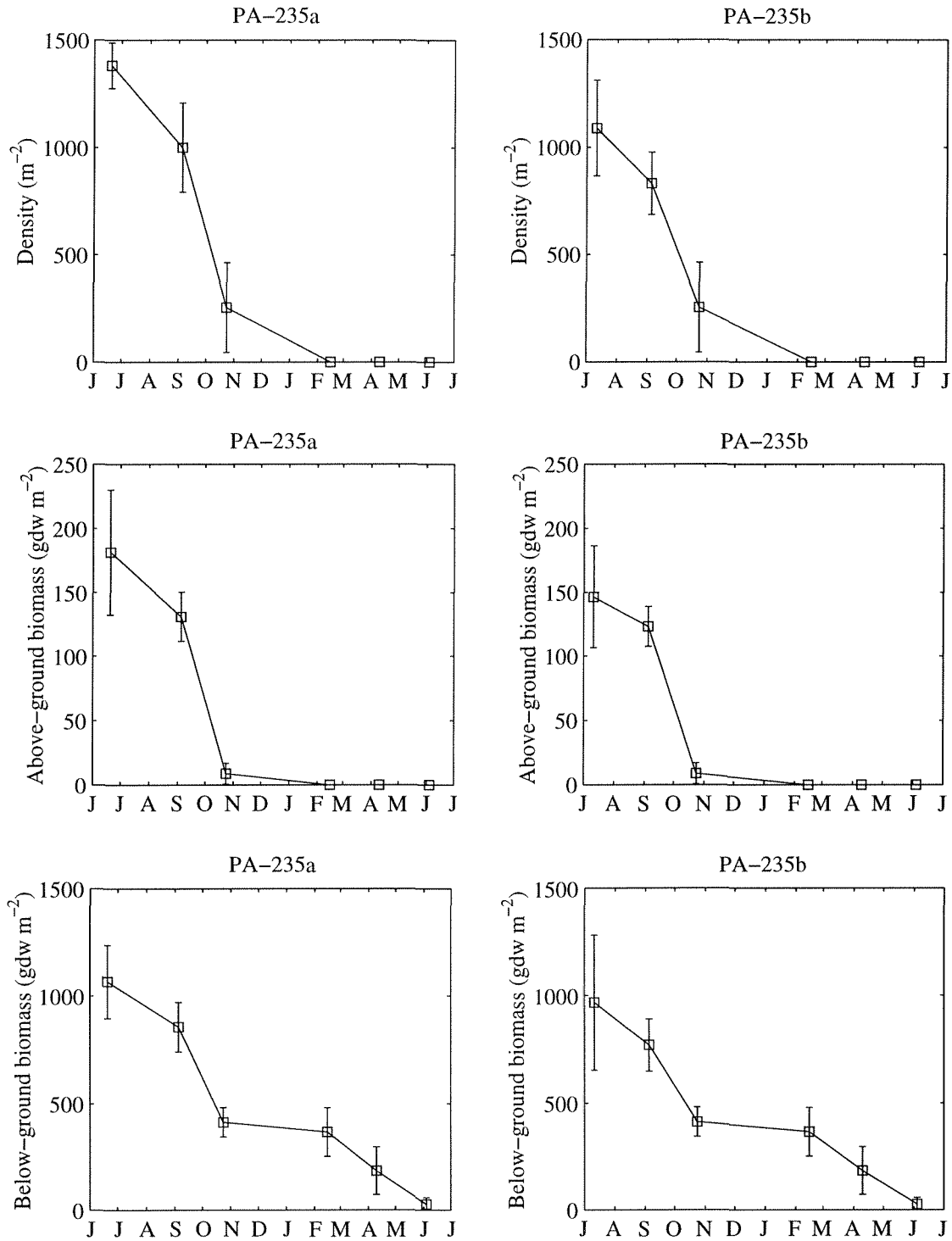


Figure 3: Measured shoot density (top row), above-ground biomass (middle row) and below-ground biomass (bottom row) at sites PA-235c (left hand column) and PA-235d (right hand column). Error bars represent standard deviations.

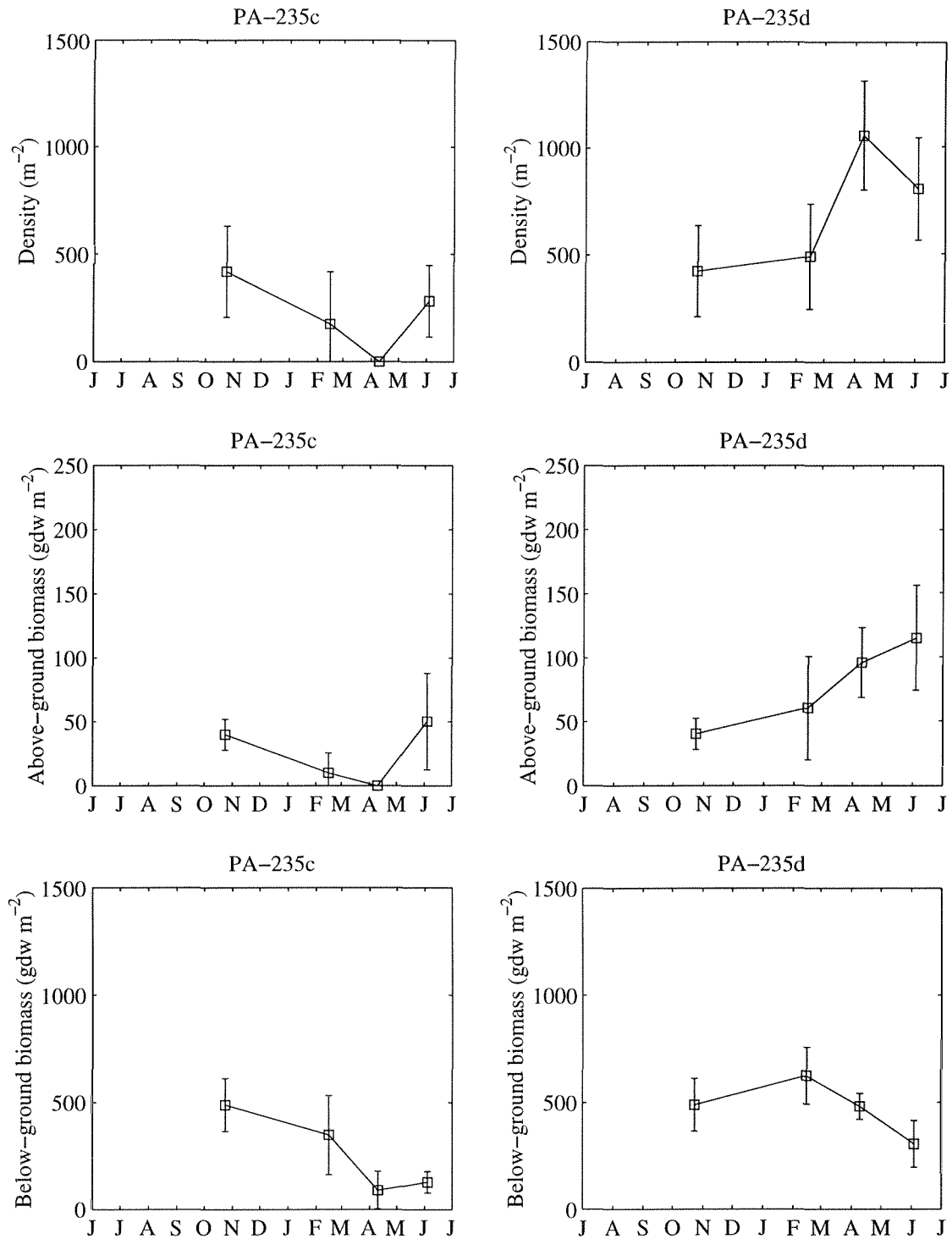
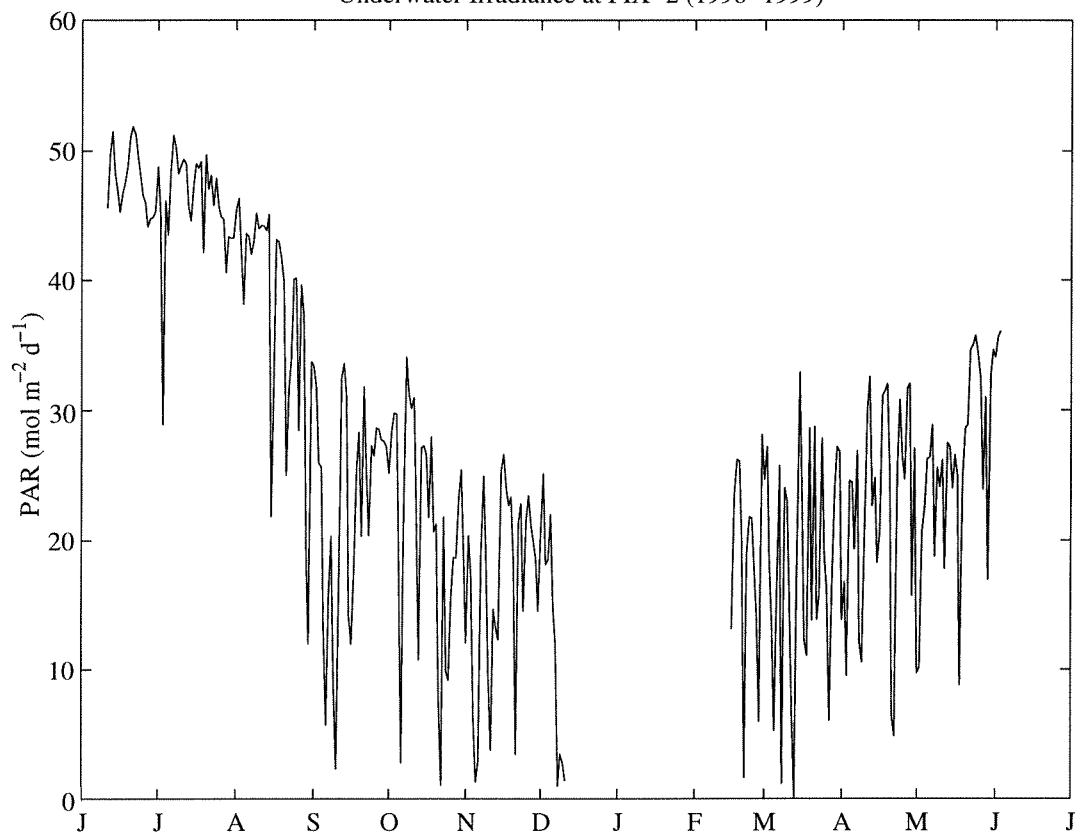
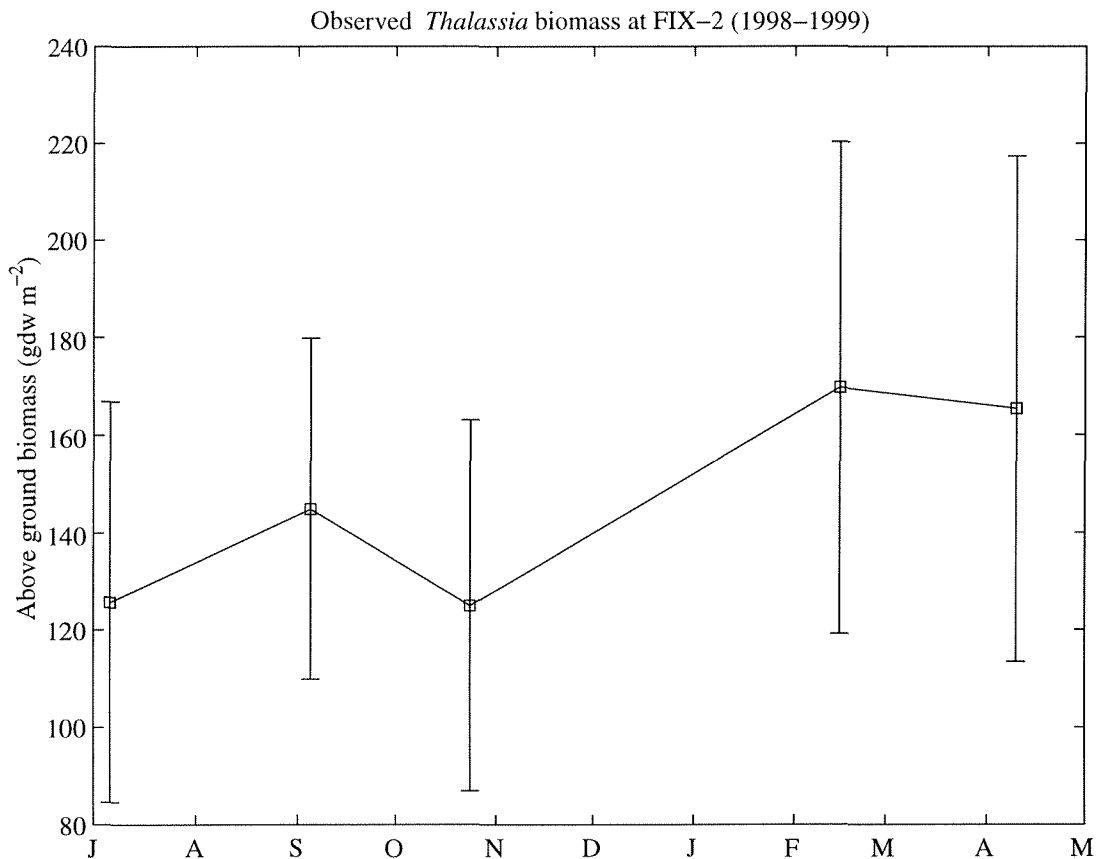


Figure 4: Measured canopy irradiance at site FIX-2
Underwater Irradiance at FIX-2 (1998-1999)



The measured irradiance at canopy level (Figure 4) showed the expected seasonal trend with a gap of two months during which data were not collected (a similar gap appears in the surface irradiance measurements, Figure 1). Since the gap in light measurements appears during the winter when the plants are least productive, one might expect that the missing light data would not be a problem. However, the measured above-ground biomass (Figure 5) at the site showed a marked increase during this time.

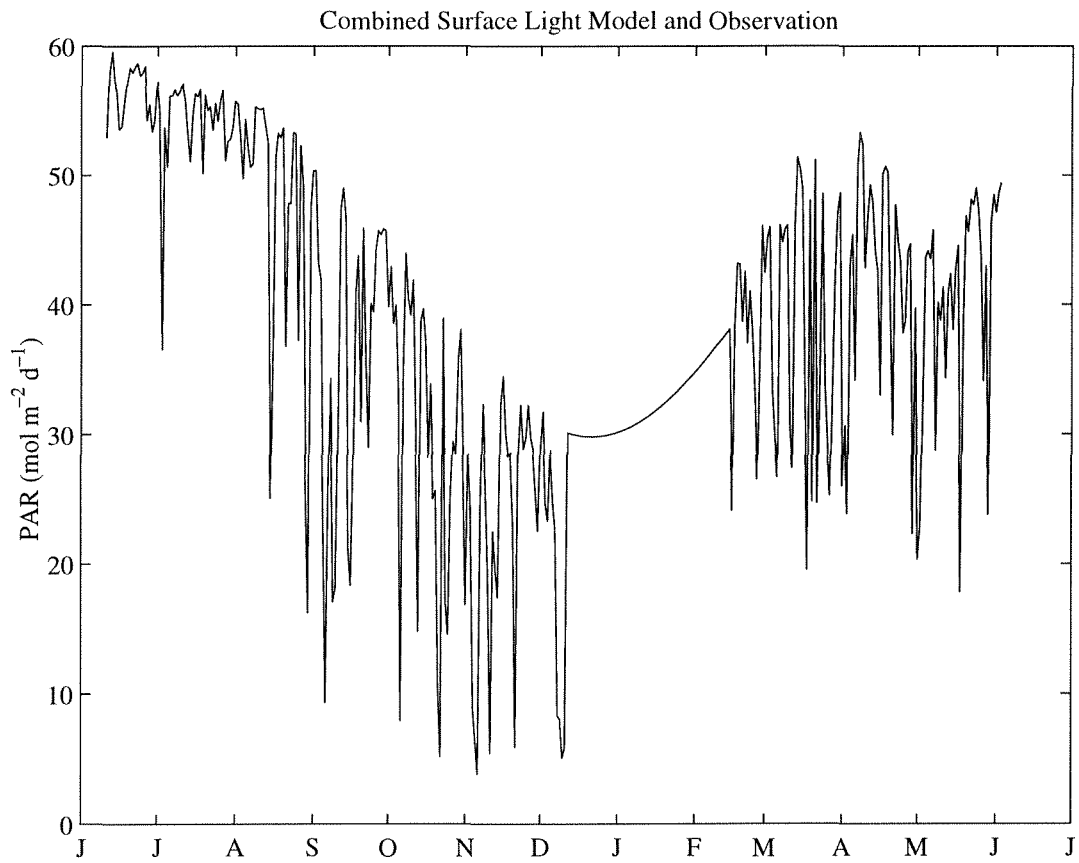
Figure 5: Measured above-ground biomass at site FIX-2. Error bars represent standard deviation.



Without a sophisticated radiative transfer model and information on the particulate material in the water column during this period, it is impossible to realistically fill a data gap of this length. We can however estimate the surface irradiance using the model described in Chapter I and with this, together with an interpolated light attenuation, arrive at an estimate for the light at the canopy level. The result of this is shown in Figure 6.

An estimate of the attenuation coefficient k_d was obtained using the available surface (Figure 1)

Figure 6: Combination of the observed surface light profile with the modeled surface light.

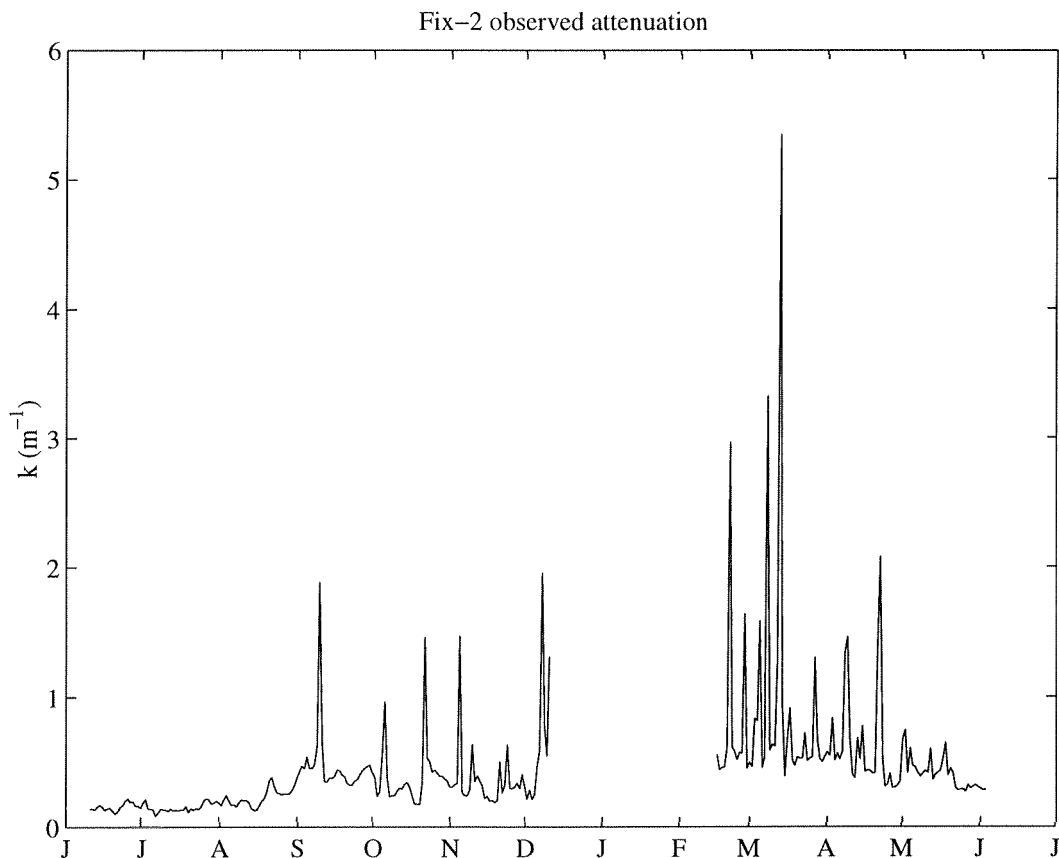


and canopy level (Figure 4) together with the formula

$$k_d = -\frac{1}{z} \log \left(\frac{I(z)}{I(0)} \right) \quad (1)$$

where $z = 1.1$ m is the depth of the canopy-level sensor below the water, $I(z)$ the measured canopy level irradiance and $I(0)$ the surface irradiance. This produces an approximate value of the diffuse attenuation coefficient (Figure 7).

Figure 7: Estimated diffuse attenuation coefficient at FIX-2



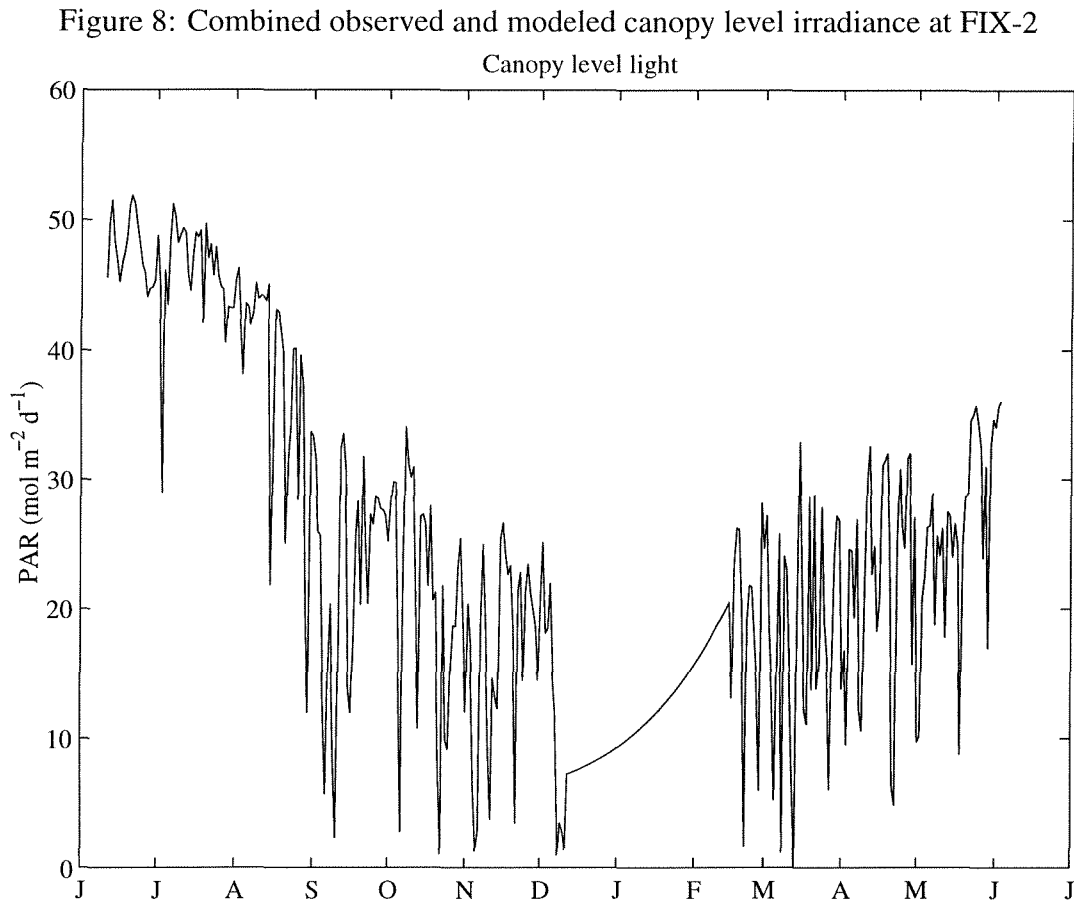
The gap in the time series of the diffuse attenuation coefficient was filled using a linear interpolation between the values either side of the gap. Different schemes for filling the gap in the k_d time series were investigated (*e.g.*, using a constant rather than a linearly interpolated value). There was no difference in the final results of the modeled plant biomass using these different schemes.

Using the time-series shown in Figure 7 for the diffuse attenuation coefficient and the surface light time-series shown in Figure 6, an estimate of the irradiance at the canopy level (Figure 8) was

obtained using a re-arranged form of equation (1)

$$I(z) = I(0) \exp(-k_d z) \quad (2)$$

where $I(z)$ is the irradiance at the canopy level (depth z), $I(0)$ is the surface irradiance and k_d is the attenuation coefficient shown in Figure 7.



The *Thalassia* seagrass model was run using the canopy-level irradiance shown in Figure 8 as a forcing function and an initial biomass equal to the first measured biomass. A comparison between the observed above-ground *Thalassia* biomass and the results of the model are shown in Figure 9.

The model does a good job of tracking changes in the above-ground *Thalassia* biomass prior to the gap in the light record (between December 1998 and February 1999). After this gap in the light record the model under-predicts the above-ground biomass. The reason for this is the

Figure 9: Comparison between modeled and measured above-ground *Thalassia* biomass at FIX-2. Error bars represent standard deviations.

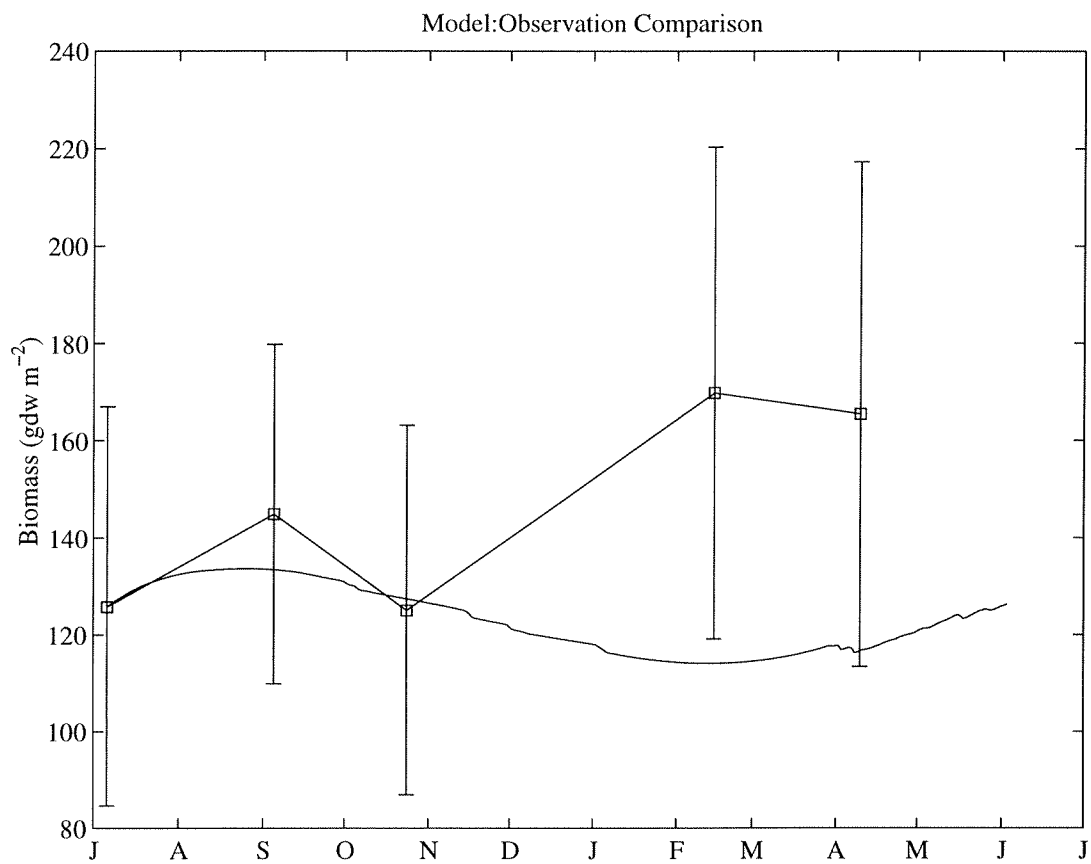
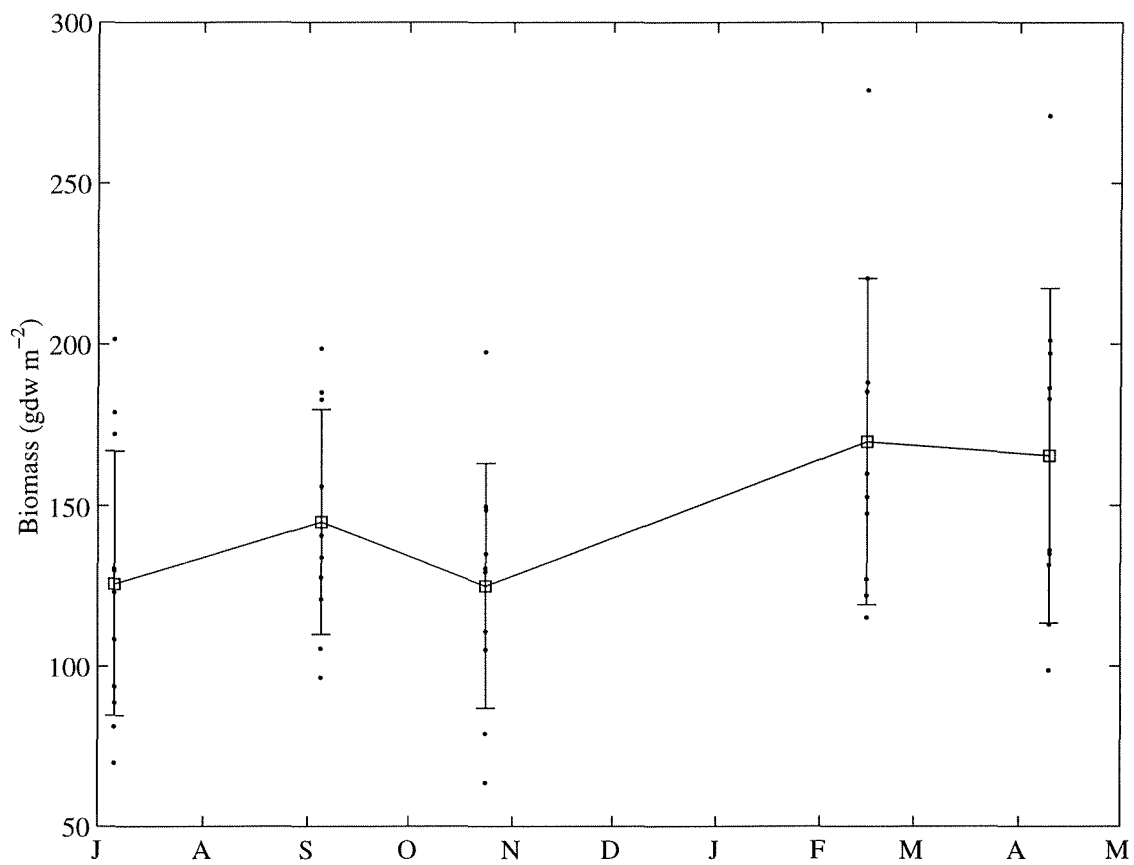


Figure 10: Observed biomass at FIX-2. The dots show the raw data values, the squares the mean values and the error bars are standard deviations.



increase in plant biomass between November 1998 and late February 1999 (Figure 9). The reason for this increase can be seen from the distribution of raw data shown in Figure 10. The biomass estimates for 199 both contain single outliers which produce the unexpectedly high mean values (February 1999 and April 1999 in Figure 10). As a result, the larger biomass measured in 1999 can be attributed to sampling heterogeneity as discussed in Chapter I of this report.

The model does reproduce changes in above-ground biomass of *Thalassia* during the first part of the verification study. During the latter half of the data record, model agreement with the data is poor. This is a result of sampling heterogeneity.

Verification for the site PA-235a

The seagrasses at sites PA-235a and PA-235b were buried by dredge deposits. This is evident from the time series of canopy irradiance (Figure 1) which show a dramatic decline to zero irradiance in September 1988; irradiance at PA-235a shows a slight return in November and December of 1998. In addition, the above-ground biomass drops from approximately 140 gdw m⁻² to almost zero between September 1998 and the end of October 1998 (Figure 2). The below-ground biomass shows a dramatic decline during the same period, followed by a gradual decline to zero biomass by June 1999.

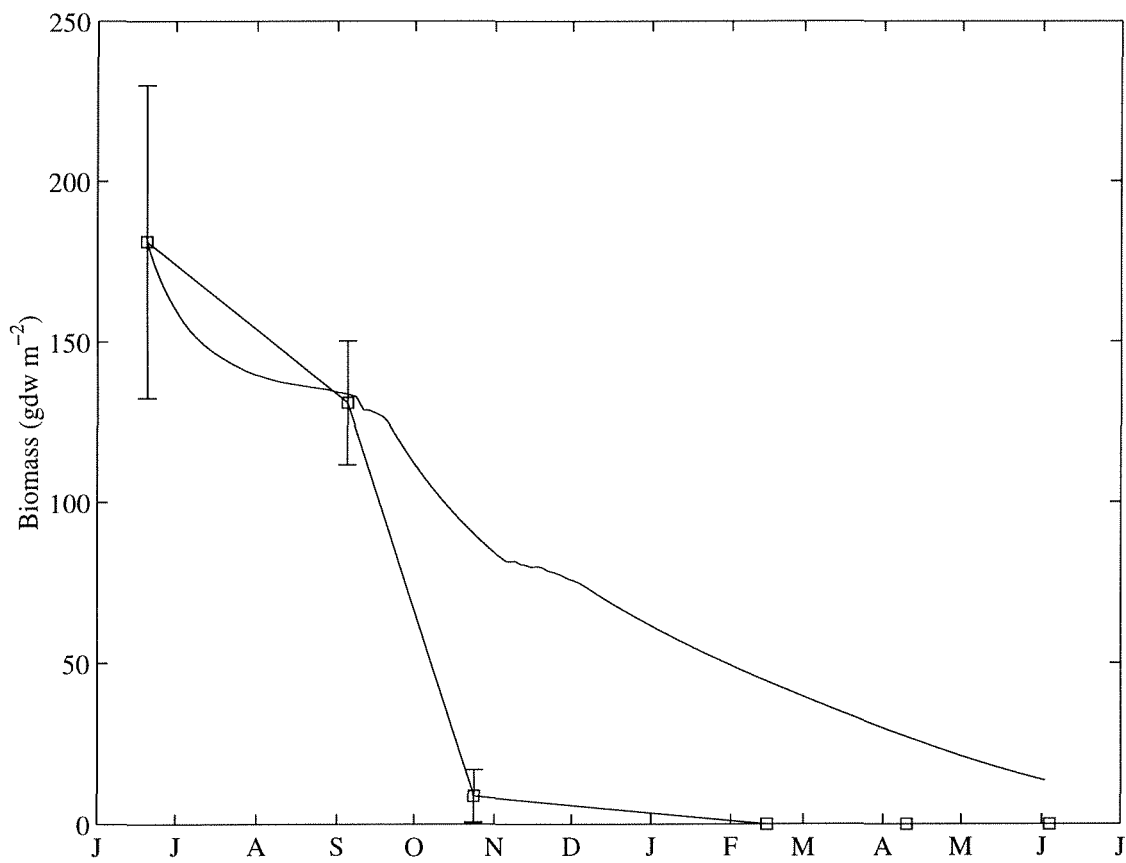
The model was run using the underwater canopy level light measured at the site PA-235a (Figure 1) and model results were compared with the measured biomass at that site (Figure 11).

The comparison between model and data shows that the whilst the model predicts a declining above-ground biomass, the rate of decline is much less dramatic than that seen in the data.

This case is difficult to model for the following reason. The model described in Chapter I was not formulated to model the behavior of seagrasses after complete burial. Under these conditions the plant will cease to photosynthesize because it is receiving no light. The resulting decline in living biomass will be dramatic. In the model, conditions are more appropriate to a chronic decline in light resulting from dredging. The rate of loss of live plant material will be very different in the two cases. This difference is akin to modeling the death of a human being from malnutrition as opposed to a sudden death by shooting; the mortality rate in the two cases is very different.

As a result, a second model was run with the mortality altered to the following according to the

Figure 11: Comparison of model (solid line) with data (solid line plus error bars). Error bars represent standard deviations.

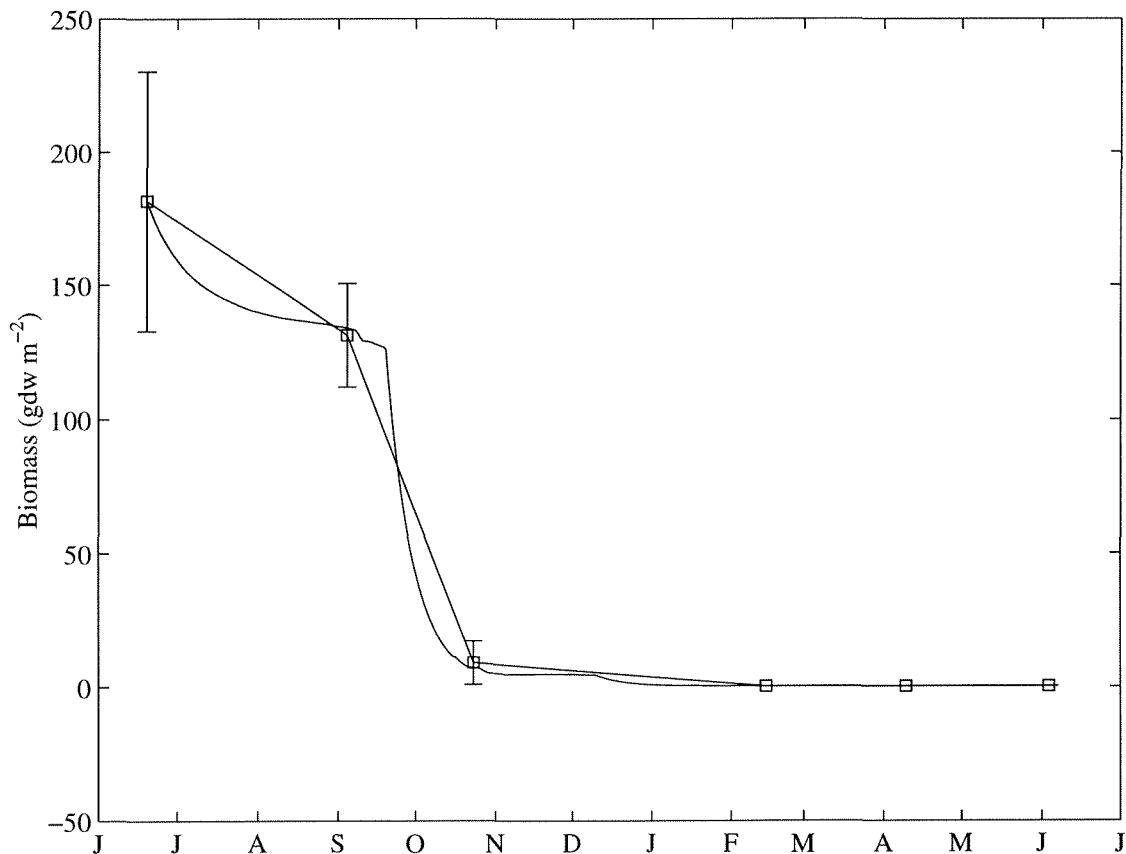


gross production $P(I)$

$$M_a = \begin{cases} 0.0052 & \text{if } P(I) \neq 0 \\ 0.1 & \text{if } P(I) = 0 \end{cases} \quad (3)$$

The value of M_a when $P(I) = 0$ was determined by trial and error in such a way that the model results agreed best with the observations by visual inspection. This new formulation provides an *ad hoc* representation of the increased rate of material loss when the plants are buried. With this new formulation, a much better agreement between data and model results was obtained (Figure 12). We stress that the model was not designed to describe sudden, catastrophic die-off resulting from (for example) burial. The modification represented in Equation 3 is an *ad hoc* formulation and only shows that the model can be modified under certain circumstances to represent different situations.

Figure 12: Comparison of model (solid line) with data (solid line plus error bars) using new loss formulation. Error bars represent standard deviations.



Full model verification: comparison with site PA-235c

The objective of this simulation is to determine how accurately the combined seagrass-sediment geochemical model can predict the results of a dredge disposal event on seagrass biomass and rhizosphere geochemistry. Both the seagrass and the sediment chemistry models were developed with data collected between 1990 and 1997 in Laguna Madre. The seagrass and rhizosphere model (sediment geochemical model) are separately described in Chapters I and III of this report. The linked model was developed by solving the seagrass and sediment geochemical equations simultaneously. This enabled us to use the outputs of the seagrass model - detritus, dissolve organic matter, etc. - as inputs to the sediment model. Further the simultaneous solution to both models allows us to formulate feedbacks between sulfide and ammonium, and seagrass production. Sulfide is toxic to seagrass at high concentrations while ammonium stimulates seagrass growth.

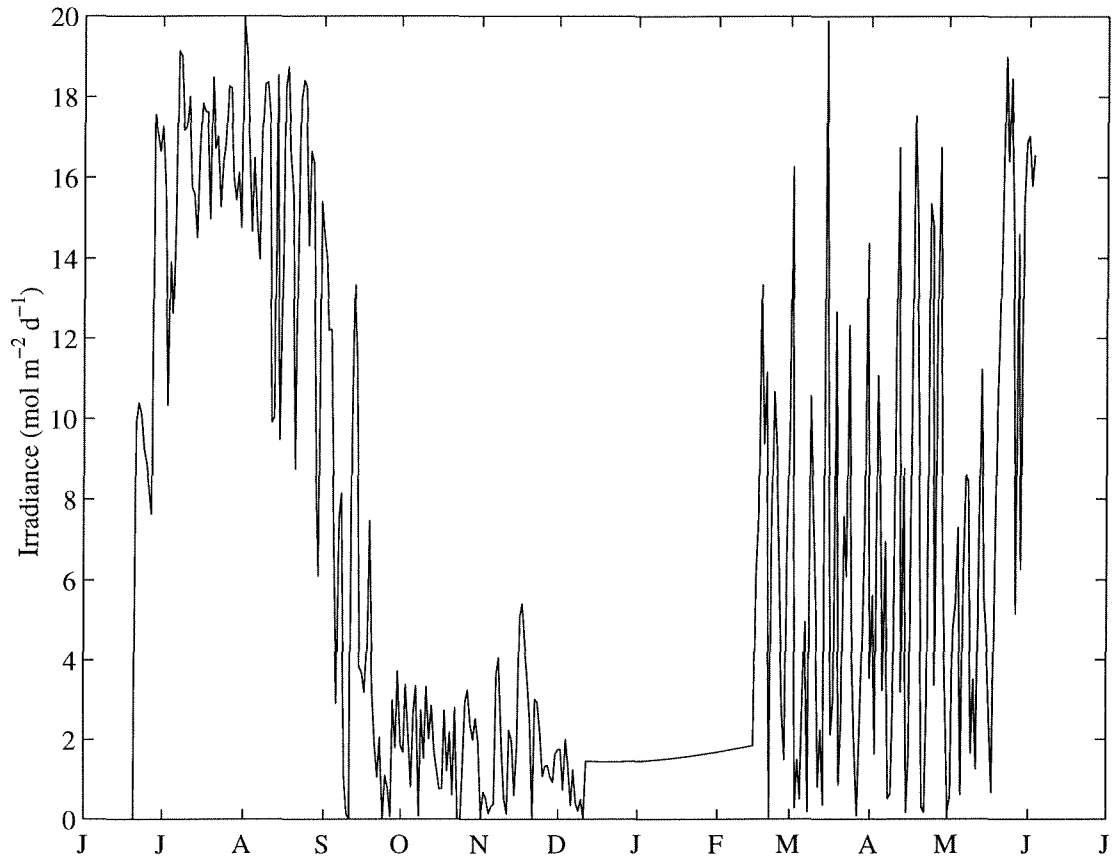
The problem facing validation of the combined seagrass/sediment model is that no single data set exists that covers light, biomass and sediment chemistry. Sediment chemistry at site PA-235c was most complete so this site was used to develop the verification. Unfortunately, at this site, light and biomass were not measured initially (Figures 1 and 3). To solve this, a data set of biomass and irradiance was compiled from data collected at sites PA-235a, PA-235b, PA-235c and PA-235d.

A time-series of light data was compiled by taking the average value of daily irradiance at each site (PA-235a, PA-235b, PA-235c and PA-235d). Two problems exist with this approach. First, the underwater irradiance at sites PA-235a and PA-235b goes to zero in late September of 1998 (Figure 1) because the light sensor was buried by material. No light data exist for the sites PA-235c and PA-235d up until late October 1998 for PA-235c and late February 1999 for PA-235d so it is hard to tell what the underwater light environment was like at these two sites. As a result, the compiled light data used for the verification at PA-235c may under-estimate the light being experienced by the plants. This gap in the underwater irradiance during September 1998 was filled using a timeseries of positive random numbers having the same mean value as the irradiance measured November and December 1998.

Secondly, the gap between December 1998 and February 1999 exists all irradiance data sets. This is a genuine gap in the data record. To fill this gap, a time series of the light attenuation coefficient at site PA-235c was estimated using the available underwater light data at that site and

the surface light data shown in Figure 1. The mean value of this light attenuation time-series was calculated. This mean value was then used to fill the gap in attenuation coefficient between December 1998 and February 1999. The underwater irradiance was then calculated using the surface light model shown in Figure 6 and the attenuation time series calculated above. The resulting underwater irradiance used in the verification is shown in Figure 13.

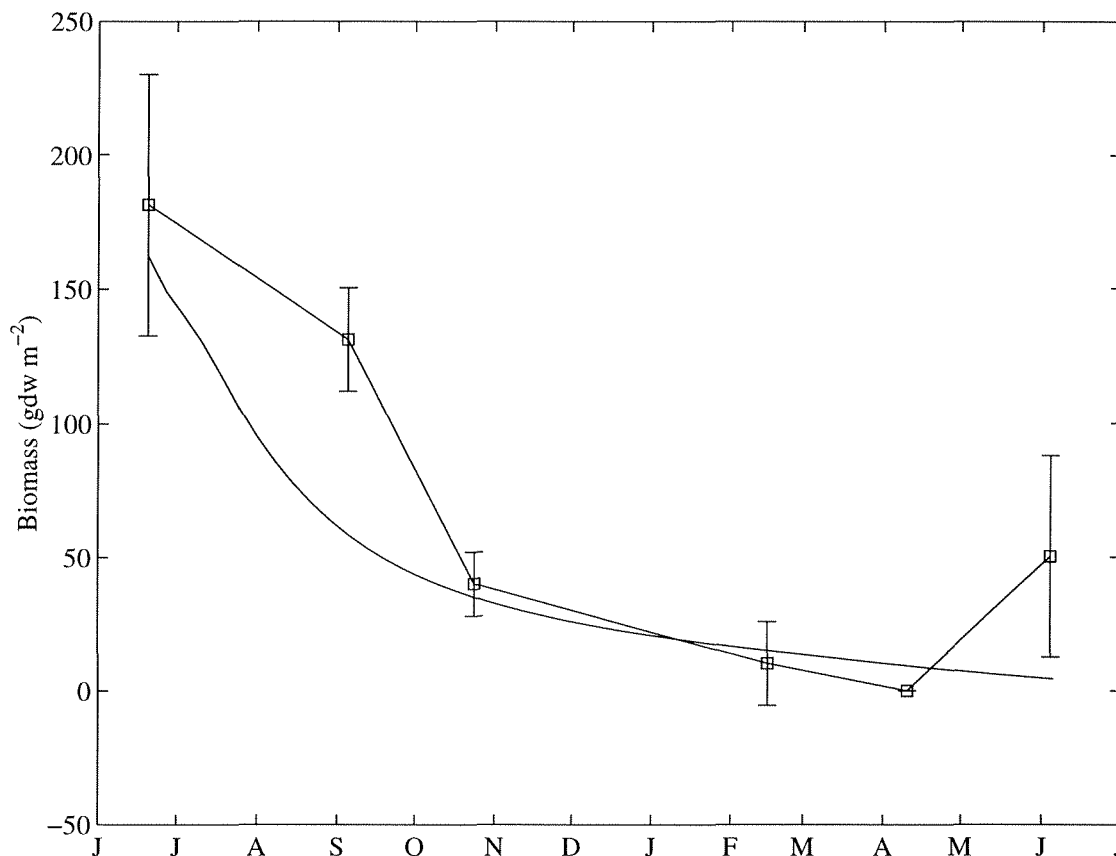
Figure 13: The compiled light profile used in the model verification for site PA-235c



The process of validation requires that the model be able to predict the outcome of the dredge event on the seagrass and rhizosphere when provided with light data, the thickness of the depositional layer from dredge material disposal and the composition of the dredged material. Although several sites were sampled after the dredge disposal event (see above), seagrass at all but PA-235c were either completely buried or were not impacted by the disposal. At PA-235c, 7 to 10 cm of new sediments were deposited over a *Thalassia* bed. Much of the leaf material remained above the sediment layer while the root/ rhizomes of the plant were buried to 9-12 cm. The usual depth

of the root/rhizome system of *Thalassia* is between 2 to 5 cm below the sediment/water interface. The new sediment contained about 0.5% organic matter. We did not have a complete record of light for this site and had to fill gaps in the light record from nearby sites (see above). Even with an incomplete light record the validation model results and the biomass data collected at PA-235c were nearly the same (Figure 14). The model slightly underestimated biomass in September during the initial decline in biomass.

Figure 14: Comparison of above-ground *Thalassia* biomass predictions from the model (solid line) with data (solid line plus error bars). The data was collected at site PA-235c. Error bars represent standard deviations.



Vertical concentration profiles of several pore-water constituents were measured ~ 10 weeks after the dredge disposal event. Pore-water sulfides had increased to 1800 to 2600 μM concentration and ammonium increased to 600 to 1000 μM . The model predicted similar concentrations of sulfides and ammonium for that time period. These modeled concentrations declined slowly over a

period of 10 months until the middle of June when the seagrass photosynthesis increased dramatically. The model suggested that dissolved oxygen from this photosynthesis moved below ground through transport tissue (lacunae) to oxidize much of the remaining sulfide (Figure 15).

Figure 15: Rootzone total sulfides (a) and rootzone NH_4 (b) model results for *Thalassia* for site PA-235c.

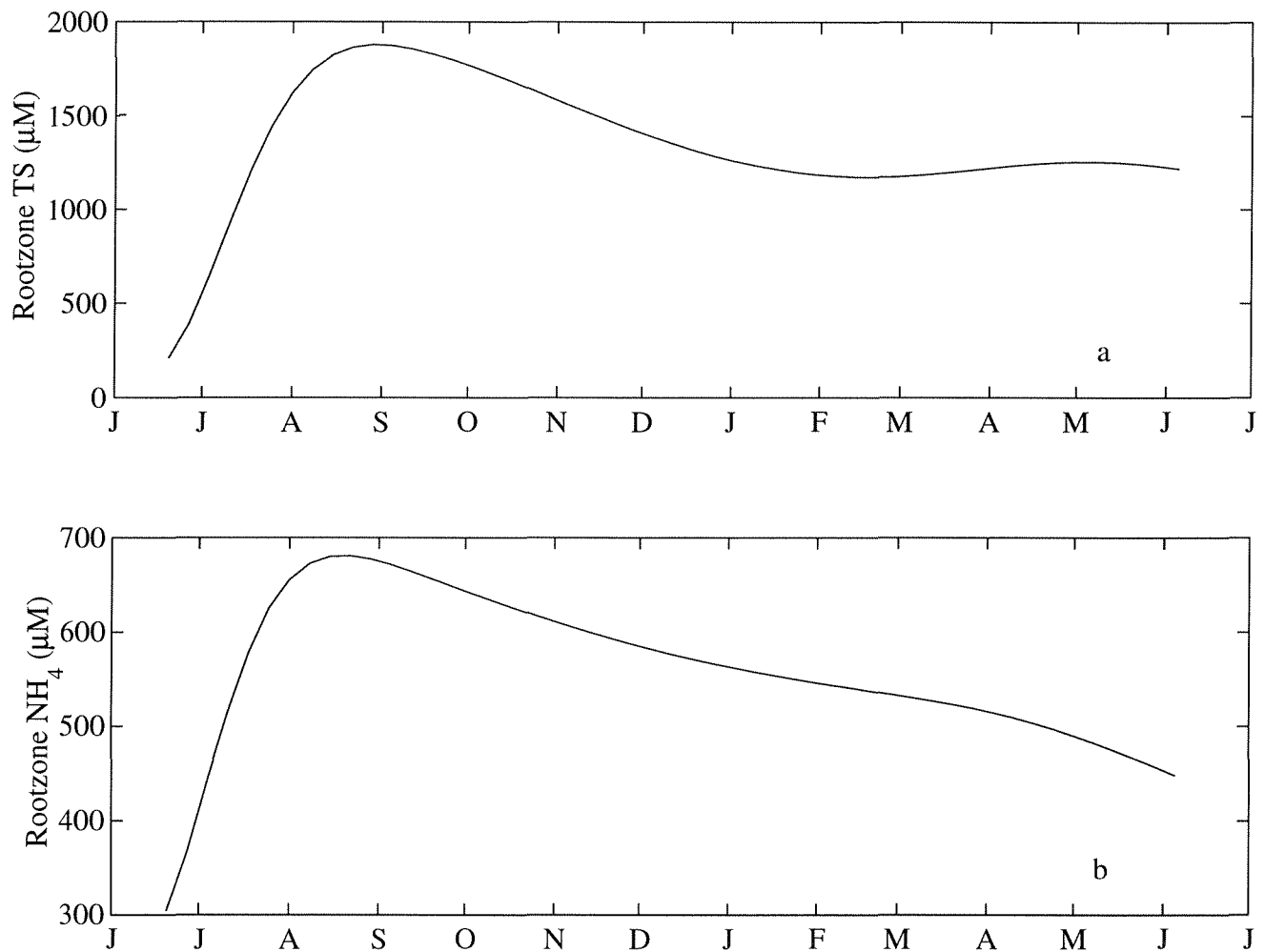


Table 2 provides an estimate of goodness of fit between the model and the vertical pore-water profiles measured after the dredge deposition at PA-235c. The best fit between the model and data occurred on the date at which the samples were taken. However, because of the slow decline in pore-water constituent, there continued to be a high goodness of fit with the data until the *Thalassia*

seagrass started to recover.

Table 2: Normalized root mean squared differences between the model and *Thalassia* field data after the dredge event.

Week	10	20	30	40	50
DIC	0.19	0.20	0.23	0.22	0.19
NH4	0.23	0.32	0.36	0.36	0.38
HS	0.26	0.30	0.41	0.41	0.39

Conclusions

Three verifications of the *Thalassia* model were run. Two verifications used only the biomass part of the model; one using the data from FIX-2 which was not affected by the dredging and a second using data from PA-235a where the seagrasses were buried. A verification of the combined seagrass/sediment diagenesis model was made using data from site PA-235c.

In spite of problems with the data records from all these sites, the verifications were generally successful. The verification at site FIX-2 produced good agreement with the observations for July 1998 through October 1998 but under-estimated the above-ground biomass that was measured in February 1999 and April 1999. Between October 1998 and late February 1999 there was an increase in observed above ground biomass that was not captured in the model. This may be due to changes in environmental circumstances, measurement error or the lack of an explicit below-ground compartment in the model.

The model verification at the site PA-235a was complicated by the fact that the plants at this site were buried by late September 1998. The model is designed to deal with chronic declines in conditions affecting seagrasses such as prolonged low irradiance levels. The model was not designed to deal with sudden, catastrophic changes in conditions, such as complete burial of the plant. However, a modification of the mortality term in the equations governing the plant dynamics shows that the model can cope with such a situation.

The verification of the combined seagrass/sediment diagenesis model at site PA-235c was also

successful. This verification was more problematic in that there was not a complete data set for this site. The model captures the decline of the seagrass biomass well, but does not capture the recovery in June 1999. This may be due to the fact that the time series ends in June and, given longer time series of light and biomass data the model may have also shown a recovery. Another possibility is that the lack of an explicit below-ground biomass compartment in the model results in an under-estimate in the plant resources available for recovery.

Part III: Biological and Chemical Measurements

CHAPTER VI: CHARACTERIZATION OF SEAGRASSES, LIGHT, AND WATER COLUMN PARAMETERS

Contents

Abstract.....	4
Introduction.....	5
Methods.....	6
Photon flux measurement	6
Seagrass density and biomass measurements	8
Water column parameters	8
Blade constituent analysis.....	10
Results.....	11
Water column characteristics.....	11
Photon flux density	17
Density and biomass	17
Blade chlorophyll.....	25
Carbon and nitrogen content.....	26
Discussion.....	27
References.....	33

Tables

Table 1. Permanent sampling stations	7
Table 2. Sampling stations along the Laguna Madre transect	10
Table 3. Average surface irradiance (SI) and diffuse attenuation coefficients (<i>k</i>) characteristic of each of the permanent sampling stations based on total daily quanta received by surface and underwater sensors.....	25

Table 4. Density and biomass changes of three seagrass species, <i>Thalassia testudinum</i> , <i>Syringodium filiforme</i> and <i>Halodule wrightii</i>	26
Table 5. Tissue carbon and nitrogen contents in different leaf parts of <i>Thalassia testudinum</i> collected from the lower Laguna Madre (LLM 2) in October 1997. Values are means \pm SE (n=3).....	27

Figures

Figure 1. Map of Laguna Madre showing the location of permanent sampling stations (ULM 1-3; LLM 1-3) and transect stations. Each COE transect site has a corresponding station # which is listed in Table 2.....	9
Figure 2. Variations in water column chlorophyll <i>a</i> with respect to other water column parameters measured along a transect from Corpus Christi Bay to Port Isabel, Texas on June 3, 1996	12
Figure 3. Variations in water column chlorophyll <i>a</i> with respect to other water column parameters measured along a transect from Corpus Christi Bay to Port Isabel, Texas on January 27, 1997	13
Figure 4. Seasonal changes in water column chlorophyll concentration in the upper Laguna Madre (ULM 1, 2, 3) and lower Laguna Madre (LLM 1, 2, 3). Values are mean \pm SE.....	14
Figure 5. Variations in water column NH_4^+ concentration at the six permanent sampling stations in the Laguna Madre over the period of this study. Values are means \pm SE (n=4).....	15
Figure 6. Variations in water column $\text{NO}_2^- + \text{NO}_3^-$ concentration at the six permanent sampling stations in the Laguna Madre over the period of this study. Values are means \pm SE (n=4).....	16
Figure 7. ULM 1. Daily integrated surface and underwater irradiance and light attenuation coefficients.....	18
Figure 8. ULM 2. Daily integrated surface and underwater irradiance and light attenuation coefficients.	19

Figure 9. ULM 3. Daily integrated surface and underwater irradiance and light attenuation coefficients.....	20
Figure 10. LLM 1. Daily integrated surface and underwater irradiance and light attenuation coefficients.....	21
Figure 11. LLM 2. Daily integrated surface and underwater irradiance and light attenuation coefficients.....	22
Figure 12. LLM 3. Daily integrated surface and underwater irradiance and light attenuation coefficients.....	23
Figure 13. <i>Thalassia</i> , <i>Syringodium</i> and <i>Halodule</i> . Shoot density, total biomass and root/shoot ratio for seagrass species along the Laguna Madre transect. Values represent means \pm SE (n=4).....	24
Figure 14. <i>Thalassia</i> , <i>Syringodium</i> and <i>Halodule</i> . Total chlorophyll and chl <i>a:b</i> ratios in seagrass leaf tissues. Values represent means \pm SE (n=6).....	28
Figure 15. <i>Thalassia</i> . Seasonal changes in carbon and nitrogen contents of leaf and rhizome tissues. Values represent means \pm SE (n=4). Where no error bars appear, SE is less than the size of the symbol.....	29
Figure 16. Correlation between water column chlorophyll estimates derived from traditional spectrophotometric and high performance liquid chromatography (HPLC) methods..	32

Abstract

Continuous measurements of photosynthetically active radiation (PAR), seagrass abundance, and water column chemical parameters were measured at several stations in Laguna Madre over an 18-month period starting in April 1996. PAR showed clear seasonal trends; lowest values were recorded in winter and highest in summer (15 and 60 mol m⁻² d⁻¹ respectively). Average water transparency was clearly highest at station LLM 2 ($k = 0.7 \text{ m}^{-1}$) which was surrounded by dense seagrass beds, and lowest at LLM 1 ($k = 2.4 \text{ m}^{-1}$), an unvegetated site. The decline in the brown tide algal bloom in the upper Laguna led to significant increases in water clarity; at ULM 3, k values over 7.0 m⁻¹ in January 1997 declined to less than 2 m⁻¹ by June. Water column chlorophyll levels were generally <10 µg L⁻¹ in the lower Laguna, and declined in the upper Laguna from 20-70 µg L⁻¹ to <10 µg L⁻¹ following the decline in the brown tide algal bloom. Nitrate and ammonium levels were generally less than 3 µM and salinity ranged from 30-45 ‰ at all sites.

The density and above- and below- ground biomass of the three predominant seagrass species (*Halodule wrightii*, *Thalassia testudinum* and *Syringodium filiforme*) showed distinct seasonal changes that reflected changes in both daylength and water temperature. Ratios of below-ground to above-ground biomass were highest in winter (3-8) and lowest in summer (2-6). *Thalassia* exhibited the highest biomass (over 900 gdw m⁻²), but highest shoot density was characteristic of *Halodule* (over 8,000 m⁻²), with *Syringodium* intermediate between the two species. Carbon content in *Thalassia* leaf and rhizome tissues averaged 36%; the nitrogen content of leaf tissues (1.7-2.7%) was higher than that of rhizomes (<1%). Both nitrogen and carbon content exhibited distinct variations as a function of leaf age.

Introduction

The distribution and primary productivity of submerged aquatic vegetation is largely regulated by variations in light attenuation within the water column. In coastal regions, declines in water quality from human encroachment have caused worldwide losses in the distribution of seagrasses (reviewed by Dennison *et al.* 1993). In Texas, the documented loss of over 140 km² of seagrasses in the lower Laguna Madre since the 1960's is attributed to decreased water transparency from maintenance dredging (Quammen and Onuf 1993, Onuf 1994); the nearly complete loss of seagrass beds in Galveston Bay (over 20 km²) is also attributed to decreased water transparency and eutrophic conditions that resulted from wastewater discharges, subsidence and dredging activities (Pulich and White 1991).

Light energy has long been recognized as the most important factor influencing seagrass habitats (Zieman and Wetzel 1980), but there are few long-term measurements of *in situ* irradiance. In addition, although the photosynthetic characteristics of several seagrasses have been determined (Drew 1979, Libes 1986, Marsh *et al.* 1986, Fouqurean and Zieman 1991, Perez and Romero 1992), this photosynthetic data has not been applied to *in situ* measurements of irradiance. The long term *in situ* measurements irradiance, plant photosynthesis, and seagrass biomass in the Laguna Madre represent a notable exception (Dunton 1994, Dunton and Tomasko 1994). The presence of these data, along with measurements of incident irradiance, growth and biomass, present a rare opportunity for modeling seagrass production and biomass with respect to changes in the underwater light field.

Changes in the amount of light that reaches the bottom are primarily regulated by concentrations of total suspended solids (TSS) and chlorophyll (chl), which can vary widely. The contribution made by TSS and chl largely determine the magnitude of the diffuse light attenuation coefficient (*k*). The relative importance of both can vary across broad spatial and temporal scales. In San Antonio Bay, the resuspension of solids contribute most to light attenuation (Dunton 1996). In other systems, high chlorophyll concentrations result from increased levels of dissolved

inorganic nitrogen that are often derived from anthropogenic inputs (sewage or fertilizers). In either case, light limitation can be assessed from increases in leaf chl content in some seagrass species (e.g., *Thalassia*) that attempt to photoacclimate to maintain high photosynthetic activity.

This chapter presents the 18-mo compilation of *in situ* measurements collected in the Laguna Madre on underwater and surface irradiance, plant biomass and density, various water column parameters (e.g., chl & nutrients), and seagrass blade constituents. The data set focuses on the three species of seagrasses prevalent in the Laguna Madre: *Halodule wrightii* in the upper Laguna and in the lower Laguna, *Thalassia testudinum* and *Syringodium filiforme*. Much of the information presented here was used in the development of an integrative productivity model for all three species.

Methods

Photon flux measurement

Photosynthetically active radiation (PAR: 400-700 nm) was collected continuously at six permanent stations (Table 1). At each site a LI-193SA spherical quantum sensor was deployed at canopy level with a LI-1000 datalogger (LI-COR Inc.). The datalogger was placed in a weighted clear polycarbonate housing (Ikelite Model 5910, Indianapolis, IN) and was wired to the sensor cables through molded underwater connectors (Crouse-Hinds Series 41 Penetrator, LaGrange, NC). Sensors were mounted on a 3-cm diameter PVC pipe at canopy level (usually 15-20 cm above the bottom) to minimize fouling by drift algae and seagrass leaves. At all sites, a clear polyethylene bag was placed over the sensor to minimize biofouling of the sensor globe and was replaced at 10-14 day periods to minimize fouling. The polyethylene bag has a negligible effect on light measurements. Photon flux density (PFD: $\mu\text{mol m}^{-2} \text{s}^{-1}$) was measured at 1-min intervals and integrated hourly. Daily PFD ($\text{mol m}^{-2} \text{d}^{-1}$) was calculated as the summation of quantum flux over each 24 hr period.

Coincident measurements of surface PFD was also collected at three stations (ULM-1, ULM-3, and LLM-2) using a LI-190SA quantum sensor and datalogger. This data was used in calculating percent surface irradiance (%SI) and values for the diffuse attenuation coefficient, k . Measurements of depth are average depths (Table 1), based on numerous soundings that were collected at the permanent study sites by field technicians. Since total tidal amplitudes generally range less than 20 cm, are significantly influenced by prevailing winds, and tide gauge information is not available throughout the Laguna, correction of k for slight changes in depth were not made. Light attenuation was calculated using the Beer-Lambert equation:

$$I_z = I_0 e^{-kz}$$

where I_0 is irradiance at the surface, I_z is irradiance at depth z and k is the attenuation coefficient (m^{-1}). The sensors used in this study were calibrated to $\pm 5\%$ (traceable to National Bureau of Standards); stability was $\pm 2\%$ over any 1 yr period, and data was recorded with a precision of $\pm 0.01 \mu mol m^{-2} s^{-1}$.

Table 1. Permanent sampling stations.

Station	Established	Latitude	Longitude	Physical Description	Biological	Depth (m)
ULM 1	6/17/96	27°41'30"	97°13'20"	ICWW	Bare	1.0
ULM 2	4/1/96*	27°25'	97°21'	100 m East of ICWW	<i>Halodule</i>	1.0
ULM 3	6/17/96	27°11'33"	97°25'42"	ICWW	Bare	1.0
LLM 1	6/4/96	26°10'45"	97°15'36"	West of ICWW	Bare	1.15
LLM 2	6/4/96	26°08'	97°12'	1.0 km East of ICWW	<i>Thalassia</i>	1.20
LLM 3	3/1/97	26°35'25"	97°22'57"	6.0 km East of Port Mansfield	<i>Syringodium</i>	1.27

*Platform not installed at this station

Seagrass density and biomass measurements

Indices of seagrass abundance (density and biomass) were measured in June 1996 at 12 stations (four stations per species) on a transect that extended the entire length of the Laguna (Fig. 1). Depths at the twelve stations ranged from 0.7 m (*Syringodium*) to 1.65 m (*Thalassia*), but were generally in the 0.8-1.1 m range (Table 2). In addition, standing stock was assessed at three stations (each representing one of the predominant species) over a 12-month period at 3-4 month intervals. On each occasion, four replicate samples were collected with a 9 cm diameter coring device for *Halodule* and *Syringodium*, while a 15 cm diameter core was used for *Thalassia*. Samples were thoroughly cleaned of epiphytes and sediments, separated into above-ground and below-ground live biomass and dried at 60°C to a constant weight. Shoot density was estimated by counting the number of shoots per core and scaling to appropriate units (shoots m⁻²).

Water column parameters

Water column physicochemical measurements were collected on two transects that extended the entire length of the Laguna on 3 June 1996 and again on 27 January 1997. Continuous measurements of chlorophyll *a* in the water column were determined using a Morgan 10-AU fluorometer equipped with a continuous flow 25 mm cuvette. In addition, monthly sampling was conducted at the six permanent stations (Table 1) over the entire period of this study. Total DIN ($\text{NO}_3^- + \text{NO}_2^- + \text{NH}_4^+$) and chlorophyll *a* were determined from four replicate water samples collected at each site. Chlorophyll *a* samples were filtered onto cellulose nitrate filters, and then extracted with 90% acetone buffered with 0.05% MgCO₃ and analyzed on a spectrophotometer at 750, 664, 647 and 630 nm following Parsons *et al.* (1984). DIN was determined colorimetrically according to Parsons *et al.* (1984). Temperature was measured *in situ* using a stem thermometer; salinity was measured using an Orion Model 140 conductivity-salinity meter.

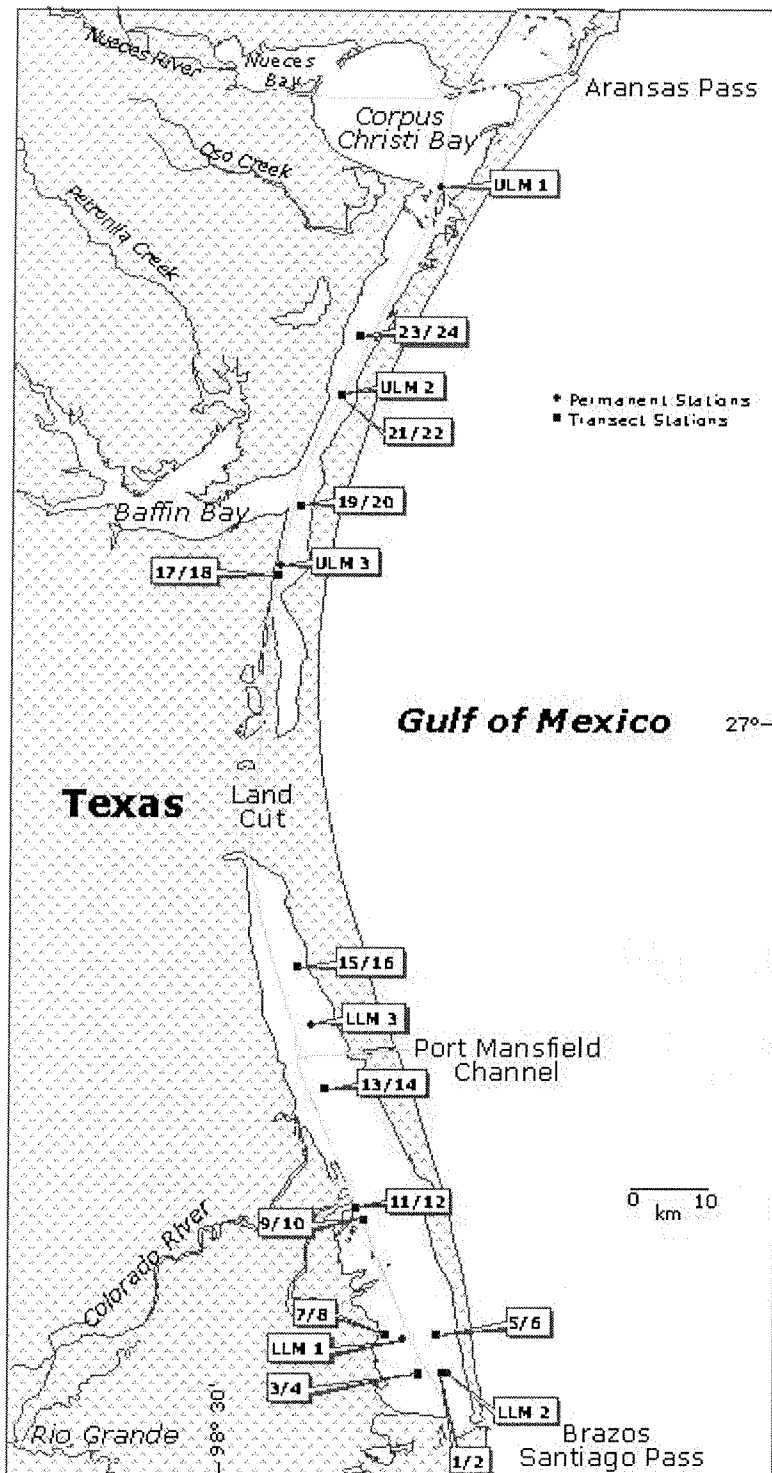


Figure 1. Map of the Laguna Madre showing the location of permanent sampling stations (ULM 1-3; LLM 1-3) and transect stations. Each COE transect site has a corresponding station # which is listed in Table 2.

Table 2. Sampling stations along the Laguna Madre transect.

COE #	Station	Marker	Latitude	Longitude	Physical Description	Biological	Depth (m)
1 / 2	30 S/B	123	26°08'06"	97°12'31"	1.0 km East of ICWW	<i>Thalassia</i>	1.2
3 / 4	29 S/B	115	26°07'57"	97°14'21"	1.0 km West of ICWW	Deep <i>Thalassia</i>	1.65
5 / 6	28 S/B	91	26°11'	97°13'	East of ICWW	<i>Thalassia</i>	1.3
7 / 8	27 S/B	91	26°11'	97°17'	West of ICWW	<i>Thalassia</i>	1.15
9/10	26 S/B	9	26°20'05"	97°18'45"	East of ICWW - on spoil bank near mouth of Arroyo Colorado	<i>Syringodium</i>	0.9
11/12	25 S/B	7	26°21'	97°19'20"	West of ICWW - natural bed near Arroyo Colorado	<i>Syringodium</i>	0.7
13/14	24 S/B	159	26°30'23"	97°21'53"	2.0 km East of ICWW	<i>Syringodium</i>	0.8
15/16	22 S/B	103	26°40'	97°24'	3.0 km East of ICWW	<i>Syringodium</i>	0.8
17/18	20 S/B	47	27°10'47"	97°25'45"	Old Blucher Remote	<i>Halodule</i>	1.1
19/20	18 S/B	3	27°16'20"	97°24'	East of ICWW	<i>Halodule</i>	1.1
21/22	16 S/B	151	27°25'	97°21'	100 m East of ICWW	<i>Halodule</i>	1.2
23/24	13 S/B	114	27°29'42"	97°19'32"	King Ranch	<i>Halodule</i>	1.2

S/B : Paired-site combination of seagrass and bare habitats

Blade constituent analysis

Blade chlorophyll (chl) content was determined for six replicate samples from each sampling date. Pre-weighed leaf tissue was ground in 90% cold acetone buffered with 0.05% MgCO₃ using chilled pestles and mortars with washed sea sand. Extracts were made up to a known volume and centrifuged. Absorbance was measured at 750, 664, and 647 nm with a Shimadzu UV 160U spectrophotometer. Chlorophyll *a* and *b* contents were determined using the equations of Jeffrey and Humphrey (1975) for 90% acetone extractions. Subsamples of dried plant

material were taken from biomass cores and used to determine total carbon and nitrogen content. Samples of 1-2 mg were weighed into tin boats for elemental analysis using a Carlo Erba EA 1108 elemental analyzer.

Results

Water column characteristics

On both June and January transects, the presence of the brown tide algal bloom was reflected in high (40-80 $\mu\text{g chl L}^{-1}$) pigment levels. The bloom was densest in the upper Laguna in June (Fig. 2), and the Land Cut area to the south in January 1997 (Fig. 3). The shift appears to be a consequence of predominant northerly winds which pushed the bloom southward in winter. Light attenuation was greatest in areas having the highest chlorophyll levels, and lowest nearest the passes. Nitrate and ammonium levels were generally less than 3 μM and salinity ranged from 30 to 45 ppt.

Water column chl concentrations from the permanent upper Laguna Madre stations (ULM 1, 2 and 3) were much higher than those of lower Laguna Madre stations (LLM 1, 2 and 3) (Fig. 4). Chlorophyll levels at ULM sites 2 and 3 exhibited their highest levels during summer and fall, but dropped precipitously by June 1997, when the seven-year brown tide bloom in Laguna Madre ended. Water column chl concentrations at ULM 1 in Corpus Christi Bay were considerably lower than at sites ULM 2 and 3 throughout the study period. In the lower Laguna Madre, the pattern was the opposite; water column chl levels reached a peak in late winter (March and April) and were lowest during the summer months. In summer, the average chl concentration in upper Laguna Madre (*ca.* 30 $\mu\text{g chl L}^{-1}$) was approximately three times that of lower Laguna Madre (*ca.* 10 $\mu\text{g chl L}^{-1}$). Except for the brief winter peak, chlorophyll concentrations in the lower Laguna were generally less than 10 $\mu\text{g chl L}^{-1}$ compared to 20-70 $\mu\text{g chl L}^{-1}$ in the upper Laguna. Ammonium (Fig. 5) and nitrate + nitrite (Fig. 6) concentrations were generally low (<3.0 μM) at all stations throughout the entire study period, with the exception of a fall peak (5-8 μM) at the ULM 1 site in October 1997.

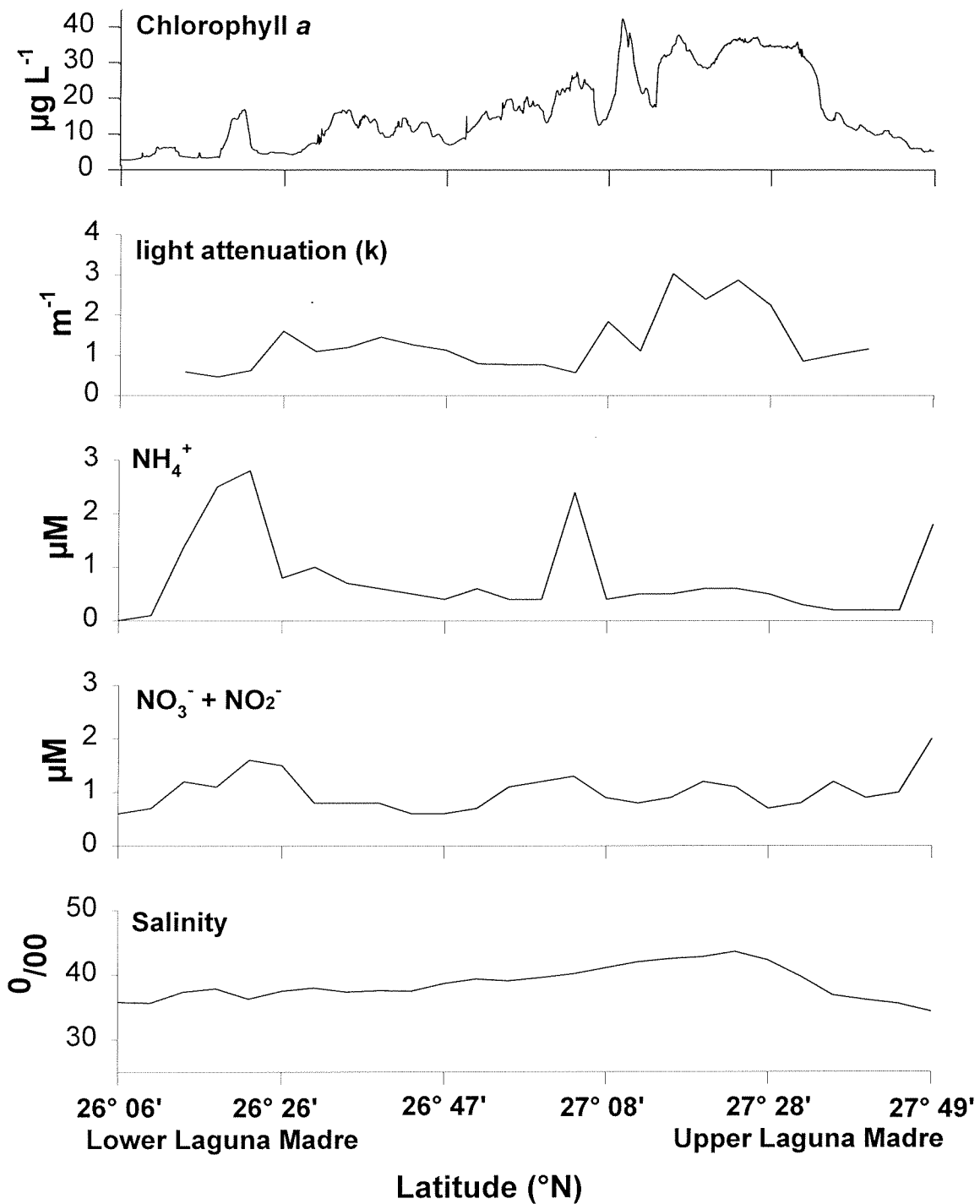


Figure 2. Variations in water column chlorophyll *a* with respect to other water column parameters measured along a transect from Corpus Christi Bay to Port Isabel, Texas on June 3, 1996.

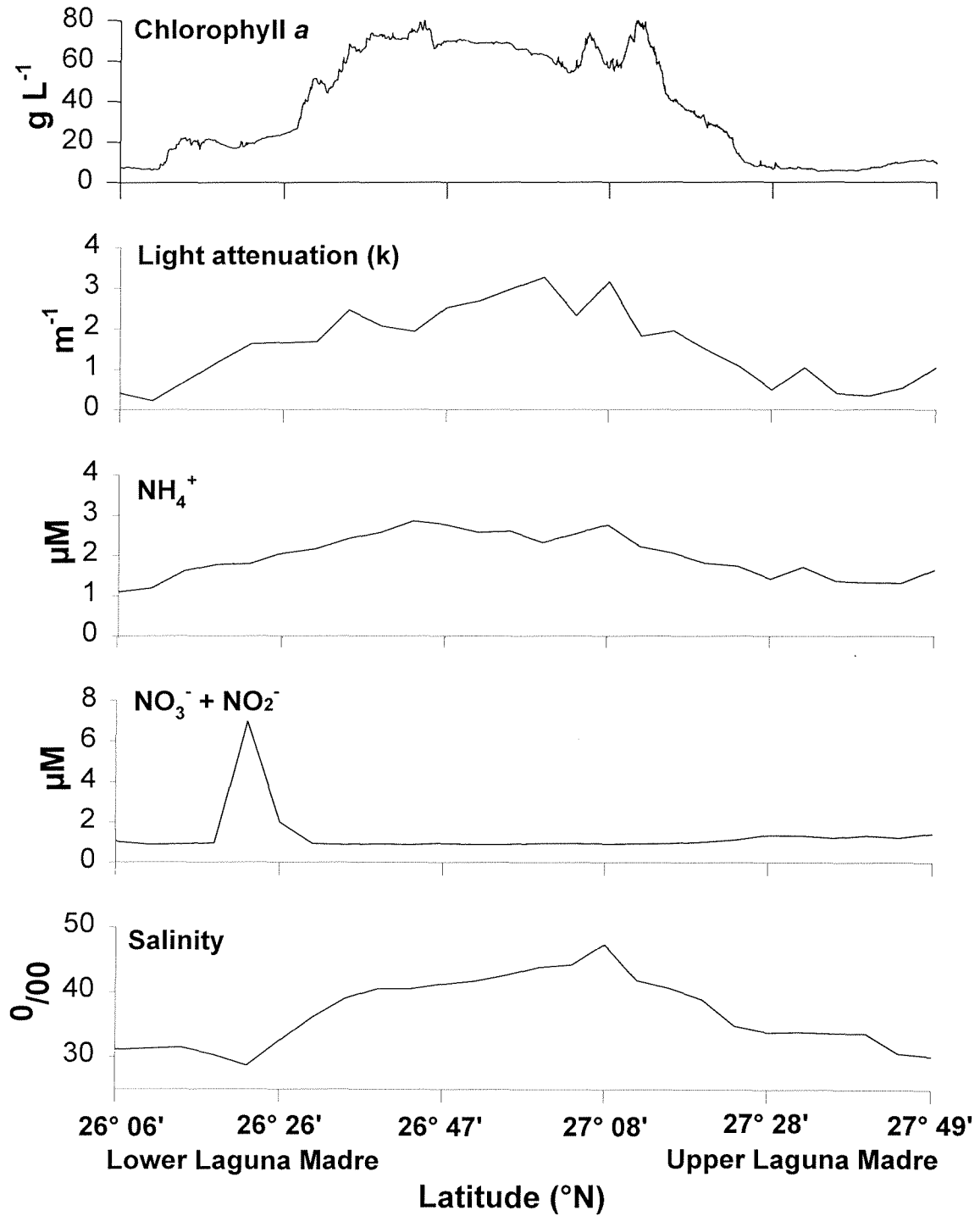


Figure 3. Variations in water column chlorophyll *a* with respect to other water column parameters measured along a transect from Corpus Christi Bay to Port Isabel, Texas on January 27, 1997.

Figure 4. Seasonal changes in water column chlorophyll concentration in the upper Laguna Madre (ULM 1, 2, 3) and lower Laguna Madre (LLM 1, 2, 3). Values are mean \pm SE.

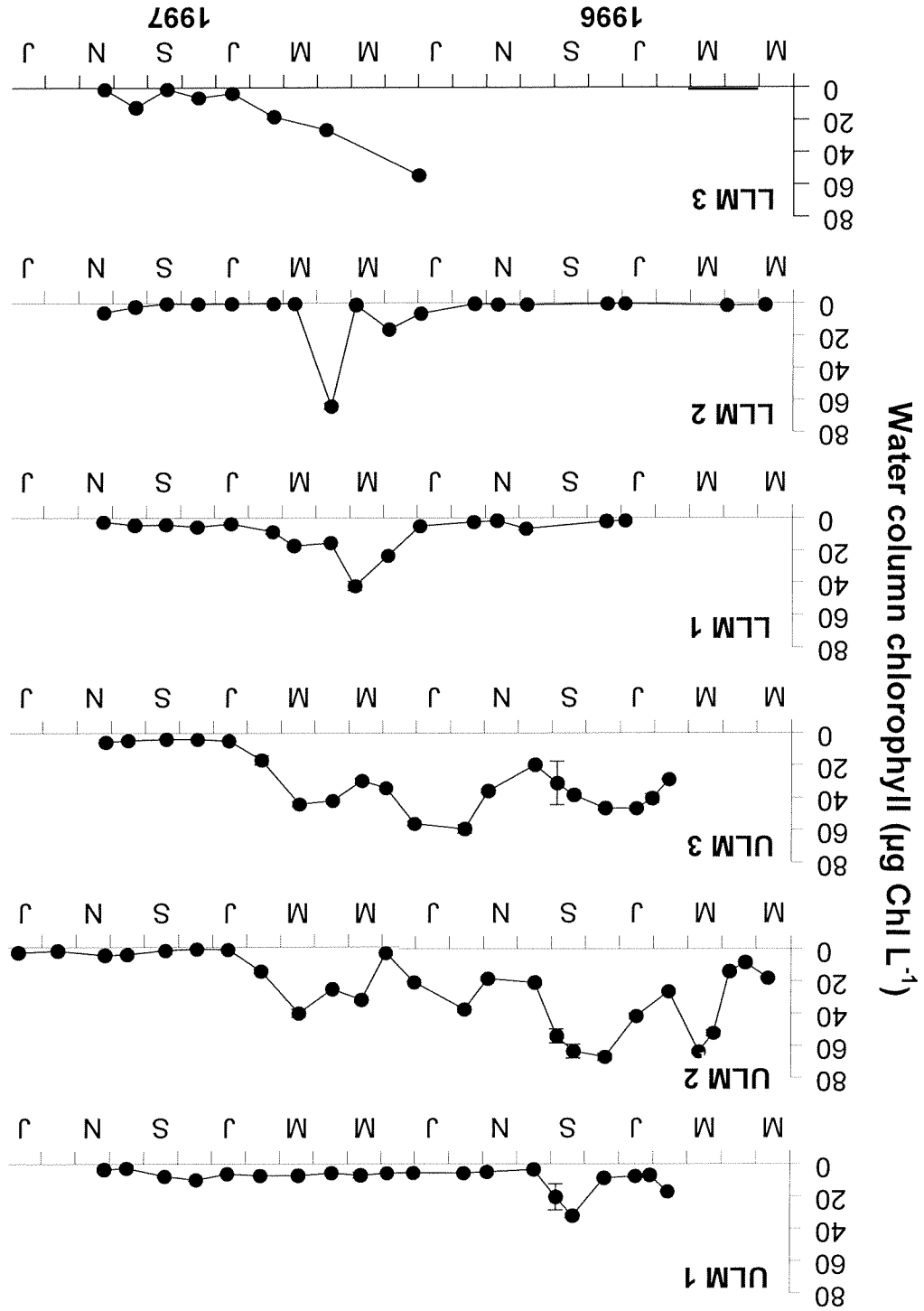
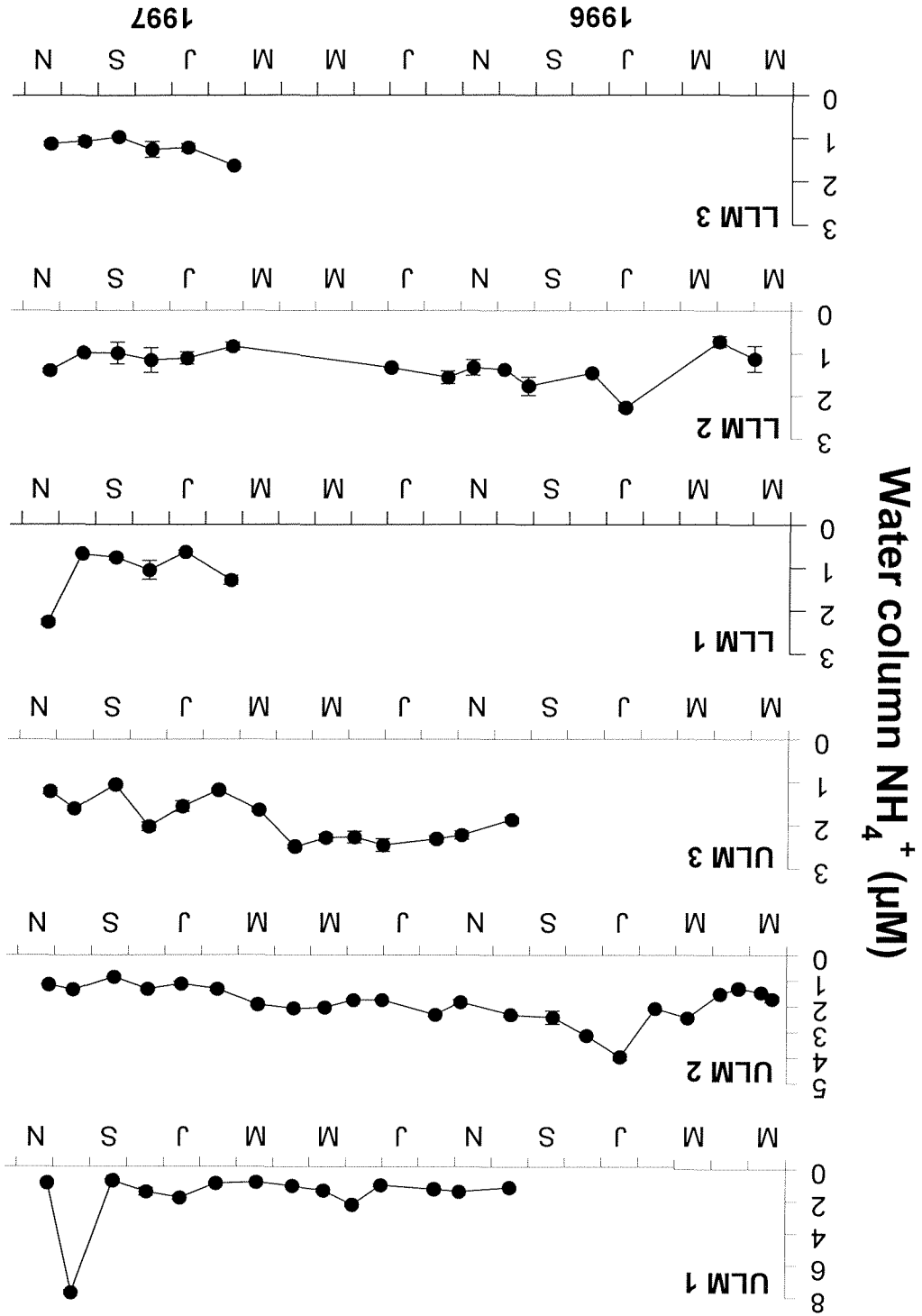


Figure 5. Variations in water column NH_4^+ concentration at the six permanent sampling stations in the Laguna Madre over the period of this study. Values are means \pm SE (n=4).



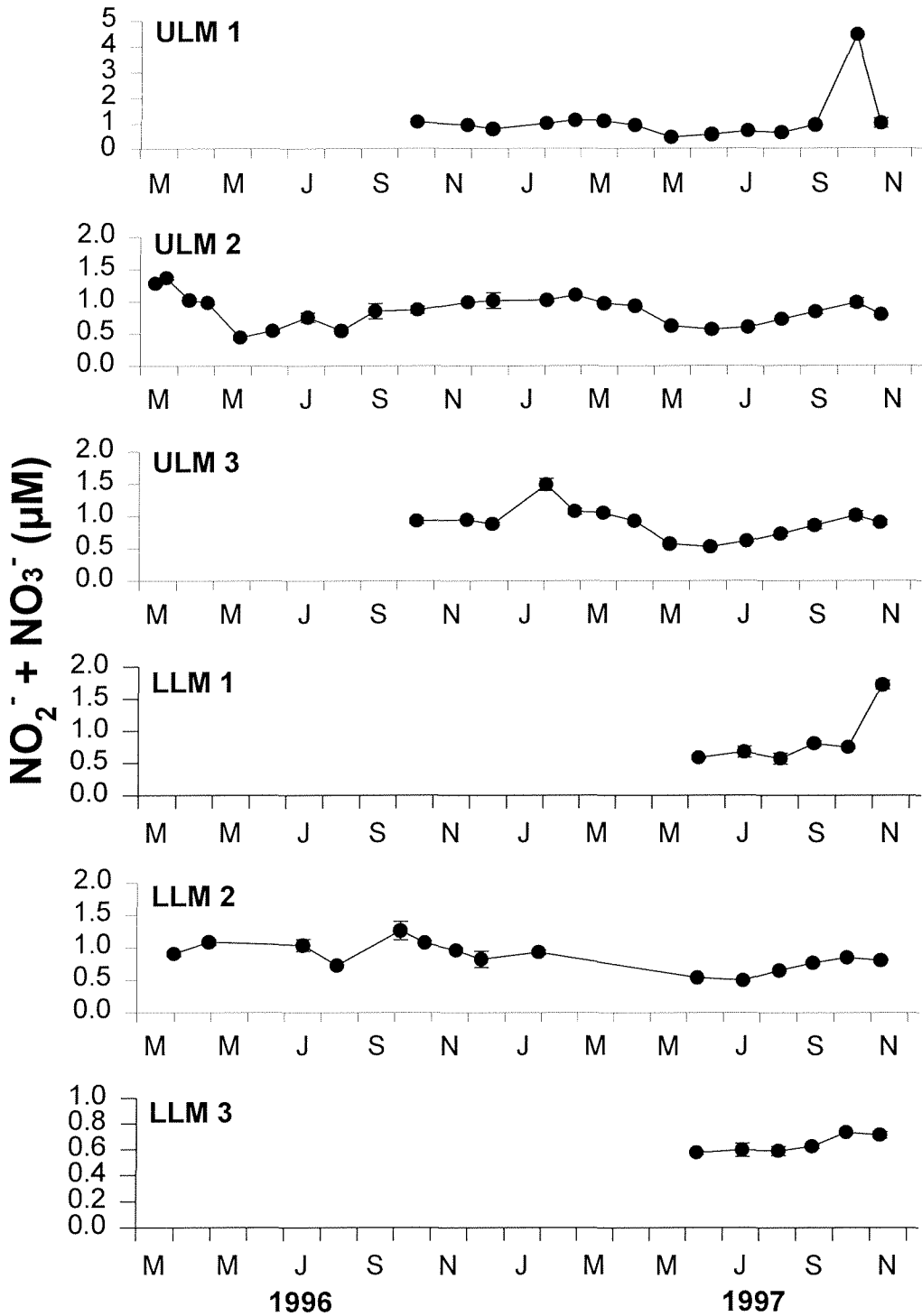


Figure 6. Variations in water column $\text{NO}_2^- + \text{NO}_3^-$ concentration at the six permanent sampling stations in the Laguna Madre over the period of this study. Values are means \pm SE (n=4).

Photon flux density

Surface irradiance (SI) exhibited a clear seasonal trend; lowest values were recorded in winter and highest in summer (*ca.* 15 and 60 mol m⁻² d⁻¹, respectively). Continuous canopy-level measurements of PAR indicated that the underwater light environment was highly variable; daily values ranged from 0 to 35 mol m⁻² d⁻¹ for upper Laguna Madre (Fig. 7-9) and from 0 to 60 mol m⁻² d⁻¹ for lower Laguna Madre (Figs. 10-12).

Diffuse attenuation coefficients (*k*) ranged from 0.1 m⁻¹ to as high as 10 m⁻¹ among the six permanent sampling stations. Average water transparency was greatest and *k* values lowest at ULM sites 1 and 2 and LLM site 2 (Table 3). The decline in the brown tide in ULM is clearly apparent after June 1997 at sites ULM 2 and 3. At ULM 3, *k* values over 7.0 m⁻¹ in January 1997 steadily declined to less than 2 by June. Light attenuation was clearly highest at LLM 1, with many values ranging between 4 and 10. The low transparency at this site clearly reflects the presence of unconsolidated sediments and dredged material deposits that are often resuspended by winds and waves--there are no seagrasses present at this site. In contrast, *k* values were generally <1.0 m⁻¹ for LLM 2 (Fig. 11) which is surrounded by dense grass beds. No underwater light data were collected at LLM 1 and 2 between February and June 1997. Missing underwater irradiance data at all sites in both 1996 and 1997 is related to rapid fouling of the underwater sensors; visits to the sites occurred every 12-14 days, but sensors were often visibly fouled after 10 days during the warmer months. Consequently, irradiance data was routinely removed from the data set after 10 days at sites where fouling was rapid (ULM 1, ULM 3, LLM 1, LLM 3).

Density and biomass

The density and above- and below-ground biomass of the three predominant seagrass species was measured at 12 stations throughout the upper and lower Laguna on a survey conducted in June 1996. *Thalassia* exhibited the lowest shoot density, ranging from 1,270 shoots m⁻² at site 30 to 1,950 shoots m⁻² at site 27 (Fig. 13). *Syringodium* and *Halodule* exhibited similar shoot densities, ranging from 2,200 to 6,800 shoots m⁻². In general, the highest shoot densities (for all species) were recorded for sites at the northern end of the sampling transect (Table 2, Fig. 13).

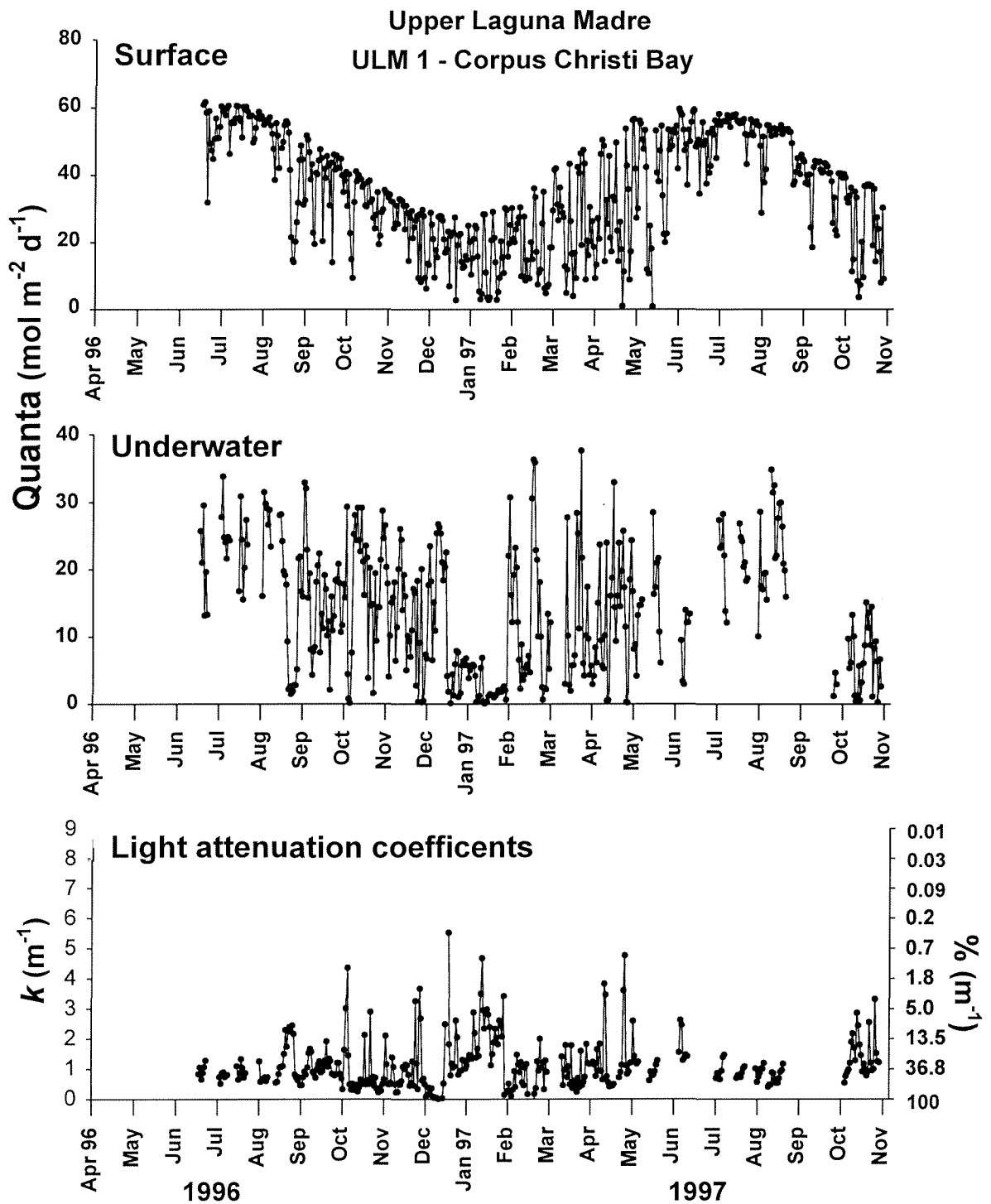


Figure 7. ULM 1. Daily integrated surface and underwater irradiance and light attenuation coefficients.

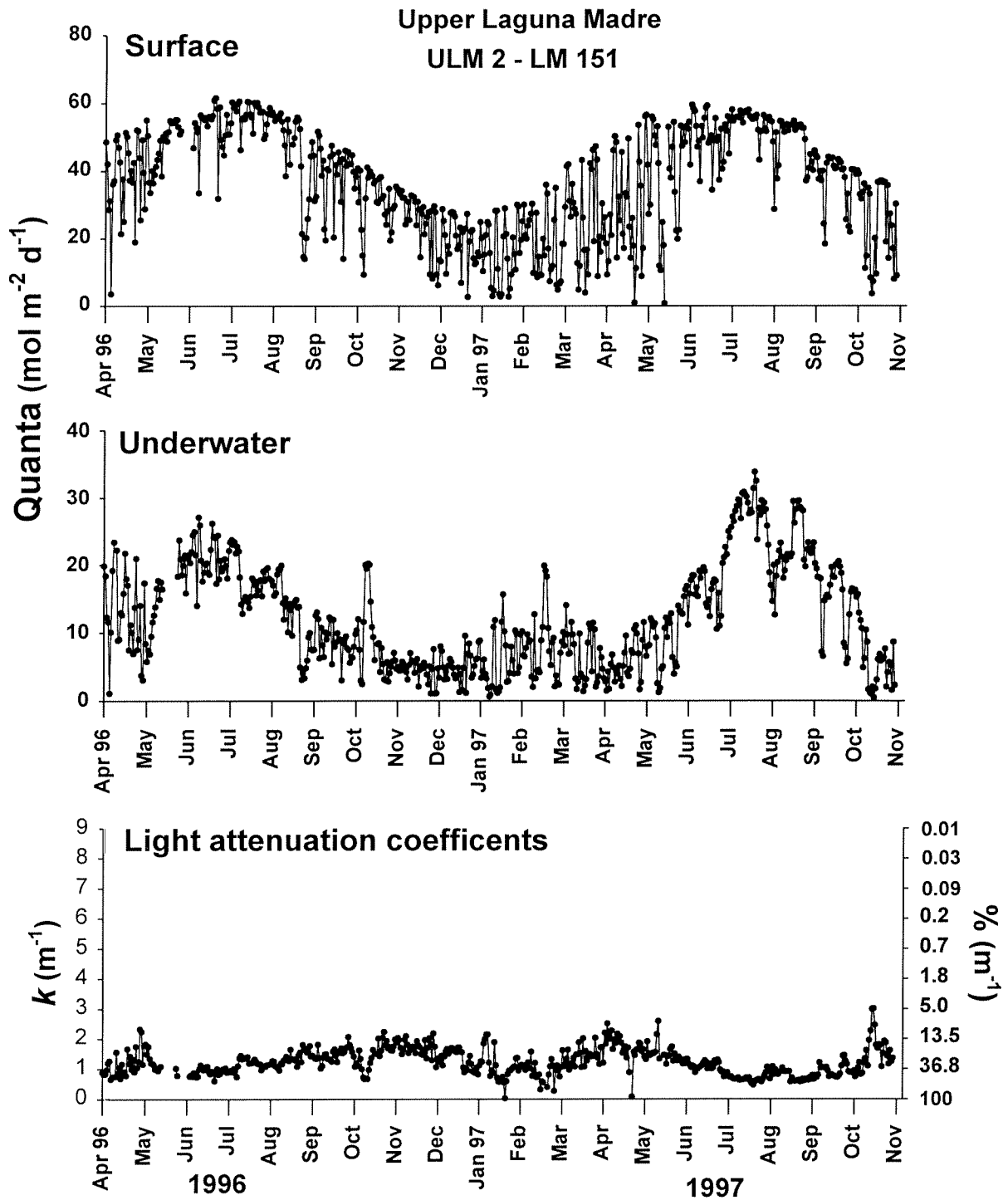


Figure 8. ULM 2. Daily integrated surface and underwater irradiance and light attenuation coefficients.

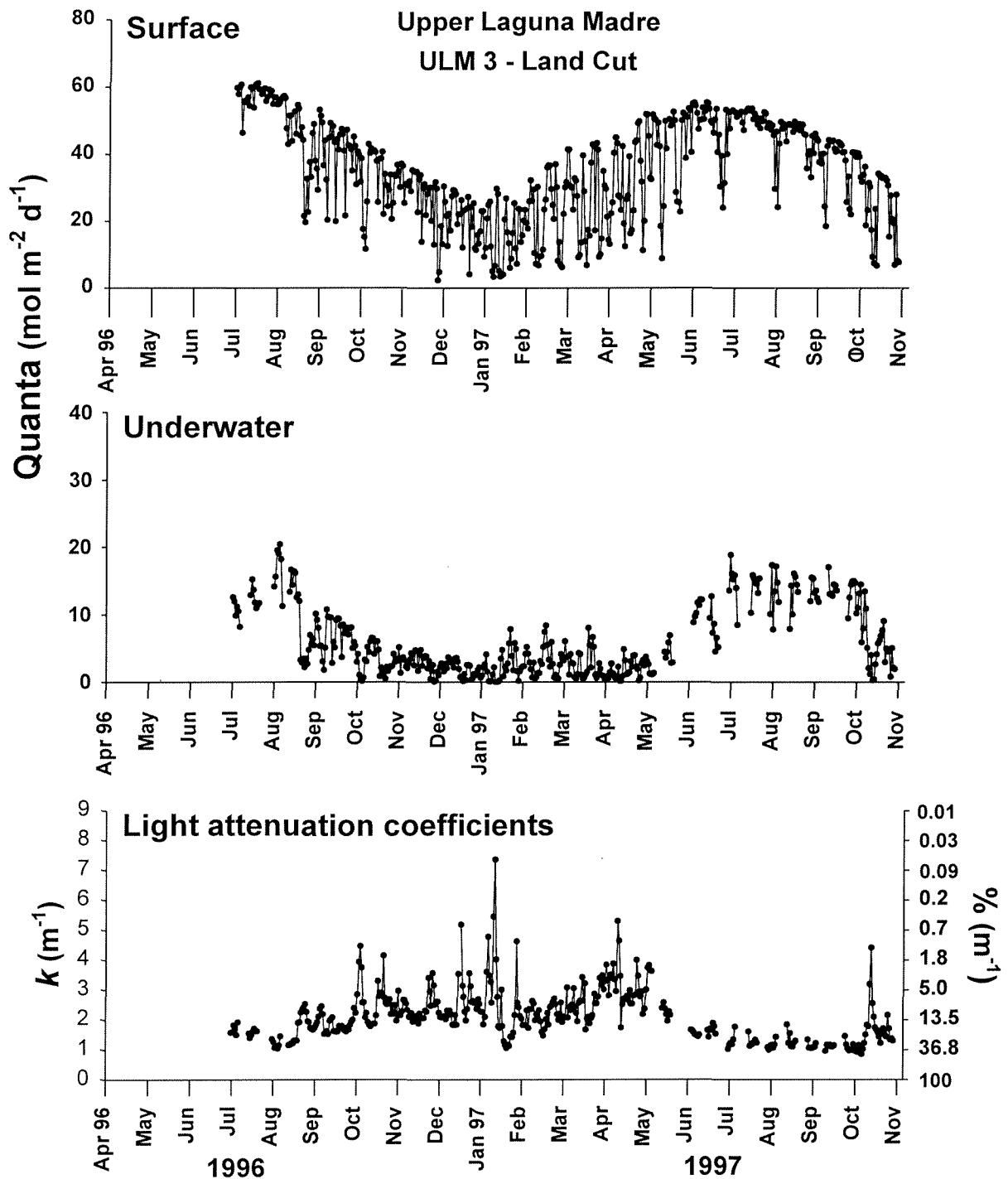


Figure 9. ULM 3. Daily integrated surface and underwater irradiance and light attenuation coefficients.

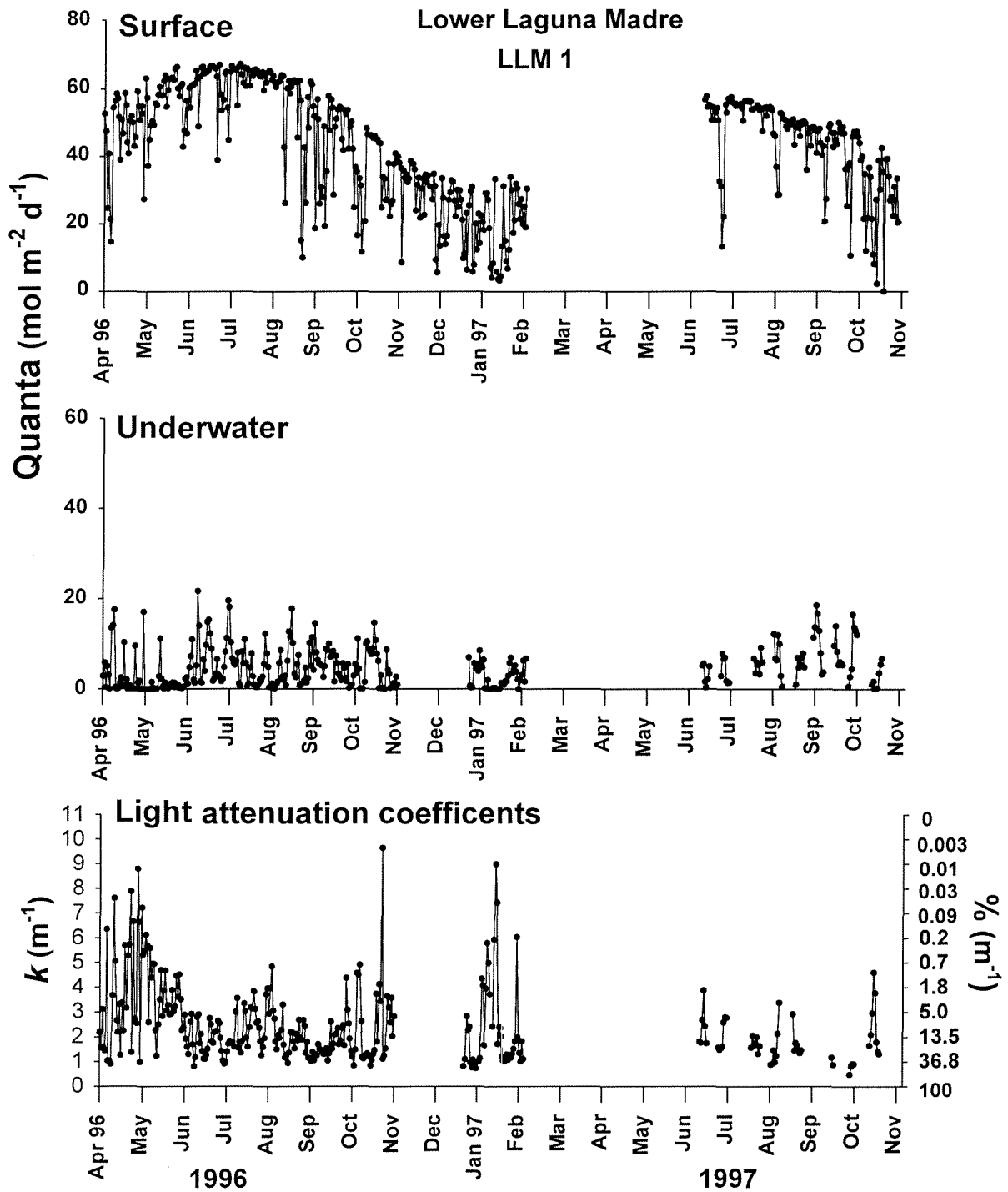


Figure 10. LLM 1. Daily integrated surface and underwater irradiance and light attenuation coefficients.

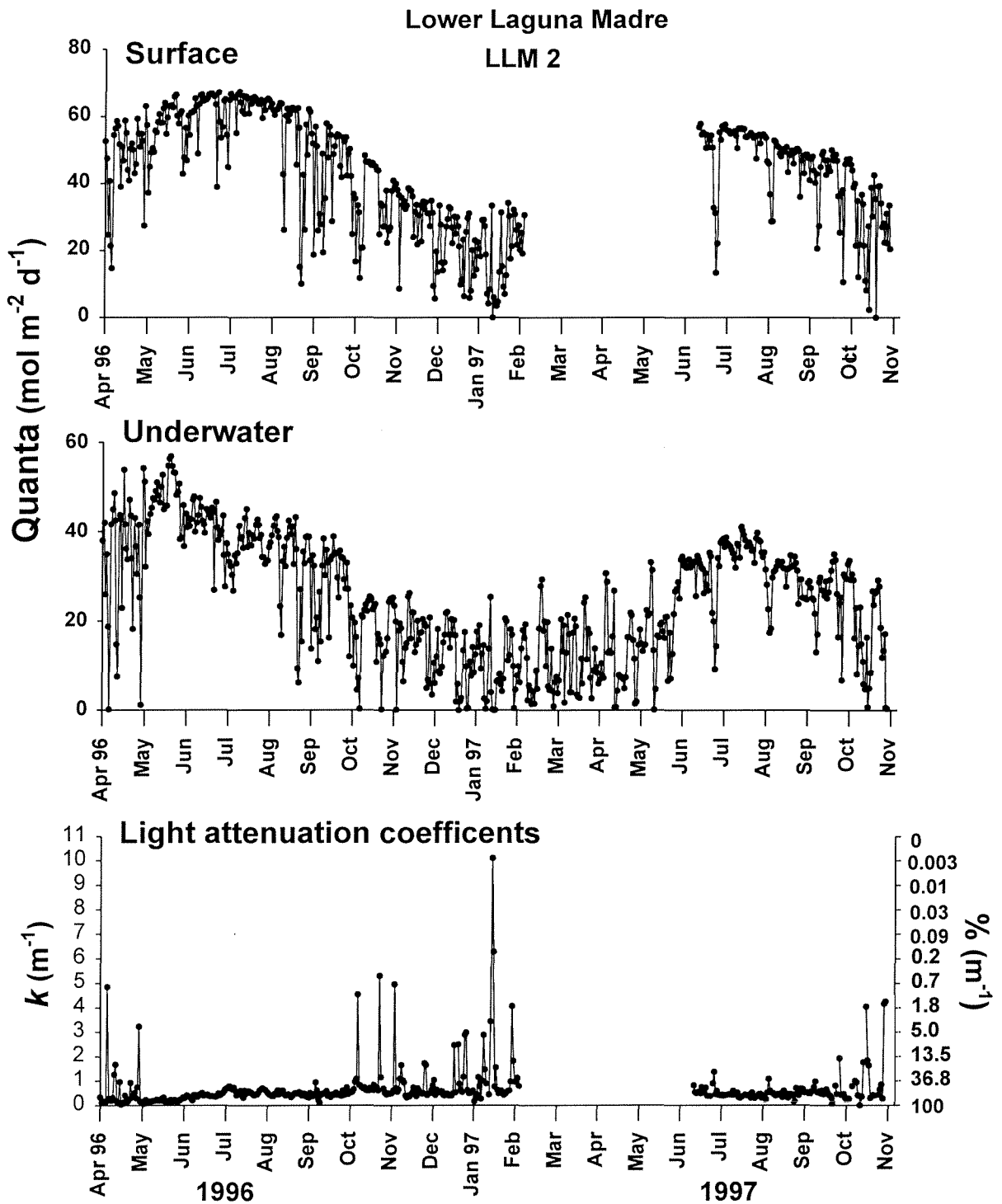


Figure 11. LLM 2. Daily integrated surface and underwater irradiance and light attenuation coefficients.

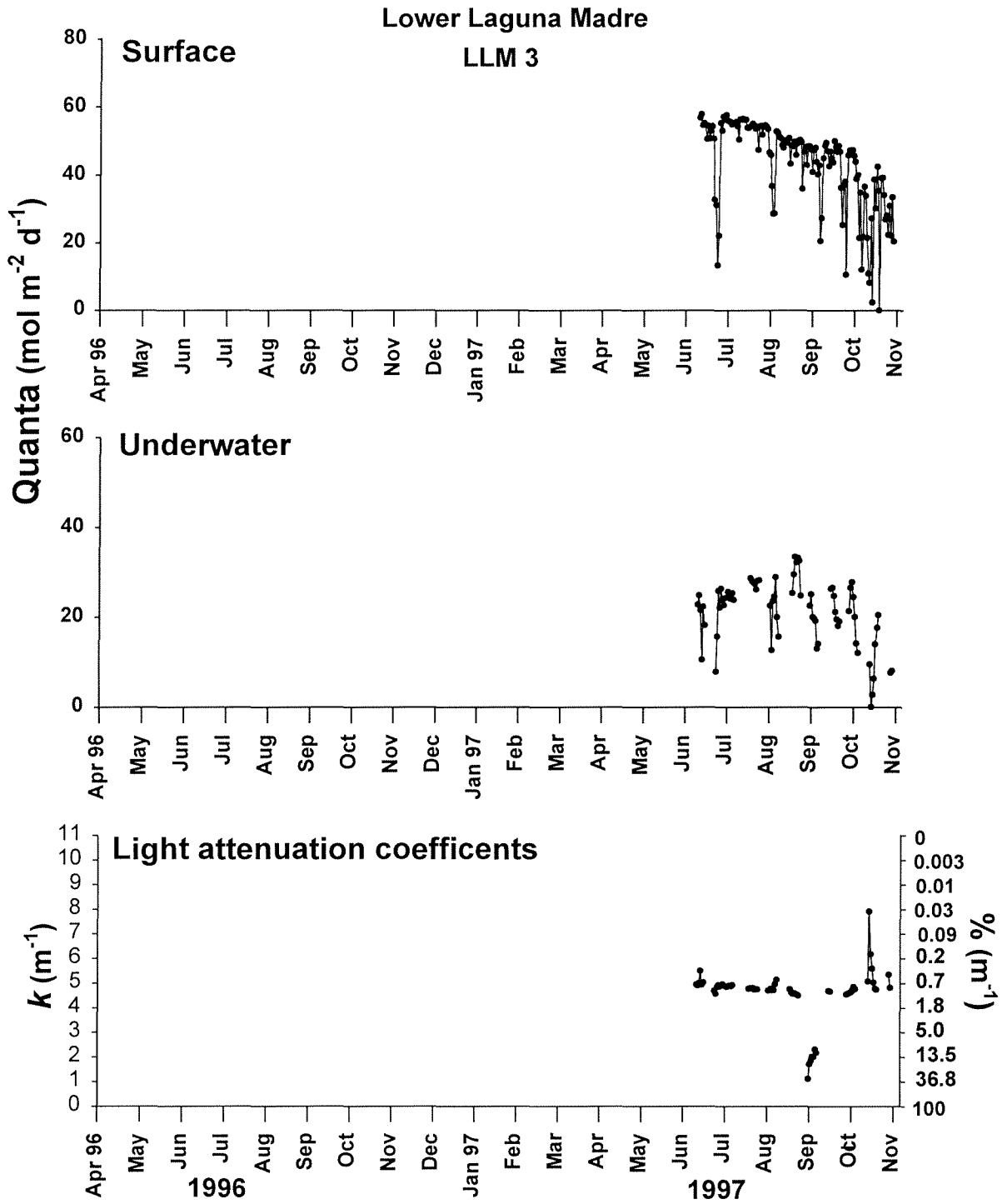


Figure 12. LLM 3. Daily integrated surface and underwater irradiance and light attenuation coefficients.

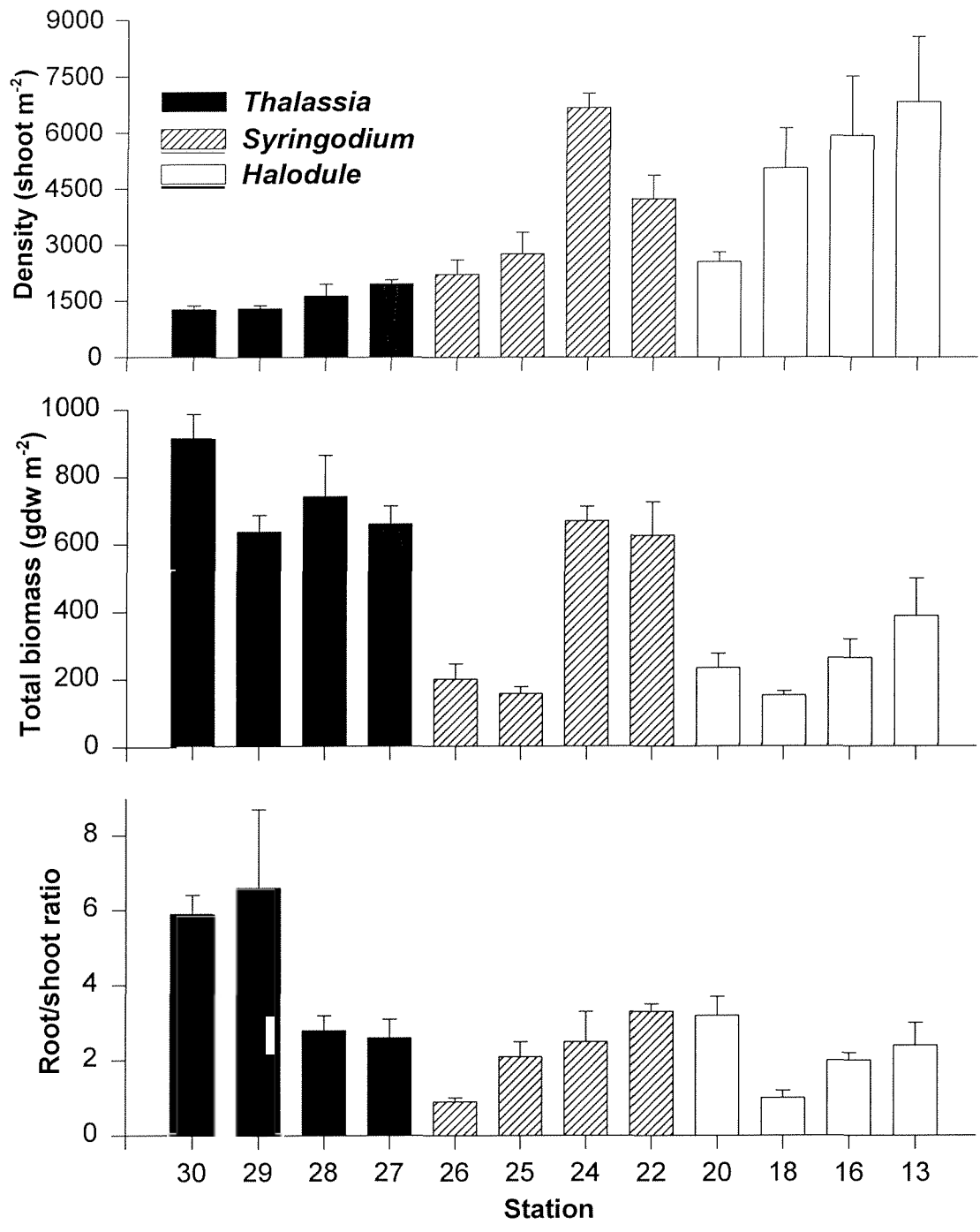


Figure 13. *Thalassia*, *Syringodium* and *Halodule*. Shoot density, total biomass and root/shoot ratio for seagrass species along the Laguna Madre transect. Values represent means \pm SE (n=4).

Table 3. Average surface irradiance (SI) and diffuse attenuation coefficients (k) characteristic of each of the permanent sampling stations based on total daily quanta received by surface and underwater sensors.

Site	Number of Days N	Mean SI (SE) %	Mean k (SE) m^{-1}
ULM 1	350	40 (1.14)	1.148 (0.04)
ULM 2	553	32 (0.55)	1.220 (0.02)
ULM 3	388	16 (0.50)	2.128 (0.04)
LLM 1	305	10 (0.54)	2.451 (0.09)
LLM 2	442	59 (0.92)	0.702 (0.04)
LLM 3	35	15 (1.86)	1.766 (0.15)

In contrast, *Thalassia* was found to exhibit the highest biomass, which ranged from 630 to 900 $gdw\ m^{-2}$. There was no evident correlation between total biomass and shoot density for this species. Biomass of *Syringodium* was highly variable with sampling site; values ranged from 150 $gdw\ m^{-2}$ at site 25 to 670 $gdw\ m^{-2}$ at site 24. *Halodule* exhibited the lowest total biomass, which ranged from 150 to 390 $gdw\ m^{-2}$. *Thalassia* also had higher root/shoot ratios (2.6-6.6), while those of *Syringodium* and *Halodule* were similar (0.9-3.3) (Fig. 13).

Temporal changes in density and biomass in *Halodule*, *Syringodium*, and *Thalassia* were measured at sites ULM 2, LLM 3, and LLM 2 respectively, between June 1996 and May 1997 (Table 4). All three species showed distinct seasonal changes in density and biomass. Ratios of below-ground to above-ground biomass were clearly highest in winter (3-8), and lowest in summer (2-6), which largely reflect the major seasonal changes in the abundance of photosynthetic shoot and leaf tissues. Consistent with the station survey results (above), *Thalassia* exhibited the highest biomass (over 900 $gdw\ m^{-2}$), but highest shoot density was characteristic of *Halodule* (over 8,000 m^{-2}), with *Syringodium* intermediate between the two species.

Blade chlorophyll

Total blade chl content of *Halodule* (7.92-11.42 $mg\ chl\ gdw^{-1}$) was higher than that of either *Syringodium* (2.26-7.33 $mg\ chl\ gdw^{-1}$) or *Thalassia* (3.62-6.35 $mg\ chl\ gdw^{-1}$). However, chl $a:b$

Table 4. Density and biomass changes in three seagrass species, *Thalassia testudinum* (LLM 2), *Syringodium filiforme* (LLM 3) and *Halodule wrightii* (ULM 2).

	Sampling Date			
	June 1996	September 1996	January 1997	May 1997
<i>Thalassia testudinum</i>				
Density (shfts m ⁻²)	1273.5 ± 96.7	2165.0 ± 58.3	1471.6 ± 189.1	1316.0 ± 155.7
Biomass (gdw m ⁻²)	909.6 ± 72.3	642.3 ± 41.5	819.3 ± 136.5	993.9 ± 97.9
Root/shoot ratio	5.9 ± 0.5	3.6 ± 0.3	7.5 ± 0.5	6.2 ± 0.9
<i>Syringodium filiforme</i>				
Density (shfts m ⁻²)	6664.7 ± 384.1	2858.3 ± 668.3	2731.0 ± 810.2	3905.4 ± 585.9
Biomass (gdw m ⁻²)	665.5 ± 43.4	246.3 ± 59.9	231.1 ± 51.5	314.5 ± 58.8
Root/shoot ratio	2.5 ± 0.8	1.5 ± 0.1	3.5 ± 0.4	3.6 ± 0.6
<i>Halodule wrightii</i>				
Density (shfts m ⁻²)	5919.1 ± 1587.0	8192.9 ± 660.2	6480.7 ± 1094.0	8235.3 ± 1124.8
Biomass (gdw m ⁻²)	265.5 ± 55.6	365.4 ± 13.4	346.9 ± 41.7	522.5 ± 75.7
Root/shoot ratio	2.0 ± 0.2	2.0 ± 0.2	8.1 ± 0.9	3.4 ± 0.8

ratios from *Thalassia* leaf tissues (3.0-3.6) were higher than those from *Syringodium* and *Halodule* (2.2-2.7) (Fig. 14). There were no clear patterns in chl content between stations for each species, except for *Syringodium*, in which total chl was higher at stations 25 and 26 than at stations 22 and 24.

Carbon and nitrogen content

Carbon content in *Thalassia* leaf tissues showed seasonal variation, with highest values (37%) in late summer compared to less than 34% in winter; rhizome tissue carbon content ranged from a high of 37% in summer to 35% during the remainder of the year (Fig. 15). Leaf tissues had higher nitrogen content (>1.7%) than rhizome tissues (<1%) throughout the study period, exhibiting lowest (1.7%) levels in summer and highest (2.7%) in late winter. Nitrogen content of

rhizome tissues showed little seasonal variation. Carbon:nitrogen (C:N) ratios ranged between 39 and 53 for rhizomes and 13 and 22 for leaves. The ratios for both tissues showed similar seasonal trends (Fig. 15).

Tissue nitrogen and carbon content exhibited distinct variations as a function of leaf age. Compared with young, newly formed tissue, both carbon and nitrogen content were lower and C:N ratio higher in older more senescent leaf parts (Table 5). Carbon content decreased from *ca.* 38% to 34%, and nitrogen, from 2.1% to 1.1%.

Discussion

Underwater light reduction has been linked to decreases in shoot density and biomass of seagrasses (Czerny and Dunton 1995, Lee and Dunton 1996). In estuarine systems, light penetration through the water column is regulated by concentrations of total suspended solids and chlorophyll. In the Laguna Madre, underwater light conditions may be predicted as a function of water column chlorophyll concentration, especially in ULM where the brown tide bloom persists. At several sites in ULM there was a strong correlation ($r^2 = 0.65$) between water column chl and k values, while there was a weak correlation ($r^2 = 0.14$) between TSS and k values (Dunton *et al.* 1994). In general, we found that light attenuation in the ULM was highest during periods when chl concentrations were high. In LLM, winter fluctuation in k values (up to 5 m^{-1}) were more site specific, in that increases in k were related to either a short brown tide event (i.e. winter increases in water column chl resulted from the movement of brown tide from ULM via winter storm fronts; e.g. stations LLM 2 and 3) or to the re-suspension of sediments

Table 5. Tissue carbon and nitrogen contents in different leaf parts of *Thalassia testudinum* collected from the lower Laguna Madre (LLM 2) in October 1997. Values are means \pm SE (n=3).

	Leaf part		
	Juvenile	Mature	Senescent
C (wt %)	37.83 \pm 2.09	37.81 \pm 2.16	33.76 \pm 2.49
N (wt %)	2.16 \pm 0.11	2.10 \pm 0.08	1.12 \pm 0.13
C/N ratio	20.41 \pm 0.19	20.98 \pm 0.51	35.48 \pm 2.07

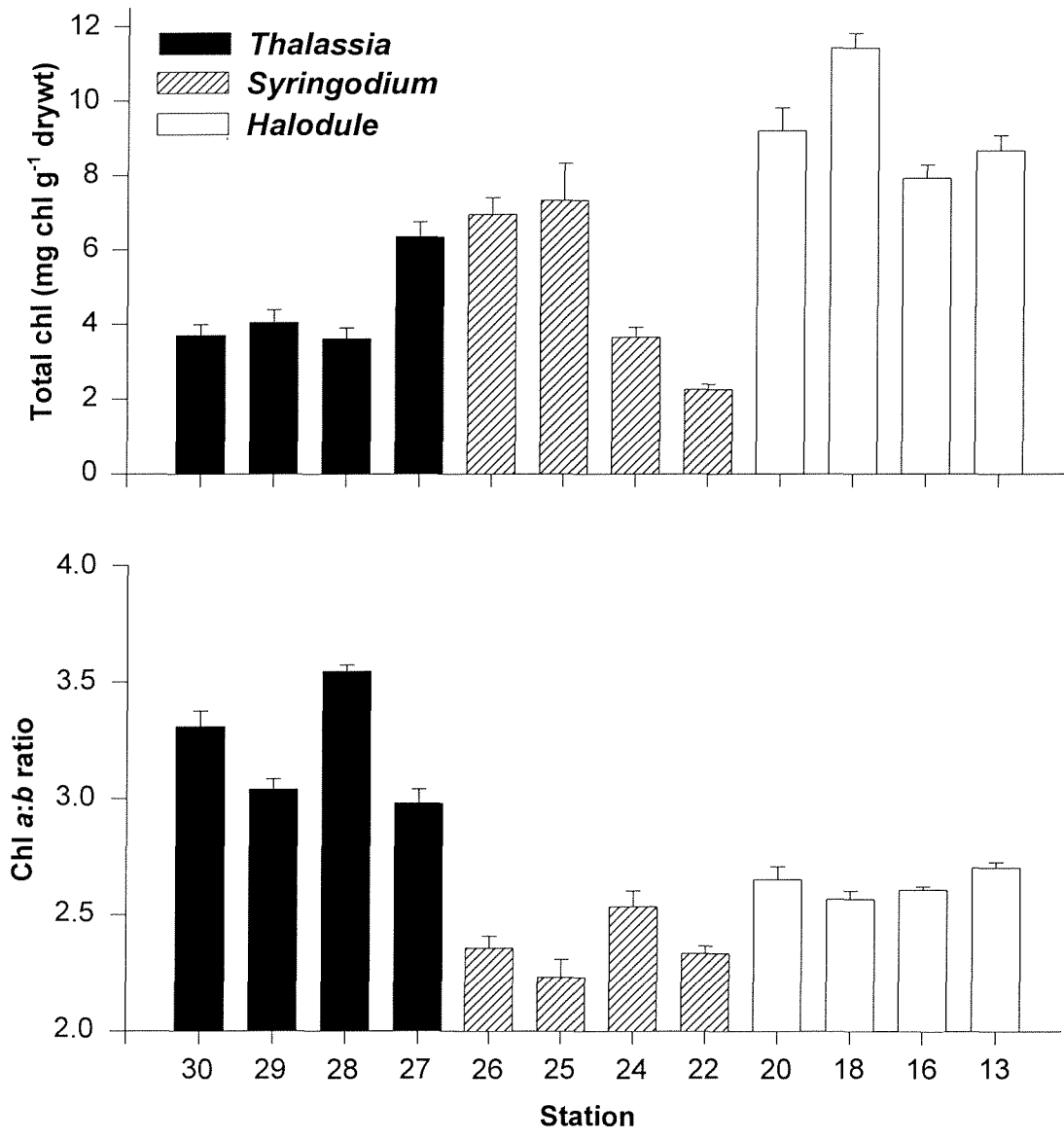


Figure 14. *Thalassia*, *Syringodium* and *Halodule*. Total chlorophyll and chl *a:b* ratios in seagrass leaf tissues. Values represent means \pm SE (n=6).

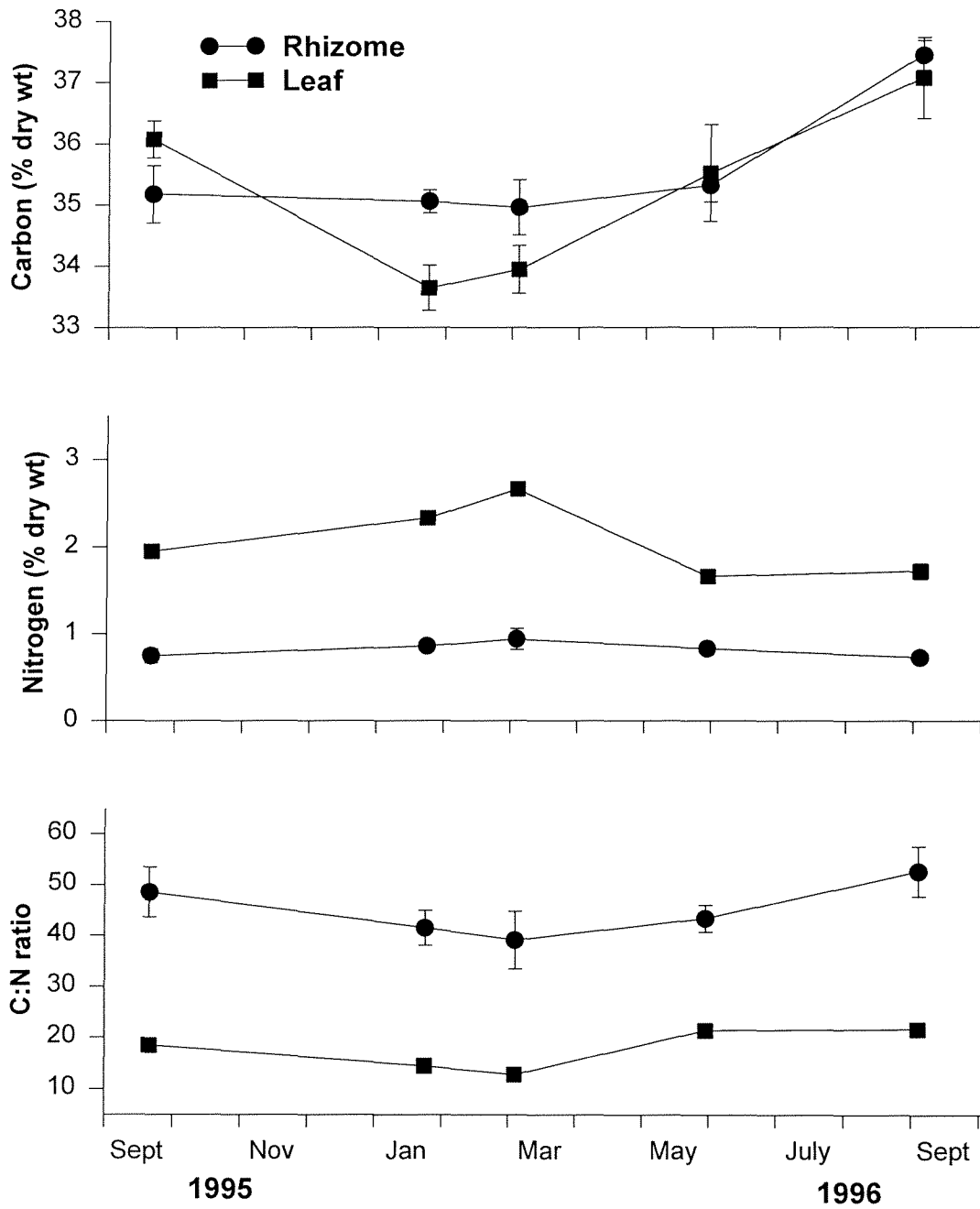


Figure 15. *Thalassia*. Seasonal changes in carbon and nitrogen contents of leaf and rhizome tissues. Values represent means \pm SE (n=4). Where no error bars appear, SE is less than the size of the symbol.

(LLM 1). Seagrass density and biomass did not exhibit pronounced negative correlations relative to water column chlorophyll. We suggest that the short-term winter appearance of brown tide in LLM does not impact seagrasses, since photosynthesis and respiration are already reduced by low water temperatures.

A pronounced spatial variation in water column chlorophyll concentration was directly correlated with the distribution of brown tide algae along the Laguna Madre transect. Although chl values exhibit seasonal variation, the lowest values from ULM were nearly two-fold higher than those from LLM. In general, ULM has much higher chl concentrations (almost 80 mg L⁻¹) and much lower underwater irradiance levels. The loss of seagrass stands from deeper portions of the ULM (Onuf 1996) have been directly attributed to a 50% reduction in underwater light caused by the brown tide (Dunton 1994).

Seagrass biomass and density patterns were similar to previously published reports (Dunton 1994, Czerny and Dunton 1995, Lee and Dunton 1996). Species-specific differences in biomass were expected, since these plants exhibit marked morphological differences. *Thalassia* has large, flat blades and a prominent rhizome system, while *Halodule* has very fine blades and rhizomes. *Syringodium* has round leaves and is intermediate in size by comparison. Large root:shoot ratios may be explained by the fact that approximately 80% of seagrass biomass is typically below ground. Patterns for carbon, nitrogen and C:N ratios were similar to those reported by Lee and Dunton (1996).

Some seagrass genera (e.g., *Zostera* and *Thalassia*) exhibit the ability to photoacclimate in response to changes in light availability by adjusting pigment content and stoichiometry (Wiginton and McMillan 1979, Dennison and Alberte 1982, 1985, Abal et al. 1994, Lee and Dunton 1996). However, the purpose of this research was to collect background information on the pigment levels of three grass species from a variety of locations. Previous work has demonstrated that *Halodule*, unlike *Thalassia*, does not exhibit a “classic” photoacclimation response (Dunton 1994, Lee and Dunton 1996) as previously reported for higher plants

(reviewed by Boardman 1977, Björkman 1981). Therefore, as indicated by the data, no distinct variations in *Halodule* pigment content were noted. *Halodule* was observed to be the dominant species and exhibited the highest total chlorophyll content. *Halodule wrightii* can be classified as an “opportunistic” species (Czerny and Dunton 1995), and the maintenance of high chlorophyll levels may contribute, in part, to this plant’s ability to tolerate environmental disturbance (i.e. reductions in light quality/availability).

High salinity values obtained in ULM were probably related to a very limited water exchange between this area and the Gulf of Mexico. Although both ULM and LLM are hypersaline, the water exchange in LLM is higher due to the proximity of the Mansfield and Brazos-Santiago Passes. Overall, nutrient levels were low. Water column ammonium exhibited two peaks, one near the mouth of Baffin Bay and again near the mouth of the Arroyo Colorado. These peak ammonium values may have resulted from agricultural run-off and/or municipal effluent into the Laguna Madre system.

Water column chlorophyll concentrations were estimated by traditional spectrophotometric (this chapter) and high performance liquid chromatography (HPLC) methods (Chapter IV). Comparison between these two techniques yielded an excellent correlation (0.832), but despite the positive correlation, chl values determined by the spectrophotometric technique consistently underestimated chl content on the same water sample (Fig. 16). Additionally, HPLC appears to be more sensitive for detecting very low levels of chlorophyll, while at high pigment concentrations (i.e., similar to those noted in ULM) traditional methods may be more sensitive.

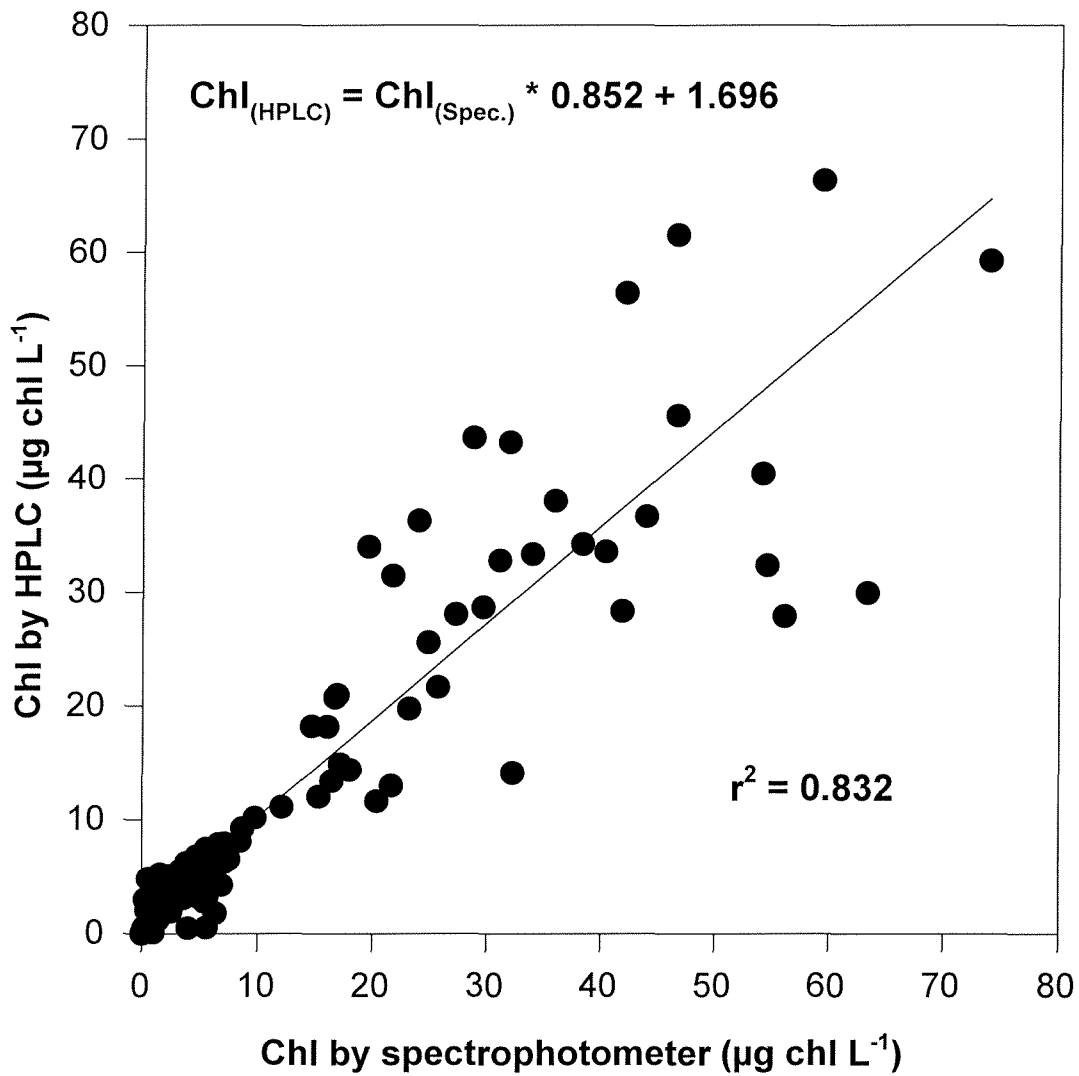


Figure 16. Correlation between water column chlorophyll estimates derived from traditional spectrophotometric and high performance liquid chromatography (HPLC) methods.

References

- Abal EG, Loneragan N, Bowen P, Perry CJ, Udy JW, Dennison WC (1994) Physiological and morphological responses of the seagrass *Zostera capricorni* Aschers to light intensity. J Exp Mar Biol Ecol 178:113-129
- Björkman O (1981) Responses to different quantum flux densities. In: Lange L, Nobel PS, Osmond CB, Ziegler H (eds) Physiological Plant Ecology I: Encyclopedia of Plant Physiology New Series. Vol 12A Springer-Verlag, Berlin, p 57-107
- Boardman NK (1977) Comparative photosynthesis of sun and shade plants. Ann Rev Plant Phys 28:355-377
- Czerny AB, Dunton KH (1995) The effects of *in situ* light reduction on the growth of two species of subtropical seagrasses, *Thalassia testudinum* and *Halodule wrightii*. Estuaries 18:418-427
- Dennison WC, Alberte RS (1982) Photosynthetic responses of *Zostera marina* L. (eelgrass) to *in situ* manipulations of light intensity. Oecologia (Berl) 55:137-144
- Dennison WC, Alberte RS (1985) Role of daily light period in the depth distribution of *Zostera marina* (eelgrass). Mar Ecol Prog Ser 25:51-61
- Dennison WC, Orth RJ, Moore KA, Stevenson JC, Carter V, Kollar S, Bergstrom PW, Batiuk RA (1993) Assessing water quality with submersed aquatic vegetation. Bio Sci 43:86-94
- Drew EA (1979) Physiological aspects of primary production in seagrasses. Aquat Bot 7:139-150

- Dunton KH (1994) Seasonal growth and biomass of the subtropical seagrass *Halodule wrightii* in relation to continuous measurements of underwater irradiance. *Mar Biol* 120:479-489
- Dunton KH (1996) Photosynthetic production and biomass of the subtropical seagrass *Halodule wrightii* along an estuarine gradient. *Estuaries* 19:436-447
- Dunton KH, Kaldy JE, Lee K-S (1994) Attenuation of light in two subtropical estuaries in Texas. Environmental Protection Agency Report - Region 6
- Dunton KH, Tomasko DA (1994) *In situ* photosynthesis in the seagrass *Halodule wrightii* in a hypersaline subtropical lagoon. *Mar Ecol Prog Ser* 107:281-293
- Fourqurean JW, Zieman JC (1991) Photosynthesis, respiration and whole plant carbon budget of the seagrass *Thalassia testudinum*. *Mar Ecol Prog Ser* 69:161-170
- Jeffrey SW, Humphrey GF (1975) New spectrophotometric equations for determining chlorophylls *a*, *b*, *c*₁ and *c*₂ in higher plants, algae and natural phytoplankton. *Biochem Physiol (Phlantz)* 167:191-194
- Lee K-S, Dunton KH (1996) Effects of *in situ* light reduction on the maintenance, growth and partitioning of carbon resources in *Thalassia testudinum*. *J Exp Mar Biol Ecol* 210:53-73
- Libes M (1986) Productivity-irradiance relationship of *Posidonia oceanica* and its epiphytes. *Aquat Bot* 26:285-306
- Marsh JA, Dennison WC, Alberte RS (1986) Effects of temperature on photosynthesis and respiration in eelgrass (*Zostera marina* L.) *J Exp Mar Biol Ecol* 101:257-267

- Onuf CP (1994) Seagrasses, dredging, and light in Laguna Madre, Texas, USA. *Estuar Cstl Shelf Sci* 39:75-91
- Onuf CP (1996) Seagrass responses to long-term light reduction by brown tide in upper Laguna Madre, Texas: distribution and biomass patterns. *Mar Ecol Prog Ser* 138:219-231
- Parsons TR, Maita Y, Lalli CM (1984) A manual of chemical and biological methods for seawater analysis. Pergamon Press, N.Y.
- Pérez M, Romero J (1992) Photosynthetic response to light and temperature of the seagrass *Cymodocea nodosa* and the prediction of its seasonality. *Aquat Bot* 43:51-62
- Pulich WM, White WA (1991) Decline of submerged vegetation in the Galveston Bay system: chronology and relationship to physical processes. *J Cstl Res* 7:1125-1138
- Quammen ML, Onuf CP (1993) Laguna Madre: seagrass changes continue decades after salinity reduction. *Estuaries* 16:302-310
- Strickland JDH, Parsons TR (1972) A practical handbook of seawater analysis. *Bull Fish Res Bd Can* 176:1-310
- Wiginton JR, McMillan C (1979) Chlorophyll composition under controlled light conditions as related to the distribution of seagrass in Texas and US Virgin Islands. *Aquat Bot* 6:171-184
- Zieman JC, Wetzel RG (1980) Productivity in seagrass: methods and rates. In Phillips RC, McRoy CP (eds) *Handbook of Seagrass Biology*. Garland STPM Press, New York, p 87-116

CHAPTER VII: SEDIMENT GEOCHEMISTRY

Contents

Abstract.....	4
Part 1: Sediment Geochemistry at Survey Sites	5
Sampling, Analyses and Data.....	5
Results.....	19
Solid Components.....	19
Pore Water Components.....	23
Relationships Between Solid and Dissolved Components.....	27
Discussion.....	30
Part 2: Sediment Geochemistry at “Super” Sites	33
Sampling and Data	33
Results.....	33
Part 3: Sediment Geochemistry at Time Series Stations	37
Sampling and Data	37
Results.....	37
Part 4: Model Verification Studies of Sediment Chemistry.....	47
Sources of Dissolved Inorganic Carbon.....	47
Impacts of Dredge Deposits on Pore Water Chemistry	48
References Cited.....	51

Tables

Table 1. Survey site solids	6
Table 2. Survey site pore waters	9
Table 3. Individual analyses	11
Table 4. Summary of samples whose data falls outside “normal” ranges	32
Table 5. “Super” site solid analytical results	34

Table 6. Concentration of pore water components at “super” sites.....	35
Table 7. Time series data.....	39
Table 8. analytical results for DIC sources study.....	48
Table 9. Calculated results for DIC source study.....	49
Table 10. Pre-dredge sediment sampling results	50
Table 11. Pre-dredge sediment sampling results	50

Figures

Figure 1. Relative abundance of samples containing different percentages of the <63 μm grain size fraction	20
Figure 2. Plot of the <63 μm grain size fraction in adjacent bare versus vegetated areas	20
Figure 3. Solid parameters relationship to grain size.....	21
Figure 4. Relationship between total reduced sulfur (TRS) and sediment grain size.....	22
Figure 5. Acid volatile sulfides (AVS) versus total reduced inorganic sulfur (TRS).....	22
Figure 6. Relationship between organic-C and TRS	24
Figure 7. The relationship between pore water ammonium concentrations in sediments covered by seagrass and in bare areas	24
Figure 8. The relationship between pore water hydrogen sulfide concentrations in sediments covered by seagrass and in bare areas	25
Figure 9. The relationship between pore water ammonium and hydrogen sulfide concentrations in sediments covered by seagrass and in bare areas	25

Figure 10. Dissolved phosphate versus dissolved ammonium	26
Figure 11. Expanded plot of dissolved phosphate versus dissolved ammonium.....	26
Figure 12. Dissolved organic carbon (DOC) concentrations in bare versus seagrass covered sediments.....	28
Figure 13. H ₂ S and NH ₄ concentrations versus DOC for seagrass and bare areas.....	28
Figure 14. Plots of H ₂ S and DOC versus organic-C.....	29
Figure 15. The relationship between dissolved hydrogen sulfide and total reduced inorganic sulfur	31
Figure 16. Depth profiles of dissolved ammonium (A) and hydrogen sulfide (B).....	36
Figure 17. LLM1 profiles	42
Figure 18. LLM2 profiles	43
Figure 19. LLM3 profiles	44
Figure 20. ULM2 profiles.....	45
Figure 21. ULM3 profiles.....	46

Abstract

The major objective of the study of Laguna Madre sediment geochemistry was to establish the general relationships among major physical and chemical components of the sediments and seagrasses as a guide to producing the "below ground" part of the seagrass productivity model. The sediment-related field efforts consisted of a major sampling cruise on the RV Longhorn in June, 1996, and a focused small boat sampling of Blucher platform and potential platform sites in September, January, and May. On the Longhorn cruise, 24 "survey" sites were studied over the length of Laguna Madre for both seagrass biology and sediment geochemistry to establish general relationships and 4 "super sites" were carefully studied using detailed depth profiles of geochemical parameters to provide guidance in constructing diagenetic models. The time series measurements at 5 sites were done in a manner similar to the "super sites" to document temporal changes and further augment the data base for model construction and testing.

Results demonstrate that most sediments in Laguna Madre are sandy with a relatively narrow range in their physical and geochemical characteristics. However, there are local major exceptions to these general relationships and in some cases both vertical and lateral heterogeneity is extreme even on a very small (cm in depth, m laterally) scale. There was generally little difference between vegetated and bare areas, except that high dissolved sulfide values were restricted to bare areas. The diagenetic pattern in these sediments is usually quite different from that in most estuarine siliciclastic muds in that virtually all diagenetic activity takes place in the upper few cm of sediment. In grass beds, this is associated with the root zone. This diagenetic pattern has demanded substantial modification of pre-existing models.

Part 1: Sediment Geochemistry at Survey Sites

Sampling, Analyses and Data

The sampling sites in Upper and Lower Laguna Madre were previously described and given in map A1. The general aim was to obtain triplicate samples at 3 depths (0-2, 6-8, 18-20 cm) from each site, except for glove bag-squeezer samples for oxygen-sensitive compounds that, because of logistic and time constraints were only sampled at 1 depth (8-10 cm). Weather and coring difficulties in hard bottom and sandy sediments, along with the very low porosity of some sediments prevented us from always obtaining our ideal goals. Sediment samples were collected by hand using plastic core liner (7 cm i.d.) and capped underwater. Cores to be used for shore-laboratory analyses of solids and some pore water components were immediately frozen on dry ice and kept frozen until time of analyses. Cores from which pore water was extracted were either sectioned and water extracted by centrifugation for non-O₂ sensitive components or placed in a glove bag under a high purity N₂ atmosphere where they were sectioned and then the sediment was loaded into Reeburgh (1967)-type sediment squeezers. The pore water from the squeezers was passed through a 0.45 μm Nuclepore filter and then into a syringe where it was stored in the dark and refrigerated until the time of its analysis.

H₂S was measured using the Cline (1969) spectrophotometric method. Chloride was measured by titration with silver nitrate and sulfate by ion chromatography. Dissolved organic carbon (DOC) was determined on an OIC carbon analyzer and dissolved inorganic carbon (DIC) was determined coulometrically. Nutrients, and dissolved iron and manganese were determined spectrophotometrically. pH was determined on the Hansson (1973) pH scale for seawater by injecting a subsample of the pore water into a flow-through combination pH electrode for January and May time series sites only. Solid sediment samples were analyzed for porosity by drying for 24 h at 110°C, grain size weight fraction less than 63 μm (the size dividing sand from silt + Clay fractions) by wet sieving, and weight percent organic-C and inorganic-C using a LECO carbon analyzer (macroscopic organic material was removed prior to analysis). Acid volatile sulfides (AVS) were determined by the HCl + SnCl₂ method of Cornwell and Morse (1987), and total reduced sulfur (TRS) was measured using the boiling Cr(II) + acid method of Canfield *et al.* (1986). "Reactive" iron and manganese were extracted by both the boiling HCl and citrate dithionite methods. Analytic results are reported as averages where replicate samples were obtained for solid phase components in Table 1 and pore water components in Table 2. Individual analyses are given in Table 3.

Table 1. Survey site solids.

COE#	Station	Depth	wt. %				μmol/gdw					
			φ	<63 μm	Org-C	CaCO ₃	TRS	AVS	CD-Fe	HCl-Fe	CD-Mn	HCl-Mn
1	30 grass	0 to 2	0.65	30	1.41	17	8.35	4.36	3.73	37.2	ND	1.56
		6 to 8	0.58	38	0.96	15	2.49	2.07	2.14	47.1	ND	1.60
		18 to 20	0.49	37	0.52	10	1.70	2.09	0.49	46.3	ND	1.50
2	30 bare	0 to 2	0.55	13	0.52	21	4.23	2.27	1.96	25.7	ND	0.87
		6 to 8	0.56	24	0.69	12	2.43	1.88	1.48	33.9	ND	1.29
		18 to 20	0.47	37	0.47	9	1.36	1.11	0.76	50.9	ND	1.58
3	29 grass	0 to 2	0.47	22	0.21	18	2.44	1.68	1.40	32.1	ND	1.15
		6 to 8	0.53	38	0.36	14	2.17	1.79	0.70	62.2	ND	2.10
		18 to 20	0.47	40	0.35	13	1.19	1.04	0.55	50.3	ND	2.23
4	29 bare	0 to 2	0.44	8	0.17	24	2.41	2.94	1.78	16.6	ND	0.71
		6 to 8	0.50	41	0.45	12	3.02	1.43	4.56	71.7	ND	2.70
		18 to 20	0.46	36	0.40	10	3.09	1.25	2.20	62.4	ND	2.67
5	28 grass	0 to 2	0.44	6	1.30	ND	3.03	1.52	1.51	19.2	ND	0.61
		6 to 8	0.47	18	0.33	12	1.92	1.13	1.72	33.9	ND	1.19
		18 to 20	0.48	42	0.43	8	1.77	1.52	0.00	40.2	ND	1.76
6	28 bare	6 to 8	0.41	13	0.22	10	3.22	1.86	0.83	21.7	ND	0.83
7	27 grass	6 to 8	0.48	22	0.43	20	2.66	1.71	0.42	27.8	ND	1.54
		18 to 20	0.53	34	0.51	15	1.33	0.89	0.50	45.8	ND	2.53
8	27 bare	0 to 2	0.46	8	0.24	14	2.89	1.70	1.24	20.2	ND	0.93
		6 to 8	0.52	29	0.56	19	1.13	0.97	ND	42.9	ND	1.91
		18 to 20	0.49	35	0.37	15	1.86	1.52	ND	51.5	ND	2.41
9	26 grass	0 to 2	0.49	19	0.33	26	2.09	1.54	1.42	53.8	ND	2.07
		6 to 8	0.55	83	0.40	19	3.14	2.70	0.87	108.5	ND	3.50
		16 to 18	0.55	86	0.42	20	1.96	1.54	0.91	129.0	ND	3.86
10	26 bare	0 to 2	0.58	53	0.51	20	2.60	1.83	1.55	60.7	ND	2.15
		6 to 8	0.56	81	0.39	19	1.79	1.57	0.94	113.8	ND	3.04
		17 to 19	0.53	96	0.27	21	4.79	1.64	0.37	171.7	ND	4.43

11	25 grass	0 to 2	0.60	60	0.47	16	5.91	3.24	2.52	75.3	ND	2.89
		6 to 8	0.54	69	0.43	18	3.32	2.64	2.52	64.9	ND	3.10
		18 to 20	0.51	77	0.37	22	2.35	1.59	2.27	101.9	ND	3.36
12	25 bare	0 to 2	0.61	53	0.43	20	5.79	2.79	1.91	67.7	ND	2.55
		6 to 8	0.54	65	0.46	18	1.97	1.71	3.36	77.2	ND	3.06
		18 to 20	0.54	93	0.25	21	2.22	1.17	0.68	130.5	ND	3.34
13	24 grass	0 to 2	0.60	19	0.57	27	3.56	1.88	2.00	23.3	ND	1.23
		6 to 8	0.51	29	0.55	17	4.96	2.85	2.58	37.8	ND	2.08
		18 to 20	0.47	14	0.24	7	1.92	1.09	0.69	19.6	ND	0.70
14	24 bare	0 to 2	0.60	27	0.66	14	5.43	2.90	3.91	30.4	ND	1.41
		6 to 8	0.58	37	0.54	16	6.25	3.43	2.69	33.3	ND	1.74
		18 to 20	0.48	12	0.29	12	3.79	1.95	0.62	21.2	ND	0.99
15	22 grass (no 23)	0 to 2	0.89	84	5.41	38	9.25	4.23	10.26	74.7	ND	2.98
		6 to 8	0.77	42	2.05	15	19.32	9.62	2.95	38.0	ND	1.39
		18 to 20	0.58	15	0.46	11	4.24	1.57	0.56	19.5	ND	0.55
16	22 bare	0 to 2	0.71	22	1.27	14	5.12	2.12	1.99	23.6	ND	0.94
		6 to 8	0.71	29	1.42	12	5.05	2.53	1.84	26.3	ND	0.89
		18 to 20	0.55	19	0.50	11	3.30	1.91	1.91	27.5	ND	0.66
17	20 grass	0 to 2	0.61	14	0.83	30	6.67	3.14	2.10	24.5	ND	1.27
		6 to 8	0.49	17	0.32	34	2.92	1.16	1.32	18.6	ND	2.42
		16 to 18	0.57	26	0.34	52	4.40	2.35	1.51	29.6	ND	2.92
18	20 bare	0 to 2	0.69	31	0.78	14	2.68	1.76	2.75	31.3	ND	1.47
		6 to 8	0.72	55	0.83	12	6.05	3.43	3.54	36.8	ND	2.04
		16 to 18	0.82	81	1.28	14	6.29	4.15	5.76	82.1	ND	6.22
19	18 grass	0 to 2	0.49	5	0.23	3	5.68	2.66	1.58	11.2	ND	0.35
		6 to 8	0.47	11	0.30	2	3.56	1.41	0.62	8.9	ND	0.14
		18 to 20	0.43	6	0.16	2	3.99	1.71	0.00	6.8	ND	0.26
20	18 bare	0 to 2	0.51	8	0.29	4	4.33	2.17	0.82	10.0	ND	0.34
		6 to 8	0.49	13	0.29	4	4.77	2.43	1.13	15.8	ND	0.59
		18 to 20	0.43	3	0.10	4	3.12	0.90	ND	3.1	ND	0.16

21	16 grass	0 to 2	0.62	17	0.92	21	6.29	2.80	1.71	17.2	ND	0.58
		6 to 8	0.53	23	0.44	20	4.67	2.41	1.64	23.7	ND	1.03
		18 to 20	0.53	20	0.63	45	7.10	3.24	1.67	23.8	ND	0.94
22	16 bare	0 to 2	0.72	25	1.56	12	6.40	3.05	1.97	21.3	ND	0.43
		6 to 8	0.57	10	0.50	10	5.84	2.35	0.44	7.8	ND	0.32
		18 to 20	0.54	19	0.54	18	3.30	2.41	1.37	17.5	ND	2.19
23	13 grass	0 to 2	0.66	12	1.13	29	7.65	3.60	1.65	10.7	ND	0.81
		6 to 8	0.52	4	0.50	26	3.48	1.11	0.40	4.6	ND	0.32
24	13 bare	0 to 2	0.56	17	0.60	29	5.42	2.42	0.61	9.8	ND	0.63
		6 to 8	0.53	18	0.43	51	3.69	1.85	0.79	15.3	ND	1.15

Table 2. Survey site pore waters.

COE#	Station	Depth	μM			mM				μM			
			NH4	NO3	Urea	PO4	SiO2	SO4	Cl	DOC	H2S	Fe	Mn
1	30 grass	0 to 2	71	0	22	5	73	28.3	550	3.72			
		6 to 8	88	0	36	5	68	26.0	529	2.17	192	2.6	2.7
		18 to 20	34	3	34	5	67	24.6	496	2.47			
2	30 bare	0 to 2	58	1	23	2	66	26.3	513	1.84			
		6 to 8	97	4	25	6	57	26.9	532	1.72	36	2.1	6.8
		18 to 20	129	5	49	5	48	23.3	466	0.87			
3	29 grass	0 to 2	44	4	40	3	19	26.5	519	2.47			
		6 to 8	50	0	43	3	33	26.7	534	3.95	58	3.5	10.5
		18 to 20	43	0	42	2	27	25.7	511				
4	29 bare	0 to 2	61	0	41	2	40	28.2	547	0.84			
		6 to 8	98	0	25	2	66	26.7	526	1.25	29	1.9	4.9
		18 to 20	88		22	2	87	27.9	543				
5	28 grass	0 to 2	70	3	36	5	12						
		6 to 8	42	2	58	6	14	28.7	551	1.49	20	1.6	1.7
		18 to 20	32	0	45	9	46						
6	28 bare	0 to 2											
		6 to 8	151	2	46	7	53				41	0.4	1.1
		18 to 20											
7	27 grass	0 to 2											
		6 to 8	70	3	33	2	72	28.0	536	2.15	21	1.4	3.1
		18 to 20	33	3	39	3	187	26.0	508	1.56			
8	27 bare	0 to 2	281	2	42	12	3	16.1	283	4.16			
		6 to 8	129	3	35	1	56				24	1.7	2.0
		18 to 20	160	2	34	10	58						
9	26 grass	0 to 2	52	0	26	5	86	29.3	555	1.51			
		6 to 8	58	0	5	6	120	29.1	560	2.75	60	3.3	3.3
		16 to 18	39	0	7	2	121	30.1	576	1.76			
10	26 bare	0 to 2	56	0	20	4	61	30.5	583	1.67			
		6 to 8	68	1	18	6	61	29.9	575	2.70	49		
		18 to 20	86	2	30	5	77	28.8	561	1.51			
11	25 grass	0 to 2	90	0	15	17	83	29.0	540	1.75			
		6 to 8	92	0	27	15	159	29.0	563	2.35	21	0.5	10.0
		18 to 20	72	0	28	14	83	28.1	555	1.28			
12	25 bare	0 to 2	65	0	21	6	50	29.2	562	2.32			
		6 to 8	101	0	22	7	38	29.1	560	1.34	29	1.0	3.3
		18 to 20	110	0	18	16	64	27.3	531	1.06			
13	24 grass	0 to 2	121	1	47	2	113	30.0	576	6.40			
		6 to 8	83	1	46	2	18	29.7	575	2.61	156	1.6	3.5
		18 to 20	65	0	23	3	68	29.9	560	1.41			
14	24 bare	0 to 2	55	2	38	1	52	30.5	581	3.67			
		6 to 8	164	2	37	3	37	29.7	580	1.33	235	1.5	0.6
		18 to 20	142	2	33	2	13	27.8	547	1.30			
15	22 grass (no 23)	0 to 2	176	0	16	8	68	31.0	594	7.56			
		6 to 8	123	0	18	10	73	31.5	597	10.77	420	2.0	4.7
		18 to 20	130	0	17	6	69	31.6	603	3.92			
16	22 bare	0 to 2	121	1	15	8	81	31.7	618	8.63			
		6 to 8	305	1	13	14	73	29.3	586	4.03	1125	2.0	4.4
		18 to 20	407	1	12	7	92	22.0	1781	2.70			
17	20 grass	0 to 2	2440	0	9	3	94	32.3	612				
		6 to 8	2050	0	16	13	63	38.3	597	23.25	39	1.8	0.7
		16 to 18	5430	0	8	22	186	29.2	596				

18	20 bare	0 to 2	213	1	13	7	73	32.5	612	1.24			
		6 to 8	213	1	10	16	134	32.3	612	2.23	591	2.4	2.7
		16 to 18	1082	1	10	44	245	28.3	616	3.90			
19	18 grass	0 to 2	15	0	10	2	60	35.3	649	3.56			
		6 to 8	44	0	12	2	34				28	1.0	1.1
		18 to 20	56	0	7	2	29	34.4	629	1.16			
20	18 bare	0 to 2	75	0	3	4	76	34.9	643	2.71			
		6 to 8	1480	0	1	3	37	34.2	626		37	0.8	0.0
		18 to 20	79	0	3	4	42						
21	16 grass	0 to 2	42	0	2	4	57	34.6	624	14.91			
		6 to 8	35	0	9	3	69	33.8	623		134	2.3	2.2
		18 to 20	35	0	5	3	51						
22	16 bare	0 to 2	43	0	7	2	32	34.8	631	4.25			
		6 to 8	1280	0	8	3	43				257	2.4	0.7
		18 to 20	1001	0	21	2	48	31.8	601	0.97			
23	13 grass	0 to 2	1150	1	17	8	58	36.2	654	4.20			
		6 to 8	1690	1	19	6	71	34.2	625	4.97	64	2.6	0.5
		18 to 20											
24	13 bare	0 to 2	51	1	26	8	49	35.4	637				
		6 to 8	57	1	18	6	51				25	3.1	0.5
		18 to 20											

Table 3. Individual analyses.

COE#	Station	Replicat	Depth	Bottle	ϕ	V Frac			wt. %						$\mu\text{mol/gdw}$			
						<63 μm	Org-C	Carb-C	TRS	AVS	CD-Fe	HCl-Fe	CD-Mn	HCl-Mn				
1	30 grass	1	0 to 2	274	0.65	28	0.84	1.66	8.03	4.35	5.41	30.0	<0.25	1.47				
			6 to 8	249	0.55	33	1.03	1.22	1.87	1.62	1.08	47.2	<0.25	1.50				
			18 to 20	257	0.48	33	0.41	1.10	0.62	0.48	0.36	38.7	<0.25	1.27				
		2	0 to 2	243	0.62	28	2.00	2.78	13.95	6.15	1.69	34.8	<0.25	1.44				
			6 to 8	276	0.63	44	0.99	2.66	3.25	2.59	3.86	59.1	<0.25	2.03				
			18 to 20	244	0.49	38	0.53	1.29	2.18	1.91	0.61	47.8	<0.25	1.55				
		3	0 to 2	264	0.68	35	1.38	1.75	3.08	2.58	4.11	46.9	<0.25	1.77				
			6 to 8	265	0.55	37	0.86	1.54	2.36	2.01	1.48	34.9	<0.25	1.28				
			18 to 20	255	0.49	40	0.62	1.36	2.29	1.93	0.50	52.5	<0.25	1.68				
2	30 bare	1	0 to 2	275	0.60	15	0.77	1.72	4.50	2.79	2.38	38.0	<0.25	1.05				
			6 to 8	236	0.58	24	0.85	1.32	1.89	1.62	1.66	41.8	<0.25	1.64				
			18 to 20	294	0.50	40	0.46	1.07	0.81	0.50	0.87	53.4	<0.25	1.73				
		2	0 to 2	237	0.45	15	0.29	4.11	3.92	1.66	1.46	14.2	<0.25	0.61				
			6 to 8	258	0.56	23	0.62	1.41	3.27	2.24	1.76	28.7	<0.25	1.22				
			18 to 20	282	0.46	35	0.44	1.22	1.93	1.66	0.73	49.4	<0.25	1.51				
		3	0 to 2	279	0.60	10	0.50	1.80	4.26	2.37	2.05	24.5	<0.25	0.95				
			6 to 8	262	0.54	26	0.59	1.73	2.12	1.79	1.04	31.2	<0.25	1.00				
			18 to 20	260	0.45	36	0.51	1.01	1.35	1.16	0.68	50.1	<0.25	1.49				
3	29 grass	1	0 to 2	253	0.47	22	0.21	2.22	2.44	1.65	1.40	32.1	<0.25	1.15				
			6 to 8	232	0.53	38	0.36	1.73	2.17	1.79	0.70	62.2	<0.25	2.10				
			18 to 20	CT8	0.47	40	0.35	1.61	1.19	1.04	0.55	50.3	<0.25	2.23				
4	29 bare	1	0 to 2	336	0.44	8	0.17	2.94	2.41	0.80	1.78	16.6	<0.25	0.71				
			6 to 8	317	0.50	41	0.45	1.43	3.02	1.69	4.56	71.7	<0.25	2.70				
			18 to 20	362	0.46	36	0.40	1.25	3.09	1.63	2.20	62.4	<0.25	2.67				
5	28 grass	2	0 to 2	148	0.44	6	1.30	0.00	3.03	1.52	1.51	19.2	<0.25	0.61				
			6 to 8	313	0.47	18	0.33	1.40	1.92	1.13	1.72	33.9	<0.25	1.19				
			18 to 20	205	0.48	42	0.43	0.96	1.77	1.52	<0.25	40.2	<0.25	1.76				
6	28 bare	1	6 to 8	220	0.41	16	0.26	0.92	3.71	2.04	0.97	21.9	<0.25	0.91				
		2	6 to 8	219	0.42	9	0.17	1.56	2.73	1.68	0.68	21.4	<0.25	0.74				
7	27 grass	1	6 to 8	251	0.48	12	0.34	2.82	2.60	1.49	0.44	15.5	<0.25	0.96				
			18 to 20	296	0.51	34	0.47	1.50	1.11	0.93	0.56	38.7	<0.25	2.10				
			6 to 8	226	0.49	31	0.51	2.02	2.72	1.92	0.40	47.4	<0.25	2.11				
			18 to 20	286	0.55	35	0.55	2.04	1.54	0.84	0.44	52.9	<0.25	2.96				
8	27 bare	1	0 to 2	268	0.46	8	0.24	1.72	2.89	1.70	1.24	20.2	<0.25	0.93				
			6 to 8	229	0.52	29	0.56	2.30	1.13	0.97	<0.25	42.9	<0.25	1.91				
			18 to 20	227	0.49	35	0.37	1.77	1.86	1.52	0.25	51.5	<0.25	2.41				

9	26 grass	1	0 to 2	196	0.49	19	0.33	3.14	2.09	1.54	1.42	53.8	<0.25	2.07
			6 to 8	188	0.55	83	0.40	2.33	3.14	2.70	0.87	108.5	<0.25	3.50
			16 to 18	161	0.55	86	0.42	2.36	1.96	1.54	0.91	129.0	<0.25	3.86
10	26 bare	2	0 to 2	180	0.58	53	0.51	2.36	2.60	1.83	1.55	60.7	<0.25	2.15
			6 to 8	151	0.56	81	0.39	2.25	1.79	1.57	0.94	113.8	<0.25	3.04
			17 to 19	154	0.53	96	0.27	2.53	4.79	1.64	0.37	171.7	<0.25	4.43
11	25 grass	1	0 to 2	356	0.59	62	0.43	2.09	3.24	2.17	2.96	70.0	<0.25	3.15
			6 to 8	348	0.52	69	0.42	1.95	1.65	1.50	1.93	65.7	<0.25	3.02
			18 to 20	360	0.51	56	0.41	2.27	2.32	1.67	1.60	53.4	<0.25	2.60
		2	0 to 2	341	0.60	60	0.49	2.03	4.36	2.48	3.23	71.1	<0.25	2.94
			6 to 8	326	0.54	63	0.45	2.15	1.90	1.61	2.79	70.8	<0.25	3.15
			18 to 20	320	0.54	77	0.46	2.35	3.24	2.73	2.19	101.7	<0.25	3.67
		3	0 to 2	202	0.61	57	0.50	1.81	10.12	5.08	1.38	85.0	<0.25	2.57
			6 to 8	204	0.57	76	0.41	2.37	6.40	4.80	2.85	58.3	<0.25	3.14
			18 to 20	344	0.49	98	0.25	3.23	1.49	0.36	1.38	150.7	<0.25	3.81
12	25 bare	1	0 to 2	195	0.62	59	0.45	2.59	6.34	3.04	2.17	77.0	<0.25	2.78
			6 to 8	357	0.51	61	0.43	2.15	1.66	1.44	1.81	62.1	<0.25	2.82
			18 to 20	200	0.54	87	0.31	2.21	2.01	1.73	0.61	119.7	<0.25	3.17
		2	0 to 2	170	0.60	50	0.43	2.48	5.06	2.61	1.89	57.1	<0.25	2.28
			6 to 8	355	0.55	70	0.53	1.97	1.74	1.44	2.46	80.2	<0.25	3.10
			18 to 20	176	0.53	94	0.23	2.82	1.73	0.78	0.90	126.3	<0.25	3.48
		3	0 to 2	177	0.61	51	0.40	2.15	5.97	2.73	1.66	69.2	<0.25	2.58
			6 to 8	167	0.57	63	0.43	2.40	2.52	2.26	1.55	89.3	<0.25	3.27
			18 to 20	182	0.55	97	0.21	2.54	2.92	1.00	0.54	145.6	<0.25	3.37
13	24 grass	1	0 to 2	540	0.60	19	0.57	3.25	3.56	1.88	2.00	23.3	<0.25	1.23
			6 to 8	515	0.51	29	0.55	2.08	4.96	2.85	2.58	37.8	<0.25	2.08
			18 to 20	507	0.47	14	0.24	0.85	1.92	1.09	0.69	19.6	<0.25	0.70
14	24 bare	1	0 to 2	531	0.65	40	0.80	1.66	6.76	3.44	1.92	35.4	<0.25	1.50
			6 to 8	509	0.61	45	0.61	2.18	8.28	3.99	2.80	35.4	<0.25	2.01
			18 to 20	537	0.44	7	0.16	1.83	4.47	1.73	0.46	12.3	<0.25	0.54
		2	0 to 2	524	0.63	26	0.75	1.90	5.37	3.00	7.12	34.3	<0.25	1.71
			6 to 8	516	0.54	44	0.51	1.68	6.26	3.64	2.01	35.4	<0.25	1.83
			18 to 20	537	0.44	7	0.16	1.83	4.47	1.73	0.46	12.3	<0.25	0.54
		3	0 to 2	517	0.53	16	0.44	1.55	4.15	2.26	2.69	21.5	<0.25	1.02
			6 to 8	522	0.60	21	0.49	1.81	4.20	2.66	3.25	29.0	<0.25	1.38
			18 to 20	556	0.52	16	0.41	1.10	3.11	2.16	0.77	30.1	<0.25	1.44
15	22 grass (no 23)	3	0 to 2	377	0.89	84	5.41	4.59	9.25	4.23	10.26	74.7	<0.25	2.98
			6 to 8	492	0.77	42	2.05	1.81	19.32	9.62	2.95	38.0	<0.25	1.39
			18 to 20	379	0.58	15	0.46	1.37	4.24	1.57	0.56	19.5	<0.25	0.55

16	22 bare	1	0 to 2	375	0.77	27	1.74	2.38	7.10	3.39	2.00	33.1	<0.25	1.29
			6 to 8	399	0.82	52	2.62	2.56	4.81	2.47	3.15	46.8	<0.25	1.77
			18 to 20	417	0.59	18	0.54	2.17	4.12	2.58	1.83	28.2	<0.25	0.77
		2	0 to 2	404	0.69	20	0.92	1.55	3.07	1.65	2.05	19.1	<0.25	0.63
			6 to 8	394	0.65	10	0.82	0.80	4.62	2.31	1.08	13.0	<0.25	0.36
			18 to 20	368	0.64	35	0.81	1.25	3.33	2.38	1.99	46.7	<0.25	1.19
		3	0 to 2	429	0.68	20	1.15	0.96	5.19	1.32	1.93	18.7	<0.25	0.90
			6 to 8	400	0.65	24	0.81	0.91	5.73	2.82	1.30	19.2	<0.25	0.54
			18 to 20	402	0.43	3	0.14	0.56	2.44	0.76	<0.25	7.6	<0.25	0.04
17	20 grass	2	0 to 2	363	0.61	14	0.83	3.57	6.67	3.14	2.10	24.5	<0.25	1.27
			6 to 8	433	0.49	17	0.32	4.06	2.92	1.16	1.32	18.6	<0.25	2.42
			16 to 18	495	0.57	26	0.34	6.29	4.40	2.35	1.51	29.6	<0.25	2.92
18	20 bare	3	0 to 2	403	0.69	31	0.78	1.63	2.68	1.76	2.75	31.3	<0.25	1.47
			6 to 8	412	0.72	55	0.83	1.48	6.05	3.43	3.54	36.8	<0.25	2.04
			16 to 18	415	0.82	81	1.28	1.67	6.29	4.15	5.76	82.1	<0.25	6.22
19	18 grass	2	0 to 2	512	0.49	5	0.23	0.32	5.68	2.66	1.58	11.2	<0.25	0.35
			6 to 8	476	0.47	11	0.30	0.22	3.56	1.41	0.62	8.9	<0.25	0.14
			18 to 20	555	0.43	6	0.16	0.20	3.99	1.71	<0.25	6.8	<0.25	0.26
20	18 bare	3	0 to 2	557	0.51	8	0.29	0.51	4.33	2.17	0.82	10.0	<0.25	0.34
			6 to 8	549	0.49	13	0.29	0.49	4.77	2.43	1.13	15.8	<0.25	0.59
			18 to 20	561	0.43	3	0.10	0.54	3.12	0.90	<0.25	3.1	<0.25	0.16
21	16 grass	2	0 to 2	411	0.62	17	0.92	2.58	6.29	2.80	1.71	17.2	<0.25	0.58
			6 to 8	638	0.53	23	0.44	2.40	4.67	2.41	1.64	23.7	<0.25	1.03
			18 to 20	629	0.53	20	0.63	5.43	7.10	3.24	1.67	23.8	<0.25	0.94
22	16 bare	2	0 to 2	646	0.72	25	1.56	1.43	6.40	3.05	1.97	21.3	<0.25	0.43
			6 to 8	637	0.57	10	0.50	1.23	5.84	2.35	0.44	7.8	<0.25	0.32
			18 to 20	410	0.54	19	0.54	2.22	3.30	2.41	1.37	17.5	<0.25	2.19
23	13 grass	2	0 to 2	270	0.66	12	1.13	3.54	7.65	3.60	1.65	10.7	<0.25	0.81
			6 to 8	315	0.52	4	0.50	3.08	3.48	1.11	0.40	4.6	<0.25	0.32
24	13 bare	3	0 to 2	585	0.56	17	0.60	3.53	5.42	2.42	0.61	9.8	<0.25	0.63
			6 to 8	622	0.53	18	0.43	6.09	3.69	1.85	0.79	15.3	<0.25	1.15

μM	mM
----	----

COE#	Station	Replicat	Depth	NH4	NO3	Urea	PO4	SiO2	SO4	Cl	DOC
1	30 grass	1	0 to 2	75	ND	15	4	63	29.2	561	4.49
			6 to 8	173	ND	53	5	69	27.7	557	2.46
			18 to 20	37	3	21	3	68	26.0	517	0.99
		2	0 to 2	61	ND	21	6	82	28.3	553	3.24
			6 to 8	51	ND	36	6	69	25.4	513	2.41
			18 to 20	32	2	42	5	71	24.8	515	
		3	0 to 2	78	ND	30	5	74	27.4	537	3.42
			6 to 8	41	ND	20	4	65	25.7	517	1.63
			18 to 20	34	ND	39	6	63	23.0	455	3.95
2	30 bare	1	0 to 2	49	1	23	4	66	26.6	524	1.35
			6 to 8	79	2	26	4	60	26.6	527	1.65
			18 to 20	140	1	38	2	55	22.9	472	0.89
		2	0 to 2	57	ND	25	1	61	26.3	513	1.81
			6 to 8	139	3	28	10	68	27.3	544	1.73
			18 to 20	138	10	50	10	69			
		3	0 to 2	68	ND	22	2	70	26.0	502	2.36
			6 to 8	73	7	21	3	44	26.8	524	1.79
			18 to 20	109	4	59	3	20	23.7	460	0.85
3	29 grass	1	0 to 2	44	4	40	3	19	26.5	519	2.47
			6 to 8	50	ND	43	3	33	26.7	534	3.95
			18 to 20	43	ND	42	2	27	25.9	511	
4	29 bare	1	0 to 2	61	ND	41	2	40	28.2	547	0.84
			6 to 8	98	ND	25	2	66	26.7	526	1.25
			18 to 20	88	ND	22	2	87	27.9	543	
5	28 grass	2	0 to 2	70	3	36	5	12			
			6 to 8	42	3	58	6	14	28.7	551	1.49
			18 to 20	32	ND	45	9	46			
6	28 bare	1	6 to 8	152	2	47	6	53			
		2	6 to 8	149	ND	44	7	53			
7	27 grass	1	6 to 8	85	3	34	2	89	28.4	553	1.72
			18 to 20	33	3	43		125	25.1	492	1.28
			6 to 8	54	3	32	2	54	26.6	518	2.57
			18 to 20	32	3	34	3	248	26.7	524	1.84
8	27 bare	1	0 to 2	281	2	42	12	3	16.1	283	4.16
			6 to 8	129	3	35	1	56			
			18 to 20	160	2	34	10	58			
9	26 grass	1	0 to 2	52	ND	26	5	86	29.3	555	1.51
			6 to 8	58	ND	5	6	120	29.1	560	2.75
			16 to 18	39	ND	7	2	121	30.1	576	1.76
10	26 bare	2	0 to 2	56	ND	20	4	61	30.5	583	1.67
			6 to 8	68	1	18	6	61	29.9	575	2.70
			17 to 19	86	2	30	5	77	28.8	561	1.51

11	25 grass	1	0 to 2	100	ND	30	41	126	28.6	539	2.62
			6 to 8	65	ND	28	10	65	28.8	552	1.85
			18 to 20	65	ND	30	17	58	27.6	549	1.47
		2	0 to 2	100	ND	10	7	70	28.3	531	1.31
			6 to 8	125	ND	27	11	148	28.5	555	3.46
			18 to 20	87	ND	24	18	136	28.4	567	1.67
		3	0 to 2	71	ND	6	2	54	29.6	551	1.32
			6 to 8	87	ND	26	25	265	29.6	581	1.73
			18 to 20	65	ND	31	6	56	28.3	550	0.70
12	25 bare	1	0 to 2	68	ND	28	5	41	29.2	544	3.33
			6 to 8	75	ND	28	7	32	29.5	557	1.68
			18 to 20	68	ND	15	2	89			
		2	0 to 2	61	ND	10	6	56	29.0	598	1.84
			6 to 8	122	ND	8	7	40	28.6	554	1.13
			18 to 20	167	116	24	40	77	26.1	526	1.21
		3	0 to 2	65	ND	24	7	54	29.5	544	1.78
			6 to 8	106	ND	30	8	41	29.1	568	1.20
			18 to 20	94	ND	14	7	25	28.4	535	0.90
13	24 grass	1	0 to 2	121	1	47	2	113	30.0	576	6.40
			6 to 8	83	1	46	2	18	29.7	575	2.61
			18 to 20	65	ND	23	3	68	29.9	560	1.41
14	24 bare	1	0 to 2	59	2	37		110	30.7	582	2.15
			6 to 8	144	2	39	2	67	30.7	593	0.68
			18 to 20	159	2	34	2	11			1.32
		2	0 to 2	53	2	39	1	41	30.6	581	5.86
			6 to 8	169	2	35	2	29	29.8	582	1.48
			18 to 20	159	2	34	2	11			1.32
		3	0 to 2	53	2	39	1	6	30.3	580	3.01
			6 to 8	178	2	38	4	16	28.8	564	1.83
			18 to 20	125	2	31		15	27.8	547	1.28
15	22 grass (no 23)	3	0 to 2	176	ND	16	8	68	31.0	594	7.56
			6 to 8	123	ND	18	10	73	31.5	597	10.77
			18 to 20	130	ND	17	6	69	31.6	603	3.92
16	22 bare	1	0 to 2	101	1	17	7	94	32.6	627	7.71
			6 to 8	409	ND	15	17	60	27.0	565	4.69
			18 to 20	377	1	13	9	110	16.3	3012	2.90
		2	0 to 2	148	1	14	8	70	30.9	610	11.06
			6 to 8	210	ND	12	9	61	31.4	603	3.89
			18 to 20	346	ND	12	7	84	27.6	549	2.49
		3	0 to 2	115	1	13	10	76	31.6	616	7.12
			6 to 8	295	1	11	16	99	29.6	589	3.52
			18 to 20	498	1	12	4	83			
17	20 grass	2	0 to 2	2440	ND	9	3	94	32.3	612	
			6 to 8	2050	ND	16	13	63	38.3	597	23.25
			16 to 18	5430	ND	8	22	186	29.2	596	
18	20 bare	3	0 to 2	213	1	13	7	73	32.5	612	1.24
			6 to 8	213	1	10	16	134	32.3	612	2.23
			16 to 18	1082	ND	10	44	245	28.3	616	3.90
19	18 grass	2	0 to 2	15	ND	10	2	60	35.3	649	3.56
			6 to 8	44	ND	12	2	34			
			18 to 20	56	ND	7	2	29	34.4	629	1.16

20	18 bare	3	0 to 2	75	ND	3	4	76	34.9	643	2.71
			6 to 8	1480	ND	1	3	37	34.2	626	
			18 to 20	79	ND	3	4	42			
21	16 grass	2	0 to 2	42	ND	2	4	57	34.6	624	14.91
			6 to 8	35	ND	9	3	69	33.8	623	
			18 to 20	35	ND	5	3	51			
22	16 bare	2	0 to 2	43	ND	7	2	32	34.8	631	4.25
			6 to 8	1280	ND	8	3	43			
			18 to 20	1001	ND	21	2	48	31.8	601	0.97
23	13 grass	2	0 to 2	1150	1	17	8	58	36.2	654	4.20
			6 to 8	1690	1	19	6	71	34.2	625	4.97
24	13 bare	3	0 to 2	51	1	26	8	49	35.4	637	
			6 to 8	57	1	18	6	51			

μM

COE#	Station	Replicat	H2S	Fe	Mn
1	30 grass	1	192	2.6	2.7
2	30 bare	1	42	4.2	14.2
		2	23	1.2	4.6
		3	43	0.9	1.7
3	29 grass	1	71	3.5	11.3
		2	45	3.5	9.7
4	29 bare	1		2.7	1.1
		2	29	2.4	8.6
		3		0.6	4.9
5	28 grass	1	25	2.1	2.0
		2	28	1.3	2.0
		3	20	1.3	1.1
6	28 bare	1	40	0.1	1.1
		2	42	0.6	1.1
7	27 grass	1	23	1.3	2.3
		2	23	1.3	3.0
		3	14	1.6	3.9
8	27 bare	1	23	0.1	1.2
		2	24	3.1	3.9
		3	24	1.8	0.9
9	26 grass	1	88	2.4	0.9
		2	47	1.1	0.9
		3	46	6.4	8.2
10	26 bare	1	40		
		2	57		
11	25 grass	1	19	0.6	8.1
		2	21	0.3	11.8
		3	22	0.6	10.2
12	25 bare	1	43	1.1	4.9
		2	22	1.3	1.8
		3	23	0.6	3.3
13	24 grass	1	236		
		2	77	1.6	3.5
		3	222		
14	24 bare	2	219	2.4	0.7
		3	250	0.6	<0.5
15	22 grass	1		3.4	9.3
		2	412	1.6	3.3
		3	428	1.1	1.5
16	22 bare	1	978	2.3	4.9
		2	1282	2.1	3.5
		3	1114	1.6	4.9
17	20 grass	1	25	1.1	<0.5
		2	72	3.4	0.9
		3	19	0.8	0.5

18	20 bare	1	625	2.1	0.9
		2	556	2.6	4.4
19	18 grass	1	23	1.3	0.7
		2	48		
		3	14	0.6	1.5
20	18 bare	1	47		
		3	27	0.8	<0.5
21	16 grass	1	154	1.6	2.1
		2	181	2.9	2.2
		3	68		
22	16 bare	1	427	2.4	0.7
		2	86		
23	13 grass	1	48	3.1	<0.5
		2	65	2.1	<0.5
		3	121		
24	13 bare	3	25	3.1	<0.5

Results

Solid Components

It is commonly observed that many sediment parameters often correlate with the portion of the sediment in the silt plus clay (<63 μm) size fraction relative to the sand component. Figure 1 shows the relative abundance of samples with different contents of the silt plus clay fraction. The sediments in Laguna Madre are far from uniform in their grain size distribution and are dominated by poorly sorted sandy sediments (79% are >50% sand fraction). Adjacent grass and bare sites have been plotted against each other for different sediment depths in Figure 2. For about 90% of the sites there is relatively good agreement between the paired values. There is no clear cut trend for other variations that probably just reflect local variability. It, therefore, does not appear that the potential baffle-effect of the seagrass beds is leading to a significantly enhanced accumulation of fine-grained sediments. The relationships of carbonate-C, organic-C and porosity to the <63 μm (silt plus clay) grain size fraction are shown in Figure 3. The data have been divided into grass and bare areas and the 3 sampling depths. Two trends are apparent in the relationship between carbonate-C and grain size. One group of data are largely confined to about 1 to 3 weight percent carbonate-C and are largely independent of grain size distribution. The other group of data exhibits a wide range of carbonate-C values, but is largely confined to sediments with >75% sand fraction. The high values are restricted to seagrass beds and probably reflect the presence of bivalves and mollusks preferentially living there. Organic-C exhibited a similar dual trend relative to grain size, one being fairly typical of what is commonly seen and another with a wide range of values in the sand-rich sediments. (Note the one value at 5.4 wt.% probably had root material in it.) The high organic-C values are generally restricted to the 0-2 cm depth samples and there appears not to be major differences between bare and grass areas when macroscopic root material is carefully removed. Although not as clear cut, porosity also exhibited a tendency to have two trends with respect to grain size. The wide range in porosities, from about 0.4 to 0.8, for sand-rich sediments does not seem to have a strong relationship as to whether or not the sediment was vegetated. TRS concentrations did not appear to bear any relationship to sediment grain size (Figure 4) and were generally at least an order of magnitude less than is typical for fine-grained siliciclastic marine sediments in the Gulf of Mexico region. HCl extractable Fe exhibited a linearly ($r^2 = 0.86$) increasing relationship with increasing silt and clay content (Fig. 5), whereas the Fe derived from the weaker citrate dithionite extraction was at very low concentrations and showed no relationship to grain size. This was also true for HCl extractable Mn. Citrate dithionite extractable Mn was below (<0.25 $\mu\text{mol/gdw}$) analytical detection limits.

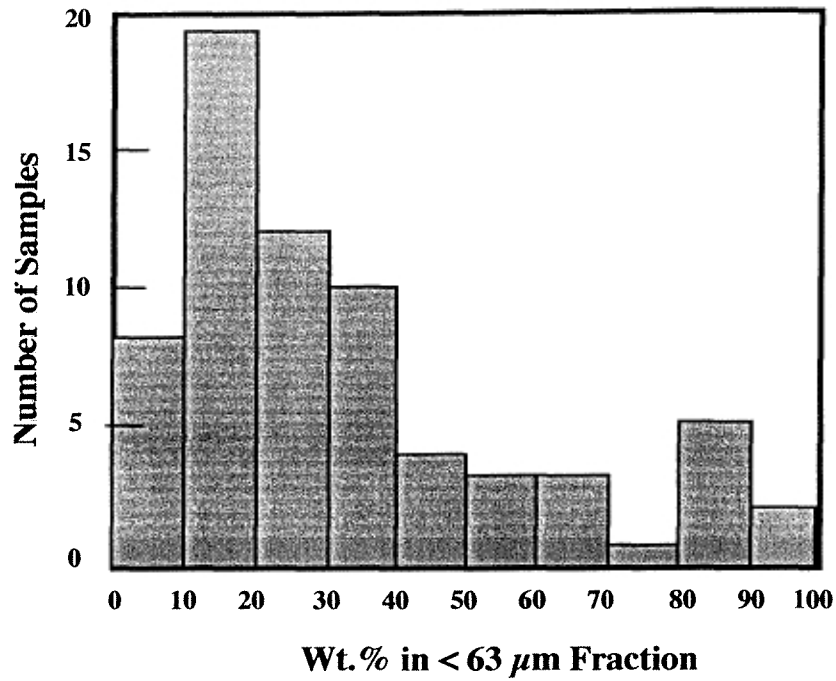


Figure 1. Relative abundance of samples containing different percentages of the <63 μm grain size fraction.

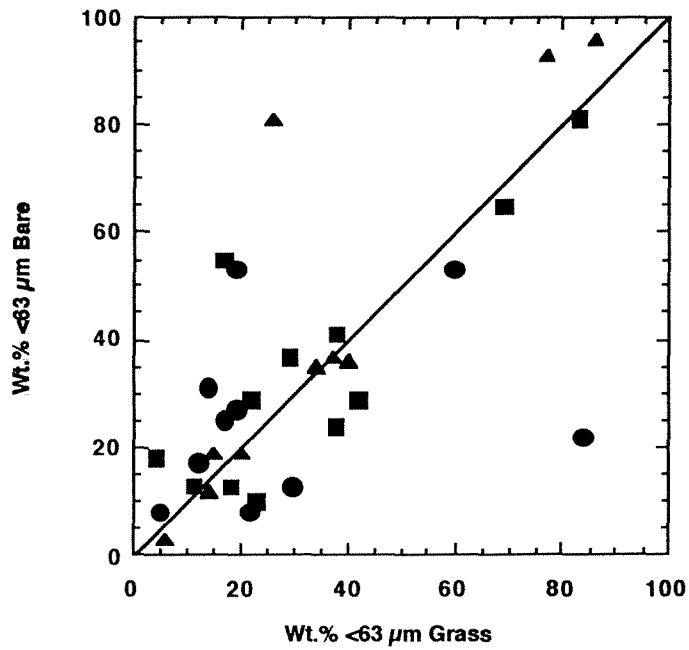


Figure 2. Plot of the <63 μm grain size fraction in adjacent bare versus vegetated areas. Circles 0-2 cm; squares 6-8 cm; triangles 18-20 cm.

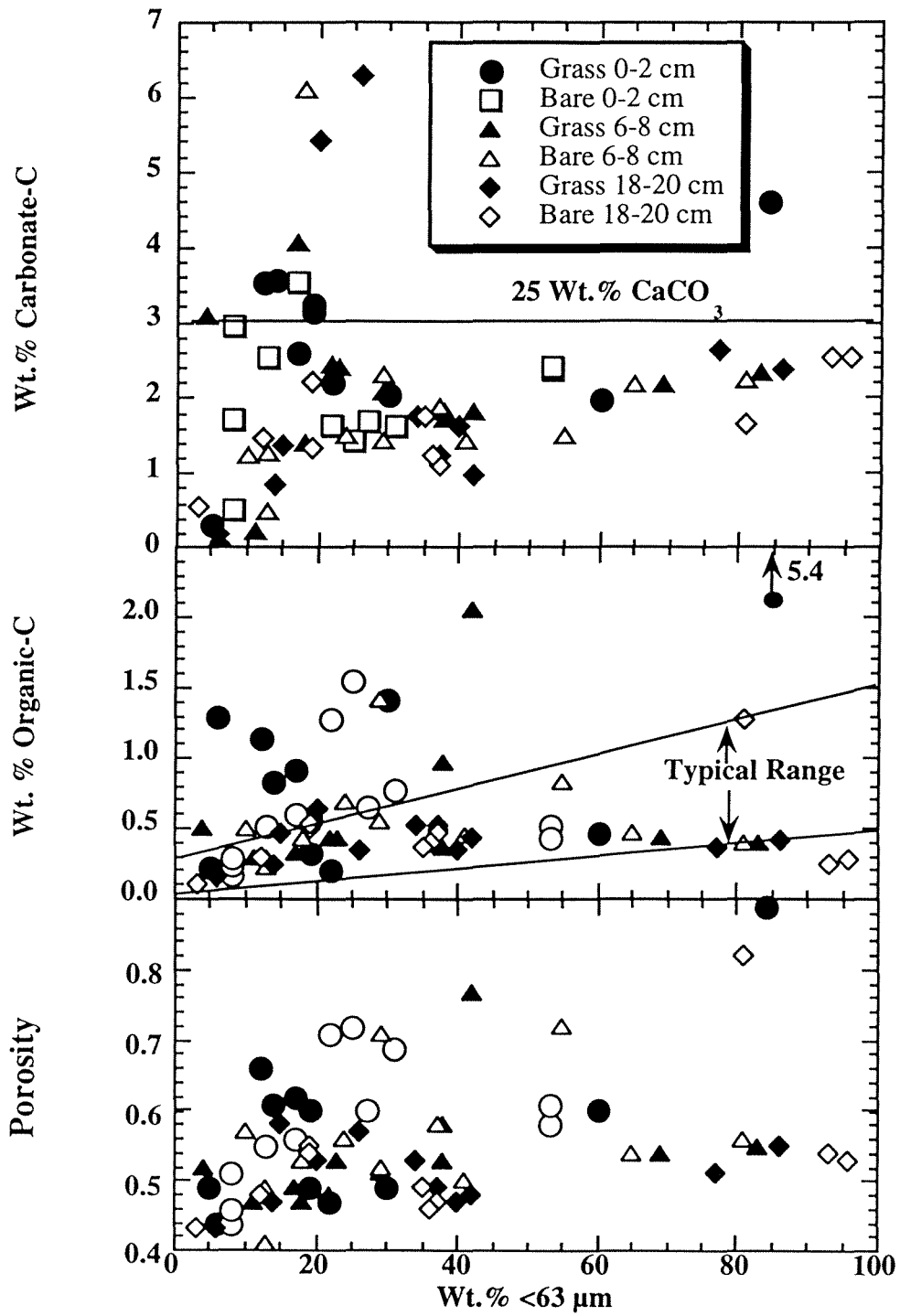


Figure 3. Solid parameters' relationship to grain size.

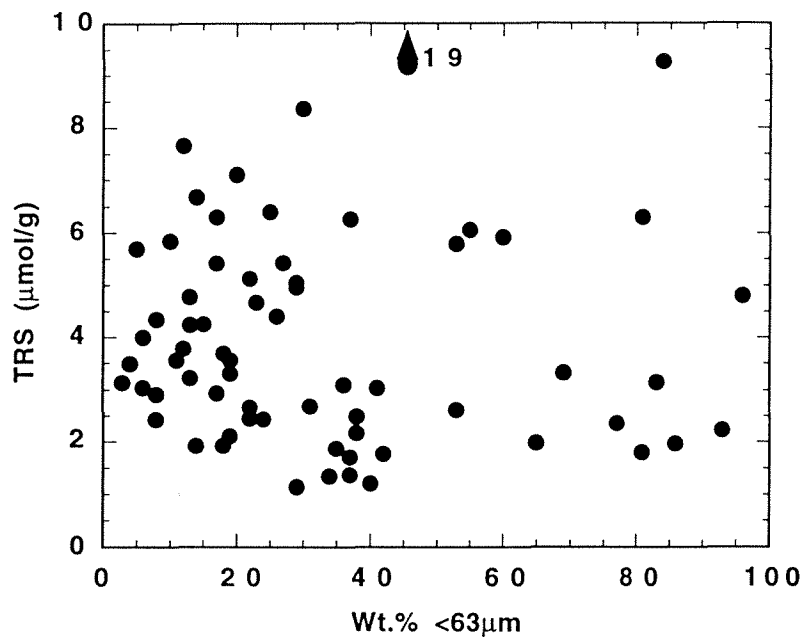


Figure 4. Relationship between total reduced sulfur (TRS) and sediment grain size.

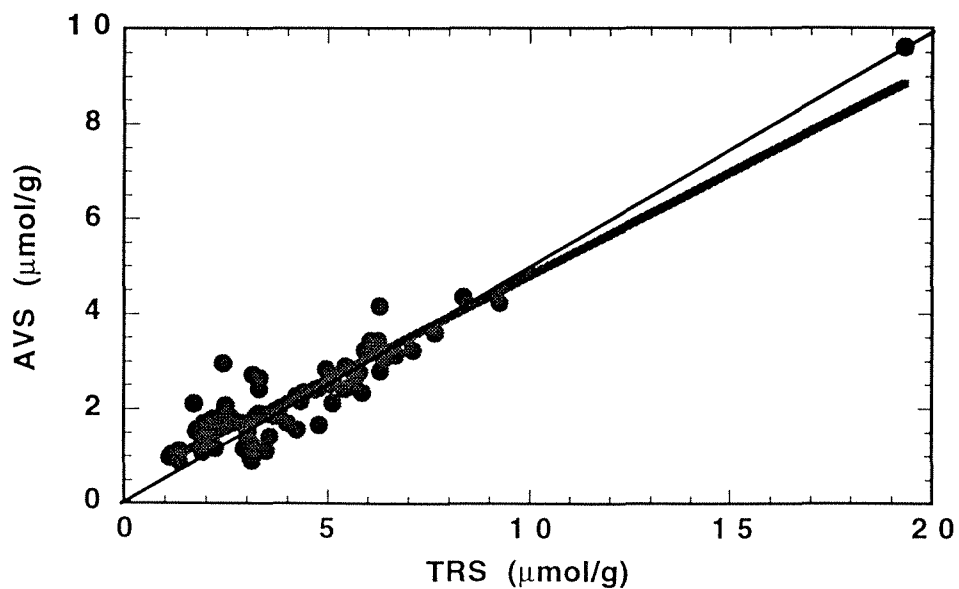


Figure 5. Acid volatile sulfides (AVS) versus total reduced inorganic sulfur (TRS). Heavy line is linear least squares fit and light line is for 50% TRS as AVS.

Two interesting relationships in the sedimentary sulfur system in Laguna Madre are shown in figures 5 and 6. The first is that the portion of TRS as AVS is very close to constant at 50% for all samples measured. This is much higher than is typical for most near sediment-water interface anoxic marine sediments where typical maximum values are about 5 to 10 percent of TRS as AVS. The lack of major differences AVS:TRS with depth, grain size, organic-C content or between vegetated and bare areas is amazing. Another commonly observed relationship is that the weight ratio of sedimentary organic-C to TRS is about 2.8 for most "normal" marine sediments. However, the C/S ratio here is about an order of magnitude higher.

Pore Water Components

The relationships among the dissolved components that were determined in sediment pore waters will be discussed in this section. In the following section the interrelationships between sedimentary solid and dissolved components will be presented. The two pore water components of central concern, for the study of the relationship between sediment chemistry and seagrasses, are ammonium and hydrogen sulfide. Figure 7 is a plot of dissolved ammonium concentrations in seagrass sediments plotted against those in adjacent bare areas. Most of the sites studied cluster tightly in the relatively low ($< \sim 300 \mu\text{M}$) region. Other sites fall into two distinctly different trends. In the first, bare areas show substantially elevated ammonium concentrations relative to seagrass sediments and, in the second, the opposite relationship is observed. The highest ammonium concentrations occur in seagrass beds.

Figure 8 is a plot of dissolved hydrogen sulfide concentrations in seagrass sediments plotted against those in adjacent bare areas. Most of the sites studied cluster tightly in the relatively low ($< \sim 100 \mu\text{M}$) region. With the exception of one site, where the seagrass hydrogen sulfide is higher than that of the adjacent bare area, in sediments with elevated hydrogen sulfide concentrations the bare areas are generally substantially higher than in sediments covered by seagrasses. The relationship between hydrogen sulfide and ammonium is shown in Figure 9 (note H_2S data are from 8 to 10 cm and NH_4^+ data are from 10 to 11 cm depth), where sediments with elevated hydrogen sulfide concentrations tend to have low ammonium concentrations and those with elevated ammonium concentrations tend to have low hydrogen sulfide concentrations. This occurs for both bare sediments and those covered by seagrasses.

The relationship between the dissolved nutrients phosphate and ammonium is also of potential interest. It is shown in figures 10 and 11. Most of the data cluster in an area of $\text{PO}_4 < 20 \mu\text{M}$ and $\text{NH}_4 < 400 \mu\text{M}$. With the exceptions of one sample (there always seems to be one) the other data

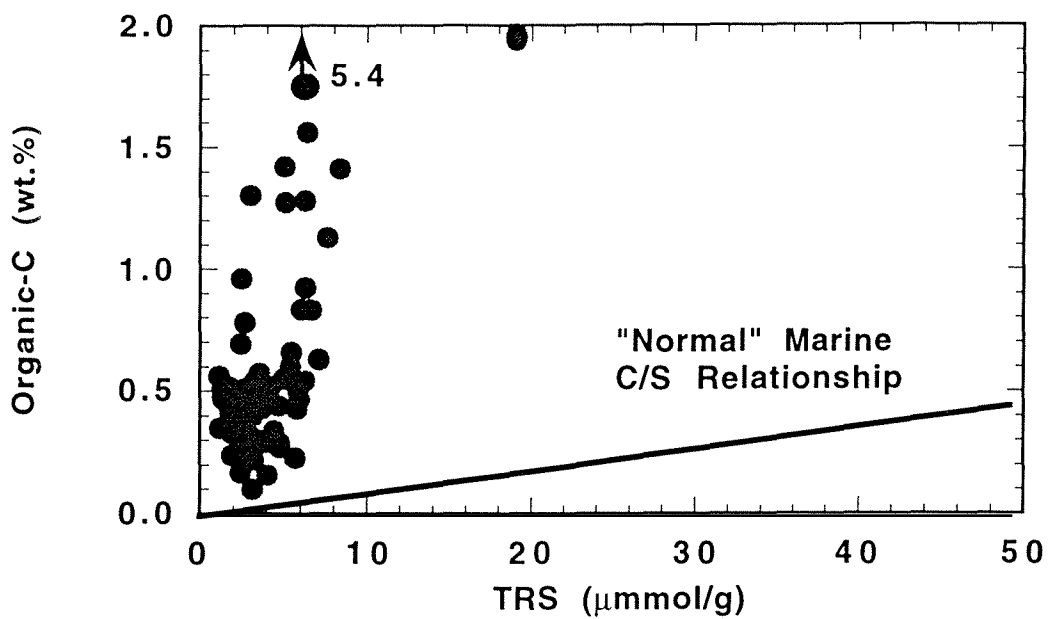


Figure 6. Relationship between organic-C and TRS. Line is for "normal marine weight ratio of 2.8.

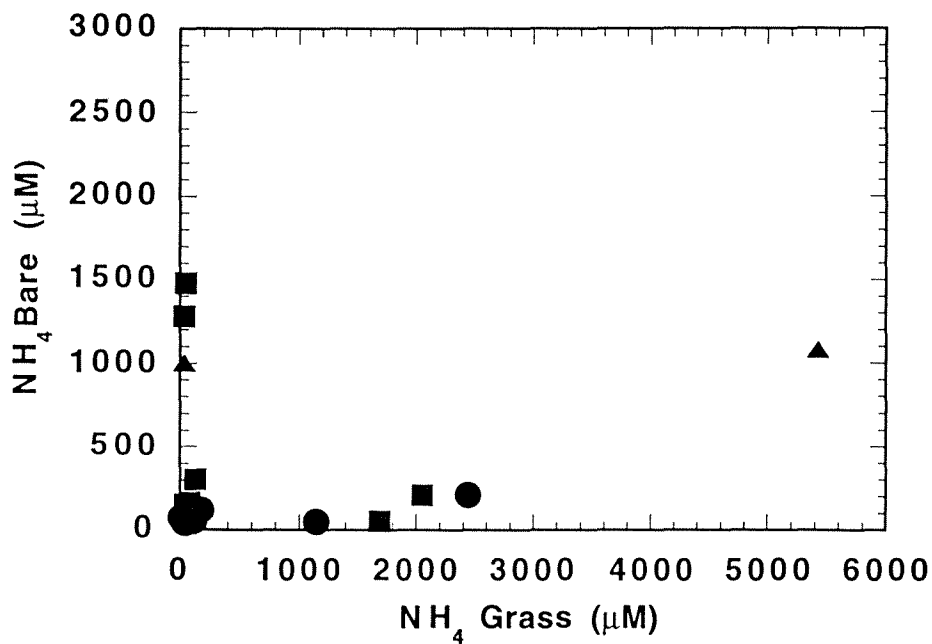


Figure 7. The relationship between pore water ammonium concentrations in sediments covered by seagrass and in bare areas. Circles 0-2 cm; squares 6-8 cm; triangles 18-20 cm.

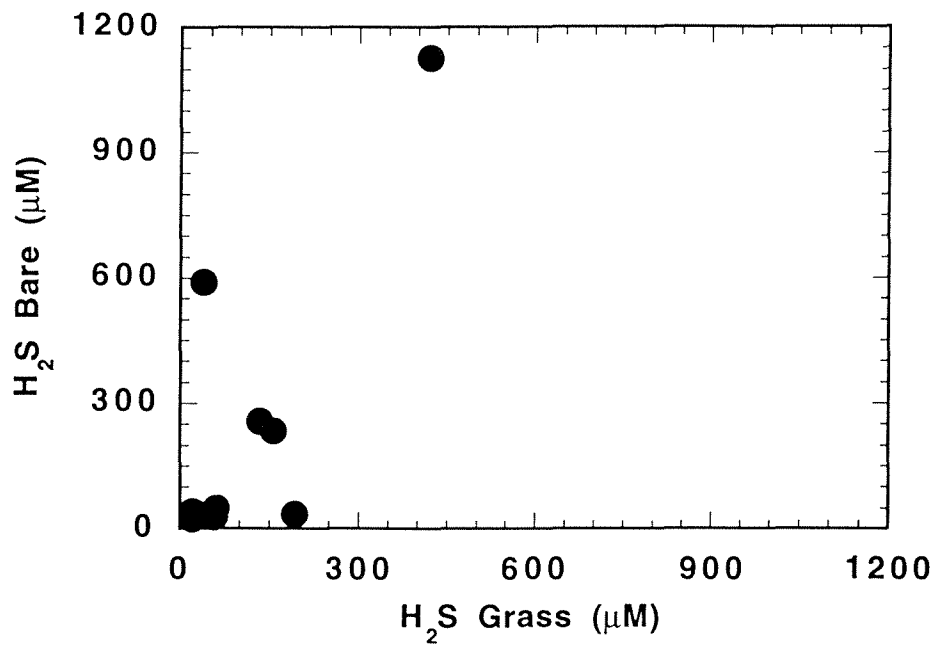


Figure 8. The relationship between pore water hydrogen sulfide concentrations in sediments covered by seagrass and in bare areas. Note that these data are all from about 8 to 10 cm depth.

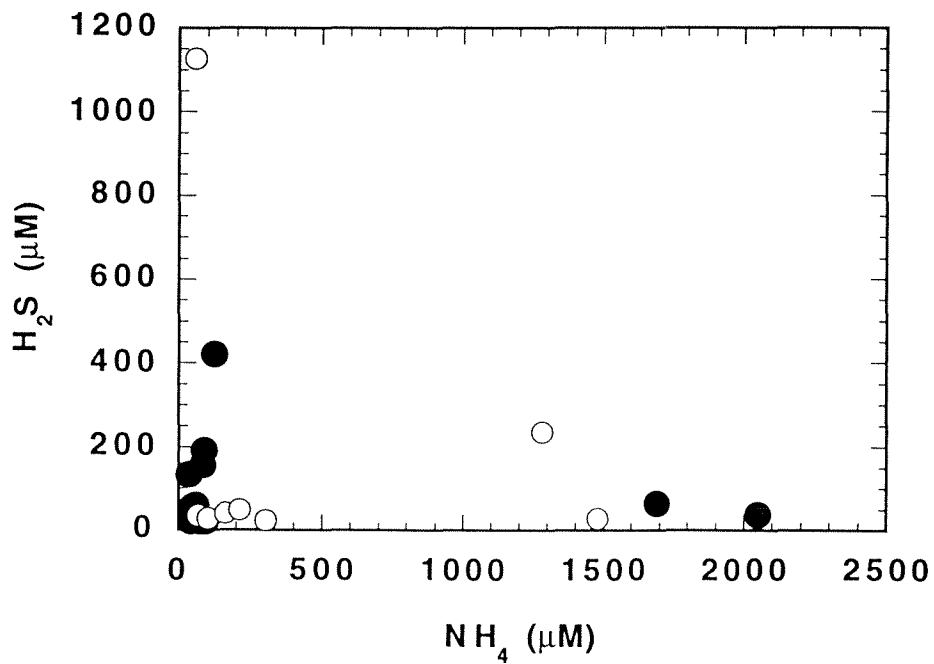


Figure 9. The relationship between pore water ammonium and hydrogen sulfide concentrations in sediments covered by seagrass (solid circles) and in bare areas (open circles).

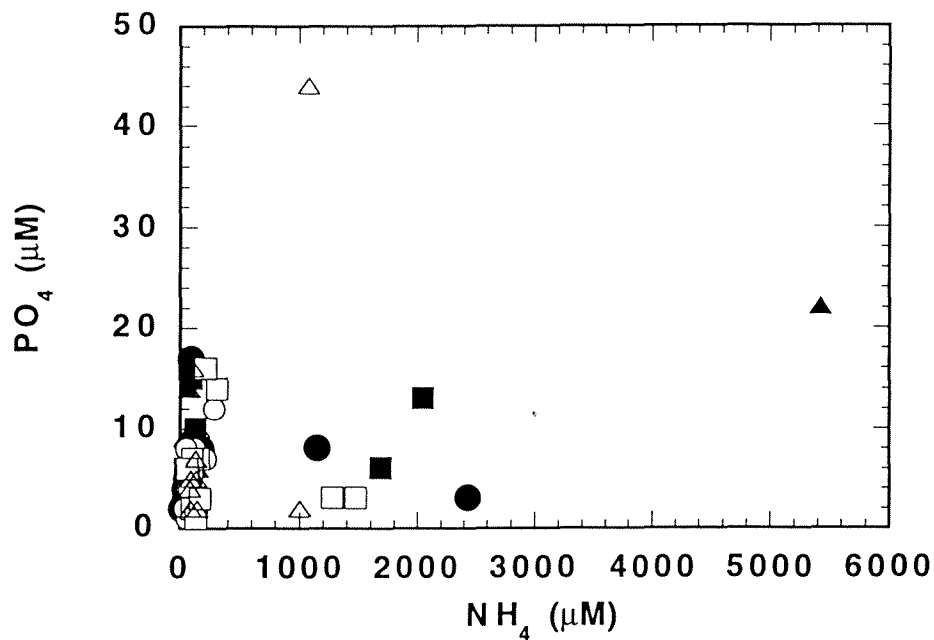


Figure 10. Dissolved phosphate versus dissolved ammonium. Circles 0-2 cm; squares 6-8 cm; triangles 18-20 cm. Solid symbols are for sediments covered with seagrass and open symbols are for sediments from bare areas.

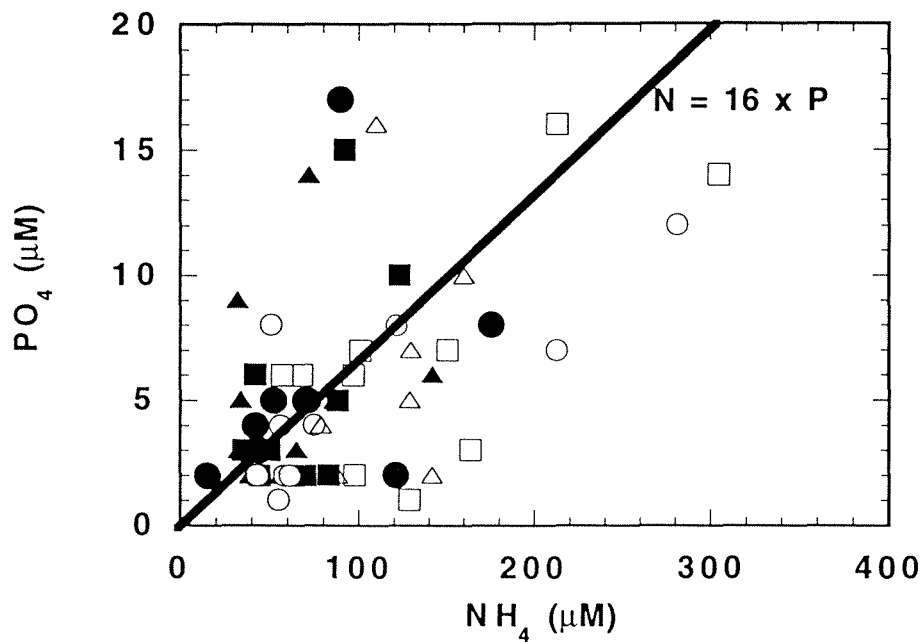


Figure 11. Expanded plot of dissolved phosphate versus dissolved ammonium. Circles 0-2 cm; squares 6-8 cm; triangles 18-20 cm. The line of $\text{N} = 16 \times \text{P}$ is for the Redfield ratio of marine organic matter. Solid symbols are for sediments covered with seagrass and open symbols are for sediments from bare areas.

remain in the same approximate phosphate concentration range but show substantially elevated ammonium concentrations. There also appears to be no strong dependence on whether an area is covered with seagrass or bare in these relationships. The expanded view of the low concentration field data (Fig. 11) shows that, although there is considerable scatter, many of the pore waters have a reasonably close N:P ratio to that of the Redfield ratio for marine organic matter. Again there is no apparent strong difference for pore waters from beneath seagrass beds and bare sediments.

Dissolved organic carbon (DOC) concentrations in bare versus seagrass covered sediments are shown in Figure 12. For most sites, there are relatively similar concentrations of DOC in bare and seagrass covered areas. However, for several sites DOC is substantially higher in the root zone of sediments from the seagrass beds. Dissolved hydrogen sulfide and ammonium concentrations have been plotted against DOC in Figure 13 (note NH_4 and DOC 6 to 8 cm; H_2S 8 to 10 cm). The elevated H_2S and NH_4 values found in a few samples are also associated with moderate ($> \sim 3000 \mu\text{M}$) to high DOC values. This probably reflects greater biologic metabolism occurring within these sediments.

Urea is at exceptionally high concentrations relative to ammonium in many sediments and may represent an important component of nitrogen in the Laguna Madre ecosystem that has not previously been considered. Dissolved iron and manganese are at very low (generally $< 10 \mu\text{M}$) concentrations in pore waters throughout the area sampled. The extent of sulfate reduction in pore waters is also small with usually less than a 5% depletion relative to Cl occurring. This low extent of sulfate reduction reflects a limitation of metabolizable organic carbon for sulfide production rather than the availability of dissolved sulfate.

Relationships Between Solid and Dissolved Components

Although a very large number of parameters could be compared from the numerous analytic data, only those most probable to be of significance to the relationship between seagrasses and sediment geochemistry will be examined here. The focus will largely be on the relation of solid sedimentary organic-C concentration and related dissolved products of its remineralization. Figure 14 shows the relationships between H_2S and organic-C, and DOC and organic-C for sediments beneath bare areas and seagrass beds (note organic-C and DOC 6 to 8 cm; H_2S 8 to 10 cm). Although the data contributing to trends at higher concentrations are rather limited and, therefore must be treated with caution, it appears that there are close to linear trends between H_2S and organic-C, that are quite

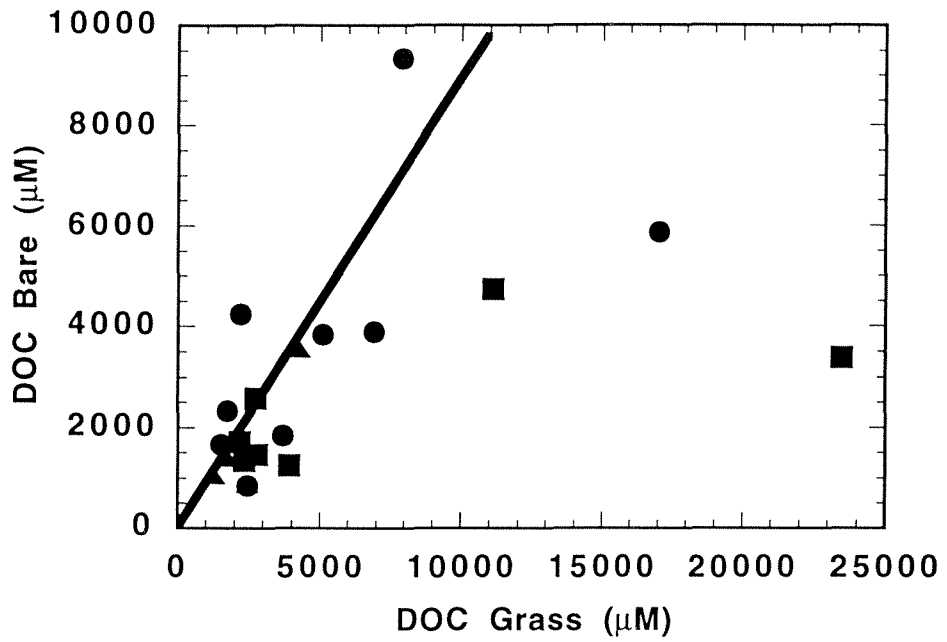


Figure 12. Dissolved organic carbon (DOC) concentrations in bare versus seagrass covered sediments. Line is for a 1:1 ratio for paired sites. Circles 0-2 cm; squares 6-8 cm; triangles 18-20 cm.

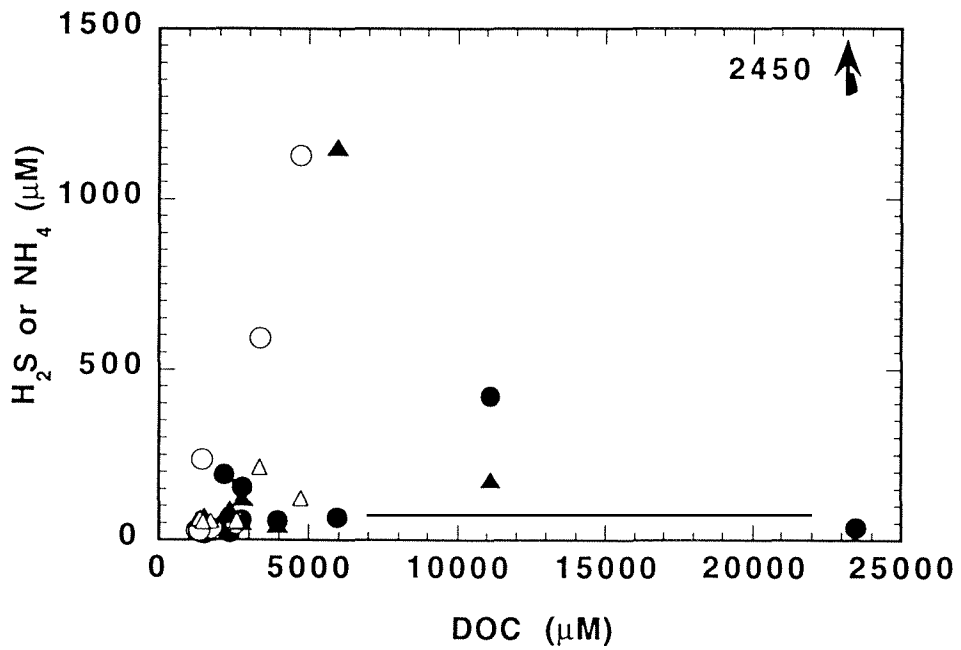


Figure 13. H_2S (circles) and NH_4 (triangles) concentrations versus DOC for seagrass (solid) and bare (open) areas.

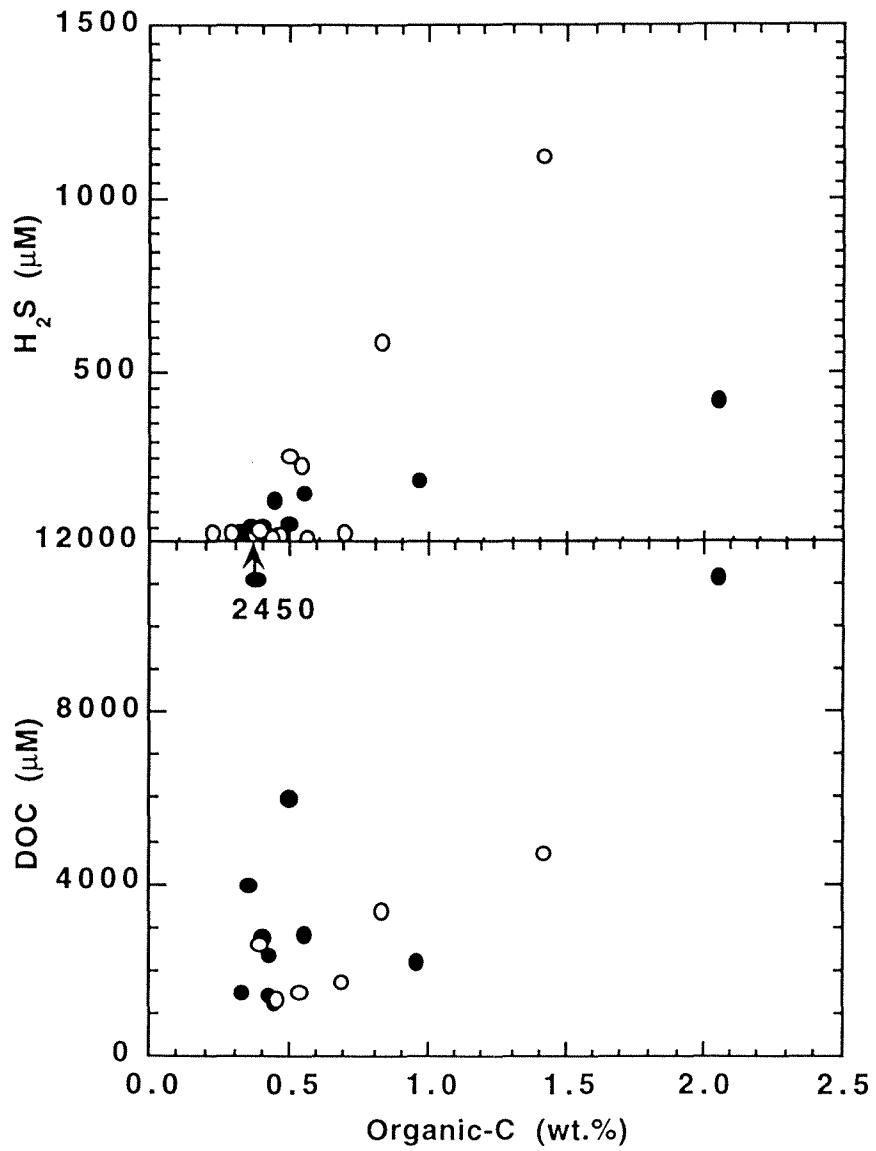


Figure 14. Plots of H₂S and DOC versus organic-C. Solid circles are from beneath seagrass beds and open circles are from beneath bare areas.

different for bare and seagrass-covered areas. Although a number of explanations are possible, two attractive ones are that supply of O_2 to seagrass sediments is depressing H_2S in these sediments or that the organic matter in these sediments is more resistant to metabolism by sulfate reducing bacteria. With the exception of the always troubling one very high-DOC point, there also is a general trend for increasing DOC with increasing organic-C. However, there does not appear to be a major difference in trends for bare and grass areas. No similar trend was observed between NH_4 and organic-C. The relationship in the sulfide system between dissolved hydrogen sulfide and total reduced inorganic sulfur (TRS) is presented in Figure 15. Most data clustered at very low values for both parameters. However, in bare areas there is a major increase in H_2S at a value for TRS of about $6 \mu\text{mol/g}$.

Discussion

For most samples, analytic values tend to be largely clustered over a narrow and often quite low range of values. After examining our current data base in light of the objective of this study, to determine the relationship between seagrass beds in Laguna Madre and sediment geochemistry, it was decided to focus on the parameters of fraction of solids in the $<63 \mu\text{m}$ size range, weight fraction organic-C, and TRS, NH_4 , PO_4 , DOC and H_2S concentrations. Based on the previously described relationships and figures "normal" ranges for these parameters were chosen for Laguna Madre sediments. They are : $<50 \text{ wt.}\%$ silt and clay fraction ($<63 \mu\text{m}$); $<1 \text{ wt.}\%$ organic-C; $<8 \mu\text{mol/g}$ TRS; $<500 \mu\text{M}$ NH_4 , , $<12 \mu\text{M}$ PO_4 , $<4000 \mu\text{M}$ DOC; and $<200 \mu\text{M}$ H_2S (the value above which it may negatively influence seagrasses). Samples with values outside these limits are summarized in Table 4 and represent "anomalous" sediments for this area. It is important to note that this terminology of "normal" is based on the observation that about 95% of the data fall within the above ranges. However, the proportion of sites having at least one data value out of the "normal" range is higher due to the large number of analyses per site.

The percent "anomalous" values for the various parameters are: grains size 21%; organic-C 10%; TRS 5%; NH_4 13%; PO_4 13%; DOC 26%; and H_2S 21%. If the spoil bank (COE sites 9 and 10, our station 26) and the nearby site which is also in the vicinity the Arroyo Colorado (COE sites 11 and 12, our station 25) are dropped from consideration, then the percent anomalous grain size drops to 5%. 69% of the anomalous DOC values are in grassbeds, none of which are *Thalassia* beds, whereas all but 1 (80%) the anomalous H_2S values are in bare areas. An interpretation of this observation is that the influence of the seagrasses is to elevate DOC, possibly as exudates, and keep H_2S down by pumping oxygen into the sediment. The composition of "typical" Laguna Madre sediments does not appear to be strongly influenced by the presence or absence of seagrass

beds. It is of central importance to the objectives of this study that these sediments contrast sharply with those found in dredged channels. Average values from six sites, 3 in lower and 3 in upper Laguna Madre, are 82% <63 μm grain size fraction, 1.9 wt. % organic-C and 2957 μM NH_4 . They are thus much finer grained and contain roughly double the organic-C and 6 times the NH_4 as the upper limits for the "typical" sediments. These major compositional differences raise the possibility that deposition of channel maintenance dredged sediments in seagrass areas has the potential to significantly alter the sedimentary environment and this may impact the vitality of grassbeds. The observation that an old dredge deposit had, with the exception of grain size, largely evolved into a geochemical composition similar to most other Laguna Madre sediments is at least suggestive that with time recolonization of such areas is possible.

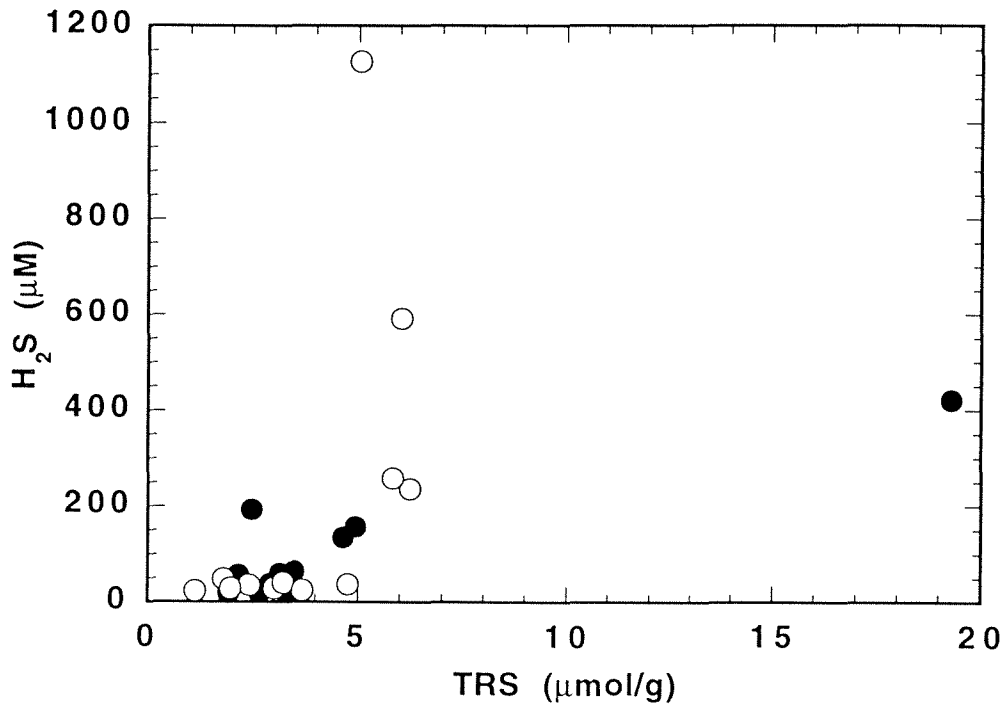


Figure 15. The relationship between dissolved hydrogen sulfide and total reduced inorganic sulfur. Solid circles are from beneath seagrass beds and open circles are from beneath bare areas.

Table 4. Summary of samples whose data falls outside prescribed "normal" ranges. L = Lower Laguna Madre; U = Upper Laguna Madre; T = Thalassia; S = Syringodium; H = Halodule.

COE#	Station	Depth	<63 μ m	Org-C	TRS	NH4	PO4	DOC	H2S
1	30 grass, L, T	0 to 2		1.41	8.35				
5	28 grass, L, T	0 to 2		1.30					
9	26 grass, L, S spoil bank	6 to 8	83						
		16 to 18	86						
10	26 bare, L spoil bank	0 to 2	53						
		6 to 8	81						
		17 to 19	96						
11	25 grass, L, S	0 to 2	60				17		
		6 to 8	69				15		
		18 to 20	77				14		
12	25 bare, L	0 to 2	53						
		6 to 8	65						
		18 to 20	93				16		
13	24 grass, L, S	0 to 2					6939		
14	24 bare, L	6 to 8						235	
15	22 grass, L, S	0 to 2	84	5.41	9.25			7920	
		6 to 8		2.05	19.32			11126	420
		18 to 20						4279	
16	22 bare, L	0 to 2		1.27				9321	
		6 to 8		1.42			14	4721	1125
17	20 grass, U, H	0 to 2				2440			
		6 to 8				2050	13	23496	
		16 to 18				5430	22		
18	20 bare, U	6 to 8	55				16		591
		16 to 18	81	1.28		1082	44	5260	
19	18 grass, U, H	0 to 2					5125		
20	18 bare, U	6 to 8				1480			
21	16 grass, U, H	0 to 2					17046		
22	16 bare, U	0 to 2		1.56				5849	
		6 to 8				1280			257
		18 to 20				1001			
23	13 grass, U, H	0 to 2		1.13		1150		5246	
		6 to 8				1690		5975	

Part 2: Sediment Geochemistry at "Super" Sites

Sampling and Data

Fortunately, largely at the urging of Dr. Eldridge, four sites were chosen for detailed depth profiles within sediments to better understand diagenetic processes and provide more detailed information for construction of seagrass-sediment interaction models. These sites were at seagrass beds representing each of the three species of seagrasses in Laguna Madre and a bare area. Multiple cores were collected at each site, some of which were frozen for subsequent analyses and others that were processed immediately for certain pore water components such as H_2S (see previous section). Where possible (3 of 4 sites), cores long enough for profiles down to 24 cm were taken. Data are presented in tables 5 and 6.

Results

There is a strong trend at all sites of decreasing porosity with depth indicating relatively rapid compaction of the sediment. The very low porosities in lower parts of the cores made extraction of pore waters in sufficient volume for all analyses often impossible. The silt and clay grain size fraction generally exhibited wide variations over short depth intervals indicating highly non-steady-state deposition, with sporadic storms (and perhaps dredging operations) causing these major variations. In the *Thalassia* and *Halodule* sites both organic and carbonate carbon exhibited major decreases with depth, probably as the result of diagenesis. Organic-C behaved similarly at the *Syringodium* site, but carbonate-C showed no major depth trends at the *Syringodium* and bare sites, and organic-C showed no distinctive depth trend at the bare site. One of the more interesting observations is that TRS instead of increasing with depth is highest near the sediment-water interface and that AVS generally makes up a much higher proportion of TRS than in most sediments.

Pore water profiles for dissolved NH_4 and H_2S are presented in Figure 17. In the seagrass beds there are elevated values of NH_4 and H_2S near the sediment-water interface in the root zone, followed by a major decrease in their concentrations below the root zone. This is probably indicative of elevated levels of biologic activity in the root zone. However, the major decreases in NH_4 and H_2S concentrations below this zone are quite unusual and indicate a major decrease in diagenetic activity. The major increases in NH_4 and H_2S with depth in the sediment from the bare area are fairly typical of what is commonly observed in anoxic marine sediments. These very different profiles from the seagrass bed sediments and bare area sediment provide important information for constructing models of sediment-seagrass interaction and how seagrasses may act

to "condition" sediments. There is only a slight extent of sulfate reduction in these sediments and the concentrations of dissolved iron and manganese are also low.

Table 5. "Super" site solid analytical results.

	V frac.	wt. %				μmol/gdw				
SS-Thal 25										
Depth	φ	<63 μm	Org-C	CaCO ₃	TRS	AVS	CD-Fe	HCl-Fe	CD-Mn	HCl-Mn
0 to 2	0.64	28	0.65	27.16	11.02	5.43	5.24	30.9	<0.25	1.54
2 to 4	0.63	26	0.58	20.41	9.98	4.92	5.29	31.5	<0.25	1.49
4 to 6	0.56	28	0.59	10.58	1.67	1.51	2.63	31.3	<0.25	1.01
6 to 8	0.51	32	0.57	8.25	1.94	1.69	1.64	28.8	<0.25	0.90
8 to 10	0.49	33	0.42	9.91	1.75	1.53	1.20	47.8	<0.25	1.22
10 to 12	0.47	35	0.39	8.91	1.57	1.33	0.77	43.6	<0.25	1.02
14 to 16	0.51	32	0.32	11.33	1.58	1.38	0.90	52.7	<0.25	1.33
18 to 20	0.46	31	0.23	8.08	1.06	0.69	0.68	36.2	<0.25	1.04
22 to 24	0.40	25	0.21	6.33	1.58	1.26	0.49	31.4	<0.25	1.10

SS-Hal 26

Depth	φ	<63 μm	Org-C	CaCO ₃	TRS	AVS	CD-Fe	HCl-Fe	CD-Mn	HCl-Mn
0 to 2	0.66	36	0.84	18.66	5.20	2.92	1.77	32.3	<0.25	1.35
2 to 4	0.61	27	0.67	26.66	3.88	2.15	1.39	23.2	<0.25	1.13
4 to 6	0.52	26	0.50	18.41	3.09	1.54	0.87	19.5	<0.25	0.93
6 to 8	0.49	12	0.34	11.08	0.86	0.09	0.56	20.4	<0.25	0.85
8 to 10	0.60	14	0.78	7.16	3.59	2.29	1.18	42.3	<0.25	2.43
10 to 12	0.52	19	0.37	3.25	5.81	3.06	0.52	29.9	<0.25	1.47
14 to 16	0.40	8	0.10	2.42	2.61	1.26	0.27	18.5	<0.25	0.66
18 to 20	0.40	7	0.06	3.42	1.41	0.29	<0.25	20.3	<0.25	1.21
22 to 24	0.39	7	0.10	10.50	1.84	0.65	<0.25	12.9	<0.25	0.58

SS-Syr27

Depth	φ	<63 μm	Org-C	CaCO ₃	TRS	AVS	CD-Fe	HCl-Fe	CD-Mn	HCl-Mn
0 to 2	0.66	21	0.78	26.99	8.57	4.06	2.32	19.4	<0.25	0.83
2 to 4	0.63	12	0.77	25.66	2.06	1.03	2.36	17.5	<0.25	0.75
4 to 6	0.55	18	0.52	16.91	3.49	1.29	1.52	10.9	<0.25	0.55
6 to 8	0.57	9	0.51	18.66	3.84	1.85	1.36	18.4	<0.25	0.79
8 to 10	0.62	36	0.77	24.66	5.22	3.27	3.55	37.1	<0.25	1.44
10 to 12	0.59	27	0.67	ND	3.69	2.13	3.30	27.7	<0.25	1.11

SS-Bare 28

Depth	φ	<63 μm	Org-C	CaCO ₃	TRS	AVS	CD-Fe	HCl-Fe	CD-Mn	HCl-Mn
0 to 2	0.75	44	1.51	10.08	13.56	6.59	4.68	25.3	<0.25	0.50
2 to 4	0.47	69	1.71	5.50	7.89	4.36	4.20	25.2	<0.25	0.38
4 to 6	0.72	29	1.36	18.83	8.67	4.43	3.12	21.3	<0.25	0.45
6 to 8	0.63	16	0.72	39.32	11.71	5.01	1.76	9.8	<0.25	0.33
8 to 10	0.52	8	1.54	30.24	3.14	1.46	0.70	8.6	<0.25	0.62
10 to 12	0.53	32	0.34	19.99	1.87	0.97	0.41	6.6	<0.25	0.63
14 to 16	0.42	7	0.18	7.16	3.51	1.69	0.49	6.1	<0.25	0.60
18 to 20	0.44	10	0.30	21.07	2.41	0.74	0.60	8.2	<0.25	0.70
22 to 24	0.40	5	0.10	32.32	3.90	1.32	<0.25	3.1	<0.25	0.34

Table 6. Concentrations of pore water components at "super" sites.

	μM					mM		μM	mM	μM		
SS-Thal												
Depth	NH4	NO3	Urea	PO4	SiO2	DOC	DIC	H2S	SO4	Cl	Fe	Mn
0 to 2	61	7	28	9	117	6.40	4.71	7	28.4	572	2.87	0.7
2 to 4	70	5	16	8	93	8.82	5.36	159	28.2	560	2.61	7.9
4 to 6	43	19	28	44	145	6.25	6.10	61	27.8	562	2.61	5.1
6 to 8	52	3	26	5	103	8.63		64	27.8	561	3.12	2.0
8 to 10	24	13	30	15	160		3.83	55			2.87	0.9
10 to 12												
14 to 16								46				
18 to 20	37		35	9	32			49				
22 to 24	30	3	57	6	95							

SS-Hal												
Depth	NH4	NO3	Urea	PO4	SiO2	DOC	DIC	H2S	SO4	Cl	Fe	Mn
0 to 2	269	2	80	18	365	136.86	4.80	72	32.8	598	2.61	0.7
2 to 4	93	3	50	2	164	9.42	4.85	161	31.6	605	2.87	1.5
4 to 6	46	1	41	1	230	3.45	4.41	92	29.8	576	5.68	3.9
6 to 8	52	1	41	1	55	2.89	3.90	101	29.6	575	1.59	1.3
8 to 10	62	1	45	1	37	3.11	4.07	58	29.0	564	1.33	<0.5
10 to 12	65	1	51	3	41	1.93	4.37	30	26.7	524	1.84	0.7
14 to 16	52	1	49	1	36		2.72	47			1.59	1.5
18 to 20								46			0.82	1.4
22 to 24							2.60	45			0.82	0.9

SS-Syr												
Depth	NH4	NO3	Urea	PO4	SiO2	DOC	DIC	H2S	SO4	Cl	Fe	Mn
0 to 2	132		9	3	108		3.59	62	34.5	634	1.33	0.5
2 to 4	210		113	5	72		4.23	132	34.2	634	1.84	1.4
4 to 6	135		7	4	74		4.79	161	34.7	641	1.84	1.4
6 to 8	92	1	7	7	142	4.15		49	34.3	635	1.59	3.9
8 to 10	51		7	6	92	3.55		29	34.1	630	2.36	10.8
10 to 12	66		10	6	153	4.08	5.01	69	33.9	628	1.84	2.8

SS-Bare												
Depth	NH4	NO3	Urea	PO4	SiO2	DOC	DIC	H2S	SO4	Cl	Fe	Mn
0 to 2	1		11	7	113	3.62		170	34.8	637	1.33	0.7
2 to 4	73	1	17	13	116	1.52	4.90	21	36.1	662	0.82	0.7
4 to 6	155	1	14	14	138	2.57	3.81	27	34.5	643	1.33	0.6
6 to 8	188	2	17	19	159	3.86	4.12	45	28.4	544	0.82	0.7
8 to 10	331		15	11	61	4.22	3.90	115	33.4	634	1.59	<0.5
10 to 12	344		15	22	357		3.16	353	31.1	618	1.59	<0.5
14 to 16	499	1	13	13	50			241			4.91	2.1
18 to 20								275			1.84	0.8
22 to 24	769		10	16	357	4.67		593			4.66	0.7

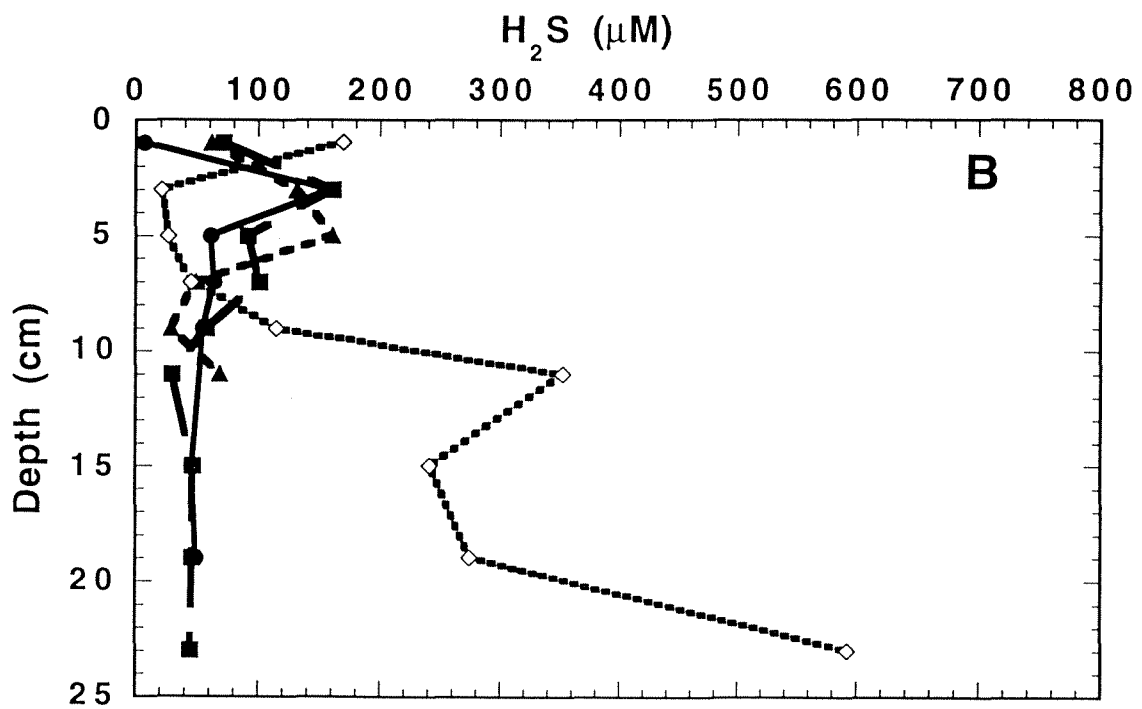
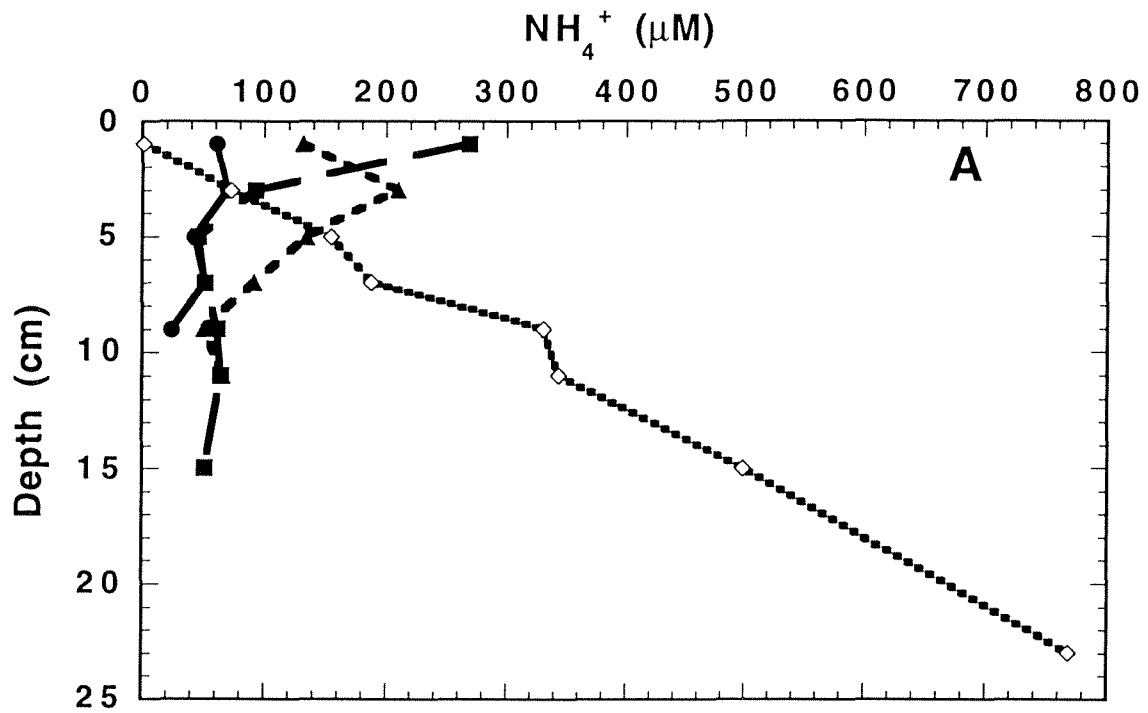


Figure 16. Depth profiles of dissolved ammonium (A) and hydrogen sulfide (B). Thalassia = solid circles; Halodule = solid squares; Syringodium = solid triangles; Bare = open diamonds.

Part 3: Sediment Geochemistry at Time Series Stations

Sampling and Data

The sampling at the time series stations was undertaken primarily to determine seasonal changes in Laguna Madre seagrasses and sediment geochemistry. Originally it was planned that this would be done quarterly for a year. However, it was decided to do the sampling in coordination with the Blucher platform sites which did not correspond to the previously described "super sites" and thus eliminated the early summer quarter. Additionally one site (ULM1) turned out to be a relatively deep water hard bare sand that could not be well sampled for sediment geochemistry. Finally, as will be subsequently discussed, some of the sites were extremely spatially heterogeneous making it impossible to unambiguously discern between spatial and temporal change. In spite of these difficulties, the large amount of data collected have proven extremely useful for refining and testing the below ground model, which was the primary purpose for making these measurements. The sampling and analytical procedures previously described were used for this part of the project as well.

Results

Analytic results are presented on a monthly basis for September, 1996, and January and May 1997, in Table 7. Monthly depth profiles for 3 parameters are plotted for each sampling site in figures 18 to 22. The 3 parameters chosen were grain size, which is relatively insensitive to diagenesis and therefore a good first order indicator of heterogeneity, and dissolved ammonium and hydrogen sulfide which are of primary interest with respect to sediment-seagrass interactions. Because these data were primarily used in model development, only a limited commentary on them will be made here.

LLM1: This site was a bare bottom sand which contained an increasing sand and silt fraction with depth. Grain size was moderately reproducible for the different sampling trips as were the fractions of organic-C and calcium carbonate. Ammonium was modest and hydrogen sulfide very low in September and May, but both exhibited a major increase in the upper sediment in May. Surprisingly, the opposite appears true for DOC and DIC.

LLM2: This site was in a *Thalassia* bed. The September and May samples were sandy with generally close to the same sand fraction. The January sample was dominated by the silt and clay grain size fraction. In spite of this observation the September and May samples have similar ammonium profiles, which are high in the root zone, and sulfide profiles, which are universally very low. There is a huge increase (to about 3000 μM) in near surface sulfide concentrations with

a concurrent drop of ammonium to about half its value at other sampling times in May. The probable explanation for this is the presence in May of a large “tumbleweed” algal mat lying on the seagrass bed. The extreme sulfide concentrations generated may provide an explanation for the production of bare areas in seagrass beds and its relatively rapid penetration throughout the root zone provided very valuable data for modeling the potential influences of dredge deposits. These elevated sulfide concentrations were accompanied by a major drop in pH, huge increase in DIC and surprisingly a very large drop in DOC.

LLM3: This site was in a *Syringodium* bed. Cores were vertically fairly homogeneous in sand fraction but exhibited a variation from almost pure sands to only about 60 wt.% sand fraction at different sampling times. September and January ammonium profiles were remarkably similar with a large maximum in the center of the root zone which was lacking in the May core. Sulfide concentrations were moderate (<25 μM) to low.

ULM2: This site was in a *Halodule* bed and extremely heterogeneous in grain size distributions with close to pure sands and muds being found on a small (meters) scale distribution and even within some cores (one ranged from no to 80 wt.% sand). Ammonium concentrations were remarkably similar and that the sandiest sediment had by far the highest (>800 μM) sulfide concentration in the upper part of the core. Given the observation at LLM2 of the impact of the mobile “tumbleweed” algal mats, it is possible that one had recently impacted the area at the time of the September sampling.

ULM3: This was a second bare site and suffers from a similar heterogeneity in grain size distribution to that observed at ULM2. Ammonium concentrations were similar throughout the sampling period and to those observed at the other bare site (LLM1). The January and May sulfide concentrations were also similar to LLM1, however, September sulfide concentrations were much greater than at LLM1 and highly variable with depth.

Table 7. Time series data.

September		<63µm wt%	φ V frac	Org-C wt%	CaCO3 wt%	pH Han.	DIC mM	H2S µM	DOC mM	NH4 µM	NO3 µM	NO2 µM	Urea µM	PO4 µM	SiO3 µM	
LLM1	0	0.13	0.50	0.13	11		4.08	<1	7.6	229	2.8	0.3	9.9	5.9	81	
	2	0.28	0.58	0.39	16		4.38	1	9.8	377	1.9	0.0	10.9	6.1	95	
	4	0.10	0.50	0.23	12		2.98	1	8.8	364	0.9	0.1	10.7	7.3	77	
	6	0.10	0.48	0.27	12		2.79	<1	8.3	326	0.7	0.2	12.9	0.1	142	
	8-	0.13	0.50	0.72	12		2.79	<1	6.6	305	2.2	0.2	12.5	5.6	84	
	10-	0.10	0.46	0.18	24		3.12	1	4.6	204	0.6	0.1	6.5	3.0	99	
	14-	0.25	0.53	0.70	21		3.59	<1	4.2	162	1.6	0.2	3.3	3.6	76	
	18-	0.41	0.52	0.57	17		4.40	1	4.6	184	6.8	0.1	2.8	4.6	134	
	22-	0.33	0.47	0.43	10		4.62	24	4.6	365	0.5	0.3	8.6	2.2	136	
	28-	0.46	0.47	0.43	10		5.49	4	3.3	177	0.7	0.1	5.6	1.2	128	
LLM2	0	0.24	0.71	1.60	21		4.84	1	36.6	513	0.7	0.3	22.9	38.3	86	
	2	0.39	0.66	1.16	11		4.28	19	53.3	613	2.2	0.2	73.4	52.2	174	
	4	0.25	0.61	1.03	8		4.33	8	58.0	551	2.2	0.2	29.0	30.5	137	
	6	0.36	0.52	0.64	8		4.88	3	54.0	546	1.2	0.2	25.1	15.9	149	
	8-1	0.39	0.48	0.62	8		5.52	3	48.6	493	1.1	0.3	13.5	9.6	108	
	10-1	0.36	0.48	0.63	9		6.20	<1	32.1	270	2.3	0.0	3.5	5.5	107	
	14-1	0.41	0.47	0.43	8		6.67	<1		104	0.3	0.4	3.3	1.5	82	
	18-2	0.37	0.41	0.31	7		5.57	<1	17.9	383	0.2	0.1	2.0	4.8	67	
	22-2	0.27	0.39	0.20	7		5.58	<1	10.5	118	0.3	0.0	0.2	1.1	84	
	28-3	0.25	0.37	0.44	4			<1	8.4	76	0.6	0.1	2.4	1.9	77	
LLM3	0-	0.09	0.38	0.31	2		3.89	6		444	0.7	0.4	0.5	54.9	206	
	2-	0.05	0.41	0.26	1		4.25	21		205	0.4	0.2	36.2	35.1	173	
	4-	0.07	0.41	0.28	3		4.09	4	72.1	566	5.6	0.3	37.9	18.8	171	
	6-	0.07	0.38	0.31	4		3.64	7	67.0	558	0.8	0.2	18.7	6.7	119	
	8-1	0.03	0.40	0.12	5		3.67	8	49.6	554	1.5	0.2	23.2	22.7	165	
	10-1	0.04	0.37	0.12	6		3.57	5	26.3	475	1.5	0.2	16.2	19.5	121	
	14-1	0.01	0.39	0.08	7		3.16	1		219	0.9	0.4	0.0	1.8	65	
	18-2	0.06	0.38	0.17	11		2.87	<1		190	0.4	0.0	0.3	2.7	60	
	22-2	0.09	0.41	0.17	10		3.22	2		139	1.0	0.1	0.4	1.9	72	
	28-3	0.11	0.42	0.21	8		2.87	10		124	3.0	0.2	8.8	1.5	40	
ULM2	0-	0.17	0.64	0.92	0		4.87	553	22.4	473	4.8	0.2	19.3	103.1	219	
	2-	0.19	0.59	0.91	3		6.39	596	24.4	503	6.6	0.1	19.6	78.9	181	
	4-4	0.21	0.62	1.09	0		7.84	732	30.7	143	1.2	0.3	25.1	81.6	195	
	6-1	0.18	0.61	1.08	8		6.18	737	24.9	538	1.4	0.1	21.1	60.4	173	
	8-10	0.23	0.55	1.24	2		4.82	240	18.3	514	2.3	0.1	24.3	39.1	145	
	10-11	0.08	0.49	0.38	10		5.83	240	20.0	542	0.5	0.5	42.1	34.8	234	
	14-16	0.04	0.41	0.28	52				227		264	2.1	0.1	8.9	1.2	78
	18-20	0.01	0.35	0.24	74				256	5.5	235	1.1	0.5	4.9	2.4	84
	22-24	0.02	0.34	0.27	66				231							
	28-30	0.02	0.38	0.17	4				226							
ULM3	0-2	0.43	0.72	0.84	29		3.64	397		511	0.7	0.3	19.7	21.6	173	
	2-4	0.42	0.62		19		3.34	392		370	1.0	0.1	8.8	22.9	112	
	4-6	0.37	0.61	1.92	22		3.00	276		373	1.8	0.1	11.0	16.0	129	
	6-8	0.58	0.69	1.50	16		3.21	233			345	1.2	0.2	8.3	9.1	109
	8-10 cm	0.75	0.72	1.40	17		3.21	17	5.6	356	1.4	0.2	6.6	7.0	121	
	10-12 cm	0.85	0.74	1.96	13		3.00	17		308	0.8	0.4	4.6	5.7	123	
	14-16 cm	0.86	0.78	2.00	10		3.07	263			227	0.9	0.4	3.6	4.3	149
	18-20 cm	0.83	0.76	1.65	18		3.27	37			251	1.2	0.2	1.4	6.4	147
	22-24 cm	0.86	0.78	1.93	19		3.51	366	3.3	297	1.9	0.0	0.3	6.9	285	
	28-30 cm						4.36	289			364	1.9	0.1	0.0	6.7	340

January

Station Number	Depth	<63µm wt%	φ V frac	Org-C wt%	CaCO3 wt%	pH Han.	DIC mM	H2S µM	DOC mM	NH4 µM	NO3 µM	NO2 µM	Urea µM	PO4 µM	SiO3 µM
LLM1	0-2 cm	0.31	0.48	0.13	12	7.88	3.46	<1	8.3	340	3.1	0.6	16.8	6.2	126
	2-4 cm	0.35	0.48	0.13	12	8.05		<1		256	3.0	1.5	11.0	3.2	72
	4-6 cm	0.36	0.49	0.15	16	8.00		<1		288	3.1	1.4	15.3	3.9	68
	6-8 cm	0.43	0.51	0.22	14	8.11		<1		245	1.7	1.2	14.2	3.4	66
	8-10 cm	0.44	0.52	0.35	13	8.09		<1	6.2	310	0.8	1.2	15.4	4.7	74
	10-12 cm	0.36	0.47	0.14	15	8.01	3.00	<1	6.1	243	1.0	1.2	9.1	2.8	67
	14-16 cm	0.57	0.53	0.42	17	7.87	3.72	1	4.3	130	3.8	0.4	1.8	4.4	77
	18-20 cm	0.47	0.50	0.47	16	7.81	3.59	<1	3.6	170	3.7	0.5	3.7	4.8	86
	22-24 cm	0.49	0.48	0.45	11	7.84	4.04	1	3.9	213	5.7	0.3	5.1	5.8	96
28-30 cm	0.60	0.53	0.42	10	7.75	4.38	<1	4.0	239	1.1	0.7	5.8	3.4	77	
LLM2	0-2 cm	0.72	0.72	0.89	18	7.66	3.54	<1	19.0	506	1.1	0.0	39.9	54.5	146
	2-4 cm	0.63	0.64	1.08	13	7.77	4.80	<1	25.4	532	0.6	0.4	46.6	56.3	140
	4-6 cm	0.61	0.59	1.07	9	7.74	6.38	19	36.0	540	1.1	0.2	31.6	67.9	60
	6-8 cm	0.55	0.55	0.72	10	7.78	6.48	<1	31.4	544	0.5	0.4	16.1	24.0	151
	8-10 cm	0.58	0.52	0.74	9	7.58	5.77	12	42.7	564	1.6	0.4	9.9	15.0	112
	10-12 cm	0.57	0.50	0.74	9	7.20	5.48	1	39.9	55	0.7	0.3	10.6	9.9	125
	14-16 cm	0.55	0.47	0.57	14	7.65	5.44	2	11.0	90	1.1	0.1	0.3	14.1	157
	18-20 cm	0.47	0.42	0.35	8	7.76	4.34	1	12.6	150	0.9	0.4	5.7	2.2	124
	22-24 cm	0.50	0.43	0.28	8	7.76	4.27	2	8.8	385	2.0	0.3	3.6	3.0	43
28-30 cm						7.82		<1	5.7	140	0.9	0.3	4.7	1.3	78
LLM3	0-2 cm	0.35	0.51	0.25	3	8.01	4.00	4	26.3	399	2.0	0.1	14.1	46.2	107
	2-4 cm	0.36	0.49	0.36	8	7.91		3	49.4	596	2.9	0.3	38.3	46.0	162
	4-6 cm	0.28	0.40	0.23	7	7.92	4.39	3	69.9	596	3.8	0.2	22.5	31.8	193
	6-8 cm	0.34	0.45	0.37	14	7.88	4.20	11	53.3	569	2.5	0.4	9.7	13.3	132
	8-10 cm	0.30	0.39	0.19	11	7.85	3.86	2	46.8	459	2.4	0.4	7.5	7.0	101
	10-12 cm	0.22	0.36	0.12	12	7.88	4.31		33.7	358	1.9	0.4	12.9	7.5	152
	14-16 cm	0.29	0.40	0.16	11	7.89	3.50			296	1.7	0.4	7.2	3.3	71
	18-20 cm	0.26	0.37	0.16	3	7.95				131	2.0	0.2	1.9	1.1	81
	22-24 cm	0.26	0.37	0.16	4	7.94				504	2.0	0.0	6.2	1.4	88
28-30 cm	0.28	0.41	0.15	4	7.96				108	1.9	0.0	9.8	1.0	32	
ULM2	0-2 cm	0.53	0.63	1.11	26	7.82	4.60	1	21.2	529	0.7	0.3	26.7	111.0	95
	2-4 cm	0.46	0.59	1.41	23	7.72	5.41	2	36.0	597	1.3	0.1	34.3	106.0	116
	4-6 cm	0.37	0.52	0.46	17	7.77	5.77	4	21.6	572	1.2	0.3	31.9	60.6	107
	6-8 cm	0.55	0.61	0.80	20	7.81	5.85	14	24.2	541	0.4	0.1	27.6	44.7	117
	8-10 cm	0.48	0.57	0.88	28	7.79	5.65	10	27.6	505	0.7	0.3	19.2	8.9	99
	10-12 cm	0.27	0.41	0.27	47	7.86	4.06	3	18.9	375	1.0	0.1	12.5	4.1	113
	14-16 cm	0.22	0.36	0.26	50	7.88		3	13.5	208	1.1	0.1	10.6	2.1	94
	18-20 cm	0.21	0.37	0.31	41	7.94		2	10.2	145	1.3	0.0	5.9	1.3	94
	22-24 cm	0.22	0.38	0.24	20			3	7.7	104	1.0	0.2	5.3	1.9	158
28-30 cm	0.21	0.37	0.23	20			11		58	2.2	0.1	5.0	1.4	53	
ULM3	0-2 cm	0.90	0.83	1.02	18	7.82	4.78	6	11.0	326	2.0	0.4	17.2	34.3	102
	2-4 cm	0.73	0.76	1.16	12	7.73	4.97	3		398	0.9	0.4	15.6	43.1	111
	4-6 cm	0.65	0.70	1.23	28	7.85	3.45	5	11.0	384	0.7	0.3	14.2	36.2	111
	6-8 cm	0.72	0.70	0.78	27	7.89	4.10	7	9.3	300	1.2	0.2	8.0	14.0	118
	8-10 cm	0.70	0.68	0.99	19	7.96	3.58	7	7.0	226	0.9	0.5	6.3	9.6	112
	10-12 cm	0.72	0.69	1.12	17	7.93	3.83	4	7.2	199	1.1	0.1	4.2	6.1	91
	14-16 cm	0.84	0.76	1.49	19	7.93	4.07	4	8.3	258	0.3	0.1	3.8	5.7	99
	18-20 cm	0.95	0.83	1.96	21	7.98	4.09	1	5.4	220	2.2	0.6	4.8	6.1	92
	22-24 cm	0.87	0.83	1.79	22	7.95	4.37		3.8	166	1.2	0.4	2.2	4.2	365
28-30 cm	0.79	0.77	1.27	15	7.90	4.98			220	1.2	0.2	0.4	6.3	465	

May

Station Number	Depth	<63µm wt%	φ V frac	Org-C wt%	CaCO3 wt%	pH Han.	DIC mM	H2S µM	DOC mM	NH4 µM	NO3 µM	NO2 µM	Urea µM	PO4 µM	SiO3 µM
LLM1	0-2 cm	0.13	0.50	0.19	14	7.70	2.87	317	3.3	670	5.6	0.1	8.8	189.7	632
	2-4 cm	0.20	0.49	0.24	15	7.84	2.72	74	4.2	669	7.6	0.1	5.9	156.7	567
	4-6 cm	0.37	0.52	0.44	17	7.87		1	3.4	675	3.8	0.1	4.0	160.4	610
	6-8 cm	0.30	0.50	0.32	18	7.83	3.63	1	3.9	674	4.8	0.2	0.2	173.9	636
	8-10 cm	0.36	0.53	0.43	18	7.83	3.13	1	3.5	653	4.0	0.1	2.5	81.8	432
	10-12 cm	0.25	0.52	0.37	18	7.83	3.57	1	14.5	402	4.0	0.1	0.2	5.6	337
	14-16 cm	0.21	0.49	0.54	20	7.92	3.59	1	11.8	259	5.6	0.1	0.2	5.6	321
	18-20 cm	0.37	0.53	0.42	14	7.94	3.79	1	5.9	627	7.4	0.1	0.7	21.5	309
	22-24 cm	0.32	0.48	0.18	10	8.03	4.04		4.4	60	3.4	0.7	5.8	3.3	168
	28-30 cm	0.54	0.58	0.46	18		4.10	1	3.9	69	3.9	0.1	0.2	5.6	244
LLM2	0-2 cm	0.67	0.88	1.82	26	6.81	20.35	2872		294	7.2	1.8	10.3	5.2	149
	2-4 cm	0.27	0.64	0.88	17	7.00	25.90	2709		297	8.2	1.5	7.2	1.9	94
	4-6 cm	0.38	0.62	0.86	17	6.88	33.95	1638		215	6.9	1.3	6.9	4.7	85
	6-8 cm	0.38	0.52	0.79	11	7.10	30.94	2176	5.8	253	6.2	0.3	7.4	4.0	85
	8-10 cm	0.34	0.49	0.60	12	7.15	28.97	2300	3.8	180	7.1	0.4	5.3	4.6	123
	10-12 cm	0.36	0.48	0.69	9	7.38	20.41	1770	0.0	142	6.7	0.5	5.7	4.6	143
	14-16 cm	0.36	0.48	0.60	12	7.25	17.89	811	0.0	155	6.3	0.4	4.2	5.2	163
	18-20 cm	0.38	0.46	0.58	9				0.0	173	7.3	0.4	4.4	2.8	167
	22-24 cm	0.38	0.44	0.44	9	7.49	11.67	512	0.0	186	8.0	1.0	5.0	1.5	184
	28-30 cm	0.26	0.38	0.28	6	7.64	6.74	459	0.0	198	7.2	0.3	5.3	0.6	208
LLM3	0-2 cm	0.16	0.51	0.28	3	7.58	5.54		18.3	509	8.5	0.4	14.6	34.4	264
	2-4 cm	0.26	0.51	0.38	6		5.49	2	14.8	306	4.7	0.5	5.8	32.8	313
	4-6 cm	0.39	0.57	0.71	7	7.55	4.72	2	16.9	323	4.7	0.5	7.2	16.7	270
	6-8 cm	0.33	0.52	0.53	8	7.51	3.96	6	10.9	161	4.1	1.1	7.2	4.0	172
	8-10 cm	0.29	0.48	0.42	9	7.65	3.78	11	9.4	337	4.3	0.8	9.6	3.6	142
	10-12 cm	0.30	0.48	0.59	7	7.61	3.36	4	9.3	202	6.8	0.4	3.3	2.1	205
	14-16 cm	0.20	0.43	0.48	8	7.42	3.55	4	5.8	58	7.3	0.4	5.8	2.4	171
	18-20 cm	0.13	0.41	0.32	11	7.69	3.31	8	7.5	67	7.5	1.9	4.8	2.1	115
	22-24 cm	0.17	0.44	0.30	9	7.48	2.88	13							
	28-30 cm	0.12	0.46	0.25	2	7.39	0.00	23	3.9	29	5.5	1.7	8.6	1.4	105
ULM2	0-2 cm	0.30	0.71		11	7.82	3.62	37	26.3	542	6.5	0.7	24.5	86.8	177
	2-4 cm	0.25	0.62		6	7.77	4.23	81	26.8	487	7.1	0.5	17.6	55.0	166
	4-6 cm	0.50	0.69	0.80	21	7.91	3.88	7	15.8	287	7.6	0.4	13.0	14.3	145
	6-8 cm	0.73	0.78	0.66	23	8.04	3.90	4		194	8.0	1.4	9.7	6.9	100
	8-10 cm	0.79	0.82	0.35	22	7.99	4.70	4		214	8.5	2.4	10.5	3.8	88
	10-12 cm	0.95	0.84	0.40	43	7.92	3.50	5							
	14-16 cm	0.99	0.86	0.48	72	7.71		6							
	18-20 cm	0.78	0.78		28	7.71		85							
	22-24 cm	0.88	0.81		42	7.59		239							
	28-30 cm	0.55	0.72	0.16	32	7.50		461							
ULM3	0-2 cm	0.25	0.60	2.99	14	7.86	3.83	209	11.4	404	4.5	0.1	13.0	62.0	296
	2-4 cm	0.21	0.57	0.54	39	7.74	3.99	210	7.9	242	4.5	0.1	7.8	21.1	173
	4-6 cm	0.21	0.57	1.94	18	7.84	3.11	118	6.4	181	4.4	0.0	6.9	12.6	170
	6-8 cm	0.15	0.54	2.08	12	7.83	3.41	114	4.4	103	4.2	0.1	3.2	6.2	174
	8-10 cm	0.12	0.47	2.21	11	7.76	3.23	123	4.3	90	4.4	0.0	2.7	4.0	186
	10-12 cm	0.08	0.37	2.47	11	7.68	3.19	117	6.2	219	4.5	0.0	6.4	3.6	199
	14-16 cm	0.04	0.35	2.02	8		3.31		0.3	108	8.3	0.1	5.0	5.7	344
	18-20 cm	0.02	0.39	1.89	9	7.66	3.36		2.6	159	6.0	0.2	3.7	4.5	360
	22-24 cm	0.03	0.42	2.76	12		4.00		2.9	225	4.2	0.1	0.3	4.7	529
	28-30 cm	0.03	0.38	1.50	22		3.34		4.0	296	5.3	0.1	2.7	5.8	339

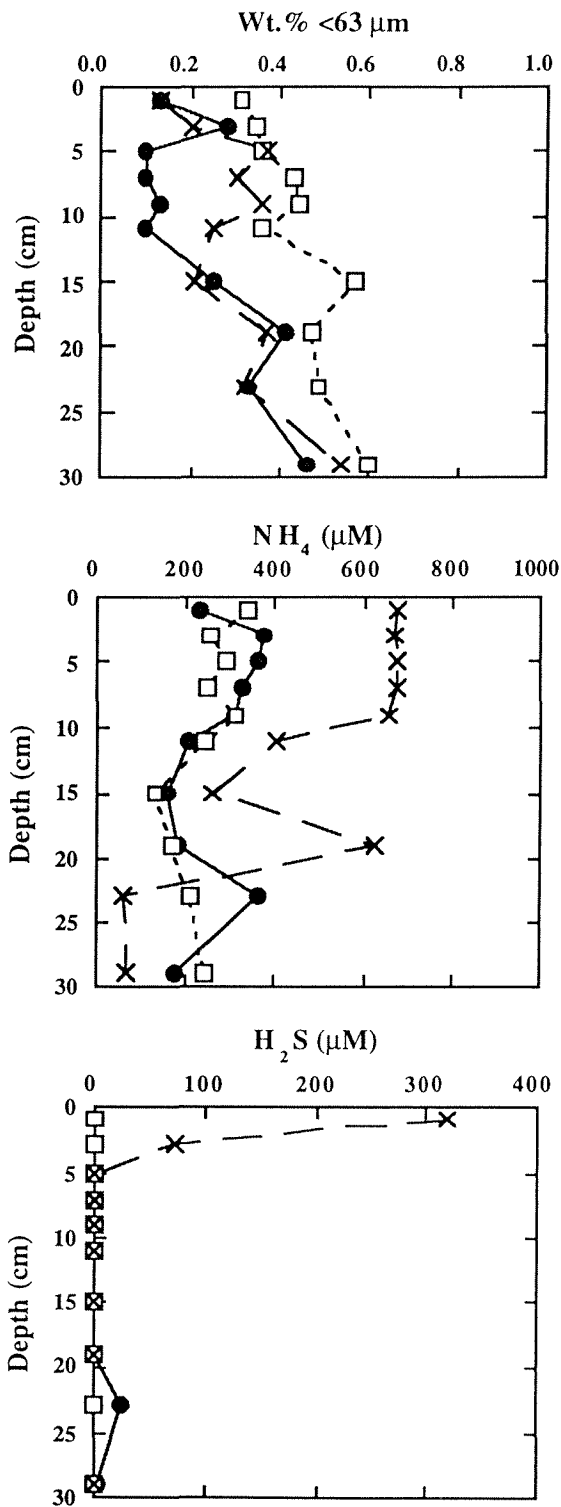


Figure 17. LLM1: solid circle= September, open square= January, X= May.

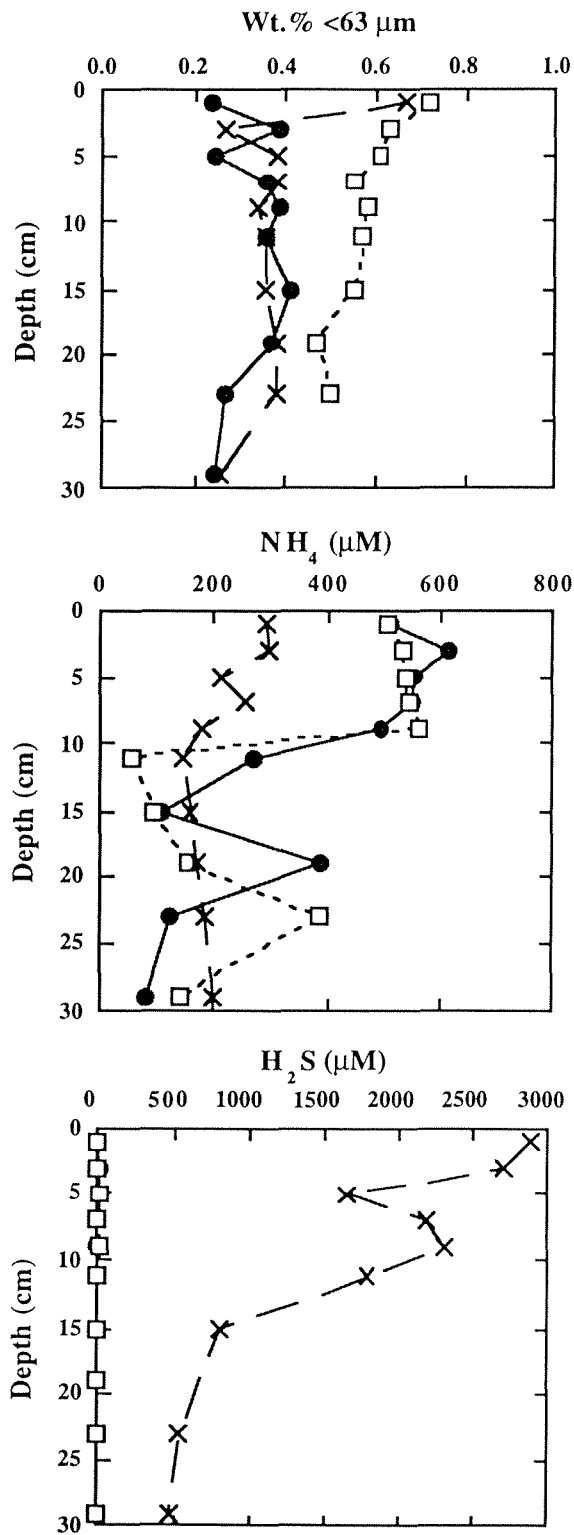


Figure 18. LLM2: solid circle= September, open square= January, X= May.

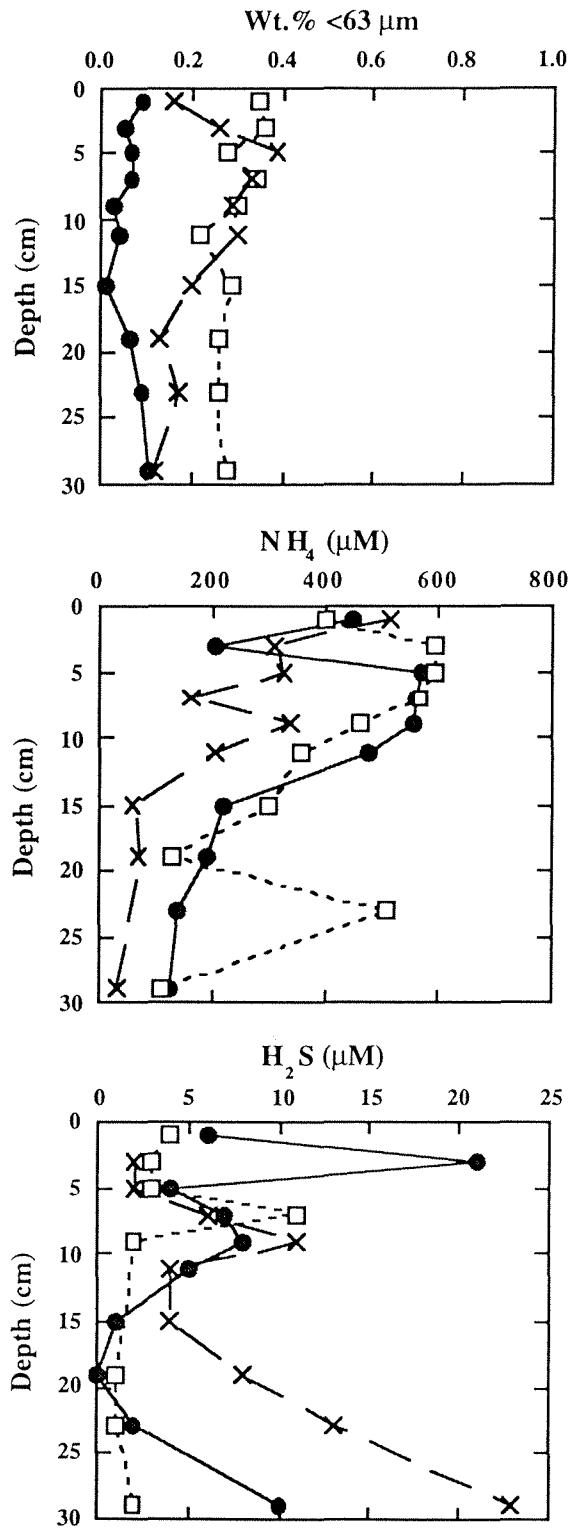


Figure 19. LLM3: solid circle= September, open square= January, X= May.

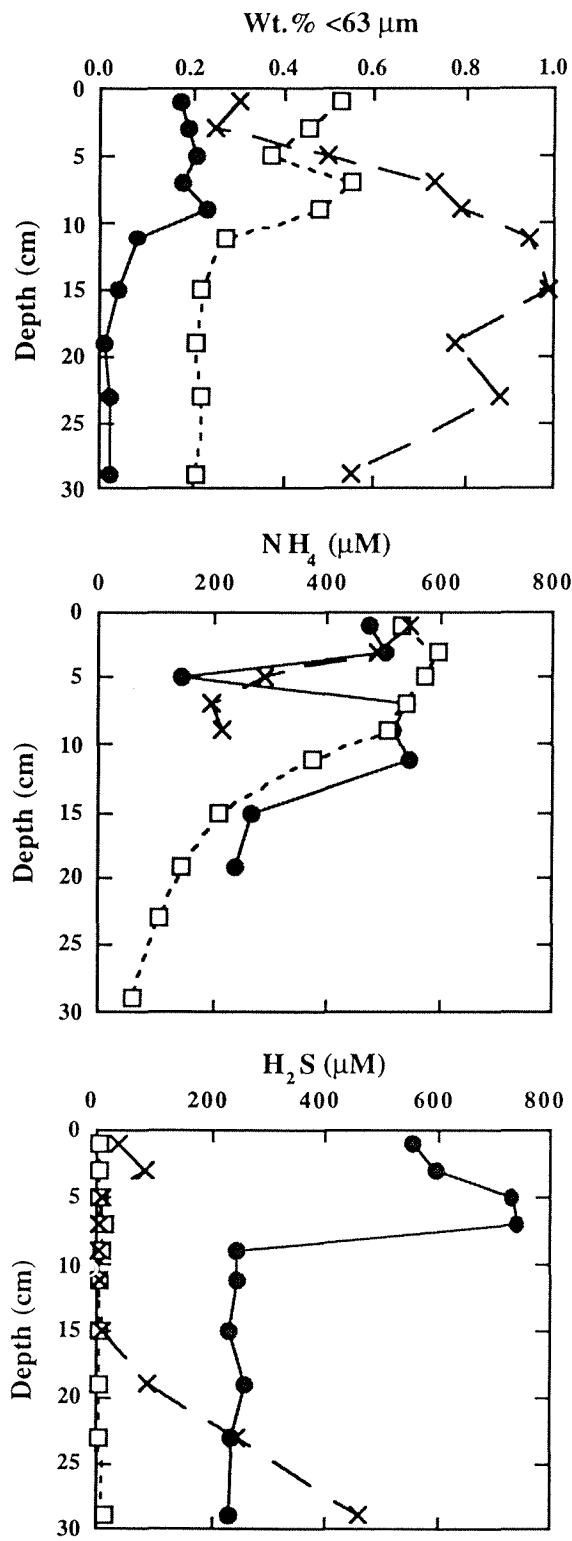


Figure 20. ULM2: solid circle= September, open square= January, X= May.

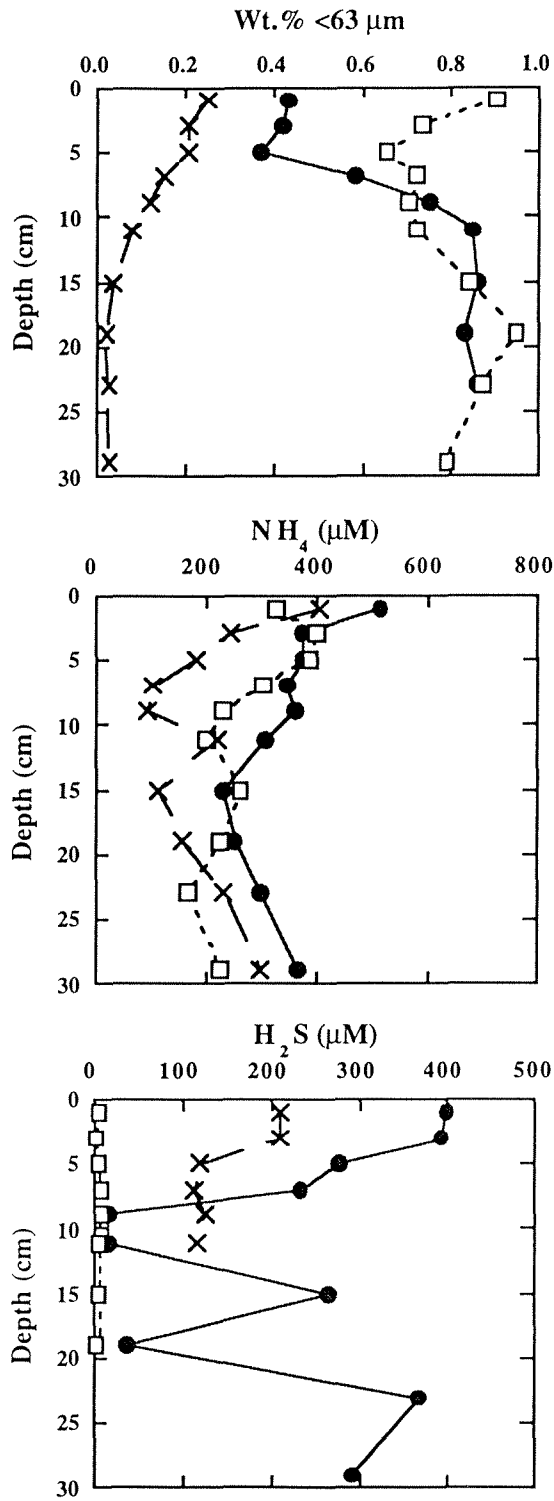


Figure 21. ULM3: solid circle= September, open square= January, X= May.

Part 4: Model Verification Studies of Sediment Chemistry

Sources of Dissolved Inorganic Carbon (DIC)

Initial attempts at modeling diagenetic processes indicated that the increase in porewater DIC concentrations could not be due entirely to the oxidation of organic matter. This raised the possibility of significant dissolution of calcium carbonate that is generally abundant in the sediments. In order to test this hypothesis, cores were taken at sites from two different *Thalassia* seagrass beds in Lower Laguna Madre, along with overlying water samples. pH values, DIC concentrations and the δC^{13} of the DIC were determined. Even though the two stations were about 2 km apart, their depth profiles were remarkably similar (Table 8). The δC^{13} of the DIC added to the pore water by diagenetic processes was determined by subtracting the concentration of the overlying water DIC with its δC^{13} value from the pore waters. Based on this calculation the δC^{13} of the diagenetically produced DIC could be calculated. An approximate calculation of the contributions of organic matter and calcium carbonate could then be made using a mixture of organically derived DIC ($\delta C^{13} = -24$) and aragonite derived DIC ($\delta C^{13} = +2$). Aragonite was used as the calcium carbonate source as it is a common biogenic carbonate component and calculations indicated that in some cases the pore water was close to being in equilibrium with this mineral. Results indicate that well over half (Table 9) the DIC added to the pore waters is coming from carbonate mineral dissolution as required from the diagenetic model.

Table 8. Analytic results for DIC source study.

Depth (cm)	pH- 1	pH-2	DIC-1 (mM)	DIC-2 (mM)	$\delta^{13}\text{C}-1$	$\delta^{13}\text{C}-2$
surface water	7.66	7.69	2.60	3.09	-3.46	-2.75
0-2	7.04	6.94	3.38	3.32	-4.23	-4.23
2-4	7.13	7.28	3.48	3.63	-4.90	-3.90
6-8	7.30	7.29	5.40	5.78	-3.45	-3.12
10-12	7.29	7.41	6.05	6.57	-2.99	-2.70

Table 9. Calculated results for DIC source study.

Depth (cm)	%DIC-Carb 1	%DIC-Carb 2	Cal Sat-1	Cal Sat-2
surface water			2.0	2.4
0-2	65	57	0.6	0.5
2-4	56	68	0.8	1.4
6-8	78	77	1.8	
10-12	81	81	1.9	

Impact of Dredge Deposits on Porewater Chemistry

A critical part of the modeling effort was to predict the impact of deposition of channel dredge material on the pore water chemistry of seagrass beds. Because of its toxicity the potential buildup and duration of abnormal concentrations of hydrogen sulfide was of particular concern. The model predicted that even relatively thin (on the order of 1 cm) dredge deposits could cause dissolved sulfide concentrations to reach critical levels for extended (months) periods of time. Because of the central importance of this model prediction to the goals of the project, it was decided that these predictions needed to be verified by direct observations. Unfortunately, the difficulties encountered in both the timing of dredging and the large amount of material deposited on the test grassbeds resulted in a less robust test of the model results than hoped for. Twice we pre-sampled the study area prior to dredging only to have the dredging put off. Results of this substantial effort are reported in Table 10. They will not be discussed in detail however as they are of limited utility to the objectives. Our discussion will focus primarily on the results presented in Table 11 where samples were obtained about 1 month after dredging took place.

Table 10. Pre-dredge sediment sampling results. Nutrient and H₂S concentrations are μM .

June 20, 1998

Site	Depth (cm)	NH4	PO4	Urea	NO3	NO2	SiO3	H2S	DIC mM	pH-NBS
FIX2	surface							0	4.16	7.65
	0-2	38.6	5.4	5.6	2.7	1.0	71.8	11	4.82	7.60
	4-6	239.1	10.8	5.6	2.6	1.2	78.0	12	6.60	7.88
	8-10	454.1	9.3	5.6	2.4	1.5	119.3	242	9.80	7.72
FA235A	surface							0	3.10	7.76
	0-2	31.1	3.3	5.6	2.6	1.5	63.5	11	5.22	7.46
	4-6	128.7	9.6	6.8	1.8	3.4	94.2	0	5.04	7.93
	8-10	127.2	3.1	5.1	2.6	3.6	62.1	0	3.71	7.98
FA235B	surface							0	3.26	7.65
	0-2	33.3	2.1	5.6	2.6	0.8	77.3	0	3.84	7.75
	4-6	121.0	4.7	5.6	2.1	0.5	75.3	0	4.21	7.94
	8-10	123.4	4.2	6.7	3.2	2.4	73.4	0	4.28	7.96

September 5, 1998

FIX2	surface	60.0	1.8	5.2	2.0	0.2	74.2	0	3.37	7.45
	0-2	68.8	2.5	6.3	3.1	2.1	112.2	162	4.12	7.69
	4-6	164.4	4.4	5.2	2.6	2.8	125.4	126	5.11	7.48
	8-10	263.8	3.9	6.2	4.3	1.2	118.7	178	6.87	7.40
FA235A	surface	213.0	7.6	9.4	4.3	0.3	132.0	181	5.44	7.31
	0-2	16.8	3.1	9.9	2.4	3.3	140.4	464	7.38	7.16
	4-6	109.3	7.0	6.2	32.2	28.5	142.4	478	8.05	7.34
	8-10	149.0	5.3	8.3	4.0	1.9	131.7	230	8.57	7.30
FA235B	surface	35.8	1.7	6.8	4.5	0.5	154.4	0	5.15	7.65
	0-2	48.8	4.9	10.4	2.5	1.5	158.0	88	6.92	7.28
	4-6	4.7	3.0	6.2	3.7	1.5	126.8	36	5.83	7.41
	8-10	30.3	1.9	5.2	0.7	3.6	75.7	125	8.25	7.26

Although both the June and September samplings (pre-dredging) were done at the same sites the June results are for directly in seagrasses whereas the September sampling was done in associated unvegetated areas. This turned out to be a good thing to have done since the dredge material unexpectedly was deposited to sufficient depths so that it was not possible to ascertain if a core was being taken in dense seagrass or a sparsely vegetated area.

In general the results are similar, but somewhat higher sulfide, DIC and lower pH values were observed in the unvegetated areas. This could be in part the result of oxic ventilation of the sediments in seagrass root zones as predicted by the model.

Table 11. Post-dredge sediment sampling results. Nutrient and H₂S concentrations are μ M.

November 3, 1998										
Site	Depth (cm)	NH ₄	PO ₄	Urea	NO ₃	NO ₂	SiO ₃	H ₂ S	DIC mM	pH-NBS
FIX2	surface	48.3	3.2	20.0	7.8	0.8	110.5	0	5.53	
	0-2	112.1	14.5	15.7	17.6	1.0	228.1	15	5.90	7.45
	4-6	104.3	3.1	25.4	19.8	1.2	232.4	151	7.29	7.47
	8-10	40.1	1.0	26.5	0.9	9.3	154.9	24	6.47	7.30
FA235C	surface	520.0	3.8	26.4	4.4	1.5	311.3	0	9.71	7.69
	0-6	932.0	27.2	5.2	3.4	1.5	544.9	1138	21.69	7.16
	8-10	1012.0	21.8	15.1	3.6	2.6	555.8	2622	28.02	7.16
	10-12	652.0	5.1	5.7	4.5	7.5	460.3	1867	24.08	7.20
	14-16	173.8	1.7	15.7	6.0	2.7	431.7	805	16.47	7.23
	18-20	33.3	1.1	16.7	9.9	12.8	384.4	386	13.29	7.38
FA235A	0	281.9	13.9	22.6	5.0	0.5	400.0	0	8.56	7.85
	13-15	1216.0	50.7	15.1	1.9	1.3	839.2	298	18.64	7.19
	15-17	1256.0	48.1	15.6	3.2	1.3	817.7	467	19.62	7.10
	19-21	1616.0	51.1	6.2	4.9	0.9	876.6	845	23.10	7.10
	23-25	1748.0	59.3	10.4	4.1	5.5	914.1	1995	29.50	6.99
	33-35	3216.0	62.5	8.8	14.7	16.8	771.6	4425	46.30	7.06
	37-39	1496.0	22.1	5.7	5.7	3.0	502.9	2134	31.79	6.95
	41-43	648.0	7.1	7.7	1.8	8.2	501.8	1933	25.97	7.10
	45-47	46.9	2.3	8.2	28.3	11.5	400.3	431	13.90	7.33

In Table 11 results are presented for samples taken at a control site with no dredge deposits (FIX2) and two sites covered with roughly 9 cm (FA235C) and 35cm (FA235A) of dredged sediments. The results at the control site are quite similar to those obtained in the pre-dredge surveys at these sites. Clearly parameters such ammonium, hydrogen sulfide and DIC are much higher, and pH lower, at the dredge deposit sites within the sediment below the pre-dredge sediment-water interface. There is a clear pattern of rapidly increasing concentration with depth within the dredge-sediment layer. This is underlain by the original sediment where concentrations rapidly decrease away from the original sediment water interface.

As discussed in the sediment modeling section this is most reasonably interpreted as substantiating our model prediction of generation of large amounts of sulfide in the dredge sediment layer and relatively rapid diffusion of the sulfide into the root zone at toxic levels. Caution should be applied however to these model verification results since they are for thick dredge deposits.

References Cited

- Canfield DE, Raiswell R, Westrich JT, Reaves CM, Berner RA (1986) The use of chromium reduction in the analysis of reduced inorganic sulfur in sediments and shales. *Chem Geol* 54: 149-155
- Cline JD (1969) Spectrophotometric determination of hydrogen sulfide in natural waters. *Limnol Oceanogr* 14: 454-458
- Cornwell JC, Morse JW (1987) The characterization of iron sulfide minerals in marine sediments. *Mar Chem* 22: 193-206
- Hansson I (1973) A new set of acidity constants for carbonic acid and boric acid in seawater. *Deep-Sea Res* 20: 461-478
- Reeburgh WS (1967) An improved interstitial water sampler. *Limnol Oceanogr* 14: 454-458

CHAPTER VIII: NUTRIENT RELEASE FROM RESUSPENDED SEDIMENTS

Contents

Abstract.....	3
Introduction.....	4
Methods.....	6
Study Area.....	6
Sediment Collection.....	7
General Sediment Characterization.....	8
Sediment NH ₄ ⁺ Extractions.....	9
Sediment Resuspension Experiments.....	9
Closed System.....	9
Open System.....	10
Dredge Operation Sampling.....	11
Results.....	11
Sediment Characteristics.....	11
Sediment NH ₄ ⁺ extractions.....	12
Closed Experiments.....	18
Open Experiments (Elutriate Test).....	19
PO ₄ ⁻³ Release During Resuspension.....	22
NH ₄ ⁺ Flux Determination and Sediment Plume Analysis.....	24
Discussion.....	25
Comparison of Release Experiments.....	25
Environmental Implications.....	28
Acknowledgments.....	30
References Cited.....	31

Tables

Table 1. Sediment sample designations and area in the Laguna Madre in which they were taken.....	7
Table 2. Sediment physical characteristics and porewater concentrations.....	14
Table 3. Yields of extractable ammonium.....	15
Table 4. Results of closed system experiments.....	21
Table 5. Results for the open, elutriate test.....	23

Figures

Figure 1. Ammonium extractions from sediments.....	13
Figure 2. Concentration of exchangeable NH_4^+	17
Figure 3. Results of closed system experiments.....	20
Figure 4. Time course PO_4^{-3} concentrations observed during resuspension.....	25
Figure 5. Data collected during a dredging event in February, 1997.....	26
Figure 6. Final equilibrium NH_4^+ concentration.....	28

Abstract

Sediments can play an important role in estuarine ecosystems by acting not only as sinks for nutrients, but also as sources of nutrients that can buffer their concentrations in overlying waters. This study examined the role surface chemistry plays in controlling the release of NH_4^+ and PO_4^{3-} from resuspended sediments in the large, but shallow, negative estuary Laguna Madre, TX. Both a generally accepted open system elutriate method and our own much more dilute closed system technique were used. The two techniques give different results that can largely be explained by the relative positions that the final solution concentrations place the systems on for an experimentally determined Langmuir-type adsorption isotherm. The closed system technique also indicated that typically approximately equal amounts of the NH_4^+ released came from porewater, loosely bound quick desorbing and tightly bound slowly released fractions. Experimental results were largely substantiated by observations of dredging activities. Model calculations indicate that resuspension of sediments by these and other human activities may cause NH_4^+ releases that approach those of NH_4^+ fluxes out of sediments over major areas of the estuary. This could potentially exacerbate environmental problems in this estuary such as the "brown tide".

Introduction

Microbially-mediated redox reactions in estuarine sediments lead to the remineralization of organic matter and recycling of nitrogen and phosphorus compounds in coastal environments (Fenchel and Blackburn 1979). Organic matter transported to the sediments is broken down by heterotrophic bacterial and fungal activity. Generally, NH_4^+ is released during remineralization of organic nitrogen compounds and subsequently oxidized to NO_2^- and NO_3^- through the bacterially mediated process of nitrification. However, in anoxic coastal sediments where dissolved oxygen is not available for nitrification, NH_4^+ can accumulate to mM concentrations in sediment porewaters. Since estuarine sediments generally are in the pH range of 7-8, concentrations of the cation NH_4^+ usually dominate ammonia speciation. This positively charged ion as well as negatively charged PO_4^{3-} can participate in adsorption-desorption reactions with sediment solids followed by incorporation into the solid phase (absorption) (Rosenfeld 1979; Froelich 1988). This process has been suggested to be a significant buffering mechanism for nutrient concentrations in estuaries (Pomeroy 1965). Under high porewater NH_4^+ concentrations, the quantity of NH_4^+ maintained in the absorbed phase is limited only by the cation exchange capacity of the sediments.

NH_4^+ loosely bound onto clay minerals is referred to as the exchangeable fraction (Rosenfeld 1979). This fraction has been quantified by Rosenfeld and others via a single 2 N KCl extraction in which adsorbed NH_4^+ is displaced by K^+ (Rosenfeld 1979; Mackin and Aller 1984; Seitzinger, Gardner *et al.* 1991). Exchangeable NH_4^+ quantification is essential for calculation of the linear adsorption coefficient (K) for NH_4^+ described by Rosenfeld (1979), and further this term is important to the model description of early diagenesis and nutrient cycling described by Berner (Berner 1976). More recently, the effectiveness of a one step extraction determination of exchangeable NH_4^+ has been questioned and the efficiency has been calculated in some cases to be less than 50% (Laima 1992).

Nutrient release from estuarine sediments is capable of supplying a significant fraction of the biologic demand of water column primary producers (Nixon 1981; Rizzo 1990). Biologically available nitrogen diffuses out of sediments as the oxidized species (NO_3^- , NO_2^-) in depositional

environments characterized by low organic matter loading rates, and as reduced NH_4^+ in regions where loading is high (Sloth, Blackburn *et al.* 1995). In shallow estuarine systems characterized by frequent resuspension of surficial sediments, NH_4^+ “stored” through solid phase exchange, can also contribute to internal cycling of nutrients, effectively delaying efforts to reduce eutrophication due to external organic matter loading (Rizzo and Christian 1996).

Diffusional processes generally dominate in undisturbed environments where sediments remain intact. In shallow marine environments, where human activity or sustained strong winds are common, another mechanism of release involves the physical resuspension of surface sediments. Radical resuspension events can relocate surface sediments and interstitial water from stable equilibrium to extreme non-equilibrium in terms of concentration gradients for both the interstitial waters and the sediment particles. Release of nutrients from resuspended porewater and sediment particles has been implicated in the stimulation of heterotrophic microplankton in estuarine waters (Wainright 1987). Considering the capacity for elevated porewater nutrient concentrations, this effect is not surprising. However, investigations into the possible alteration of nutrient release and influence on geochemical processes due to resuspension have been rare until recently (Blackburn 1997; Rutgers, van der Loeff and Boudreau 1997; Wainright and Hopkinson 1997). These investigations have mainly concentrated on enhanced biological activity, such as organic matter mineralization and mineral dissolution during natural periodic resuspension of surficial sediments. Sediment relocation due to yearly maintenance of the channel and waterway network in the coastal United States is a particular example of resuspension which can result in the relocation of large volumes of anaerobic, sub-surface porewater and particles. Chemical exchange between these resuspended sediments and surrounding waters is of primary concern to the U. S. Army Corps of Engineers who are responsible for the maintenance of the coastal waterways. Previous investigations of dredging related sediment resuspension and subsequent nutrient release have tenuously concluded that biologically available nitrogen release during dredging events does not adversely alter water column concentrations (Jones and Lee 1979). Conclusions of this investigation were based on the elutriate test which involves resuspension of dredge sediments in overlying water (volume ratio 1:5). Here, we report contradictory results along with a comparison of the different experimental approaches. Nutrient concentrations during these events are altered locally due to porewater dilution. In addition, the relatively fast release of particle surface bound ions as well as slower exchange with ions diffused inside clay particles, can contribute to concentration alterations.

The present work investigates the release of NH_4^+ from highly anoxic sediments taken from the bottom of the Gulf Intracoastal Waterway (GIWW) between Corpus Christi, TX. and Port Isabel, TX. Dilution experiments using different dry weight to volume ratios of sediment (0.1, 1.0 and 10.0 grams per L) were conducted with a comparison to the U.S. Army Corps of Engineers elutriate test. In addition, GIWW sediments were extracted through multiple (5) treatments with 2 N KCl to determine total extractable NH_4^+ . The results from the extraction are compared to results from resuspension experiments to investigate the effect of varying solid to solution ratios which occur in natural systems.

Methods

Study Area

Laguna Madre is a seasonally hypersaline, shallow (ca. 1 m) estuary located in the southern region of Texas. Phytoplankton production has been estimated to be $78 \text{ g C m}^{-2} \text{ yr}^{-1}$, while above ground seagrass (*Halodule wrightii*) production has been measured at $723 \text{ g C m}^{-2} \text{ yr}^{-1}$ (Chin-Leo and Benner, 1991). The estuary is transversed along its north to south extent by the GIWW which averages a depth of approximately 4 meters. The GIWW is basically a channel constructed and maintained by the U. S. Army Corps of Engineers to accommodate barge traffic from industrial centers from Port Isabel, Texas to Corpus Christi, Texas. Maintenance of the channel requires frequent dredging operations that involve the relocation of deposited sediments to other regions of the estuary or along the sides of the waterway. The relocation and subsequent resuspension of sediments causes the mixing and dilution of interstitial waters associated with the channel sediments with overlying waters. Dredging events can result in the release of high concentrations of dissolved components contained in sediment porewaters. Barge traffic in general can be responsible for additional and perhaps more frequent resuspension of channel sediments as well. Sediment slumping into the channel reduces the clearance depth (shoaling) along the channel lanes. During sample collection in June of 1996 we observed large sediment plumes created by passing barges. This also implies that at least the surficial sediments inside the channel are periodically resuspended and deposited. We collected sediments inside the GIWW channel along the Northern and Southern sections of the Laguna Madre and from shallow bare areas outside the channel. These sediments were used in resuspension experiments to assess the potential for NH_4^+ released during dredging operations.

Table 1: Sediment sample designations and area in the Laguna Madre in which they were taken.

Sediment Sample	Location	Location Description
1	Marker 91	GIWW Lower LM
2	Marker 157	GIWW Lower LM
3	Marker 41	GIWW Lower LM
4	COE Sta.5	Top 10 cm Bare Sediment
5	COE Sta.28	Top 10 cm Bare Sediment
6	Marker 45	GIWW Upper LM
7	Marker 59	GIWW Upper LM
8	Marker 151	GIWW Upper LM
9	COE Sta.16	Top 10 cm Bare Sediment
10	COE Sta.13	Top 10 cm Bare Sediment

Water samples collected in lower and upper Laguna Madre were filtered to 0.2 μm immediately for experiments using sediments from different parts of Laguna Madre.

Sediment Collection

Sediment cores (7.0 cm diameter) from potential dredge sites along the channel bottom were collected using a gravity coring mechanism on a winch line. The top 10 cm of each sediment core was quickly homogenized, sealed in Nalgene containers and stored at 4°C for transfer back to the lab at College Station, TX.. Sediments taken outside of the channel were collected by hand in shallow, bare sections of Laguna Madre using large (30.5 cm), hand held coring mechanisms. The top 10 cm of sediment was homogenized and placed in 1 liter Nalgene containers. Table 1 defines the region to which each of the sediment designations correspond. Only the outer channel sediments COE Station #28 and #13 were tested for NH_4^+ release. Overlying water samples were collected in close proximity to each site for use in the resuspension experiments. The water was

filtered through a 1.0 μm milliguard cartridge filter, in line with a 142 mm, 0.2 μm membrane filter (Millipore) into large Nalgene carboys and kept cold during transport. All sediments and overlying water were stored at 4° C until experiments were conducted.

Cores were collected by divers from 12 stations in both upper and lower Laguna Madre in order to determine concentration profiles and calculate potential NH_4^+ flux into overlying waters. Sediment cores (7.0 cm diameter, 30 cm length) were taken both within grass covered areas and in bare areas. Sediments were sectioned at 2 cm intervals to 12 cm and again at 14, 20, 24 and 28 cm, placed in 50 ml tubes and centrifuged at 3000 rpm for 1 hour. The porewater was drawn off with a glass 10 ml syringe and passed through 0.45 μm syringe filters. Liquid samples were collected in 20 ml scintillation vials and frozen (-20 °C).

General Sediment Characterization

Porosity measurements were performed immediately on small subsamples from each site in order to calculate mass additions for the resuspension experiments (by weight fraction). Duplicate sediment subsamples were weighed into pre-tared Pyrex beakers and placed in a drying oven overnight (80°C). When samples appeared thoroughly dried they were weighed again to determine the solid weight fraction. In addition, weight fraction <63 μm and percent carbon content was determined. The <63 μm fraction was determined by washing out the smaller fraction through a 63 μm sieve, collecting and drying the retained fraction, and measuring the weight. Duplicate subsamples were split into two equal quantities for carbon analysis. One quantity was combusted directly in a Leco Organic Carbon Analyzer for total carbon content and the other was acidified with 10% HCl prior to combustion for analysis of organic carbon. Inorganic carbon was calculated by difference. Interstitial waters from each sample were collected by centrifuging approximately 20 ml of sample at 2500 rpm, for one hour, in a fixed angle centrifuge rotor. Pore water was drawn off with a small glass syringe and filtered through a 0.45 μm membrane filter into pre-cleaned 20 ml scintillation vials with Teflon caps. The water was immediately frozen on dry ice and stored at -20° C. Pore water NH_4^+ concentrations were determined using the spectrophotometric methods of Strickland and Parsons (1972). NH_4^+ measurements were also performed on all overlying water samples.

Sediment NH₄⁺ Extractions

Total NH₄⁺ content was determined on duplicate subsamples using a modification of a method used by Laima (Laima 1992). Ten grams of sediment was first centrifuged at 2500 rpm for one hour to remove the porewater. The porewater supernatant was then drawn off with a large glass syringe through a Teflon tube and filtered through 0.45 μm Millipore syringe filters into 20 ml scintillation vials. A 20 ml volume of 2N KCl and 0.1% azide was then added to the sediment and the mixture was homogenized in 250 ml centrifuge bottles using a benchtop vortexer. The samples were shaken at 150 rpm overnight in a 25 °C incubator, then centrifuged. The supernatant was removed and filtered, stored as above, and immediately frozen. This extraction procedure was repeated 5 times for each sample. Total NH₄⁺ from each extraction was determined spectrophotometrically (phenol blue method) and summed for all extractions. An asymptotic relationship was observed when accumulated volume through the sequence of extractions was compared to the accumulated NH₄⁺. This relationship can be described by the mathematical formulation:

$$[NH_4^+] = [NH_4^+]_{Max} (1 - e^{-kv}) \quad (\text{eqn. 1})$$

where $[NH_4^+]_{Max}$ is equal to the maximum accumulated amount of NH₄⁺, k is a desorption constant, and v is the accumulated volume. Total NH₄⁺ was predicted by fitting a line described by the above equation to the data and extrapolating the maximum value. The line fit was determined using a non-linear optimization routine in MATLAB™.

Sediment Resuspension Experiments

Closed system

Experiments were carried out for each sediment collected from inside and outside the channel. Using the porosity to calculate sediment dry weight per volume, duplicate sediment addition of 10.0, 1.0, and 0.1 grams were resuspended in six 1 liter Erlenmeyer flasks containing 1000 ml. of 0.1% azide amended overlying water. These sediment additions were made with wet sediment resulting in significant addition of porewater to each experiment. Porewater volumes were calculated using the porosity and were accounted for in concentration calculations. Prior to sediment addition, overlying water sub-samples were filtered into scintillation vials for determination of background nutrient concentrations. The experiments were carried out in flasks

sealed with rubber stoppers fitted with syringe needle ports, and stirred vigorously with Teflon stir bars throughout the duration of the experiments (48 hr.). At regular intervals (5, 15, 60, 120, 240, 720, 1440, 2160, and 2880 min), 10 ml of the sediment water mixture was removed and filtered into scintillation vials using syringe filters. Liquid samples for nutrient concentration determination were immediately placed on dry ice until frozen, then transferred to a -20°C freezer. All experiments were maintained at room temperature (approx. 23°C) throughout their duration.

NH_4^+ analyses were carried out spectrophotometrically as described above. High concentrations of NH_4^+ required that each sample was diluted (in duplicate) for NH_4^+ measurement. NH_4^+ release measured at 5 minutes was considered to be fast release. This quantity represents the sum of background concentration, porewater concentration, and loosely bound nutrient concentration. Sub-samples were also analyzed for PO_4^{3-} concentration. PO_4^{3-} determinations were also carried out spectrophotometrically according to the methods of Strickland and Parsons (1972). The experiments were monitored over a two day time period and the maximum measured concentration of both PO_4^{3-} and NH_4^+ was considered to be the total released. These experiments were considered closed as dissolved oxygen concentrations were not maintained. The consumption of dissolved oxygen was possibly significant in some cases, but NH_4^+ mobility generally is not strongly dependent on oxygen concentration. Conversely, the release and solution mobility of PO_4^{3-} is dependent on oxygen consumption specifically due to the formation of iron oxy/hydroxides. For this reason we will concentrate mainly on the observations and analysis of NH_4^+ .

Open system

The open system experiments were carried out according to the U. S. Corps of Engineers (COE) method described by Plumb (1980). The experiments were similar to our closed experiment procedure, with notable exceptions. Sediment additions were made on a volume basis in a 1:5 sediment to solution ratio (100 ml sediment: 400 ml overlying water), and release experiments were conducted in 500 ml Pyrex Erlenmeyer flasks. Each flask was sealed with a rubber stopper containing two syringe needle ports. One port was used to withdraw samples of the slurry, while the other was connected to an air pump. The slurries were aerated throughout the experiment duration. We refer to this method of resuspension experiment as “open” because the slurry was aerobic. Background samples were taken as above, prior to sediment addition. Sediment was maintained in suspension by securing the flasks on a shaker table (150 rpm). After one hour of shaking, sediment was allowed to settle. Samples were collected at 10, 20, 40, and 60 minutes as

described by the COE method, and a 1440 minute sample was taken for comparison to the closed system experiments. Storage and nutrient analysis of the time series samples was performed as described.

Dredge Operation Sampling

During a February 1997 sampling trip we were able to sample several points located in close vicinity to an active dredging operation being conducted near Port Mansfield, Texas in the lower Laguna Madre. The dredging operation was interrupted temporarily so that samples could be taken from the pipe carrying sediment. Samples were also collected approximately 30 meters (near) from the opening of the pipe and at approximately 300 meters (far). Water volumes were collected and filtered for nutrient analysis as well as samples frozen for determination of total suspended solids. Samples collected for suspended solid quantification were later thawed, resuspended and filtered onto pre-tared 47 mm GF/F filters. The filters were dried and weighed until no change was detected.

Results

Sediment Characteristics

Sediments collected from the channel bottom had a significantly larger silt and clay size fraction than those from shallow bare area outside of the channel. Table 2 presents measured sediment characteristics for both channel bottom and bare area sediments. Sediments collected inside the channel displayed evidence of active sulfate reduction (dark black color with sulfurous odor). NH_4^+ concentrations were all very high in the channel bottom samples (mM), while concentrations in sediments collected outside the channel were an order of magnitude lower. Channel bottom sediments had roughly twice as much organic carbon as the outer sediments.

Sediment NH_4^+ Extractions

The total sediment NH_4^+ is composed of the dissolved porewater fraction and that associated with the sediment solid phase. We determined this value by performing multiple (5 total) exchangeable NH_4^+ extractions with 2N KCl on each sediment after the porewater was removed. Accumulated NH_4^+ quantities derived from each successive extraction displayed close dependence on the accumulated extraction volume. This dependence can be accurately represented mathematically by

equation 1. Figures 1a and 1b demonstrate this relationship for the sediments collected from the channel bottom at Marker #45 in the upper Laguna Madre. These graphs illustrates typical results observed for all sediments. The first data point on each plot represents the ammonium content and the measured porewater volume. The dotted horizontal line at the top of each figure represents the asymptotic maximum concentration ($[\text{NH}_4^+]_{Max}$) of NH_4^+ approached by each function. This value was taken as the total amount of NH_4^+ obtained from the extracted sample. In order to establish “goodness” of fit for the analysis procedure, we calculated the sum of residuals (sum total difference between the measured points and equation predictions) for each sediment extraction. In all inner channel sediment extraction the sum of residuals was less than 5% of the asymptotic maximum. The summed residuals in one of the duplicate analysis for the outer sediment at Station 13 was 14% of the asymptotic maximum. The sediments collected outside the channel in general were not as well represented by the equation used in the line fit procedure, though the summed residuals calculated for all outer sediment extractions, with the above exception, were at most 7% of the asymptotic value.

The total amount of NH_4^+ associated with each sediment sample was normalized to a per gram (dry weight) sediment added basis for each sample (Table 2). Total NH_4^+ (ΣNH_4^+) refers to the combined quantity associated with the porewater plus that loosely bound to surfaces and dissolved inside clay particles. Sediments taken from the GIWW channel bottom contained much more ΣNH_4^+ associated with the solid phase.

The ΣNH_4^+ content of sediments inside and outside the intracoastal waterway was examined to assess the amount of NH_4^+ available for desorption and to assess what fraction of the total might be released during a resuspension event. Table 3 shows the NH_4^+ yield from the first two extractions with 2N KCl and a comparison to the final yield obtained from the optimization routine. Efficiencies for the first extraction did not exceed 50% for any sediment and were as low.

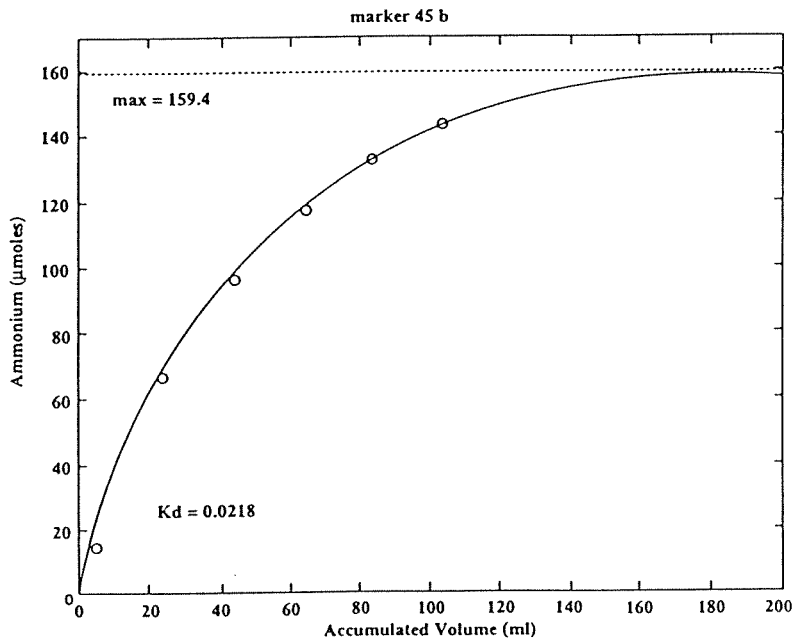
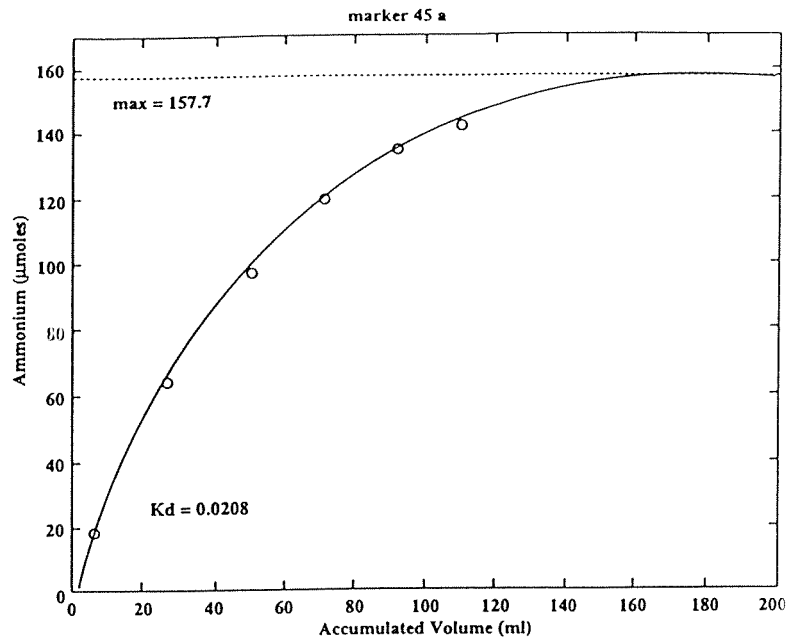


Figure 1. Sediment NH_4^+ extractions from sediments collected at Marker 45 in Laguna Madre. Accumulated NH_4^+ was compared to accumulation of total extraction volume. The solid lines represent the exponential equation using the fitting technique to the data (circles) as described in the methods (eqn. 1). Dotted lines represent the value for the total NH_4^+ associated with the sediment. K_d is the constant which also results from this fitting technique.

Table 2. Sediment physical characteristics and some porewater concentrations measured in the interstitial water for the sediments collected at the channel bottom and outside in bare areas. Outside sediments are given station designations and are listed at the bottom.

Station	ϕ	<63 μm (%)	Inorganic Carbon (%)	Organic Carbon (%)	Total Carbon (%)	Pore water PO4 (mM)	Porewater NH4 (mM)	Total NH4 ($\mu\text{moles}/$ gdw)
Inner Channel								
Marker 157	0.8	99	2.60	1.00	3.59	0.106	1.73	11.61
	0							
Marker 151	0.9	81	1.18	4.53	5.71	0.034	3.85	32.50
	0							
Marker 59	0.7	60	0.36	0.93	1.28	0.124	3.62	8.04
	2							
Marker 45	0.8	65	1.84	1.59	3.42	0.061	2.90	15.80
	3							
Marker 41	0.8	94	2.44	2.37	4.81	0.035	2.66	20.60
	7							
Marker 91	0.7	91	2.40	1.06	3.45	0.015	2.07	10.90
	8							
Outer Channel								
Stat 13 (N)	0.4	5	4.81	0.42	5.23	0.008	0.352	1.61
	7							
Station 28 (S)	0.4 3	6	1.24	0.52	1.76	0.008	0.450	2.70

Table 3. Yields of extractable ammonium after the first two treatments with 2 N KCl. Linear diffusion coefficient (K) was calculated according to Rosenfeld for each of the first two extractions and for the Total. Upper values are for inner channel sediments and lower numbers are for outer channel sediments.

<i>Exchangeable Ammonium</i>								
Station	After first extraction ($\mu\text{moles/gdw}$)	Percent of Total	K (slope= 2.18)	After second extraction ($\mu\text{moles/gdw}$)	Percent of Total	K (slope= 3.53)	Predicted Total ($\mu\text{moles/gdw}$)	K (slope= 6.81)
Marker 157	3.51	30.2	1.4	5.68	48.9	2.3	11.61	4.50
Marker 151	8.71	26.8	0.7	14.42	44.4	1.1	32.5	2.10
Marker 59	3.94	49.0	2.3	5.96	74.1	3.7	8.04	7.10
Marker 45	4.84	30.6	1.2	7.82	49.5	2.0	15.8	3.80
Marker 41	5.62	27.3	0.9	9.61	46.7	1.4	20.6	2.70
Marker 91	4.04	37.1	1.6	6.39	58.6	2.6	10.9	5.10
Station 13 (N)	0.75	46.6	6.7	1.05	65.2	10.8	1.61	20.90
Station 28 (S)	0.48	17.9	7.7	1.53	56.7	12.4	2.7	23.90

as 18% for the sandy sediment collected at Station 28. After the second extraction only half of the yields exceeded 50%, and the highest yield was 74% for one of the inner waterway sediments. No correlation was obvious between extraction efficiency and the sediment porosity.

Using the relationship presented by Rosenfeld (1979), we calculated the NH_4^+ adsorption coefficient, K, for the first extraction, second extraction and for the total amount determined by multiple extractions. The porewater concentration of each sediment compared to the yield of extractable NH_4^+ after the subsequent extractions (1st, 2nd and final) are presented in Figure 2. Inset in each graph are the regression curves determined for each relationship. The slope of the line fits ranged from 2.18 for the first extraction to 6.81 for the total extractable NH_4^+ content, and y intercept values were negative for each extraction. This result is in contrast with earlier data (Rosenfeld 1979; Boatman and Murray 1982; Mackin and Aller 1984). Positive y-intercepts observed in previous investigations have been attributed to sediment pre-treatment designed to

remove organic material. "Excess" NH_4^+ associated with positive y-intercepts was explained by the release of NH_4^+ from readily hydrolyzable sources (e.g. surface bound amines). No attempts to remove organic material from the sediments were performed in this study. Another possible explanation for this observation is that, as the extractable NH_4^+ approaches zero, some dissolved NH_4^+ should remain in the porewater. When y is set equal to zero for each regression curve (implying total removal of extractable NH_4^+), the porewater concentration can be calculated. This value is 0.168, 0.118 and 0.233 mmol/L for the first, second and final extraction, respectively. The slopes of each regression were used in the relationship presented by Mackin and Aller (1984), to determine the apparent adsorption coefficient (K^*):

$$K^* = \hat{C}_N / C_N \quad (\text{eqn. 2})$$

where \hat{C}_N is the sediment exchangeable NH_4^+ concentration ($\mu\text{mole/gdw}$ sediment) and C_N is the porewater concentration of NH_4^+ (mM). Units for K^* are given in ml porewater/gdw sediment.

The linear adsorption coefficient can be calculated following the relationship derived by Krom (1980) using the value for K^* , the measured porosity for each sediment and the sediment density ρ_s (2.65 g/ml).

$$K = \frac{(1 - \phi)}{\phi} \rho_s K^* \quad (\text{eqn. 3})$$

Adsorption coefficients calculated for each set of extractions are presented along with the extraction yields in Table 3. Although K values were extremely variable and showed a strong dependence on the number of extractions, these values fell well within the range of adsorption coefficients measured in various coastal systems by Laima (Laima, 1992).

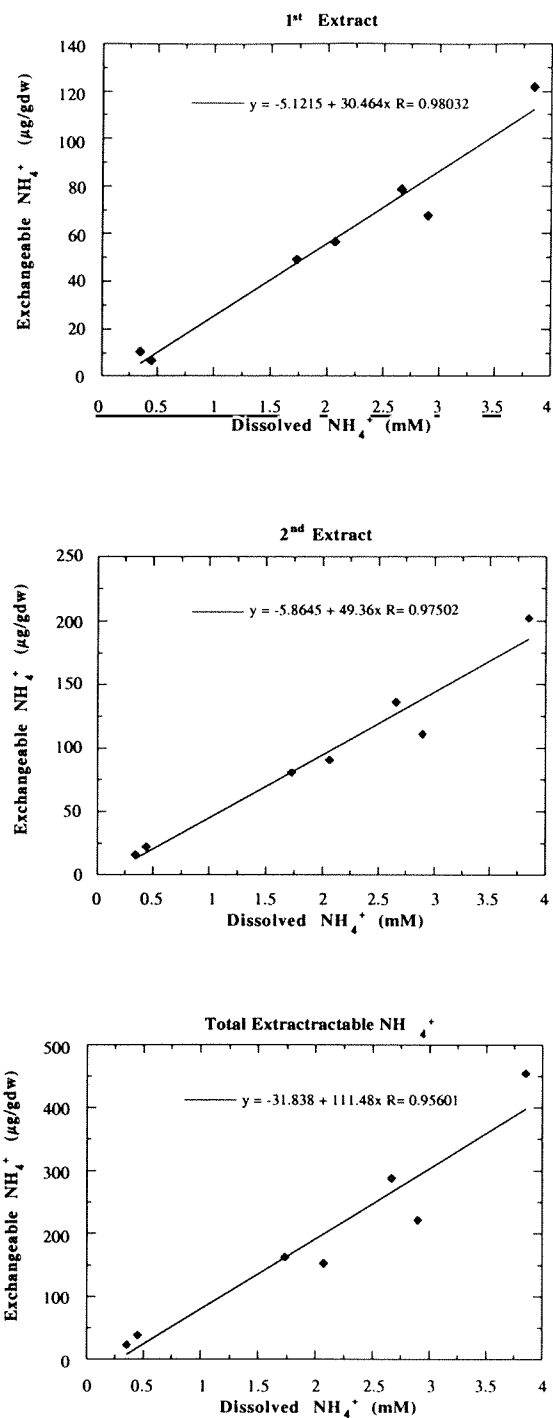


Figure 2. Concentration of exchangeable compared to porewater NH_4^+ in sediments collected in bare areas and the GIWW in Laguna Madre. Inset equations are regression curves fit to the data. Slopes are used in the calculation of the linear diffusion coefficient presented in Table 3.

Closed Experiments

Results for the closed system NH_4^+ release experiments are presented in Table 4. The channel bottom sediment results are displayed in the upper region of the tables and the bare area (outside channel) results are located below the shaded area. Data are presented as the average of duplicate sediment additions in the rows beneath the location designation. NH_4^+ concentrations in the dilution waters increased rapidly over the first 20 minutes of the experiments and then exhibited slow increases over the remainder of the experiment. The background concentration of NH_4^+ in the overlying water was added to the total NH_4^+ associated with the porewater volume (added with sediment) to arrive at a seawater + porewater NH_4^+ concentration. This value represents the concentration of NH_4^+ expected at the instant resuspension occurs due to porewater dilution. The difference between this quantity and the measured quantity at 5 minutes represents the "fast" release fraction of loosely bound NH_4^+ . The maximum measured concentration was considered to be the total quantity of NH_4^+ in the sediment sample. The fast release and seawater + porewater components were subtracted from the total to determine the "slow" release quantity. NH_4^+ released from the channel sediments generally greatly exceeded the release from the sediments collected in bare areas of the Laguna Madre, with one exception. Sediments collected at marker 157 released less NH_4^+ in the 0.1 gram addition experiment than both bare area sediments. In the higher dilutions (1.0 and 10.0 gram additions) Marker 157 sediments released more NH_4^+ gdw^{-1} added. Porewater concentrations of NH_4^+ in the marker 157 sediments were the lowest for the sediments collected inside the channel.

The "fast" and "slow" release patterns are shown in Figures 3a and 3b. These graphs illustrate typical replicate results for 10.0 gram addition experiments on sediments collected in the upper and lower Laguna Madre. The horizontal lines on each graph are described on the right side, corresponding to the seawater (background) + porewater concentrations, fast release fraction and slow release fraction. The inset graph displays the first 300 minutes of the experiments. It is apparent that significant release occurs after the first two hours of resuspension. Averages of the fast and slow release fractions for each experiment normalized to per gram sediment added are shown in Table 3. In two of the closed experiments in which 0.1 gram of sediment were added,

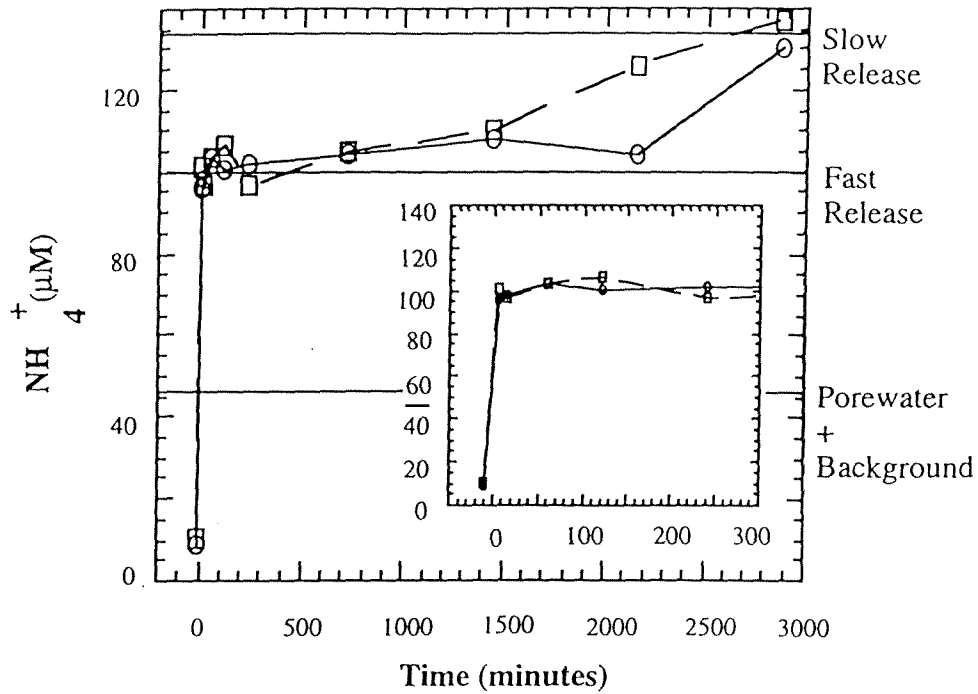
the NH_4^+ concentration actually dropped in the first five minutes (see Marker 151 and Station 28, 0.1 gram addition). This could be due to an increase in the concentration of adsorption sites due to the rapid dilution of particulate matter or possibly because of error introduced in measuring small quantities of sediment. These sediments were the only two which exhibited this type of behavior. In general, the quantity of rapidly released NH_4^+ was dependent on the quantity of sediment added. The rapid release NH_4^+ for each sediment however did not increase in a manner directly proportional to the mass of sediments. In most cases the NH_4^+ gdw^{-1} release was greatest for the lowest sediment addition. This relationship was also observed for the total released fraction and particularly for the slow release quantity. The last three columns of Table 4 deal with total NH_4^+ content of each sediment (from above extractions), the maximum NH_4^+ measured for each experiment, and the fraction of the total measured in the closed system experiments. The calculations of greater than 100% of the total NH_4^+ (porewater + extractable) determined for some sediments is attributed to the varying ratios of solid to solution and will be addressed in the discussion.

Open Experiments (Elutriate Test)

Results for the experiments conducted according to the Corps of Engineers method are displayed in Table 5. Many of the calculations are the same as those used in the closed experiments.

Background seawater NH_4^+ concentrations were added to the porewater concentrations of NH_4^+ to determine an expected quantity released at the instant of resuspension. This was followed by a maximum NH_4^+ concentration measured over the successive sampling times. The background + porewater concentration was subtracted from the maximum measured NH_4^+ to calculate the amount associated with the solids in each sediment. This measurement was normalized to weight of solid sediment added (per gram). The value was compared to the extraction determination of ΣNH_4^+ to generate a percentage released. The dynamics of NH_4^+ release as a function of time for the open system experiments were very similar to those observed in the closed systems Corps experiments. NH_4^+ concentrations rapidly increased during the first time samples, then showed a relatively small increase between the 60 minute sample and the final sample taken at 24 hours. This final increase in the nutrient concentration in the overlying water occurred after the sediments had settled, indicating that release of NH_4^+ can continue after particles have sedimented out of the

Northern
Laguna Madre



Southern
Laguna Madre

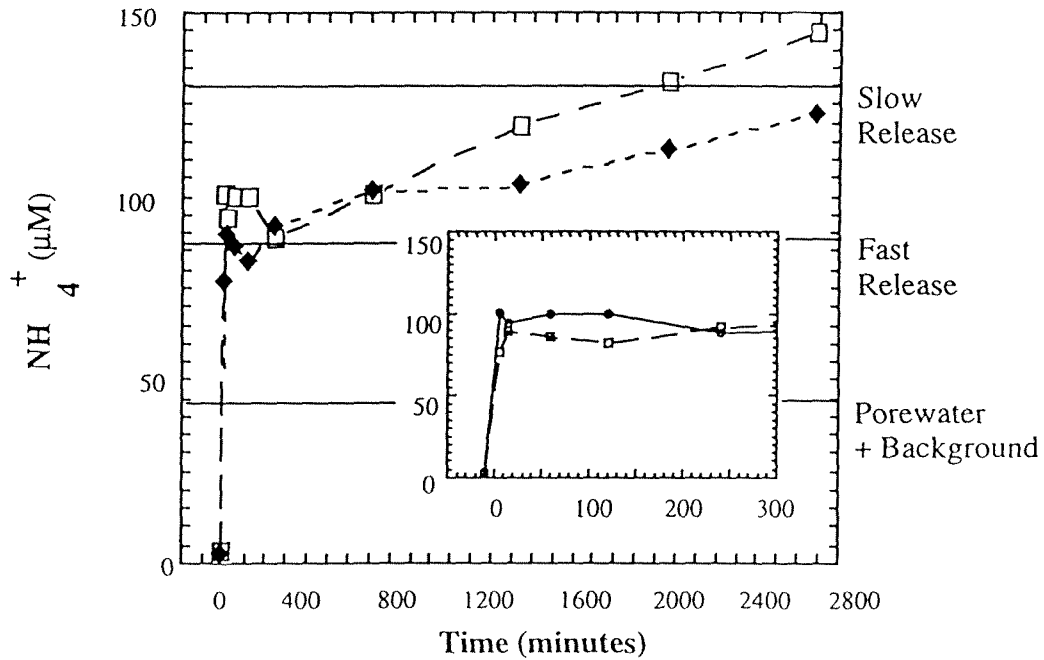


Figure 3. Results from two of the closed system experiments using sediments taken from the Northern and Southern Laguna Madre. The graphs display time series NH_4^+ concentrations for the duplicate experiments, with an inset graph to highlight the first 300 minutes of data. Horizontal lines represent concentrations in terms of release of NH_4^+ .

Table 4. Results for the closed experiments conducted by adding 0.1, 1.0, 10.0 grams of sediment by dry to one liter volumes of overlying water. Outer channel sediment results are displayed at the bottom and inner sediments at the top of the table.

Location and sediment addition (g/L)	Seawater initial concentration (μM)	Seawater + Porewater ammonium (μM)	Initial NH ₄ t = 5mins (μM)	Fast release in μM	NH ₄ max (μM)	Slow Release (μM)	Fast Release (μmoles/gd w)	Slow Release (μmoles/gd w)	Total NH ₄ (μmoles/gd w)	Released as % of total (μmoles/gdw)	Total Released (μmoles/gdw)
Marker 151									32.50		
0.1	7.5	8.8	7.9	-0.9	12.6	3.8	nd	37.8		116.39	37.83
1.0	11.6	24.9	45.1	20.2	57.2	12.1	20.2	12.1		99.39	32.30
10.0	11.3	144.0	325.6	181.7	373.5	47.9	18.2	4.8		70.63	22.96
Marker 157									11.60		
0.1	1.0	1.3	1.4	0.1	2.5	1.1	1.0	11.0		103.44	12.00
1.0	1.9	4.6	9.2	4.5	13.7	4.5	4.5	4.5		77.74	9.02
10.0	1.2	28.7	86.8	58.1	123.5	36.7	5.8	3.7		81.72	9.48
Marker 45									15.80		
0.1	4.2	4.8	7.1	2.3	9.5	2.5	22.8	24.9		301.39	47.62
1.0	3.4	8.8	21.3	12.5	29.6	8.3	12.5	8.3		131.85	20.83
10.0	3.9	57.8	150.7	92.9	218.8	68.1	9.3	6.8		101.90	16.10
Marker 59									8.00		
0.1	10.1	10.5	10.7	0.2	12.6	1.9	2.3	19.4		270.90	21.67
1.0	7.6	11.2	16.1	4.9	24.9	8.8	4.9	8.8		171.09	13.69
10.0	9.6	45.7	98.6	52.9	133.8	35.1	5.3	3.5		110.00	8.80
Marker 91									10.90		
0.1	3.3	3.6	5.3	1.7	6.8	1.5	17.3	15.3		298.79	32.57
1.0	2.2	5.2	10.8	5.7	18.5	7.7	5.7	7.7		122.40	13.34
10.0	3.1	32.3	95.3	63.0	133.2	37.9	6.3	3.8		92.64	10.10
Marker 41									20.60		
0.1	6.6	7.3	8.1	0.7	13.4	5.3	7.4	28.8		175.52	36.16
1.0	6.4	13.5	22.5	9.1	23.9	1.4	9.1	1.4		50.83	10.47
10.0	5.7	76.0	160.4	84.5	171.8	11.3	8.4	1.1		46.51	9.58
Station 13									1.60		
0.1	7.2	7.2	7.8	0.6	8.9	1.1	6.4	11.1		1092.7	17.48
1.0	6.7	6.8	8.3	1.5	15.5	7.2	1.5	7.2		545.17	8.72
10.0	7.1	8.2	31.9	23.7	43.5	11.5	2.4	1.2		220.23	3.52
Station 28									2.41		
0.1	8.0	8.0	7.7	-0.4	9.9	2.2	nd	22.0		762.22	18.37
1.0	8.5	8.6	9.5	0.9	10.5	1.0	0.9	1.0		78.40	1.89
10.0	6.6	7.9	9.7	1.8	12.8	3.1	0.2	0.3		20.31	0.49

water column. In several of the experiments, the release after sediments had settled was in excess of 10% of the total release. One exception to this was the results Marker 151 sediments where NH_4^+ concentration decreased between the one hour sample and final sample. This station's sediments also had the highest release of NH_4^+ in the open experiments and are characterized by the highest total NH_4^+ content.

NH_4^+ release from bare area sediments in the elutriate experiments was more than an order of magnitude less than for the inner sediments. Final calculations of mass normalized release in the open experiments exhibited similar trends to the mass normalized calculations for the closed systems. In both types of experiments Marker 151 sediments had a very high release of NH_4^+ , where as sediments collected inside the channel at Marker 157 and Marker 59 released the least. Marker 59 and 91 sediments released the highest percentage of the ΣNH_4^+ contained in the sediments (determined by extraction). This was true for both the open and closed experiments. Marker 45 sediments in the closed experiments also released a large portion of the total contained in the sediments.

Experiments where the largest fraction of ΣNH_4^+ was released were also characterized by the highest mass of sediments added. Sediment mass additions in the open experiments exceeded at least twice the mass addition in closed experiments. Porewater additions in open experiments also far exceeded the additions in the closed experiments, and were considered in final calculations of NH_4^+ concentrations and ΣNH_4^+ release.

PO_4^{-3} Release During Resuspension

The sediments collected inside the GIWW were all black in color and sulfide could be detected when the sediments were exposed. Anoxic estuarine sediments characterized by high concentrations of sulfide, particularly in the Laguna Madre generally have high concentrations of acid volatile sulfide composed mainly of reactive iron-sulfide compounds. These compounds are rapidly oxidized upon exposure to oxygenated environments. The oxidation of reduced iron compounds results in the formation of metal oxides and hydroxides which are known to strongly adsorb phosphate from solution. This explains the general trend observed in the time course PO_4^{-3}

concentrations measured for the various resuspension experiments. Figure 4 displays typical results which were observed in almost every case. An initial rapid increase in the PO_4^{-3} concentration was followed by a rapid decrease. PO_4^{-3} released initially by porewater dilution was probably readsorbed due to the simultaneous formation of oxide minerals in the experiments. Unfortunately this complicates the interpretation of the PO_4^{-3} data. In some cases where 1.0 or 0.1 grams of sediment were added the PO_4^{-3} concentration actually decreased to below the background level by the end of the experiment.

Table 5. Results for the open, elutriate test. Data is presented with inner sediments at the top of the chart and outer sediments in the lower section

Location	NH4 max measured (μM)	Grams Sediment added	μMoles of NH4 released	NH4 released ($\mu\text{M/gdw}$)	Total NH4 ($\mu\text{M/gdw}$)	Released as % of total
Marker 151	1449.30	26.75	528.45	19.75	32.50	60.78
Marker 157	692.32	52.00	169.67	3.26	11.60	28.13
Marker 45	929.80	45.19	305.03	6.75	15.80	42.72
Marker 59	1074.30	73.63	279.97	3.80	8.00	47.53
Marker 91	982.40	57.17	242.37	4.24	10.90	38.89
Marker 41	828.00	33.70	0.30	0.01	20.60	0.04
Station 13 (N)	705.60	139.54	186.43	1.34	1.60	83.50
Station 28 (S)	99.00	146.67	26.96	0.184	2.41	7.63

NH₄⁺ Flux Determination and Sediment Plume Analysis

Sediment NH₄⁺ profiles were determined in cores taken from seagrass beds and from bare areas. Flux estimations were calculated using Fick's first law along with modifications suggested by Boudreau (1996). Concentration gradients were calculated using the difference between concentrations of NH₄⁺ in the overlying water and at 2 cm sediment depth. The diffusivity was considered a function of porosity and adjusted using the reciprocal of $(1 - \ln(\phi^2))$. NH₄⁺ flux estimations were all positive and ranged from 229 to 622 $\mu\text{M m}^{-2} \text{ dy}^{-1}$ for bare areas, and from 175 to 612 $\mu\text{M m}^{-2} \text{ dy}^{-1}$ in grass covered regions. These estimates were used to calculate a total NH₄⁺ flux from sediments in Southern Laguna Madre, considering a total sediment surface area of 487 km² and approximately 70% seagrass coverage. A conservative estimate of NH₄⁺ flux will be presented in the discussion with calculations of potential release associated with a dredging event.

Results of the sediment plume sampling collected in February of 1997 are presented in Figure 5. The column graph at the top of the figure displays the NH₄⁺ concentration and suspended solid quantities measured at the three points [at the dredge pipe, 30 meters away (near), and 300 meters away (far)] . Both NH₄⁺ and suspended solid concentration increase with distance from the dredge pipe. The increase in suspended solids with distance from the source was due to the interruption of sediment flow from the outlet during sampling allowing the sediment plume to move with the current away from the area of disposal. NH₄⁺ concentrations increased from approximately 20 μM near the dredge pipe terminus to over 130 μM in the sediment plume. At the bottom of Figure 5 suspended particle concentration is compared to NH₄⁺ concentration. The comparison appears to reflect a non-linear relationship between the amount of suspended solid and quantity of NH₄⁺ released. As the suspended particle load in the water increased the concentration of NH₄⁺ seemed to follow an exponential increase. It should be kept in mind that the higher concentration of particles also corresponds to an increase in distance from the dredge pipe, and thus an increase in the amount of time the sediments had been resuspended.

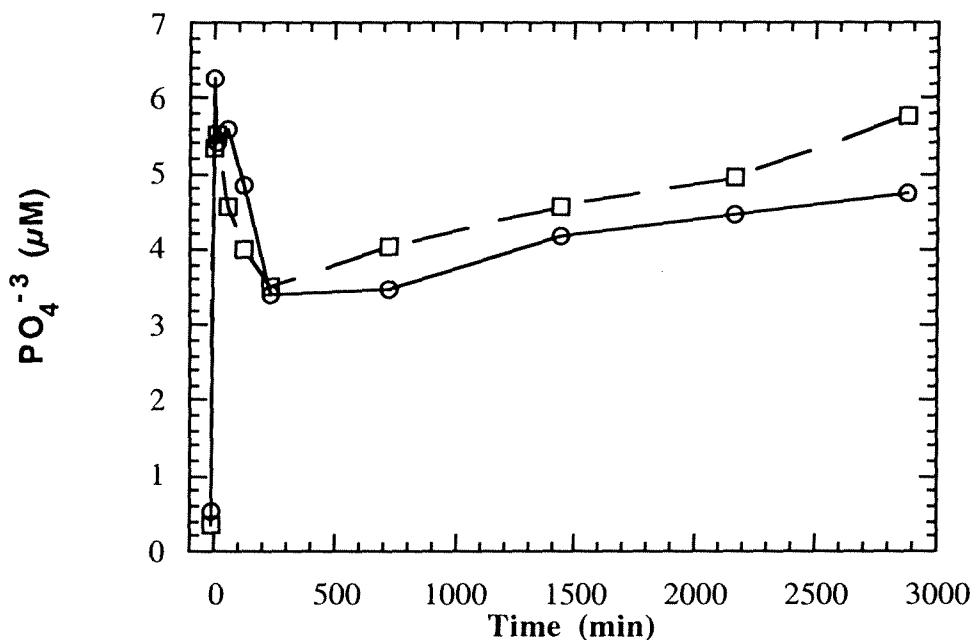


Figure 4. Time course PO_4^{-3} concentrations observed during resuspension of Marker 59 sediments from Laguna Madre. Squares and circles represent duplicate release experiments.

Discussion

Comparison of Release Experiments

The impetus for this study was to compare the currently accepted method of NH_4^+ release assessment to a method that may more accurately represent open water environments. We found that our closed system experiments resulted in much larger values of released NH_4^+ when compared to the elutriate method. Major differences between the two methods are the constant aeration of the sediment resuspensions in the elutriate experiments and terminating the agitation of the sediment water mixture after one hour. Although these differences in methodology influenced

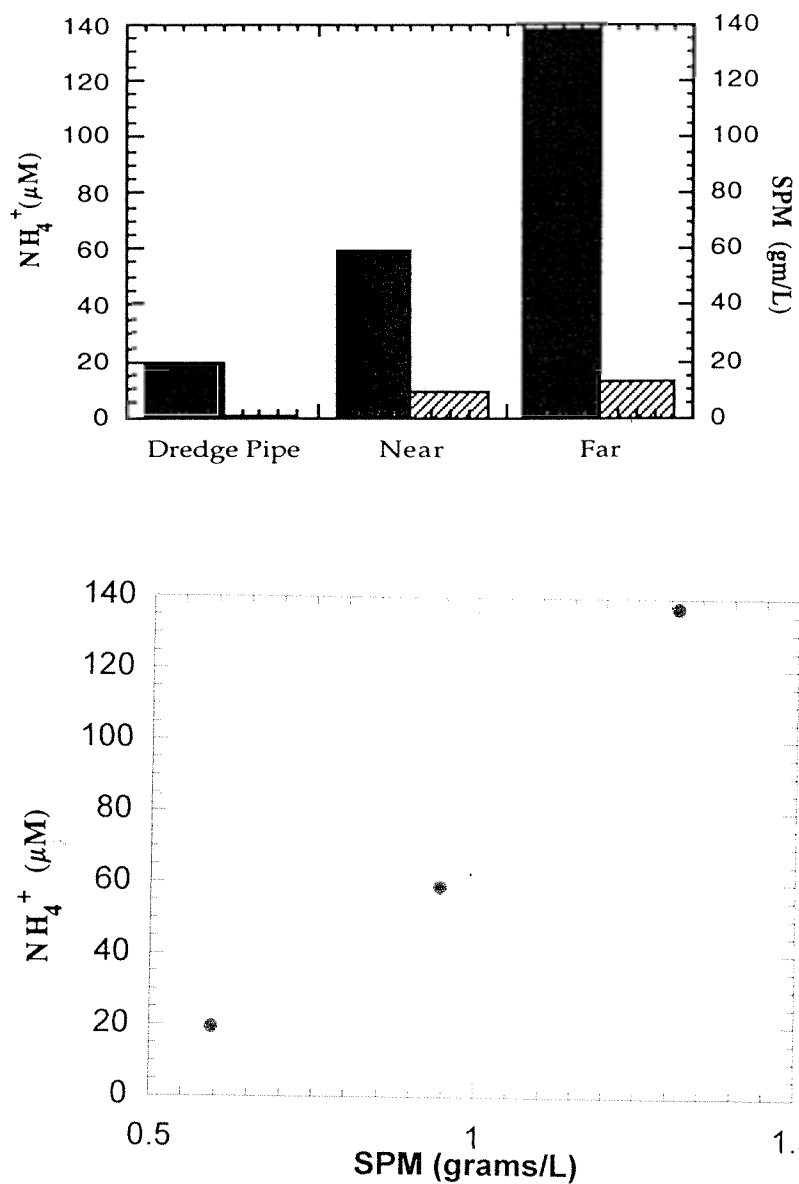


Figure 5. Data collected during a dredging event in February, 1997. The upper column graph displays NH_4^+ concentrations (shaded column) as well as suspended particulate matter (SPM)(cross hatched column) at points 300 meters from the dredge pipe (far), 30 meters from the dredge pipe(near, and immediately adjacent to the pipe. The lower graph compares NH_4^+ concentrations to suspended particle load. The points are results of duplicate samples at each location.

the experimental results, they are probably of secondary importance to the relative amount of sediment added in the two techniques.

In the elutriate experiments the sediment dry weight to volume ratio ranged from 52.4 grams to 249 grams L⁻¹. In contrast, sediment dry weight addition in the closed system experiments were 10 grams, 1 gram and 0.1 grams per liter. Figure 6 displays the final concentration [assumed to be the equilibrium concentration (μM)] measured at the end of each resuspension experiment using sediments collected at Marker 45. The concentration is plotted against the sediment dry weight addition normalized to one liter of overlying water. The graph resembles a typical Langmuir isotherm with the closed experiment values found on the linear part of the curve while the elutriate experiment measurements are closer to the saturation part of the curve. This type of relationship was observed for all sediments. Elutriate experiments were largely designed to imitate conditions inside dredge pipes during the sediment relocation process where very high sediment to water ratios occur. After sediments are expelled into open waters the ratio of sediment to water volume rapidly decreases as the sediment plume moves away from the source. Thus our closed system experiments may better represent conditions in open water where sediment plume dilution and persistence of the particles in suspension for extended periods of time allows for greater nutrient release.

Measurements taken in the field during a dredging event appear to support this conclusion. The data presented in Figure 5 illustrate the release of NH_4^+ after the initial dilution of porewater. Instead of a linear increase of NH_4^+ with suspended particle concentration, we observed more of an exponential relationship. This would seem to indicate that NH_4^+ release continues after porewater dilution. In both the elutriate and closed experiments large quantities of NH_4^+ associated with the "fast" release of loosely bound ions were released in the first five minutes of sediment resuspension. This fraction will be important in the early stages of particle resuspension, releasing NH_4^+ to the surrounding water following the initial dilution of pore water dissolved NH_4^+ . In addition, smaller particles capable of remaining in suspension for long time periods (on the order of hours) will continue to desorb NH_4^+ until removal by sedimentation.

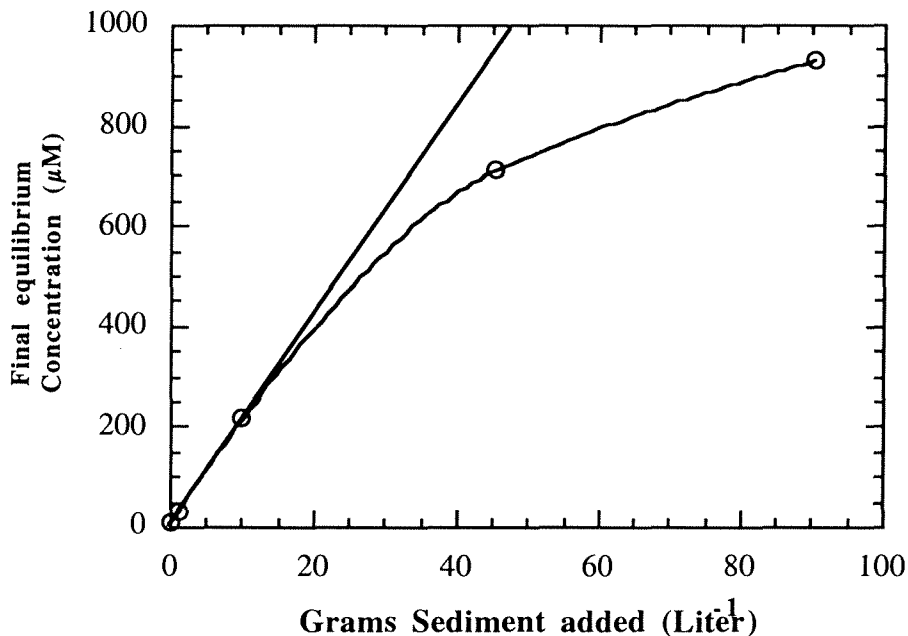


Figure 6. Final equilibrium NH_4^+ concentration vs. sediment (dry weight) normalized to the volume of overlying water used in resuspension experiments with Marker 45 sediments. The data points fall on a typical Langmuir type curve. Data collected from the closed experiments fall on the linear section of the curve near the origin. The points falling closer to the saturation part of the relationship are results generated from the open, elutriate test.

Environmental Implications

We have established that sediments collected from the bottom of the GIWW have very large quantities of NH_4^+ associated with the porewaters and solid fraction and that their resuspension could result in release of possibly environmentally significant quantities of NH_4^+ , particularly in very shallow regimes. A recent investigation by Blackburn (1997) using a simulation model of sediment resuspension concluded that resuspension of up to 2.4 cm of surficial sediment and porewater would have inconsequential effects on the overlying water nitrogen concentration, and thus no effect on primary producers in the water column. In a mesocosm experiment, Sloth et al. observed a slight increase in NH_4^+ concentrations where an estimated 6 mm of surficial

sediments were resuspended and the liberated NH_4^+ nitrogen was assumed to be relatively rapidly absorbed by planktonic algae (Sloth 1996). The present investigation concentrates on the affect of large scale dredge operations which are characterized by removal of sediments to depths of 1 meter (Technical report, Cheryl A. Brown and N. C. Kraus. for U.S. Army Corp. of Engineers 1996). A similar investigation conducted by Jones and Lee using the elutriate procedure concluded that dredge associated nutrient release would rarely have an adverse effect on water quality (Jones and Lee 1979). These authors determined that the relatively short-lived duration of these events would prevent any significant affects on the dump site surroundings, though they admit that this conclusion should be evaluated on a site-by-site basis.

Using the data collected in the present study we calculated a potential release of NH_4^+ during a dredging operation near Port Mansfield Texas in 1989 where over 318,000 m^3 of sediment were removed from the channel and deposited outside. Considering the volume fraction determination of the sediments, this would result in the dilution of over 5.3×10^8 liters of porewater. These calculations should be considered as rough estimates of the conditions which actually occur during large scale sediment relocation. Using the porewater concentration of NH_4^+ , and the volume fraction of water we calculated a release of NH_4^+ through porewater dilution. In addition we added the quantity associated with the loosely bound fraction of NH_4^+ which was released within 5 minutes of resuspension. The potential release in this relatively small area of estuary was in excess of 46 metric tons of NH_4^+ over a time period of approximately two months. For comparison, we used flux calculations estimated from 12 nutrient profiles obtained from sediment cores collected in the lower Laguna Madre in both grass covered and bare areas. Calculated NH_4^+ release from the sediments on a monthly basis was approximately 80 metric tons. These numbers should be considered as conservative in that we have not taken into account the release of additional NH_4^+ associated with a slow release fraction. In our laboratory studies we determined that this fraction can contribute a significant amount of the total release occurring during sediment resuspension. In addition we have only considered physical diffusion of NH_4^+ from sediments and have not attempted to include biological factors such as bioirrigation. Sediment cores taken during sampling trips in the Laguna Madre displayed an biologically active surficial zone. The macrobenthos found in surficial sediments has been determined capable of significantly altering the flux of materials out of and into the sediment (Aller, 1982)

The potential for nitrogen enrichment during channel maintenance operations has significant implications for the Laguna Madre estuary. Alterations in the NH_4^+ concentration, specifically the ratio of available NH_4^+ to available NO_3^{-2} , may influence the structure of the planktonic algal communities which inhabit the Laguna Madre. A well known phenomena referred to as “the brown tide” has been occurring in this south Texas estuarine system for the last seven years. Street et al. described the brown tide event and isolated the organism responsible for the bloom (Street, 1997). This organism is a member of the Chrysophyceae family and is closely related to an organism associated with brown tide in Long Island Sound and Naragansett Bay, *Aureococcus anophagefferens*. Unlike the organism isolated in the Northern Atlantic coastal systems, the Laguna Madre species cannot utilize nitrate as a N source (DeYoe and Suttle 1994). Lomas et al. have characterized the nitrogen uptake dynamics of the organism isolated from Long Island Sound and Naragansett Bay (Lomas 1996). The authors determined that *A. anophagefferens* is well adapted to low light, highly turbid environments, and in these types of conditions, preferentially take up NH_4^+ as nitrogen source. This could be due to the fact that NO_3^{-2} uptake requires light (energy) whereas NH_4^+ uptake does not.

The onset of the brown tide in south Texas was associated with a large die-off of fish and benthos during severe freezes in the estuary in the winter of 1989 (DeYoe and Suttle 1994). This event caused NH_4^+ concentrations to increase to $69 \mu\text{M}$ in the Southern Laguna Madre and coincided with a collapse of the micro- and macro- zooplankton communities. These events taken together with the physiological characteristics of the Texas brown tide organism created exceptionally favorable conditions for the mono-specific bloom. NH_4^+ inputs during dredging events combined with a reduction in light penetration could simulate the substrate alterations of the original event, at least in a localized fashion. Due to the geographical structure of the Laguna Madre estuary, nutrient concentration perturbations are not transported rapidly outside of the estuary and eliminated. These localized alterations can persist, essentially acting to exacerbate the brown tide bloom.

Acknowledgments

We would like to thank Samantha Joye, George Jackson, Jeffrey Kovacs, Roswell C. Downer, Chris Garcia, Jennifer Wormuth, D. C. Cooper, and L. Cifuentes for technical and creative assistance.

References Cited

- Aller RC (1982) The effects of macrobenthos on chemical properties of marine sediments and overlying water. In: *Animal Sediment Relations*. Ed. P. L. McCall and M. J. S. Tevesz. Plenum Publications, New York, NY. 53-102.
- Berner RA (1976) Inclusion of adsorption in the modeling of early diagenesis. *Earth Planet Sci Lett* 29:333-340.
- Blackburn TH (1997) Release of nitrogen compounds following resuspension of sediment: Model predictions. *J Mar Sys* 11:343-352.
- Boatman CD, Murray JW (1982) Modeling exchangeable NH_4^+ adsorption in marine sediments: Process and controls of adsorption. *Limnol Oceanog* 27: 99-110.
- Boudreau B (1996) The diffusive tortuosity of fine grained unlithified sediments. *Geochim Cosmochim Acta* 60:3139-3142.
- Chin-Leo G, Benner R (1991) Dynamics of bacterioplankton abundance and production in seagrass communities of a hypersaline lagoon. *Mar Ecol Prog Series* 73:219-230
- DeYoe HR, Suttle CA (1994) The inability of the Texas "Brown Tide" alga to use nitrate and the role of nitrogen in the initiation of a persistent bloom of this organism. *Jour Phycology* 30:800-806.
- Fenchel T, Blackburn TH (1979) *Bacteria and Mineral Cycling*. New York, Academic Press.
- Froelich PN (1988) Kinetic control of dissolved phosphate in natural rivers and estuaries: A primer on the phosphate buffer mechanism. *Limnol Oceanog* 33:649-668.
- Jones RA, Lee GF (1979) The significance of dredging and dredged material disposal as a source of nitrogen and phosphorus for estuarine waters. In: *Estuaries and Nutrients* Eds. B. J. Neilson, L. E. Cronin. Clifton, New Jersey, Humana Press. 636.
- Krom MD, Berner RA (1980) Adsorption of phosphate in anoxic marine sediments. *Limnol Oceanog* 25:797-806.

- Laima MJC (1992) Extraction and seasonal variation of NH_4^+ pools in different types of coastal marine sediments. *Mar Ecol Prog Ser* 82:75-84.
- Lomas MWP, Gilbert M, *et al.* (1996) Characterization of nitrogen uptake by natural populations of *Aureococcus anophagefferens* (Chrysophyceae) as a function of incubation duration, substrate concentration light and temperature. *Jour Phycology* 32:907-916.
- Mackin JE, Aller RC (1984) Ammonium adsorption in marine sediments. *Limnol Oceanog* 29:250-257.
- Nixon SW (1981) Remineralization and nutrient cycling in coastal marine ecosystems. In: *Estuaries and Nutrients* Eds. B. J. Neilson and L. E. Cronin. Clifton, New Jersey, Humana Press. 636.
- Plumb RH (1980) Sampling, Preservation and Analysis of Sediment Samples: State-of-the-art Limitations. Springfield, VA, National Technical Information service.
- Pomeroy LR, Smith EF, *et al.* (1965) The Exchange of phosphate between estuarine water and sediments. *Limnol Oceanog* 10:167-172.
- Rizzo M (1990) Nutrient exchanges between the water column and a subtidal benthic microalgal community. *Estuaries* 13: 219-226.
- Rizzo WM, Christian RR (1996) Significance of subtidal sediments to heterotrophically-mediated oxygen and nutrient dynamics in a temperate estuary. *Estuaries* 19:475-487.
- Rosenfeld JK (1979) Ammonium adsorption in nearshore anoxic sediments. *Limnol Oceanog* 24:356-364.
- Rutgers van der Loeff MM., Boudreau BP (1997) The effects of resuspension on chemical exchanges at the sediment-water interface in the deep sea - A modeling and natural radiotracer approach. *Jour Mar Sys* 11:305-342.
- Seitzinger SP, Gardner WS, *et al.* (1991) The effect of salinity on ammonium sorption in aquatic sediments: Implications for benthic nutrient cycling. *Estuaries* 14:167-174.

- Sloth NP, Blackburn TH, *et al.* (1995) Nitrogen cycling in sediments with different organic loading. *Mar Ecol Prog Ser* 116:163-170.
- Sloth NP, Riemann B, *et al.* (1996) Resilience of pelagic and benthic microbial communities to sediment resuspension in a coastal ecosystem, Knebel Vig, Denmark. *Estuar Coast Shelf Sci* 42:405-415.
- Street GT, Montagna PA, *et al.* (1997) Incorporation of brown tide into an estuarine food web. *Mar Ecol Prog Ser* 152:67-78.
- Strickland JD, Parsons TR (1972) A practical hand book of seawater analysis. Ottawa, Fisheries Research Board of Canada.
- Wainright SC (1987) Stimulation of heterotrophic microplankton production by resuspended marine sediments. *Science* 238:1710-1712.
- Wainright SC, Hopkinson CS Jr. (1997) Effects of resuspension on organic matter processing in coastal environments: a simulation model. *Jour Mar Sys* 11:353-368.

CHAPTER IX: RESPONSE OF *THALASSIA* *TESTUDINUM* TO A DREDGING EVENT

Contents

Abstract.....	3
Introduction.....	4
Materials and methods.....	5
Study sites.....	5
Photon flux measurement.....	5
Water column and sediment characteristics.....	7
Biological measurements.....	8
Statistics.....	9
Results.....	9
Underwater irradiance and light attenuation coefficient.....	9
Water column and sediment characteristics.....	9
Seagrass shoot density and biomass.....	14
Leaf production rates and blade chlorophyll.....	14
Discussion.....	20
References.....	24

Tables

Table 1. Sediment grain size distribution at control (Fix 2) and buried (PA235a & b) and non-buried (PA235c & d) dredge disposal sites.....	13
---	----

Figures

Figure 1. Study area at lower Laguna Madre, Texas.....	6
Figure 2. Surface and underwater photon flux density at Fix 2 (control) and PA235c & d (dredge disposal sites) during pre- and post-dredging.....	10

Figure 3. Light attenuation coefficients at Fix 2 and PA235c & d	11
Figure 4. Water temperature (A), salinity (B) and depth (C) at Fix 2 and PA235 sites	12
Figure 5. Water column chlorophyll (A), NH_4^+ (B) and $\text{NO}_2^- + \text{NO}_3^-$ (C) at Fix 2 and PA235 sites..	15
Figure 6. Sediment pore water NH_4^+ concentrations at control (Fix 2) and buried (PA235a & b) and non-buried (PA235c & d) dredge disposal sites.....	16
Figure 7. <i>Thalassia testudinum</i> . Changes in shoot density at the control site (Fix 2) in comparison to PA235 sites adjacent to the deposition of dredged materials, both before and after dredging began.....	17
Figure 8. <i>Thalassia testudinum</i> . Above- and below-ground biomass at the control site (Fix 2) in comparison to PA235 sites adjacent to the deposition of dredged materials, both before and after dredging began.....	18
Figure 9. <i>Thalassia testudinum</i> . Leaf production rates at the control site in comparison to PA235 sites.	19
Figure 10. <i>Thalassia testudinum</i> . Blade chlorophyll content and chl <i>a:b</i> ratios of plants from Fix 2 and PA235 sites.....	21

Abstract

The effects of dredging on the production and survival of the seagrass *Thalassia testudinum* were assessed in lower Laguna Madre, Texas. Underwater photosynthetically active radiation (PAR), shoot density, biomass and blade chlorophyll content were monitored before and after the dredging event at a station (PA235) located near the disposal site and at an adjacent but unaffected control site (Fix 2). Dredging of the Gulf Intracoastal Waterway (GIWW) and placement of dredged materials in Placement Area 235 (PA235) began in early September, 1998. Two of the sampling sites at the placement area (PA235a & b) were buried by dredge materials and all plant shoots disappeared within 2 months after dredging; two remaining sites (PA235c & d), located within 200 m distant of the buried sites were exposed to heavy siltation but not buried. Underwater irradiance at the PA235 sites was reduced significantly compared to the control during and following dredging activity. This increased light attenuation was sustained for over 9 months. Water column chlorophyll and NH_4^+ concentrations increased significantly after dredging. Increases in water column NH_4^+ concentrations at the PA235 sites were coincident with increases in water column chlorophyll concentrations, suggesting high re-mineralized nitrogen flux from the sediment, which had NH_4^+ values exceeding 500 μM after dredging. Shoot density and biomass declined significantly, and leaf production rates decreased to a third of those at the control site after dredging.

Dredging activity was deleterious to seagrass growth and survival as a result of direct burial and increased light attenuation caused by sediment suspension. Burial was severe but more localized in comparison to the increased light attenuation, which potentially affects extensive areas of seagrass beds for long periods due to continuous re-suspension of dredged materials by wind-generated waves.

Introduction

Significant declines in seagrass coverage are related to human activities (Cambridge & McComb 1984, Cambridge et al. 1986). Pollution, ship and barge traffic, sewage dumping and dredging activities can reduce seagrass growth and consequently cause declines in seagrass coverage. While dredging activities are critical for maintaining shallow channels and harbors, the shallow bay and coastal areas near the channels and harbors usually contain flourishing seagrasses and other submerged aquatic macrophytes. Therefore, dredging activities can remove submerged aquatic vegetation directly by burial and indirectly through increases in light attenuation from sediment suspension.

Laguna Madre has the most extensive seagrass beds in Texas coastal regions. The Gulf Intracoastal Waterway (GIWW), which passes through Laguna Madre, provides an essential connection for the transportation of products vital to the economy of Texas (Texas Department of Highway and Public Transportation 1980). Some areas of the GIWW have relatively high shoaling rates and require maintenance dredging by the U. S. Army Corps of Engineers (USACE) approximately every 2 years (Brown and Kraus 1997). The present study examined the effects of dredging activities on seagrasses in an open-bay dredged material placement area along the GIWW in the lower Laguna Madre.

The productivity and physiological responses of seagrasses to environmental changes caused by dredging activities have been little documented despite the immediate and direct impacts on seagrass growth and survival (Onuf 1994). The main cause of seagrass loss resulting from maintenance dredging is underwater light reduction (Onuf 1994). Seagrasses respond morphologically and physiologically to reduced underwater irradiance by increasing chlorophyll content, narrowing blade width, and decreasing chl *a:b* ratio, biomass and density (Czerny and Dunton 1995, Lee and Dunton 1997).

We hypothesized that dredging and the disposal of dredged materials would affect seagrass

productivity and survival through burial with dredge spoils and through severe light reduction with periods of high light attenuation extending for several months as dredged materials become continually re-suspended by winds and currents. To test this hypothesis, we monitored the underwater light regime before and after dredging. Additionally, we characterized water column and sediment environments and assessed the changes in productivity, shoot density, biomass and blade chlorophyll content of the seagrass *Thalassia testudinum*.

Materials and methods

Study sites

This study was conducted in an open-bay dredged material placement area (PA235) along the Gulf Intracoastal Waterway (GIWW) in lower Laguna Madre (Fig. 1). *Thalassia testudinum* is the dominant seagrass species in this area. We established four sampling sites within a 0.5 km² area at a station (PA235) located west of the placement area. Sites PA235a (26° 07' 05"N, 97° 13' 50"W) and PA235b (26° 07' 11"N, 97° 13' 56"W) were located near the edge of the dredged material placement area, and two additional sites PA235c (26° 07' 13"N, 97° 13' 40"W) and PA235d (26° 07' 21"N, 97° 13' 48"W) were placed ca. 200 m west of the first two. A nearby but unaffected *T. testudinum* bed (Fix 2; 26° 08' 06"N, 97° 12' 29"W) was chosen as a control (Fig. 1). Lower Laguna Madre is characterized by strong winds predominantly from the southeast (Brown and Kraus 1997). These winds carry the dredged sediments to the northwest, leaving the control site (Fix 2; located to northeast of the dredged material placement area), unaffected. Dredging of the Gulf Intracoastal Waterway (GIWW) and placement of dredged materials in PA235 began in early September 1998.

Photon flux measurement

Underwater photosynthetically active radiation (PAR; 400-700 nm) was collected continuously during pre- and post-dredging periods (June 1998 to June 1999) using a LI-193SA spherical quantum sensor at seagrass canopy level, which provided input to LI-1000 data-logger (LI-COR). Since

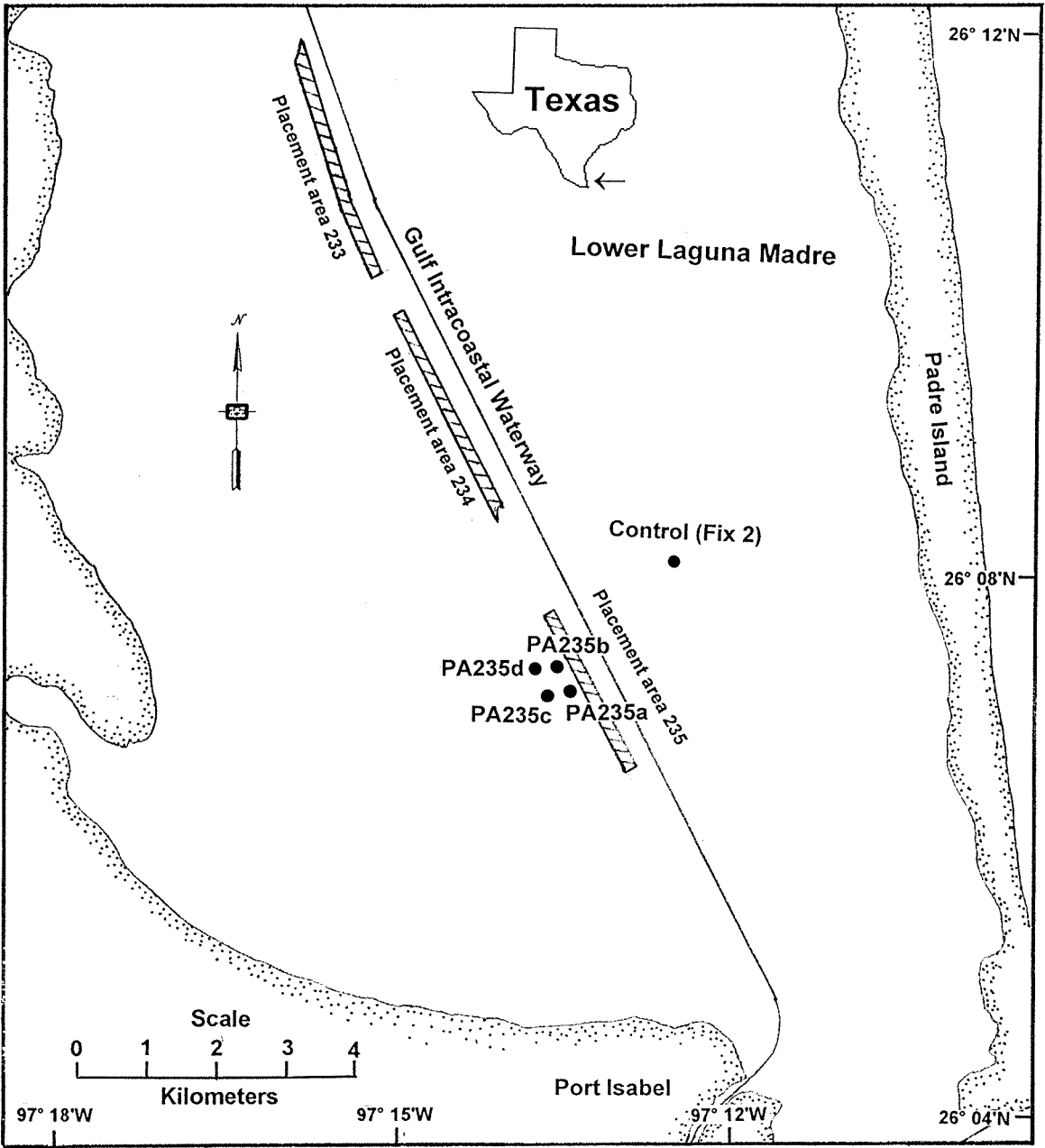


Figure 1. Study area at lower Laguna Madre, Texas.

seagrass beds at sites PA235a and PA235b were unexpectedly and rapidly buried by dredge materials that were not retained in the placement area, underwater PAR was monitored from the control site (Fix 2) and sites PA235c and PA235d following burial of the quantum sensors at PA245a and PA235b. Underwater PFD at PA235c and PA235d were averaged to represent underwater light condition at PA235 sites. The underwater light sensor was cleaned every two weeks to minimize fouling. Coincident measurements of incident surface PAR were made at Fix 2. Daily attenuation coefficient was calculated from the integrated daily surface and underwater irradiance and water depths using the Beer-Lambert equation:

$$I_z = I_0 e^{-kz}$$

where I_z is underwater Photon flux density (PFD) at depth z , I_0 is surface PFD and k is the light attenuation coefficient (m^{-1}). Average water depths were determined by pooling data from one to several independent measurements that occurred during distinct lunar tidal cycles. There is no light data for the period December 1998 to February 1999 when the instruments were retrieved for servicing.

Water column and sediment characteristics

Water temperature, salinity and depth were measured every 2 weeks during pre- and post-dredging periods from control and dredge disposal station. Since all sites were located within a 0.5 km² area, we assumed that water column characteristics were homogeneous among the four PA235 sites. Four replicates surface water samples were collected monthly at the control site and site PA235c to determine water column NH_4^+ and $NO_3^-+NO_2^-$ concentrations. Sediment pore water NH_4^+ concentrations were determined from four replicate sediment samples collected with a 2.5 cm-diameter corer to a depth of 13 cm. Sediment pore water was obtained by centrifugation (5000xg for 15 min) and then diluted (1:5, v/v) with low NH_4^+ seawater (< 0.1 μ M) collected offshore in the Gulf of Mexico. Water column NH_4^+ and $NO_3^-+NO_2^-$ and sediment pore water NH_4^+ concentrations were determined using standard colorimetric techniques following the methods of Parsons et al. (1984).

Sediment grain size distribution was determined from four replicate sediment samples using standard geologic procedures (Folk 1964). Percent distribution by weight was measured for components, rubble (e.g., shell hash), sand, silt and clay. A 20 ml homogenized sediment sample was mixed with 100 ml 3 % hydrogen peroxide to digest the organic materials in sediment. The sample was wet sieved through a 62 μm stainless steel screen using a vacuum pump to separate rubble and sand from silt and clay. The rubble and sand were separated using a 125 μm screen after drying. The silt and clay fractions were measured using a pipette method that samples sediment suspension at 10-cm depth after specific time intervals.

Biological measurements

For shoot density and biomass, 5-10 replicate samples from each sampling site were collected using a 15 cm diameter corer driven approximately 20 cm into the sediments. Samples were cleaned of epiphytes and sediments, separated into leaf (above-ground) and root and rhizome (below-ground) tissues, and dried at 60°C to a constant weight. Shoot density was estimated by counting the number of shoots in the core samples. Shoot density and biomass were expressed as areal estimates: shoots m^{-2} and g dry wt m^{-2} , respectively. For determination of blade chlorophyll content, 10 to 20 shoots from each site were collected and then cleaned of epiphytes in the laboratory. Ten replicate pre-weighed center portions of green leaves were extracted for 3-4 days with 10 ml of N,N-dimethyl formamide (DMF) following Dunton and Tomasko (1994). Absorbance of the extracts was measured at 750, 664 and 647 nm on a spectrophotometer (Shimadzu UV160U). Contents of chl *a* and *b* were determined using the equations of Porra et al. (1989). Leaf production rates were estimated using the blade marking technique (Zieman 1974, Kentula and McIntire 1986). Five to fifteen randomly chosen shoots from each site were marked just above the bundle sheath with a hypodermic needle and collected after approximately 2 weeks. Leaf material was separated into tissue produced before and after marking, and was dried at 60°C to a constant weight. The rate of leaf production (g dry wt $\text{m}^{-2} \text{d}^{-1}$) was determined by dividing the dry weight of new leaf tissue produced after marking by the number of days elapsed since marking and multiplying by its corresponding shoot density. Since all shoots disappeared after dredging, leaf production rates and blade chlorophyll concentrations were measured in control and non-buried dredge disposal station.

Statistics

All values are reported as means \pm 1SE. Statistical analyses were performed using a general linear procedure (SAS Institute, Inc 1989). Data were tested for normality and homogeneity of variance to meet the assumptions of parametric statistics, and assumptions were satisfied for all data tested.

To examine the effects of dredging activities, significant differences in underwater PFD, water column and sediment characteristics, seagrass biomass, leaf growth rate and blade chlorophyll content among study sites and sampling times were tested using a two-way ANOVA with time as a block. When a significant difference among variables was observed, the means were analyzed with a Tukey multiple-comparison test to determine where the significant differences occurred among variables.

Results

Underwater irradiance and light attenuation coefficient

Sites on the edge of the placement area (PA235a & PA235b) were buried by dredged materials. Average underwater PAR at PA235c and PA235d decreased significantly ($P < 0.001$) after dredging began and then remained highly variable (especially in contrast with the control site) for the remainder of the study (to June 1999; Fig. 2). Light attenuation coefficients at PA235c and PA235d increased significantly ($P < 0.001$) and were also highly variable following the initiation of dredging compared to the control site (Fig. 3)

Water column and sediment characteristics

Water temperature, salinity and depth were not significantly ($P = 0.59, 0.82$ and 0.81 , respectively) different between the control and dredge disposal sites during pre- and post-dredging periods (Fig. 4). Rubble, sand, silt and clay content at the control site did not change significantly ($P = 0.33, 0.15, 0.22$ and 0.47 , respectively) after dredging (Table 1). At PA235, rubble and sand content decreased significantly ($P < 0.001$), but silt and clay content increased significantly ($P < 0.001$) after dredging.

Water column chlorophyll and NH_4^+ concentrations were not significantly ($P = 0.14$ and 0.61 ,

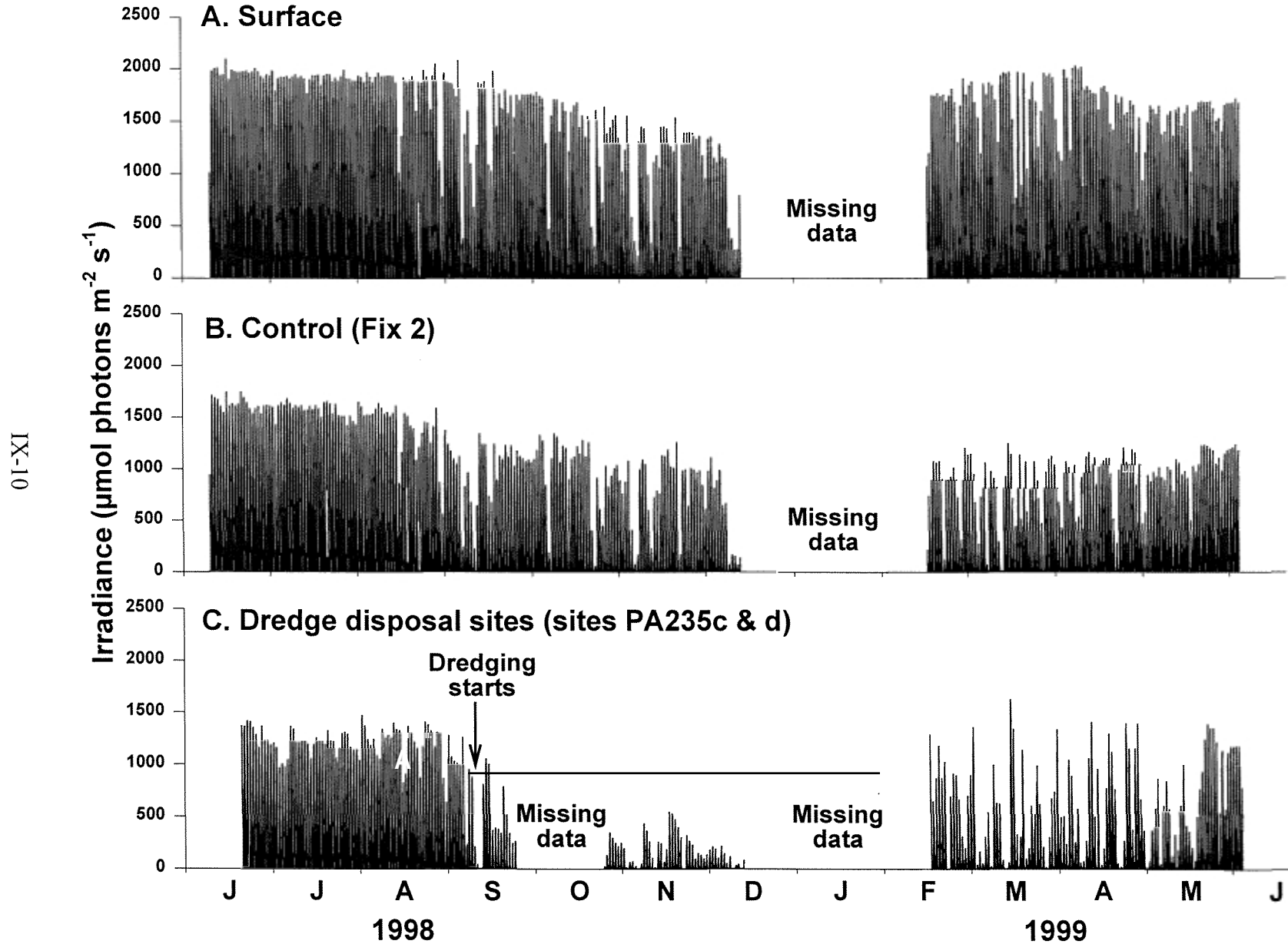


Figure 2. Surface and underwater photon flux density at Fix 2 (control) and PA235c & d (dredge disposal sites) during pre- and post-dredging.

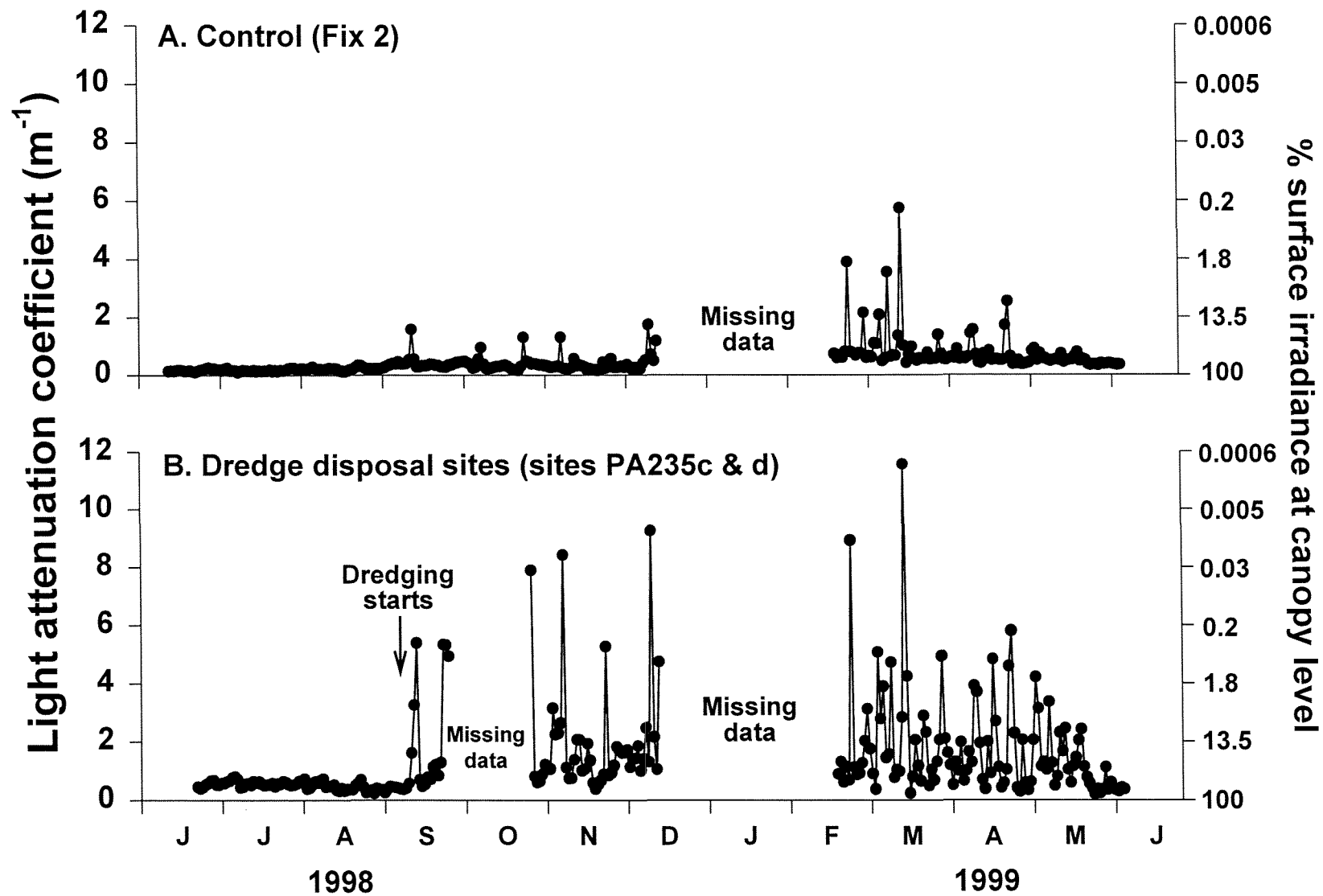


Figure 3. Light attenuation coefficients at Fix 2 and PA235c & d.

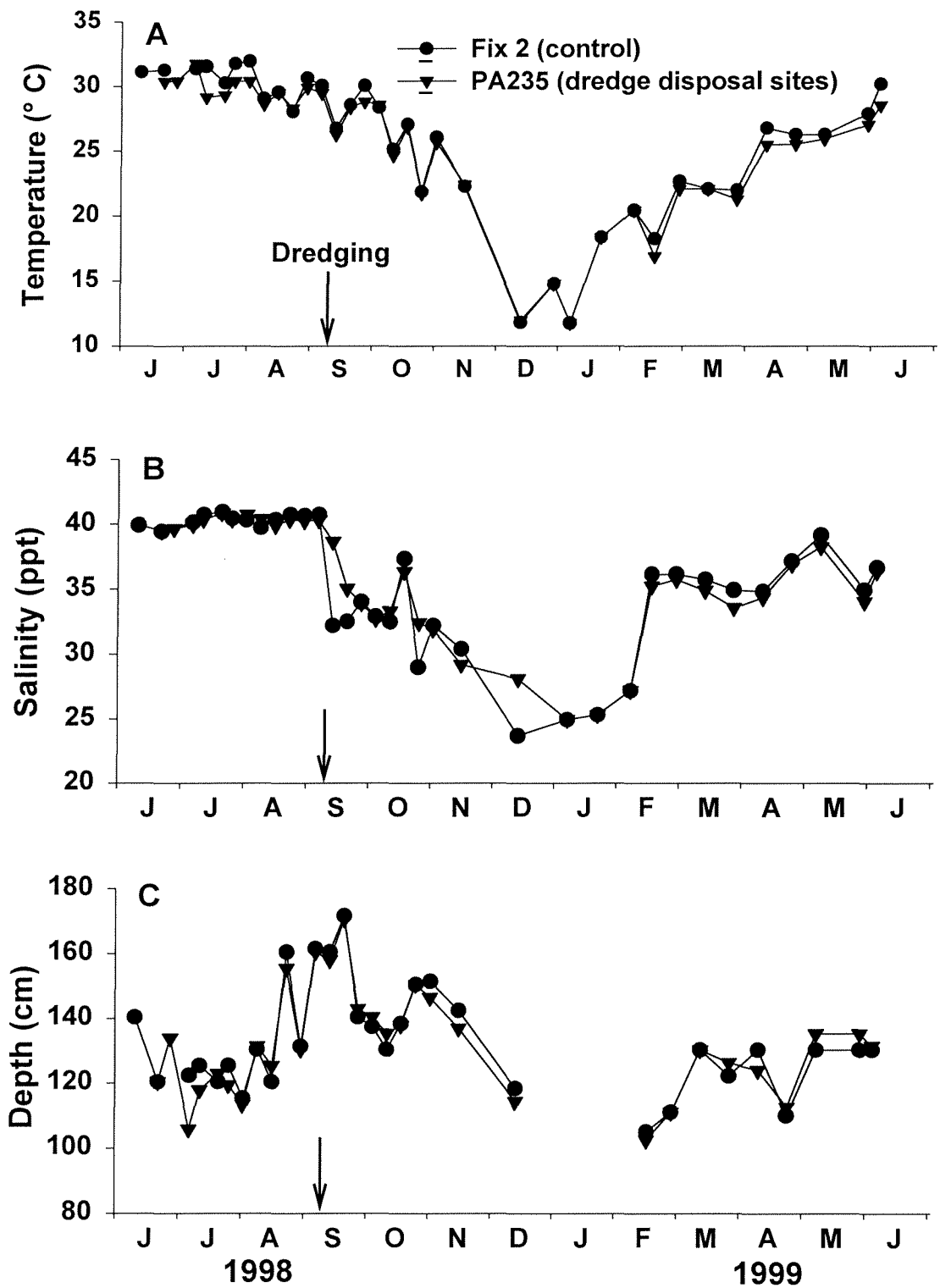


Figure 4. Water temperature (A), salinity (B) and depth (C) at Fix 2 and PA235 sites.

Table 1. Sediment grain size distribution at control (Fix 2) and buried (PA235a & b) and non-buried (PA235c & d) dredge disposal sites.

		Site		
		Control (Fix 2)	Dredge disposal site	
			PA235a & b	PA235c & d
Pre-dredging (June 1998)	Rubble	16.8 ± 9.5	3.1 ± 0.3	-
	Sand	50.3 ± 6.3	25.7 ± 1.8	-
	Silt	12.3 ± 1.4	37.0 ± 1.5	-
	Clay	20.6 ± 2.0	34.2 ± 0.7	-
Post-dredging (February 1999)	Rubble	6.0 ± 0.7	0.1 ± 0.1	7.6 ± 1.5
	Sand	61.5 ± 2.5	0.7 ± 0.3	41.3 ± 2.0
	Silt	10.0 ± 1.0	47.6 ± 5.7	29.4 ± 3.8
	Clay	22.6 ± 1.6	51.7 ± 5.9	21.7 ± 3.6

respectively) different between the control and dredge disposal sites at PA235 during pre-dredging periods (Fig. 5A, B). However, chlorophyll and NH_4^+ concentrations at PA235 sites increased significantly ($P < 0.001$) after dredging compared to the control site. Water column $\text{NO}_3^- + \text{NO}_2^-$ concentrations were not different significantly ($P = 0.21$) between the control and PA235 sites during pre- and post-dredging periods (Fig. 5C). In addition sediment pore water NH_4^+ concentrations were not significantly ($P = 0.17$) different between control and dredge disposal station before the initiation of dredging started (Fig. 6). However, following dredging, pore water NH_4^+ concentrations were significantly ($P < 0.001$) higher at PA235 than the control site at Fix 2. At PA235, buried sites (PA235a & b) had significantly ($P < 0.001$) higher pore water NH_4^+ concentrations than the non-buried sites (PA235c & d) following dredging (Fig. 6).

Seagrass shoot density and biomass

At the control site, shoot density did not significantly ($P = 0.21$) change after dredging (September to October). However, shoot density at sites PA235a & b decreased by 75%, and by 55% at sites PA235c & d one month after dredging began (Fig 7). All seagrass shoots disappeared about 2 months after dredging at sites PA235a & b, which were buried by sediment accumulations of 10 cm or more (Fig. 7). Above- and below-ground and total seagrass biomass were not significantly ($P = 0.41, 0.97$ and 0.99 , respectively) different between the control and PA235 sites before dredging (Fig. 8). However, above-ground biomass decreased by about 95% at sites PA235a & b, and by 70% at sites PA235c & d compared to the control site one month after dredging. Below-ground biomass decreased by 55% and 45% compared to the control site one month after dredging at PA235a & b and PA235c & d sites, respectively. Below-ground biomass continuously decreased at PA235 sites throughout the experiment, while above-ground biomass at sites PA235c & d increased at the end of the experiment (Fig. 8).

Leaf production rates and blade chlorophyll concentrations

Leaf production rates at the control site exhibited a significant ($P < 0.001$) seasonal trend (Fig. 9). Production rates were not different significantly ($P = 0.49$) between control and dredge disposal station before dredging started. However, leaf production rates at the dredge disposal station (0.7-

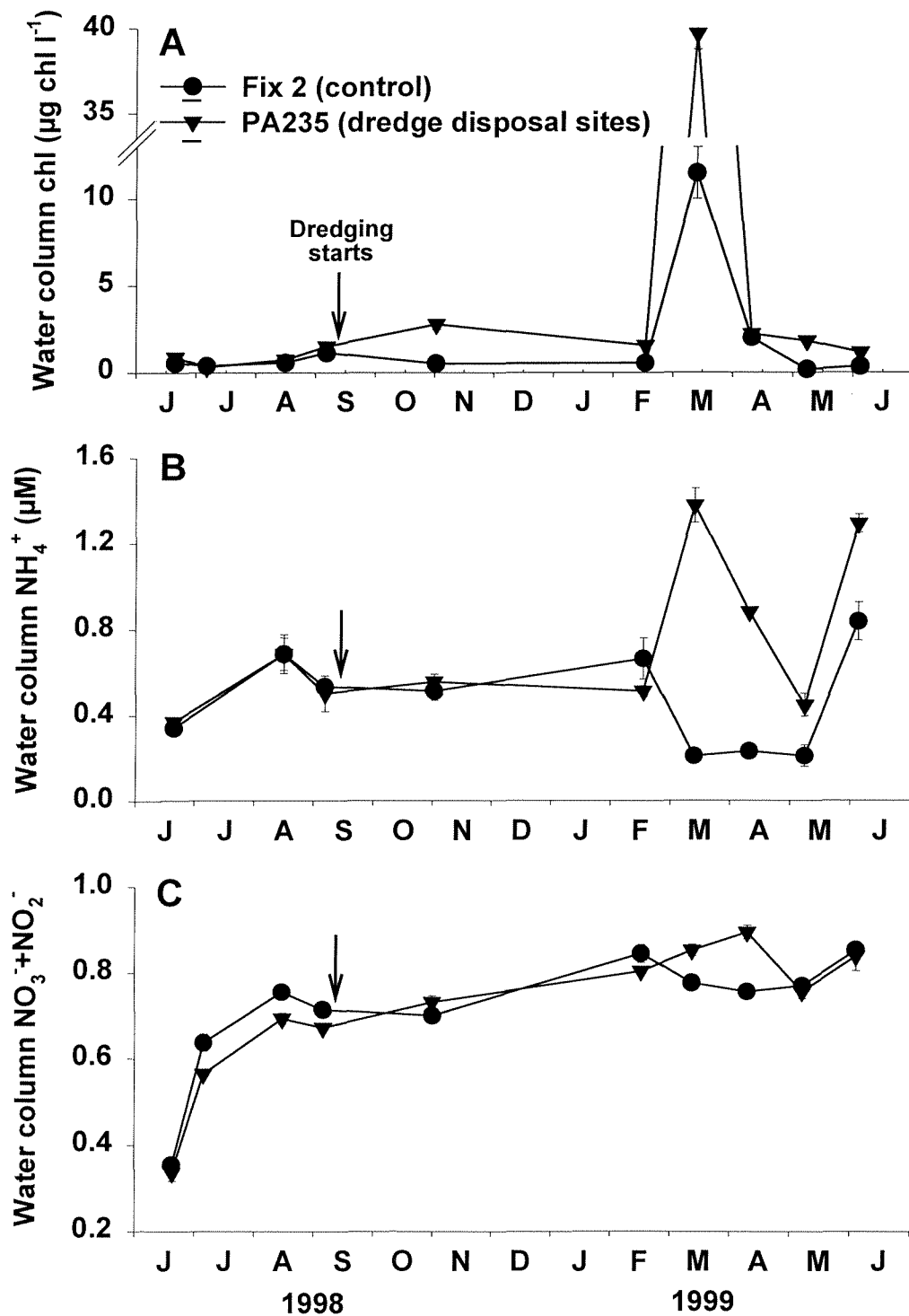


Figure 5. Water column chlorophyll (A), NH_4^+ (B) and $\text{NO}_3^- + \text{NO}_2^-$ (C) at Fix 2 and PA235 sites.

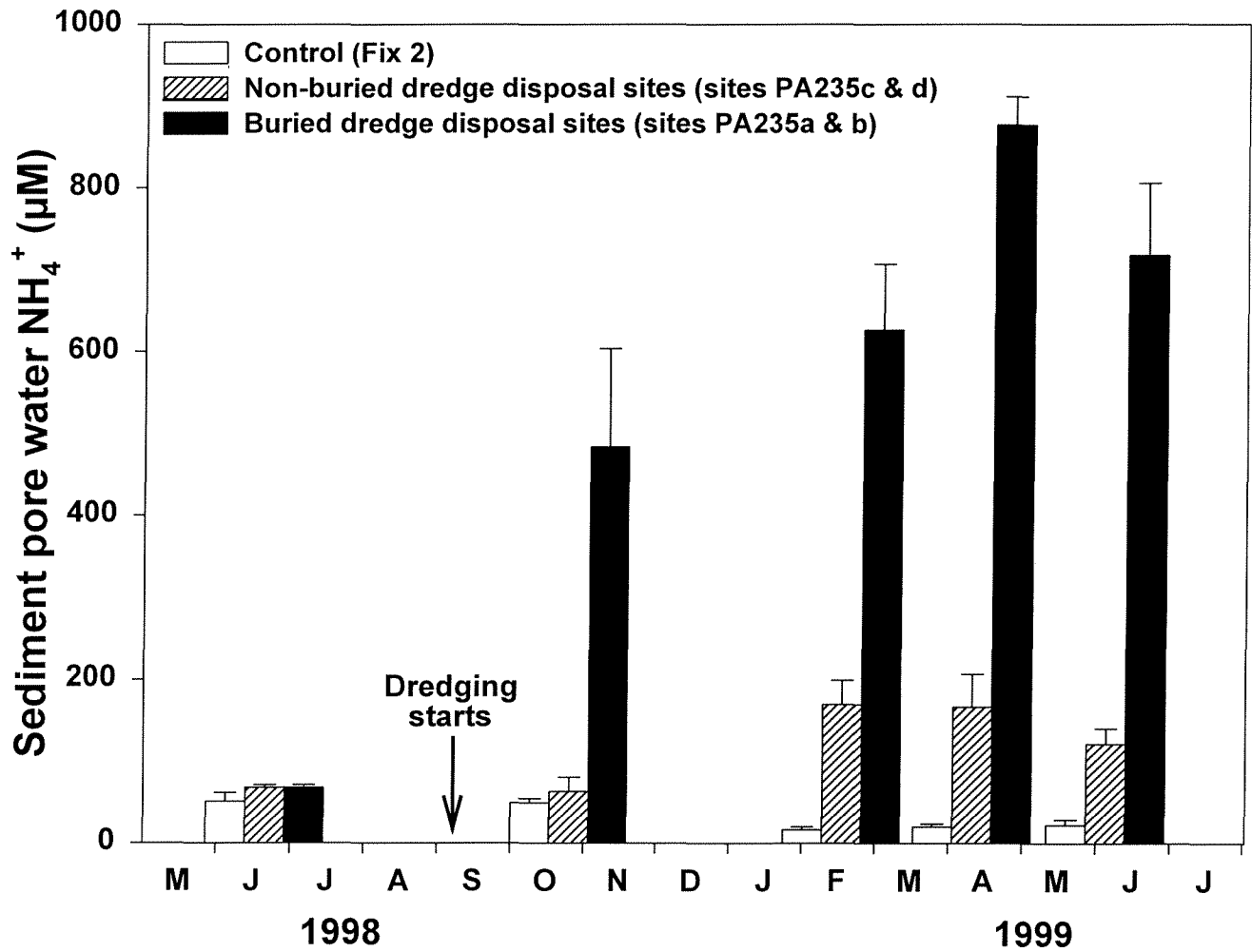


Figure 6. Sediment pore water NH₄⁺ concentrations at control (Fix 2) and buried (PA234a & b) and non-buried (PA235c & d) dredge disposal sites.

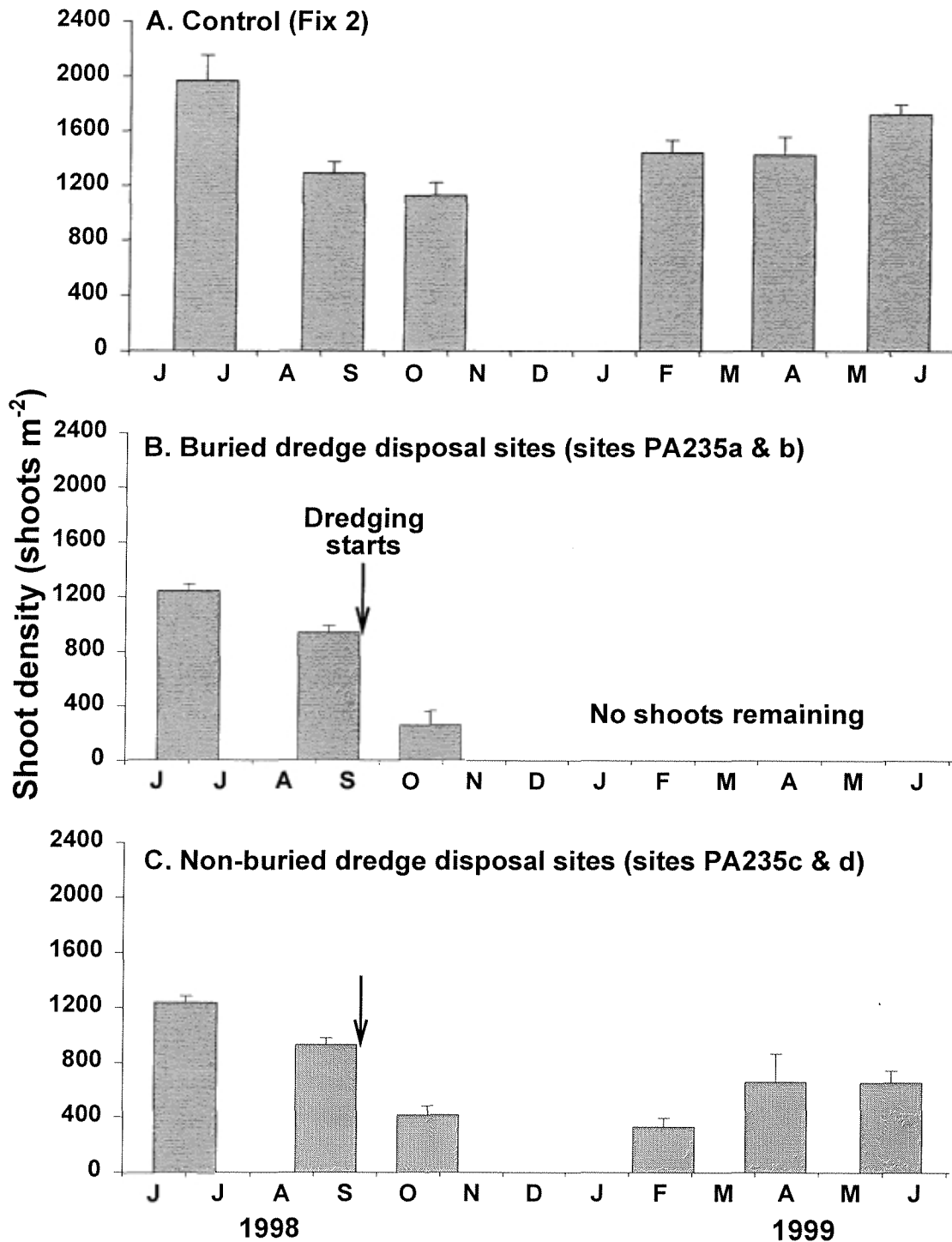


Figure 7. *Thalassia testudinum*. Changes in shoot density at the control site (Fix 2) in comparison to PA235 sites adjacent to the deposition of dredged materials, both before and after dredging began.

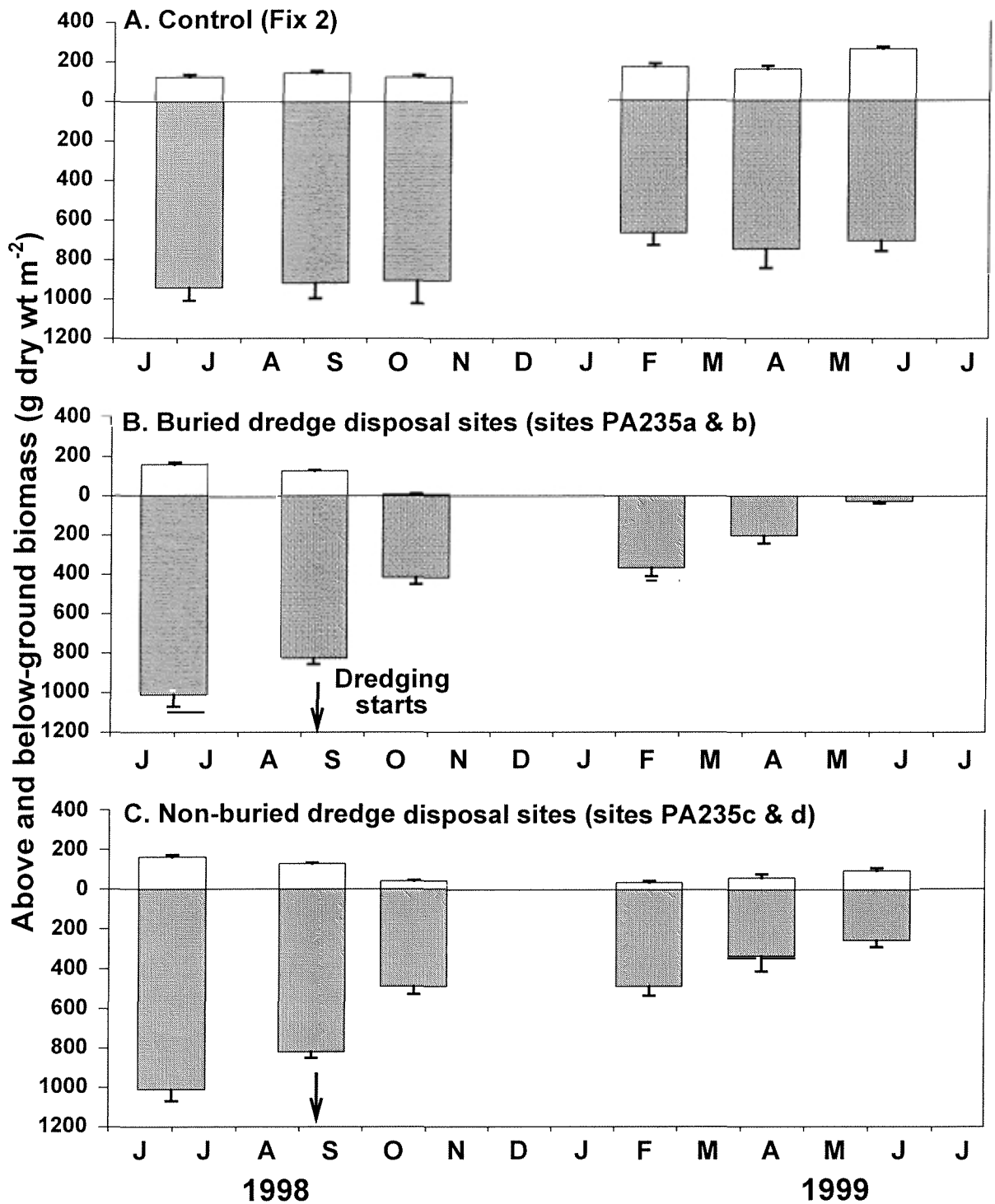


Figure 8. *Thalassia testudinum*. Above- and below-ground biomass at the control site (Fix 2) in comparison to PA235 sites adjacent to the deposition of dredged materials, both before and after dredging began.

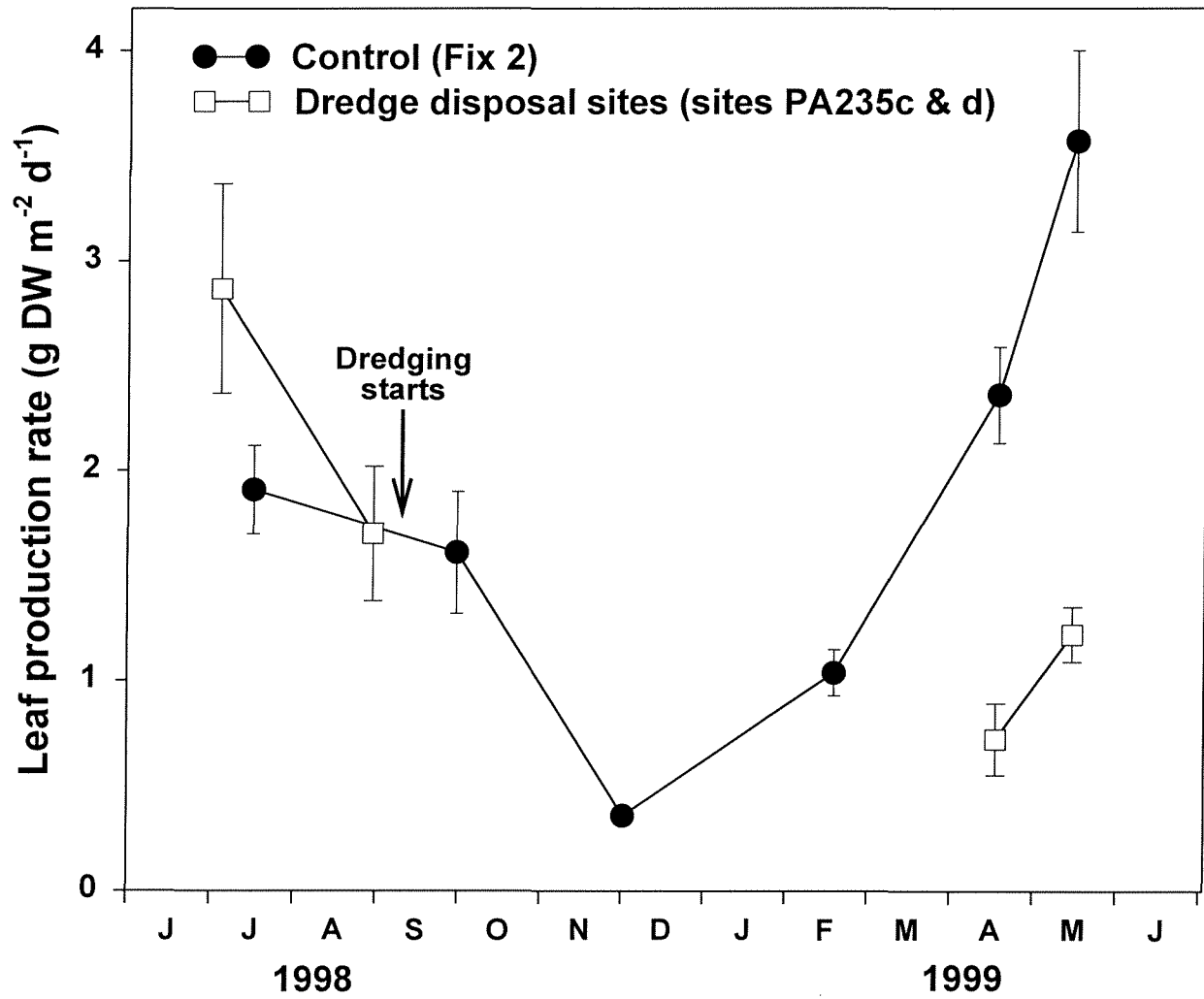


Figure 9. *Thalassia testudinum*. Leaf production rates at the control site in comparison to PA235 sites.

1.2 g dry wt m⁻² d⁻¹) were significantly ($P < 0.001$) lower than at the control site (2.4-3.6 g dry wt m⁻² d⁻¹) after dredging started. Total blade chlorophyll concentrations were significantly ($P < 0.001$) higher and chl. *a:b* ratios were significantly ($P < 0.001$) lower at PA235 compared to the control during pre- and post-dredging periods, except June 1999 (Fig. 10).

Discussion

Dredging activities and open-bay dredge material disposal significantly decreased production and survival of the seagrass *Thalassia testudinum* through direct burial by dredge materials and through significant decreases in underwater PAR levels. Seagrasses on the edge of the dredge placement area were buried by dredge materials, and all plants disappeared within 2 months after dredging. Within 200 m of Placement Area 235, underwater PFD significantly decreased after dredging due to suspension and re-suspension of dredge materials. Underwater irradiance and the light attenuation coefficients at PA235 sites fluctuated highly and were characterized by extremely low underwater PFD and high attenuation coefficient for the duration of the study. These fluctuations suggest re-suspension of the dredged materials during days with high winds and currents. Brown and Kraus (1997) reported that wind-generated waves and currents were the dominant mechanisms for sediment re-suspension in lower Laguna Madre. Approximately 99% of the disposed dredge materials were silt and clay, which are easily re-suspended.

Decreases in growth and biomass as a result of light reduction have been reported in *Thalassia testudinum* (Czerny and Dunton 1995, Lee and Dunton 1997). In this study, decreases in leaf production rate, shoot density and biomass were probably due to the reduction of underwater light caused by dredging activities. Above-ground biomass decreased more rapidly than the biomass of below-ground tissues. Rapid reductions of leaf biomass are normal responses of terrestrial and submerged plants to reduced light levels (Addicott and Lyon 1973, Backman and Barilotti 1976, Lee and Dunton 1997). After dredging, seagrasses at the sites PA235c & d received an average of 27% of surface irradiance (% SI), while plants in the control site received approximately 60% SI. Czerny

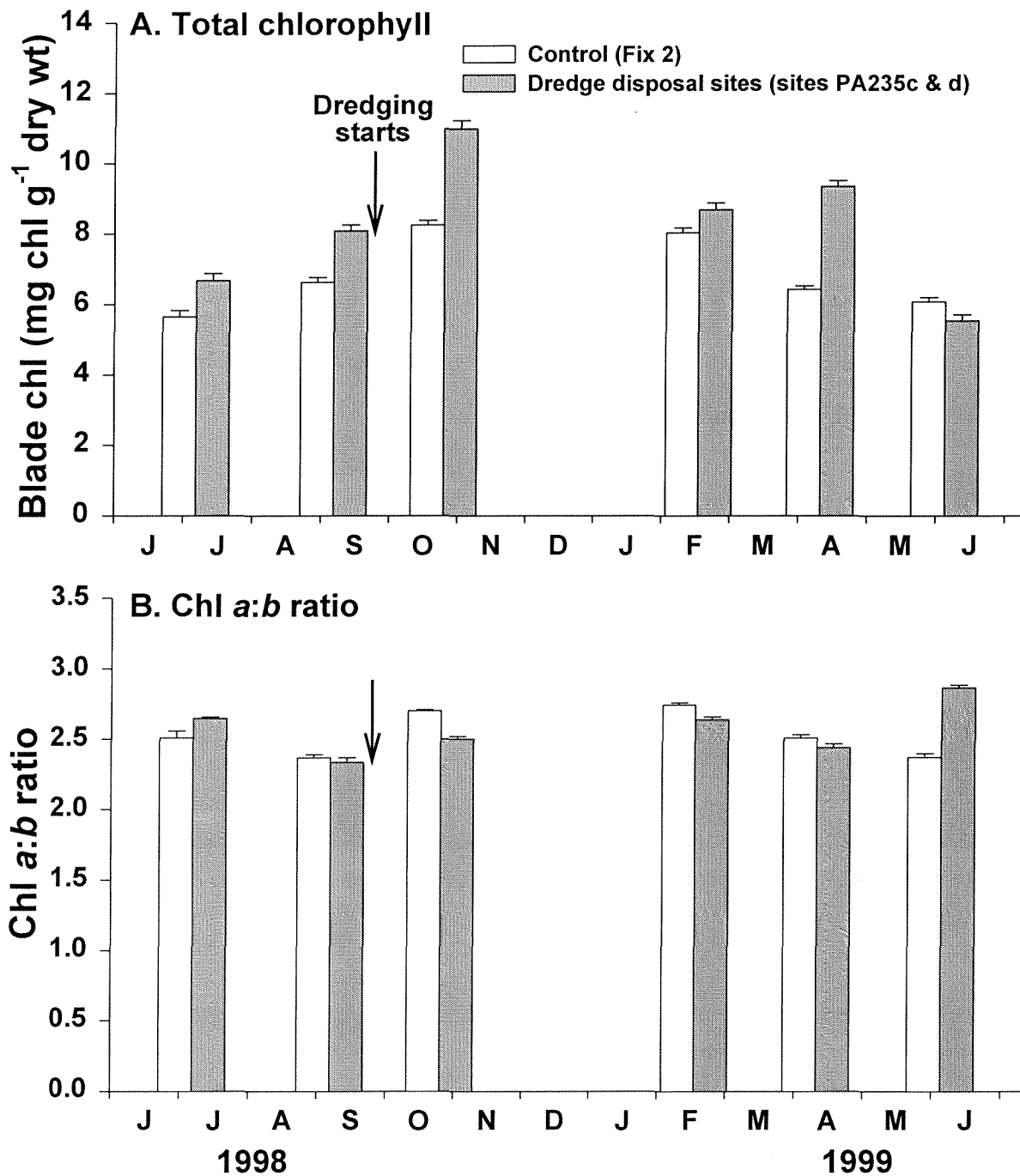


Figure 10. *Thalassia testudinum*. Blade chlorophyll content and chl a:b ratios of plants from Fix 2 and PA235 sites.

and Dunton (1995) and Lee and Dunton (1997) demonstrated that *T. testudinum* did not survive under a light reduction equivalent to 14% SI. The minimum light requirement of 15 to 25% SI for *T. testudinum* was reported by Dennison et al. (1993). Therefore, *T. testudinum* at PA235 appears to receive the minimum PAR for survival after dredging.

Water column chlorophyll and NH_4^+ concentrations at the dredge disposal station increased compared to the control site after dredging, while water column $\text{NO}_3^- + \text{NO}_2^-$ concentrations were not significantly different with those at the control site (Fig. 4). Increased water column NH_4^+ concentrations probably reflect high re-mineralized NH_4^+ flux from sediment, which then stimulated phytoplankton growth as reflected by the rise in chlorophyll levels. Increased sediment pore water NH_4^+ concentrations in reduced light conditions have been attributed to increased decomposition of seagrass detritus and decreased nitrogen uptake by seagrass roots (Lee and Dunton 1997). Similarly, high sediment pore water NH_4^+ concentrations at PA235 sites following dredging probably reflected increases in decomposition and decreases in nitrogen uptake.

Leaf biomass at PA235c and PA235d (non-buried dredge disposal sites) had begun to return to pre-dredging levels nine months after the initiation of dredging. This restoration of leaf biomass was probably due to high sediment nutrients and decreased light attenuation. Fluctuations in underwater PFD were lowest and water transparency highest in June 1999, approximately 9 months after dredging (Fig. 3). During this period, dredge materials became compacted and incorporated into the sediments surrounding the seagrasses at sites PA235c and PA235d, reducing the proportion that could become re-suspended into the water column. Patterns of total blade chlorophyll content and chl *a:b* ratio did not change significantly after dredging (Fig. 3), probably because these plants previously exhibited pigment characteristics that were reflective of low light conditions (high chlorophyll content and low chl *a:b* ratio) prior to dredging (Wiginton and McMillan 1979, Dennison and Alberte 1982, 1985, Abal et al. 1994, Lee and Dunton 1997).

In conclusion, dredging and disposal of dredged materials had a distinct quantitative impact on seagrass production and survival. Seagrasses disappeared rapidly as a result of burial by dredge

materials and production significantly decreased in seagrass beds adjacent to the disposal area for over 9 months in response to continuous re-suspension of dredged materials by wind-generated waves.

References

- Abal EG, Loneragan N, Bowen P, Perry CJ, Udy JW, Dennison WC (1994) Physiological and morphological responses of the seagrass *Zostera capricorni* Aschers. to light intensity. *J Exp Mar Biol Ecol* 178: 113-129.
- Addicott FT, Lyon JL (1973) Physiological ecology of abscission. In, *Shedding of plant parts*, edited by Kozlowski TT, Academic Press, New York.
- Backman TW, Barilotti DC (1976) Irradiance reduction: effects on standing crops of the eelgrass *Zostera marina* in a coastal lagoon. *Mar Biol* 34: 33-40.
- Brown CA, Kraus NC (1997) Environmental monitoring of dredging and processes in Lower Laguna Madre, Texas. Final Report to US Army Corps of Engineers District, Galveston, Galveston Texas. TAMU-CC-CBI-96-01. 118 p.
- Cambridge ML, Chiffings AW, Brittan C, Moore L, McComb AJ (1986) The loss of seagrass in Cockburn Sound, Western Australia. II. Possible causes of seagrass decline. *Aquat Bot* 24: 269-285.
- Cambridge ML, McComb AJ (1984) The loss of seagrass in Cockburn Sound, Western Australia. I. The time course and magnitude of seagrass decline in relation to industrial development. *Aquat Bot* 20: 229-243.
- Czerny AB, Dunton KH (1995) The effects of in situ light reduction on the growth of two species of subtropical seagrasses, *Thalassia testudinum* and *Halodule wrightii*. *Estuaries* 18: 418-427.
- Dennison WC, Alberte RS (1982) Photosynthetic responses of *Zostera marina* L. (eelgrass) to in situ

- manipulations of light intensity. *Oecologia* 55: 137-144.
- Dennison WC, Alberte RS (1985) Role of daily light period in the depth distribution of *Zostera marina* (eelgrass). *Mar Ecol Prog Ser* 25: 51-61.
- Dennison WC, Orth RJ, Moore KA, Stevenson JC, Carter V, Kollar S, Bergstrom PW, Batiuk RA (1993) Assessing water quality with submersed aquatic vegetation. *BioScience* 43: 86-94
- Dunton KH, Tomasko DA (1994) *In situ* photosynthesis in the seagrass *Halodule wrightii* in a hypersaline subtropical lagoon. *Mar Ecol Prog Ser* 107: 281-293
- Folk RL (1964) Petrology of sedimentary rocks. Hemphill's Press. Austin, Texas.
- Kentula ME, McIntire CD (1986) The autecology and production dynamics of eelgrass (*Zostera marina* L.) in Netarts Bay, Oregon. *Estuaries* 9: 188-199
- Lee K-S, Dunton KH (1997) Effects of *in situ* light reduction on the maintenance, growth and partitioning of carbon resources in *Thalassia testudinum* Banks ex König. *J Exp Mar Biol Ecol* 210: 53-73.
- Onuf CP (1994) Seagrasses, dredging and light in Laguna Madre, Texas, U.S.A. *Est Coastal Shelf Sci* 39: 75-91
- Parsons TR, Maita Y, Lalli CM (1984) A manual of chemical and biological methods for seawater analysis. Pergamon Press, New York.
- Porra RJ, Thompson WA, Kriedemann PE (1989) Determination of accurate extinction coefficient and simultaneous equations for assaying chlorophylls a and b extracted with four different solvents: verification of the concentration of chlorophyll standards by atomic absorption spectroscopy. *Biochem Biophys Acta* 975: 384-394

SAS Institute, Inc. (1989) SAS/STAT guide for personal computers, version 6, SAS Institute, Cary, NC, 4th edition

Texas Department of Highways and Public Transportation (1980) The Gulf intracoastal waterway in Texas. 195 p.

Wiginton JR, McMillan C (1979) Chlorophyll composition under controlled light conditions as related to the distribution of seagrass in Texas and US Virgin Islands. *Aquat Bot* 6: 171-184.

Zieman JC (1974) Methods for the study of the growth and production of turtle grass, *Thalassia testudinum* König. *Aquaculture* 4: 139-143.

CHAPTER X: PHOTOSYNTHESIS IN THE MANATEE GRASS, *SYRINGODIUM FILIFORME*

Contents

Abstract	3
Introduction.....	4
Methods	6
Study Sites	6
Pigment Content	6
Photosystem Density and Size	8
Photosystem I.....	8
Photosystem II	8
Photosynthetic Measurements.....	9
In Situ Measurements	9
Laboratory Measurements	10
Statistical Analysis.....	10
Results.....	11
Underwater Irradiance and Temperature.....	11
Blade Chlorophyll and Photosystem Contents	11
Photosynthetic Physiology	14
Discussion.....	18
Photosynthetic Apparatus Structure and Performance	18
In Situ vs. Laboratory Photosynthetic Physiology.....	21
Conclusion	22
References.....	23

Tables

Table 1. *Syringodium filiforme*. Seasonal changes in pigment content, photosynthetic unit size, reaction center density and ratios13

Table 2. *Syringodium filiforme*. In situ estimates of dark respiration based on whole-chamber and separate incubations of photosynthetic (PS) and non-photosynthetic (NPS) tissues at Station 2, LLM.....17

Table 3. Comparison of estimates for photosynthetic unit sizes in aquatic macrophytes.....19

Figures

Figure 1. *Syringodium filiforme*. Map of study site, designated Station 2, in lower Laguna Madre, Texas. Mean depth is ~1.2 m.7

Figure 2. *Syringodium filiforme*. Seasonal changes in (A) daily-integrated underwater irradiance and (B) ambient seawater temperature at Station 2, Lower Laguna Madre, Texas (1996-1997). Vertical bars denote SE of means.....12

Figure 3. *Syringodium filiforme*. Photosynthesis-irradiance curves derived from field incubations for the months of (A) September 1996 and (B) July 1997. Data are expressed on a per gram dry weight basis. Vertical bars denote SE of means (n = 4).....15

Figure 4. *Syringodium filiforme*. A comparison of laboratory and field-collected photosynthetic data for late-summer (30EC) and late-spring (28EC) 1996-1997. White bars represent laboratory measurements for August 1996 and May 1997. Shaded bars represent in situ measurements for September 1996 and July 1997. Data are expressed on a per gram dry weight basis. Vertical bars denote SE of means; those with the same letter are not significantly different ($p>0.05$; n = 4).16

Abstract

Syringodium filiforme does not exhibit physiological compensation as a function of season. This has important implications with respect to the diversity and spatial distribution of seagrass species, with *Syringodium*-like physiological characteristics, that are exposed to chronic low light conditions common to estuarine environments. Adult *Syringodium filiforme* plants were sampled at bimonthly intervals between August 1996 and August 1997 from a site in Lower Laguna Madre, Texas with a mean depth of ~1.2 m. Photosynthesis-irradiance (PI) experiments were conducted at ambient temperatures, in conjunction with measurements of reaction center density and size, to characterize photosynthetic apparatus structure and performance. Values for relative quantum yield (α ; O₂ evolved per *incident* photon), compensation point (I_c), saturation point (I_k), dark respiration (R_d) and light-saturated photosynthesis (P_{max}), collected during late-summer 1996, exhibited no significant differences from those collected in late-spring 1997. Changes in pigment concentration, exhibiting no distinct seasonal pattern, were manifested in adjustments of both photosystem density and size. Densities for photosystem I (PSI) were highest during winter months (*ca.* 0.5 pmol mm⁻³); densities for photosystem II (PSII) exhibited no seasonal trend, ranging from 0.2 to 0.7 pmol mm⁻³. Little variation was noted regarding the size of PSI (PSU_{P700}), whereas, size estimates for PSII (PSU_{O2}) were largest during winter and early-spring (*ca.* 5400 Chl-a P680⁻¹). These data indicate that *S. filiforme* may have some capacity for altering photosynthetic apparatus structure. However, since α , I_c and I_k did not change with season, the benefit of such adjustments is not obvious. We suggest photophysiological parameters may not be reliable indicators of environmental stress in *Syringodium filiforme*, as this species does not exhibit a great potential for phenotypic plasticity. This work serves as a basis for future studies designed to address physiological compensation in seagrasses and the ability of coastal macrophytes to respond to environmental change (e.g., reductions in light availability).

Introduction

South Texas is distinguished by some of the world's most productive coastal marine communities (McRoy and McMillan 1977). Seagrass populations extend over approximately 730 km² of the Texas coast (Quammen and Onuf 1993) and are of key ecological and economical importance (reviewed by Zieman 1982). Seagrasses serve as major primary producers and provide habitat for various species of invertebrates, fishes and waterfowl (Cornelius 1977, Fry and Parker 1979, Rooker *et al.* 1997). As they grow and senesce, seagrasses release both particulate and dissolved organic matter, providing a vast organic carbon source for assemblages of pelagic and benthic suspension feeders. However, these populations have recently exhibited notable declines, including 150 km² of habitat loss in lower Laguna Madre (Quammen and Onuf 1993, Onuf 1996). Declines have been attributed to underwater light reduction (Dunton 1994) and increased turbidity as a consequence of anthropogenic disturbances such as dredging practices (Onuf 1994). In some areas, light levels have been reduced by as much as 50% (Dunton 1994). Increases in our understanding of seagrass photo-physiology may provide an opportunity to detect stress in seagrasses before the effects of light limitation are manifested.

Plants and algae exhibit considerable variation in photosynthetic response(s) to environmental change. Although the variation may reflect genetic adaptation to growth regimes (e.g., Kübler *et al.* 1991), most represent phenotypic acclimation responses (reviewed by Berry and Björkman 1980). Not only does acclimation result in optimization of photosynthesis and growth, but in some cases, it may increase tolerance to and/or ability to recover from extreme exposures (Dudgeon *et al.* 1990, Pearson and Davison 1994). Species adapted to habitats characterized by great environmental variation tend to possess a higher, genetically determined potential for photosynthetic acclimation, which enables them to shift their metabolism in concert with seasonal changes in temperature and/or light (reviewed by Berry and Björkman 1980, Falkowski and LaRoche 1991). When grown under low light, species with the ability to photoacclimate exhibit relatively high rates of light-limited photosynthesis, high relative quantum yields and high pigment concentrations; the reverse is found when grown under high light (Baker and McKiernan 1988, Falkowski and LaRoche 1991).

Previous research has shown that some seagrass genera (e.g., *Zostera* and *Thalassia*) can photoacclimate by adjusting pigment content and stoichiometry (Dennison and Alberte 1985, Abal *et al.* 1994).

This study targeted *Syringodium filiforme*, which is common in coastal waters of South Texas, inhabiting areas that are 1-2 m in depth. Limitations in the distribution of Texas seagrasses have been attributed to a notable decline in water clarity observed in the Laguna Madre over the last 8-9 years (Onuf 1996). It is largely unknown how efficiently *Syringodium* responds to changes in the environment. A co-existing species, *Halodule wrightii*, does not demonstrate a clear ability to photoacclimate (Dunton 1994, Dunton and Tomasko 1994). The implications are enormous with regard to this lack of phenotypic plasticity; if light availability continues to decline in coastal waters, we may witness further disappearance of seagrass-dominated habitats and consequent declines in species diversity.

The main objective of the following research was to characterize changes in photosynthetic performance and light-harvesting characteristics as a function of season in *Syringodium filiforme*. A secondary objective was to evaluate the usefulness of photophysiological parameters as environmental indicators in seagrass systems. In addition, photosynthesis-irradiance characteristics derived from laboratory studies were compared to those derived from field-collected data to assess the appropriateness of each approach when addressing the impact of anthropogenic disturbance on seagrass populations.

Methods

Study Site

Adult *Syringodium filiforme* Kützing plants were sampled between August 1996 and August 1997 from a site (Station 2, marker 123) in lower Laguna Madre, Texas with a mean depth of ~1.2 m. Station 2 (26°08' N, 97°12' W) is located east of the Gulf Intracoastal Waterway (GIWW), off the coast of South Padre Island, and lies approximately 15 km north of the Rio Grande (Fig. 1). Although this population of *S. filiforme* forms a monotypic stand, *Thalassia testudinum* Banks ex König, *Halodule wrightii* Ascherson and *Halophila engelmannii* Ascherson are common in surrounding areas. Low epiphyte abundance and water column chlorophyll concentrations made this an ideal site for conducting *in situ* experiments.

Underwater irradiance was monitored at Station 2 between August 1996 and August 1997. To measure ambient photon flux density, a LICOR LI-193SA spherical quantum sensor was positioned at canopy height (i.e., ~25 cm from the sediment surface), providing continuous input to a LICOR LI-1000 datalogger (LICOR, Inc., Lincoln, NE, USA) sealed in a watertight underwater housing. As described by Dunton (1994), data were collected at 1 min intervals and integrated on an hourly basis.

Pigment Content

Pigments were quantified spectrophotometrically following extraction with dimethyl formamide (DMF) as described by Dunton and Tomasko (1994). Chlorophyll-a and -b concentrations were determined using the equations of Porra *et al.* (1989).

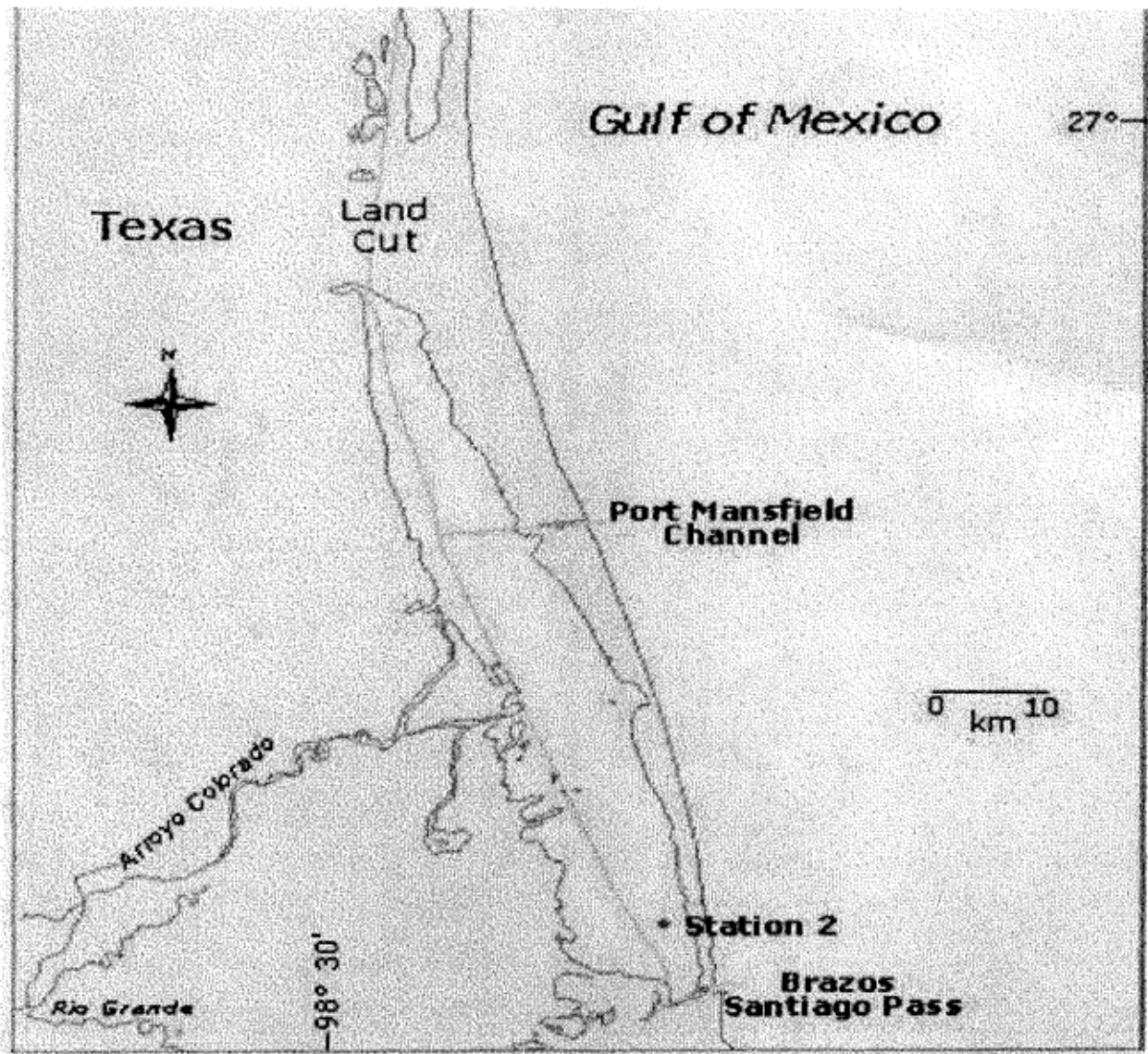


Figure 1. *Syringodium filiforme*. Map of study site, designated Station 2, in lower Laguna Madre, Texas. Mean depth is ~1.2 m.

Photosystem Density and Size

Photosystem I

Photosystem I (P700) was isolated using a modification of the procedure outlined by Smith and Melis (1987; see also Henley and Dunton 1997). Whole *Syringodium* plants were collected at bimonthly intervals from Station 2 as described above. Segments (~ 2-14 cm sections) were cut from seagrass blades above the sheath and chopped into small fragments with a sharp razor blade. Tissue fragments (~2.0 g fresh weight per sample) were homogenized with 15 mL cold isolation buffer (40 mM Tricine; 0.4 M sucrose; 2% PVP-40; 10 mM NaCl; 2 mM MgCl₂; 2 mM Na₂EDTA; 5 mM DTT; 20 mM methylamine; 5 mM Na₂-ascorbate; 0.1% BSA at pH 7.6) for ~30 s, using a Polytron tissue homogenizer, gradually increasing the speed from 5 to 14,000 rpm. Homogenates were filtered through miracloth and thylakoid membranes were pelleted by centrifugation for ~10 min at 4°C and 10,000 x g. Supernatants were discarded and remaining pellets were resuspended with 3 mL cold suspension buffer (20 mM Tricine (pH 7.6); 200 mM sucrose; 10 mM NaCl; 5 mM MgCl₂). Samples were centrifuged for ~10 min at 4°C and 10,000 x g. Supernatants were once again discarded and 3 mL cold solubilization buffer (20 mM Tricine (pH 7.6); 200 mM sucrose; 10 mM NaCl; 5 mM MgCl₂; 0.2% Triton-X 100) were added to each sample. Thylakoids were solubilized using a vortex, transferred to microfuge tubes and spun for ~2 min at 10,000 x g in an Eppendorf microfuge. Samples were maintained on ice, in complete darkness, and analyzed spectrophotometrically within 30 min of isolation. Concentrations of P700 were determined from light-induced absorption differences at 697 nm relative to 720 nm with an extinction coefficient of 64 mol⁻¹ m² (Falkowski *et al.* 1981, Smith and Melis 1987). Aliquots were also taken and diluted (3-8 fold) with 20 mM Tricine (pH 7.6) for Chl determination (see Henley and Dunton 1997).

Photosystem II

Photosystem II (P680) reaction center densities were measured by the O₂ --flash technique (Mishkind and Mauzerall 1980, Falkowski *et al.* 1981). Segments (~2-14 cm sections) were cut

from field-collected *Syringodium* blades above the sheath. These segments were then cut into smaller, 2-cm sections and allowed to wound respire for 1-1.5 h prior to use. Measurements were made with a Clark-type oxygen electrode (Rank Brothers, Bottisham, England) and high intensity strobe (Stroboslave, Genrad) at flash frequencies of 15-20 Hz. The length of incubation in flashing light was ~10 min per frequency, which was sufficient in duration to obtain a stable rate of O₂ production. Photosystem II reaction center densities were calculated from average O₂ evolution per flash divided by four; photosynthetic unit size was calculated from PSII density and total Chl-a content (mol Chl-a mol O₂⁻¹).

Photosynthetic Measurements

In Situ Measurements

Whole-plant PI experiments were conducted during September 1996 and July 1997. Four 5 L plexiglas chambers were randomly placed in the *Syringodium* bed at Station 2. Measurement of ambient irradiance and photosynthesis were made following the protocol of Dunton and Tomasko (1994). A total of 15 irradiance levels between 4 and 1200 mmol photons m⁻² s⁻¹ were used for the construction of PI curves. Photosynthesis-irradiance parameters were calculated on the basis of dry weight using the Bannister (1979) function and the curve-fitting program Sigma-Plot (Herzka and Dunton 1997). Mean rates of P_{max} were calculated from light-saturated rates of photosynthesis achieved in all chambers and expressed in terms of gross oxygen evolution. Respiration rates of photosynthetic and non-photosynthetic tissues and whole-plant respiratory requirements were estimated as described by Herzka and Dunton (1997). Measurements of water column respiration were negligible. Relative quantum yield (α ; O₂ evolved per *incident* photon) was the slope of the light-limited region of the PI curve, representing an estimate of light-harvesting efficiency. The compensation (I_c) and saturation (I_k) points were defined as the PFD required to achieve rates of net photosynthesis and light-saturated photosynthesis, respectively.

Laboratory Measurements

Whole *Syringodium* plants were collected at bimonthly intervals using a 15 cm diameter corer. Intact cores were placed in 19 L seawater-filled buckets that were immediately transported to the laboratory and provided access to flowing seawater to maintain ambient growth temperatures. An irradiance of $\sim 150\text{-}200 \mu\text{mol photons m}^{-2} \text{ s}^{-1}$ was provided by an overhead bank of fluorescent lights as measured with a LICOR LI-192SA flat cosine sensor.

Segments ($\sim 2\text{-}14$ cm sections) were cut from seagrass blades above the sheath. These segments were then cut into smaller, 2-cm sections and allowed to wound respire for 1-1.5 h prior to use. Measurements were made with a Clark-type oxygen electrode (Rank Brothers, Bottisham, England) and a custom-built chamber with flat Plexiglas windows, containing 14 mL Millipore-filtered (0.45 mm) seawater as described by Dunton and Tomasko (1994). Photosynthesis was measured at 11 irradiance levels between 4 and 1500 $\mu\text{mol photons m}^{-2} \text{ s}^{-1}$. Rates of oxygen production (total $\mu\text{mol O}_2 \text{ chamber}^{-1}$) were derived from a Rank Brothers digital output and recorded on a Zenith PC computer over a period of $\sim 5\text{-}10$ min at each irradiance.

Photosynthesis-irradiance (PI) parameters were calculated on the bases of both Chlorophyll-a and dry weight using the inverse-quadratic transformation of Jassby and Platt (1976) and the curve-fitting program Sigma-Plot. Rates of light-saturated photosynthesis (P_{max}) were expressed in terms of gross oxygen evolution. Relative quantum yield, I_c and I_k were defined as described above. No data were available for December 1996.

Statistical Analysis

Statistical significance of seasonal effects was determined using a single-factor ANOVA (Analysis of Variance). The null hypothesis was rejected at the level of $p \leq 0.05$. Multiple comparisons were made using the Ryan-Q test (Zar 1984, Day and Quinn 1989). All statistical analyses were performed on a Gateway 2000 (Pentium II) computer with Microsoft Excel 97 software.

Results

Underwater Irradiance and Temperature

Ambient daily integrated irradiance followed a distinct seasonal pattern (Fig. 2A). Values for underwater irradiance were highest during summer months (i.e., July and August), averaging *ca.* 33 mol photons m⁻². Lowest underwater irradiance levels were observed from January to March 1997 (*ca.* 11 mol m⁻²). Annual integrated photon flux density was approximately 8100 mol m⁻² from August 1996 to August 1997.

There was approximately a 12°C annual shift in ambient seawater temperatures at Station 2 (Fig. 2B). Temperatures declined from 30°C in August 1996 to a minimum of 19°C in January 1997. Laguna Madre waters warmed rapidly after March, reaching 27°C in May and the annual maximum of 31°C in August 1997.

Blade Chlorophyll and Photosystem Contents

No distinct seasonal variations in major light-harvesting pigment concentrations were observed from pigment data (Table 1). Chlorophyll-a content was highest in August 1996 and March 1997 and lowest in October 1996 and August 1997. Concentrations of Chl-b followed a similar pattern to that of Chl-a. Chlorophyll-a:b ratios ranged between 2.46 and 2.79, exhibiting no apparent variation with season.

Changes in the photosynthetic apparatus followed those of pigment and exhibited high variability throughout the year (Table 1). Densities of both photosystem I (PSI) and photosystem II (PSII) ranged from 0.1 to 0.7 pmol mm⁻³. However, PSI densities exhibited a greater degree of change between March and August 1997, resulting in high PSII:PSI ratios in May and August 1997. Seasonal variation in photosynthetic unit (PSU) size was less obvious. Estimates for PSU_{P700} were higher during January 1997 (775 mol Chl-a mol P700⁻¹) than those obtained during any other month (*ca.* 520 mol Chl-a mol P700⁻¹), excluding August 1997. No other differences in PSU_{P700} were observed. Estimates for PSU_{O₂} ranged between 3448 and 5927 mol Chl-a mol O₂⁻¹, with minimum and maximum PSU sizes noted in October 1996 and March 1997, respectively.

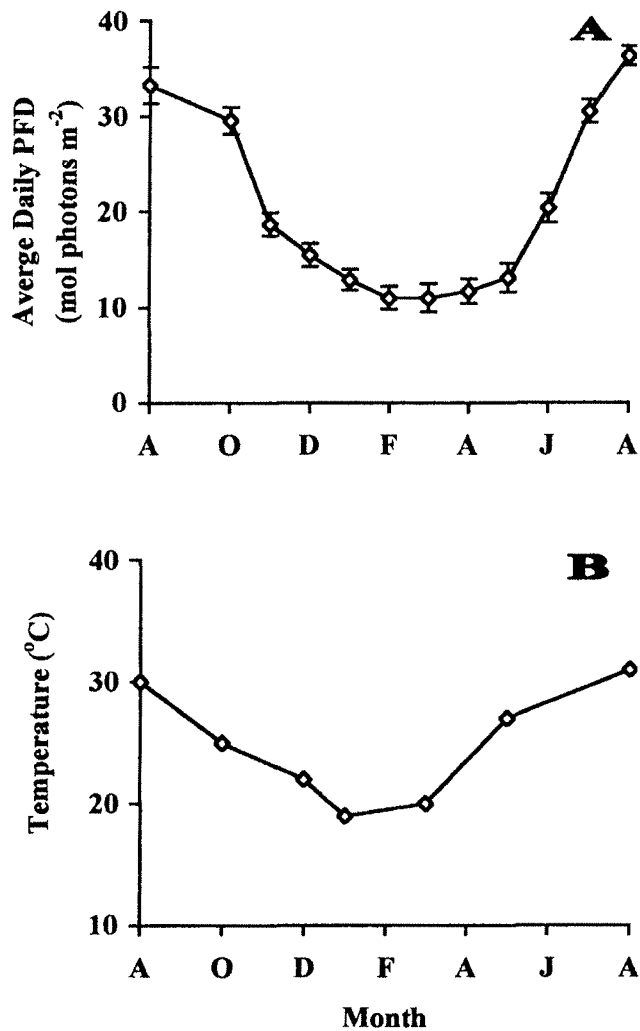


Figure 2. *Syringodium filiforme*. Seasonal changes in (A) daily-integrated underwater irradiance and (B) ambient seawater temperature at Station 2, Lower Laguna Madre, Texas (1996-1997). Vertical bars denote SE of means.

Table 1. *Syringodium filiforme*. Seasonal changes in pigment content, photosynthetic unit size, reaction center density and ratios. Values are means (SE); those with the same letter are not significantly different ($p > 0.05$).

Month	n	Chl-a	Chl-b	Chl-a:Chl-b	PSII	PSU _{O₂}	n	PSI	PSU _{P700}	PSII:PSI
		mg g ⁻¹ dw	mg g ⁻¹ dw	mg g ⁻¹ dw	pmol mm ⁻³	Chl-a O ₂ ⁻¹		pmol mm ⁻³	Chl-a P700 ⁻¹	
Aug-96	4	3.61 (0.17) ^a	1.38 (0.09) ^a	2.63 (0.05) ^{ab}	ND	ND	ND	ND	ND	ND
Oct-96	4	2.32 (0.06) ^c	0.95 (0.04) ^c	2.46 (0.06) ^b	0.7 (0.04) ^a	3448 (233) ^b	ND	ND	ND	ND
Dec-96	ND	ND	ND	ND	0.4 (0.05) ^{cde}	5525 (170) ^a	3	0.4 (0.03) ^a	537 (12) ^b	1.0
Jan-97	4	2.82 (0.36) ^{ac}	1.01 (0.13) ^c	2.79 (0.00) ^a	0.5 (0.03) ^c	4898 (98) ^{ac}	3	0.5 (0.06) ^a	515 (48) ^b	1.0
Mar-97	4	3.42 (0.23) ^a	1.36 (0.09) ^a	2.52 (0.01) ^{ab}	0.3 (0.0) ^{be}	5927 (77) ^a	3	0.5 (0.03) ^a	775 (38) ^a	0.6
May-97	4	2.78 (0.24) ^{ac}	1.06 (0.10) ^{ac}	2.62 (0.05) ^{ab}	0.3 (0.0) ^{bd}	5427 (413) ^a	3	0.2 (0.0) ^b	518 (25) ^b	1.5
Aug-97	4	1.15 (0.06) ^b	0.42 (0.02) ^b	2.74 (0.14) ^{ab}	0.2 (0.03) ^b	4221 (329) ^{bc}	3	0.1 (0.03) ^b	637 (70) ^{ab}	2.0

Photosynthetic Physiology

Photosynthesis-irradiance parameters derived from field-collected data in September 1996 exhibited no significant differences from those collected in July 1997 (Fig. 3A, 3B). When comparing laboratory and *in situ* estimates of PI parameters, values for a were nearly 1-3 times higher in laboratory-incubated plants (1.3-2.0 cf. 0.6-0.7 $\mu\text{mol O}_2 \text{ g}^{-1}\text{dw h}^{-1}/\mu\text{mol photons m}^{-2} \text{ s}^{-1}$, respectively) during both late-summer and -spring (Fig. 4A). In contrast, laboratory oxygen evolution measurements underestimated I_k by nearly 40% when compared to values calculated for whole-plant incubations (*ca.* 144 cf. 370 $\mu\text{mol photons m}^{-2} \text{ s}^{-1}$, respectively; Fig. 4B). A similar trend was noted for I_c where laboratory estimates were 9-18% lower than *in situ* estimates (Fig. 4C).

Although not statistically different, rates of whole-plant gross P_{max} were lower than laboratory-derived rates in late summer; no differences were noted in late spring (Fig. 4D). Whole-plant dark respiration rates (*ca.* 70 $\mu\text{mol O}_2 \text{ g}^{-1}\text{dw leaf h}^{-1}$ for September 1996 and July 1997), calculated from tissue-specific values for R_d and ratios of non-photosynthetic to photosynthetic tissues (NPS:PS; after Herzka and Dunton 1997), were 1.5 times higher in late summer and five times higher in late spring than those exhibited by laboratory-incubated blades (Table 2, Fig. 4E). In addition, photosynthetic tissue exhibited respiratory demands that were approximately 3-4 times higher than those of non-photosynthetic tissue (Table 2). Estimates of whole-plant and chamber oxygen consumption per gram dry weight of leaf tissue yielded similar values, demonstrating that chamber respiration (excluding that of seagrasses) was negligible (Table 2).

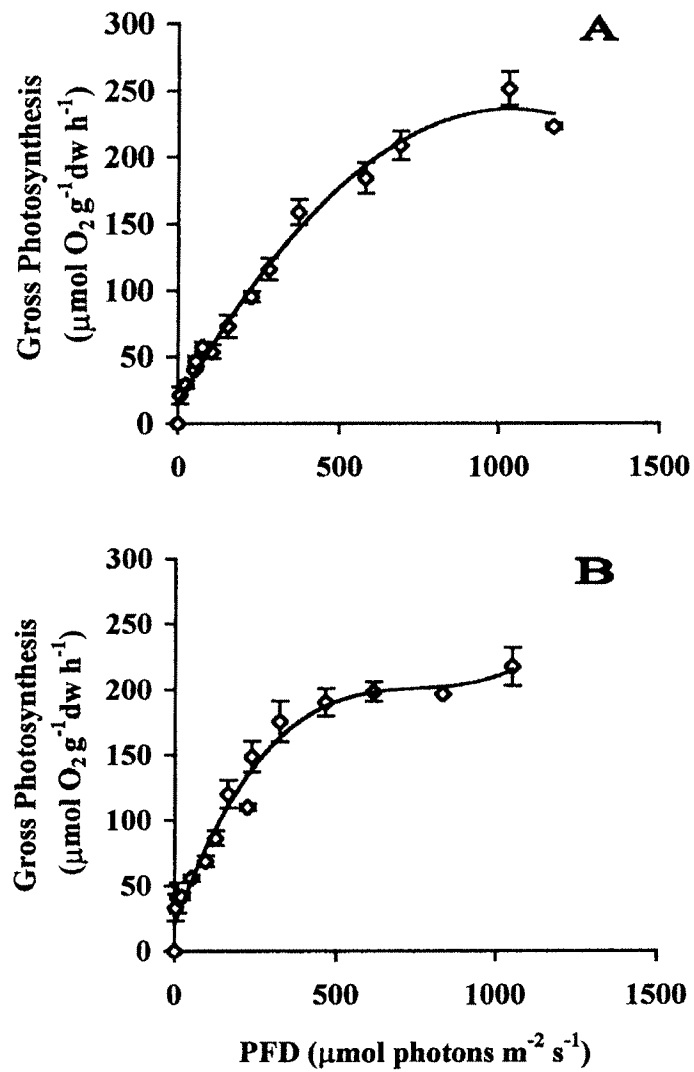


Figure 3. *Syringodium filiforme*. Photosynthesis-irradiance curves derived from field incubations for the months of (A) September 1996 and (B) July 1997. Data are expressed on a per gram dry weight basis. Vertical bars denote SE of means (n = 4).

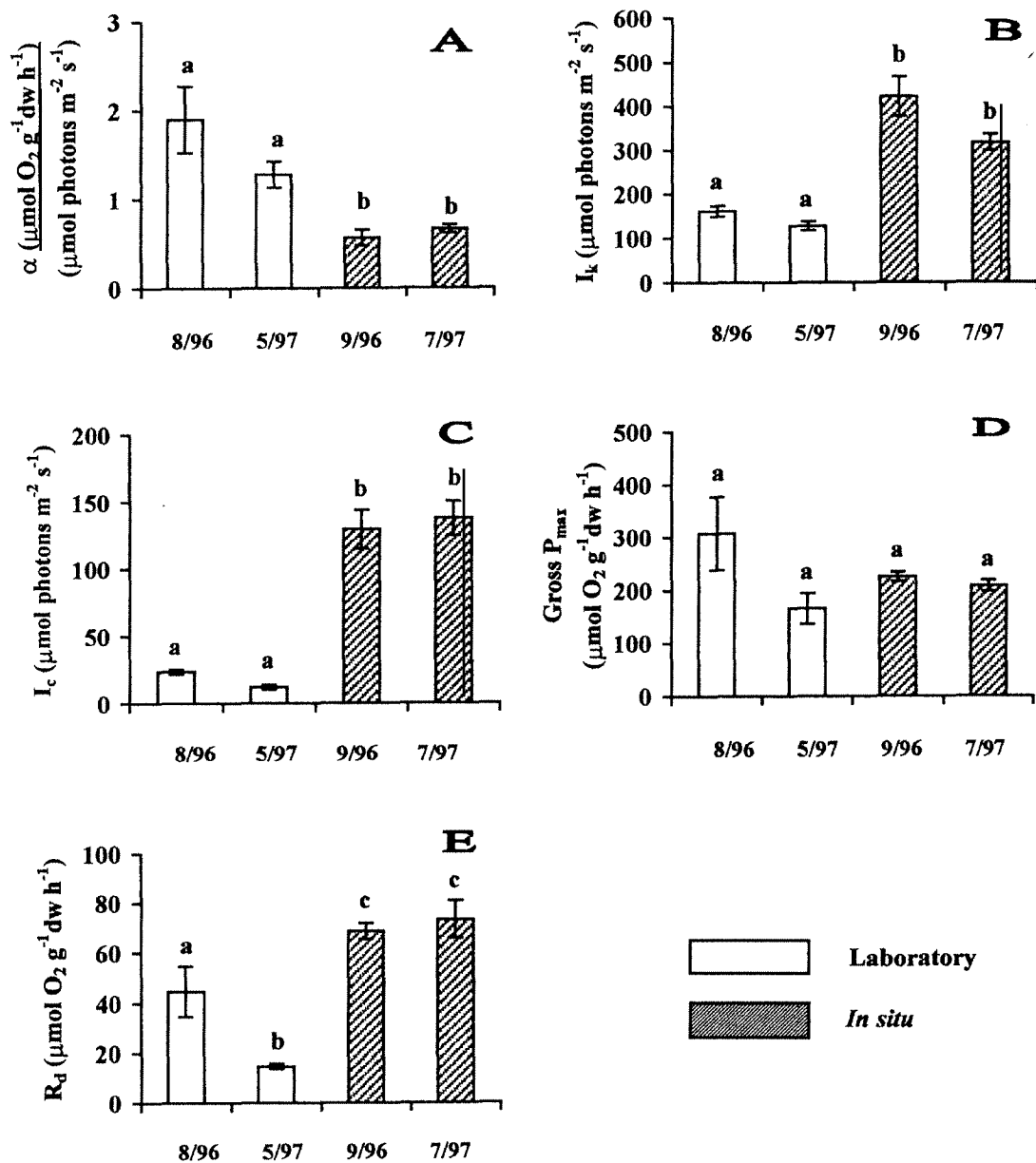


Figure 4. *Syringodium filiforme*. A comparison of laboratory and field-collected photosynthetic data for late-summer (30°C) and late-spring (28°C) 1996-1997. White bars represent laboratory measurements for August 1996 and May 1997. Shaded bars represent *in situ* measurements for September 1996 and July 1997. Data are expressed on a per gram dry weight basis. Vertical bars denote SE of means; those with the same letter are not significantly different ($p > 0.05$; $n = 4$).

Table 2. *Syringodium filiforme*. *In situ* estimates of dark respiration based on whole-chamber and separate incubations of photosynthetic (PS) and non-photosynthetic (NPS) tissues at Station 2, LLM. Values are means (SE) (n = 4).

Month	Chamber R_d	PS R_d	NPS R_d	NPS:PS	Whole-plant R_d	Net $P_{max}:R_d$
	$\mu\text{mol O}_2 \text{ g}^{-1} \text{ dw leaf h}^{-1}$	$\mu\text{mol O}_2 \text{ g}^{-1} \text{ dw h}^{-1}$	$\mu\text{mol O}_2 \text{ g}^{-1} \text{ dw h}^{-1}$	$\text{gdw g}^{-1} \text{ dw}$	$\mu\text{mol O}_2 \text{ g}^{-1} \text{ dw leaf h}^{-1}$	
Sep-96	69.1 (4.5)	36.5 (2.0)	10.3 (1.0)	3.1	68.6 (3.2)	3.5
Jul-97	89.8 (5.2)	29.0 (0.5)	7.7 (0.6)	5.5	73.3 (7.5)	1.6

Discussion

Photosynthetic Apparatus Structure and Performance

We suggest *Syringodium filiforme* probably lacks the phenotypic plasticity to metabolically compensate for changes in the environment. This species is able to achieve high rates of photosynthesis and production only when temperature and irradiance are relatively high (i.e., during warm seasons of late-spring and summer). In contrast, this species "endures" sub-optimal conditions. Like other seagrass species (e.g., *Thalassia testudinum*; Herzka and Dunton 1997), *S. filiforme* "shuts down" during winter months, exhibiting very slow growth and production. Clearly, this has important implications for the long-term survival of *Syringodium*, and other aquatic macrophytes, in systems that are chronically exposed to anthropogenic and natural disturbances.

In this study, variability in chlorophyll and accessory pigment content was not correlated with seasonal changes in temperature and irradiance. Pigment stoichiometry remained relatively constant throughout the year, indicating that adjustments of Chl-a and Chl-b were proportional (i.e., changes in pigment content offered no clear adaptive advantage). Chlorophyll concentrations were associated with alterations in both reaction center density and size. *Syringodium filiforme* exhibited a greater number of functional PSI reaction centers between December 1996 and March 1997, with little seasonal change in the photosynthetic unit size of PSI (PSU_{P700}). In contrast, no seasonal trend was noted in PSII density, but estimates for PSU_{O_2} were larger during winter months. These data indicate that *S. filiforme* may have some capacity for adjusting pigment packaging. However, considering the lack of seasonality observed in other light-harvesting parameters (e.g., a , I_k and I_c), the benefit of such adjustments is not obvious and may warrant further investigation. The data presented here are the first estimates regarding photosynthetic apparatus structure in *Syringodium*, and are consistent with those from other seagrass systems, using the O_2 -flash (PSU_{O_2}) and absorption-difference (PSU_{P700}) techniques (Mishkind and Mauzerall 1980, Mazella *et al.* 1981, Dennison and Alberte 1982, Dennison and Alberte 1985, Dennison and Alberte 1986, Major and Dunton Unpubl.; Table 3). We suggest that the high degree of variability associated with measurements of photosystem density and size resulted from plant-plant variation and the variation often inherent in such biochemical assays.

Table 3. Comparison of estimates for photosynthetic unit sizes in aquatic macrophytes.

Species	PSU _{O₂}	PSU _{P700}	Source
	Chl- <u>a</u> O ₂ ⁻¹	Chl- <u>a</u> P700 ⁻¹	
<i>Thalassia testudinum</i>	4000-7000	400-700	Major & Dunton Unpubl.
<i>Zostera marina</i>	1500	ND	Mishkind & Mauzerall 1980
<i>Zostera marina</i>	1900-2300	ND	Dennison & Alberte 1982
<i>Zostera marina</i>	1800-5300	ND	Dennison & Alberte 1985
<i>Zostera marina</i>	2700-3900	ND	Dennison & Alberte 1986
<i>Zostera marina</i>	2150	525	Mazzella <i>et al.</i> 1981

Little seasonal variation was observed in light-harvesting characteristics (α , I_c and I_k), whether derived from either field or laboratory incubations, in *Syringodium filiforme* from 1996 to 1997. Similar to other studies involving seagrass systems (e.g., Dunton and Tomasko 1994, Herzka and Dunton 1997), this lack of variability is likely attributable to the small range of environmental fluctuation typical of coastal South Texas. Although adult *S. filiforme* exhibited changes in photosynthetic performance throughout the year, the pattern of change was not consistent with physiological compensation (reviewed by Berry and Björkman 1980, Davison 1991, Falkowski and LaRoche 1991). Overall, rates of respiration and photosynthesis were high during -late-spring/summer seasons and low during winter (data not shown), suggesting this species does not have the ability to overcome the effects of environmental change. *S. filiforme*, like many other seagrasses, exhibits a drastic decline in metabolic activity during winter, achieving rapid rates of growth and production when high irradiance levels are coincident with the hottest temperatures of the year. Presumably, this pattern of performance is the resultant effect of temperature on the enzymatic reactions of respiratory and photosynthetic pathways (reviewed by Bulthuis 1987).

Photosynthesis-irradiance parameters presented here for *Syringodium filiforme* are within the range of those reported for other seagrass genera (Dawes and Tomasko 1988, Pérez and Romero 1992, Dunton and Tomasko 1994, Herzka and Dunton 1997) and aquatic macrophytes (Nielsen and Sand-Jensen 1989). For *Halodule wrightii*, Dunton and Tomasko (1994) report field-collected rates of light-saturated photosynthesis of 533 and 331 $\mu\text{mol O}_2 \text{ g}^{-1}\text{dw leaf h}^{-1}$ for May 1989 and July 1990, respectively. Corresponding to similar seasons (i.e., late-spring and late-summer), Herzka and Dunton (1997) report P_{max} values of 122 and 195 $\mu\text{mol O}_2 \text{ g}^{-1}\text{dw leaf h}^{-1}$ for *Thalassia testudinum*. In addition, estimates for pigment content, rates of dark respiration, relative quantum yield and other PI parameters are consistent with results for a variety of other seagrass studies (Dennison and Alberte 1985, Dawes and Tomasko 1988, Abal *et al.* 1994, Dunton and Tomasko 1994, Herzka and Dunton 1997, Dawes 1998, Lee and Dunton 1999).

In Situ vs. Laboratory Photosynthetic Physiology

When PI parameters calculated from laboratory and *in situ* experiments were compared, values for a were grossly overestimated using laboratory-incubated plants. In contrast, values for I_k and I_c were underestimated by as much as 40%. Similar results were noted for *Thalassia testudinum* (Fourqurean and Zieman 1991, Herzka and Dunton 1997) and *Halodule wrightii* (Dunton and Tomasko 1994). As noted by Herzka and Dunton (1997), unidirectional light sources typically used for laboratory photosynthesis-irradiance experiments are not reflective of ambient underwater irradiance regimes. In nature, light availability may be affected, and hence, reduced by the presence of a dense plant canopy, epiphyte abundance and/or self-shading (Pérez and Romero 1992, Massini *et al.* 1995). Reductions in light availability are often effected through shifts in spectral quality (Tomasko 1992), which in turn, may determine photosynthetic performance in the field. We present further evidence for the merit of designing field experiments, to coincide with laboratory studies, particularly when addressing questions concerning the natural environment and its effect on light-use characteristics in seagrasses.

Similar to trends reported for *Halodule wrightii* (Dunton and Tomasko 1994) and *Thalassia testudinum* (Herzka and Dunton 1997), values of gross P_{max} for whole-plant incubations of *Syringodium filiforme* were not significantly different from those derived from incubated blades in late-summer or -spring. Whole-plant respiratory rates were 1.5-5 times higher than those exhibited by laboratory-incubated blades. This was expected because estimates of whole-plant respiratory demands include the consumption requirements of non-photosynthetic tissues. Consequently, ratios of $P_{net}:R_d$ were nearly 3 times higher in laboratory-incubated blades than those calculated for *in situ*-incubated whole plants (*ca.* 8 cf. 3, respectively). This is consistent with data reported for *Halodule wrightii* in upper Laguna Madre (ULM), Texas (Dunton and Tomasko 1994); $P_{net}:R_d$ ratios were much higher for laboratory-incubated plants.

Conclusion

Photophysiological parameters may be difficult to use as indicators of environmental stress in *Syringodium filiforme*, as this species does not display a great capacity for phenotypic plasticity. Not only was there no discernable seasonal variation in pigment content and/or stoichiometry, but photosynthesis-irradiance parameters (I_c , I_k , Gross P_{max} and R_d) were all highest during months characterized by high temperature and irradiance. Unlike temperate species, which exhibit a unique strategy for overcoming large environmental fluctuations through acclimation, tropical and subtropical plants have no clear mechanism for compensation. As expected, photon flux densities necessary to achieve net and light-saturated photosynthesis (I_c and I_k , respectively) increase with increasing temperature, while rates of light-limited photosynthesis necessarily decrease. These relationships appear to be a general phenomenon in higher plants and some macroalgae (Marsh *et al.* 1986, Davison *et al.* 1991), suggesting that light-limited plants might achieve lower rates of photosynthesis. In part, this may explain the recent widespread disappearance of seagrass habitat coincident with underwater light reduction.

Similar to recent studies addressing *in situ* photosynthesis in seagrass systems (e.g., Dunton and Tomasko 1994, Herzka and Dunton 1997), we suggest that PI parameters derived from whole-plant incubations are more representative of seasonal photosynthetic performance than those derived from laboratory blade incubations. While blade incubations provide useful physiological information regarding seasonal trends in photosynthesis, they may significantly underestimate light requirements (i.e., I_k and I_c). In contrast, although costly and time-consuming, *in situ* measurements provide invaluable information with reference to the natural environment and increase our predictive capabilities when used to assess coastal ecosystem health and productivity.

References

- Abal EG, Loneragan N, Bowen P, Perry CJ, Udy JW, Dennison WC (1994) Physiological and morphological responses of the seagrass *Zostera capricorni* Aschers. to light intensity. *J Exp Mar Biol Ecol* 178:113-129
- Baker NR, McKiernan M (1988) Modifications to the photosynthetic apparatus of higher plants in response to changes in the light environment. *Biol J Linn Soc* 34:193-203
- Bannister TT (1979) Quantitative description of steady state, nutrient-saturated algal growth, including adaptation. *Limnol Oceanogr* 24:76-96
- Berry J, Björkman O (1980) Photosynthetic response and adaptation to temperature in higher plants. *Annu Rev Plant Physiol* 31:491-543
- Björkman O (1981) Responses to different quantum flux densities. In: Lange OL, Nobel PS, Osmond CB, Ziegler H (eds) *Encyclopedia of Plant Physiology*, n s vol 12A. Springer-Verlag, Berlin, p 57-107
- Bulthuis DA (1983) Effects of temperature on the photosynthesis-irradiance curve of the Australian seagrass, *Heterozostera tasmanica*. *Mar Biol Lett* 4:47-57
- Bulthuis DA (1987) Effects of temperature on photosynthesis and growth of seagrasses. *Aquat Bot* 27:27-40
- Chapman ARO, Craigie JS (1977) Seasonal growth in *Laminaria longicuris*: relations with dissolved inorganic nutrients and internal reserves of nitrogen. *Mar Biol* 40:197-205

- Chapman ARO, Markham JW, Lüning K (1978) Effect of nitrate concentration on the growth and physiology of *Laminaria saccharina* (Phaeophyta) in culture. *J Phycol* 14:195-198
- Cornelius SE (1977) Food and resource utilization by wintering redheads on Lower Laguna Madre. *J Wildl Mgmt* 41:374-385
- Davison IR (1991) Environmental effects on algal photosynthesis: temperature. *J Phycol* 27: 2-8
- Davison IR, Greene RM, Podolak EJ (1991) Temperature acclimation of respiration and photosynthesis in the brown alga *Laminaria saccharina*. *Mar Biol* 110:449-454
- Dawes CJ (1998) Biomass and photosynthetic responses to irradiance by a shallow and deep water population of *Thalassia testudinum* on the west coast of Florida. 62(1):89-96
- Dawes CJ, Tomasko DA (1988) Depth distribution of *Thalassia testudinum* in two meadows on the west coast of Florida: a difference in effect of light availability. *PSZN I: Mar Ecol* 9: 123-130
- Day RW, Quinn GP (1989) Comparisons of treatments after an analysis of variance in ecology. *Ecol Monogr* 59:433-446
- Dennison WC, Alberte RS (1982) Photosynthetic responses of *Zostera marina* L. (Eelgrass) to *in situ* manipulations of light intensity. *Oecologia* 55:137-144
- Dennison WC, Alberte RS (1985) Role of daily light period in the depth distribution of *Zostera marina* (eelgrass). *Mar Ecol Prog Ser* 25:51-61
- Dennison WC, Alberte RS (1986) Photoadaptation and growth of *Zostera marina* L. (eelgrass) transplants along a depth gradient. *J Exp Mar Biol Ecol* 98:265-282

- Dudgeon SR, Davison IR, Vadas RL (1990) Freezing tolerance in the intertidal red algae *Chondrus crispus* and *Mastocarpus stellatus*: relative importance of acclimation and adaptation. *Mar Biol* 106:427-436
- Dunton KH (1994) Seasonal growth and biomass of the subtropical seagrass *Halodule wrightii* in relation to continuous measurements of underwater irradiance. *Mar Biol* 120:479-489
- Dunton KH, Tomasko DA (1994) *In situ* photosynthesis in the seagrass *Halodule wrightii* in a hypersaline subtropical lagoon. *Mar Ecol Prog Ser* 107:281-293
- Falkowski PG, LaRoche J (1991) Acclimation to spectral irradiance in algae. *J Phycol* 27:8-14
- Falkowski PG, Owens TG, Ley AC, Mauzerall DC (1981) Effects of growth irradiance levels on the ratio of reaction centres in two species of marine phytoplankton. *Plant Physiol* 68: 969-973
- Fourqurean JW, Zieman JC (1991) Photosynthesis, respiration and whole plant carbon budget of the seagrass *Thalassia testudinum*. *Mar Ecol Prog Ser* 69:161-170
- Fry B, Parker PL (1979) Animal diet in Texas seagrass meadows: $d^{13}C$ evidence for the importance of benthic plants. *Est Coast Mar Sci* 8:499-509
- Gerard VA (1988) Ecotypic differentiation in light-related traits of the kelp *Laminaria saccharina*. *Mar Biol* 97:25-36
- Henley WJ, Dunton KH (1997) Effects of nitrogen supply and continuous darkness on growth and photosynthesis of the arctic kelp *Laminaria solidungula*. *Limnol Oceanogr* 42 (2): 209-216

- Herzka SZ, Dunton KH (1997) Seasonal photosynthetic patterns of the seagrass *Thalassia testudinum* in the western Gulf of Mexico. *Mar Ecol Prog Ser* 152:103-117
- Jassby AD, Platt T (1976) Mathematical formulation of the relationship between photosynthesis and light for phytoplankton. *Limnol Oceanogr* 21(4):540-547
- Kübler JE, Davison IR, Yarish C (1991) Photosynthetic adaptation to temperature in the red algae *Lomentaria baileyana* and *Lomentaria orcadensis*. *Br Phycol J* 26:9-19
- Lee K-S, Dunton KH (1999) Influence of sediment nitrogen-availability on carbon and nitrogen dynamics in the seagrass *Thalassia testudinum*. *Mar Biol* 134:217-226
- Machalek KM, Davison IR, Falkowski PG (1996) Thermal and photoacclimation of photosynthesis in the brown alga, *Laminaria saccharina*. *Plant, Cell and Environ* 19:1005-1016
- Marsh JA, Dennison WC, Alberte RS (1986) Effect of temperature on photosynthesis and respiration in eelgrass (*Zostera marina* L.). *J Exp Mar Biol Ecol* 101:257-267
- Massini RJ, Cary JL, Simpson CJ, McComb AJ (1995) Effects of light and temperature on the photosynthesis of meadow-forming seagrasses in Western Australia. *Aquat Bot* 49:239-254
- Mazzella L, Mauzerall D, Lyman H, Alberte RS (1981) Protoplast isolation and photosynthetic characteristics of *Zostera marina* L. (eelgrass). *Bot Mar* 24:285-289
- McRoy CP, McMillan C (1977) Production ecology and physiology of seagrasses. In: McRoy C P, Helfferich C (eds) *Seagrass ecosystems: a scientific perspective*. Dekker, New York, p 53-81

- Mishkind M, Mauzerall D (1980) Kinetic evidence for a common photosynthetic step in diverse seaweeds. *Mar Biol* 56:261-265
- Nielsen SL, Sand-Jensen K (1989) Regulation of photosynthetic rates of submerged rooted macrophytes. *Oecologia* 81:364-368
- Onuf CP (1994) Seagrasses, dredging and light in Laguna Madre, Texas, USA. *Estuar Coast Shelf Sci* 39:75-91
- Onuf CP (1996) Seagrass responses to long-term light reduction by brown tide in upper Laguna Madre, Texas: distribution and biomass patterns. *Mar Ecol Prog Ser* 138:219-231
- Pearson GA, Davison IR (1994) Freezing stress and osmotic dehydration in *Fucus distichus* (Phaeophyta): Evidence for physiological similarity. *J Phycol* 30:257-267
- Pérez M, Romero J (1992) Photosynthetic response to light and temperature of the seagrass *Cymodocea nodosa* and the prediction of its seasonality. *Aquat Bot* 43:51-62
- Porra RJ, Thompson WA, Kriedemann PE (1989) Determination of accurate extinction coefficients and simultaneous equations for assaying chlorophylls *a* and *b* extracted with four different solvents: verification of the concentration of chlorophyll standards by atomic absorption spectroscopy. *Biochim Biophys Acta* 975:384-394
- Quammen ML, Onuf CP (1993) Laguna Madre: seagrass changes continue decades after salinity reduction. *Estuaries* 16:302-310

- Ramus J, Lemons F, Zimmerman C (1977) Adaptation of light-harvesting pigments to downwelling light and the consequent photosynthetic performance of the eulittoral rockweeds *Ascophyllum nodosum* and *Fucus vesiculosus*. *Mar Biol* 42:293-303
- Rooker J, Holt J, Holt S (1997) Condition of larval and juvenile red drum (*Sciaenops ocellatus*) from estuarine nursery habitats. *Mar Biol* 127:387-394
- Smith BA, Melis A (1987) Photosystem stoichiometry and excitation distribution in chloroplasts from surface and minus 20 meter blades of *Macrocystis pyrifera*, the giant kelp. *Plant Physiol* 84:1325-1330
- Tomasko DA (1992) Variation in the growth form of shoal grass (*Halodule wrightii*) due to changes in the spectral composition of light below a canopy of turtle grass (*Thalassia testudinum*). *Estuaries* 15:241-247
- Zar JH (1984) *Biostatistical Analysis* (2nd ed). Prentice Hall, New Jersey, p 522-537
- Zieman JC (1982) The ecology of seagrasses of South Florida: a community profile. US Fish Wildl Serv USFWS/OBS-82/25:158